Skeletal element elongation and interdigital tissue regression in developing bat limbs: a gene expression analysis

Mandy Kelly Mason

Thesis Presented for the Degree of

DOCTOR OF PHILOSOPHY

in the Department of Molecular and Cell Biology

UNIVERSITY OF CAPE TOWN

May 2016

Declarations

I know the meaning of plagiarism and declare that all of the work in the dissertation (or thesis), save for that which is properly acknowledged, is my own

Signed by candidate
Signature Removed

Mandy Mason

2 February 2016

Date

I hereby:

(a) grant the University free license to reproduce the above thesis in whole or in part, for the purpose of research;

(b) declare that:

(i) the above thesis is my own unaided work, both in conception and execution, and that apart from the normal guidance of my supervisor, I have received no assistance apart from that stated below;

(ii) except as stated below, neither the substance nor any part of the thesis has been submitted in the past, nor is being, nor is to be submitted for a degree at this University or any other University.

(iii) I am now presenting the thesis for examination for the Degree of PhD.

Signed by candidate
Signature Removed

Mandy Mason

2 February 2016

Date

Acknowledgements

I would like to acknowledge and thank the following people and institutions for playing an integral part in my research journey and academic development.

My supervisors, Prof. Nicola Illing and A/Prof. David Jacobs, who have supported me throughout my Doctoral research, providing valued input and feedback regarding the work. My lab (in the Molecular and Cellular Biology Department, UCT) and visiting researchers, both past and present: Dr. Arthur Shen, Dr Christiane Nday, Rafe Lyall, Stephen Schlebusch, Lyle Lathe Curry, Yolande Grobler, Liezl le Roux, Zoe Gill and Ash Parker, a fantastic and dynamic team of people who have helped, supported and challenged me throughout this project. The Molecular and Cellular Biology Department, for creating a nurturing academic environment and providing a variety of opportunities to learn and grow. A special mention goes to Faezah Davids, Madhu Chauhan, Di James, Pei-yin Liebrich and Shakiera Sattar who have provided vital services, support and experienced technical advice.

The Animal Evolution & Systematics Group, in the Biological Sciences Department, UCT, for providing tissue samples for five additional bat species: *Cloeotis percivali*; *Hipposideros commersoni*; *Pteronotus parnellii*; *Mystacina tuberculata*; *Rhinolophus clivosus*. Special thanks go to Dr. Samantha Stoffberg and Dr. Lizelle Kruger for providing encouragement and advice to support the fieldwork component of this project. Thanks to the Biological Sciences Department, for the use of their facilities, specific thanks go to Granville Faulmann and George Du Plessis for their help with vehicle bookings and Petra Muller for her essential role in training and running the digital imaging unit, and for allowing me many fun hours on the microscope getting things 'just right'.

I would also like to thank the Logan Group, in the MRC-NIMR, Division of Developmental Biology (2000-2013) for allowing me to join their lab for a year. Thank you to Dr. Malcolm Logan for sage advice, Sue Miller for her kindness, Satoko Nishimoto, Natalie Butterfield, Veronique Duboc and Laurianne Besse for constructive criticisms, Sorrel Bickley for her patience and support, Fatima Sulliman for her instruction, and thanks to Ania Kucharska for everything. I would like to extend my thanks to the people in the NIMR administration, who provided valuable support during this time.

I acknowledge that several components of this work were performed with the assistance of the following people: Quantitative PCR experiments were performed in conjunction with Lyle Curry, Liezl le Roux and Zoe Gill. Whole mount *in situ* staining experiments of *Hoxa11* and *Hoxa13* were performed in conjunction with Zoe Gill. RACE, HiFi PCR and Skeletal element staining experiments were

performed in conjunction with Liezl le Roux. WISH experiments on *Rdh10*^{trex} transgenic mouse embryos were performed by Dr. Thomas Cunningham and Dr. Gregg Deuster.

During this project I was supported by the following bursaries, scholarships and awards: SARChi Grantholders Linked Bursary, the UCT Twamley Postgraduate Bursary, NRF Doctoral Package Project Award, UCT Research Associate Award, Harry Crossley Foundation Postgraduate Scholarship, UCT Doctoral Research Scholarship, WhiteSci Travel Award, Commonwealth Split-site Scholarship, DST /NRF Innovation Doctoral Scholarship. Thanks go to the associated organisations, institutions and companies. The financial assistance of the National Research Foundation towards this research is acknowledged. Opinions expressed in this thesis and the conclusions arrived at, are those of the author, and are not necessarily to be attributed to the National Research Foundation.

I also want to acknowledge the bats and mice that were killed for this work to be performed, and give thanks to the UCT Faculty of Health Sciences Animal Ethics Committee, the University of Cape Town Faculty of Science Animal Experimentation Committee and the Western Cape Nature Conservation Board, for the ethical guidance in this regard. Thanks also go to Jaap Visser at the UCT Research Animal Facility, for his assistance in sampling mouse embryos. Thank you to Callum Beattie, Conservation Manager, De Hoop Nature Reserve for facilitating field trips.

Finally thanks go to my family (both close and extended) and friends (you know who you are) who have provided a bottomless pool of support and encouragement through this time. My partner Robyn for taking this journey with me and for being besides me every step of the way, I owe you a great debt, one that I look forward to paying. My mother Shirley and sisters, Kate and Nienke for their patience, support and tough love. The Verrinders, with special mention to Cedric, and his Lamarckian jests, you have taught me the most in this time. Jenny, Noel and Roanna, thank you for being such a wonderful team. Thanks to my gran, so recently passed, who would always ask: 'How are the bats?' and to the Braithwaite family for all of their encouragement, interest and pragmatic support. Thank you all for keeping things together while I chased an ephemeral truth, like a fleeting bat in the night sky.

Table of Contents

List of Figures and Tables

List of Abbreviations

AER	apical ectodermal ridge
AP	anteroposterior
BLAST	basic local alignment search tool
BLAT	BLAST-like alignment tool
BMP	bone morphogenic protein
BMPR	BMP receptor
bp	base pairs
CDS	coding sequence
CS	*Carollia* stage
Cq	quantification cycle
Ct	cycle threshold
DE	differentially expressed
DI	digit I
DV	dorsoventral
E	efficiency (qPCR experiments)
E	embryonic day (developmental staging)
EC	embryonal carcinoma
ECM	extracellular matrix
ELCR	early limb control region
FGF	fibroblast growth factor
FISH	florescent *in situ* hybridisation
FL	forelimb
GCR	global control region
GLI3R	GLI3 repressor form protein
GLI3A	GLI3 activator form protein
H	humerus
HDAC	histonedeacetylases
HL	hindlimb
HMR	human mouse rat
ICD	interdigital cell death
ID	interdigit / interdigital
IGF	insulin-like growth factors
IIBA	branchial arch II
IPTG	isopropyl β-D-1-thiogalactopyranoside
ISH	*in situ* hybridisation
IVT	*in vitro* transcription
LB	lysogeny broth
LPM	lateral plate mesoderm
LRT	likelihood ratio test
M	metacarpal / metatarsal
MAPK	mitogen-activated protein kinase
Mc	metacarpals
Mt	metatarsals
NTC	no template control
P	phalange
P1	phalange 1
PCD	programmed cell death
PCR	polymerase chain reaction
PD	proximodistal
PFR	phalanx-forming regions
PKA	protein kinase A
PWI	pairwise identity
qPCR	quantitative PCR
R	radius
RA	retinoic acid
RAR	retinoic acid receptor
RARE	retinoic acid response element
RXR	retinoic acid receptor
RE	restriction enzyme
RG	red-green
SD	standard deviation
SE	standard error
SHH	sonic hedgehog
TF	transcription factor
WGS	whole genome shotgun
WISH	whole-mount *in situ* hybridisation
WNT	wingless-related integration site
WT	wildtype
ZPA	zone of polarising activity
ZRS	ZPA regulatory sequence

Abstract

Skeletal element elongation and interdigital tissue regression in developing bat limbs: a gene expression analysis

Mandy Kelly Mason
January 2016

Vertebrate limbs classically illustrate the morphological diversity of homologous structures, with the form of each adapted to its function. Bat limbs exemplify this, having strikingly divergent forelimbs and hindlimbs, suited to flying and grasping respectively. The bat wing is composed of highly elongated skeletal elements, supporting expansive membranes, while the hindlimbs are reduced, with short, symmetrical, typically free digits, features that are evident during embryonic development. An understanding of the genes, interactions and events that shape bat limbs, will inform conventional models of development and allow us to describe deviations from these in a natural and stable limb variant. This thesis outlines key processes involved in limb development, focusing on autopod formation, and integrates this with current research on bat limb development. Two genes that are differentially expressed between developing bat limbs, *Meis2* and *Hoxd11*, were characterised during autopod development, digit formation and interdigital regression in the bat (CS15-CS18) and equivalently staged mice.

Meis2 is involved in limb bud proximodistal patterning, with its role in the context of autopod development currently unexplored. Comparisons of autopod *Meis2,* by qPCR, and WISH, found strong expression in the expanding interdigital regions of the bat forelimb, with lowered expression in mouse interdigits and loss of expression in the bat hindlimb. This did not correspond with *Hoxa13* expression, which was reduced in the forelimb. Interdigital expression of *Meis2* was independent of retinoic acid (RA) signalling, with genes involved in RA synthesis (*Rdh10*, *Aldha2*), degradation (*Cyp26b1*) and signalling (*Rarβ*) expressed in bat limbs. Altered expression patterns of *Aldha2* and *Cyp26b1*, indicate that this pathway may be modulated in the forelimb. *Meis2* is suggested to play a role in interdigital tissue retention, enhancing cell proliferation and contributing to wing expansion.

5'HoxD genes (*Hoxd10-13*) are involved in limb patterning, digit formation and growth. Their modular autopod expression domains correspond to the adult bat skeletal element phenotype, with strong overexpression of *Hoxd10*, *11* (and to a lesser extent *Hoxd12*) in the forelimb posterior elements (digits II-V), which are highly elongated, and a loss of expression of these genes in the hindlimb digits, which are proportionately shortened and highly symmetrical. These genes were not expressed in a

typical reverse collinear relationship, with absolute qPCR revealing highest expression of *Hoxd10*. While the protein coding sequence of these genes appeared highly conserved between bats and other mammals, several changes were found in a conserved sequence region (termed the CsC) of the digit enhancer Prox, some of which were associated with alterations in transcription binding sites. These findings indicate that *Hoxd10-12* expressions contribute to the altered skeletal element morphologies of bat forelimbs and hindlimbs.

In conclusion, I find that the upregulation of *Meis2* in the interdigital tissues of the developing bat wing suggests a role for *Meis2* in shaping the autopod. This expression is RA-independent, and, in the bat wing, interdigital tissue retention is not due to a suppression of RA-induced cell death. In this context RA signalling may, play a role in interdigital tissue thinning in the bat forelimb, while *Meis2* has the potential to interact with other factors during both bat and mouse autopod development to maintain a pool of interdigital cells that contribute to interdigital growth. Based on the examination of the 5'HoxD genes, I conclude that there has been an alteration in their regulation in both the bat FL and the HL, with modifications of one of their enhancer sequences, potentially playing a small part in modulating these interactions. This study makes a valuable contribution to the growing body of work that explores the bat limb development and the genetic adaptations that underlie the evolution of these unique structures.

1. Origins and extremes: fins, limbs and the evolutionary development of the bat wing

1.1. Limbs are complex structures that can be used to understand the process of evolutionary change

Vertebrate limbs are remarkable structures that exhibit deep homology, evidenced by a common, basic skeletal template and a conserved gene set that governs their initial formation and growth during embryonic development (Shubin *et al.* 1997). Their modular structure is a product of their evolutionary origins: the employment of body axis developmental pathways that allowed the body wall to bud outwards, and, in an iterative, mutable fashion, to form an appendage (Coates and Cohn 1998). Over their 500 million years of evolutionary history, tetrapod limbs have repeatedly diverged into an astonishing assortment of forms, each with a unique morphology that is adapted to perform a specific set of functions (Darwin 1859). They are classic models of evolutionary variation, commonly used to examine and understand processes that underlie (and principles that can be used to explain) evolutionary change (Shubin *et al.* 1997). They remain a fascinating system, and have been recently used to examine evolutionary novelty within the framework of evolution and development otherwise known as evo-devo (Carroll 2008; Shubin *et al.* 2009). In this section I give a brief overview of the origins of the vertebrate limb, highlight how these have become diversified and then focus on the bat as an example of limb morphological variation.

1.1.1. Limbs and the rise of the autopod

The tetrapod limb has three distinct regions consisting of the stylopod, the zeugopod and the autopod (Figure 1.1). The skeletal elements of the stylopod (humerus/femur) and zeugopod elements (ulna/fibula and radius/tibia) have clear homology with the proximal elements of the fin in lobe-finned fish (Sarcopterygii), which includes the extant *Coelacanth* (Figure 1.1) (Shubin 2002; Schneider and Shubin 2013). The autopod, the most distal structure, has been broadly described as a structural evolutionary 'novelty' (Shubin *et al.* 1997; Wagner and Lynch 2010), a distinguishing feature of tetrapods, with its appearance in the fossil record originally used as a landmark in the fin to limb (and the ancestral fish to tetrapod) transition. However, closer examinations of extant lobe-fin fish (e.g. *Coelacanth*, Friedman *et al.* 2007) and advanced transitional forms (Tetrapodomorpha) have revealed that they share features of both fish and tetrapods (e.g. *Tiktaalik*, Shubin *et al.* 2006), with simple wrist

regions and distal radials that appear to become transformed into digit-like rays (Figure 1.1) (as found for *Acanthostega*, Coates 1996).

In addition to this, recent examination of gene expression and regulatory elements that are specifically involved in vertebrate autopod formation have shown that there is deep homology between these and the distal radials of basal Actinopterygii that have retained their metapterygium (Figure 1.1) (Davis *et al.* 2007; Johanson *et al.* 2007; Davis 2013; Gehrke *et al.* 2015). These experiments highlight the fact that the tetrapod autopod is a distinct evolutionary and developmental module, with deep homology of conserved regulatory elements and pathways, which have become adapted to take on a variety of forms.

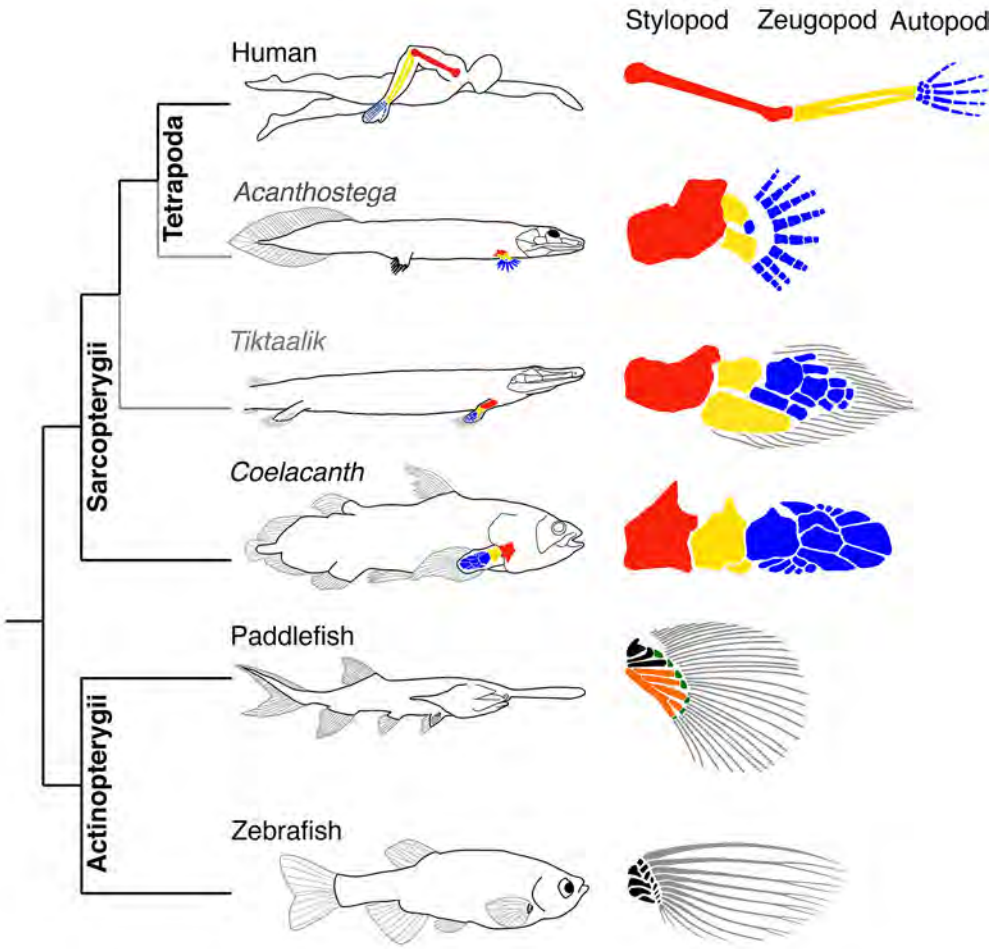

Figure 1.1: The evolution of the limb and its relationship to the fin. The deep homology of fins and limbs has been well illustrated (Shubin *et al.* 1997, 2009), with the transformation of water-propelling fin structures into load-bearing limbs representing a crucial turning point in vertebrate evolution that enabled terrestrial colonisation and subsequent expansion (Hall 2007). Limbs evolved within the Sarcopterygii and are derived from the elaborated fins of the lobed-fin fish (represented by the extant *Coelacanth*). Tetrapodomorpha (represented by the *Tiktaalik*) had extended distal radials, while early tetrapods (*Acanthostega*) had more digit-like rays. These fins and limbs of Sarcopterygii do not show structural homology with the fins of Actinopterygii. Tetrapod autopods have deep homology to the metapterygium (orange) and the distal radials (green), a feature that has been lost in Teleostei (represented by the zebrafish, black). Homology among Sarcopterygii (extinct lineages indicated in grey) forelimbs stylopod (red), zeugopod (yellow) and autopod (blue) is shown. Image adapted from Schneider and Shubin (2013) and Davis *et al.* (2013).

1.1.2. Autopod morphologies differ both within and across vertebrate species

The modern tetrapod autopod has a basic structure that can be represented by the highly modified human hand and foot (Figure 1.2). The proximal portion (basipod) is made up of nodular bones forming the forelimb wrist (carpus) or hindlimb ankle (tarsus). In extant tetrapod limbs these bones vary widely in shape, size and number as they have become lost or fused to provide support, enable articulation and aid locomotion (reviewed by Johanson *et al.* 2007). The distal portion (mesopod and acropod, together known as the metapod) is made up of columns of articulating, elongate 'spool-shaped' bones (or cartilages) that form the metacarpals/metatarsals and phalanges. The proximal metacarpals/metatarsals form the base of the digit ray while the more distal phalanges form the portion of the digit ray that is free in primates (the digit). The autopod conventionally has five morphologically distinct digit rays, a feature termed pentadactyly, classed as digits I–V Figure 1.2). The addition of digits (polydactyly) is considered anomalous, and is attributed to specific genetic mutations that affect development (congenital disorders) rather than species-specific traits (Galis *et al.* 2001; Biesecker 2011). Loss or fusion of digits is more common, and is mediated during early embryonic development through the re-patterning or destruction of digit ray anlages (Lande 1978; Shapiro *et al.* 2003; Cooper *et al.* 2014).

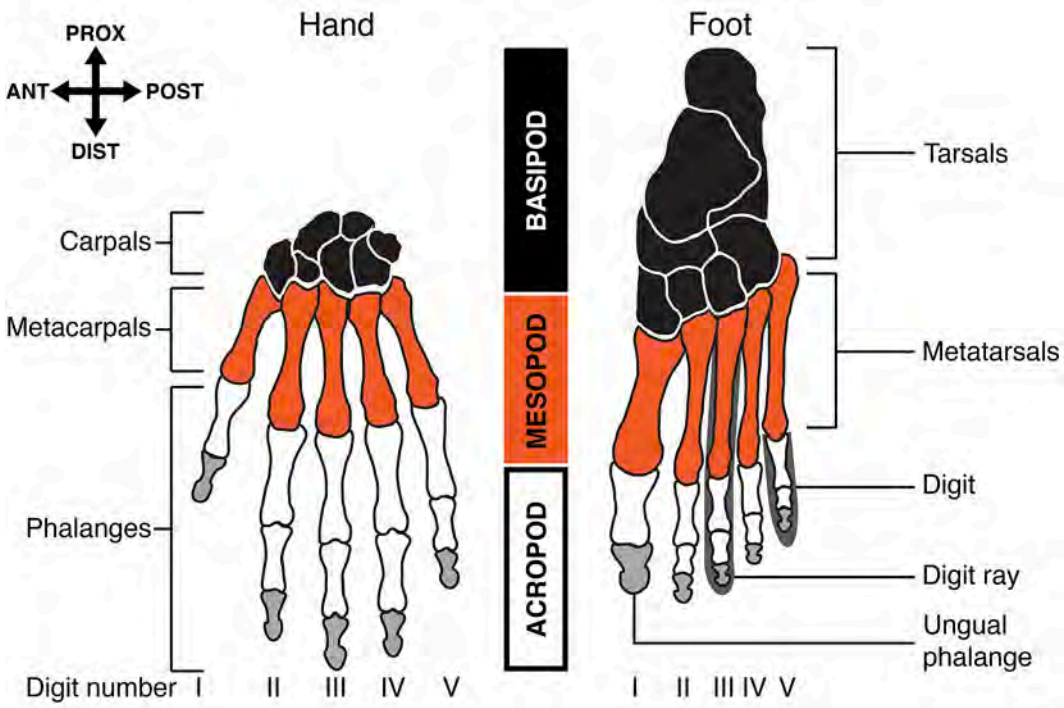

Figure 1.2: Skeletal structure of the human hand and foot. This schematic illustrates the basic structure of the autopod skeletal elements and their respective terminology. It also highlights the differences between these components in the human forelimb (hand) and hindlimb (foot). Dorsal surface shown, autopods are not to scale.

While each digit ray has one metacarpal/metatarsal element, the numbers of phalanges (phalangeal formula) differs across vertebrates. The ancestral amniote (reptiles, birds and mammals) phalangeal formula (2/3/4/5/4) has become reduced in the majority of mammals (primitive formula of 2/3/3/3/3; Figure 1.2) while being increased in some groups (hyperphalangy in cetaceans e.g. dolphins) (Figure 1.3) (reviewed by Fedak and Hall 2004). Phalanges are numbered proximally to distally (P1; P2; P3), with the single proximal phalanx of the mammalian thumb given an intermediate term (P1/2). Both the length and number of phalanges affect the length and flexibility/strength of the digit in an interdependent manner. The most terminal (ungual) phalanx is often covered by specialised keratinised structure (nail, claw, hoof) that interfaces with the environment, protects the digit tip and can perform a diverse range of functions (Hamrick 2001).

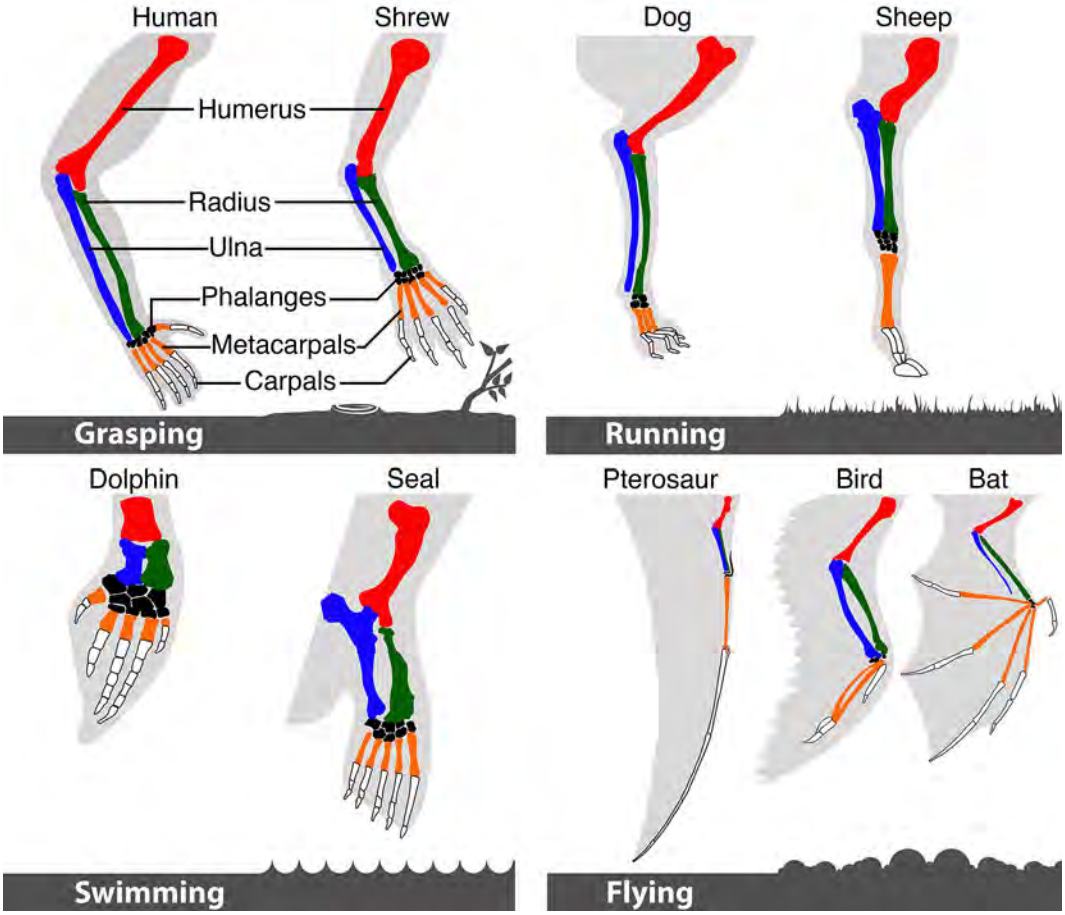

Figure 1.3: Vertebrate forelimb skeletal elements are highly diverse. The functional requirements of the limb (how it is used to interact with the environment) correspond to its basic structure with species that manipulate objects (grasping) typically having five free digits; those that run (running) having elongate fused elements; those that swim (swimming) showing shortened robust elements that support a webbed structure; and those that fly (flying) exhibiting several means of supporting an enlarged surface to form a wing. The basic skeletal elements are shared amongst all vertebrates with the humerus (red) radius (green); ulna (blue); metacarpals (orange) and phalanges (white) indicated. Adapted from Audesirk and Audesirk (1999), limbs not to scale.

In addition to the skeletal structure described above, the autopod is comprised of soft-tissue (that includes networks of connective tissue, vasculature, nervous tissue, musculature and epidermis) to form the most highly complex and adaptable portion of the tetrapod limb.

Autopods are an essential part of the limb. Each is exquisitely adapted to the specific function of arboreal, terrestrial, aquatic or aerial locomotion (in addition to other activities). Their structure appears to be highly labile and they have been adapted to a variety of forms (Figure 1.3). Most familiar are our own primate hands, with their flexible wrist and fingers that are joined by muscular palms, and feet, that have supportive ankles, padded elongate metatarsals and short toes (Figure 1.2). Primates and some rodents have metacarpals connected by muscular tissue, forming a supportive palm with free digits to aid in climbing and gripping objects (Figure 1.3). Quadrupeds that run for long distances at high speed often have a reduced number of digits that make contact with the ground (Figure 1.3). Secondarily aquatic tetrapods (e.g. cetaceans) have modified digits that form strong, thickly webbed, flippers that are used as paddles or rudders when swimming (Figure 1.3).

Striking autopod adaptations are found in the three vertebrate lineages that have independently evolved the ability to fly. In the extinct Pterodactyloidea, the wing membrane was extended using the highly elongated, thickened phalanges of digit IV, while digit V was lost and digits I-II were truncated and reduced (Figure 1.3) (Bennett 2000; Tokita 2015). In the class Aves (birds) there has been a similar loss, with flying birds having only three morphologically distinct digit rays in their forelimb, homologous to mammalian digits I-III (Wang, Young, *et al.* 2011). The metacarpals are fused and the phalanges are truncated, providing a stiff framework to support the wing feathers (Figure 1.3). The bat is the only mammal that has evolved the capability of powered flight. It is the only flying vertebrate to have maintained its pentadactyl condition, with its four highly elongated posterior digits used as a framework to support a flexible wing membrane (Neuweiler 2000). This pentadactyl support structure allows multiple degrees of freedom during flight, giving the bat active control over the shape and tension of the wing membrane (Swartz *et al.* 2007). The skeletal element proportions differ amongst bat families, with the wing dimensions being an important determinant of the physical flight capabilities of each (Norberg 1969, 1981; Norberg and Rayner 1987). The Order Chiroptera is named for this “hand-wing” and remains a classic example of autopod variability, which has been long used as an example of the remarkable outcomes of evolutionary processes over time (Darwin 1859).

1.1.3. The unique adaptations of bat limbs facilitate flight

Bat forelimbs are specifically adapted for highly manoeuvrable, powered flight (Vaughan 1970). The forelimb skeletal elements of digits II-V are disproportionality elongated; in adult *Miniopterus natalensis* they are more than twice the head body length (Figure 1.4). The more proximal elements (that form the arm-wing) have an increased diameter, this becomes reduced in the more distal elements (hand-wing), with corresponding lower cortical bone mineralisation as compared to nonvolant mammals (Swartz 1997; Swartz and Middleton 2008). Together these characteristics give the wing reach, structural strength and flexibility. While the stylopod and zeugopod elements of the forelimb elements are highly robust, their hindlimb counterparts are comparatively thinner. The zeugopod shares a reduced ulnar (in the forelimb) and fibula in the (in the hindlimb). Both the carpals and the tarsals are also highly specialised allowing limited degrees of freedom to resist torsion during flight (Vaughan 1970). The forelimb digit I (pollex) is short, clawed and free, and extends perpendicularly from the wrist. It is used for grasping and crawling, and in many species, it shares a tendon locking mechanism with the digits of the hindlimb (Quinn and Baumel 1993; Neuweiler 2000). The elements of the other digits are asymmetrically elongated, and do not have claws (with the exception of many of the Pteropodidae, which have a claw on digit II) (Vaughan *et al.* 2011). Digit II is the shortest of these proximal digits, and in *M. natalensis*, only the proximal phalange is ossified, with a ligament extending from the distal end of this digit to the base of the second phalanx of digit III (Figure 1.4), creating a stiff frame to support the leading edge of the hand-wing (Norberg 1969). Digit III is the most elongated digit, extending to provide length to the wing. Digits III-V become progressively shorter and contain only the proximal and intermediate phalanges (P1 and P2) with each digit capped by a flexible cartilage tip (Figure 1.4) (Hockman *et al.* 2009).

The bat forelimb is incredibly divergent, both from that of other mammals, and from its own hindlimb, which is reduced in size and strength when compared to terrestrial mammals (Howell and Pylka 1977; Swartz 1997; Riskin *et al.* 2005; Swartz and Middleton 2008). For the most part, bat hindlimbs have five symmetrical digits that are short, free, and clawed (Figure 1.4), these aid in crawling and roosting i.e. clinging to perches (Swartz 1997; Neuweiler 2000; Schutt Jr. and Simmons 2006). Two families deviate from this form: Myzopodidae have toes with fused metatarsals and only two phalanges; and Thyropteridae have syndactyly of digit III and IV and only two phalanges (Vaughan *et al.* 2011). These species are 'exceptions to the rule', relying on foot-pads or disks that allow the bats to adhere to the smooth surface of leaves where they roost (Riskin and Fenton 2001; Riskin and Racey 2010).

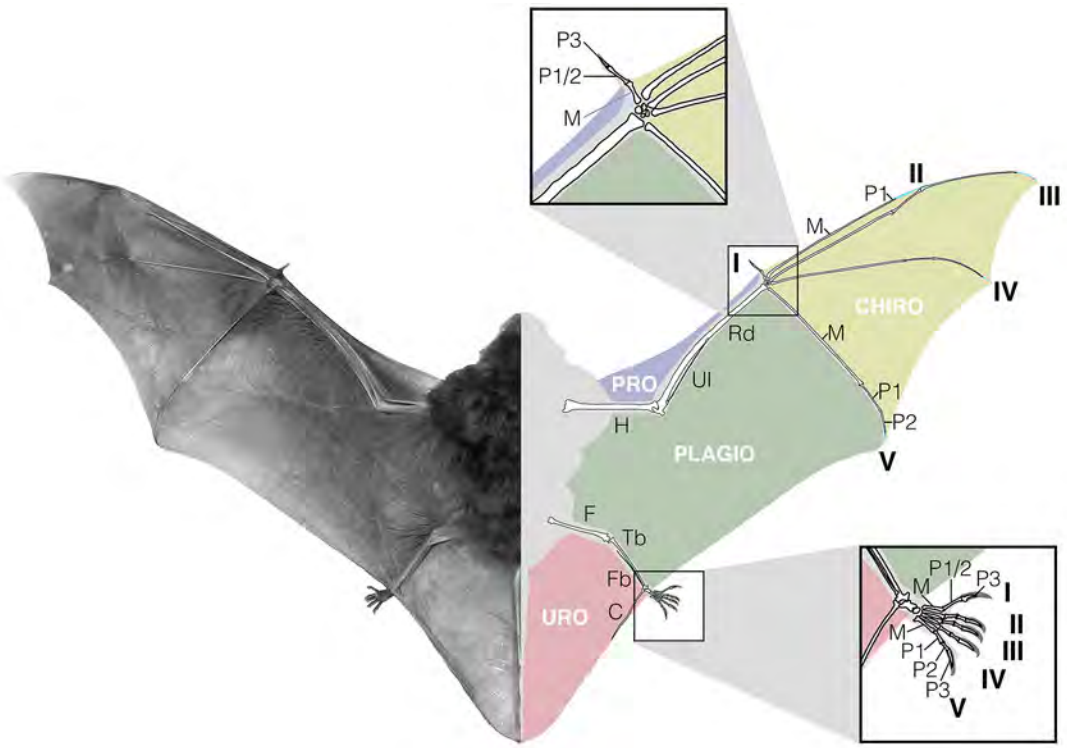

Figure 1.4: An image and corresponding schematic of the ventral surface of an adult bat, *Miniopterus natalensis*. The membranous components that make up the wing surface, the chiropatagia (CHIRO, yellow); propatagia (PRO, purple); plagiopatagium (PLAGIO, green) and uropatagium (URO, red) are shown. Digit numbers are given and the skeletal elements of the arm (H, humerus; Ul, ulna; Rd, radius), forelimb digits (M, metacarpal; P, phalange) and hindlimb (F, femur; Tb, tibia, Fb, fibula; C, calcar) are given with the skeletal elements of the foot shown inset.

In addition to the dramatic differences seen in the appendicular skeleton of the bat, unique changes are also seen in the skin associated with these structures. An extensive, compliant membrane encompasses the entire forelimb and proximal hindlimb (Figure 1.4). This comprises of a complex network of muscles, tendons and nerves that serve to tension the membrane and provide sensory feedback while in flight (Sterbing-D'Angelo *et al.* 2011; Cheney *et al.* 2014). The arm-wing area consists of the propatagia, which runs from the shoulder of the bat to the wrist to form the leading edge (Norberg 1969) and the plagiopatagium, which is the membrane extending from the flank that joins the forelimb to the hindlimb (Figure 1.4). The hand wing is formed from chiropatagia (also known as dactylopatagia), which are membranes found between digits II-V (Figure 1.4). While the pro- and plagiopatagium provide most of the lift during flight, the chiropatagia generates the thrust that propels the bat forwards (Vaughan 1970). Another membrane, the uropatagium, runs from the hindlimb (excluding the foot) to the tail (Figure 1.4). This membrane does facilitate, but is not required for, flight while some species use this to assist in catching prey on the wing (Vaughan 1970).

1.1.4. The evolutionary enigma of bat flight

Bats are thought to have evolved from small nocturnal insect-eating arboreal mammals, with transitional behaviour and forms following a leaping, gliding and then flying trajectory, possibly in response to predation or to aid foraging and locomotion (Darwin 1859; Norberg 1990; Giannini 2012). This is suggested to initially correspond with the evolution of features that supported gliding, such the extension of the body wall to form a membrane that can be spread out, supported by the forelimb and the hindlimb, and the retention of interdigital webbing; features that are found, and are highly specialized, in colugos, gliding, tree-climbing mammals (Dudley *et al.* 2007; Bishop 2008; Giannini 2012; Panyutina *et al.* 2015).

Consensus has not been reached on how the transition between gliding and powered flight may have occurred without concurrent reductions in the overall fitness of successive intermediate organisms (Darwin 1859; Norberg 1990; Bishop 2008; Adams and Shaw 2013). This cannot be resolved through the current fossil record, which is incomplete and does not capture the transition of ancestral, possibly tree-climbing (arboreal), mammals into ones capable of powered flight (Teeling *et al.* 2005; Eiting and Gunnell 2009). Based on molecular phylogenetic reconstructions, the last common ancestor of extant bats is estimated to have occurred ~64 million years ago (Teeling *et al.* 2005). However, the most basal bat fossil found to date (*Onychonycteris finneyi*, 52.5 mya) was already capable of powered flight (Simmons *et al.* 2008).

The earliest transitions in bat evolution may have initially occurred through the modification of key genes that regulate in limb developmental processes (e.g. skeletal element formation and interdigital webbing retention) to allow for the gradual formation of a weight-bearing wing (Giannini 2012). New insights into these genetic mechanisms have come from comparative studies that examine the processes involved in bat limb development in the context of the well described mouse developmental model (Cretekos *et al.* 2001). These studies have identified specific genes and pathways that have altered activities during bat limb development (reviewed by Sears 2008; Cooper and Sears 2013). It is hoped that this evo-devo approach will reveal key molecular changes to gene regulatory networks that have resulted in the morphological evolution of the bat wing. In addition, this research has the potential to extend current knowledge of limb developmental processes in general and, more broadly, the generation of morphological diversity (Cretekos *et al.* 2001; Carroll 2008). An overview of limb development with a focus on autopod formation follows.

1.2. Vertebrate limbs are patterned by conserved genetic interactions among signalling centres

Vertebrate limb development is a complex process that involves orchestrated cellular specification, differentiation and proliferation events (reviewed by Capdevila and Izpisúa Belmonte 2001; Zeller *et al.* 2009). Several vertebrate model systems, including the mouse (*Mus musculus*) and the chick (*Gallus gallus*) in addition to the zebrafish (*Danio rerio*), axolotl (*Ambystoma mexicanum*) and the frog (*Xenopus laevis*) have been used as benchmarks to identify and understand the gene regulatory networks that are involved in these processes. The integration of this work, typically focused on stages of early limb bud formation and outgrowth or regeneration, has identified a common 'toolkit' of genes, encoding proteins that are often involved in gene transcription and/or cell signalling events that pattern the limb (Carroll 2008; Zeller *et al.* 2009). The power of these models lies in the initial focus on conserved gene regulatory pathways that form the basis of this developmental system and then examination of subsequent variation within, and permutation of, that system. For example, through functional experiments in mice and chicks and clinical human limb abnormalities (Cohn and Bright 1999; Zeller 2010). In this section I outline basic models of limb bud development as understood in these conventional model organisms.

1.2.1. Limb bud outgrowth is mediated by the antagonism between proximal and distal factors that separate the limb into the stylopod, zeugopod and autopod regions

Early limb buds form in specific regions along the embryonic flank as dorsoventrally flattened semi-circular projections of tissues, consisting of an outer layer of ectodermal cells and an inner-mass of proliferating mesenchymal cells (reviewed by Tanaka 2013). The distal limb bud is capped by a thickened ridge of tissue (the apical ectodermal ridge; AER), which runs along the anteroposterior (AP) axis (Figure 1.5A). The AER is a signalling centre, creating a positive, growth-promoting feedback loop with the underlying mesenchymal tissue, through Fibroblast Growth Factor (FGF) signalling (Ohuchi *et al.* 1997). This signalling controls the outgrowth of the limb bud along the proximodistal (PD) axis through the promotion of cell survival in addition to specifying distal cell fates (Sun *et al.* 2002; Mariani *et al.* 2008). This distal FGF signalling is thought to be antagonised by proximal factors, suggested to be RA signalling from the embryonic flank (Cooper *et al.* 2011; Roselló-Díez *et al.* 2011) that together specify PD identities along the outgrowing limb bud (Figure 1.5A-B) (Mercader *et al.* 2000).

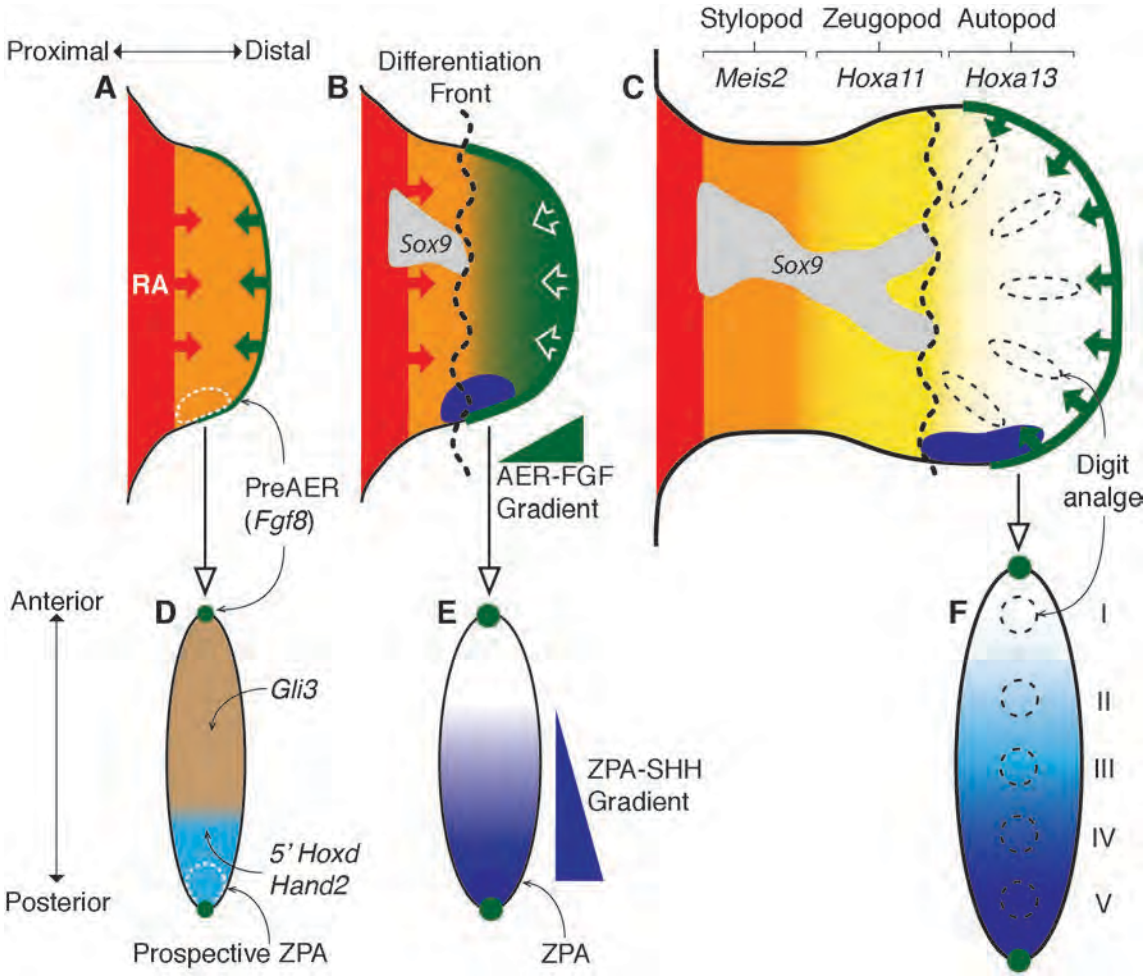

Figure 1.5: The outgrowing limb bud undergoes integrated patterning events along both its proximodistal (A-C) and anteroposterior (D-F) axes. During early limb bud formation an antagonistic interaction is set up between distal (FGF signalling from the AER, green) and proximal (suggested to be RA signalling from the flank, red) factors (**A**). As the limb develops a gradient of activities is formed through diffusion, coupled with tissue growth. This creates a proximal domain that undergoes differentiation events, whereby a portion of cells located within the centre of the limb bud change from a loosely connected network of homogenous mesenchymal cells, into closely packed cell condensations that subsequently differentiate into chondroblasts (grey). This process of chondrogenesis forms the cartilage primordia, templates for the limb skeletal elements (**B**). As outgrowth continues there is progressive formation of the stylopod, zeugopod and autopod cartilage primordia, marked by the expressions of *Meis2* (orange), *Hoxa11* (yellow) and *Hoxa13* (white) respectively. These condensations are initially distinguished through the initial expression of the *Sox9* and *Col2a1* genes, which are involved in regulating chondrocytic differentiation events and cartilage matrix synthesis respectively (**C**). Anteroposterior (AP) patterning is initially set up through the localised expression of the 5'HoxD genes and *Hand2* in the posterior region of the bud (**D**). The 5'HoxD genes induce the expression of *Shh* in the ZPA, and SHH protein forms a gradient of expression across the AP axis of the limb bud (**E**). The progenitor pool that contributes to the posterior zeugopod (ulna/fibula) and digits II-V, is made up of cells that have experienced SHH signalling (paracrine for digit II and the anterior half of digit III, autocrine for the posterior half of digit III, in addition to digits IV and V) while digit I is made up of cells that have not been exposed to SHH signalling (**F**). Adapted from Zeller *et al.* (2009) and Zeller (2010).

This 'two-signal' gradient model (Mercader *et al.* 2000) has been refined, with the inclusion of the dynamic 'differentiation-front' model (Tabin and Wolpert 2007) to describe the temporal dependence of cell identity specification (Roselló-Díez *et al.* 2014). In this model diffusion of RA from the flank through the nascent limb bud forms a gradient that is reinforced by the distal inhibition of its synthesis by FGF in the AER (Mercader *et al.* 2000) and degradation by the distally expressed RA metabolising genes, predominantly *Cytochrome P450 26B1* (*Cyp26b1*) (Yashiro *et al.* 2004). It is possible that cells localise themselves within the protracting axis by interpreting the RA gradient as a dual-threshold, with a high threshold limit specifying the stylopod-zeugopod boundary and a lower threshold limit (together with a timing mechanism that is based on histone acetylation) informing the zeugopod-autopod boundary (Figure 1.5C) (Mercader *et al.* 2000; Yashiro *et al.* 2004; Mariani *et al.* 2008; Roselló-Díez *et al.* 2011, 2014). This dynamic process would result in the formation of a differentiation front, which demarcates the boundary between proximal, differentiated tissue and the distal 'undifferentiated zone' that is maintained by FGF signalling. As cells pass across the differentiation front they become determined, express specific *Hox* gene markers (*Hoxa11* then *Hoxa13*) and acquire an identity based on the gene expression combination that they experience at that time (Tabin and Wolpert 2007; Roselló-Díez *et al.* 2014). However, the requirement for a proximalising agent in PD specification of the limb bud has been contested. Genetic studies in the mouse have revealed that limb bud patterning does not require RA signalling, instead it is suggested that RA must be excluded from the limb bud to prevent RA-induced teratogenesis (Zhao *et al.* 2009; Cunningham *et al.* 2011, 2013). In the absence of a proximal factor, a 'one-signal progress-zone' model is proposed, whereby distal FGF signalling in conjunction with autonomous collinear *Hox* gene expression specifies PD patterning (Cunningham and Duester 2015). The progressive patterning of the limb bud can be visualised through the separation of the expression of four transcription factors: *Meis1/2* mark the presumptive stylopod, while the expressions of *Hoxa11* and *Hoxa13* separate into the distinct proximal and distal domains with *Hoxa11* marking the zeugopod region and *Hoxa13* marking the autopod region (Figure 1.5C) (Tabin and Wolpert 2007; Zeller *et al.* 2009).

1.2.2. Interactions between the limb bud organisational centres play a role in subsequent limb morphology

During the phase of early limb bud outgrowth, a second organisational centre, the zone of polarising activity (ZPA), plays a predominant role in regulating outgrowth and patterning. It becomes established in the posterior portion of the bud, demarcated by the localised, mesenchymal expression of *Sonic hedgehog* (*Shh*) (Figure 1.5D). This regionalised expression is activated by the expression of genes on the 5' end (posterior or centromeric) of the HoxD gene cluster, namely *Hoxd13*, *12*, *11* and *10* (Nelson *et al.* 1996; Zákány *et al.* 2004; Zákány and Duboule 2007). The 5'HoxD genes are collinearly expressed (nested from *Hoxd10* to *Hoxd13*, with the expression domain of each gene becoming progressively distally restricted) in the posterior portion of the limb bud during early outgrowth (Dollé *et al.* 1989; Nelson *et al.* 1996). This pre-patterning leads to the direct activation of both *Shh* and *dHand* (also known as *Hand2*) in this region (Figure 1.5D-E) (Zákány *et al.* 2004). SHH signalling initiates the polarisation of the limb along the AP axis through the antagonism of a repressive form of GLI3 (GLI3R) protein (Figure 1.5D) (Litingtung *et al.* 2002; Harfe *et al.* 2004; Zhu *et al.* 2008, reviewed by Suzuki 2013). In addition to its involvement in AP patterning, the SHH signalling pathway also controls digit number and identity (Figure 1.5E-F) (Riddle *et al.* 1993; Litingtung *et al.* 2002 reviewed by Suzuki 2013).

The AER and ZPA organisational centres form a positive feedback loop co-ordinated through SHH signalling (known as the FGF-SHH feedback loop); creating an integrated regulatory network that patterns the limb (Bénazet *et al.* 2009; Zeller *et al.* 2009). Changes in the expressions of the genes that demarcate these regions in early limb bud growth have the power to alter the gross morphology of the limb, resulting in digit loss, duplications, and the loss of skeletal elements (Saunders 1948; Summerbell 1974; Riddle *et al.* 1993; Chiang *et al.* 2001). In addition, the AER and overlying ectoderm of the limb bud secretes Wingless-related integration site family (WNT) proteins, and together these factors keep the underlying mesenchyme in a proliferating and undifferentiated state that is pre-specified to a chondrogenic (cartilage cell) fate (ten Berge *et al.* 2008; Zeller *et al.* 2009). As the limb grows, the inner core of cells loses contact with FGF signalling from the AER and WNT signalling from the ectoderm. These cells undergo cell-cycle arrest and differentiate into chondrocytes (expressing *SRY box 9*, *Sox9*, as the first marker of this fate) (Figure 1.5B). Cells still within range of ectodermal WNT signalling alone maintain their proliferative state and become re-specified towards a connective tissue fate (ten Berge *et al.* 2008; Zeller *et al.* 2009). The activities of these two factors and their downstream targets play an important role in modulating the shape of the limb and in specifying the cartilage anlages within.

1.3. Autopod development involves the divergence of digital and interdigital fates

The autopod (also known as a handplate or footplate) is a highly complex structure. It initially develops as a dorsoventrally flattened region of the distal limb that experiences a symmetrical proliferative expansion along its AP axis. Its subsequent development encompasses several processes, including the specification of the digital and interdigital regions, formation of the digit rays (initiation, condensation and differentiation events), and finally the shaping of the interdigital tissue (through cell migration, proliferation and death events) (reviewed by Tamura *et al.* 2008).

1.3.1. Digit and interdigital regions are patterned by a Turing mechanism and their identities are initially specified through SHH signalling

The developing autopod consists of alternating digit and interdigital (ID) regions that have divergent fates, but which are highly integrated in terms of processes that underlie their specification, differentiation, growth and shape (Chimal-Monroy *et al.* 2011). The partitioning of the mesenchyme into digital and interdigital tissues has recently been shown to be under the control of a self-organising Turing reaction-diffusion model (Turing 1952; Newman and Frisch 1979; Raspopovic *et al.* 2014). This involves the diffusible interaction of two morphogenic pathways, namely the BMP and WNT β-catenin signalling pathways, with the SOX9 transcription factor. These proteins have auto- and cross-regulatory interactions with each other. Initial imbalances in genes expressions are amplified by the differences in the rate of diffusion of BMP factors (faster) and WNT β-catenin signalling factors (slower) through the presumptive autopod. This forms a periodic pattern of nascent digit (*Sox9* expressing) and interdigital (exposed to *Bmp* expression and WNT β-catenin signalling) regions in the autopod (Raspopovic *et al.* 2014, reviewed by Zúñiga and Zeller 2014; Cooper 2015).

Digit numbers and identity are described using a temporal-gradient model of SHH signalling across the limb bud prior to digit initiation (Litingtung *et al.* 2002; Harfe *et al.* 2004; Zhu *et al.* 2008, reviewed by Suzuki 2013). Autocrine SHH signalling specifies the more posterior digits (posterior half of digit III, and digits IV and V), while the more anterior digits (anterior half of digit III and digit II) experience long range SHH (paracrine) signalling. In most models, digit I (anterior digit) is specified in the absence of SHH signalling (Harfe *et al.* 2004; Zeller *et al.* 2009), with exposure to SHH having a negative effect on the positional identity of this progenitor population (Figure 1.5F) (Akiyama *et al.* 2005; Li *et al.* 2014; Zhulyn *et al.* 2014).

1.3.2. Digit formation is regulated by multiple gene networks through the process of chondrogenesis

As described above, *Sox9*, expression in the nascent digit rays is the first marker of digit development. This gene is a key regulator of the chondrocyte (cartilage cell) lineage, playing multiple roles in the process of chondrogenesis (Akiyama *et al.* 2005; Kozhemyakina *et al.* 2015), whereby mesenchymal cells condense, differentiate into chondrocytes, and deposit a characteristic extracellular matrix (ECM) (Hall and Miyake 2000). After digit specification, prechondrocytic mesenchymal cells aggregate and undergo compaction to form prechondrogenic condensations (also known as precartilage condensations) (Figure 1.6A) (Hall and Miyake 1992; Barna and Niswander 2007). In the mouse, these are seen as regions of relatively denser tissue that form digit rays between stages E11.25 and E12.5 (Wanek *et al.* 1989; Martin 1990). These aggregations form through cell-cell and cell-ECM interactions, produced by the expression of genes controlling the generation of both cell adhesion molecules (such as N-cadherin and N-CAM) and ECM (hyaluronan, tenascin and fibronectin and collagen type I and IIA) (Hall and Miyake 1992; Hall and Miyake 1995; reviewed by Goldring *et al.* 2006; and Egawa *et al.* 2014). The size of the initial condensation plays a part in determining the eventual size of the final skeletal element (Hall and Miyake 2000). Their relative growth is based on the aggregation of cells into the condensation and failure of cells to disperse, as, at these early stages, the rate of cell proliferation within the condensation is similar to that of the surrounding mesenchyme (Hall and Miyake 1992, 2000).

The next step in cartilage formation involves the differentiation of the prechondrogenic mesenchymal cells into small, rounded, immature chondrocytes (Figure 1.6B) (Bi *et al.* 1999; Smits *et al.* 2001; Akiyama *et al.* 2002). In addition to *Sox9*, these cells begin to express *Sox5* and *Sox6*, and deposit a matrix that is composed mainly of collagen (typically type II, IX and XI collagens) and proteoglycans (e.g. aggrecan) into the surrounding region (Kosher *et al.* 1986; Kulyk *et al.* 1991; see Goldring *et al.* 2006 for an overview). The proliferation of, and matrix deposition by these cells at this stage modulates interstitial growth (growth in the length) of the skeletal element, and appears to be under the control of insulin-like growth factors (IGF) (Fisher *et al.* 2005). In the cartilage template core these cells, known as proliferating chondrocytes, become radially flattened at later stages, appearing stacked, and are known as columnar chondrocytes (Figure 1.6C-D) (Rooney and Archer 1992).

As chondrogenesis progresses, cells express genes encoding Runt family transcription factors, *Runx2* and *Runx3*, which are required for chondrocyte maturation (Komori 2015). These transcription factors promote the expression of *Indian hedgehog* (*Ihh*), which positively regulates cell proliferation (St-Jacques

et al. 1999). Chondrocytes leave the proliferative pool and undergo hypertrophy, becoming prehypertrophic chondrocytes that synthesize the hypertrophic chondrocyte marker, type X collagen (by expressing *Col10a1*) (St-Jacques *et al.* 1999; Yoshida *et al.* 2004). Cells expand along their longitudinal axis, becoming rounded in shape; lose expression of *Sox9*, eventually differentiating into large hypertrophic chondrocytes (Figure 1.6D) (reviewed by Lefebvre and Bhattaram 2010; Long and Ornitz 2013). In turn, *Ihh* enhances the expression of *Runx2* in the perichondrium, a layer of cells surrounding the cartilage template that forms adjacent to the maturing chondrocytes (Kim *et al.* 2013) (Figure 1.6C-D). In this context, *Runx2* promotes the differentiation into osteoblasts and is involved in the formation of the bone collar (Komori 2011).

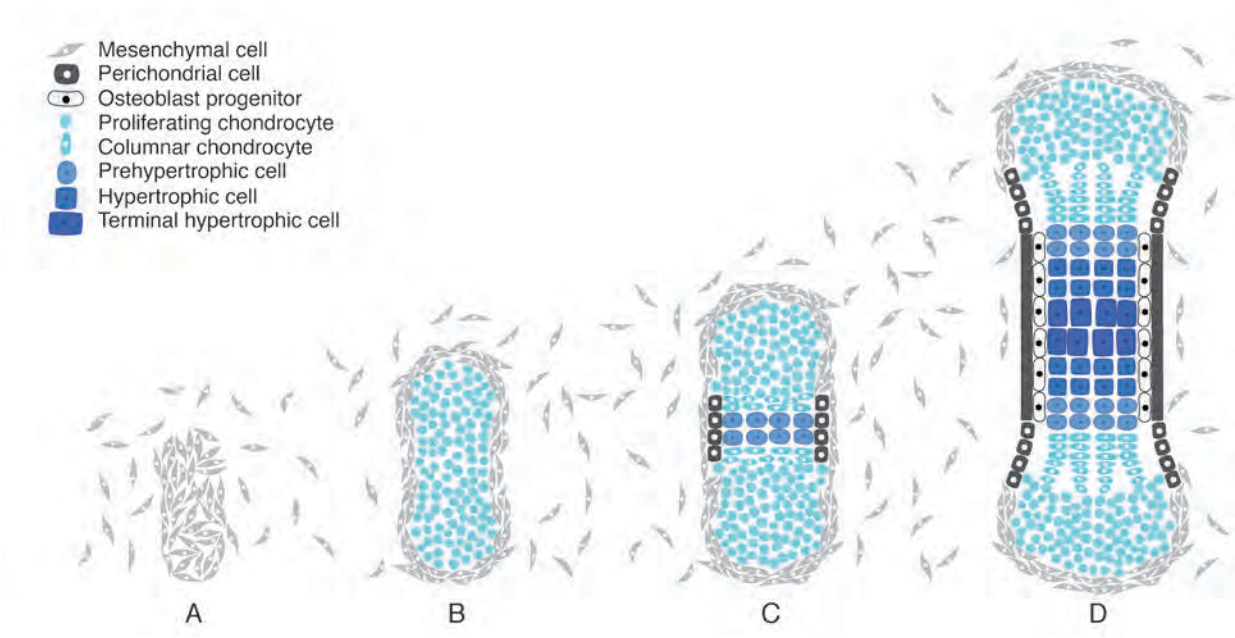

Figure 1.6: Chondrogenesis is a progressive process that results in the formation of a cartilage template. Mesenchymal tissue initially becomes condensed to form a tightly packed aggregate of prechondrogenic cells (**A**). The cells within this aggregate differentiate into chondrocytes that synthesise and maintain their surrounding cartilage matrix (**B**). Chondrocytes flatten, forming distinct, columnar stacks. They then stop secreting cartilage matrix proteins and undergo terminal differentiation to become hypertrophic cells (**C**). The outer layer of mesenchymal cells differentiates to form the perichondrium that consists of cells orientated perpendicular to the longitudinal axis of the cartilage template. As cells undergo hypertrophy they grow, expanding along their longitudinal axis this extension is constrained by the perichondrium (**D**). Due to this growth, perichondrial cells become realigned along the longitudinal axis of the element. The inner layer of the perichondrium gives rise to a cell line fated to become osteoblasts (bone forming cells), which secrete a matrix to form a supportive bone collar in the regions undergoing hypertrophy.

1.3.3. The perichondrium provides directional growth to the cartilage elements

The perichondrium is a fibrous sheath that forms around the cartilage template during chondrogenesis and is key to mediating their directional, longitudinal growth. Perichondrial cells form from undifferentiated mesenchymal cells that directly surround the core of flattened columnar chondrocytes (Figure 1.6C). As these underlying chondrocytes expand during hypertrophy, the tightly associated perichondrial cells act as a 'constraining sheath or corset' that confers directionality to the growth of the cartilage element, restricting expansion across the radial axis in favour of that along the longitudinal axis (Rooney and Archer 1992). The perichondrium becomes organised into a outer (fibroblastic) layer of fibrous tissue, that has a structural role, and an inner (cambial) layer of loose progenitor cells that contribute to appositional growth (growth in diameter) of the cartilage template through the division and subsequent differentiation of surrounding cells (Rooney and Archer 1992; Bandyopadhyay *et al.* 2008).

These differentiation events occur in the midpoint of the cartilage template that extends to form a long shaft (diaphysis), capped by bulbous ends (epiphyses), which are made up of the rapidly proliferating chondrocytes. Together, chondrocyte proliferation, ECM deposition and hypertrophy, in conjunction with the mechanical restriction of the perichondrium, result in longitudinal growth of the cartilage template and the eventual formation of a distinct region of cell turnover known as the growth (or epiphyseal) plate (Kronenberg and Kronenberg 2003). Molecular interactions with the perichondrium are important in controlling proliferation rates, and in regulating chondrocytes differentiation events (Di Nino *et al.* 2001; Bandyopadhyay *et al.* 2008). The perichondrium demarcates the cartilage template, separating the condensations from the surrounding mesenchyme, excluding the distal end, which, during this time, experiences progressive mesenchymal aggregation and subsequent differentiation (Shubin and Alberch 1986; Rooney and Archer 1992).

1.3.4. Digit cartilage formation and growth occurs in a progressive proximodistal fashion that is coordinated with joint and digit tip formation

In digit rays, chondrogenesis occurs in a proximal-distal fashion, with loosely connected mesenchyme on the distal end of the condensation progressively contributing to its formation (Pitsillides and Ashhurst 2008; Suzuki 2013). The distal digit-tip regions are termed phalanx-forming regions (PFR), and act as digit signalling centres, maintaining expression of *Sox9* and expressing *BmpR1b* (Suzuki *et al.* 2008; Witte *et al.* 2010). Each PFR has a unique activity of phosphorylated SMAD1/5/8, an indicator of BMP-receptor (BMPR) mediated signalling, with cells in this region appearing to receive positional

cues from their posterior interdigital region (from BMP family members) as they become incorporated in to the phalanx (Dahn and Fallon 2000; Suzuki *et al.* 2008; Witte *et al.* 2010). PFR cells are replenished by the movement of distal proliferating cells that lie directly beneath the AER (Suzuki *et al.* 2008; Witte *et al.* 2010). Dynamic encoding of this information into the developing phalanges, possibly through a cellular 'memory' of SHH signalling, results in the generation of a digit with a specific morphology and thus a unique identity (Harfe *et al.* 2004; Suzuki 2013).

The formation of digit condensations is coordinated with their segmentation to form a pattern of phalanges specific to each digit identity (Casanova and Sanz-Ezquerro 2007). Cartilage elements form distinct regions, known as interzones, of compacted, flattened mesenchymal cells that express *Gdf5* and undergo differentiation events to form the tissues of the synovial joint, first seen at E12.5 in the mouse autopod (reviewed by Decker *et al.* 2014). It is thought that these digit joints form at specified distances from the AER and other joints, due the repression of both a distal inhibitory program and an auto-inhibitory mechanism. In this manner condensations are allowed to form and elongate to a certain point at which time a threshold that allows the activation of the joint formation program is reached (Casanova and Sanz-Ezquerro 2007).

A separate developmental program underlies the development of the most distal phalanx, the digit tip, (Casanova and Sanz-Ezquerro 2007). These form at ~E15 in the mouse, have a distinct 'pointed shape' and, in the chick, are marked by the ectodermal expression of *Bambi* and *Sp8* (Grüneberg and Lee 1973; Sanz-Ezquerro and Tickle 2003; Casanova and Sanz-Ezquerro 2007; Casanova *et al.* 2012). Digit tips have unique characteristics that includes: the presence of both intramembranous and endochondral ossification (Dixey 1880; Grüneberg and Lee 1973), a distal ossification centre (Casanova *et al.* 2012), the inclusion of ectodermal derivatives (nails, claws or hooves) (Hamrick 2003), and a limited ability to regenerate (Han *et al.* 2008).

1.3.5. Bone deposition takes place through perichondrial and endochondral ossification with the formation of a single growth plate in digit elements.

Digit ray cartilage templates are transformed into bony tissue through two closely linked processes, namely endochondral ossification (the replacement of the template with trabecular bone) and perichondrial ossification (the formation of cortical bone surrounding the template) (reviewed by Farnum 2007). This occurs when hypertrophic cells reach a terminal size, direct the surrounding matrix to mineralise and promote vascularisation of the element. The majority of these cells undergo apoptosis and are replaced by osteoprogenitor cells, which migrate into the element. These differentiate into

osteoblasts that direct the process of bone matrix deposition and mineralisation to form trabecular bone. Hypertrophic cells direct the adjacent perichondrial cells to differentiate into osteoblasts, which either travel to the centre of the template to form trabecular bone, or stay on the periphery to form cortical bone, contributing to the periosteal bone collar. These processes usually occur during development and are initiated from the centre of the template diaphysis (known as the primary ossification centre) while chondrogenesis continues to drive elongation towards the epiphyses as a result of the combined effect of cell proliferation, matrix deposition and hypertrophic growth events (reviewed by Farnum 2007; Kronenberg 2003; Kronenberg 2007; Egawa *et al.* 2014). In this manner, each element becomes stratified into regions of: ossification; calcification; maturation (hypertrophy); proliferation and resting/reserve cartilage cells (Kronenberg and Kronenberg 2003).

In mammals, secondary ossification centres form later (typically postnatally) in the epiphysis. The growth plate forms as compact region between these two regions of ossification, and retains highly organized zones of resting, proliferating, columnar and hypertrophic chondrocytes (Kronenberg and Kronenberg 2003). The growth plate continues to contribute new cartilage that is progressively replaced by bone, with the rate of proliferation, matrix synthesis (by proliferating and hypertrophic chondrocytes), and cellular growth driving bone elongation after birth (Wilsman *et al.* 1996). Digit ray elements are notable in that they only form a single growth plate. In the metacarpals/metatarsals this is found in the distal epiphysis (with the exception of digit I where it is located in the proximal portion), while in phalanges, they form in the proximal epiphyses (Reno *et al.* 2006, 2013). Epiphyses that do not form distinct growth plates do not develop a secondary ossification centres, instead undergoing direct ossification as found in nodular bones (such as carpals or tarsals) (Reno *et al.* 2006).

1.3.6. Interdigital tissue is shaped by differential growth and cell death events

During its formation the mouse autopod experiences differential growth, whereby the digit regions extend distally at a greater rate than the interdigital (ID) regions, which appear to regress (Hernández-Martínez and Covarrubias 2011). These interdigital regions (conventionally named from anterior to posterior as ID1, ID2, ID3 and ID4) are composed of loosely connected mesenchymal tissue found between the digit ray anlages, these are not clearly distinguished at early stages of autopod formation (E12.5; limb S7). In this interdigital tissue, interactions between proximal and distal factors take place to mediate proliferation, differentiation and cell death events. Early in autopod formation, *Fgf8* expression is still found in the AER, where it promotes the survival and proliferation of the underlying mesenchymal cells (Figure 1.7A) (Mariani *et al.* 2008; ten Berge *et al.* 2008). This effect appears to be

mediated through the mitogen-activated protein kinase (MAPK) signalling pathway that exerts a protective effect on cells through the suppression of the expression and/or activities of pro-apoptotic factors (Figure 1.7B) (Hernández-Martínez *et al.* 2009). Mesenchymal cells are thus maintained in an undifferentiated state that have the potential to undergo chondrogenesis (i.e. form digits) (Gañan *et al.* 1998).

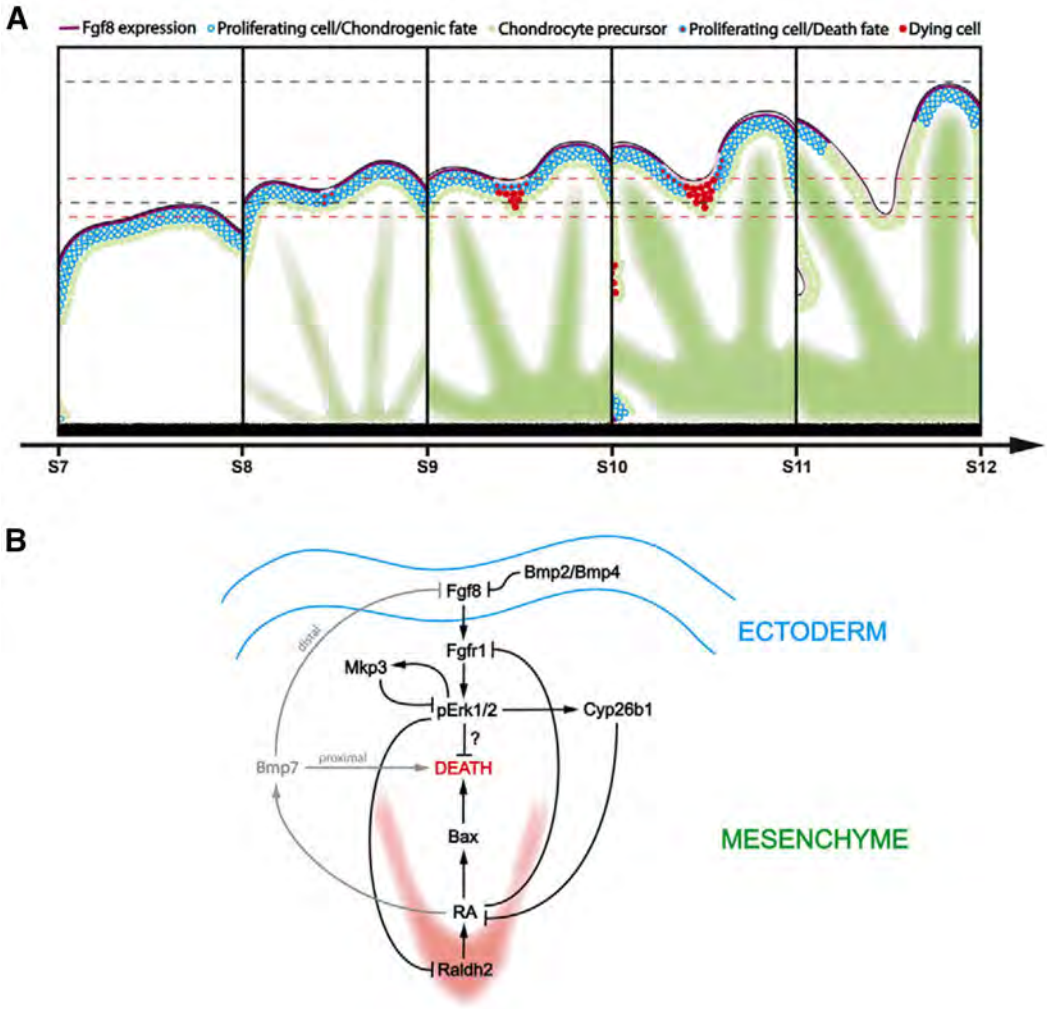

Figure 1.7: Differential growth events shape the autopod. Tissues are progressively shaped through the death of proliferating cells along the distal edge of the interdigital regions and survival of proliferating cells overlying the digit regions. Interdigital regression in the mouse occurs through the process of differential growth of the digit (black dashed lines) and interdigital (red dashed lines) regions in addition to cell death events in the distal edge of the interdigital mesenchyme (red dots) (**A**). This results in the relative extension of the digits beyond the distal boundary of the interdigital tissue and the thinning of the interdigital tissue. These processes are mediated through a balance in the levels of distal FGF signalling (that maintains the underlying distal mesenchymal cells in a proliferating state) and more proximal interdigital RA signalling (that modulates several processes, including cell death and digit formation) (**B**). *Fgf8* expression is lost in the AER overlying the distal interdigital mesenchyme through downregulation by BMP signalling in both the ectoderm and mesenchyme. This results in an increase in the availability of RA in the interdigital regions, which promotes cell death events. Limb stages S7-S12 correspond to E12-E16 (Wanek *et al.* 1989). Schematics taken from Hernández-Martínez *et al.* (2009).

RA signalling becomes activated in the ID tissue through the localised expression of genes encoding enzymes that synthesise RA (*Rdh10* and *Aldh1a2*), and is excluded from the digit regions through degradation by CYP26B1 (Figure 1.7B) (Zhao *et al.* 2010; Shou *et al.* 2013). This ID RA signalling antagonises FGF signalling from the overlying AER, both directly (through the inhibition of *Fgfr1* expression in the mesenchyme) and indirectly (through the promotion of *Bmp* expression which downregulates *Fgf8*) and promotes the expression of a proaptotic factor *Bax* (Figure 1.7B) (Rodriguez-Leon *et al.* 1999; Pajni-Underwood *et al.* 2007; Hernández-Martínez *et al.* 2009). This results in the inhibition of MAPK signalling (through the loss of phosphorylated ERK1/2 protein and downregulation of *Mkp3* expression), and an associated increase in programmed cell death (PCD) in the interdigital regions. This process appears to be regulated by a feedback loop as FGF8 activity decreases RA availability through the down-regulation of *Aldh1a2* expression in the ID regions, and upregulation *Cyp26b1* expression in the digit regions (Hernández-Martínez *et al.* 2009).

Due to this process ID tissue thins and appears to regress, while the distal digit condensations continue to form, causing the autopod to become scalloped, with the digit rays appearing as ridges on the dorsal surface and projecting slightly from the distal edge (Salas-Vidal *et al.* 2001). This process is known as interdigital cell death (ICD), and it extends proximally as development continues (E13.5; limb S8, Figure 1.7A) (Hernández-Martínez *et al.* 2009).

ICD is preceded by the vascularisation of the interdigital tissue (Eshkar-Oren *et al.* 2015). This process increases oxygen availability in these tissues, and is associated with an increase in the generation of reactive oxygen species (ROS), chemically reactive molecules (free radicals) derived from oxygen, that disrupt and damage proteins and contribute to PCD (Covarrubias *et al.* 2008; Eshkar-Oren *et al.* 2015). The vascularisation of the ID tissue, and its exclusion from the cartilage templates contributes to the restriction of PCD to the ID regions, functioning as an additional permissive control mechanism in addition to the genetic network described above (Eshkar-Oren *et al.* 2015). Cell death is followed by the degeneration of the ID tissues, including this network of vasculature and the extracellular matrix. This contributes to ID thinning and distal regression, with the formation of distinct regions of webbing at later stages of development (E14; limb S9) and the separation of digits by E15 (limb S11) (Wanek *et al.* 1989; Salas-Vidal *et al.* 2001).

1.4. Vertebrate limb development is informed by the study of non-model organisms including that of the bat

A complementary approach to study limb development is through the evo-devo framework. This involves the characterisation of the physical and molecular processes that underlie the development distinctive limb morphologies from alternative vertebrates (such as the bat). These studies have the potential to identify differences in the activities of critical genes in the common developmental toolkit, and inform how these may alter conventional models of limb development (Carroll 2008; Sears 2011).

The bat has become an instructive 'non-model' developmental system, resulting in a number of findings that describe the molecular evolution of the bat wing, while informing an understanding of the general principles underlying vertebrate limb development (Chen *et al.* 2005; Sears *et al.* 2006; Weatherbee *et al.* 2006; Cretekos *et al.* 2008; Hockman *et al.* 2008; Ray and Capecchi 2008; Sears 2011; Tokita *et al.* 2012; Dai *et al.* 2014; Wang *et al.* 2014). The morphological process of bat limb development has been well described in several species, (*Carollia perspicillata,* Cretekos *et al.* 2005; *Rousettus amplexicaudatus*, Giannini *et al.* 2006; *Pipistrellus abramus*, Tokita 2006, *Molossus rufus*, Nolte *et al.* 2009) and *Miniopterus natalensis*, (Hockman *et al.* 2009) (Figure 1.8). The outgrowing bat limb bud appears to have a similar morphology to the equivalently staged mouse (CS13-CS14; Figure 1.8A-H). At later stages of autopod formation (CS15), while the bat footplate retains its similarity to the mouse autopods, being fairly symmetrical across its AP axis, the bat handplate becomes distinctly asymmetrical (Figure 1.8I-L). On digit formation (CS16), the anterior portion of the bat forelimb autopod forms a thumb primordia that projects perpendicularly from the handplate. The posterior portion of the bat handplate initially expands outwards, first over the posterior-distal region where digit IV will form and then over the distal region where digit III will form (Figure 1.8O) (Hockman *et al.* 2009). At later stages (CS17) the thumb becomes progressively free, and is comparable to the toes of the bat hindlimb, which undergo interdigital regression (Figure 1.8S-T). (Cretekos *et al.* 2005).

Examination of the genetic regulation underlying the formation of these distinct bat forelimb and hindlimb phenotypes has the potential to offer insight into the molecular mechanisms that control processes such as limb patterning, bone elongation and interdigital webbing formation (Cretekos *et al.* 2001; Cooper *et al.* 2012). In this section I introduce what is currently known of these processes.

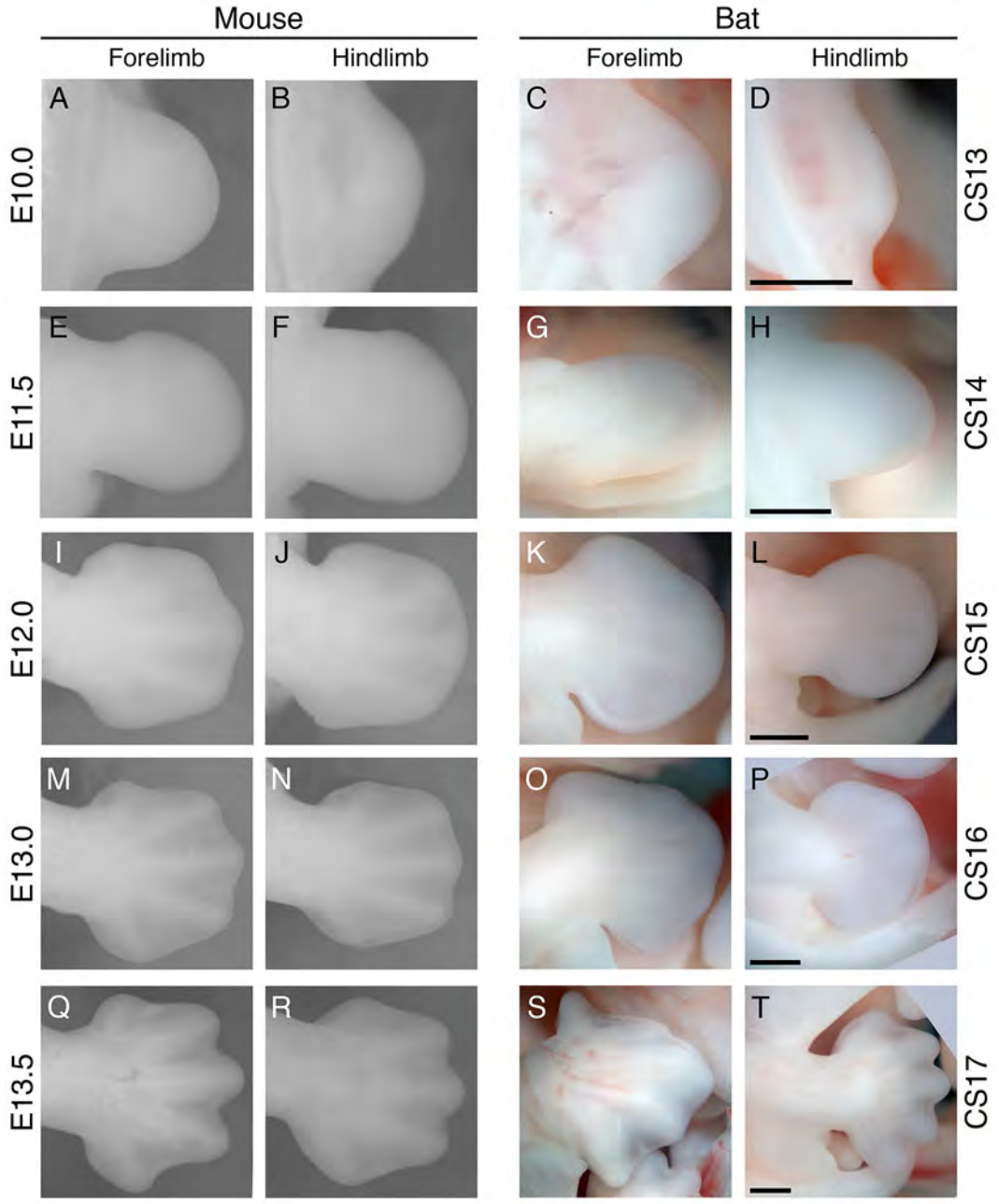

Figure 1.8: Limb development in the mouse and the bat (*M. natalensis*). These encompass the stages of early limb bud outgrowth (**A**-**H**) and over the stages of autopod formation (**I**-**L**) and digit formation (**M**-**T**). Adapted from Hockman *et al.* 2009. Dorsal surface of forelimbs and hindlimbs shown, scale bar in bat limbs is 500 μm.

1.4.1. Enlargement of the bat forelimb is not due to heterochronic differences between the bat forelimb and hindlimb during limb bud initiation and growth.

Alterations in the timing and rate of formation of a developmental structure can result in changes to its relative size or shape (heterochrony) (Hall 2003). This is seen in the developing emu (*Dromaius novaehollandiae*) where a delay in forelimb budding and the modulation of limb field gene expression (due to transcriptional heterochrony) results in a reduced forelimb with one residual digit (Richardson *et al.* 2009; Nagai *et al.* 2011; Bickley and Logan 2014). In most vertebrates, the forelimb field is specified earlier than that of the hindlimb, due to the delay in specification of the posterior portion of the embryo, resulting in a developmental lag of the hindlimb (Wanek *et al.* 1989; Bininda-Emonds *et al.* 2007). In bats, the limb buds form at a similar location and at an equivalent developmental stage, and are initially of a comparable relative size, to those of the mouse (Cretekos *et al.* 2005, 2008; Sears *et al.* 2006; Hockman *et al.* 2009). The developmental lag of the bat hindlimb is slightly less than that of the mouse, with both species having relatively synchronous limb morphological development (Bininda-Emonds *et al.* 2007; Sears 2009). This indicates that subsequent differences in the size of the bat forelimb and hindlimb, apparent at later stages of development, are unlikely to be as a result of changes in the timing of limb bud initiation, nor of alterations in the sequence of developmental events that occur during early limb bud formation (Bininda-Emonds *et al.* 2007; Richardson *et al.* 2009).

1.4.2. Upregulation of the FGF-SHH signalling feedback loop during early limb bud outgrowth

The alteration of the spatial pattern of gene expression during development (heterotopy) is another evolutionary developmental mechanism underlying changes in morphologies. This is illustrated in the limb bud by the generation of mirror image duplications of chick digits through the ectopic expression of *Shh,* which emulates the ZPA and initiation of the FGF-SHH feedback loop in the anterior region (Riddle *et al.* 1993; Niswander *et al.* 1994). The FGF-SHH feedback loop, is a vital signalling component of limb bud outgrowth and patterning (reviewed by Duboc and Logan 2009) and has been shown to be strengthened in the developing bat forelimb bud, with the expansion of the *Shh* expression domain in the region of the ZPA (Hockman *et al.* 2008) and the broadening of the *Fgf8* expression domain in the AER (Cretekos *et al.* 2008). This is thought to result in an increase in cell proliferation in the posterior portion of the forelimb autopod that results in the expansion of this tissue at later stages of development (Figure 1.8K-L) (Hockman *et al.* 2008). This indicates that influential events during early limb bud patterning are modulated in the bat forelimb, altering a key signalling node that has the potential to affect later autopod formation and digit growth.

1.4.3. Reactivation of the FGF-SHH feedback loop during autopod formation may lead to interdigital retention and associated digit growth

In addition to this early alteration of the FGF-SHH feedback loop, a remarkable reactivation of these genes occurs during later bat autopod formation (Hockman *et al.* 2008). *Fgf8* expression, normally restricted to the distal AER, is found within the autopod mesenchyme of the CS15 forelimb and is clearly seen in the interdigital regions at later stages of development (Hockman *et al.* 2008). This is associated with the novel re-activation of *Shh* expression in the interdigital (ID3) mesenchyme of the forelimb at CS16 VE. The strong co-incident, and anterior-posteriorly graded expressions of these two genes in the interdigital regions of the bat forelimb are suggested to result in increased proliferation and cell survival in this mesenchymal tissue (Hockman *et al.* 2008). Their expressions in this region are associated with the graded expression of *Bmp2* and the activation of the BMP antagonist, *Gremlin*, in the interdigital tissues of *C. perspicillata* (Weatherbee *et al.* 2006). Interactions amongst these genes are proposed to operate through similar feedback loops as found during early development, whereby BMP signalling in the limb bud initiates the FGF-SHH feedback loop through the initial upregulation of *Gremlin* (in the subdermal mesenchyme), which then feedbacks to reduce BMP repressive activity on *Fgf* gene expression. SHH signalling, initiated independently, upregulates *Gremlin* further, reinforcing interactions between the ZPA and AER, to promote proliferation and expansion of the outgrowing limb. The growth of the autopod and subsequent separation of these signalling centres and the domain of *Gremlin* expression appears to attenuate their interactions over time, and *Shh* expression is lost in the bat by CS17 (Hockman *et al.* 2008; Bénazet and Zeller 2009; Bénazet *et al.* 2009; Zeller *et al.* 2009).

By maintaining the interdigital mesenchyme in an undifferentiated, proliferative state the interactions among these genes may result in the retention of interdigital webbing in the bat wing. The repression of BMP signalling in the bat autopod (through the expression of *Gremlin*) should result in decreased cell death, as has been shown for duck interdigits, which are retained as webbing (Merino *et al.* 1998; Weatherbee *et al.* 2006). This is supported by bead implantation experiments in the bat wing, which have shown that the enhancement of BMP signalling (BMP soaked bead) and repression of FGF signalling (FGF inhibitor, SU5402, bead), results in increased interdigital cell death in the bat distal interdigits (Weatherbee *et al.* 2006). Interestingly, cell death was not increased by the enhancement of BMP signalling alone, as found in mouse interdigits (Weatherbee *et al.* 2006; Hernández-Martínez *et al.* 2009). It is proposed that BMP signalling is modulated by the expression of *Gremlin* in bat autopods, while the continued expression of *Fgf8* in the interdigital mesenchyme of the bat forelimb and hindlimb acts to promote cell survival in these region. Subsequent loss of *Fgf8* expression in the

hindlimb interdigits at CS17 corresponds to the apparent regression along the distal edge of the interdigital mesenchyme. At this later stage the interdigital tissue between forelimb digits II-V thins and expands, appearing slightly scalloped along the distal edge at later stages while digit I is free (Cretekos *et al.* 2005; Hockman *et al.* 2009).

While not directly implicated in interdigital retention events, the expression of *Shh* in this region is also suggested to play possible roles in promoting cell survival, enhancing proliferation in the digit ray anlages while regulating joint formation, and assigning the digit symmetry of the hindlimb (Hockman *et al.* 2009). In the early limb bud SHH signalling from the ZPA during early limb development encodes digit identity. The posterior interdigital mesenchyme progressively signals to the anterior digit anlage to mediate growth and joint formation events, conferring their digit identity (Harfe *et al.* 2004; Suzuki 2013). Interdigital BMP signalling is thought to relay this information through signalling to the distal PFR prior to their involvement in apoptotic events (Suzuki *et al.* 2008; Suzuki 2013). It is possible that the modulation of BMP signalling in the bat interdigits, through graded expression of *Shh* in the forelimb and uniform expression in the hindlimb, contributes to the assignment of a specific morphology to each digit ray.

1.4.4. The digits of the bat forelimb have conserved specification and increased chondrogenic parameters

The upregulation of *Fgf* and *Shh* in signalling centres at early stages of limb outgrowth does not appear to noticeably affect the relative length of the forelimbs at stages of initial autopod formation (CS15) (Cretekos *et al.* 2008). However, differences at these stages may be slight, and a comprehensive morphological analysis of cartilage elements in the early autopod has not been performed. The formation of the stylopod, zeugopod and autopod elements does appear to progress normally in bat forelimbs (Hockman *et al.* 2009) implying that the PD axis specification and subsequent early patterning events in the bat do not affect the gross organisation of the elements at these stages. Bat limbs have also maintained their pentadactyl condition, indicating that the mechanisms underlying the periodic separation of the autopod into interdigit and digital regions are not altered, as suggested for some ungulate mammals (Cooper 2015). Examination of digit development is currently limited to Alcian Blue staining of limbs, which demarcates the digit ray cartilage templates from CS15 (in the forelimb) onwards and Alizarin Red staining of limbs at later stages of development to describe the ossification of the elements (Adams 1992; Adams and Pedersen 2000; Cretekos *et al.* 2005; Hermanson and Wilkins 2008; Hockman *et al.* 2009).

An examination of *C. perspicillata* wing cartilage condensations (CS16) have suggested that they are similar in size and patterning to those of the mouse, with the proportions of the different limb elements thought to be under constraint due to early patterning events, however, this has not been quantified (Sears *et al.* 2006). Noticeable differences in the lengths of the cartilage templates are seen between the bat forelimb and hindlimb cartilage templates, with those of the forelimb appearing asymmetrically elongated throughout their development (Figure 1.9). It is notable that the formation of the bat footplate appears to be slightly delayed in *C. perspicillata* as compared to other Eutherians and Marsupials (Sears 2009) and though small, this developmental lag between the limb types must be considered in comparisons between the CS15 forelimb and hindlimb.

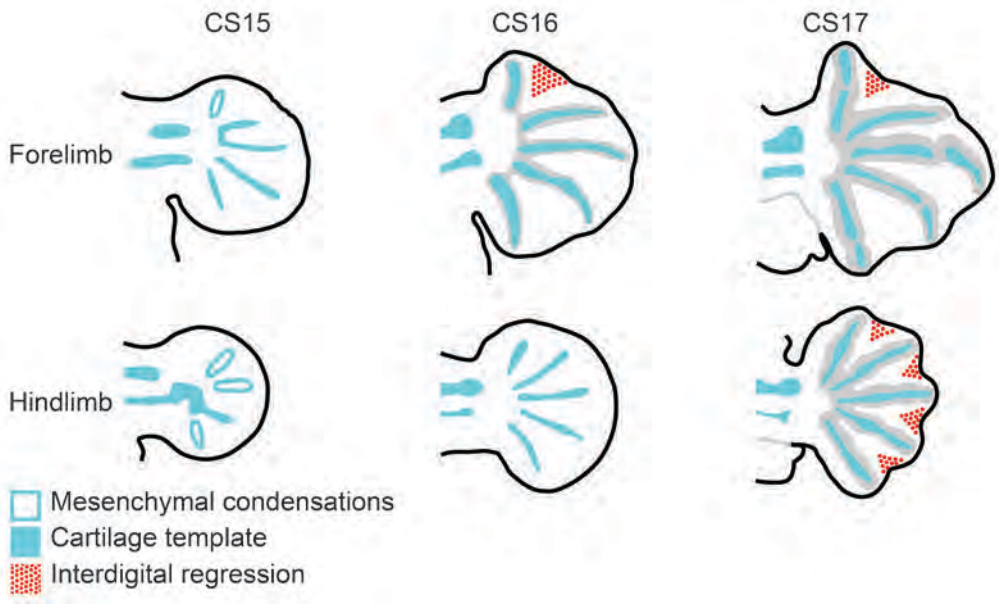

Figure 1.9: The progression of skeletal element formation in the bat *M. natalensis* is shown over stages of digit formation and interdigital apoptosis. At developmental stage CS15 digit rays are evident as cartilage templates in the forelimb and mesenchymal condensations in the hindlimb. The opposing extension of digit I anteriorly and that of digit V posteriorly gives the bat handplate an asymmetrical spade shape that is clearly seen at CS16. In addition to these differences in shape, it is double the size and has an advanced state of differentiation as compared to the footplate. Clear differences in the size of these cartilage anlages are evident from their initial formation. Regression of the interdigital regions occurs between digits I and II in the CS16 and CS17 bat forelimb and occurs at CS17 between the digits of the bat hindlimbs.

All cartilaginous digit rays are evident by CS16 (Figure 1.9). The developmental differences between the size of the bat forelimb and hindlimb are attributed to differential growth (allometric heterochrony), specifically that driven by chondrogenic proliferation and differentiation, rather than differences in its chondrogenic patterning (limb development heterochrony) (Bininda-Emonds *et al.* 2007). Measurements of whole limbs during autopod formation reveal that while similar during early

development (CS15), the relative lengths of the forelimb of *C. perspicillata* at later stages (CS19) is nearly three times that of the mouse (when normalised to crown rump length) (Cretekos *et al.* 2008). This indicates that over these intermediate stages, processes leading to the growth and elongation of the forelimb are present. These data also indicate that the initial formation of pre-cartilaginous anlage is not altered in the bat forelimb, rather, events occurring during cartilage formation and growth (chondrogenesis) likely contributes to the initial elongation of these elements over stages of autopod formation. This is not to discount the fact that the majority of digit elongation does occur during fetal development, with late stage bats (CS18-CS22) having both increased rates of proliferation and extended hypertrophic zones in their elongating metacarpals as compared to equivalently staged mice (Sears *et al.* 2006; Sears 2008; Richardson *et al.* 2009). This is attributed to the increased expression of *Bmp2* and associated BMP signalling in the bat metacarpals as compared to their metatarsals or mouse metacarpals (Sears *et al.* 2006). Additional allometric elongation of bat limb skeletal elements occurs post-natally and this is associated with the enhancement of all chondrocytic parameters associated with elongation events (e.g. cell height, cell volume) in the bat forelimb, with hypertrophic cells achieving their final height early leading to enhanced interstitial growth as compared to the mouse (Adams and Pedersen 2000; Farnum *et al.* 2008a).

1.5. Large scale transcriptome studies in bat limb development

The majority of studies on bat limb development have focused on a candidate gene approach that describe the expression and assess the function of genes that are known to play a role in limb development in the mouse or the chick (including *Hoxd13*, *Shh*, *Fgf8*, *Bmp2/4/7*, *Gremlin*, *Prrx1*) (Chen *et al.* 2005; Sears *et al.* 2006; Weatherbee *et al.* 2006; Cretekos *et al.* 2007, 2008; Hockman *et al.* 2008; Ray and Capecchi 2008). The arrival of high-throughput transcriptional profiling allows entire gene expression networks to be characterised at different stages of limb development and in different limb types or tissues in both the mouse and the chick (Margulies *et al.* 2001; Shou *et al.* 2005; Gyurján *et al.* 2011; Wang, Young, *et al.* 2011). These studies have the potential to expose activity of genes previously unexamined during limb development and have been applied to the bat limb developmental system (Dai *et al.* 2014; Wang *et al.* 2014; Mason *et al.* 2015). In this section I describe the findings of a high throughput transcript analysis that forms the foundation of this work, introduce the genes that were identified, and highlight the additional work that has recently been published in this field.

1.5.1. Cross-species microarray analysis of bat autopods revealed a set of genes that were robustly differentially expressed

Cross-species microarray analysis was an early technique used to examine the transcriptomes of non-model organisms (Bar-Or *et al.* 2007). One such study, involved the physical hybridisation of bat (*Miniopterus natalensis*) transcripts to a platform containing catalogued mouse gene probes (Mason 2009; Mason *et al.* 2015). Comparisons were made among developing bat FL and HL autopods at stages of digit formation and interdigital regression, (CS16-CS17, Figure 1.10O-P, S-T) with mouse FL autopods (E13.5; Figure 1.10Q) being used as a reference sample, facilitating a 3-way comparison. While comparisons between the bat and the mouse samples (interspecies comparisons) revealed a large number of differentially expressed (DE) genes (Figure 1.10A (i)-(ii)), only 107 up-regulated genes and 5 down-regulated genes were unique to the bat FL analysis (Figure 1.10A (iii). Very few genes were found to be DE between the bat FL and HL (intraspecies comparison; Figure 1.10B (i)-(ii)), with only 15 genes significantly DE at CS17 and only six at CS16 (Figure 1.10B (iii)). Two genes were significantly and robustly upregulated at both developmental stages and across all comparisons. The most significantly DE gene found, was a probe to RIKEN clone AK043601 that mapped upstream of the *Myeloid ectopic insertion site* (*Meis2*) locus while the second was *Homeobox D11* (*Hoxd11*) (Mason 2009; Mason *et al.* 2015).

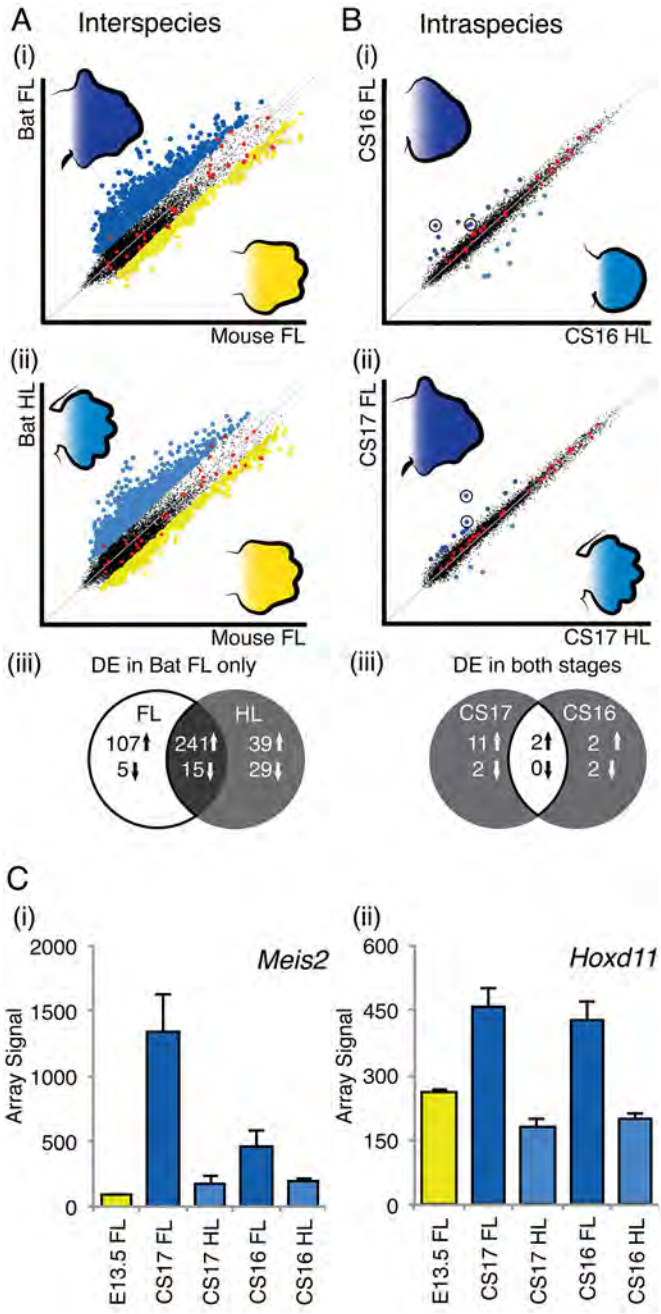

Figure 1.10: A microarray comparison of bat forelimb and hindlimb autopod transcript abundance with the mouse forelimb. Two direct analyses between the array signal between bat and the mouse samples revealed many genes that were significantly differentially expressed (DE) (**A**). Two indirect analyses comparing the bat FL and HL at stages CS16 and CS17 show few differences between the array signals of these limb types (**B**). *Hoxd11* and *Meis2* (circled) were identified as highly DE in these comparisons (**C**).

The *Meis2* probe had higher array signal for the CS17 bat FL than in the E13.5 mouse FL (over 9 fold) and was higher in the bat FL at both stages of development examined (over 2 fold in CS16 and over 6 fold in CS17) (Figure 1.10C (i)). *Hoxd11* also showed this pattern of differential expression, however these differences were more modest, with expression being just under two fold higher in the CS17 bat FL than in the E13.5 mouse FL and over two fold higher in the other comparisons (Figure 1.10C (ii)).

These findings were recently supported by more advanced methods of RNA sequencing (RNA-seq) in the developing autopods of the bat *Miniopterus schreibersii*, a sister group of *M. natalensis* (Wang *et al.* 2014). This study found that both *Meis2* and the 5'HoxD genes were upregulated in the bat forelimb at stages of autopod formation and growth and (during CS15-CS17) (Dai *et al.* 2014; Wang *et al.* 2014). A key feature of this highly informative dataset is that, autopods were separated into tissue groups (digit I, digit II-V and interdigits), providing insight into the genes that may be involved in digit elongation, and interdigital apoptosis. In this dataset the 5'HoxD genes were the most differentially expressed genes in the digits of the CS15-CS17 bat (Wang *et al.* 2014), while *Meis2* was the most differentially expressed gene in the interdigital webbing of the bat forelimb at CS15-CS17 (Dai *et al.* 2014).

Meis2 and *Hoxd11* are both key developmental genes that encode transcription factors, proteins that bind to DNA to regulate the expression of downstream genes. They belong to Superclass called the homeobox genes, best known for directing downstream cascades of gene expression that control the developmental patterning and formation of body structures in animals, plants and fungi (Holland 2013).

1.5.2. Meis2 is a transcription factor that is involved in proliferation events and is found in interdigital tissues of the mouse

Meis2 (Nakamura *et al.* 1996) is a TALE (Three Amino acid Loop Extension) class homeobox gene that encodes a protein, which acts as a HOX protein co-factor, together with the closely related PREP (PBX Regulatory Protein) protein family, to increase the binding specificity of HOX transcription factors to DNA targets (reviewed by Moens and Selleri 2006; Longobardi *et al.* 2013). *Meis2* has a complex regulatory strategy underlying its activity (Bürglin 1997; Huang *et al.* 2005; Sánchez-Guardado, Irimia, *et al.* 2011). It plays a role in olfactory bulb, inner ear and eye formation and brain pattering, where its protein product regulates cell proliferation and differentiation.

During limb development, *Meis2*, together with its closely related ortholog, *Meis1* (Moskow *et al.* 1995), serve as proximalising agents in the outgrowing bud. They are initially expressed throughout the bud, ostensibly activated by high levels of RA synthesised in the flank (Capdevila *et al.* 1999; Mercader *et al.* 1999; Roselló-Díez *et al.* 2011). *Meis1/2* maintain high levels of RA by repressing the activity of *Cyp26b1* (Roselló-Díez *et al.* 2014). As the limb bud extends *Meis1/2* gene expression becomes restricted proximally to the presumptive stylopod region, corresponding to cells that maintain high levels of RA signalling (Mercader *et al.* 2000; Cooper *et al.* 2011). This promotes the initiation of

Homeobox A11 (*Hoxa11*) expression throughout the '*Meis*-free' undifferentiated distal region, along with expression of the gene, *Homeobox A13* (*Hoxa13*) (Cooper *et al.* 2011). *Meis1* and *Meis2* are clearly excluded from the autopod during early stages of its formation (Capdevila *et al.* 1999; Mercader *et al.* 1999; Roselló-Díez *et al.* 2011). However, there have been reports of *Meis2* expression occurring in the interdigital region of the E12.5 (Oulad-Abdelghani *et al.* 1997) and E14.5 mouse autopods (EMAGE:29320; (Richardson *et al.* 2014). The role that this gene may play in this context is currently unknown, however the expression of this gene in the interdigital region, and its high expression in the bat forelimb indicates that it may be involved in interdigital membrane formation in the bat.

1.5.3. Hoxd11, in conjunction with neighbouring 5'HoxD genes, plays a role in skeletal element formation and growth

Hoxd11 is one of 39 classic *Hox* homeobox genes that are clustered within the vertebrate genome, namely HoxA, HoxB, HoxC and HoxD. These are homeotic genes, with the remarkable ability to confer segment identity in developing embryos (Lewis 1978). They have predominant roles in organogenesis and morphogenesis in a variety of systems, both indirectly thorough the control of regulatory networks (activating or repressing multiple transcription factors), and directly through the regulation of genes that are involved in specific cellular processes (i.e. cell proliferation, cell survival, cell shape, cell growth and localisation) (Castelli-Gair Hombría and Lovegrove 2003).

In the developing limb, genes within the HoxD cluster appear to regulate cell proliferation, cartilage condensation and growth plate organisation (Duboule 1995, 2007; Goff and Tabin 1997; Jung and Tsonis 1998; Villavicencio-Lorini *et al.* 2010; Gross *et al.* 2012; González-Martín *et al.* 2014). The four Hox clusters are composed of paralogous genes, all transcribed in the same direction and conventionally numbered from the 3' to the 5' end of the cluster (Scott 1993). *Hoxd11* is co-regulated and expressed with neighbouring genes, *Hoxd13*, *Hoxd12* and *Hoxd10* (a group hereafter referred to as 5'HoxD genes) (Zákány and Duboule 2007). Loss of function of these genes in mice results in shortened or absent skeletal elements, thought to be the result of alterations in both limb patterning and growth (Duboule 1995; Nelson *et al.* 1996; Zákány and Duboule 1996; Goff and Tabin 1997). These results indicate that the 5'HoxD genes are well positioned to mediate the formation of distinct skeletal morphologies between the forelimb and the hindlimb (Chen *et al.* 2005; Ray and Capecchi 2008; Chew *et al.* 2012).

Hoxd11, originally known as *Hox-5.5* (Dollé *et al.* 1989) and *Hox-4.6* (Morgan *et al.* 1992), was first characterised in terms of its early co-ordinated expression with the neighbouring HoxD genes (then

known as the Hox-5 complex) in the outgrowing limb bud (Dollé and Duboule 1989; Dollé *et al.* 1989). This and subsequent studies suggest that these genes co-operatively pattern the early limb bud and mediate its outgrowth together with other factors (Zákány and Duboule 2007).

The 5'HoxD genes act as a functional unit, forming a 'meta-gene' with integrated expressions, activities and functions (Duboule 2007). This is a result of their shared ancestry, in conjunction with the evolution and retention of a common regulatory strategy (Tschopp *et al.* 2011). While the loss of single genes in the cluster leads to mild defects in certain skeletal elements, combinatorial loss of these genes generates more severe phenotypes (Davis and Capecchi 1996; Zákány and Duboule 2007). To complicate the matter, *Hox* genes are involved in the regulation of multiple processes during limb development in a tissue and time dependant manner, playing important roles in early AP and PD limb patterning (Morgan and Tabin 1994; Zákány *et al.* 2004; Sheth *et al.* 2013), autopod patterning (Fromental-Ramain *et al.* 1996; Sheth *et al.* 2012), growth plate formation and long bone growth (González-Martín *et al.* 2014; Kuss *et al.* 2014). The differential expression of *Hoxd11* in bat limbs, and compelling phenotypes of *Hoxd11* mouse mutants, indicate that this gene may be involved in bone elongation events in the bat forelimb autopod. However, based on their integrated regulation and function, the characterisation of all of the 5'HoxD genes in the bat limb is required to understand the potential role that they play in the development of their unique morphologies.

1.6. Thesis Aims

The genes, interactions and events that pattern the early limb bud are well characterised (Tabin and Wolpert 2007). Due to its late development and structural complexity, those of the autopod are less well understood, with integrated models of patterning, digit formation and interdigital apoptosis only recently being described (Suzuki 2013; Díaz-Hernández *et al.* 2014; Raspopovic *et al.* 2014). This is conventionally done through the analysis of phenotypes and molecular events during normal and mutant chick and mouse embryos, providing standardised systems in which to characterise these processes. Characterisation of these, and exploration of gene expressions in non-model organisms, such as the bat, takes advantage of natural and stable variations in limb morphologies to further understand developmental systems (Cretekos *et al.* 2001; Sears 2011).

The identification of differential gene expression in limb types and/or tissues is a well-established method to characterise incongruent processes and pathways that may underlie their divergent developmental fates (Shou *et al.* 2005; Gyurján *et al.* 2011; Wang *et al.* 2014). In this thesis I characterise the expression of *Meis2* and *Hoxd11*, in conjunction with associated genes, in the autopods of the bat, *M. natalensis* over stages of digit formation, elongation and interdigital regression (CS15-CS18), to understand the roles these genes play in the formation of the unique limb phenotypes of the bat, specifically in context of interdigital membrane formation and skeletal elongation.

The first component of this thesis examined *Meis2* expression in bat and mouse autopods in the context of genes that are involved in interdigital apoptosis. I aimed to:

(i) validate the overexpression of *Meis2* in the bat forelimb during autopod formation using qPCR and examination of RNA-seq data;

(ii) characterise *Meis2* expression pattern in both bat and mouse autopods over a developmental series by WISH, to determine the localization of overexpression in the bat forelimb;

(iii) determine if RA signalling (as indicated by *Rarβ* expression) in the autopod could be corresponded to *Meis2* expression pattern using WISH in CS17 bat limbs and those of transgenic (*Rdh10*^{trex}) mice;

(iv) characterise the expressions of genes that encode enzymes involved in RA synthesis, metabolism, and signalling (*Rdh10*, *Aldh1a2*, *Cyp26b1* and *Rarβ*) in both bat and mouse autopods over a developmental series by using WISH and examination of RNA-seq data to determine if these were altered in bat limbs at CS17;

(v) characterise *Hoxa11* and *Hoxa13* expression levels and patterns in both bat and mouse autopods over a developmental series by using qPCR and WISH, to determine whether these were altered by the overexpression of *Meis2* in the forelimb.

The second component of this thesis characterises the 5'HoxD genes activity in bat autopods in the context of skeletal development. I aimed to:

(i) examine the limb and autopod skeletal element lengths of bat forelimb and hindlimbs to compare these to the mouse, to determine if elongated elements correspond to regions of 5'HoxD gene activities;

(ii) quantify both the relative and absolute expressions of the 5'HoxD genes in the bat and the mouse autopods over a developmental series, to compare their expressions in different limb types and correspond these to changes in morphologies over development;

(iii) describe the 5'HoxD gene expression patterns in the bat autopod;

(iv) characterise the bat 5'HOXD protein coding sequences to determine if any changes were evident with the potential to alter protein function;

(v) characterise the highly conserved sequence region (CsC) in the bat Prox *cis*-regulatory region, which controls limb specific expression of the 5'HoxD genes, to identify bat specific mutations in these regions that may be responsible for the altered expressions of these genes in the bat.

2. Materials and methods

2.1. Study samples

2.1.1. Ethics approval

Ethical approval for work on ICR (UCT strain 1) mice (*Mus musculus*) at the University of Cape Town was approved by the UCT Faculty of Health Sciences Animal Ethics Committee (006/040; 012/052). Ethical approval to sample wild-caught bats (*M. natalensis*) was given by the University of Cape Town Faculty of Science Animal Experimentation Committee (2006/V4/DJ; 2008/V16/DJ; 2012/V39/NI) and additional sampling permission granted by the Western Cape Nature Conservation Board (AAA004–00030–0035; AAA007-00041-0056).

2.1.2. Field work

M. natalensis embryos were collected from wild-caught, pregnant females in September to October of 2006, 2008 and 2012 from the maternity colony of the De Hoop Guano Cave, De Hoop Nature Reserve, Western Cape Province, South Africa. Bats were trapped during emergence using an Austbat 3 Bank Harptrap (Faunatech Austbat, Victoria, Australia), were placed in black cloth bags for transport to a field station, killed and dissected on site as previously described (Hockman *et al.* 2008, 2009; Mason 2009).

2.1.3. Embryo preparation and storage

Embryos were staged with *M. natalensis* given the nomenclature CS to designate *Carollia* Stages (Chen *et al.* 2005; Giannini *et al.* 2006; Hockman *et al.* 2009) and *M. musculus* embryos given the nomenclature E to designate embryonic day. Tissues used for RNA extraction were put in RNA*later* RNA Stabilisation Reagent (QIAGEN, Valancia, CA, USA) at 4 °C overnight and stored at -80 °C. Embryos used for *in situ* hybridisation were fixed in 4% Paraformaldehyde (PFA) overnight, rinsed in Phosphate Buffered Saline (PBS), put through a Methanol (MeOH) dehydration series (25%, 50%, 75%, 100%, 100% MeOH in PBS) rocking at room temperature for 15 min each wash, and stored at -20 °C. Adult bats were stored in 70% ethanol (EtOH) at -20 °C.

2.2. Quantitative real time PCR

Quantitative real time PCR (hereafter referred to as qPCR) experiments were performed according to the Minimum Information for Publication of qPCR Experiments, the MIQE guidelines (Bustin *et al.* 2009).

2.2.1. Overview of experimental design

Quantitative PCR was performed to measure both the relative and the absolute level of selected mRNA transcripts in developing bat and mouse autopods. Samples consisted of amplified mRNA (aRNA) that was extracted from individual bat forelimb (FL) and hindlimb (HL) autopods (left and right pooled) at stages CS15, CS16, CS17 and CS18 and mouse forelimb autopods at E13.5, with three biological repeats per stage (Table 2.1).

Relative qPCR was performed to validate the microarray signal data for *Meis2* (two regions hereafter referred to as 5' *Meis2* and 3' *Meis2*), *Hoxd10*, *11*, *12* and *13* mRNA transcripts and to characterise abundance of these transcripts over sequential stages of autopod development. The reference gene *TATA Box binding protein-like 1*, *Tbpl1*, was used for normalisation of data. Complementary DNA (cDNA) were synthesised in batches and a serial dilution generated by pooling a portion of each sample and diluting these. Four bat developmental stages (CS15, CS16, CS17, CS18) and one mouse stage (E13.5), with three biological repeats of each, were examined. Each biological sample was measured in triplicate using the RotoGene6000 (QIAGEN). Developmental stages were run together, 42 samples and 2 no template controls (NTC), with biological repeats being performed separately. All pipetting steps were performed manually.

Absolute qPCR was performed to measure the absolute levels of *Hoxd10, 11, 12* and *13* and *Hoxa11* and *13* mRNA transcripts for the bat samples indicated above. cDNA were synthesised in one batch. Each gene was tested together with a generated standard curve of quantified target DNA and all samples were measured in triplicate alongside four NTC samples. Each qPCR experiment was performed as one run of 100 samples with the aid of the QIAgility robotic workstation (QIAGEN).

Table 2.1: Summary of experimental samples and their downstream applications. The average and standard deviation of measurements for each staging group are given. The concentration of the total RNA extraction and aRNA yield for each limb type is given.

Experiment	Sample Code	Stage (CS)	Biological Repeat	Uterus Length (mm)	CR Length (mm)	Embryo Weight (mg)	Total RNA Conc. (ng/µl)		aRNA Yield (µg)	
							FL	HL	FL	HL
qPCR	Mn06-35	15	1	8.5	8	0.13	60±0	29±4	50.5	48.2
	Mn06-38	15	2	8	7.5	0.10	22±2	46±3	36.1	47.4
	Mn06-46	15	3	8	9	0.10	56±1	95±1	33.3	34.2
Microarray / qPCR	Mn06-60	16	1	-	-	0.17	90±1	72±0	109.1	101.0
	Mn06-49	16	2	8.5	9.5	0.16	77±1	45±0	102.8	105.5
	Mn06-59	16	3	8	9.5	0.13	101±4	49±2	107.3	96.8
Microarray	Mn06-39	16	4	9	9	0.12	75±3	40±1	101.6	104.9
Microarray / qPCR	Mn06-45	17	1	8	11	0.23	146±0	71±2	110.9	100.9
	Mn06-44	17	2	9.5	10	0.20	112±3	77±1	102.6	101.7
	Mn06-31	17	3	9	11	0.16	135±3	76±1	103.1	83.3
Microarray	Mn06-40	17	4	8.5	10.5	-	130±3	54±1	95.0	110.2
qPCR	Mn06-56	18 E	1	9	11	0.28	89±0	111±2	104.3	82.9
	Mn06-32	18 L	2	10.5	12	0.33	92±1	80±4	50.2	90.4
	Mn06-58	18 VL	3	10	15	0.46	115±2	80±3	120.1	131.0

2.2.2. Sample preparation

Autopods were dissected from embryos using forceps while submersed in RNA*later* solution. The autopod was distinguished as the dorso-ventrally flattened tissue on the distal portion of the limb and was dissected along the point of constriction of the presumptive wrist or ankle, excluding the tissue associated with the stylopod and the zeugopod as well as that associated with the proto- and plagiopatagium. This autopod tissue is subsequently referred to as either the forelimb (FL) or the hindlimb (HL).

Total RNA was purified from paired autopod tissues using the RNeasy Lipid Tissue Mini Kit (QIAGEN) as per manufacturer's instructions with the following modification: homogenisation in the QIAzol Lysis Reagent was performed by grinding tissue with a plastic microfuge tube pestle, and the sample was maintained in this solution for a minimum of 15 min. RNA was eluted in 50 µl RNase-free

water, and quantified using the Nanodrop ND-1000 UV-Vis Spectrophotometer (Nanodrop Products, Thermo Scientific, Wilmington, DE, USA). The average RNA concentration differed among the limb types, reflecting the variation in input tissue sizes (Table 2.1). RNA samples appeared pure (A_{260}/A_{280} < 2.0) and intact. RNA integrity was assessed by denaturing gel electrophoresis, (Figure 2.1) with a subset of samples were quality checked using the Agilent 2100 Bioanalyser using the Agilent RNA 6000 Nano Kit (Agilent Technologies Inc., Santa Clara, CA, USA), confirming high quality total RNA (RIN < 9.6). RNA samples were aliquotted and stored at -80°C.

RNA samples were amplified using the Amino Allyl MessageAmp II Cy3 aRNA Amplification Kit (Ambion®, Life Technologies, Carlsbad, CA, USA), as per manufacturer's instructions, using a fixed amount of 0.5 µg of input RNA with the IVT reaction being maintained for 16 hrs. aRNA samples had expected yields, aside from CS15 samples which were lower (Table 2.1), and A_{260}/A_{280} readings within an acceptable ranges (1.98 – 2.35). The nucleotide size distributions of each sample were comparable (ranged from 250 nt to 3 000 nt with the highest density found at 1 400 nt), when 1 µg aRNA was run on a denaturing gel.

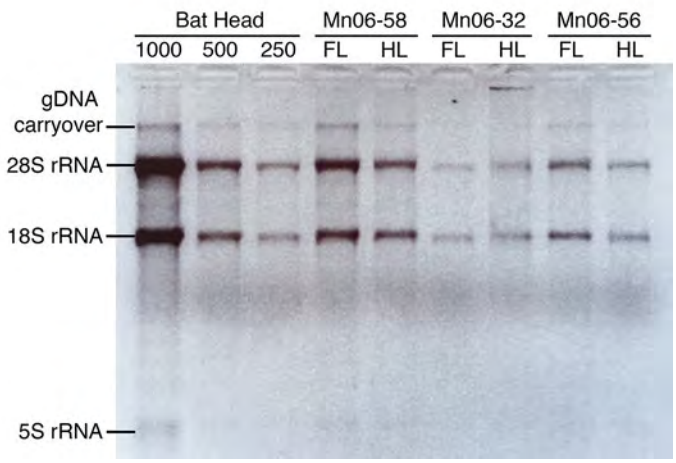

Figure 2.1: An example of a denaturing RNA gel (1.2%). This shows the ribosomal bands (rRNA) that give an indication of the integrity of the total RNA for the CS18 forelimb (FL) and hindlimb (HL) biological repeats (**A**). These are shown alongside a series of decreasing RNA amounts (1000 ng, 500 ng, 250 ng) of high quality bat head RNA.

2.2.3. qPCR primer sets

Primers were designed for each gene of interest using alignments of predicted transcripts from *Mus musculus* (NCBI37/mm9 and GRCm38/mm10), *Myotis lucifugus* (Broad Institute Myoluc2.0/myoLuc2) and *Pteropus vampyrus* (Broad/pteVam1) (Table 2.2). Sequences were obtained from the Ensembl Genome Browser (ver. 59 to 83) (Flicek *et al.* 2014) or the UCSC genome browser (Kent *et al.* 2002). Sequences were aligned using ClusterW in BioEdit (Ibis Biosciences, Carlsbad, CA, USA) and regions of interspecies conservation, suitable for primer design for amplification of *M. natalensis* were noted, while unsuitable regions of high conservation amongst paralogs were excluded. Primer design was performed using the *M. lucifugus* sequence, using IDT's PrimerQuest (Integrated DNA Technologies, Inc., Coralville, IA, USA), which incorporates Primer3 software (ver. 2.2.3) (Untergasser *et al.* 2012). Oligo hairpins, homodimers and heterodimers were characterised using OligoAnalyzer 3.1 (Integrated DNA Technologies, Inc.).

Table 2.2: Summary of qPCR primer sets used in both relative and absolute experiments. Primer names, sequences and melting temperatures are given. Melting temperatures were calculated using OligoAnalyzer 3.1 (IDT). The amplicon sizes are indicated.

Primer Name	Primer Sequence (5'- 3')	nt	GC (%)	Tm (°C)	Amplicon Size (bp)
5'-Meis2_qPCR_Fwd	CTA TGG CCA CCA CGA CTT C	19	57.9	55.6	118
5'-Meis2_qPCR_Rvs	TGT CAG TAG GTG TTG GCA GG	20	55	57	
3'-Meis2_qPCR_Fwd	GAA GAA ACA GTT AGC GCA AGA CA	23	43.5	55.7	175
3'-Meis2_qPCR_Rvs	ACC ATC CAA CAC AAA GCT CC	20	50	55.6	
Hoxd10_qPCR_Fwd	ATG TAC CTC ACC CGC GAG T	19	57.9	58.5	146
Hoxd10_qPCR_Rvs	AGG TTG GCG GTC AGT TCT CG	20	60	59.8	
Hoxd11_qPCR_Fwd	ATG AAC GAC TTT GAC GAG TGC GG	23	52.2	59.7	93
Hoxd11_qPCR_Rvs	ATT GCT GGC GAA GTC CGA CG	20	60	60.5	
Hoxd12_qPCR_Fwd	AGA TTG CGG AGC TGG AGA ACG	21	57.1	59.6	110
Hoxd12_qPCR_Rvs	ACA GAT TTT GAC CTG CTG GTC GC	23	52.2	60	
Hoxd13_qPCR_Fwd	AGC TAC CAC TTC GGC AAC GG	20	60	60.1	130
Hoxd13_qPCR_Rvs	ACA CGT CCA TGT ACT TCT CCA CCG	24	54.2	60.5	
Lnp_qPCR_Fwd	GAT CCC CTG CTA CTT CAG T	19	52.6	59.4	130
Lnp_qPCR_Rvs	TGT GGA CCA TCA CCA ACT A	19	47.4	59.1	
Hoxa11_qPCR_Fwd	GAA GCT ATT CAA TCT CCA AAC C	22	40.9	51.5	122
Hoxa11_qPCR_Rvs	CTA GTC CAG TCG TCT TTC AC	20	50	52.3	
Hoxa13_qPCR_Fwd	CTC TTT CTC CTT GGT GGA ATC	21	47.6	52.9	137
Hoxa13_qPCR_Rvs	CTG AAA CTG CGT ACT TAG GG	20	50	52.9	
Tbpl1_qPCR_Fwd	GGC AGA CAG TGA TGT TGC ATT GGA C	20	52	60.5	190
Tbpl1_qPCR_Rvs	GGT TCC TGA GGA CCA AAT TGC AGC TG	26	53.8	62	

Primer sequences were checked for target specificity using Primer-BLAST, National Centre for Biotechnology Information (NCBI), both against the nucleotide (nr), Refeq RNA (refseq_rna) or Genome (chromosomes from all organisms) (Ye *et al.* 2012). In addition, target regions were verified using *in silico* PCR, UCSC Genome Browser (min match 15 bp), performed against *M. lucifugus* (Broad Institute Myoluc2.0/myoLuc2), *P. vampyrus* (Broad/pteVam1), *M. musculus* (GRCm38/mm10) and *H. sapiens* (GRCh37/hg19). If primers were not found using the above analyses (due to size limits), nucleotide BLAST (NCBI) (Altschul *et al.* 1990) on the nucleotide collection (nt/nt) and BLAT, (UCSC) (Kent 2002) analyses were performed using *in silico* generated amplicons to confirm the target identity (Appendix A.1). Primers (Table 2.2) were synthesised by the UCT MCB DNA Oligonucleotide Synthesis Lab (University of Cape Town). Target specificity was confirmed by: the amplification of a single product of the expected size when visualised on an agarose gel; the presence of melt curves with a single peak, and sequencing of the amplified product (Bustin *et al.* 2009; Derveaux *et al.* 2010)

2.2.4. Relative qPCR experimental run

cDNA was synthesised from 1 µg aRNA using a modification of the SuperScript III First-Strand synthesis system (Invitrogen™, Life Technologies, Carlsbad, CA, USA) in a Techne Genius PCR Thermal Cycler (Model FGEN02TP, Bibby Scientific Ltd., Stone, Staffordshire, UK). Template was primed using 250 ng of second round primers (Ambion®, Life Technologies) incubated with 25 mM of dNTPs at 65 °C for 5 min. Samples were kept on ice for 1 min, after which First Strand Buffer, 0.25 M DTT, 100 U RNaseOUT Recombinant Ribonuclease Inhibitor and 500 U Superscript III Reverse Transcriptase were added to make up a 50 µl reaction. Reactions were incubated at 25 °C for 10 min, 50 °C for 60 min and 70 °C for 15 min. *E. coli* Ribonuclease H (2 U) was added for a final volume of 51 µl and samples were incubated at 37 °C for 20 min. Newly synthesised cDNA was stored at 4 °C and used within two weeks. A pooled sample was generated from combining 15 µl of each cDNA synthesis reaction. This was diluted in series (1; ½; ¼; ⅛; $^1/_{16}$) using molecular grade water to generate standard curve samples. An equal volume (36 µl) of water was added to each limb cDNA template sample. qPCR was performed in 0.1 ml strip tubes (Gene Target Solutions, Dural, NSW, AU). The SensiMix SYBR Kit (Bioline Reagents Ltd, London, UK) was used at 20 µl reactions with a final concentration of 3 mM $MgCl_2$, and 250 nM primers, and 2 µl of template. qPCR reactions were performed on a RotorGene 6000 (QIAGEN) using a three-step cycling protocol: 10 min. at 95 °C, 40x (15 s at 95 °C, 15 s at 60 °C) and 15 s at 72 °C followed by a melting analysis that acquired the fluorescence readings from 60 °C to 95 °C in steps of 1 °C.

2.2.5. Relative qPCR analysis

Data were obtained using the RotorGene 6000 real time rotary analyser software (Ver. 1.7, QIAGEN). Melt curve peaks were examined for amplicon homogeneity. Background fluorescence was removed using Dynamic Tube Normalisation and Noise Slope Correction. The quantification cycle (Cq; also known as threshold cycle, Ct) was calculated using an automatically generated threshold that excluded the first 10 cycle readings. Raw data were manually examined and technical repeats with amplification profile irregularities, such as non- or very poor amplification were noted. Standard curves were plotted and the efficiency (E) and Cq values calculated for each run (Table 2.3).

Data were analysed using Microsoft® Excel® for Mac 2011 (ver. 14.4.3; Microsoft Corporation). Outliers attributable to failed amplification reactions were discarded and technical repeats were averaged. Though optimal to use at least three normalisation genes in the analysis of these experiments (Bustin *et al.* 2009), limitations on the sample availability precluded this. *Tbpl1* had constant expression levels across the microarray data and in qPCR experiments and performed well as a reference gene (Appendix A.2). Data were analysed using the efficiency correction method (Pfaffl 2004): data were corrected for the efficiency of the run calibrating against the average Ct value of the standard curve, and normalised to the reference gene (*Tbpl1*) as per the following equation:

$$N = \frac{(E_G + 1)^{(G - S_G)}}{(E_R + 1)^{(R - S_R)}} \tag{2.1}$$

Where:
N = Normalised sample
E = Efficiency of qPCR run
G = Average Ct value of gene of interest sample
R = Average Ct value of normalisation gene sample
S = Average Ct value of all standards of the qPCR run

The normalised data for each sample of each biological repeat (B1, B2 and B3) were then calibrated to the normalised average CS15 HL value of all biological repeats as per the following equation:

$$C = \frac{N}{\frac{1}{3}(H_{B1} + H_{B2} + H_{B3})} \tag{2.2}$$

Where:
C = the calibrated value of each sample
H = the normalised value of the CS15 HL sample
B1, *B2*, *B3* indicates each biological repeat

Normalised data for each biological repeat were averaged to get a single value to represent each sample and standard errors (SE) were calculated. Statistical analyses were performed in IBM® SPSS Statistics ver. 22 (IBM Corporation, Armonk, NY, USA).

Table 2.3: Summary of the relative qPCR experiments performed. For each gene and experimental run the threshold at which the cycling threshold values (Ct) were obtained, the Ct values of the NTC, the E values and r^2 values of the standard curve are given. The threshold used to determine the melt peak is given and the average melt peaks (standard deviation) of the mouse, bat and Standards (Std.) and no template controls (NTC) are shown.

Gene	cDNA synthesis	Bio	Ct Threshold	NTC Ct	E val.	r^2	Melt Thresh.	Melt Peak			
								Mouse	Bat	Std.	NTC
Tbpl1	cDNA1	1	0.026	29.8; 29.13	1.06	0.98194	20	81.5 (0.0)	81.0 (0.1)	81.1 (0.1)	NA
		2	0.1614	31.5; 31.42	1.07	0.96893	20	81.1 (0.1)	80.6 (0.1)	80.9 (0.1)	NA
		3	0.3734	36.0; NA	0.89	0.99003	20	80.2 (0.0)	80.0 (0.2)	80.3 (0.2)	NA
	cDNA2	1	0.2512	NA; NA	1.11	0.99531	10	79.7 (0.0)	79.5 (0.1)	79.5 (0.0)	NA
		2	0.0555	NA: NA	0.99	0.99209	10	79.6 (0.1)	79.5 (0.1)	79.6 (0.1)	NA
		3	0.34	34.0; 33.71	0.84	0.97678	7	80.7 (0.1)	80.2 (0.1)	80.5 (0.1)	77.3; 77.5
	cDNA3	1	0.0615	19.3; 35.19	0.94	0.99371	10	79.8 (0.2)	79.6 (0.1)	79.7 (0.1)	NA
		2	0.1145	34.4; 37.67	0.97	0.98637	20	80.6 (0.1)	80.1 (0.2)	80.4 (0.1)	NA
		3	0.0626	NA; NA	0.94	0.96674	20	80.5 (0.0)	80.0 (0.2)	80.3 (0.1)	NA
5'-Meis2	cDNA3	1	0.0008	12.7; NA	1.00	0.99862	10	89.0 (0.0)	89.0 (0.1)	89.0 (0.1)	NA
		2	0.1015	NA; 38.55	1.02	0.96568	10	89.5 (0.0)	88.9 (0.1)	88.9 (0.2)	NA
		3	0.002	22.5; 26.35	0.99	0.99875	10	88.8 (0.2)	89.0 (0.1)	89.0 (0.1)	NA
3'-Meis2	cDNA1	1	0.0522	NA; 30.67	0.94	0.99188	20	85.7 (0.2)	84.7 (0.2)	85.0 (0.2)	NA
		2	0.16	NA; 33.43	1.13	0.99509	15	85.3 (0.1)	84.0 (0.1)	84.2 (0.1)	NA
		3	0.0988	NA; NA	1.01	0.98414	20	85.8 (0.1)	84.5 (0.1)	84.7 (0.1)	NA
Hoxd10	cDNA3	1	0.004	28.82; 28.8	1.00	0.99892	20	86.0 (0.0)	86.3 (0.1)	86.4 (0.1)	NA
	cDNA1	2	0.0032	28.5; 25.78	1.02	0.99841	20	86.3 (0.3)	86.5 (0.1)	86.5 (0.2)	NA
		3	0.1599	30.8; 31.04	0.97	0.9888	15	86.3 (0.1)	86.6 (0.1)	86.6 (0.2)	85.7; 85.7
Hoxd11	cDNA3	1	0.0008	NA; NA	1.00	0.99697	10	89.6 (0.1)	88.6	88.7 (0.1)	NA
	cDNA1	2	0.1168	36.5; 38.39	1.22	0.98537	10	90.1 (0.1)	89.0 (0.0)	89.1 (0.1)	NA
		3	0.0044	31.7; 23.27	1.10	0.99642	20	90.2 (0.0)	88.8 (0.2)	89.0 (0.2)	NA
Hoxd12	cDNA2	1	0.0176	NA; NA	0.97	0.96704	10	84.6 (0.2)	84.9 (0.1)	84.7 (0.1)	NA
	cDNA1	2	0.0008	NA; NA	1.01	0.99908	5	83.9 (0.1)	84.4 (0.1)	84.2 (0.0)	NA
		3	0.0036	29.7; NA	1.08	0.99904	15	83.9 (0.1)	84.2 (0.1)	84.2 (0.1)	NA
Hoxd13	cDNA1	1	0.002	NA; NA	0.98	0.99887	15	88.4 (0.1)	89.5 (0.1)	89.5 (0.1)	78.3, 78.0
		2	0.0792	30.1; 29.62	1.08	0.97428	10	88.1 (0.1)	89.4 (0.1)	89.1 (0.1)	77.8; 78.0
		3	0.0192	26.4; 30.7	1.05	0.99854	15	88.4 (0.1)	89.3 (0.1)	89.4 (0.1)	79.0
Lnp	cDNA3	1	0.0204	NA; NA	0.98	0.95617	20	84.6 (0.1)	84.3 (0.1)	84.5 (0.2)	NA
		2	0.0076	31.5; 29.85	1.00	0.97497	15	84.8 (0.2)	84.3 (0.1)	84.5 (0.1)	NA
		3	0.1548	NA; NA	1.10	0.96262	20	85.2 (0.2)	84.8 (0.1)	84.9 (0.1)	NA

Microarray data (RG values; N = 4) and qPCR data (N = 3) were calibrated to the E13.5 mouse and graphed (Microsoft Corporation). Uncalibrated data were tested for differences between: the mouse E13.5 FL and the bat CS17 FL (Independent-samples T-tests) and between bat FL and HL of each stage (CS17 and CS16; Paired-samples T-test). The *p*-values were adjusted for multiple testing (30 tests) using a Bonferroni correction. Fold changes were graphed as median values, with error bars indicating the minimum and maximum values. These were tested for significance (one-sample T-test) and *p*-values were adjusted for multiple testing using a Bonferroni correction. Differences among the limb types and developmental stages were tested using a two-way ANOVA ensuring that assumptions of normality and homogeneity of variances held. All data were analysed using standard tests in IBM® SPSS Statistics ver. 22 (IBM Corporation).

2.2.6. Absolute qPCR experimental run

Absolute qPCR relies on the measurement of a known standard to calibrate the readings of the sample among the different genes tested. This method removed SYBR-based primer and amplicon bias to be excluded allowing multiple genes to be directly compared. To do this a quantified standard curve was generated by cloning the target amplicon product into a plasmid. qPCR products were run on a 2% agarose gel, the single band was cut out, extracted and purified using the Wizard® SV Gel and PCR Clean-up System (Promega, Madison, WI, USA), and rechecked on a second gel for specificity. Purified products were ligated into the pGEM®-T Easy vector using the using the pGEM®-T and pGEM®-T Easy vector system (Promega) according to the manufacturer's instructions, using a 16 hr ligation step at 4 °C. Ligations were transformed into XL1-Blue competent cells and plated onto fresh LAIX plates (Lysogeny Broth, LB; plates containing ampicillin, IPTG and X-Gal) at two dilutions (10^{-2}, 10^{-1}) and culturing, plating and blue/white selection were performed as recommended. Five to ten white colonies and one blue colony were selected from each plate, re-streaked onto a master plate and left to grow at 37 °C overnight.

Colony PCRs were performed on all selected colonies to check for the presence of an insert of the estimated size using SP6 and T7 primers. PCR amplifications were performed using KAPA Taq Ready Mix (KAPA Biosystems, Wilmington, MA, USA) in 20 µl reactions with primers at a final concentration of 0.5 µM, and run at the following cycling parameters: 5 min at 94 °C, 30x(1 min at 94 °C, 30 s at 55 °C, 30 s at 72 °C), 5 min at 72 °C. For each amplicon, three positive colonies were inoculated into a 5 ml starter LB amp culture and left to grow for 4-8 hrs. These were re-inoculated into a 200 ml LB amp culture and grown for 16 hrs. Plasmids were purified from cultures using either

the QIAprep® Spin Miniprep Kit (QIAGEN) or the Promega Pure Yield™ Plasmid Miniprep System (Promega) as per manufacturer's instructions. A sample of each culture was stored as a 1 ml glycerol stock (25% sterile glycerol) at -80 °C. Purified plasmid yields were determined using the Nanodrop 1000 (Nanodrop Products, Thermo Scientific Inc.). Purified plasmids were sent for sequencing using both T7 forward and SP6 sequencing primers to the Central Analytical Facility (Stellenbosch University, Stellenbosch, RSA).

Raw sequences were trimmed to remove vector sequences. Forward (T7 forward) and reverse (SP6) sequences were aligned and a consensus sequence generated using the sequence with the highest quality scores when calling ambiguous nucleotides (Geneious ver. 7.1.5, Biomatters Ltd., Auckland, NZ). The transcript identity of each consensus sequence was confirmed by using the NCBI BLAST (megablast), against the nucleotide collection (nt/nr) of the mouse and the bat (Appendix A.1). The top hit was taken as the sequence identity. Each amplicon was mapped to the genome of *M. lucifugus* (Jul 2010 Broad Institute Myoluc2.0/myoLuc2) using UCSC Genome Browser BLAT analysis to confirm its identity.

Purified plasmids were linearised using restriction enzyme (RE) digestion with *Sac1* (Fermentas, Thermo Fisher Scientific, Pittsburgh, PA, USA) and visualised on a 0.8% agarose gel run to confirm that they were digested to completion. These restricted linearised plasmids were cut out and purified using the Wizard® SV Gel and PCR Clean-up System (Promega). They were used as a template to amplify the insert along with the flanking plasmid sequences using KAPA HiFi PCR kit (KAPA Biosystems) with M13 Fwd and Rvs primers using the following cycling parameters: 2 min at 95 °C, 30x (20 s at 98 °C, 15 s at 45 °C, 30 s at 72 °C), 2 min. at 72 °C. PCR products were visualised on a 2% agarose gel, gel extracted and purified as described above. These pure standard curve templates were quantified using the Nanodrop 1000 (Nanodrop Products, Thermo Scientific Inc.) and the nucleotide concentrations (ng/µl) were converted to copies/µl using the following equation:

$$\text{Template (copies/µl)} = \frac{6.022141\times10^{23}\times \text{ Template concentration (ng/µl)}}{\text{Transcript length} \times 660\text{Da}} \tag{2.3}$$

A quantified standard curve was generated for each gene. These consisted of eight ten-fold dilutions that ranged from $1x10^8$ (Stock 1) to $1x10^1$ (Stock 8) copies/µl. These serial dilutions were generated using 100 ng/µl carrier tRNA and were diluted 4-fold to allow 4 µl to be added to each qPCR reaction. All pipetting steps were performed using the QIAgility robotic workstation (QIAGEN).

To generate the qPCR sample template 6 µg of aRNA from each limb sample (24) was DNase treated using DNA-free™ as per the manufacturer's instructions (Ambion®, Life Technologies). These were split into two, 3 µg aliquots that were stored at -80 °C and processed separately. The first was used to examine 5'HoxD gene expression levels while the second was used to examine 5'HoxA gene expression levels. cDNA synthesis reactions were set up using a modification of the SuperScript III First-Strand synthesis system (Invitrogen™, Life Technologies). The aRNA template was first primed using 0.5 M random nonamers (Sigma-Aldrich, St Louis, MO, USA) and incubated with 1 µl of dNTPs (10 mM) at 70 °C for 10 min. Samples were kept on ice for 1 min after which 4 µl First Strand Buffer (5x), 1 µl DTT (0.1 M), 40 U RNaseOUT Recombinant Ribonuclease Inhibitor (Invitrogen™, Life Technologies) and 200 U Superscript III Reverse Transcriptase (Invitrogen™, Life Technologies) were added to make up a 20 µl reaction. Reactions were incubated at 25 °C for 15 min, 50 °C for 60 min and finally 70 °C for 15 min. The newly synthesised cDNA was diluted with 60 µl of Nuclease-Free Water (Sigma-Aldrich), stored at 4 °C and used within one week.

Absolute qPCR was performed using the RotorGene SYBR green PCR Kit Mix (QIAGEN) in 20 µl reactions. Primers (1 µM) were added to a master mix and 4 µl of each template was added to each qPCR reaction to ensure precision of template pipetting step. The QIAgility pipetting robot (QIAGEN) was used to perform all qPCR pipetting steps. The RotorGene 6000 (QIAGEN) was used to perform all experimental runs using the following two-step cycling protocol: 5 min at 95 °C, 40x (5 s at 95 °C, 10 s at 60 °C). Automatic gain calibration was performed on the first sample and the fluorescence readings were acquired after the annealing step. After each run a melt analysis was performed, and the fluorescence readings acquired from 60 °C to 95 °C in steps of 1 °C.

2.2.7. Absolute qPCR analysis

Background fluorescence was removed using Dynamic Tube Normalisation and the threshold cycle model was used to calculate the quantification cycle (Cq) using an automatically generated threshold. Absolute qPCR data were cleaned and technical repeats averaged as previously described (Section 2.2.5). Calibration curves were calculated for each qPCR run. Average r^2 and efficiency (E) values and the Ct values for the NTCs of each experiment, in addition to the average melt curve peak of the samples are given in Table 2.4. Data were analysed using absolute quantification by calibration to the known standard curve. Biological repeats were averaged to get a single value that represented each sample and the standard errors (SE) were calculated and graphed. All data were analysed using standard tests in IBM® SPSS Statistics ver. 22 (IBM Corporation).

Table 2.4: Summary of the absolute qPCR experiments performed. For each gene and experimental run the quantification cycle thresholds (Cq) are given, the Cq values of the NTC, the E values and r^2 values of the standard curve are given. The threshold used to determine the melt peak is given and the average melt peaks (standard deviation) of the mouse, bat and Standards (Std.) and no template controls (NTC) are shown.

Gene	cDNA	Bio	Cq	NTC Cq	E val.	r^2	Melt Thresh.	Melt Peak		
								Bat	Std.	NTC
Tbpl1	cDNA5	1,2,3	0.2792	35.80; 35.57	1.00	0.99825	1.5	80.2	80.2	79.2; 79.2
Hoxa11	cDNA5	1,2,3	0.2368	35.58; 34.38	1.00	0.9996	1	84.6	84.8	74.8; 75.0
Hoxa13	cDNA5	1,2,3	0.3048	32.53; 32.03	1.01	0.99977	2	82.5	82.7	75.8; 76.0
Tbpl1	cDNA4	1,2,3	0.3298	34.17 (0.68)	0.88	0.99979	1.5	80.2	80.3	78.8 (0.2)
Hoxd10	cDNA4	1,2,3	0.1840	30.65 (0.21)	0.93	0.99959	1.5	86.4	86.4	81.2 (0.0)
Hoxd11	cDNA4	1,2,3	0.2020	29.38 (1.23)	0.99	0.99978	1	88.6	88.9	82 (0.0)
Hoxd12	cDNA4	1,2,3	0.1252	32.13 (2.71)	0.98	0.99991	1.5	84.5	84.2	79.7 (0.2)
Hoxd13	cDNA4	1,2,3	0.3396	27.92 (0.84)	1.00	0.99995	1.5	89.1	89.2	78.7 (0.1)

2.2.8. RNA-seq data

The qPCR data were compared to RNA-seq normalised read counts for *M. schreibersii* (Wang *et al.* 2014). Data were obtained from the Gene Expression Omnibus (GSE50699) (Barrett *et al.* 2013). Gene IDs were extracted from the bat sequence dataset (GSE50699_GeneNameSeq.fasta) through a custom BLAST (blastn, word size: 11, Gap cost [open extend]: 5 2, low complexity filter, scoring [match mismatch]: 2-3) using the longest mouse (GRCmm38) coding transcript sequence (cDNA, Ensembl release 75) as the query (Eval. < 1e-100 and Grade > 45% and pairwise similarity > 75%). In the case of the highly similar *Meis* paralogs, where queries had overlapping hits, GeneIDs were assigned to the query with the best hit. Normalised read counts (GSE50699_GeneCounts_Normalized.txt) were extracted for each Gene ID. Where multiple Gene ID were found for a gene of interest, the normalised read count of each limb sample was taken as the sum of all Gene IDs: *Meis1*: comp14476_c0_seq1, comp13769_c0_seq1; *Meis2*: comp4463_c0; *Meis3*: comp12264_c0_seq1; *Rdh10*: comp2095_c0; *Aldh1a2*: comp3518_c0; *Cyp26b1*: comp6517_c0, comp2661_c0; *Rarβ:* comp848_c0; *Hoxa9:* comp913_0; *Hoxa10:* comp1556_c0, comp3291_c0; *Hoxa11:* comp3606_c0, comp6025_c0; *Hoxa13:* comp1324_c0. For the 5'HoxD genes, normalised read counts were taken as published with the inclusion of the additional contig found for *Hoxd9*, as follows: *Hoxd9*: comp1699_c0, comp10336_c0; *Hoxd10*: comp11192_c0; *Hoxd11*: comp3957_c0, comp7027_c0; *Hoxd12*: comp1220_c0, comp1181_c0; *Hoxd13*: comp611_c0.

2.3. Whole-mount *in situ* hybridisation (WISH)

The following section describes the methods used to generate bat specific DIG-labelled WISH probes and protocols followed for *in situ* hybridisation. Details are also included for the probe templates that were kindly given by various labs.

2.3.1. ISH primer sets and PCR amplification

Primers were designed to amplify 500 to 1000 bp of transcript sequence of interest for subsequent cloning and *in situ* probe generation (Table 2.5).

Table 2.5: Summary of *in situ* hybridisation (ISH) probe PCR primer sets used to amplify target sequences for bat and mouse. Primer names, sequences and melting temperatures are given. Melting temperatures were calculated using Primer3 (ver. 2.3.4) using the Santalucia 1998 formula and salt correction concentration settings: monovalent salt (50 mM), divalent salt (1.5 mM), oligo (0.8 mM), dNTP (0.8 mM). The amplicon sizes are indicated. **Aldh1a2*..

Primer Name	Primer Sequence (5'- 3')	nt	GC (%)	Tm (°C)	Amplicon Size (bp)
ISH_b5'-Meis2_Fwd	CTC GGC GCG GCG CGC TCC	18	89	75.8	511
ISH_b5'-Meis2_Rvs	CAG TAA AAA CTC CGC GAG GGG TTT CTG CGT C	31	55	72.9	
ISH_3'-Meis2_Fwd	ACC CGT TGT TTC CTC TGT TAG CTC T	25	48	66.8	1 255
ISH_3'-Meis2_Rvs	GCA TGA ATG TCC ATA ACC TGT CCG C	25	52	67.2	
ISH_bHoxa11_Fwd	GGT GGT TCA TTC TTG GTG ACT G	22	50	62.7	631
ISH_bHoxa11_Rvs	CTT CCA TTA AGT GTG GCA GAG G	22	50	62.2	
ISH_bHoxa13_Fwd	CAG AAC AGG AGG GTC AAA GAG	21	52	61.3	477
ISH_bHoxa13_Rvs	AAG GGT GGG CAG ATG TTT AC	20	50	61.4	
ISH_bRdh10_Fwd	AAT GGC GAG GAA GAA ATC CT	20	45	60.5	647
ISH_bRdh10_Rvs	AAC CGA TAC ATG CAC ACG AC	20	50	62.1	
ISH_bRaldh2_Fwd(i)*	AGG ATA AGC TCG CAG ACT TGG	21	52	63.2	697
ISH_bRaldh2_Rvs(ii)*	CTC ACA AAC TCC TCG TAG ATG G	22	50	61.4	
ISH_bCyp26b1_Fwd	AGG CCA TCA ACG TGT ACC AG	20	55	62.6	774
ISH_bCyp26b1_Rvs	AGA AGG GGA GGT AAT GGA AGC	22	50	62.6	
ISH_bRarB_Fwd	CAG AAG TGC TTT GAA GTG GG	20	50	60.4	796
ISH_bRarB_Rvs	GAA TGA GAG GTG GCA TTG ATC C	22	50	62.3	
ISH_bHoxd10_Fwd	CCA ACA GCT CTC CTG CTG CTA ATA CT	26	50	67.2	920
ISH_bHoxd10_Rvs	GAC CTG CCT GTC GGT GAG GTT A	22	59	67.2	
ISH_bHoxd11_Fwd	TCG GAC TTC GCC AGC AAG CCG TC	23	65	72.5	+736
ISH_bHoxd11_Rvs	GCC GGT CAG TGA GGT TGA GCA TCC GAG	27	63	73.1	
ISH_bHoxd12_Fwd	ACT CCT TCT ACT TCT CCA ACC TGC G	25	52	66.8	645
ISH_bHoxd12_Rvs	TTG GAC AAT TCC TTG CGC TTC TGC	24	50	67.5	
ISH_bHoxd13_Fwd(iii)	ACG GCT ACC ACT TCG GCA ACG	21	62	68.8	501
ISH_bHoxd13_Rvs(i)	CGT TCT CCA GTT CTT TGA GC	20	50	60.2	

Primer design was performed as described in Section 2.2.3, using the customisable assay with the following parameters: Design - PCR (2 primers); Tm – 60 °C (opt), GC – 50% (opt), Size – 24 nt (opt), 3' GC clamp – 2 nt; Amplicon Size – 500-1200 nt, with primer focus regions constrained to regions of interest previously identified in alignments. Primers were synthesised by the UCT MCB DNA Oligonucleotide Synthesis Lab (University of Cape Town, Cape Town, WC, RSA) or by Source Bioscience (Nottingham, UK). PCR amplifications were performed as summarised (Table 2.6).

Table 2.6: Summary of successful PCR protocols for amplifying probes for the synthesis of WISH templates. **Aldh1a2*.

Gene	Template	Reagents	Primer Conc. (µM)	Other	PCR cycling parameters
b5'-Meis2	Bat Head cDNA (CS16)	Kapa2G Robust Ready Mix	1	NA	2' @ 94 °C 30x(30'' @ 94 °C, 30'' @ 65 °C, 30'' @ 72 °C) 10' @ 72°C
b3'-Meis2	Bat Head cDNA (CS16)	MyTaq Mix (Bioline)	0.4	NA	1' @ 94 °C 30x(15'' @ 94 °C, 15'' @ 70 °C, 1' @ 72 °C) 10' @ 72°C
m3'-Meis2	Mouse Head cDNA (E13.5)	MyTaq Mix (Bioline)	0.4	NA	1' @ 94 °C 30x(15'' @ 94 °C, 15'' @ 70 °C, 1' @ 72 °C) 10' @ 72°
bHoxa11	Adult muscle gDNA	Kapa Ready Mix	0.4	NA	2' @ 94 °C 30x(30'' @ 94 °C, 30'' @ 55 °C, 30'' @ 72 °C) 2' @ 72°C
bHoxa13	Adult muscle gDNA	Kapa Ready Mix	0.4	NA	2' @ 95 °C 35x(30'' @ 95 °C, 30'' @ 56 °C, 30'' @ 72 °C) 4' @ 72°C
bRdh10	Bat Head cDNA (CS17)	Kapa Ready Mix	0.4	NA	2' @ 94 °C 30x(30'' @ 94 °C, 30'' @ 55 °C, 30'' @ 72 °C) 2' @ 72°C
bRaldh2	Bat FL cDNA (CS17)	Taq polymerase	0.4	1.5 mM $MgCl_2$	2' @ 95 °C 35x(30'' @ 95 °C, 30'' @ 56 °C, 30'' @ 72 °C) 4' @ 72°C
bCyp26b1	Bat FL cDNA (pooled CS15-CS18)	Kapa2G Robust Hot Start Ready Mix	0.5	NA	2' @ 95 °C 35x(15'' @ 94 °C, 15'' @ 55 °C, 15'' @ 72 °C) 10' @ 72°C
bRarb	Bat FL cDNA (CS17)	Taq polymerase	0.4	1.5 mM $MgCl_2$	2' @ 95 °C 35x(2' @ 95 °C, 30'' @ 70 °C, 30'' @ 72 °C) 4' @ 72°C
bHoxd10	Bat FL cDNA (CS17)	MyTaq Mix (Bioline)	0.4	NA	1' @ 94 °C 30x(15'' @ 94 °C, 15'' @ 70 °C, 1' @ 72 °C) 10' @ 72°
bHoxd11	Bat FL cDNA (CS17)	MyTaq Mix (Bioline)	0.4	5% DMSO	1' @ 94 °C 30x(15'' @ 94 °C, 15'' @ 70 °C, 1' @ 72 °C) 10' @ 72°
bHoxd12	Bat FL cDNA (CS17)	MyTaq Mix (Bioline)	0.4	Buffer Q	1' @ 95 °C 30x(30'' @ 94 °C, 30'' @ 55 °C, 1' @ 72 °C) 7' @ 72°
bHoxd13	Bat FL cDNA (CS17)	MyTaq Mix (Bioline)	0.4	3 mM $MgCl_2$	1' @ 95 °C 30x(30'' @ 94 °C, 30'' @ 60 °C, 1' @ 72 °C) 7' @ 72°

2.3.2. Probe template generation and probe synthesis

Amplicons of the expected sizes were gel extracted using Wizard® SV Gel and PCR Clean-up System (Promega), quantified, checked on a gel, and ligated into pGEM-T easy (Promega), sequenced and their identity verified as described previously (Section 2.2.6, Appendix A.3).

Mouse *in situ* probe templates were received from M. Logan, M. Kmita and G. Deuster, and have been previously published: mHoxd10, mHoxd11; mHoxd12 and mHoxd13 (Dollé, Izpisúa-Belmonte, Brown, *et al.* 1991); mHoxa11 (Scotti and Kmita 2012); mHoxa13 (Warot *et al.* 1997); mRdh10 (Sandell *et al.* 2007), mAldh1a2 (Mic *et al.* 2002), mCyp26b1 (MacLean *et al.* 2001) and mRarβ (Giguère *et al.* 1990). These were recovered by transforming into competent XL-Blue *E. coli* cells, culturing, performing a colony PCR and purifying as described above (Section 2.2.6).

Antisense and sense probes were generated by linearising plasmids (10 µg) using a unique restriction enzyme (RE) sites (5' of the insert sense strand sequence for antisense probes and 3' of this for sense probes) as recommended (Fermentas, Thermo Fisher Scientific) (Table 2.7). Linearized plasmids were purified using Wizard® SV Gel and PCR Clean-up System (Promega).

In vitro transcription (IVT) was performed using 1 µg of purified, linearized plasmid in 20 µl reactions using 40 U of the required RNA polymerase (Table 2.7) in 1x Transcription Buffer (Roche, Basel, CH), 1x DIG labelling mix (Roche), 40 U RNAse Out RNaseOUT Recombinant Ribonuclease Inhibitor (Invitrogen™, Life Technologies), 0.01 M DTT (Roche).

Table 2.7: Summary of *in situ* probe templates generated for WISH experiments. The plasmid name and vector name and insert size are given along with the restriction enzyme and polymerase used to linearise and transcribe the antisense probe. **Aldh1a2*.

Name	Vector	Size (bp)	RE	Polymerase
m5'-Meis2_ISHprobe	pFLC1	473	SmaI	T3
m3'-Meis2_ISHprobe	pGEM-T easy	1200	SacII	SP6
b5'-Meis2_ISHprobe	pGEM-T easy	511	NcoI	SP6
b3'-Meis2_ISHprobe	pGEM-T easy	1255	SacII	SP6
bHoxa11_ISHprobe	pGEM-T easy	631	*NotI*	SP6
bHoxa13_ISHprobe	pGEM-T easy	477	*NotI*	SP6
bRdh10_ISHprobe	pGEM-T easy	647	NcoI	SP6
bRaldh2_ISHprobe*	pGEM-T easy	698	SacII	SP6
bCyp26b1_ISHprobe	pGEM-T easy	775	SpeI	T7
bRarB_ISHprobe	pGEM-T easy	796	SpeI	T7
bHoxd10_ISHprobe	pGEM-T easy	920	NcoI	SP6
bHoxd11_ISHprobe	pGEM-T easy	+736	SphI	SP6
bHoxd12_ISHprobe	pGEM-T easy	645	SphI	SP6
bHoxd13_ISHprobe	pGEM-T easy	501	SphI	SP6

IVT reactions were incubated at 37 °C for 2 hrs, DNase treated using DNA-free™ as per the manufacturer's instructions (Ambion®, Life Technologies) and purified using a SigmaPrep™ Spin Column (Sigma-Aldrich). After each step, 1 µl of each reaction was kept aside and run together on a 1% agarose denaturing gel alongside a RiboRuler High Range RNA ladder when possible (ThemoScientific, Thermo Fisher Scientific) to ensure that the IVT, DNA digestion and purification steps were successful. Newly synthesised probes were stored in 50% Hybridisation buffer at -20 °C.

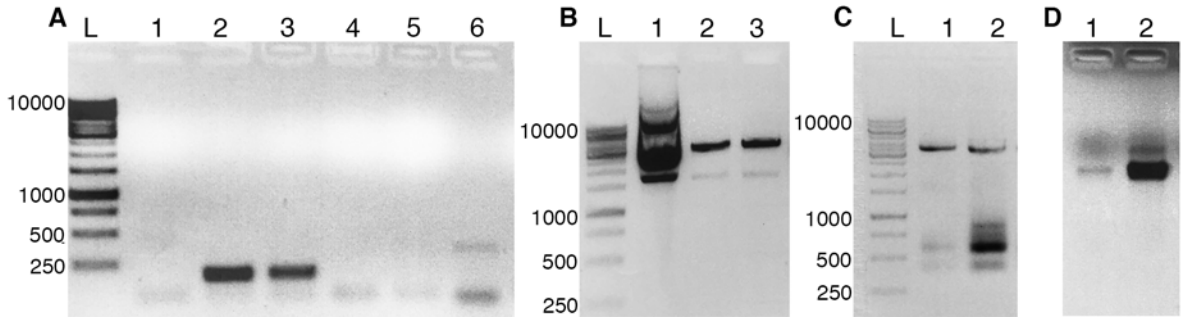

Figure 2.2: Gel images showing examples of the different gel checking steps for the 5'-*Meis2 in situ* probe generation. PCR amplification of the region of interest is first performed (**A**) the DNA agarose gel (1.2%) shows bands at >200 bp for the positive control *Tbpl1* for both mouse (lane 2) and bat (lane 3) cDNA templates. A positive band of the expected size (~500 bp) was found for 5'-*Meis2* primer set for the bat cDNA (lane 6), but was not amplified for the mouse cDNA (lane 5). Lanes 1 and 4 are no template controls, which, aside from faint primer-dimers, do not show amplification. The bat amplicon was inserted into the pGEM-T easy plasmid (**B,** lane 1 shows the uncut plasmid) and this was linearised to form a sense (lane 2) and an antisense (lane 3) probe template (~4000 bp). After IVT (**C**), in addition to the linearised plasmid (~4000), the synthesised labelled RNA probes can be found (between 250-1000). The sense product (lane 1) appeared fainter than the antisense product (lane 2). Both RNA probe bands can be seen after DNA digestion (**D**), while the sense probe appeared as a weak band (lane 1), a faint upper band was also apparent in the antisense probe (lane 2), possibly due to poor denaturation on the gel. **A**, **B** and **C** are DNA agarose gels (1.2%) while **D** is a RNA denaturing gel (1.2%). L indicates the 1 kb DNA ladder (G571A, Promega).

2.3.3. WISH experiments

The *in situ* protocol used was a modification of Riddle *et al.* (1993) (Appendix A.4). Sense probes (no signal control) were generated and tested in mouse embryos only (Appendix A.5). Bat heads were removed prior to the protocol (while submerged in MeOH), and embryos bisected along the longitudinal axis (after the first rehydration step of day 1 while submerged in ice cold PBT). The proteinase K digestion times (day 1) were optimised for staining within the limb tissue, and differed for species and stage (Rasweiler *et al.* 2009). Colour reactions were stopped when it was determined that they had reached a required colouration (or saturation) in a specific tissue while still maintaining a low background signal. For some experiments the TBST wash of the Post-AB hybridisation washes (day 3) was extended from an overnight wash to 1 or 2 days.

Table 2.8: A guideline for the timing of proteinase K digestion (day 1) in bat and mouse embryos. Note that the timing of this step is also dependent on the strength of the original PFA fixation of the sample and the strength of the proteinase K utilised. Timings based on those given by Rasweiler *et al.* (2009).

Species	Stage	Time (min.)
Mus musculus	E10.5	15
	E11.5	20
	E12.5	25
	E13.5	30-35
	E14.5	40
Miniopterus natalensis	CS14	20
	CS14L-CS15E	25
	CS15	30
	CS15L-CS16E	33
	CS16	35
	CS16L-CS17E	37
	CS17	40
	CS17L-CS18E	43
	CS18	45

Embryos were examined, and digital photographs taken under either a Leica MZ7S microscope equipped with a Leica DFC 320 camera using Leica Firecam software (Leica Microsystems AG, Wetzlar, DE) or under a Nikon Stereoscopic Zoom Microscope SMZ1500 equipped with a Nikon Digital Sight Camera Control Unit (DS-U2) and a DS-5M Camera head (Nikon Instruments Inc., Melville. NY, USA) and NIS-Elements digital 3D imaging software (Nikon Instruments Inc.). Photographs were taken from 1x to 9x magnification while the embryos were submerged in 1x PBT. Photographs were edited (limited to cropping, resizing and adjusting levels, brightness, or colour balance, across the full image) in Adobe® Photoshop® CS6 (ver. 13.0.6, Adobe Systems Inc., San Jose, CA, USA).

2.4. Random amplification of cDNA ends (RACE)

The following section describes the methods used to determine the sequence of the 5'HoxD genes. This was done to obtain the full sequence of the *Hox* transcripts expressed in the bat forelimb.

2.4.1. Experiment and primer design

The 5'HoxD transcripts of *M. natalensis* were sequenced using RACE analyses. Sets of nested primers were designed as described (Section 2.2.3). Where possible, primers were designed using the following parameters: Design - PCR (2 primers); Tm – 70 °C (opt), GC – 50% (opt), Size – 24 nt (opt), 3' GC clamp – 2 nt; Amplicon Size – 500-1200 nt, with primer focus regions constrained to regions of interspecies conservation. These were designed to amplify both the 5' and 3' ends of each transcript.

Table 2.9: Summary of RACE primer sets used to amplify probes for both the bat 5'HoxD genes. Primer names, sequences and melting temperatures are given. Melting temperatures were calculated using Primer3 (ver. 2.3.4) using the Santalucia 1998 formula and salt correction with the following concentration settings: monovalent salt (50 mM) divalent salt (2.0 mM), oligo (0.3 mM), dNTP (0.3 mM).

Primer Name	Primer Sequence (5'- 3')	nt	GC (%)	Tm (°C)
RACE_Hoxd10_GSP1	TAA TGT TGG TGG TGA AGG AGC AGG TGG	27	52	69.9
RACE_Hoxd10_NGSP1	TCG GGT CTG TCC AAC TGT CTA CTT GAG GTA T	31	48	70.8
RACE_Hoxd10_ GSP2	GGC TGA GGT CTC CGT GTC CAG TCC	24	67	71.7
RACE_Hoxd10_ NGSP2	TCA AGT CTG ATA CTC CAA CCA GCA AT	26	42	65.5
RACE_Hoxd11_GSP1	GCC GCG TAG TAG GGA GCG TAG CC	23	70	72.3
RACE_Hoxd11_NGSP1	GTT CCT GTC GCA GCC GTC GTC CT	21/23	65	72.4
RACE_Hoxd11_ GSP2	CTG AGA AGA GCG GCG GCA CAG TG	23	65	71.3
RACE_Hoxd11_ NGSP2	GCT GTC CCT ACA CCA AGT ATC AGA TC	26	50	65.8
RACE_Hoxd12_ GSP1	TAG GGC TGC GAG AAG CTG CCG AAG	24	63	72.2
RACE_Hoxd12_ NGSP1	GCG CCG CGA GGG TAT GAG ATG G	22	68	71.2
RACE_Hoxd12_ GSP2	CGA CCA AAG TAC GAC TAC GCA GGT GTG	27	56	70.3
RACE_Hoxd12_ NGSP2	ACT TGA ACA TGA CAG TGC AGG CAG CG	26	54	71.2
RACE_Hoxd13_ GSP1	CCG ACA CGT CCA TGT ACT TCT CCA CC	26	58	69.9
RACE_Hoxd13_ NGSP1	AGG AGT GCG GCG ACG ACT TGA GAG	24	63	71.8
RACE_Hoxd13_ GSP2	GGC ACG AGG CGT ACA TCT CTA TGG AGG	27	59	71.2
RACE_Hoxd13_ NGSP2	CCA GGT GTA CTG CGC CAA GGA CCA	24	63	72.2

2.4.2. RACE-ready cDNA generation, RACE PCR, cloning and sequencing

SMARTer™ first strand syntheses were performed to generate 5' RACE-Ready cDNA and standard first strand synthesis was used to generate 3' RACE-Ready cDNA using the SMARTer RACE cDNA Amplification Kit and 500 ng of bat (*M. natalensis*) forelimb (Mn06-31 FL) total RNA (Clontech Laboratories, Inc., Mountain View, CA, USA). RACE-ready cDNA was diluted with 100 µl Tricine-EDTA buffer, aliquotted and stored at -80 °C. RACE and Nested RACE PCR reactions were performed using the Advantage 2 PCR Kit as recommended (Clontech Laboratories). RACE reactions were performed as follows: 5x (30 sec at 94 °C, 3 min at 72 °C), 5x (30 sec at 94 °C, 30 sec at 70 °C, 3 min at 72 °C), 20x (30 sec at 94 °C, 30 sec at 68 °C, 3 min at 72 °C), 5 min at 72°C. RACE PCR products were visualised, and specific bands were cut out from an extraction gel. RACE PCR products were diluted 1: 49 in Tricine-EDTA buffer and 5 µl was used as the nested RACE PCR template. This was performed using the following cycling conditions: 20x (30 s at 94 °C, 30 s at 68 °C, 3 min at 72 °C). PCR products were visualised and specific bands were cut out and purified using the Wizard® SV Gel and PCR Clean-up System (Promega) as described (Section 2.2.6).

PCR products were cloned using either the pGEM®-T Easy Vector System (Promega) or the CloneJET PCR Cloning Kit (Thermo Scientific). Transformations were performed as recommended with cells containing pJET vector being plated onto LBamp plates. Colony PCRs, cell cultures and plasmid purifications were performed as described (Section 2.2.6). PCRs and sequencing reactions were performed using the pJET Fwd and pJET Rvs sequencing primers or T7 Fwd SP6 sequencing primers.

2.4.3. RACE sequence alignment and analyses

Raw sequences were processed and consensus sequences of all vector inserts were generated as described previously (Section 2.2.6). Sequences were discarded if RACE primer sets were not identified or if sequences were low quality. Forward and reverse sequences that did not overlap were joined using polyN to indicate the gap. The top BLAST hit of each consensus sequence was recorded (Appendix A.6-A.9) and sequences were aligned to the gene locus sequence of *M. lucifugus* using a Geneious Multiple Alignment (Global Alignment with free end gaps, Cost matrix: 93% similarity, Gap open penalty: 8, Gap extension penalty: 2). These alignments were manually edited and automatically annotated using a sequence similarity cut-off of 90% recorded (Appendix A.6-A.9). A consensus sequence for *M. natalensis* was generated using the sequence nucleotide majority to call ambiguities.

Multiple species alignments were generated using the CDS of *M. natalensis*, *M. schreibersii* and additional bat species with those of other mammals and vertebrates (Appendix A.10-A.13). If only genomic sequences could be obtained, these were edited to represent the expected transcript sequence by alignments to the Ensemble CDS (KNOWN protein coding) of the Human and Mouse. The CDS for all species were aligned using a Cluster W multiple alignment (BLOSUM cost matrix, Gap open cost: 10, Gap extend cost: 0.1, free end gaps allowed). These alignments were manually edited and pairwise sequence similarity (percentage of bases/residues that are identical) was calculated using Geneious (Biomatters Ltd).

Sequence alignment analyses were performed using Datamonkey (*http://www.datamonkey.org*), a public webserver application that implements specific HyPhy (Hypothesis testing using PHYlogenies) packages and analyses on CDS alignments (Pond and Frost 2005; Delport *et al.* 2010). Sequences that were misaligned and/or contained internals stop codons were removed and remaining sequences were edited to exclude stop codons. A custom nucleotide substitution bias model was automatically selected (Model string *Hoxd10*: 010120; *Hoxd11*: 010212; *Hoxd12* and *Hoxd13*: 010010), a phylogenetic tree was imposed (Ensembl, Agnarsson *et al.* 2011), and a combination of tests performed to determine if the nucleotide alignment of the CDS contained evidence of selection events. The entire alignment was

tested for evidence of positive selection using the PARtitioning approach for Robust Inference of Selection (PARRIS) method with the full alignment being considered as a single partition (Scheffler *et al.* 2006). Four independent codon-based maximum likelihood methods: SLAC (p = 0.1), FEL (p = 0.1), REL (Bayes factor cut-off = 50) and FUBAR (Posterior probability cut-off = 0.9) were used to estimate and test the dN-dS (ω) at each codon site. Mixed Effects Model of Evolution (MEME) analysis was performed (p = 0.1) to identify instances of both pervasive (evident in all branches) or episodic (evident in selected branches) positive selection at specific sites of the alignment (Murrell *et al.* 2012). An integrated selection analysis was used to identify selection events that were robust to testing.

2.5. High fidelity PCR of genomic regions

This section describes the methods followed to amplify the conserved CsC1 and CsC2 sequence region from the Prox enhancer of the 5'HoxD gene cluster from a variety of bat species.

2.5.1. Experiment and primer design

The CsC1 and CsC2 regions were identified from Gonzalez *et al.* (2007). Sets of nested primers were designed as described (Section 2.2.3) to outer, unconserved regions (set A) and inner, highly conserved regions (set B). Where possible, primers were designed by using the customisable assay with the following parameters: Design - PCR (2 primers); Tm – 65 °C (opt), GC – 50% (opt), Size – 24 nt (opt), 3' GC clamp – 2 nt; Amplicon Size – 500-1200 nt, with primer focus regions constrained to regions of interest previously identified by alignments.

Table 2.10: Summary of primer sets used to amplify the CsC1 and CsC2 regions from bat genomic DNA. Primer names, sequences and melting temperatures are given. Melting temperatures were calculated using Primer3 (ver. 2.3.4) using the Santalucia 1998 formula and salt correction with the following concentration settings: monovalent salt (50 mM), divalent salt (2.0 mM), oligo (0.3 mM), dNTP (0.3 mM).

Primer Name	Primer Sequence (5'- 3')	nt	GC (%)	Tm (°C)
CsC1_Fwd_A	AAC TGA ATA ATT GAA AAA AAG AGA TAG CTC AAG CA	35	29	65.7
CsC1_Rvs_A	ATA ACT TAT CTT ACA TTA TAA ATT CCA GTA GGG TG	35	29	62.9
CsC1_Fwd_B	ATC TGC TAA TAA GTT TTG CCC AGC TTG G	28	43	67.3
CsC1_Rvs_B	TGT GGT GTT CTG GCT TAT CTT GCC TAA G	28	46	68.1
CsC2_Fwd_A	AGT TCC AAG TTT TGC ATG AAA ATG TTA AAT ACC	33	30	65.3
CsC2_Rvs_A	ATC CAC CCA TCT GCA GAC AAT TAA GAC C	33	27	62.8
CsC2_Fwd_B	ATT TGA ATG ACA GTA TCA AAG AAA ATA TGT CTG	28	46	68.0
CsC2_Rvs_B	TGG GAC TAT TTT CTT ACT AAG CCT GTA ACA G	31	39	65.7

2.5.2. Genomic DNA extraction HiFi PCR, cloning and sequencing

DNA was extracted from adult bat muscle tissue from *M. natalensis* and wing membrane biopsies from five additional bat species: *Cloeotis percivali*; *Hipposideros commersoni*; *Pteronotus parnellii*; *Mystacina tuberculata*; *Rhinolophus clivosus* (acquired from Assoc. Prof. David Jacobs, Biological Sciences, UCT). Extractions were performed using the DNeasy® Blood & Tissue Kit (QIAGEN), Nanodropped and run on a 1.2% agarose gel to determine concentration and quality.

Purified DNA (200 ng) was used as the template to amplify the CsC1 and CsC2 region using touchdown PCR and the KAPA HiFi PCR Kit (Kapa Biosystems) under the following cycling conditions: 5 min at 95 °C, 20 s at 98 °C; 15 s at (68 °C, 66 °C, 64 °C, 62 °C) for 5 cycles each and then 15 s at 60°C for 10 cycles; 8 min at 72°C. PCR products were visualised on agarose gels and amplicons were gel extracted, purified, ligated into the pJET cloning vector (Thermo Scientific), cloned and sequenced as described in Section 2.2.6.

2.5.3. Csc1 and CsC2 sequence analysis

Raw sequences were processed and consensus sequences generated as described (Section 2.2.6). A multiple species alignment was generated using consensus sequences, and including additional bat species and selected mammals (Appendix A.14). Highly conserved regions (HCRs) within the alignment were identified as sequence regions with average identities (sliding window of 25 bp in either direction) that were > 80% (gaps < 10 bp were tolerated). Nucleotide changes that were specific to bats were manually identified and potential transcription factor binding sites, based on the TransFac database 7.0 (Matys *et al.* 2003), were annotated using the Emboss 6.5.7 (Rice *et al.* 2000) tool tfscan in Geneious R7 (Biomatters). Additional limb specific transcription factor binding sites, for TBX4, TBX5 and PITX1 (JASPER Database Ver. 5.0_ALPHA, Quirk *et al.* 2001) (Ghosh *et al.* 2001) were manually identified and annotated.

2.6. Skeletal lengths

The following section describes the methods used to double stain mouse and bat skeletal elements for bone and cartilage.

2.6.1. Skeletal element staining

The right-hand side forelimbs and hindlimbs were removed from the body of stored (70% EtOH at -20 °C) adult *M. natalensis* bats and freshly sampled mice. Soft tissue was removed from the upper limb regions, limbs were soaked in 1x PBS overnight, and skin was then removed from the autopod. Limbs were rinsed in Acetone overnight, postfixed in 70% EtOH overnight and stained with a solution of 0.3% Alcian Blue prepared in EtOH:Glacial Acetic Acid (7:3) for 2 days. Stained limbs were washed in EtOH:Glacial Acetic Acid (7:3) for 1 hour and left to soak in 100% EtOH overnight. They were soaked in distilled H_2O for 2 days, and treated with 1% trypsin prepared in 30% saturated Borate solution. They were restained with Alazarin Red prepared in 0.5% KOH. Double stained limbs were put through a series of 0.5% KOH:glycerol (2:1, 1:1, 1:2) washes that contained 1.5% H_2O_2 and finally into 100% glycerol (2 days per wash). Fully cleared, specimens were stored in 100% glycerol at 4 °C (Hanken and Wasersug 1981).

2.6.2. Photography and measurements

Skeletal elements were photographed at high resolution (4288 x 2848) using a Nikon D90 macro digital camera (Nikon Instruments Inc.) while submerged in glycerol and flattened using a glass plate (Figure 2.3). Measurements were taken using the NIS-Elements digital 3D-imaging software (Nikon Instruments Inc.) and calibrated to an imaged ruler. Lengths (mm) of skeletal elements were measured along the central axis of the elements (Figure 2.3) at the highest resolution using the following morphological landmarks. Stylopod: in the FL this was taken from the humoral head to the distal trochlea, in the HL it was taken from the greater trochanter to the intercondylar fossa. Zeugopod: in the FL this was taken from the oleocranon process and lateral styloid process of the mouse ulnar, the head and trochlea of the bat radius, and in the HL it was taken from the intercondylar eminence and lateral malleolus. The sum of multiple linear measurements was taken of the zeugopod element to account for its curvature (Figure 2.3D). Measurements were taken of intact digit elements placed laterally using the base of the metacarpal/metatarsal, the metacarpophalangeal joints, the proximal interphalangeal joints, the distal interphalangeal joints, and the distal tip of P3, as landmarks. Measurements performed three times and averaged. In the bat FL the median standard deviation (SD) of each sample was below 0.05 mm with the maximum SD of each group as follows; Bat FL: 0.79 mm; Bat HL: 0.14 mm; Mouse FL: 0.22; Mouse HL: 0.32. The averages of these three technical repeats were used and the variances presented in the analyses represent that of the biological repeats.

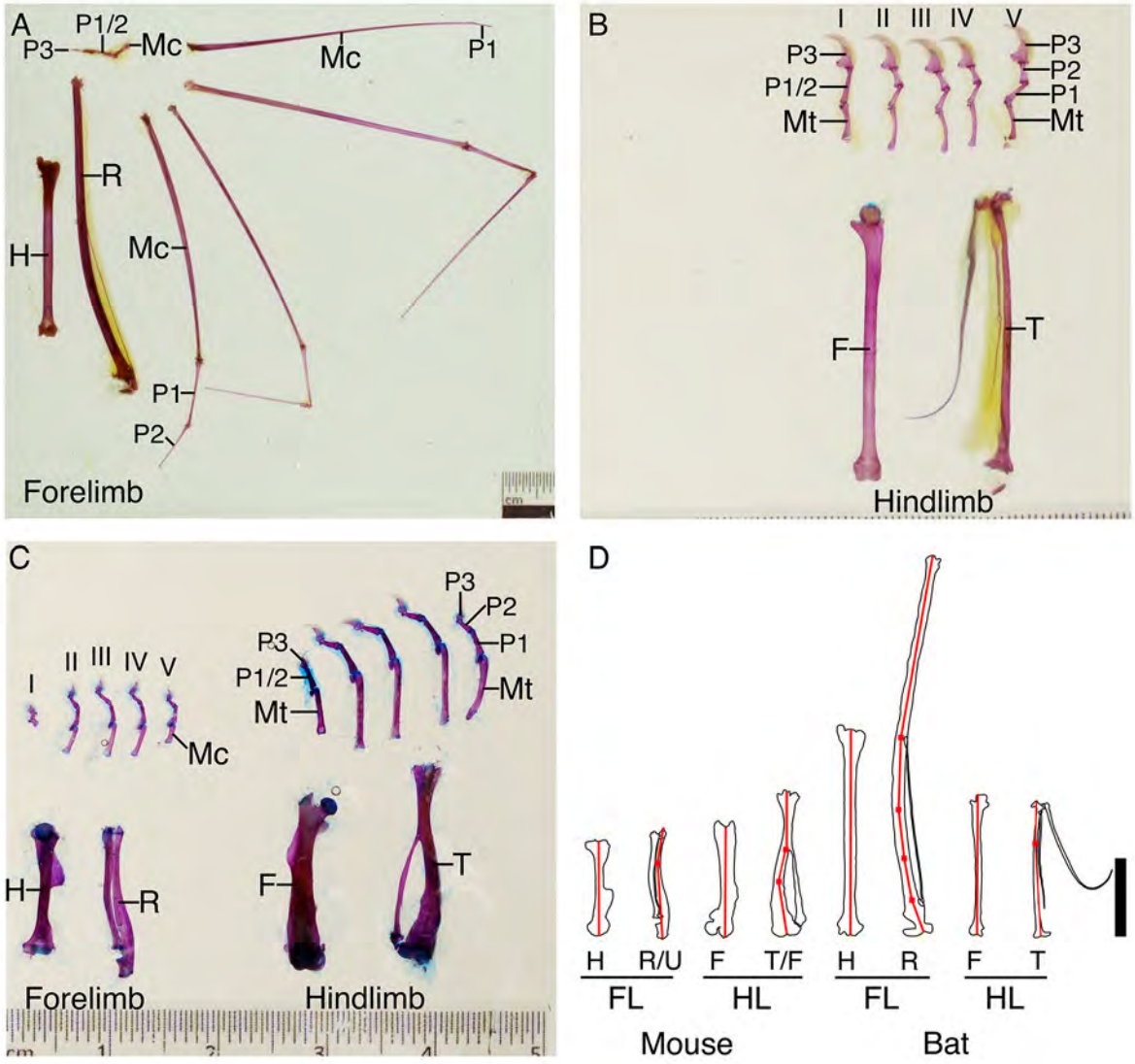

Figure 2.3: An example of the Alazarin red and Alcian blue stained skeletal elements measured in adult bats and mice. The lengths of the humerus (H), radius (R), the metacarpals (Mc) and phalanges (P) were taken. In digit I the central element is termed P1/2 while in digits II-V the phalanges are numbered in a proximal to distal fashion. In the bat FL (**A**) multiple linear measurements were taken along the central axis of the metacarpals and phalanges due to their length and curvature The skeletal elements of the bat HL (**B**) were short, however two linear measurements were taken along the central axis of the metatarsals due to their curvature. The mouse FL and hindlimb (**C**) had fairly straight digits and only one linear measurement was used along their length. A schematic (**D**) approximating how measurements in the stylopod and zeugopod were taken in each element. Curvatures of the zeugopod elements were taken into account by maintaining the line of measurement along the central axis of the bone as indicated in each sample. Scale bar represents 1 cm.

2.6.3. Statistical analyses

Mouse element lengths were normalised for the relatively larger body size of the mouse using the average head-body length: mouse mean = 83.1 mm, SD = 1.81 mm, N = 8 (Ackert-Bicknell *et al.* 2011) bat: mean = 62.7 mm, SD = 3.3 mm, N = 20 (Miller-Butterworth *et al.* 2005).

All data were tested for normality (slight deviations were tolerated), and homogeneity of variances. Outliers were noted and excluded where appropriate. Data were square-root transformed when they did not meet the above assumptions. Significance testing of a single variable among the limb types was performed through a one-way ANOVA, using pairwise comparisons, with a Bonferroni adjustment, to identify comparisons that were significantly different. When variances were significantly different the Welch ANOVA was interpreted and the Games-Howell post hoc test was used to identify pairwise differences. Significance testing of multiple variables was performed using a two-way ANOVA. An Analysis of Covariance (ANCOVA) was performed to compare the relative sizes of elements; groups that did not have a linear relationship were excluded from the analysis. Tests were performed using IBM® SPSS Statistics ver. 22 (IBM Corporation).

3. *Meis2* expression marks the retained interdigital webbing of the bat autopod and is independent of Retinoic Acid signalling

3.1. Background

Meis genes are key transcription factors that regulate a variety of developmental processes through the promotion of cell proliferation and survival and the repression or activation of cell differentiation events. These genes appear to be involved in patterning and it has been suggested that the modulation of their expression and subsequent activity may be a mechanism underlying the formation of species-specific organ morphologies among vertebrates (Heine *et al.* 2008).

The MEIS family has three vertebrate paralogs (*Meis1, Meis2*, and *Meis3*) that share conserved sequences and specificities (Nakamura *et al.* 1996; Cecconi *et al.* 1997; Biemar *et al.* 2001; Waskiewicz *et al.* 2001; Zerucha and Prince 2001; Sánchez-Guardado, Irimia, *et al.* 2011). *Meis* genes are complex loci, with each gene having multiple alternative splice variants that contribute to a diverse range of protein products, which mediate a complex repertoire of activities (Bürglin 1997; Huang *et al.* 2005; Sánchez-Guardado, Irimia, *et al.* 2011). Consequently, like their *Drosophila* ortholog *Homothorax* (*Hth*), they should not be thought of as a single functional entity (Corsetti and Azpiazu 2013). The mouse *Meis2* locus spans over 200 000 bp, is transcribed and processed into 19 splice variants, with six of these known to encode functional protein isoforms using 14 exonic regions (GRCm38, Ensembl release 83). Alternative splicing of the coding region of *Meis* transcripts occurs in the more variable 3' end (coding exon 10' to exon 12b), and, as a result, several isoforms that differ in their C-terminal region can be produced (Irimia *et al.* 2011). Two well characterised *Meis* splicing events, show that processed transcripts differ by the presence (A) or absence (B) of exon 12a and by the presence (.1) or absence of (.2) of Exon 11' resulting in four possible isoform combinations that differ in their C terminal domains (Irimia *et al.* 2011; Sánchez-Guardado, Irimia, *et al.* 2011). Splicing variants that exclude the DNA binding domains or homeodomain have also been characterised, with these variants being proposed to function in a dominant negative fashion (Yang *et al.* 2000).

MEIS proteins have the ability to interact directly with the Pre-B Cell family of transcription factors (PBX proteins) and the posterior HOX paralogs (HOX11-13) through their N-terminal and C terminal domain respectively, allowing them to form dimeric and trimeric complexes both with and without making contact with DNA (Chang *et al.* 1997; Knoepfler *et al.* 1997; Berthelsen *et al.* 1998; Shanmugam *et al.* 1999; Williams *et al.* 2005). The association of MEIS with PBX relieves its auto-

inhibitory activity (Hyman-Walsh *et al.* 2010) increases its stabilisation (Longobardi and Blasi 2003), drives nuclear localisation (Abu-Shaar *et al.* 1999; Berthelsen *et al.* 1999), and allows complexes to bind to DNA targets with higher affinity and sequence specificity than can be achieved by monomeric proteins (Jacobs *et al.* 1999; Ryoo *et al.* 1999). PBX/HOX complexes that include MEIS have a binding preference for promoter-remote (e.g. enhancer) sequences and tend to regulate developmental genes and HOX target sequences (Penkov *et al.* 2013). Modulation of enhancer binding in selective tissue regions during development has the potential to mediate the formation of anatomical structures. For example, in the developing branchial arches of the mouse, cooperative binding of MEIS and HOXA2 in the second arch (IIBA) confers its identity through increased binding affinity to multiple enhancer regions and the promotion of an IIBA specific transcription program (Amin *et al.* 2015; Merabet and Lohmann 2015). While PBX proteins appear to have HOX proteins from paralogs groups 1-9 as their preferred binding partners, MEIS proteins form complexes with those from 10-13 when bound to DNA (Chang *et al.* 1995, 1997; Shen *et al.* 1997). In the reproductive tract MEIS2 isoforms co-occur with HOXA13 in the nuclei of mesenchymal cells, with these proteins shown to directly interact in yeast two-hybrid assays (Williams *et al.* 2005). However, *Meis2* and *Hoxa13* are not co-expressed during early limb development, and it has been argued that HOXA13 proteins function as monomers, or through interacting with alternative cofactors, in the autopod (Williams *et al.* 2005).

The role that *Meis* genes play during development is complicated by the multiplicity of splice-variants, protein isoforms and partners that have the potential to participate in binding events. However, it is this depth of complexity that allows MEIS proteins to regulate a variety of processes in different organs and tissues at several stages of development. This is evident by the broad range of expressions patterns seen for these genes throughout development. *Meis1* and *Meis2* are expressed in both distinct and overlapping regions in the vertebrate nervous system and are involved in regionalisation of the developing brain through patterning and cell specification events (Toresson *et al.* 2000; Waskiewicz *et al.* 2001; Ferran *et al.* 2007; Sánchez-Guardado, Irimia, *et al.* 2011). During early embryonic development, in several organisms, *Meis1* is expressed in the somites and mesoderm. This expression becomes posteriorly restricted in the mesoderm and neural tube during later development, and is also found in the anterior regions of the midbrain, hindbrain, optic area, in addition to limb buds and branchial arches (Maeda *et al.* 2001; Waskiewicz *et al.* 2001; Choe *et al.* 2002; Coy and Borycki 2010; Pillay *et al.* 2010). In the mouse, its expression appears to be coordinated with that of *Hox* genes, *Hoxa7* and *Hoxa9* in particular (Nakamura *et al.* 1996; Afonja *et al.* 2000). *Meis1* is known to play a vital role in haematopoiesis (the formation of blood cells) and angiogenesis (the formation of blood vessels from pre-existing vasculature), with loss of function mutant embryos not surviving beyond

E14.5 (Hisa *et al.* 2004; Azcoitia *et al.* 2005). This gene is required for proliferation and subsequent self-renewal of haematopoietic stem cells and is known to regulate the genes that control cell fate specification in these tissues (Hisa *et al.* 2004; Pillay *et al.* 2010; Amali *et al.* 2013). *Meis2* has been shown to be specifically involved in mesencephalic development and olfactory bulb neurogenesis (Shim *et al.* 2007; Agoston and Schulte 2009; Agoston *et al.* 2012, 2014). Both *Meis1* and *Meis2* are involved in the development and organisation of sensory organs such as the eye, where they promote rapid proliferation of the retinal progenitor cells prior to their specification (Hisa *et al.* 2004; Heine *et al.* 2008; Conte *et al.* 2010; Sánchez-Guardado, Irimia, *et al.* 2011), the olfactory system where they maintain the slowly dividing, multi-potent olfactory epithelium precursor cells (Hisa *et al.* 2004; Tucker *et al.* 2010) and the inner ear where they have been suggested to play a role in cell proliferation and survival (Oulad-Abdelghani *et al.* 1997; Sánchez-Guardado, Ferran, *et al.* 2011). *Meis2* is required for cardiac morphogenesis in the developing zebrafish (Paige *et al.* 2012). Several congenital defects are associated with the partial loss (haploinsufficiency) of *Meis2* expression including orofacial clefting, cardiac septal defects and varying degrees of intellectual disability, with an intragenic mutation resulting in foot defects that include a widened gap between digits I and II and syndactyly of digits II-III (Erdogan *et al.* 2007; Crowley *et al.* 2010; Johansson *et al.* 2014; Louw *et al.* 2015). *Meis3* expression has been well characterised during zebrafish gastrulation and patterns the anterior endoderm of the developing pancreas through the regulation of *Shh* (Sagerström *et al.* 2001; Vlachakis *et al.* 2001; DiIorio *et al.* 2007). *Meis3* is also involved in neural plate development and is found in the neural tube, somites and pectoral fin primordia and the pectoral fin (Sagerström *et al.* 2001; Waskiewicz *et al.* 2001). It plays a role in hindbrain development in both *Xenopus* and the zebrafish (Salzberg *et al.* 1999; Waskiewicz *et al.* 2001; Choe *et al.* 2002), and functions to promote neuronal differentiation through the regulation of gene expression via its interaction with HOXB1B and PBX4 (Vlachakis *et al.* 2000, 2001).

Meis1 and *Meis2* are co-expressed during chick development, exhibiting slightly modulated levels and patterns suggesting redundancy, with slight spatio-temporal differences in their regulation suggested to refining their activity (Sánchez-Guardado, Irimia, *et al.* 2011). Their expressions are well characterised in vertebrate limb development with conservation of the pattern and progression of expression (Cecconi *et al.* 1997; Oulad-Abdelghani *et al.* 1997; Sánchez-Guardado, Irimia, *et al.* 2011). Initially, widespread expression is found in the embryonic trunk mesenchyme (E8.0-8.5; HH16) with localised expressions found throughout the budding forelimb (E9.5) that appears graded with strong proximal expression. On limb bud outgrowth (E10.5, HH18), expression is clearly restricted to the proximal limb, and remains so during later stages of development (Figure 3.1A; Capdevila *et al.* 1999). The proximal

localised expressions of these two genes are similar in the limb and they are used interchangeably to mark the presumptive stylopod (Figure 3.1B; Capdevila *et al.* 1999; Mercader *et al.* 1999; Tabin and Wolpert 2007; Bénazet *et al.* 2009).

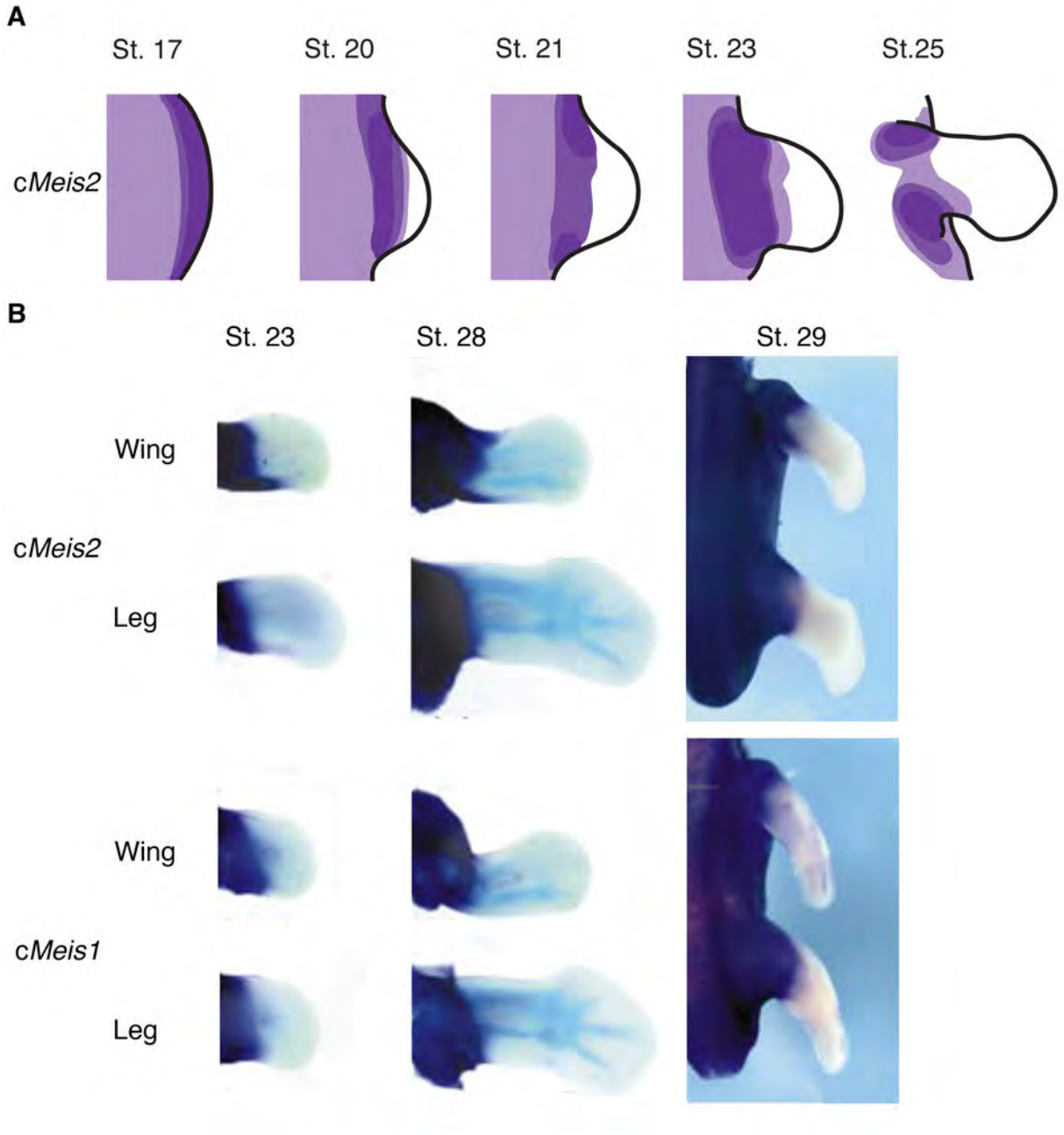

Figure 3.1: *Meis1* and *Meis2* expression is restricted to the proximal limb bud in the developing chick. A schematic of *Meis2 in situ* expression (**A**) in the developing chick limb illustrating the progressive restriction of expression to the proximal region of the limb bud from stages early limb budding to stages of autopod formation (adapted from Capdevila *et al.* 1999). Whole mount *in situ* of both *Meis1* and *Meis2* (**B**) show that they are expressed in the trunk, lateral plate mesoderm and proximal limb bud of St. 29 chick embryos. Examination of expression in conjunction with Alcian blue staining (to show cartilage) indicates that it is absent from the distal limb regions that form the zeugopod and autopod (images taken from Mercader *et al.* 1999).

Meis1 and *Meis2* expressions are upregulated by retinoic acid signalling (Oulad-Abdelghani *et al.* 1997). Retinoic acid signalling involves the binding of all-*trans*-retinoic acid (hereafter referred to as RA), a

small, diffusible molecule, to nuclear retinoic acid receptors (RAR and RXR dimers). These receptors are bound to regions of DNA known as retinoic acid response elements (RAREs), which control the expressions of different sets of genes in their bound and unbound state (Niederreither and Dollé 2008; Rhinn and Dollé 2012; Cunningham and Duester 2015). Mouse *Meis2* contains three RAREs two of which have been shown to be functional (occupied by RAR:RXR dimers), and which confer a low efficiency, delayed response to RA signalling in F9 cell lines (Lalevée *et al.* 2011).

RA is an active metabolite of retinol (vitamin A), a nutrient that is maternally supplied during development and is found throughout the embryo. RA is a potent teratogen; its availability is therefore tightly regulated through both its synthesis and degradation. In the embryonic flank (somites and LPM) and interdigital tissues, endogenous retinol is oxidised into retinaldehyde by retinaldehyde dehydrogenase 10 (RDH10), which is then irreversibly oxidised into RA by retinaldehyde dehydrogenase 2 (ALDH1A2, also known as RALDH2). RA is converted into inactive forms by cytochrome P450 RA-degrading enzymes namely: CYP26A1, CYP26B1 and CYP26C1, of which *Cyp26b1* encodes the predominant form expressed in limbs. In this manner RA levels can be finely tuned in different tissue regions of the developing embryo (Cunningham and Duester 2015).

RA signalling has been suggested to underlie PD patterning in the limb bud, and is described by a 'two-signal gradient' model of limb outgrowth (Tabin and Wolpert 2007; Bénazet and Zeller 2009). RA is thought to specify proximal limb fate. Its loss causes the limb bud mesenchyme to fail to form proximal structures (Cooper *et al.* 2011), while increased levels result in limb truncations, attributed to the proximalisation of the distal limb (Mercader *et al.* 2000, 2005; Qin *et al.* 2002). A link between RA signalling and *Meis2* expression in the limb is supported by pharmacological studies in the chick, with proximal expression of this gene is attributed to its activation by a threshold level of RA that diffuses from the embryonic flank (Mercader *et al.* 2000; Roselló-Díez *et al.* 2011). However, studies in mice do not support this model. Pharmacological and genetic inactivation of RA signalling in the mouse limb do not affect *Meis1* and *Meis2* expressions (Cunningham *et al.* 2013; Cunningham and Duester 2015). These data suggest that RA signalling is unnecessary for proximal patterning; instead, its exclusion from the distal limb is required to prevent massive teratogenic effects that result in distal truncation. Based on this evidence, limb bud outgrowth can be described by a 'one-signal model' mediated by distal FGF signalling. This activates distal *Cyp26b1* expression, which excludes teratogenic RA activity from this region (Cunningham and Duester 2015).

Though the role of RA signalling in early limb bud patterning is contentious, the later phase of activity in autopods is known to be important for interdigital apoptosis and inter-digit formation (Dupé *et al.*

1999; Zhu *et al.* 2010; Hernández-Martínez and Covarrubias 2011; Díaz-Hernández *et al.* 2014). This has been well described in the mouse where, from early stages of autopod formation, the expression of genes encoding RA synthesising enzymes (*Rdh10* and *Aldh1a2*) are found in the interdigital regions. This is contrasted by predominant expression of the gene encoding the RA metabolising enzyme, *Cyp261b*, in the digit regions. Though RA is difficult to assay directly, these expression patterns indicate that RA is restricted to the undifferentiated interdigital mesenchyme, and excluded from digit rays undergoing chondrogenesis (Díaz-Hernández *et al.* 2014). This localisation can be confirmed through monitoring the expression of the Retinoic Acid Receptor (*Rarβ*), which is upregulated in response to RA (Mendelsohn *et al.* 1991).

In the developing limb of *M. natalensis*, *Meis2* is overexpressed in the forelimb autopod during stages when digits elongate and interdigital webbing expands (Mason 2009). Characterisation in the mouse has shown that it is expressed in the interdigital tissue during autopod formation and a recent study in the closely related bat species, *M. schreibersii,* has confirmed upregulation of this gene in the interdigital webbing (Oulad-Abdelghani *et al.* 1997; Dai *et al.* 2014). A role for *Meis2* in autopod formation has not been explored and it is unknown how the high levels of expression in the bat wing can be integrated with the current understanding of its development. Overexpression of *Meis2* in the developing chick limb actually results in distal limb defects, including limb axis proximalisation, reductions in element lengths and, interestingly, the persistence of interdigital webbing (Capdevila *et al.* 1999; Mercader *et al.* 1999). Similar phenotypes can be found in transgenic mouse lines that ectopically express *Meis1* in the distal limb bud (Mercader *et al.* 2009). Interestingly, both mouse and chick overexpression experiments show alterations in the pattern of expression of the zeugopodal marker, *Hoxa11* and the autopodal marker *Hoxa13*, possibly due to alterations in early limb patterning events (Mercader *et al.* 1999, 2009). In the autopod *Hoxa13* has been shown to be involved in RA signalling (through direct activation of *Aldh1a2* expression) in the interdigital regions to facilitate interdigital apoptosis (Knosp *et al.* 2004; Shou *et al.* 2013). Characterisation of *Meis2* expression within the context of RA signalling and HoxA gene expression in the developing bat will provide a greater understanding of how the pathways involved in interdigital webbing regression or retention are modulated. In this chapter I characterise the expressions of *Meis2*, genes that control RA availability (*Rdh10*, *Aldh1a2*, *Cyp26a1*) and signalling (*Rarβ*) and *Hoxa13* in the developing autopods of both the bat (*M. natalensis*) and the mouse to determine whether they have alternative expression in the bat wing and to understand their potential to interact in this tissue.

3.2. *Meis2* is expressed in the interdigital region of the autopod and is overexpressed in the bat forelimb as compared to the hindlimb

A microarray analysis on bat autopods, over stages of digit formation and hindlimb interdigital regression (CS16-CS17) indicated that *Meis2* expression was highly elevated in the bat forelimb autopods (FL) as opposed to the hindlimb autopods (HL) (Mason 2009). These data were intriguing, as *Meis2* is known to be a proximal marker of the outgrowing limb bud, thought to be excluded from the distal limb region (Mercader *et al.* 2000; Roselló-Díez *et al.* 2014), although is there evidence for interdigital expression of this gene in the mouse (Appendix B.1). In this section I examine the expression of *Meis2* using relative qPCR analysis performed on the E13.5 mouse FL and the FLs and HLs of an extended range of bat developmental stages (CS15-CS18, Figure 3.2A), and through visualisation of the expression patterns using whole mount *in-situ* hybridisation (WISH) experiments.

3.2.1. qPCR analysis confirms the elevated expression of Meis2 transcripts in the developing bat forelimb

Meis2 transcript abundance was quantified over two regions that corresponded to OPERON microarray probes binding sites (5'*Meis2*: M400017713 and 3'*Meis2*: M400000987). Relative qPCR levels of different amplicons are not directly comparable, but a strong positive correlation existed between the two datasets (Pearson Correlation: $r = 0.95$, N = 24, $p < 0.001$). In both there was a relatively low abundance in CS15 FL that peaked in CS17 FL, and dropped slightly in CS18 FL. The relative abundance remained low in the HL throughout development (Figure 3.2B). The transcript abundance was higher in the FL as compared to the HL from CS16 onwards, with the largest fold difference (over five-fold) seen at CS17 (Table 3.1). These qPCR data confirmed that *Meis2* is upregulated in the bat FL with fold differences of both amplicons corresponding to the more 5' microarray probe (M400017713) data (Table 3.1).

Overall pairwise differences between the FL and HL samples indicated that while FL transcript abundance was larger in both experiments, it was only significantly so for the 3'*Meis2* amplicon. There were significant differences among developmental stages, attributable to the significantly lower abundance in CS15 as compared to late developmental stages (CS17 and CS18). For the 5'*Meis2* amplicon, the developmental stage examined had an effect on the limb type abundance, attributable to significantly increased expression in the FL across developmental stages CS16, CS17 and CS18, with no significant differences found amongst HL samples (Appendix B.2).

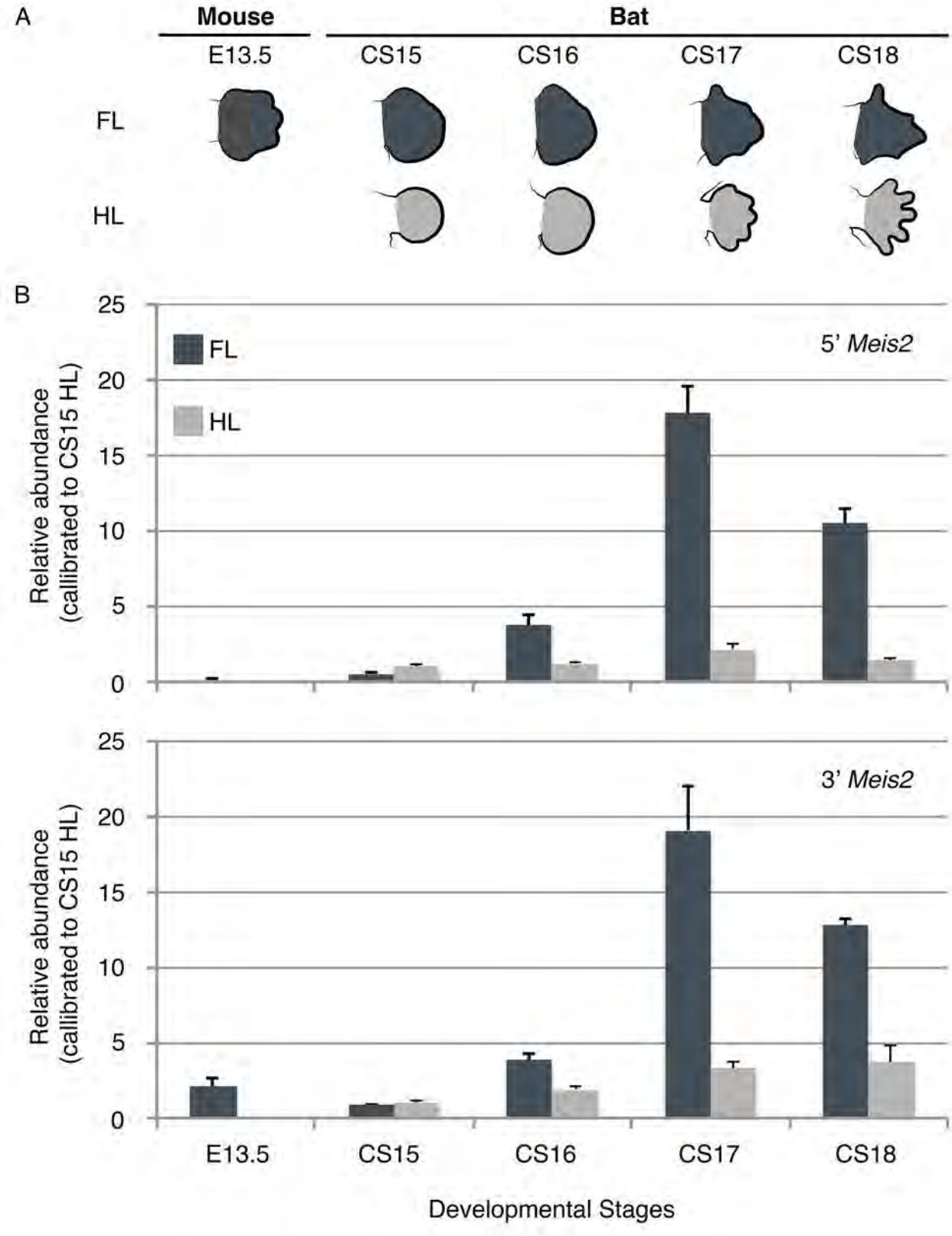

Figure 3.2: The abundance of *Meis2* transcripts was quantified by relative qPCR in the E13.5 mouse forelimb autopods and in bat forelimb (FL) and hindlimb (HL) autopods (**A**). This was measured from early stages of autopod patterning (CS15) to late stages of autopod differentiation and growth (CS18). The relative qPCR signal for primers specific to the 5' region and the 3' region of the *Meis2* gene (**B**) are similar, with FL samples being over 2 fold higher than the hindlimb from CS16 onwards and peaking in CS17 FLs. All samples represent the average of 3 biological samples with error bars indicating the standard error (SE).

Table 3.1: Fold change data for *Meis2* transcripts over both the 5'-*Meis2* and the 3'-*Meis2* region. Median fold changes of biological repeats are given with minimum and maximum fold changes bracketed. Four biological repeats were tested in the microarray experiments (Mason 2009) and three in the qPCR experiments. NA indicates that the experiment was not performed.

Transcript Region	Experiment	Bat (CS17) vs. Mouse (E13.5)	FL vs. HL			
		FL	CS15	CS16	CS17	CS18
5'*Meis2*	qPCR	287.1 (56.5-829.9)	0.5 (0.7-0.5)	3.0 (2.3-3.9)	8.4 (7.7-8.5)	7.9 (5.8-8.4)
(M400017713)	Microarray	9,9 (8.4-11.7)	NA	2 (1.5-3.3)	6,1 (5,4-12.6)	NA
3'*Meis2*	qPCR	8.6 (8.3-12.3)	0.9 (0.6-1.2)	1.9 (1.6-2.6)	5.9 (5.5-6.0)	4.9 (2.2-5.1)
M400000987	Microarray	1,5 (1.2-2.3)	NA	1 (0.6-1.2)	1,4 (1.2-2.6)	NA

Comparisons between the E13.5 mouse FL and the CS17 bat limbs revealed that these were significantly different for the 5'*Meis2* amplicon, due to its relatively higher expression in the bat FL (over 250 fold) (Table 3.1; Appendix B.2-B.3). Though not significant, the relationship among transcript abundance was similar in the 3'*Meis2* amplicon, with the bat FL having 8 times the transcript abundance as that of the mouse (Table 3.1). These latter fold changes were within the range of values obtained for the more 5' microarray probe (M400017713) (Table 3.1).

These results validate microarray experiments that show higher transcript abundance in the CS17 bat FL as compared to equivalently staged (E13.5) mouse FLs. They support evidence that transcripts containing both the 5' and 3' OPERON binding region are expressed in the bat limb (Curry 2014) and illustrate how, in the bat, *Meis2* transcripts are overexpressed in the FL from developmental stage CS16 onwards, peaking in CS17.

3.2.2. Meis2 is expressed in the proximal region of the developing bat and mouse limb buds

The spatial and temporal expression pattern of *Meis2* was examined using WISH, with probes encompassing either the 5'*Meis2* or 3'*Meis2* OPERON probe binding region. This was performed over a series of developmental stages in both bat (CS15 to CS18) and mouse (E11.5 to E14.5) embryos, with both probes showing the expected pattern of *Meis2* expression in E11.5 mouse embryos. Staining was apparent along the trunk of the embryo, and in the proximal limb bud, with no evidence of expression in the distal limb (Figure 3.3A-B). The early expression of *Meis2* in the CS15 bat was comparable (Figure 3.3C-D), confirming a recent reports on the expression of *Meis2* (Dai *et al.* 2014), and indicating that the bat-specific probes generated gave a clear positive signal for this gene.

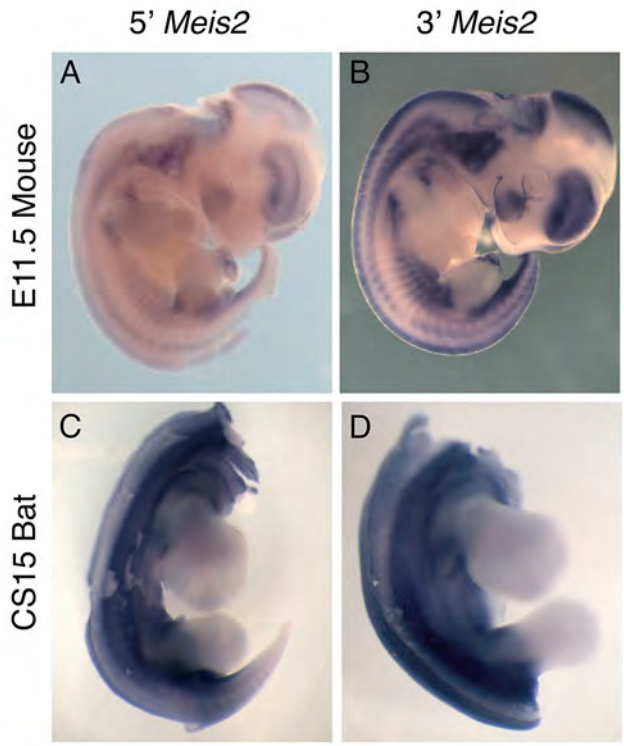

Figure 3.3: Expression of *Meis2* transcripts during early limb development in the mouse and the bat. The signal from the 5'*Meis2* probes recapitulated that of the 3'*Meis2* probes. The expression confirms the restriction of *Meis2* expression to the proximal region of the developing limb bud during outgrowth in both the mouse (**A**, **B**) and the bat (**C**, **D**).

3.2.3. Meis2 expression is found in the interdigital region of the developing bat and mouse autopod

The earliest indication of *Meis2* expression in the distal limb was found in the E12.5 mouse HL where a distinct 'comma-shaped' region was stained immediately proximal of the presumptive digit IV and V and was still evident at E13 (5'*Meis2*: 13/15 embryos) (Figure 3.4F and Appendix B.4). In the mouse FL, expression was first observed in the interdigital (ID) region at E13 when examining the distal limb from a frontal orientation (Figure 3.4A'-B') and became visible in the dorsal orientation at E13.5 FL as a faint stripe restricted to the proximal interdigital region (Figure 3.4I, Figure 3.5C). Interdigital expression was maintained in the E14.5 autopods, as a strong proximally restricted interdigital domain (Figure 3.4N). Similar expression patterns were found for both WISH probes (Appendix B.5-B6).

In the bat, no 'comma-shaped' domain was found (Figure 3.4H), instead the first evidence of autopodal *Meis2* expression was found at CS16 FL in the tissue between digits IV and V (ID4; Figure 3.4G). A less intense region of staining distinguished the ID3 tissue, while no staining was evident in ID1 or ID2 at this stage (Figure 3.4G). Strong expression of *Meis2* was found in the presumptive plagiopatagium and uropatagium from this stage onwards (red arrows in Figure 3.4G-P). At later stages, *Meis2*

expression was evident in all ID tissues of the FL, with a proximal bias in signal being noted in CS17 interdigits (Figure 3.4K-L). In the HL no (CS17) to very faint (CS18) interdigital expression was seen in the autopods ID tissue (Figure 3.4O-P). Though the *in situ* signal for the shorter 5'*Meis2* probe was faint in comparison to that of the longer 3'*Meis2* probe in the proximal limb bud region of early stages, both probes appeared to have similar expression patterns (Appendix B.5-B6).

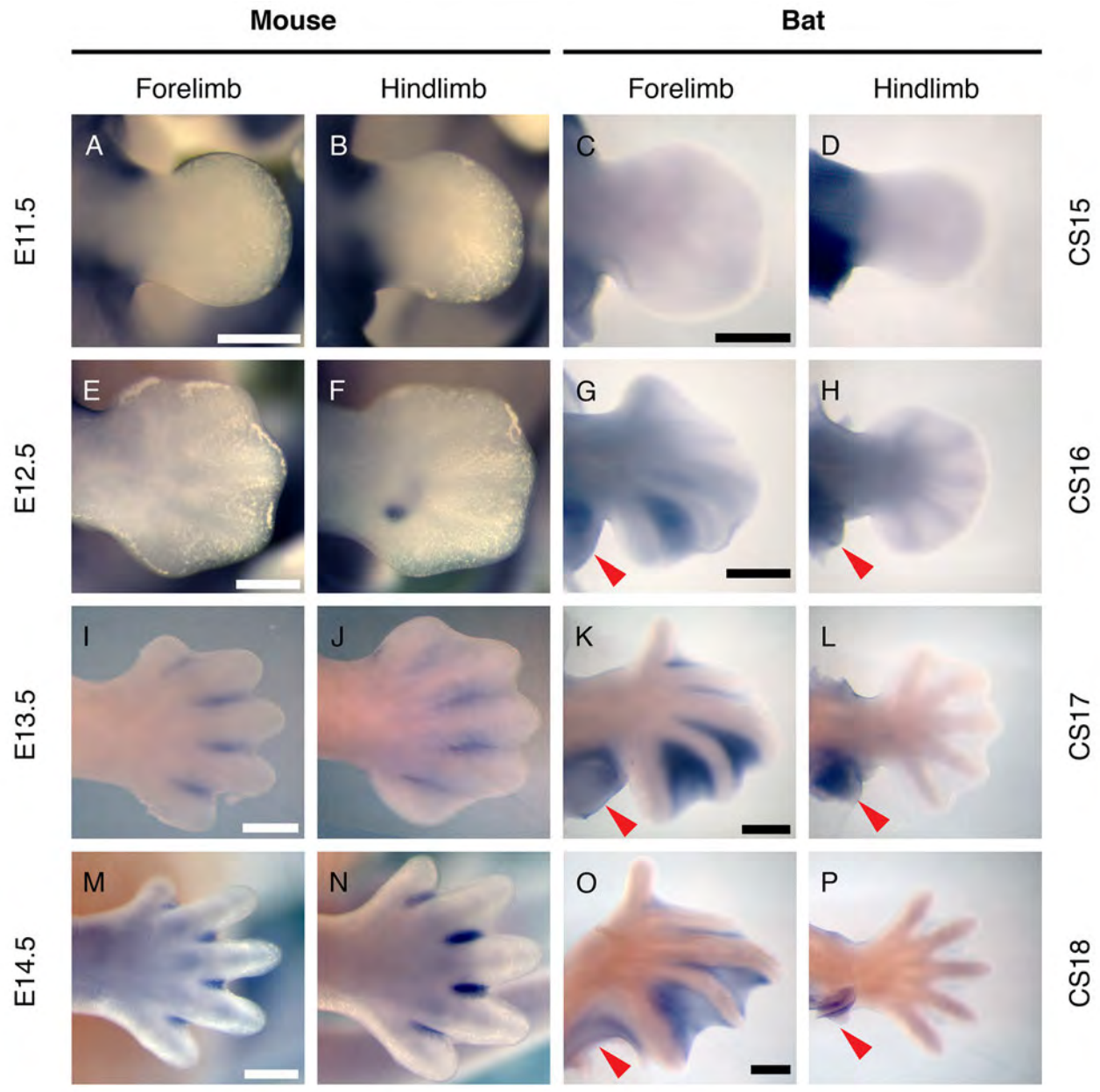

Figure 3.4: *Meis2* has novel distal expression in developing mouse and bat limbs during autopod development. In the mouse *Meis2* expression was found in the proximal region of the early limb bud (**A**, **B**). A similar pattern was seen in equivalently staged bat limbs (**C**, **D**). During autopod formation, *Meis2* was not seen in the mouse FL (**E**) but a small domain of expression was evident in the HL (**F**). In the bat, expression was found in the FL, restricted to the region between digits IV and V (**G**), but was absent in the HL (**H**). At later stages of digit formation *Meis2* was found in the interdigital regions of the mouse (**I**, **J**), and the bat FL (**K**), but was not in the bat HL (**L**). In the E14.5 mouse, expression occured in the proximal interdigital mesenchyme (**M**, **N**), but was maintained in the webbing of the bat FL (**O**), with a faint stripe of expression seen in the bat HL interdigital region (**P**). It is notable that *Meis2* expression can be found in the bat FL and HL patagia throughout their development (red arrows, **G**, **H**, **K**, **L**, **O**, **P**). Scale bars represent 500 μm.

A detailed developmental series of the *Meis2* expression in the mouse FL and HL gave an indication of the progression of *Meis2* expression in these tissues (Figure 3.5). *Meis2* transcript signal was initially seen in the slightly depressed junctions of the digit regions (Figure 3.5A', B', H'-I'). As the digits became distinct and extended, *Meis2* expression was evident in the indented interdigital regions that undergo thinning (Figure 3.5A'-L'). It appeared to be excluded from the more distal interdigital regions in both the FL the HL (Figure 3.5D, J-L). A schematic of limbs over these stages illustrates the relative domains of *Meis2* expression amongst the stages shown suggesting that interdigital tissue that is lost, did not appear to express *Meis2* (Figure 3.5M-N).

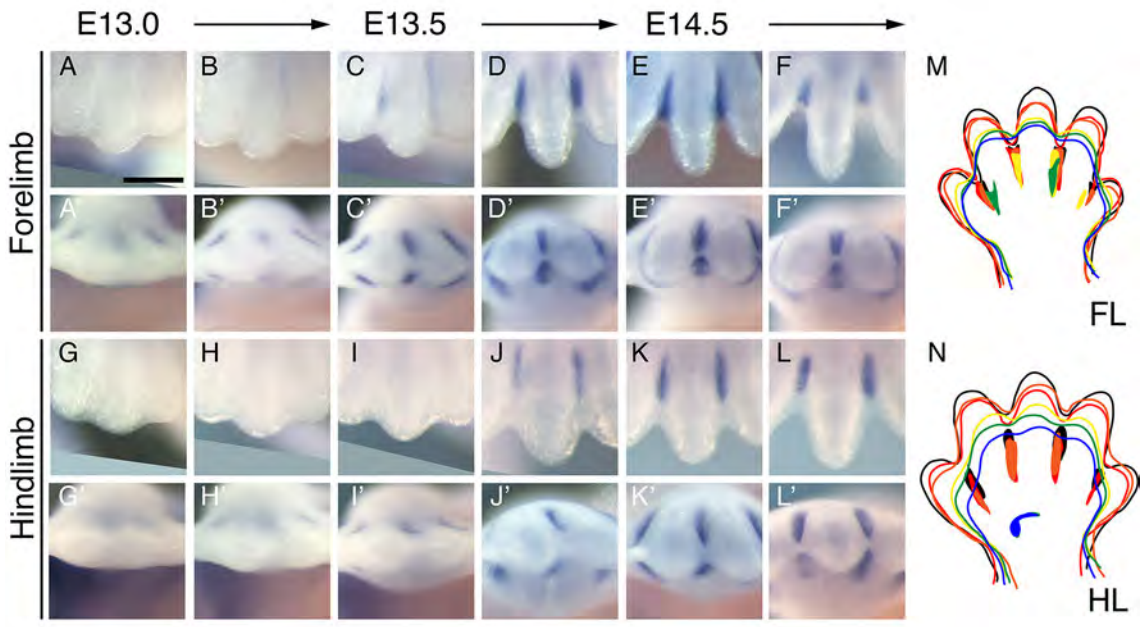

Figure 3.5: Expression of *Meis2* in the developing mouse autopod is limited to interdigital tissue that is retained. A time series of the expression in both the forelimb (**A**-**F**) and the hindlimb (**G**-**L**) indicates that *Meis2* is expressed in both the dorsal and ventral surface of the autopod, in the region of the interdigits, over the period of interdigital thinning. A schematic of the staining over these stages gives an indication of the growth of the autopod and the regression of the interdigital tissue during this time. Scale bar represents 1 mm.

3.2.4. Meis2 is the most highly expressed Meis gene in the limb

Normalized read counts for *Meis1*, *Meis2* and *Meis3* for both the CS14 and pooled CS15-17 bat limbs (Dai *et al.* 2014; Wang *et al.* 2014) were extracted to examine their transcript abundance and confirm upregulation in the interdigital regions of the closely related bat, *M. schreibersii*. These indicated that *Meis2* was the predominant *Meis* gene in bat limbs, both in early development (CS14), when *Meis* gene expression is found in the proximal limb bud (Figure 3.6A), and during later development (pooled CS15-17) when expression was found in autopod interdigital tissues (Figure 3.6B).

Care should be taken when interpreting these normalize read counts due to biases introduced by differences in contig sizes. This did not account for the difference found amongst these genes. *Meis1* values were given by two separately annotated contigs (combined length of 2697 nt), *Meis2* values were given by two overlapping sequences that encoded isoform 2 (2752 nt) and isoform 4 (2773 nt) and *Meis3* was represented by one contig (1652 nt). The smaller contig size of *Meis3* introduced a bias, with slightly lowered normalized read counts than should be expected. However, when adjusted to account for this, *Meis3* values maintained the lowest values for most tissue comparisons.

During early development (CS14), *Meis2* transcripts were asymmetrically distributed in both limb buds, with the majority found in the anterior and posterior samples (Figure 3.6A). Overall, normalised read counts were highest in the HL tissues, with between 4 fold (medial) and 12 fold (anterior) higher expression in this limb type. During later autopod development (represented by pooled CS15-17 autopod tissues), *Meis2* transcripts were most abundant in the FL webbing as compared to the FL digits or HL tissues (Figure 3.6B). In the FL, transcripts were asymmetrically distributed, with lower signal found in the anterior tissues (FL (I)) as compared to the posterior tissues (FL (II-V)). This bias may reflect the posteriorly restricted expression found at CS16. It is notable that WISH analyses did not detect expression of *Meis2* in the anterior FL autopod nor in the HL at these stages; while RNA-seq analysis showed low normalized read counts values for all of these tissues.

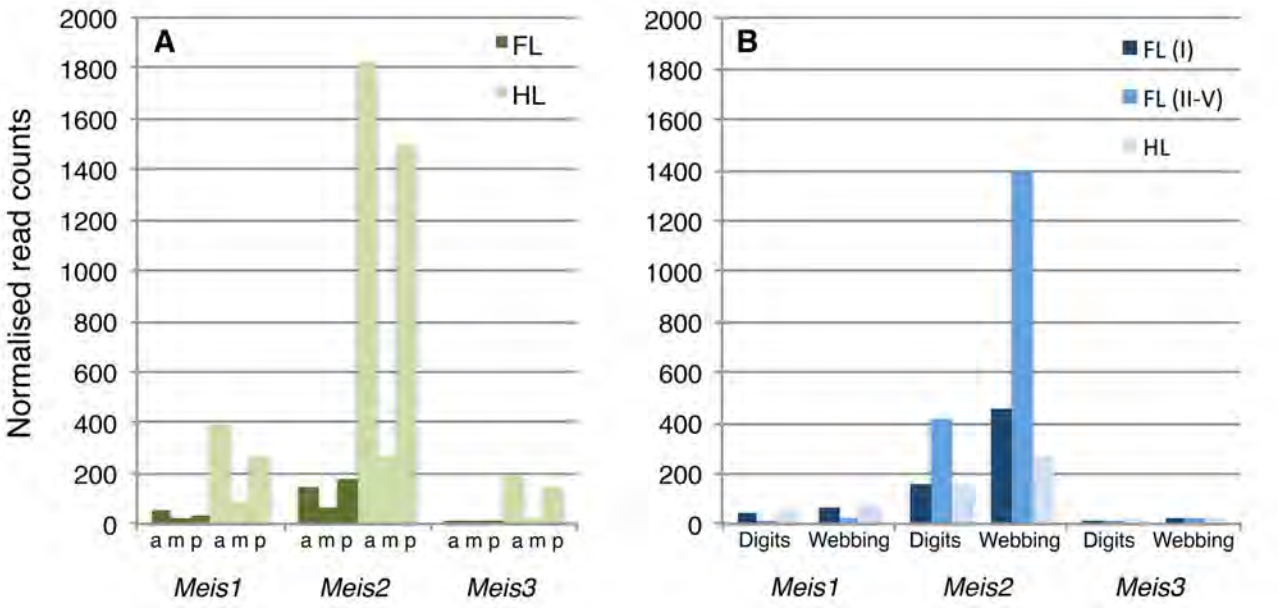

Figure 3.6: RNA-seq normalised read counts for *Meis* genes in the bat, *M. schreibersii*. Of these three genes, *Meis2* has the highest expression in the limb. At early stages of limb bud outgrowth, CS14 (**A**); *Meis2* expression was asymmetrically expressed in the limb bud with expression being strongest in the anterior and posterior (p) portion of the limb bud in comparison to the medial region (m). Overall, expression was higher in the HL (light green) than the FL (dark green). At later stages of development (pooled CS15-17) (**B**), digit and webbing tissue of both the FL (dark blue - digit I/ID1; blue - digits II-V/ID2-4) and the HL (light blue) were examined, showing that FL webbing had the highest expression, particularly in the posterior autopod. Data extracted from the GEO dataset (GSE50699) of Wang et al. (2014).

3.3. Retinoic acid signalling does not underlie the differential expression of *Meis2* in bat autopods but shows modulation of its synthesis at the digit-interdigit junction

Based on evidence that *Meis2* is a RA activated gene (Mercader *et al.* 1999, 2000; Roselló-Díez *et al.* 2014), the strong expression of *Meis2* in the bat forelimb interdigital regions may indicate that there is a high level of RA signalling in this tissue. The loss of/lower level of *Meis2* expression in the bat hindlimb interdigital regions suggests that RA signalling may be low or absent in this region. However, this does not agree with transgenic mouse experiments. Instead, a loss of RA synthesis in the interdigital regions of the mouse hindlimb in *Rdh10* mouse mutant (*Rdh10^{trex}*) results in a reduction in apoptosis and subsequent retention of interdigital webbing (Sandell *et al.* 2007; Cunningham *et al.* 2011). In this section, to understand the relationship between RA signalling and *Meis2* expression in the interdigits, I examine the expression of *Meis2* and *Rarβ* (a RA inducible gene that is used to mark regions of active RA signalling (Mendelsohn *et al.* 1991)), in the CS17 bat autopods and the HL of wildtype (WT) and *Rdh10^{trex}* mutant mice. I then examine whether the retention of interdigital webbing can be linked to alterations in genes involved in RA signalling in bat forelimb autopods.

3.3.1. Meis2 expression does not correspond to RA signalling in the bat or the mouse

A direct comparison (left and right limb samples) of *Rarβ* and *Meis2* WISH signal in the bat (Figure 3.7A-B) indicated that these two genes had overlapping expression domains in the interdigital regions of the FL, the plagiopatagium and the uropatagium (green in Figure 3.7D-H). However, this was not the case in the bat HL autopod, where strong interdigital *Rarβ* expression was present with the absence of *Meis2* expression (Figure 3.7E-F). Together these suggest that the retention of the interdigital membrane in the bat FL autopod is not a consequence of a loss of RA signalling, and that RA signalling in the hindlimb interdigital tissue does not activate *Meis2* expression.

Expression of *Rarβ* in the wild type (WT) E14.5 mouse bordered the developing free digits and was concentrated at the intra-digit junction where the presumptive joints form (Figure 3.7I). In the *Rdh10^{trex}* mouse HL, expression was absent confirming that RA signalling was absent (Cunningham *et al.* 2011, Figure 3.7M). *Meis2* was strongly expressed alongside the digits and in the proximal interdigital regions of the WT mouse HL (Figure 3.7J), overlapping with the expression of *Rarβ* (green in Figure 3.7L). However, strong *Meis2* expression was retained throughout these retained interdigital tissues (Figure 3.7N) in the *Rdh10^{trex}* mutant, indicating that *Meis2* does not require RA signalling to be expressed in this domain.

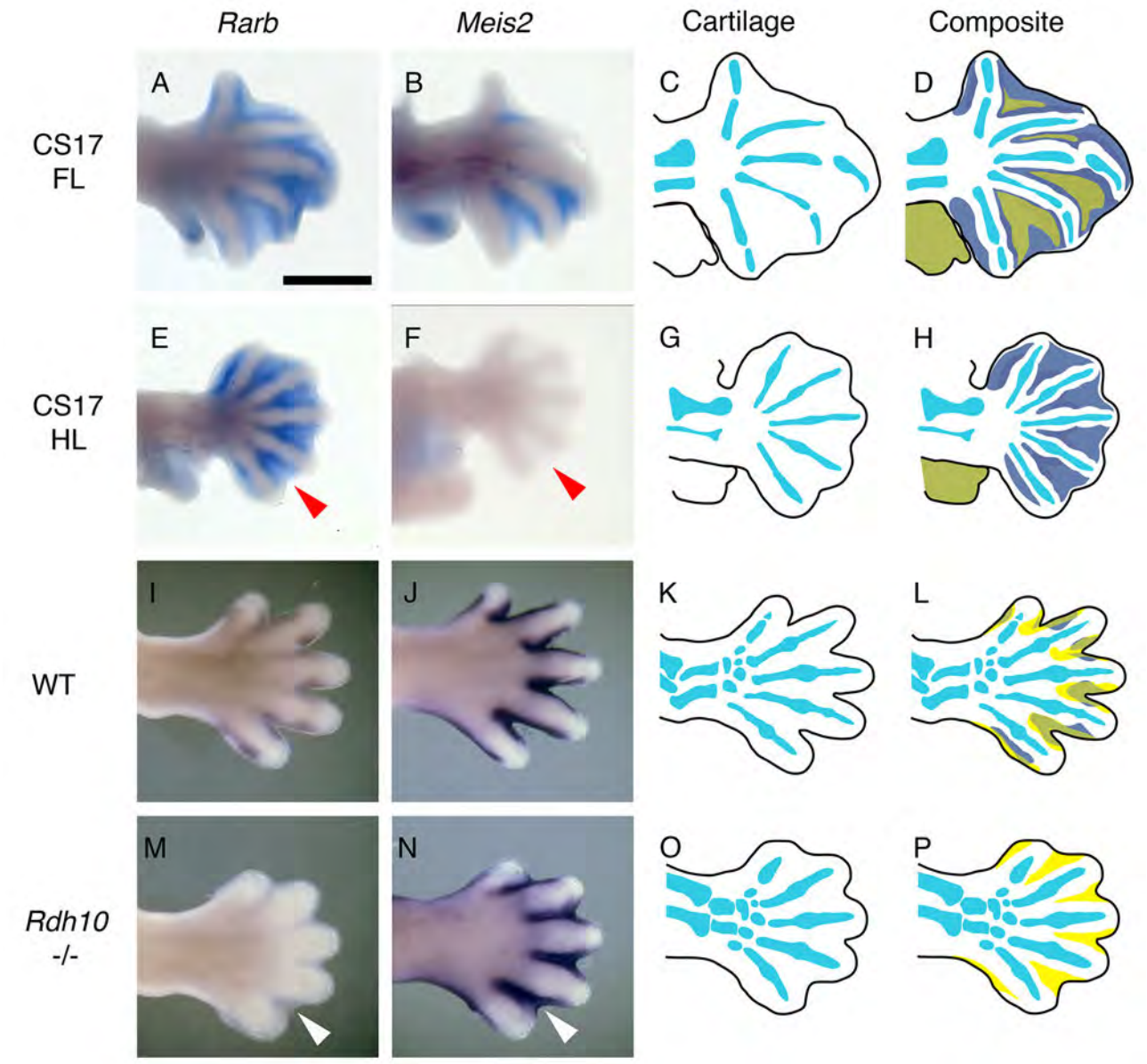

Figure 3.7: *Meis2* expression domains do not correspond to RA signalling. The expression pattern of the RA receptor (*Rarβ*) in the interdigital tissue of bat forelimbs (FL) at CS17 appears similar to that of *Meis2* (**A**-**B**) with mostly overlapping expressions (green in **D**) that correspond to the interdigital regions. Expression of *Rarβ* was found in the bat HL (**E**) in the absence of *Meis2* expression (**D**), indicating that RA signalling does not activate *Meis2* in this tissue. Overlapping expressions of *Rarβ* are seen in the WT mouse HL (**I**, **J**), green in **L**). *Rarβ* expression is absent in the retained interdigital tissue of the *Rdh10*^{trex} mutant mouse HL (white arrow, **M**), however, *Meis2* expression is present (**N**), indicating that its expression is not dependent on RA signalling (yellow in **P**). Scale bat represents 1 mm.

Cross-sections of the bat FL and HL (CS17) illustrated the restriction of *Meis2* and *Rarβ* expression to the interdigital tissues of the bat forelimb, with predominant expression of *Meis2* in the membrane between digits IV and V, localised to a dorsal and a ventral band of tissue (Figure 3.8A). There is no evidence of *Meis2* expression in the HL (Figure 3.8B). RA signalling was strongly expressed in the mesenchymal tissue of the interdigital region in both the FL and the HL and surrounded the digit rays, also appearing strongest in the dorsal and ventral bands (Figure 3.8C-D).

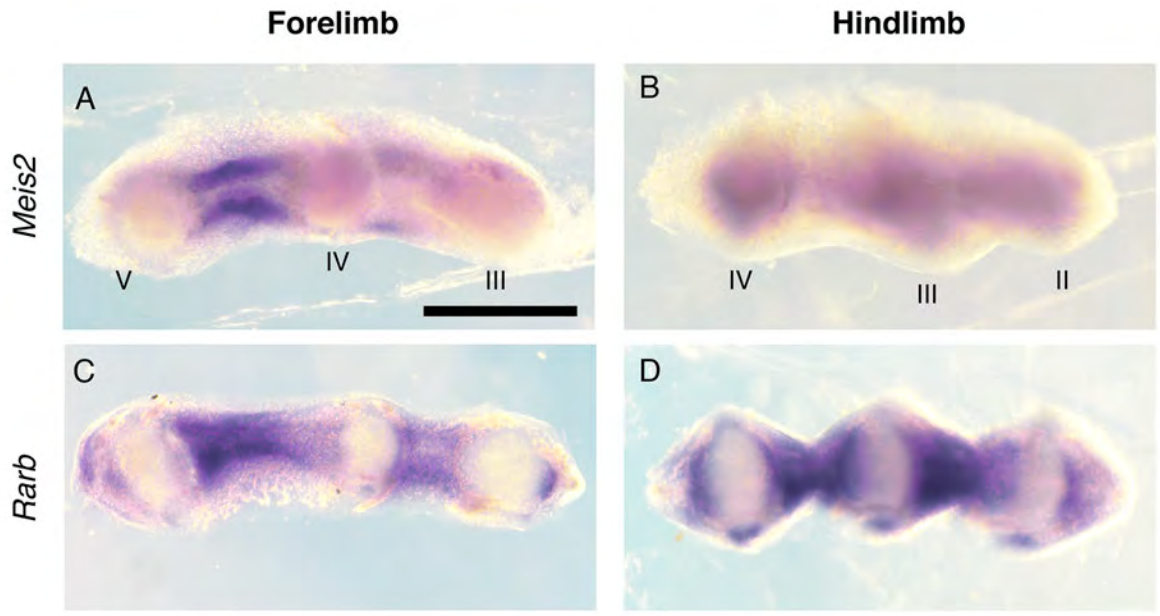

Figure 3.8: Macro-sections of bat FL and HL showing *Meis2* and *Rarβ* expression in interdigits. Scale bar represents 500 μm.

Though there is some overlap between the expressions of *Meis2* and *Rarβ* (used as a marker of RA signalling), the lack of *Meis2* expression in the presence of *Rarβ* in the bat HL, and presence of *Meis2* expression in the absence of RA signalling in the *Rdh10*^{trex} HL, indicates that *Meis2* expression is independent of RA signalling in mammalian interdigital tissue.

3.3.2. Expression of RA signalling pathways in the mouse and bat autopod

Interdigital RA signalling (as indicated by *Rarβ* expression) appears similar in bat forelimb and hindlimb autopods at CS17. I examined the expression pattern of genes that encode proteins involved in RA synthesis and degradation in the bat to confirm that these correspond to that of *Rarβ* expression.

In the mouse the RA synthesising genes (*Rdh10*, Figure 3.9A-D and *Aldha2*, Figure 3.9E-H) were restricted to the interdigital tissue. The RA degrading enzyme (*Cyp26b1*) had strong expression in the digits (strongest in digit I) and weaker expression in interdigital tissue (Figure 3.9I-L). *Rarβ* expression was restricted to the more proximal regions of the interdigital tissue and included a region posterior to digit V (Figure 3.9M-P), and corresponded strongly with *Rdh10* expression.

In the bat strong *Rdh10* expression (Figure 3.9Q-T) surrounded the digits with weaker expression evident in all interdigital regions. *Aldh1a2* followed this pattern in the CS17 HL (Figure 3.9V) but was notable for weak interdigital expression in the FL, with a clear posterior bias (Figure 3.9U). This was most evident in slightly older embryos, which had only faint expression alongside the distal phalanges of FL digits III, IV and V and HL digits II, III, IV and V (Figure 3.9W-X). *Cyp26b1* had weak

expression in the distal digit rays and interdigital tissue of the CS17 FL (Figure 3.9Y). However, its expression was strong in the hindlimb, focused in the tendons and digit tips, with notable expression in the interdigital webbing (Figure 3.9Z). *Cyp26b1* expression became less evident at CS17L and was restricted to the digit tips of the FL and the growing tip of the plagiopatagium, while it remained strongly expressed in the digit tips and tendons of the HL (Figure 3.9AA-AB). The loss of *Aldh1a2* and *Cyp26b1* in the CS17L bat digits was similar to that found in later stages (E14.5) of mouse FL, which also have weaker expressions of *Rdh10* and *Rarβ*. In agreement with previous experiments, *Rarβ* was expressed throughout the interdigital tissue of both the bat FL and HL (Figure 3.9AC-AF), with stronger proximal expression. This gene was also expressed throughout the plagio- and uropatagium (red arrow in Figure 3.9AC-AF), in the absence of the expression of *Rdh10* and *Aldh1a2,* but was excluded from *Cyp26b1* expressing domains.

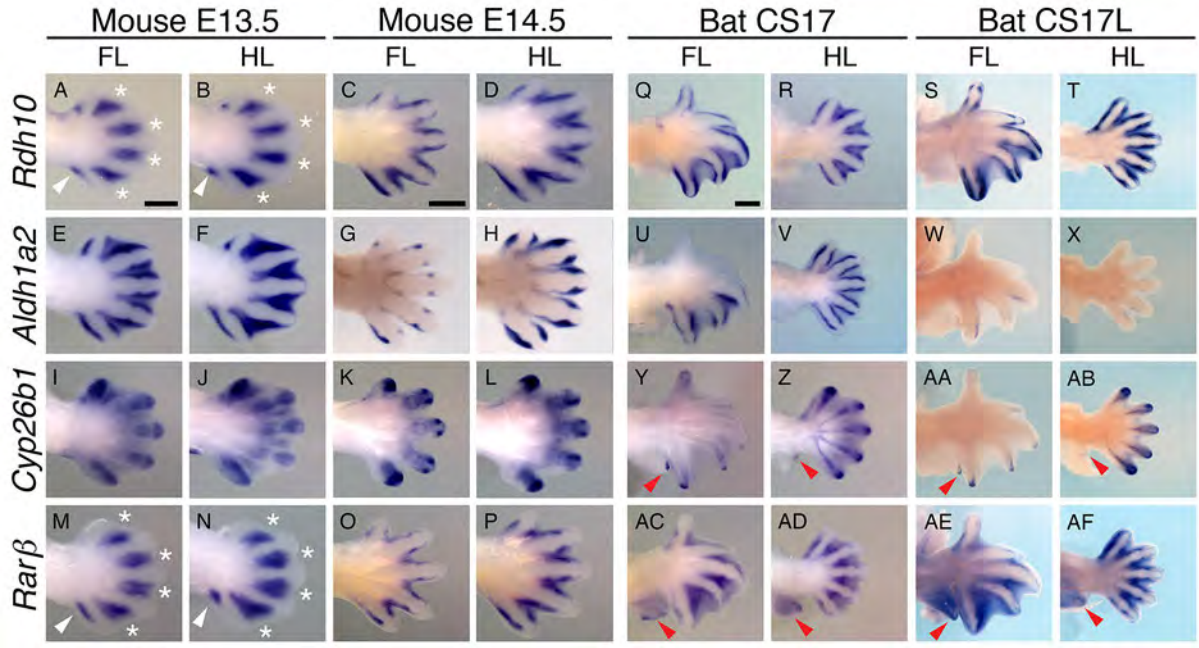

Figure 3.9: Expression of genes involved in Retinoic Acid (RA) synthesis and degradation. Comparison among the bat (CS17) and mouse (E13.5-E14.5) autopods indicates that this pathway is active in both FL and HL interdigital tissues. In the mouse FL the RA synthesising genes (*Rdh10*, **A-D** and *Aldh1a2*, **E-H**) are restricted to the interdigital tissue, while the RA degrading enzyme gene (*Cyp26b1*) has strong expression in the digits (strongest in digit I) and weaker expression in the interdigital tissue (**I-L**). RA signalling in these limbs is conventionally visualised through the expression of *Rarβ* (**M-P**), which, similar to *Rdh10*, is restricted to the more proximal regions of the interdigital tissue and a region posterior to digit V. *Aldh1a2* expression appears to differ in the bat FL (**U**, **W**), while maintaining a conventional pattern of expression in the HL (**V**, **X**). *Cyp26b1* also shows weak expression in the distal digit rays and interdigital tissue of the FL (**Y**, **AA**), Expression is also seen in the tip of the plagio- and uropatagium (**Y-AB**). The expression of *Cyp26b1* in the bat HL appears more prominent, and is strongest in the tendon and digit tips, with notable expression in the interdigital webbing (**Z**, **AB**). *Rarβ* is expressed throughout the interdigital tissue of both the bat FL and HL (**AC-AF**). It is interesting to note that this gene is also expressed throughout the plagiopatagium, in the absence of expression of *Rdh10* and *Aldh1a2*. Scale bars represent 500 μm.

3.3.3. *Retinoic acid synthesis, degradation and signalling genes to not appear to be differentially expressed between the bat FL and HL*

Normalised read counts for *Rdh10*, *Aldh1a2*, *Cyp26b1* and *Rarβ* for pooled CS15-17 bat limbs were examined to determine their expressions in *M. schreibersii* (Wang *et al.* 2014). These data show that, as expected, expressions of *Rdh10, Aldh1a2* were highest in the interdigital webbing than in the corresponding digit regions (Figure 3.10A). Expressions were also higher in the bat FL as compared to HL webbing. The anterior FL (digit I and its associated webbing) had the lowest transcript abundance among the tissue regions indicating an asymmetry of RA synthesis in the autopod. In contrast to this, *Cyp26b1* expression was highest in anterior tissues, and was slightly higher in the digits as compared to the webbing (Figure 3.10A). These transcript levels give support to an autopod environment with relatively higher RA availability in the posterior, as compared to the anterior FL tissues. This is confirmed by the expression of *Rarβ* in the webbing, which has slightly higher normalised read counts in the posterior FL region, however this relationship is not apparent in the digits. The highest normalised read counts for *Rarβ* were found in the webbing of the HL, with the HL digits also having a greater transcript abundance than those of the FL (Figure 3.10A). When averaged normalised read counts were generated to give a view of overall abundance across the full FL and HL autopod, the strong differences found for *Rdh10*, were lost, however the expressions of the other genes supported an environment where RA signalling is strongest in the HL (Figure 3.10B).

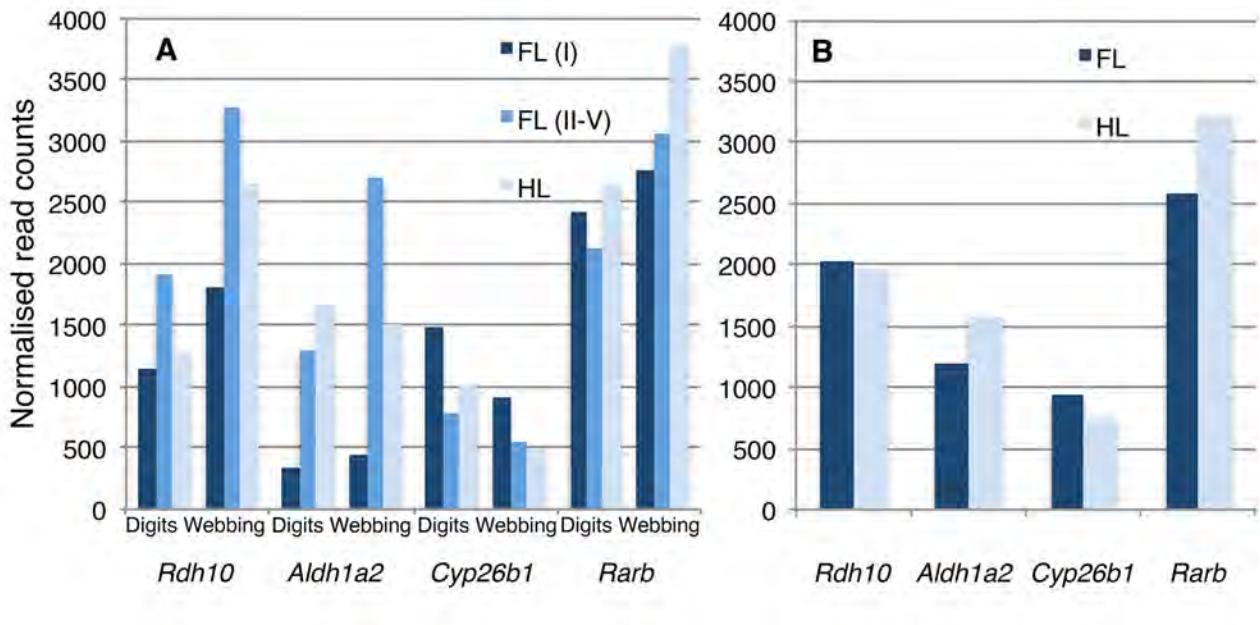

Figure 3.10: RNA-seq normalised read counts for genes involved in RA signalling in the bat, *M. schreibersii*. Normalised read counts for these genes from different tissue regions of the FL (dark blue - digit I/ID1; blue - digits II-V/ID2-4) and the HL (light blue) indicated that the posterior FL webbing favored higher, while the anterior FL tissues favored lower RA availability (**A**). The averaged normalized read count of the FL and HL showed fewer differences (**B**). Data extracted from the GEO dataset (GSE50699) of Wang et al. (2014).

3.4. *Hoxa13* is underexpressed in the developing bat forelimbs as compared to the hindlimbs

Meis2 is reported to indirectly control the spatial distribution of *Hoxa13* activity through RA signalling, in addition to other possible mechanisms (Roselló-Díez *et al.* 2014). However, the relationship between these genes is not clear-cut as they also have the potential to act as co-factors (Williams *et al.* 2005). In the outgrowing limb bud, *Meis1* and *Meis2* mark the proximal region (presumptive stylopod) (Mercader *et al.* 1999; Cooper *et al.* 2011), while *Hoxa11* and *Hoxa13* mark the zeugopod and autopod respectively. These exclusive domains of expression may play a role in patterning these distinct regions (Tabin and Wolpert 2007; Zeller *et al.* 2009). *Hoxa11* and *Hoxa13* are a part of the 5'HoxA cluster of genes, which are co-regulated in the developing limb with neighbouring genes, *Hoxd9* and *Hoxd10* (Woltering *et al.* 2014). In the autopod *Hoxa13* expression is required for digit formation (Yoshida *et al.* 2004; Hinoi *et al.* 2006; Villavicencio-Lorini *et al.* 2010) and in the interdigital tissue, mediates cell death through the regulation of BMP signalling and RA signalling (Knosp *et al.* 2004, Shou *et al.* 2013). In this section, I compare the expression pattern of *Hoxa13* over several stages of bat and mouse and correspond these with *Meis2* expression to determine whether there is potential for them to have antagonistic or collaborative interactions in this region. I also explore *Hoxa11* expression to determine whether the distal boundary of its expression domain is altered and confirm expressions of these genes alongside the neighbouring 5'HoxA genes (*Hoxa9*, *Hoxa10*, *Hoxa11* and *Hoxa13*) (Wang *et al.* 2014).

3.4.1. Hoxa13 has a decreased expression in the bat forelimb autopod as compared to that of the hindlimb.

During early stages of FL and HL autopod formation, the expression of *Hoxa13* is similar in the E11.5 mouse (Figure 3.11A-B), showing no potential for overlap with *Meis2* expression, which is only expressed proximally during these stages. Over stages of digit development *Hoxa13* expression appears equivalent in both the FL and the HL of the mouse, with expression becoming weaker in the regions of condensing mesenchyme (Figure 3.11H), and concentrated in the regions surrounding the distal digit ray (Figure 3.11G). At later stages (E13.5) *Hoxa13* expression is maintained in both the FL and the HL autopod, with regionalisation within the autopod becoming more apparent, with strong expression found surrounding the distal phalanges (Figure 3.11K-L). Expression appears weaker by E14.5, but is still maintained in the regions surrounding all digits in both the FL and the HL, with faint expression found in the remaining interdigital tissue of the HL (Figure 3.11O-P). In the mouse, *Meis2* and *Hoxa13* expressions overlap in the interdigital mesenchyme and regions surrounding the digit rays.

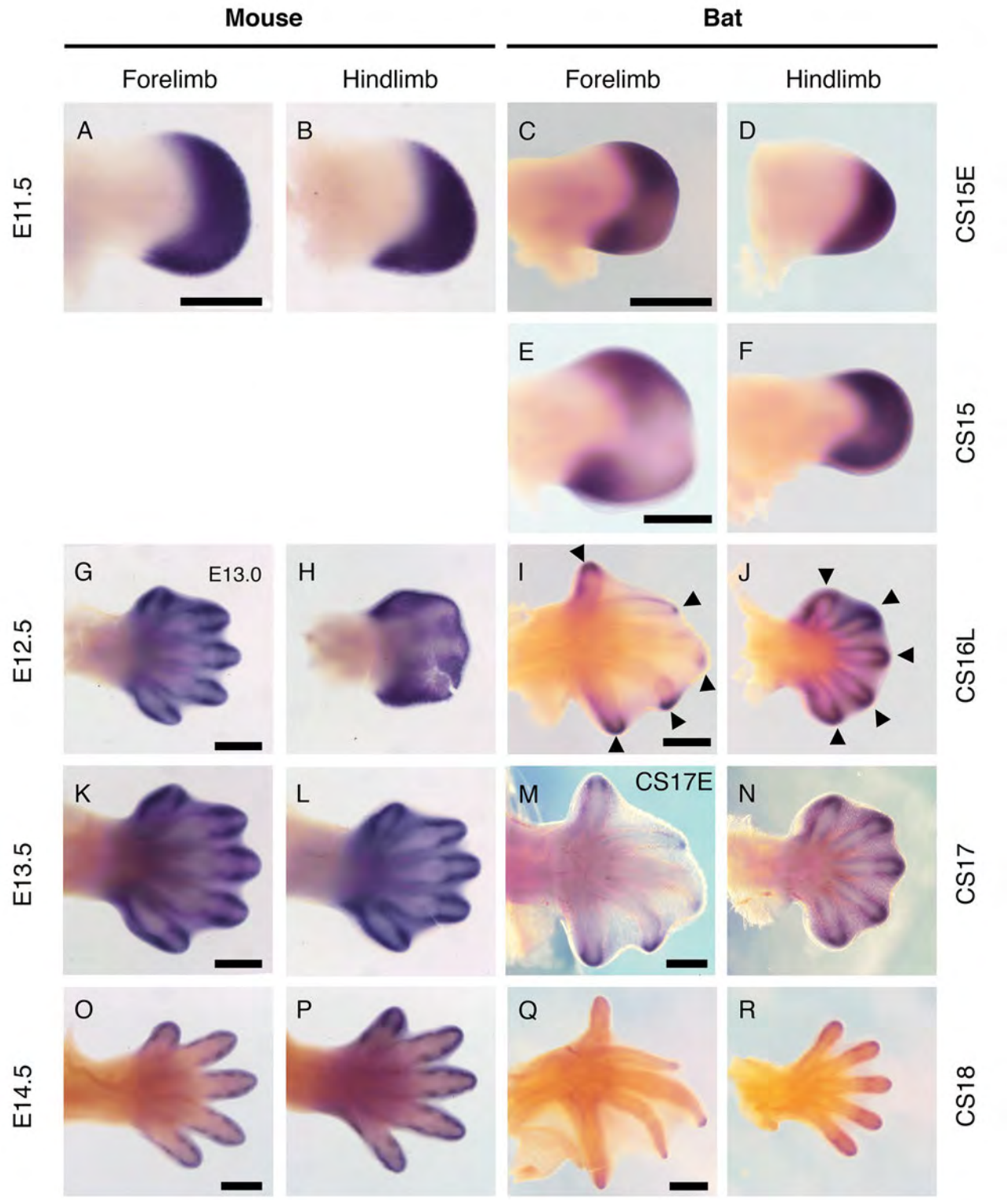

Figure 3.11: The expression of *Hoxa13* in mouse and bat forelimb (FL) and hindlimb (HL) at stages of autopod formation. During early stages of development, *Hoxa13* demarcates the autopod (**A**-**D**). In the bat, expression was lost in the FL (**E**), while being maintained in the HL (**F**). This trend continued during later stages of digit formation where FL expression was found in the distal digits but was absent in the more proximal digits and became lost in the interdigital tissue (**I**, M). In contrast, the bat HL had expression throughout the autopod, which was strongest in the digit tips (**J**, **N**), black arrow). Similarly, expression was strong throughout the mouse FL (**G**, **K**) and HL (**H**, **L**) autopods, with expression focused in the tissue surrounding the distal phalanges. Interdigital expression was lost at later stages of mouse development (**O**, **P**), while in the bat expression was only found in the most distal phalanges of the FL (**Q**) and HL (**R**). Expression was not found in the bat patagia. Scale bars represent 500 μm.

While expression of *Hoxa13* in the bat is similar to that of the mouse during early limb bud out growth (CS14), over stages of digit formation and growth it differs. Close examination at stages of autopod formation (CS15) shows a slight decrease in staining in the FL, over the region where digits III and IV form, it was notable that the proximal expression boundary at CS15, did not correspond to the dissection point used to dissect off the autopod in qPCR analyses (Figure 3.11E). Anterior expression of *Hoxa13* was maintained along the presumptive basipod region. In the bat HL only a slight loss of expression is evident in the region where digit IV forms (Figure 3.11F). These differences became more apparent in the FL of later stages (CS16), where expression was lost in the more proximal autopod region and the interdigital tissues. Weak expression was seen in digit ray I, digit ray V and the proximal portion of digit ray II and IV, while strong expression was restricted to the digit tips (black arrows in Figure 3.11I). This expression strongly contrasted with that of the HL, where *Hoxa13* was expressed across the autopod and focused in the regions surrounding the distal digits (Figure 3.11J). Weak signal was found in distal digit tips of the CS17FL where it was still evident at CS18, while signal from other regions was lost (Figure 3.11M & Q). In the HL, expression was similar to the mouse FL and HL, with a loss of the interdigital, and maintenance of distal digit ray expression at CS18 (Figure 3.11N & R). It was notable that, at all stages examined, staining was never observed in the developing patagia.

In the bat FL *Meis2* expression was found in the interdigital regions (initially ID4) from CS16 onwards. This corresponds to a loss of *Hoxa13* expression from this region, clearly indicating that these two genes are not co-expressed in the bat FL. In addition, *Meis2* expression is not seen in the bat HL interdigital tissue. These results show that while there may be potential for interactions between MEIS2 and HOXA13 in the interdigital regions of mouse autopods, where they are co-expressed, this is unlikely to occur in the bat FL and HL.

To confirm the loss of expression found in the bat FL over these stages I examined the absolute level of *Hoxa13* expression in bat autopods at sequential stages of development (CS15-CS18). In agreement with the WISH results, the *Hoxa13* transcript abundance was markedly lower in the bat FL than the HL, and was significantly different for all stages examined (Figure 3.12, Appendix B.7). The CS15 HL had the highest number of transcripts of all stages examined. Transcript abundance decreased over development, with a significantly lower number of transcripts found in the CS18 HL as compared to earlier stages. At all stages, FL expression was less than half that of the HL (Appendix B.8). While FL transcript levels were similar at earlier stages (CS15 and CS16), these dropped slightly in the CS17 FL, and significantly in the CS18 FL (Figure 3.12).

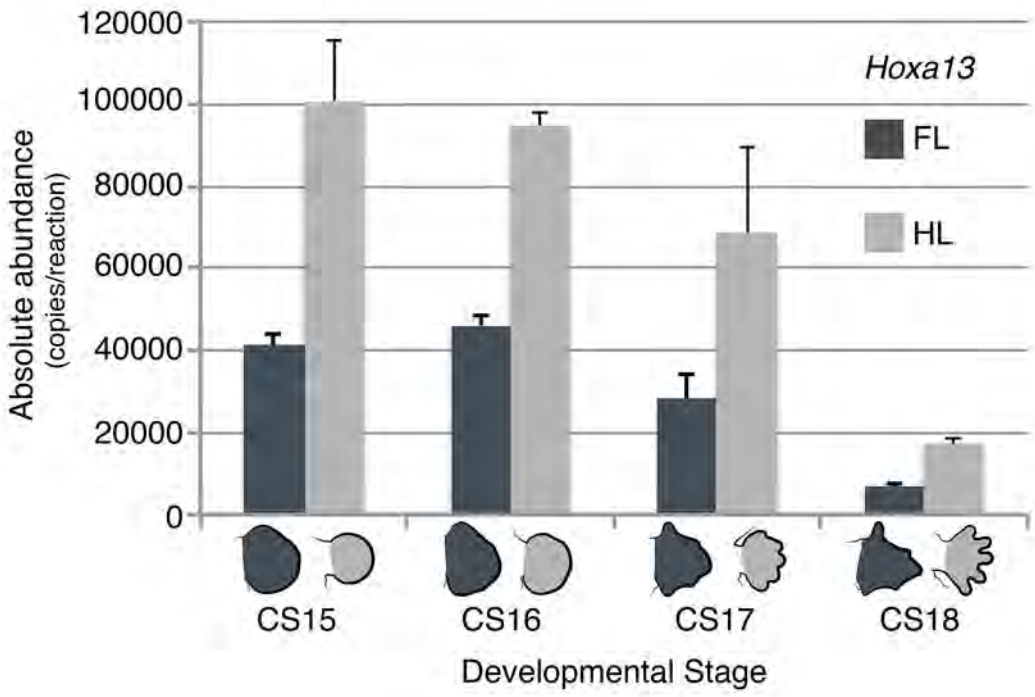

Figure 3.12: *Hoxa13* transcript abundance as quantified by absolute qPCR in the bat forelimb (FL) and hindlimb (HL) autopods. Measurements were performed over successive stages of development from autopod formation and patterning (CS15) to late stages of autopod differentiation and growth (CS18). All samples represent the average of 3 biological samples with error bars indicating the standard error (SE).

A weak positive correlation existed between FL and HL expressions (Spearman's correlation: r_s = 0.692, N = 12, p = 0.013), indicating that, as development continued, expression of this gene in both the FL and the HL decreased together. These experiments indicate that *Hoxa13* expression is lowered in the bat FL over all stages of autopod formation examined, and that as development progresses expression is reduced in both the FL and the HL, likely due to its absence from the proximal regions of the digit rays and the interdigital tissue.

3.4.2. Hoxa11 is not differentially expressed between the bat FL and HL autopod but can be seen in the digit tips and patagia at later stages of development

Hoxa11 showed a similar spatial and temporal pattern of expression in both the mouse and bat autopods during early autopod development. This was restricted to the presumptive zeugopodal region in both the FL and HL with no distal expression evident during early development (CS15) (Figure 3.13A, B, C-D). In agreement with WISH analysis of *Hoxa13* expression, the distal boundary of *Hoxa11* expression extended within the dissection point used to demarcate the autopod in both the FL and the HL (Figure 3.13E-F). At later stages (CS16, CS17 and CS18), this was not the case, suggesting that there is minimal inclusion of this region into these later samples.

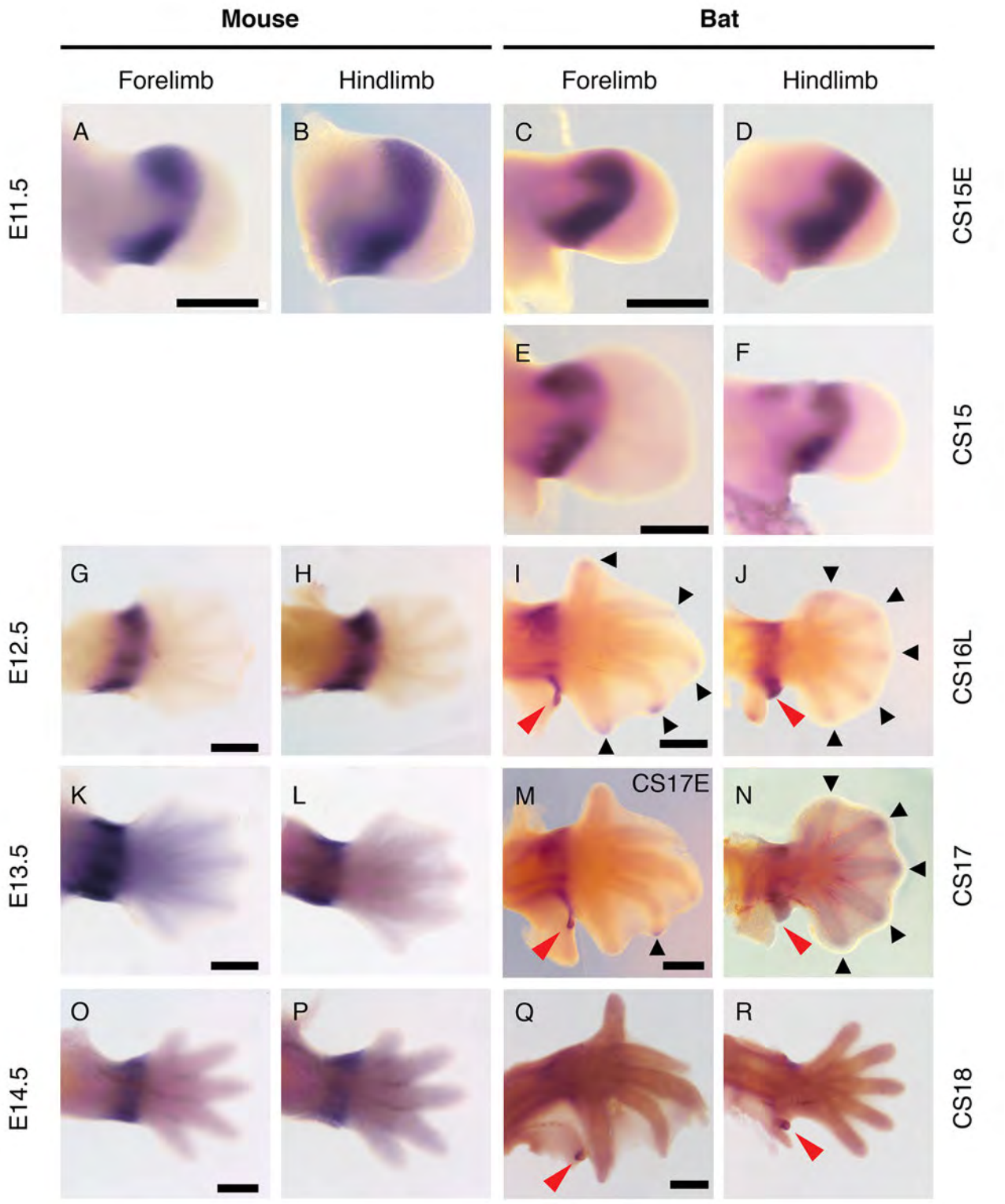

Figure 3.13: *Hoxa11* expression in the mouse and bat forelimb (FL) and hindlimb (HL) at stages of autopod formation. *Hoxa11* was restricted to the presumptive zeugopod of the mouse FL and HL. While this domain of expression is also seen in the bat embryos novel regions of expression are found in the distal edge of the plagiopatagium and uropatagium in later stages examined (red arrow, **I**, **J**, **M**, **N**, **Q**, **R**) and faint expression is also found in the digit tips of both the FL and the HL (black arrows, **I**, **J**, **M**, **N**). Scale bars represent 500 μm.

In both mouse and bat, the distal boundary of *Hoxa11* zeugopod expression did not overlap with *Hoxa13* expression, and no distal expansion of the *Hoxa11* expression domain was evident. However, novel domains of *Hoxa11* expression were seen in the digit tips of the bat FL and HL, and these corresponded to regions where *Hoxa13* was found (black arrows, Figure 3.13I-J). At later stages (CS17) these were evident in FL digit IV and HL digit I-V (Figure 3.13M-N), but were not found at CS18 (Figure 3.13Q-R). This distal, digit tip expression was not seen in the mouse (Figure 3.13G, H, K, L, O-P). In the bat, expression was also found along the anterio-distal edge of the plagiopatagium (red arrows, Figure 3.13I & M) and in the distal portion of the uropatagium (red arrows, Figure 3.13J & N). Patagial expression was still evident, restricted to the distal tips of the patagia at later stages of development (red arrows, Figure 3.13Q-R). Unlike *Meis2* and *Hoxa13*, *Hoxa11* was not differentially expressed between the FL and HL (Figure 3.14 Appendix B.9). In agreement with WISH results, *Hoxa11* expression was significantly higher in the CS15 FL and HL samples (Appendix B9). Transcripts measured at later stages likely originate from the distal digit tip domain, or through incorporation of trace distal zeugopod tissues. These two experiments indicate that there is a significant portion of distal zeugopodal tissue incorporated into the autopod samples at CS15, however this is minimal at later stages of development (CS16, CS17 and CS18) and this inclusion is equivalent in the FL and the HL samples at all stages.

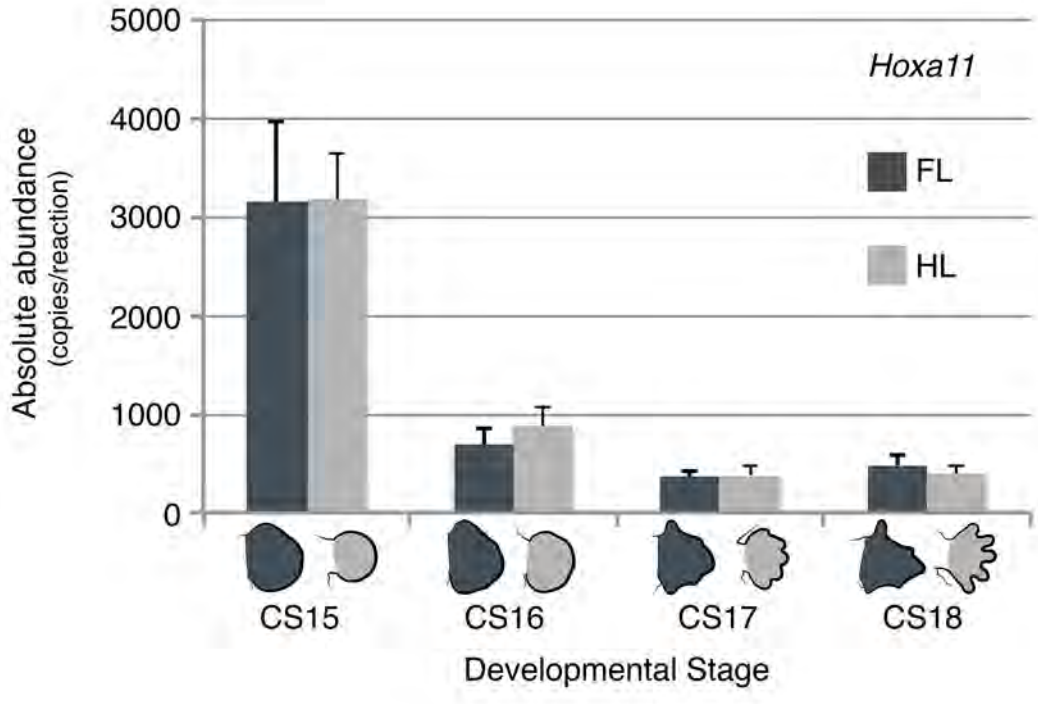

Figure 3.14: *Hoxa11* transcript abundance as quantified by absolute qPCR in the bat forelimb (FL) and hindlimb (HL) autopods. Measurements were performed over successive stages of development from autopod formation and patterning (CS15) to late stages of autopod differentiation and growth (CS18). All samples represent the average of 3 biological samples with error bars indicating the standard error (SE).

3.4.3. *Hoxa13 has strong differential expression in as while Hoxa9-11 appear similarly expressed between the developing bat FL and HL*

Interestingly, *Hoxa13* appears to be the only 5'HoxA gene to be strongly differentially expressed in bat autopods. During early limb bud development (CS14), it is more highly expressed in the bat FL than in the HL, showing asymmetric expression, with high levels in anterior and posterior regions of the FL, while in the HL, highest levels were found in the medial region (Figure 3.15A).

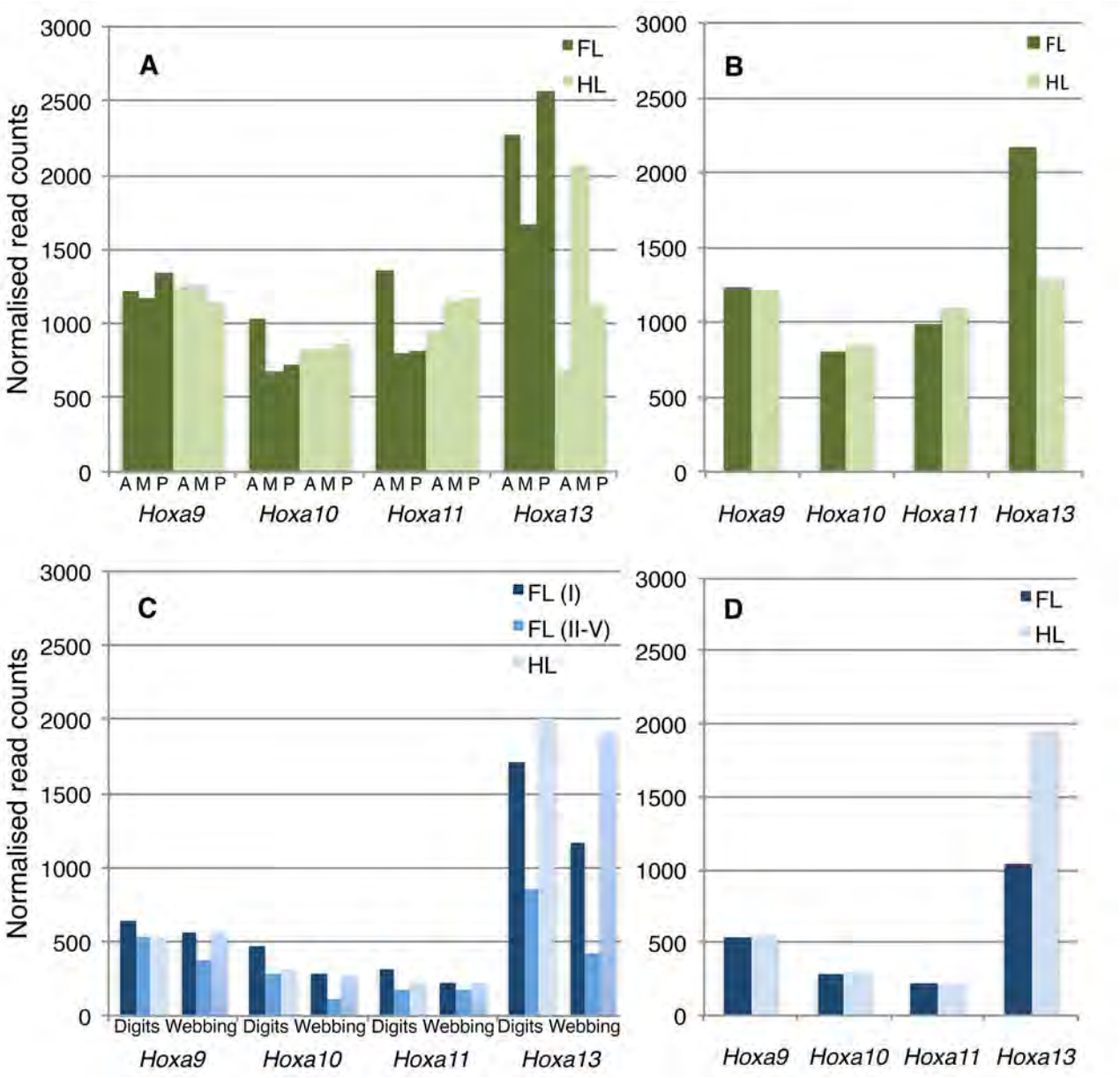

Figure 3.15: RNA-seq normalised read counts for the bat, *M. schreibersii* for genes in the HoxA gene cluster. At early stages of limb bud outgrowth (**A**; CS14), *Hoxa9*, *10* and *11* were not differentially expressed between the forelimb (FL) and hindlimb (HL), however *Hoxa13* was more highly expressed in FL tissues. This was clearly evident in the averaged expression data for these genes (**B**). In later staged digit and webbing tissues (**B;** CS15-CS17), there were few differences between the FL (dark blue - digit I/ID1; blue - digits II-V/ID2-4) and HL (light blue) expressions for *Hoxa9*, *10* and *11*. *Hoxa13* expression was slightly lower in posterior FL tissues. *Hoxa13* expression was clearly lower in the FL when examining averaged read counts (**D**). Data extracted from the GEO dataset (GSE50699) of Wang et al. (2014).

The normalised read counts of *Hoxa13* remained high in later development (pooled CS15-17). These measurements are consistent with the WISH data for *M. natalensis*. The HL tissues showed the highest transcript levels, with equivalent expression found in the digit and webbing tissues. In the FL, elevated levels were apparent in the anterior tissues (digit I and its associated webbing), and reduced levels in the posterior FL, with lowest expression found in the webbing of this region (Figure 3.15C). The transcript abundance of *Hoxa9*, *10* and *11* digits appear to be similar between the FL and HL, with slightly increased normalised read counts found in the anterior FL (digit I and its associated webbing).

3.5. Discussion

Meis2 is well known as a marker of the proximal limb bud, with studies in the chick suggesting that, in this context, it is activated by RA signalling to proximalise the limb bud, indirectly restricting expressions of more distal markers (*Hoxa11* and *Hoxa13*) (Tabin and Wolpert 2007; Zeller *et al.* 2009; Roselló-Díez *et al.* 2014). A role for this gene in autopod development has not been explored. In this chapter I characterised the expression of *Meis2* in developing bat and mouse autopods over several stages of development, and explore the correspondence of its gene expression with RA signalling in this tissue. I complement this by characterising the expressions of genes that regulate RA availability. In addition, I explore the potential effects of high levels of *Meis2* expression in the developing autopod by characterising the expressions of genes that are perturbed by overexpression of *Meis2* in the distal limb bud (*Hoxa11* and *Hoxa13*). These results are discussed in the context of both digit and interdigital development.

3.5.1. Early proximal expression of Meis2 may alter proximodistal patterning events in the bat hindlimb bud

Meis2 is the predominant *Meis* paralog expressed in developing bat limbs. Its early proximal expression pattern is conserved, appearing similar to that described in the chick and the mouse (Oulad-Abdelghani *et al.* 1997; Capdevila *et al.* 1999; Mercader *et al.* 1999; Coy and Borycki 2010; Sánchez-Guardado, Irimia, *et al.* 2011). During early limb bud outgrowth (CS14), it is strongly expressed in the anterior and posterior regions of *M. schreibersii* limbs, with highest expression in the hindlimb tissues (Dai *et al.* 2014). At this early stage of development, forelimb and hindlimb comparisons must be interpreted with caution due to the developmental lag of the hindlimb, with dilution effects in the forelimb (due to relatively larger '*Meis*-free' distal domain expected) likely resulting in relatively lowered expression in this tissue (Chen *et al.* 2005; Hockman *et al.* 2009; Mercader *et al.* 2009; Gyurján *et al.* 2011). Expansion of *Meis2* expression in the hindlimb bud does have the potential to alter early proximodistal patterning events and should be further examined. In the chick and the mouse, overexpression and distal ectopic expression of *Meis1/2* is accompanied by shortening and truncations of zeugopod and/or autopod elements (Capdevila *et al.* 1999; Mercader *et al.* 1999). Mice that conditionally express distal ectopic *Meis2* in the limb bud show a deregulation of distal *Hoxa11* repression, through the inhibition of *Hoxa13,* that results in a distal expansion of the zeugopod/autopod boundary (Roselló-Díez *et al.* 2014). In the adult bat hindlimb, the lengths and proportions of the zeugopod and autopod elements are shorter than those of the forelimb (Chapter 4). An early increase in *Meis2* expression in the bat

hindlimb bud at this stage may confer (or indicate) a greater proportion of cells that have a proximal fate. It would be useful to examine the expression of all of these genes at early stages of limb bud outgrowth (CS13 to CS15), and correspond their expressions to models of limb bud outgrowth (Uzkudun *et al.* 2015) to understand their potential interactions in bat forelimbs and hindlimbs.

3.5.2. Meis2 is overexpressed in the bat forelimb interdigital regions and is positioned to drive cell proliferation

Most interesting was the finding of *Meis2* expression in the interdigital tissue of the autopod during later limb development. The mouse autopod had robust expression in the proximal interdigital mesenchyme, which undergoes thinning, but not cell death (Salas-Vidal *et al.* 2001; Hernández-Martínez *et al.* 2009; Hernández-Martínez and Covarrubias 2011). The distal edge mesenchyme, which experiences cell death, due to the loss of FGF signalling from the AER, appeared to have low to no expression of *Meis2* in the samples examined, while *Meis2* was absent in the digit regions.

This is congruent with what is found in the *M. natalensis* where strong *Meis2* expression was associated with interdigital retention and expansion of the forelimb, while there was a dramatic reduction of expression in these regions of the hindlimb, which experiences interdigital tissue loss (Cretekos *et al.* 2005; Hockman *et al.* 2009). These observations extend to other bat species. *Meis2* transcripts were abundantly expressed in *M. schreibersii* embryos in the interdigital tissue of FL digits II to V over stages CS15L-CS19 (Dai *et al.* 2014; Wang *et al.* 2014). Elevated expression of *Meis2* has also been noted in later (fetal) stages in *Myotis ricketti* and *Hipposideros armiger*, in tissues taken from FL digits and interdigital tissue (II to V) compared to forelimb digit I or the hindlimb (digits I-V) (Wang *et al.* 2010). *Meis2* expression was also found in the patagia of both the forelimb and the hindlimb, and was maintained during their growth and expansion. The hindlimb autopods provide a stark contrast. These undergo interdigital regression to form free digits and have low *Meis2* expression that, at earlier stages (CS15 and CS16) was only detectable by qPCR in *M. natalensis*. Expression levels did increase at later stages of development, and faint but detectable signal was visible in hindlimb interdigital tissues of *M. schreibersii* (Dai *et al.* 2014). The low *Meis2* expression in this region appeared to be close to the level of detection of these WISH experiments, which may account for the discrepancies between these two species.

The strong expression of *Meis2* in the forelimb interdigital tissue and patagia coincides with their thinning and growth into expansive webbing, a process that begins during autopod formation and continues throughout fetal development (Cretekos *et al.* 2005; Hockman *et al.* 2009). *Meis2* expression

may mark and determine the fate of this region by keeping these cells in a rapidly proliferating, undifferentiated state, similar to the role of *Meis1* and *Meis2* in retinal progenitor cell populations in the chick (*G. gallus*) and *Hth* in *D. melanogaster* (Bessa *et al.* 2002; Domínguez and Casares 2005; Heine *et al.* 2008). In these systems, competitive blocking of MEIS activity or interference of *Meis2* expression in this tissue, reduces the overall size of the eye. The size of the proliferating progenitor cell pool is decreased but the apoptotic cell death parameters remain unchanged. These results indicate that *Meis1* and *Meis2* function synergistically to control proliferation, regulating the expression of genes involved in cell cycle processes (Heine *et al.* 2008). In the eye, species-specific differences in *Meis* gene expression are associated with differences in its final size, with the modulation of *Meis* gene expressions, and resultant regulation of rapid proliferation in the progenitor cell pools, presented as a mechanism underlying the evolution of this feature (Heine *et al.* 2008).

In human cancers, *Meis2* appears to have similar molecular role, with high expression in neuroblastoma cell lines required for their continued survival and proliferation (Zha *et al.* 2014). The loss of *Meis2* expression in neuroblastoma (BE(2)-C) cell lines resulted in non-apoptotic cell death due to M-phase arrest and mitotic catastrophe, this was associated with the downregulation of multiple late cell-cycle genes, including those involved in DNA replication, G2-M checkpoint control, M-phase progression and mitotic sister chromatid segregation (Sadasivam *et al.* 2012). It is likely that the continued expression of *Meis2* in the bat interdigital tissues is positioned to drive proliferation events to both maintain and feed the expansion of this tissue and their associated digits.

3.5.3. Meis2 expression is independent of RA signalling in the bat and the mouse

Due to limited characterisation of this gene during later stages of the mouse development, a role for *Meis2* in shaping the autopod has not been explored. *Meis2* expression is known to be induced by ectopic retinoic acid (RA) both in cell lines (mouse P19 embryonal carcinoma, EC, Bouillet *et al.* 1995; NT2/D1 EC, Freemantle *et al.* 2002) and mouse embryonic tissues (E8.5 presomatic mesoderm, Savory *et al.* 2014; E11.0 limbs Qin *et al.* 2002). Its expression should therefore be considered in the context of RA signalling (Díaz-Hernández *et al.* 2014).

During limb bud outgrowth *Meis1/2* are conventionally described in terms of their role in specifying the most proximal limb (stylopod) region with their proposed dependence on RA signalling from the embryonic flank being an important component of the two-signal model of proximal-distal patterning (Mercader *et al.* 2000; Tabin and Wolpert 2007; Zeller *et al.* 2009; Roselló-Díez *et al.* 2011). The role of RA signalling in this model is supported by pharmacological work in the chick limb, but has been

challenged in mouse models (reviewed by Cunningham and Duester 2015). Genetic loss-of-function experiments show that *Meis1/2* expression is maintained in the proximal limb buds of *Raldh2*$^{-/-}$; *Raldh3*$^{-/-}$ (loss of *Aldh1a2*) and *Rdh10*$^{trex/trex}$ mouse embryos, and even in *Rdh10*$^{trex/trex}$ embryos treated with an RAR antagonist (Zhao *et al.* 2009; Cunningham *et al.* 2011, 2013). These mutants show no endogenous limb-field RA signalling as indicated by a *RARE-lacZ* transgenic reporter, shown to be sensitive to 0.25 nM RA (~100 fold lower than endogenous RA) (Cunningham *et al.* 2013). While these studies show that RA signalling is required for mouse FL bud initiation, they show that RA is not required for HL bud initiation, or for the proximal expression of *Meis1/2* in either the FL or HL (Zhao *et al.* 2009; Cunningham *et al.* 2013; Kawakami 2013).

In this study *Meis2* is shown to be expressed in the interdigital membrane of *Rdh10*$^{trex/trex}$ mice, despite the absence of RA signalling (clear from the prominent defect syndactyly and lack of RARE-lacZ activation/expression) (Cunningham *et al.* 2011). This observation is consistent with a model of limb patterning in which the expression of *Meis2* does not require RA signalling (Cunningham and Duester 2015).

3.5.4. RA signalling is present in the bat forelimb interdigital tissues.

RA signalling is known to play an important role in autopod patterning by regulating the expression of genes that activate cell death and inhibit cell differentiation in the interdigital regions, as well as in controlling tissue specification events at the digit-interdigit junction (Zhao *et al.* 2010; Cunningham *et al.* 2011; Díaz-Hernández *et al.* 2014). Mouse mutants deficient in RA signalling display soft tissue syndactyly (Díaz-Hernández *et al.* 2014), have impaired cell death with an increase in cell proliferation (Dupé *et al.* 1999), raising the possibility that diminished RA signalling in the bat FL might explain the retention of the interdigital membrane. This was not the case. The RA-responsive gene, encoding a RA receptor (*Rarβ*), showed clear expression in the interdigital tissues of both autopods in addition to the patagia, indicating that RA signalling is active in these tissues at CS17.

While RA availability appears to be similar, several signalling pathways exist to transduce its activity. RA receptors (RARs: *Rarβ*, *Rarα*, *Rarγ* and retinoid X receptors, RXRs: *Rxrα*, *Rxrβ* and *Rxrγ*) propagate the RA signal in complex co-ordinated manner in different tissues (reviewed by Cunningham and Duester 2015). Interdigitally expressed *Rarβ* has been suggested to be involved in digit separation or the suppression of a chondrogenic fate (Dollé *et al.* 1990; Jiang *et al.* 1995). However, inactivation of *Rarβ* alone does not appear to affect interdigital tissues nor show chondrogenic defects. Compound mutants (*Rarβ*$^{-/-}$ *Rarγ*$^{-/-}$ and *Rarβ*$^{+/-}$ *Rarγ*$^{-/-}$) do exhibit soft tissue syndactyly that is attributable to a loss of

interdigital mesenchyme ingression (Ghyselinck *et al.* 1997). These mutants, and those that have a loss of RA synthesis (*Raldh2*$^{-/-}$ and *Rdh10*), have reduced cell death and the maintenance of cell proliferation in this interdigital mesenchyme (Dupé *et al.* 1999; Zhao *et al.* 2010; Cunningham *et al.* 2011; Cunningham and Duester 2015). Due to the complex transduction of RA signalling in the autopod it is necessary to examine the expressions of the genes encoding alternative RA receptors before concluding that this pathway is unaltered in bat autopod development.

While RA availability appears to be equivalent in the bat forelimb and hindlimb, it is possible that the bat forelimb experiences a suppression or lack of the downstream response to RA signalling required for the complete removal of interdigital tissue. Another possibility is that RA signalling in the bat FL is modulated, or stratified, within the wing mesenchyme, allowing the thinning but not the complete removal of the bat wing interdigital membranes. This is supported by the findings that BMP-mediated cell death, activated by RA signalling in the interdigital regions, is present in the bat (*C. perspicillata*) forelimb, in addition to purported markers of apoptosis (*Msx1* and *Msx2*) (Weatherbee *et al.* 2006; Díaz-Hernández *et al.* 2014). This apoptotic pathway appears to be limited in the bat by the expression of *Gremlin* (a BMP antagonist) in the FL at CS16 and CS17. In this system, the continued expression of *Fgf8* in the interdigital mesenchyme of the bat (CS16 and CS17) forelimb is suggested to limit apoptosis of the distal edge, preventing the ingression of interdigital tissue adjacent to digits II to V (Weatherbee *et al.* 2006). While RA-mediated apoptosis is likely occurring in the bat interdigital membranes, this process appears to be modulated by the presence of *Gremlin* and *Fgf8* in the forelimb, with subsequent cell death events likely playing a role in the thinning and shaping of this of the interdigital tissue rather than the complete regression of the membranes as found in the mouse.

3.5.5. Modulation of RA availability occurs in the bat forelimb at later stages of autopod development

While RA signalling appeared to be similar in bat forelimbs and hindlimbs, notable differences were found in the expressions of two genes involved in RA metabolism. There was a dramatic loss of *Cyp26b1* expression in the posterior digits of the forelimb, and loss of *Aldh1a2* (*Raldh2*) expression in the most anterior interdigits. This was supported by RNA-seq data (Wang *et al.* 2014). Together these alterations in expressions could be expected to result in increased exposure to RA activity in forelimb digit rays II-V (due to a loss of degradation in this region) and a reduction of RA availability in the anterior forelimb (due the loss of synthesis in this region) (Dranse *et al.* 2011). The expression patterns

and levels of *Rarβ*, conventionally used as readouts of RA signalling, did not support this at developmental stage CS17.

The loss of *Cyp26b1* expression in the posterior forelimb digits is an intriguing finding. In the two-signal/differentiation front model of limb bud outgrowth, exclusion of *Cyp26b1* from the proximal limb by *Meis2* allows high levels of RA signalling to be maintained in this region, which is suggested to repress *Hoxa11* and *Hoxa13* expressions. In the distal limb bud, ectopic expression of *Meis2* (in HB6:R26RM2 transgenic mice) results in a loss of *Cyp26b1* expression in this region and downregulation of *Hoxa13* (Roselló-Díez *et al.* 2014). When these interactions are extended to the bat forelimb autopod it would suggest that the overexpression of *Meis2* in the interdigital tissues mediates the downregulation of *Cyp26b1* in these regions. This loss would be expected to result in increased interdigital RA availability, and subsequent downregulation of *Hoxa13*. However this is not the case, as *Rarβ* expression (an indicator of RA signalling) was not elevated in these tissues and localised *Hoxa13* downregulation was already evident in the CS15 bat forelimb, prior to the activation of *Meis2* expression. In addition, these genetic interactions have been shown to occur in a cell autonomous manner in the limb bud (Roselló-Díez *et al.* 2014), implying that the loss of *Cyp26b1* and *Hoxa13* expressions should only occur in the interdigital tissues where *Meis2* is expressed, which is not the case. Therefore this model does not account for the loss of *Cyp26b1* in the proximal digit rays.

It is unknown what factors may be responsible for the down regulation of *Cyp26b1* in the CS17 bat forelimb. In fact, in the bat there is robust interdigital expression of *Fgf8* (Weatherbee *et al.* 2006; Hockman *et al.* 2008), which, based on interactions found in the mouse limb bud, would be expected to promote the expression of *Cyp26b1*, resulting in a reduction of *Meis2* expression and RA signalling (Mariani *et al.* 2008; Probst *et al.* 2011). Based on these findings, interactions amongst these patterning genes in the bat autopod are unlike those described in the developing mouse limb bud. This may be a result of the advanced differentiation of autopod tissues that separate regions of activity, or due to the other genetic factors at play. For example, *Cyp26b1* expression is antagonised by the expression of *Forkhead box L2* (*Foxl2*) during gonadal development (Kashimada *et al.* 2011). Similar mechanisms may be at play during bat forelimb development to modulate the expression of this gene and subsequent regional RA availability within the autopod.

At these late stages *Aldh1a2* expression is absent or decreased in the anterior half of the bat forelimb. This was not associated with a loss of *Rarβ* expression, or with the retention of interdigital webbing (in fact interdigital tissue is lost in the first interdigit). *Fgf8* expression also appears relatively lower across this region (Weatherbee *et al.* 2006) making it an unlikely candidate for this suppression (Hernández-

Martínez *et al.* 2009). *Aldh1a2* expression has been shown to be directly induced by either HOXD13 or HOXA13, with these proteins binding to promoter and enhancer regions respectively (Kuss *et al.* 2009; Shou *et al.* 2013). Their downstream functions differ, with HOXD13 mediated activation implicated in chondrogenesis (Kuss *et al.* 2009), while HOXA13 mediated activation maintains (but does not appear to initiate) interdigital cell death (Shou *et al.* 2013). At this stage *Hoxa13* expression is fairly low in the regions corresponding to *Aldh1a2*, in contrast, *Hoxd13* expression is strong, focussed in digit rays III-V (Chapter 4). The maintenance of *Aldh1a2* expression at this stage, in the absence of *Hoxa13* expression, may therefore be mediated by *Hoxd13*, which promotes strong expression alongside digits that are undergoing elongation. In this role RA signalling specifies the digit interdigit junction (Zhao *et al.* 2010; Díaz-Hernández *et al.* 2014). Mutants that lack *Aldh1a2* expression (*Raldh2*$^{-/-}$) show a loss of expression of several associated genes that are expressed in digit interdigit junctions (*Rarβ*, *Bmp7*, *Fgf18*) of the E13.5 mouse, in addition to the downregulation of *high mobility group N1* (*Hmgn1*) (Shou *et al.* 2013). The loss of *Aldh1a2* in the anterior digits of the bat forelimb likely results in the downregulation of tissue remodelling genes, specifically *Hmgn1*, which downregulates *Sox9*, and *Fgf18*, regulators of chondrogenesis and osteogenesis (Zhao *et al.* 2010). This might result in slight differences in the maturation of skeletal elements, which will have an impact on their growth and shape. The slight modulation, in the expression patterns of genes encoding products involved in RA metabolism, indicates that differences within the autopod regions do occur. This may play a role in digit specific growth through altering differentiation events.

3.5.6. Hoxa13 expression is lost in the forelimb during digit chondrogenesis

During limb bud outgrowth the separation of *Meis1/2*, and *Hoxa13* expressions is required for early proximodistal patterning (Zeller *et al.* 2009). *Hoxa13* is a key regulatory gene in this context, modulating the expressions of multiple developmental cascades to control several processes involved in shaping the autopod, including interdigital cell death, mesenchymal cell adhesion, chondrogenesis and skeletal element formation (Stadler *et al.* 2001; Knosp *et al.* 2004, 2007; Salsi and Zappavigna 2006). In the bat, *Hoxa13* is initially expressed throughout both autopods, becoming lost in the interdigital and posterior digital regions of the forelimb on digit formation (CS15 and CS16). *Meis2* is expressed in the interdigital regions subsequent to this loss (CS16). It is notable that in the mouse autopod these two genes have overlapping expressions in the interdigital regions, supporting the argument *Hoxa13* downregulation is not attributable *Meis2* overexpression in this region. This is supported by the fact that *Hoxa13* expression is lost after initial autopod specification and is not associated with an expansion of *Hoxa11* into this domain as found in ectopic expression studies (Mercader *et al.* 1999, 2009).

In the autopod interdigital tissue HOXA13 mediates interdigital cell death through the regulation of *Bmp* gene expressions (specifically *Bmp2* and *Bmp7*) and the direct promotion of *Aldh1a2* expression (Knosp *et al.* 2004). In this role *Hoxa13* expression increases the availability of RA in the interdigital regions and promotes interdigital cell death and subsequent regression. In homozygous *Hoxa13*$^{-/-}$ mutants, *Aldh1a2* expression is delayed and reduced, corresponding to a smaller autopod, loss of interdigital cell death and absence of digit I (Shou *et al.* 2013). While the loss of expression of *Hoxa13* in the bat forelimb autopod, does correspond to the retention of this interdigital tissue, there is no concomitant loss of *Bmp2* and *Bmp7* expression (Weatherbee *et al.* 2006), and downregulation of *Aldh1a2* expression is only found in the anterior portion of the forelimb autopod.

Hoxa13 expression is required for digit formation, its protein is capable of directly promoting expression of *Runx2* an essential transcription factor that inhibits chondrocyte proliferation and is required for their maturation (Yoshida *et al.* 2004; Hinoi *et al.* 2006; Villavicencio-Lorini *et al.* 2010). Loss of *Runx2* expression in bat forelimb digit elements has the potential to increase chondrocyte proliferation and alter timing of their transition to hypertrophy. This is supported by examinations of the bat (CS18) metacarpal growth plates, which had a greater proportion of resting cells (proliferating immature chondrocytes) as compared to equivalently staged mice (Sears *et al.* 2006).

4. *5'* HoxD gene expression is associated with the formation and development of elongated skeletal elements in the bat wing

4.1. Background

Hox genes are widely known for their role in specifying patterning events during development (Durston 2012). They are thought to have arisen coincident with the formation of three germ layers (triploblasty) and have undergone *cis*-duplication and divergence events to form clustered groups of genes (Garcia-Fernández 2005; Gehring *et al.* 2009). The expansion of these clusters, and subsequent genome duplication events in vertebrates has resulted in four cluster complexes, HoxA, HoxB, HoxC and HoxD (though teleosts, and *Xenopus laevis* have eight clusters), each containing 9 to 11 genes with 39 genes in total (Figure 4.1A) (Hueber *et al.* 2010; Soshnikova *et al.* 2013). The paralogous genes within these clusters are conventionally referred to as anterior (3' genes *Hox1*-5), central (*Hox6-8*) or posterior (5' genes, *Hox9-13*), classified into functional groups that share homology (Figure 4.1A) (Hueber *et al.* 2010). Genes in these clusters are strongly conserved, highly organised and tightly co-regulated in vertebrates, with the remarkable feature of having their temporal and spatial expression pattern reflect their genomic organisation, a feature referred to as collinearity (Figure 4.1A) (reviewed by Noordermeer and Duboule 2013). They are well known for patterning the vertebrate body plan during early development, with their 3'–5' arrangement corresponding to the order (spatial collinearity) and timing (temporal collinearity) in which they are expressed along the anterior-posterior body axis, which defines region specific structures (functional collinearity) (Figure 4.1A) (Durston 2012). These gene clusters are strictly organised in mammals, they are compact and uninterrupted, have limited small introns, are transcribed in the same orientation, and have few repetitive elements (Noordermeer and Duboule 2013). Genes in these clusters have the ability to act as co-ordinated, functional subunits (known as meta-genes) to specify the patterning along axes (Figure 4.1A) (Duboule 2007; Durston 2012). The HoxA and HoxD clusters are involved in both the organisation and the growth of the limb, and have been shown to have distinctive early and late expression patterns (Figure 4.1B) (Morgan and Tabin 1994; Deschamps *et al.* 1999; Zákány and Duboule 2007).

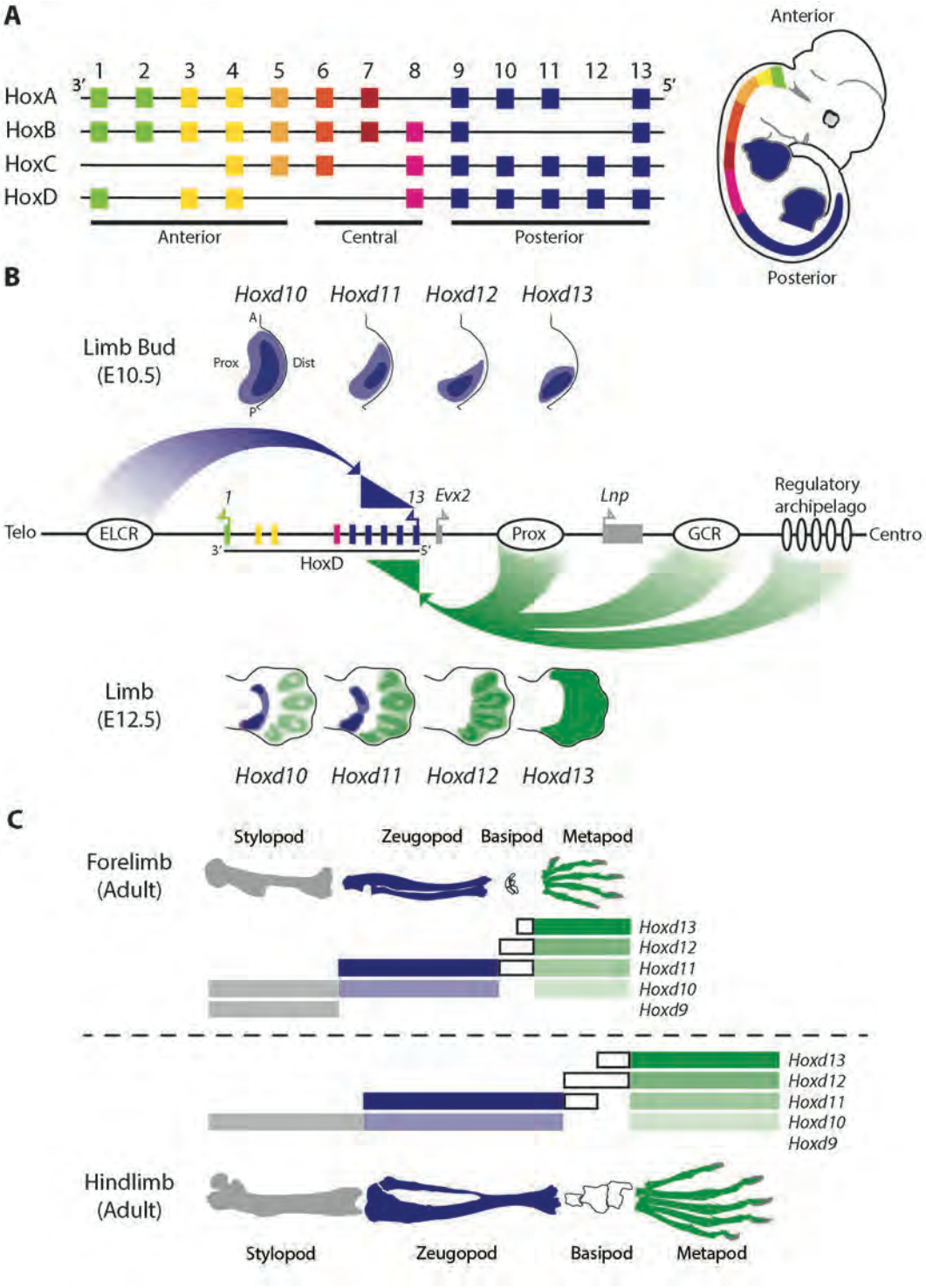

Figure 4.1: Hox gene clusters are highly organised with their genomic arrangement underlying their temporal and spatial expression patterns. Genes are arranged into 13 paralogous groups that can be broadly categorised into anterior, central and posterior Hox genes, the genomic position of these genes reflects their spatio-temporal expression along the anterior posterior axis of the developing embryo (**A**). *Hoxd10-13* are known as 5'HoxD genes and are expressed in a collinear fashion in the early limb bud (blue) driven by an Early Limb Control Region (ELCR) that lies telomeric (Telo) to the cluster. During later development, autopodal expressions (metapod in green) are driven in a reverse-collinear fashion by the co-ordination of several enhancer regions located centromeric (Centro) to the cluster (**B**). The spatio-temporal expression domains of these genes, in the early limb bud, is represented alongside the final adult mouse morphology (**C**). Figure adapted from (Wellik and Capecchi 2003; Montavon *et al.* 2008).

In the early limb bud, expression of central and posterior genes (*Hoxd8-11*) occurs in a spatio-temporal collinear manner and is driven by enhancer regions found on the telomeric side of the cluster (3' of *Hoxd1*) termed the Early Limb Control Region (ELCR) (Figure 4.1B) (Spitz *et al.* 2001). The 3' genes are expressed across the limb bud prior to their 5' neighbours and are spatially restricted with the 5' genes being expressed during later limb bud outgrowth, in progressively distally restricted domains that are nested within the posterior half of the limb bud mesenchyme (Figure 4.1B) (Dollé and Duboule 1989; Haack and Gruss 1993; Nelson *et al.* 1996; Zákány and Duboule 2007; Noordermeer and Duboule 2013). At this early stage of development these genes are involved in setting up A-P patterning in this region, playing a role in the growth of the undifferentiated mesenchyme (Morgan and Tabin 1994), mediated through the activation of *Shh* expression in the ZPA (Zákány *et al.* 2004).

At later stages of development, during autopod formation, reverse collinear expression of the 5'HoxD genes (*Hoxd9-13*) occurs. This involves a reversal of the spatial expression of these genes and has a quantitative component, with *Hoxd13* being expressed at high levels throughout the autopod digit forming region (Nelson *et al.* 1996), while *Hoxd12-10* expressions are posteriorly restricted and expressed at successively lower levels (Figure 4.1B) (Zákány and Duboule 2007; Montavon *et al.* 2008; Noordermeer and Duboule 2013). This alteration of expression results from a switch in the regulatory strategy of the HoxD cluster to centromeric long-range enhancers (5' of *Hoxd13*). These include Prox, the Global Control Region (GCR), in addition to conserved regulatory elements that are found within an 800 kb gene desert, 5' of the cluster, termed a regulatory archipelago (Figure 4.1B) (Spitz *et al.* 2003; Zákány *et al.* 2004; Gonzalez *et al.* 2007; Montavon *et al.* 2008, 2011). At these later stages of development HoxD genes participate in events that regulate digit formation and growth.

Limb regions (stylopod, zeugopod and autopod) are specified during early outgrowth and are marked and patterned by combinations of HoxA and HoxD cluster gene expression (Figure 4.1B). Targeted loss of HoxA cluster gene expression in the mouse forelimb results in deformations of the zeugopod and autopod elements, with the loss of digit I and reduction of digits II-V (Kmita *et al.* 2005). Targeted loss of HoxD cluster gene expression (specifically those of the 5' portion), by genomic inversion, deletion, or inhibition of activity, leads to the reduction of digits, the loss and/or fusion of phalanges and a delay in ossification (Spitz *et al.* 2001; Kmita, Fraudeau, *et al.* 2002; Villavicencio-Lorini *et al.* 2010; Montavon *et al.* 2011). HoxA/HoxD double mutants (targeted to the forelimb) have reduced stylopods and loss of the distal forelimb structures (zeugopod and autopod), with these phenotypes thought to be a result of an early developmental arrest of limb bud outgrowth and patterning (Kmita *et al.* 2005).

Hox10 paralogs are involved in patterning the stylopod and zeugopod (Wellik and Capecchi 2003; Boulet and Capecchi 2004), *Hox11* the zeugopod (Davis and Capecchi 1994; Davis *et al.* 1995; Kmita *et al.* 2005) and *Hox13* the autopod (Figure 4.1C) (Fromental-Ramain *et al.* 1996; reviewed by Zákány and Duboule 2007). The area where the carpal and tarsal elements will form (presumptive basipod) is regionalised by the expression of *Hoxa13* in the absence of other Hox gene expressions, and the region within which the digit rays will develop (presumptive metapod) by the combination of *Hoxa13* and *Hoxd13* expressions (Woltering and Duboule 2010). The functional expression domains of these genes differ between the mouse FL and HL, with that of *Hoxd9* involved in the specification of the stylopod of the FL (Figure 4.1C) (reviewed by Wellik and Capecchi 2003). The autopod itself is modular, with unique Hox signatures found in regions that specify digit ray I (*Hoxd13* and *Hoxa13*) and the posterior digit rays (II-V) (*Hoxa13*, *Hoxd13-10*) (Reno *et al.* 2006; Deschamps 2008; Montavon *et al.* 2008; Woltering and Duboule 2010).

The expressions of *Hoxa13* and *Hoxd13* in the autopod plays an essential role in its formation (reviewed by Zákány and Duboule 2007; Woltering and Duboule 2010). These genes have some redundancy, with compound mutants exhibiting more severe phenotypes, but their activity is not functionally equivalent (Fromental-Ramain *et al.* 1996). *Hoxa13* regulates multiple processes during autopod development, organising cells that contribute to the carpal and tarsal elements and those of digit I, controlling processes during condensation and boundary formation in chondrogenic mesenchyme and facilitating interdigital cell death (Perez *et al.* 2010; Shou *et al.* 2013). *Hoxd13* is involved in skeletogenesis, binding to and regulating the expression of genes that are involved in chondrogenic differentiation, maturation and joint formation (Salsi *et al.* 2008). A loss of *Hoxd13* expression alone results in notable retardation of digit cartilage and loss of some elements (Dollé *et al.* 1993; Davis and Capecchi 1996; Fromental-Ramain *et al.* 1996). While *Hoxd13* has an essential function, all 5'HoxD genes collectively modulate digit length, with *Hoxd12-10* loss of function mutants exhibiting shortened digit elements (Davis and Capecchi 1996; Delpretti *et al.* 2012). This is attributed to a gene dosage effect of the total HOX activity on these elements, with expression of *Hoxd12-10* altering the phenotype of the posterior four digits in conjunction with *Hoxd13* expression (Goff and Tabin 1997; Zákány *et al.* 1997; Deschamps 2008; Montavon *et al.* 2008).

The 5'HoxD genes have long been known to be involved in growth plate formation and bone elongation, regulating the rate of cell proliferation in cartilage templates (Davis and Capecchi 1996; Goff and Tabin 1997; Reno *et al.* 2008). Loss of 5'HoxD gene expressions (or of protein product activities) results in the arrest of chondrocyte differentiation prior to their transition into

prehypertrophy and a loss of growth plate formation, causing the growth of the cartilage element to become isotropic (uniform in all directions) (Villavicencio-Lorini *et al.* 2010; González-Martín *et al.* 2014). Recently, examination of the *synpolydactyly homolog* (*Spdh*) mouse mutant, which exhibits a loss in the activity of all 5'HoxD genes (due to the dominant negative activity of a mutated HOXD13 protein), has revealed that these genes help organise the growth plate and establish the perichondrium (Kuss *et al.* 2014). The reduction of 5'HoxD expression downregulates the Wnt/PCP pathway (through the downregulation of *Wnt5a* and *Wnt5b*) resulting in the loss of cell polarity and causing cells in the growth plate to become misorientated (Kuss *et al.* 2014). Subsequently, metacarpals/metatarsals do not form cortical bone, but instead undergo secondary ossification during later postnatal development, exhibiting a phenotype more closely resembling that the carpals/tarsals which do not form growth plates (Villavicencio-Lorini *et al.* 2010; Kuss *et al.* 2014).

It has been suggested that alterations in the regulation and expression of *Hoxd13* in the bat may underlie the elongation of their forelimb digits, however examinations of protein coding sequence, expression patterns and the GCR enhancer sequence in bats (*C. perspicillata*, *M. lucifugus*, *R. ferrumequinum*) have revealed few differences as compared to the mouse (Chen *et al.* 2005; Ray and Capecchi 2008). In this Chapter, I explore the skeletal element phenotype of adult bat limbs finding that the autopod of the bat forelimb is proportionately longer, while that of the hindlimb is proportionately shorter than those of the mouse. I characterise the expressions of four 5'HoxD genes (*Hoxd10*, *Hoxd11*, *Hoxd12* and *Hoxd13*), examining their expression levels, in conjunction with their respective patterns showing that *Hoxd10* and *Hoxd11* expression are upregulated in the bat forelimb as compared to the mouse forelimb, and that *Hoxd12-10* are downregulated in the bat hindlimb as compared to the bat forelimb from CS16 onwards. Finally I show that while the protein sequence of these genes appears conserved, several changes are found in the digit enhancer region (Prox) that are specifically unique to bats.

4.2. Characterisation of digit element lengths in the adult bat reveals changes associated with 5' HoxD gene expression domains

The 5'HoxD genes are involved in the specification and the elongation of long bones (Villavicencio-Lorini *et al.* 2010; González-Martín *et al.* 2014; Kuss *et al.* 2014). Loss of function (*Hoxd11*, *Hoxd12* and *Hoxd13*) and gain of function (*Hoxd11*) experiments result in the relative shortening or elongation of specific autopod skeletal elements (Dollé *et al.* 1993; Davis and Capecchi 1996; Fromental-Ramain *et al.* 1996; Delpretti *et al.* 2012). I examined the lengths of the bones that undergo endochondral ossification in adult bat limbs, comparing these with those of the mouse, to determine how the skeletal elements lengths differed both within limb types, and from the mouse, a comparative model organism (Cretekos *et al.* 2001). I asked the question as to whether limb regions and autopod elements lengths were disproportionately elongated in the bat forelimb, and whether these differences were associated with 5' HoxD gene expression domains during development.

4.2.1. The autopods of the bat are disproportionately longer in the forelimb and shorter in the hindlimb as compared to the mouse

The differences in overall average length among adult bat and mouse forelimb (FL) and hindlimb (HL) elements are immediately apparent, with the bat having extraordinarily long skeletal elements as compared to the other limb types (Figure 4.2). Together, the bat FL elements were more than three times longer than those of the bat HL and more than six times longer than those of the mouse FL (when scaled for differences in body size) (Figure 4.3A). The total length of the bat HL elements was only 1.3 times longer than their mouse counterparts (Figure 4.3A). The relationship between the FL and the HL differed in the mouse, with HL elements being 1.4 times longer than those of the FL (Figure 4.3A). The normalised limb lengths showed significant differences amongst one another (Table 4.1); this was attributable to significant differences between each pairwise comparisons ($p < 0.001$).

It was notable that the lengths of the three limb regions (stylopod, zeugopod and autopod) elements followed this relationship (longest in the bat FL, then the bat HL, then the mouse HL and smallest in the mouse FL) with the exception of the bat HL autopod, which was shorter than that of the mouse HL but larger than the mouse FL autopod (Figure 4.3A).

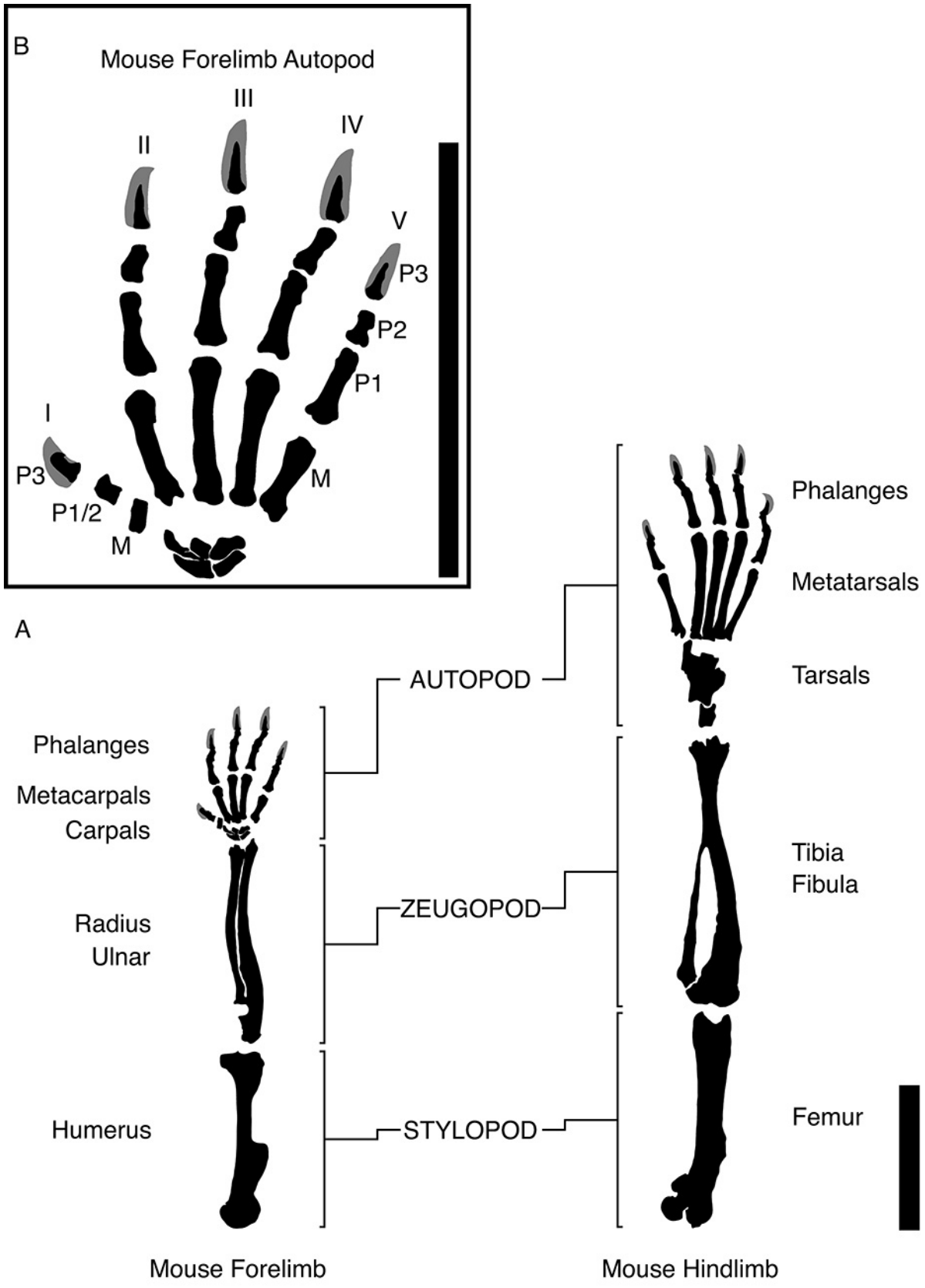

Figure 4.2: Schematic of the forelimb and hindlimb skeletal elements of the mouse and the bat. The three main limb regions and the various skeletal elements within the limb (**A**). In the mouse autopod (**B**) elements are marked in the mouse forelimb autopod (inset), indicating the proximal metacarpals (M) and distal phalanges (P1to P3). Digit I (equivalent to the human thumb) differs from digits II-V, in that it has only two phalanges (P1/2 and P3).

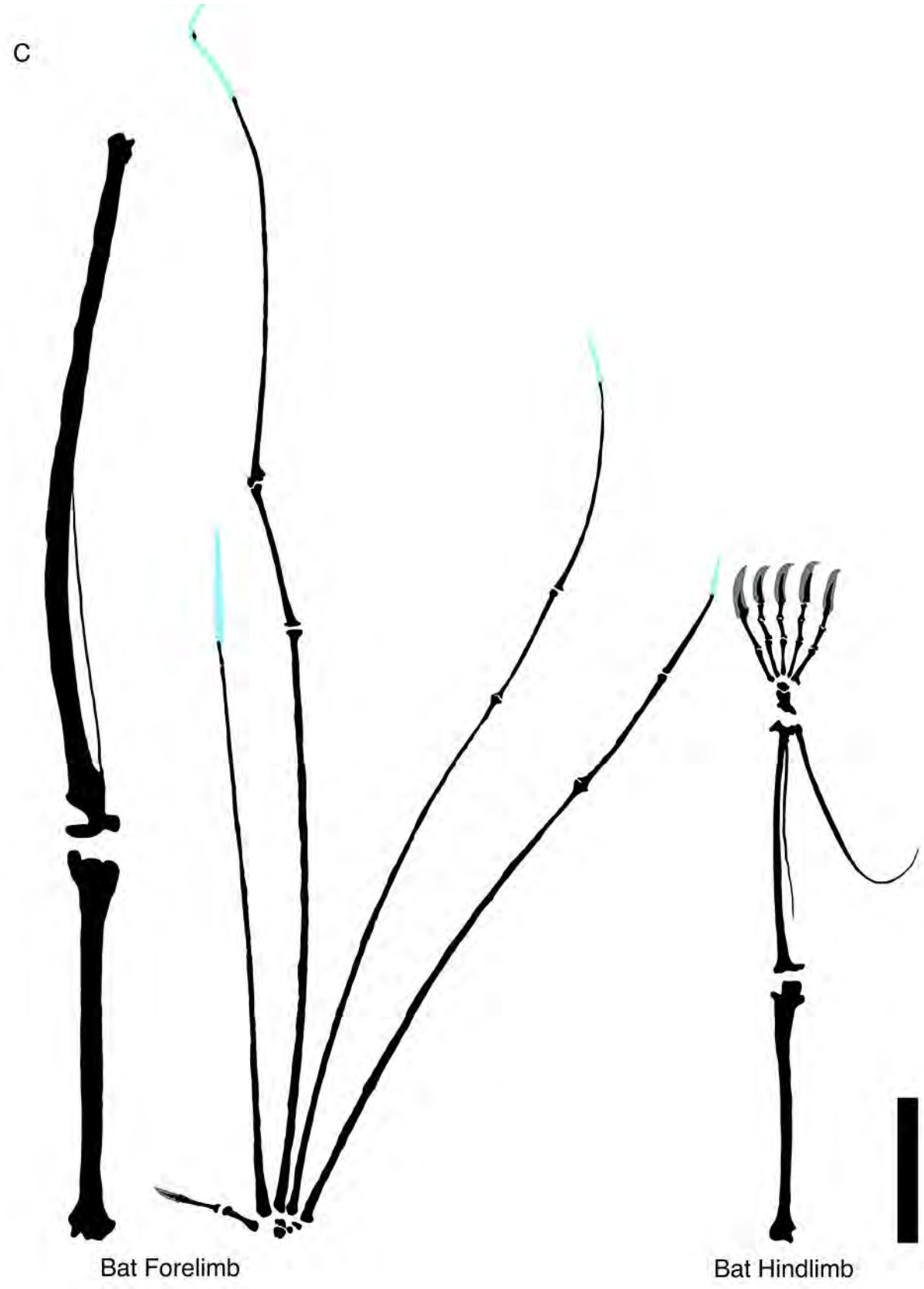

The skeletal elements of the bat forelimb and hindlimb are shown (**C**), skeletal elements are not marked but are comparable to those of the mouse The exceptions are the loss of the distal phalange of P2 and P3 in digit II and the loss of P3 in digits III-V in the FL, and the addition of the calcar in the HL. Regions of cartilage are shown in blue, claws are shown in grey. Scale bars represent 1 mm.

To understand the origin of these differences in total element lengths, the limb elements: stylopod (S), zeugopod (Z) and autopod (A; given by digit ray III), were compared amongst limb types (Figure 4.3A). All normalised limb element lengths were significantly different, with pairwise comparisons revealing that this was attributable to significant differences between each pair-wise comparison ($p < 0.001$) (Table 4.1). All bat FL elements were significantly larger than those of the other limb types. The bat HL had significantly longer stylopod and zeugopod elements than either of the mouse comparisons (corresponding to its significantly longer limb); however, its autopod was significantly shorter than that of the mouse HL. The mouse FL had significantly shorter elements than all other limb types (Table 4.1).

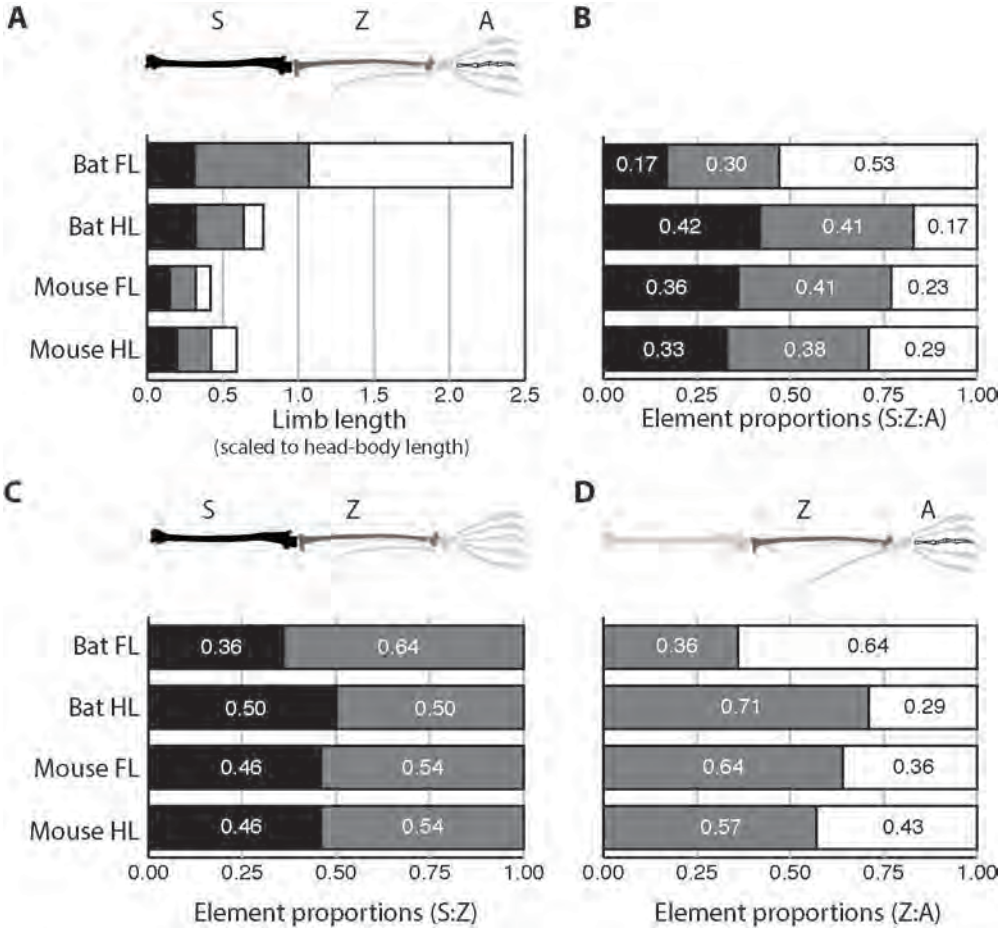

Figure 4.3: Bar graphs of the skeletal element lengths of the bat and mouse forelimb (FL) and hindlimb (HL). The total scaled limb lengths show that the bat FL is extremely elongated (**A**). The proportion of each limb region (illustrated by the bat HL) against the total limb length shows that the bat FL autopod is disproportionately larger than that of the other limb types (**B**). The proportion of the stylopod (S) and zeugopod (Z) (**C**) and the zeugopod with the autopod (**D**) show that the distal elements of the bat forelimb are disproportionately longer.

Table 4.1: Statistical analyses used to assign significance to the differences in skeletal element lengths and proportions. Analyses determined the differences between the lengths of the different limb types and elements (One Way ANOVA, scaled length in mm), and the relationships of limb element proportions among the limb types examined (ANCOVA). For the ANCOVA, data are transformed for the stylopod (Log_{10}), zeugopod (SqRt) and autopod (Log_{10}). For all analyses N = 10.

Scaled lengths				
	Bat FL	**Bat HL**	**Mouse FL**	**Mouse HL**
Limb	157.89 ± 2.41	48.19 ± 0.99	26.29 ± 0.47	37.18 ± 0.87
	One Way ANOVA: $F(3,36) = 20776$, $p < 0.001$			
Stylopod	26.15 ± 0.54	20.20 ± 0.27	9.36 ± 0.17	12.27 ± 0.54
	One Way ANOVA: $F(3,36) = 3191$, $p < 0.001$			
Zeugopod	47.44 ± 1.21	19.84 ± 0.57	10.82 ± 0.24	14.28 ± 0.26
	Welch's $F(3,18.658) = 3209$, $p < 0.001$			
Autopod	84.29 ± 1.42	8.14 ± 0.24	6.11 ± 0.20	10.62 ± 0.22
	Welch's $F(3,19.263) = 9665$, $p < 0.001$			
Relative length				
	Bat FL	**Bat HL**	**Mouse FL**	**Mouse HL**
Stylopod	1.245 ± 0.026	1.327 ± 0.004	1.244 ± 0.022	NA
	ANCOVA: $F(3, 35) = 944.98$, $p < 0.001$, partial $\eta^2 = 0.986$			
Zeugopod	3.938 ± 0.345	5.226 ± 0.091	5.245 ± 0.171	5.071 ± 0.085
	ANCOVA: $F(3, 35) = 55.24$, $p < 0.001$, partial $\eta^2 = 0.826$			
Autopod	1.500 ± 0.062	1.008 ± 0.014	1.148 ± 0.035	1.236 ± 0.013
	ANCOVA: $F(3, 35) = 2011$, $p < 0.001$, partial $\eta^2 = 0.994$			

Relative limb element lengths were significantly different among the limb types (Figure 4.3B, Table 4.1). The bat HL stylopod was significantly larger than those of the other limb types tested (bat FL: p = 0.026; mouse FL: p = 0.026), and the proportion of the proximal element lengths (S:Z) were equivalent (Figure 4.3C). The relative length of the bat FL stylopod was smaller that of other comparisons (Figure 4.3B). Though the mouse HL was excluded from the analysis of the stylopod, the proportions of its proximal limb elements lengths were very similar to those of the mouse FL (Figure 4.3B-C). The relative length of the bat HL zeugopod was significantly larger than the bat FL (p = 0.033) and the mouse HL (p < 0.001), but other pair-wise comparisons were not significantly different (Table 4.1). Autopod relative lengths were significantly different amongst limbs (Figure 4.3B, Table 4.1), with the bat FL being larger (mouse FL: p = 0.006; mouse HL: p = 0.008), while the bat HL was significantly smaller than all other autopods (p < 0.001) (Figure 4.3B, Table 4.1). In the mouse, the HL autopod was significantly larger than that of the FL (p = 0.003) (Figure 4.3B, Table 4.1). When examining the relative proportions of the two most distal elements (Z:A) this pattern can clearly be seen, with the bat FL autopod being almost double the length of the zeugopod while the bat HL autopod comprises less than a quarter of this length (Figure 4.3D). These analyses show that in addition to changes in overall lengths, bat limb proportions have diverged from those of the mouse, finding that the autopod of bat FLs is disproportionately longer, while that of bat HLs is disproportionately shorter.

4.2.2. Digit ray elements show asymmetrical elongation in the bat FL and are symmetrical in the bat HL

The 5'HoxD genes are known to affect autopod skeletal element lengths, most notably those of the metacarpals, with loss of function mutants showing that these genes have combinatorial effects (Davis and Capecchi 1996; Delpretti *et al.* 2012). To understand the differences in the skeletal element lengths of bat and mouse limbs, I examined and compared their lengths and proportions among the different limb types, focusing in particular on the metacarpal/metatarsal and an examination of digit ray (D) symmetry.

The skeletal elements of the bat forelimb autopod were dramatically longer than those of the other limb types, with DIII (the longest digit ray in the bat FL) over 10 times longer than that of the bat HL and the mouse FL (Figure 4.4A). The posterior digit rays (DII-V) of the bat FL were unique in this comparison, having lost their most distal phalanx (with DII having lost the last two phalanges, only retaining a shortened, seemingly truncated proximal phalange, P1) (Figure 4.2). All posterior digit ray skeletal elements were longer than those of the other limb types. All bat HL elements were shorter than their counterparts in the mouse HL, with the exception of DV P1 (which was similar in size), DV P2 (which was larger) and P3 of all digit rays (which were larger) (Figure 4.4A).

The lengths of the posterior digit rays of the bat FL were significantly different, with a short DII, highly elongated DIII and successively shorter posterior digit rays (Figure 4.4A, Table 4.2). This asymmetry did not stem from the metacarpals, which had weak differences as compared to those found amongst P1 and P2 elements (all comparisons: $p < 0.001$). In fact, the metacarpals of DII and DIV were not significantly different from one another, and the differences between DII and DIII were weakly supported ($p = 0.044$), while the differences between all other comparisons were strongly supported ($p < 0.001$). In contrast to this, bat HL posterior digit rays were highly symmetrical, with no significant differences found among their lengths (Figure 4.4A, Table 4.2). Interestingly, while the metatarsal of DV was significantly shorter than that of the other digits ($p < 0.001$), P1 and P2 of this digit were significantly longer than their counterparts ($p < 0.01$). Differences between other digit ray elements were small, P1 and P2 elements of digit II were significantly shorter than digit IV ($p < 0.05$) and P2 of digit III was significantly different to that of digit IV ($p < 0.05$). No differences could be found among P3 elements (Table 4.2).

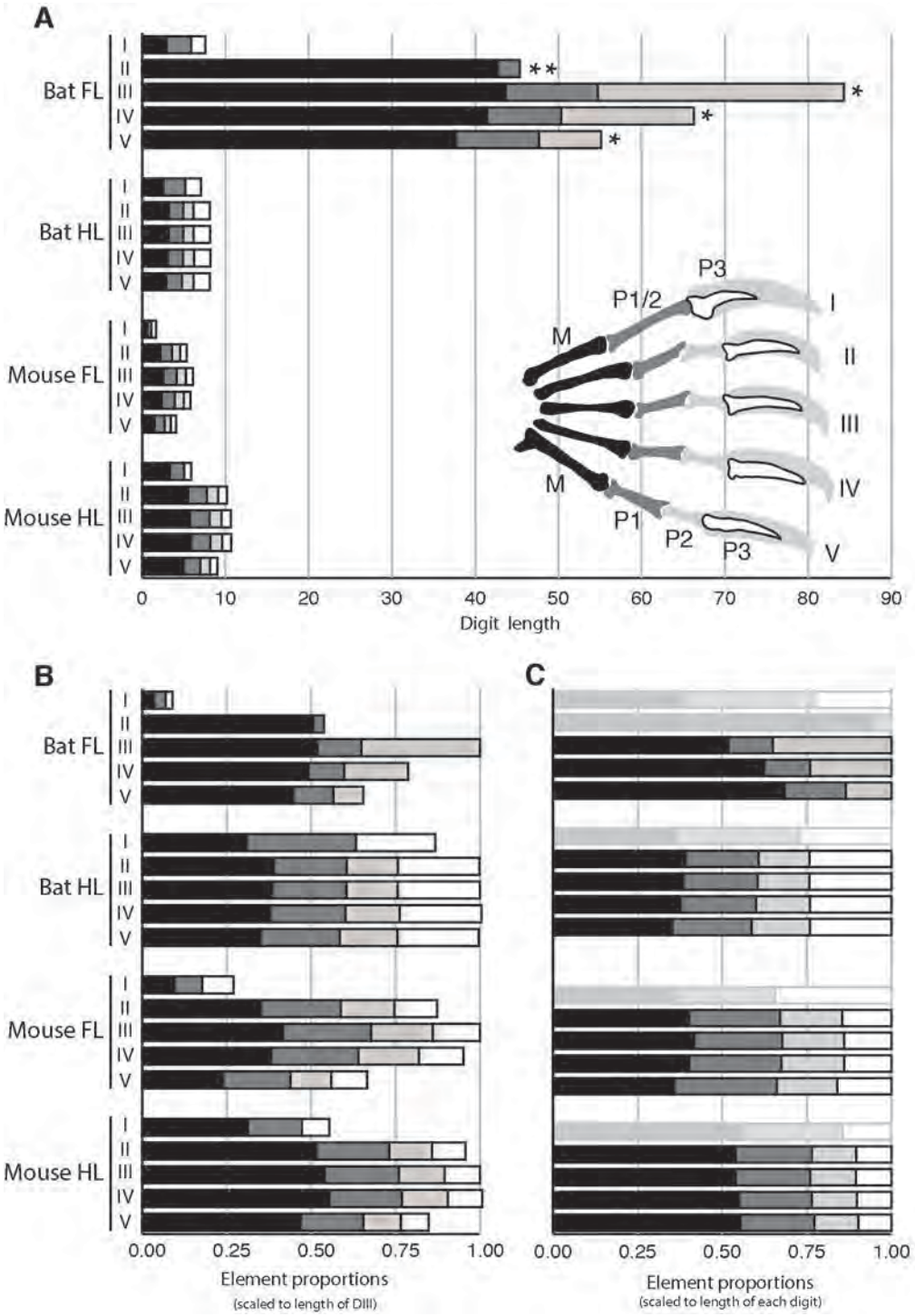

Figure 4.4: Bar graphs of the autopod skeletal element lengths of the bat and mouse forelimb (FL) and hindlimb (HL). The total scaled limb lengths show that the bat FL autopod has dramatically longer skeletal elements (illustrated with a key of the bat HL) (**A**). The proportion of each element against the total digit III length highlights the symmetry found in the bat hindlimb (**B**). The proportion of each element as compared to individual digit lengths shows the loss of symmetry in the bat FL digits (**C**). Digits I (and digit II in the bat FL) greyed out to facilitate comparisons among the more posterior digits. Asterisks indicate phalange loss.

Table 4.2: Statistical analyses used to assign significance to the differences among digit ray lengths. Analyses determined the differences among the digit ray lengths within the different limb types and that of the elements (metacarpal/metatarsal, M; phalange 1, P1; phalange 2, P2; phalange 3, P3). Tests in grey indicate those that did not pass significance testing. For all analyses N = 10.

Digit lengths				
	Digit II	**Digit III**	**Digit IV**	**Digit V**
Bat FL	45.37 ± 0.70	84.29 ± 1.42	66.83 ± 0.97	56.10 ± 0.73
	Welsh: $F(3, 19.55) = 2338.8$, $p < 0.001$, partial			
Bat HL	8.12 ± 0.15	8.15± 0.24	8.18 ± 0.20	8.11± 0.28
	One-Way ANOVA: $F(3, 36) = 0.171$, $p = 0.915$			
Mouse FL	5.33 ± 0.16	6.10 ± 0.20	5.80 ± 0.14	4.06 ± 0.10
	One-Way ANOVA: $F(3, 36) = 329.7$, $p < 0.001$			
Mouse HL	10.16 ± 0.21	10.62 ± 0.22	10.69 ± 0.28	9.00 ± 0.22
	One-Way ANOVA: $F(3, 36) = 112.7$, $p < 0.001$			
Element lengths				
Bat FL	M	One-Way ANOVA: $F(3, 36) = 90.1$, $p < 0.001$		
	P1	One-Way ANOVA: $F(3, 36) = 2208.2$, $p < 0.001$		
	P2	*Welsch*: $F(3, 16.63) = 5116.6$, $p < 0.001$		
Bat HL	M	One-Way ANOVA: $F(3, 36) = 15.1$, $p < 0.001$		
	P1	One-Way ANOVA: $F(3, 36) = 16.6$, $p < 0.001$		
	P2	One-Way ANOVA: $F(3, 36) = 19.5$, $p < 0.001$		
	P3	One-Way ANOVA: $F(3, 36) = 0.491$, $p = 0.691$		
Mouse FL	M	One-Way ANOVA: $F(3, 36) = 419.1$, $p < 0.001$		
	P1	One-Way ANOVA: $F(3, 36) = 82.1$, $p < 0.001$		
	P2	One-Way ANOVA: $F(3, 36) = 62.6$, $p < 0.001$		
	P3	One-Way ANOVA: $F(3, 36) = 50.1$, $p < 0.001$		
Mouse HL	M	One-Way ANOVA: $F(3, 36) = 540.3$, $p < 0.001$		
	P1	One-Way ANOVA: $F(3, 36) = 23.9$, $p < 0.001$		
	P2	One-Way ANOVA: $F(3, 36) = 43.7$, $p < 0.001$		
	P3	One-Way ANOVA: $F(3, 36) = 64.6$, $p < 0.001$		

Mouse autopod digit rays were asymmetrical, with significant differences found between all pairwise comparisons of DII-V (p <0.005) with the exception of between DIII and DIV of the mouse HL. These differences could be attributed to strong differences among all digit ray elements, particularly those of the metacarpals and metatarsals ($p < 0.001$) (Figure 4.4A, Table 4.2).

When controlled for digit size, significant differences were still found among the relative lengths of the metacarpals/metatarsals both within each limb type, and that of DIII among limb types (Figure 4.4C, Appendix C.1). The relative length of the metacarpal/metatarsal followed the same pattern as found for the scaled length of DIII (bat FL > mouse HL > mouse FL > bat HL) with significant differences being found between all pairwise comparisons with the exception of those that included the bat FL (p < 0.001; Figure 4.4C).

To simplify comparisons among limbs and to remove the confounding effect of phalange loss in bat digits, the ratios between the more proximal and the more distal digit elements were examined and compared (M:P1; P1:P2; P2:P3), both within and among limb types. Significant differences were found among proximal digit region proportions (M:P1) within all limb types (Figure 4.5A; Table 4.3). In the bat FL the metacarpal proportion of DII was significantly larger than all other comparisons ($p < 0.001$), DIV was larger than DIII and V ($p < 0.001$), however DIII and V (the longest and shortest metacarpal respectively) were not significantly different. The increased metacarpal proportion for DII was attributed to the overall reduction in this digit ray's length, due to the shortened P1 and loss of P2. Bat HL metatarsal proportions of DII-III were similar, however the proportion of the DV metatarsal was significantly smaller than all other digit rays ($p < 0.001$), while that of DII was slightly, but significantly larger than that of DIV ($p < 0.018$). The strongly asymmetrical mouse FL digit rays had significantly different metacarpal proportions ($p < 0.001$) with the exception of that between DII and IV. In the mouse HL, significant differences were found between DII, with both DIV and DV ($p = 0.001$), while all other digits did not have significantly different metatarsal proportions.

When examining the proximal (P1) and central (P2) phalanges (Figure 4.5B; Table 4.3), the proportions of P1 within the bat FL were significantly different, with the lowest values found in DIII and successively larger values in the more posterior digit rays (IV and V). The proportions of this element were not significantly different among bat HL digit rays and only small differences were found within mouse autopods, with DV of mouse FLs having a significantly larger proportion of P1 than the other digit rays ($p < 0.001$) and the proportion of P1 in DII of mouse HLs being slightly larger than that of DIV ($p = 0.047$) (Figure 4.5B; Table 4.3).

When examining the lengths of the central (P2) and distal (P3) phalanges, proportions were very similar within each limb type (Figure 4.5C, Table 4.3). In the bat HL, P2 was proportionately longer in DV as compared to the other digit rays ($p < 0.05$), and the proportion of P2 in DIV was significantly, if slightly, longer than DIII ($p = 0.033$). In the mouse FL the proportion of P2 in DV was significantly smaller than that of DIV and DIII ($p < 0.05$), and no significant differences were found among these proportions in the mouse HL (Figure 4.5C, Table 4.3.

When comparing the proportions of the all digit ray elements (selected elements that did not have significantly different proportions within a limb type) among limb types, significant differences were found among all comparisons (Figure 4.5, Table 4.3). Metacarpals/metatarsals were all significantly different from one another ($p < 0.001$), following the same relationship among limb types as that of total limb length (bat FL > mouse HL > bat HL > mouse FL). However, the bat FL had

proportionately smaller P1 elements ($p < 0.05$) while those of the mouse HL were significantly larger than all other comparisons ($p < 0.001$) and those of the mouse FL and bat HL were not significantly different. The proportion of P2 in the bat HL was significantly lower than those of the mouse ($p < 0.001$) with no significant differences found between mouse limbs (Figure 4.5, Table 4.3).

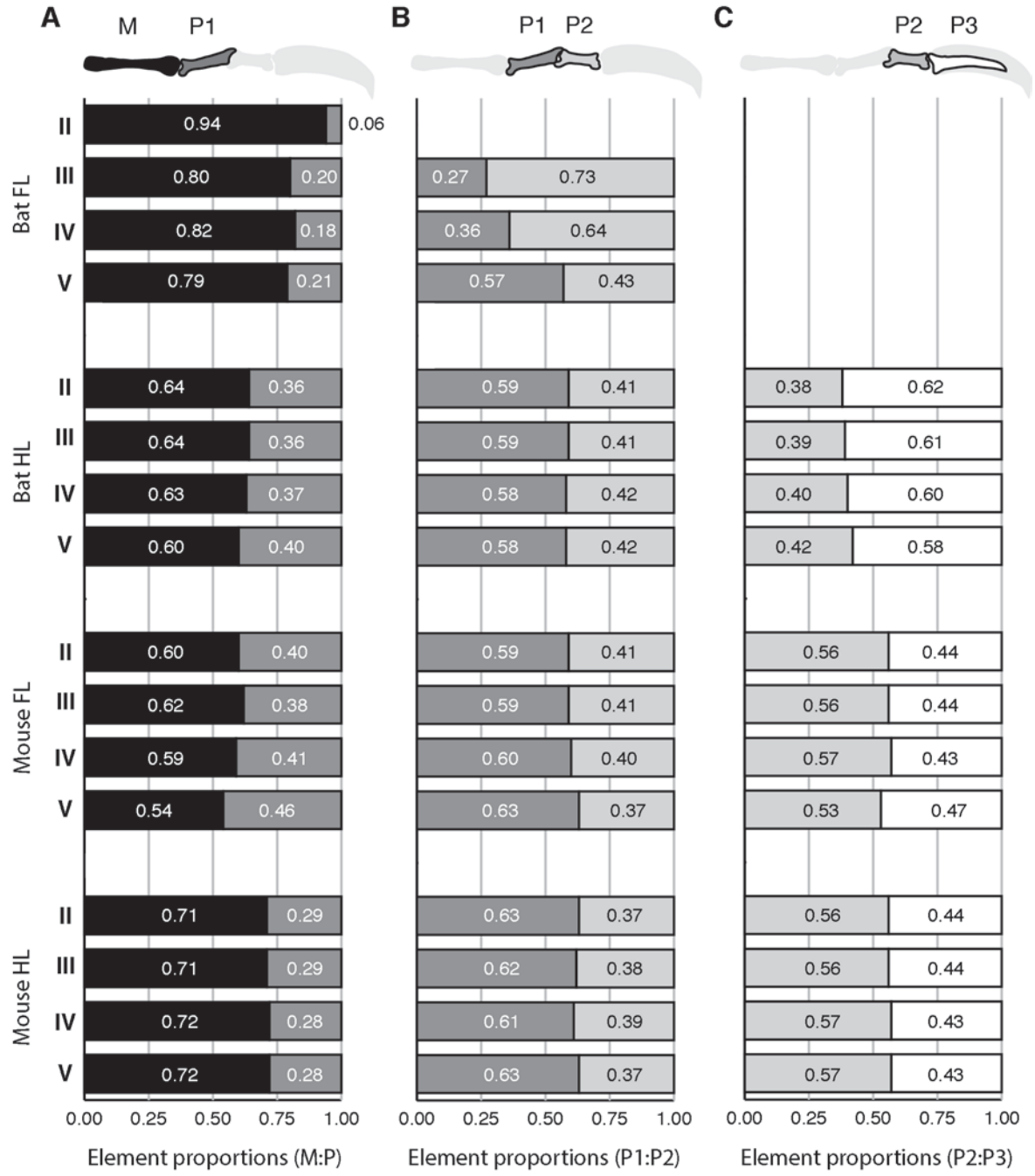

Figure 4.5: Bar graphs of digit II-V skeletal element lengths of the bat and mouse forelimb and hindlimb. Proportions of (**A**) the proximal (metacarpal / metatarsal, M; phalange 1; P1), (**B**) the intermediate (P1 and P2) and (**C**) the more distal (P2 and P3) elements (illustrated with the bat HL digit III). The bat FL digits have asymmetrical and disproportionately elongated central phalanges (P2), while the proportions of the other limb autopods are similar.

Table 4.3: Statistical analyses used to assign significance to the differences in autopod skeletal element proportions. Analyses determined the differences between the proportions of (**A**) the Metacarpals/metatarsals in the proximal digit, (**B**) Phalange 1 in the intermediate digit, and (**C**) Phalange 2 in the distal digit within the different limb types (One-Way ANOVA). For all analyses N = 40. Values in grey did not pass significance testing.

A: Proportion of metacarpal / metatarsal in proximal digit region				
	Digit II	**Digit III**	**Digit IV**	**Digit V**
Bat FL	0.941 ± 0.005	0.798 ± 0.001	0.824 ± 0.002	0.794 ± 0.004
		Welch: $F(3, 17.92) = 2324.33$, $p < 0.001$		
Bat HL	0.645 ± 0.008	0.636 ± 0.008	0.633 ± 0.012	0.600 ± 0.007
		One Way ANOVA: $F(3, 36) = 51.020$, $p < 0.001$		
Mouse FL	0.598 ± 0.008	0.617 ± 0.006	0.596 ± 0.009	0.544 ± 0.006
		Welch: $F(3, 19.24) = 56.107$, $p < 0.001$		
Mouse HL	0.704 ± 0.008	0.712 ± 0.005	0.720 ± 0.011	0.720 ± 0.010
		One Way ANOVA: $F(3, 36) = 9.537$, $p < 0.001$		
B: Proportion of P1 in intermediate digit region				
	Digit II	**Digit III**	**Digit IV**	**Digit V**
Bat FL		0.272 ± 0.003	0.360 ± 0.006	0.572 ± 0.011
		Welch: $F(3, 14.75) = 3850.55$, $p < 0.001$		
Bat HL	0.587 ± 0.102	0.592 ± 0.174	0.581 ± 0.127	0.578 ± 0.122
		One Way ANOVA: $F(3, 36) = 2.201$, $p = 0.105$		
Mouse FL	0.597 ± 0.009	0.587 ± 0.011	0.593 ± 0.013	0.627 ± 0.030
		Welch: $F(3, 19.36) = 5.572$, $p = 0.006$		
Mouse HL	0.633 ± 0.022	0.618 ± 0.014	0.609 ± 0.013	0.627 ± 0.025
		One Way ANOVA: $F(3, 36) = 3.057$, $p = 0.041$		
C: Proportion of P2 in distal digit region				
	Digit II	**Digit III**	**Digit IV**	**Digit V**
Bat HL	0.385 ± 0.013	0.380 ± 0.011	0.398 ± 0.017	0.416 ± 0.014
		One Way ANOVA: $F(3, 36) = 13.353$, $p < 0.001$		
Mouse FL	0.556 ± 0.012	0.567 ± 0.010	0.571 ± 0.017	0.529 ± 0.035
		Welch: $F(3, 19.15) = 5.123$, $p = 0.009$		
Mouse HL	0.558 ± 0.023	0.563 ± 0.022	0.575 ± 0.021	0.570 ± 0.040
		One Way ANOVA: $F(3, 36) = 0.777$, $p = 0.515$		
D: Comparison of proportions among limb types				
	Bat FL	**Bat HL**	**Mouse FL**	**Mouse HL**
M:P1	0.79.6 ± 0.001	0.641 ± 0.009	0.597 ± 0.008	0.708 ± 0.007
		Welch: $F(3, 38.655) = 4592.144$, $p < 0.001$		
P1:P2	0.572 ± 0.015	0.587± 0.014	0.592 ± 0.011	0.626 ± 0.021
		Welch: $F(3, 37.172) = 37.707$, $p < 0.001$		
P2:P3		0.388 ± 0.015	0.565 ± 0.014	0.565 ± 0.022
		One Way ANOVA: $F(2, 89) = 989.659$, $p < 0.001$		

These analyses indicate that the metacarpals of the bat FL are relatively elongated, however the massive asymmetry of the wing appears to be determined by the growth of the P2 elements. In contrast the bat HL metatarsals appear shortened in comparison to the mouse HL and exhibit a relative elongation of DV P1 that results in highly symmetrical digits.

4.2.3. Elements lengths of digit I are different amongst the limb types but their proportions appear similar in bats

Digit ray I has unique element patterning in mammals. It has been suggested to result from a separate developmental module as it experiences a unique Hox gene expression profile during development, with exposure to *Hoxa13* and *Hoxd13*, subsequently experiencing a low dose of HOX activity during its formation and growth (Deschamps 2008; Montavon *et al.* 2008). It lacks a central phalanx with its most proximal phalanx given an intermediate identity (P1/2) (Figure 4.2B). The DI of the bat FL is remarkable as it appears to be unaffected by elongation events that occur in the more posterior digit rays (DII-V) (Figure 4.2C). Though it appears similar in size to that of the bat HL the normalised total lengths of DI, and the lengths of each element were significantly different among all limb types, and can be attributed to differences between each comparison ($p < 0.001$) (Figure 4.6A; Table 4.4).

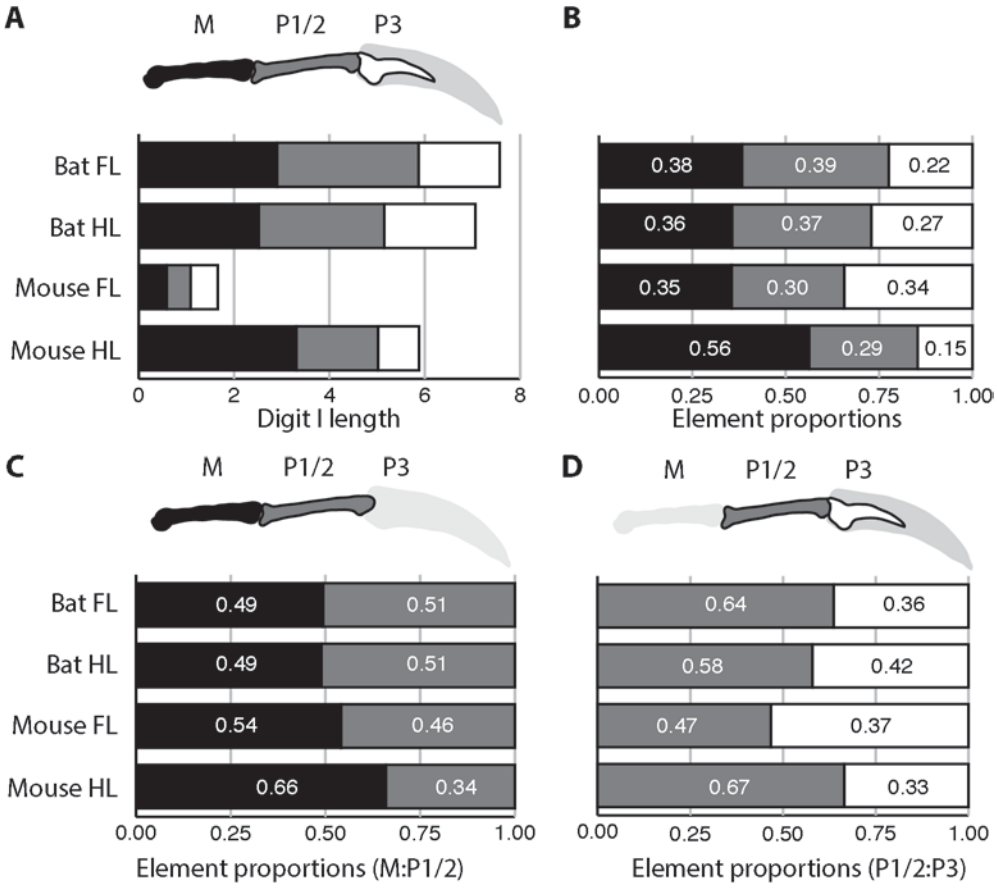

Figure 4.6: Bar graphs of digit I skeletal element lengths of the bat and mouse forelimb (FL) and hindlimb (HL). The total scaled limb lengths show that the bat digits are fairly similar, while the mouse FL digit I is highly reduced (**A**). The proportion of each element, metacarpal/metatarsal (M), phalange (P) against the digit length (illustrated with the bat HL digit I) (**B**), shows that the metatarsal of the mouse HL is elongated in comparison to those of the other digits.

Table 4.4: Statistical analyses used to assign significance to the differences among digit I elements lengths and proportions. Analyses determined the differences between the lengths Digit I (One Way ANOVA, scaled length in mm) both among and within the skeletal elements (Two Way ANOVA). The relationship of Digit I element proportions (One Way ANOVA) of the limb types are also examined. N = 10. Metacarpal / Metatarsal (M); Phalange (P).

		Scaled Length		
	Bat FL	**Bat HL**	**Mouse FL**	**Mouse HL**
Digit I	7.55 ± 0.12	7.15 ± 0.07	1.65 ± 0.15	5.88 ± 0.13
		One Way ANOVA: $F(3,34) = 4665$, $p < 0.001$		
		Scaled Length		
	Bat FL	**Bat HL**	**Mouse FL**	**Mouse HL**
		Two Way ANOVA: $F(4,75) = 406.9$, $p < 0.001$, partial $\eta^2 = 0.958$		
M	2.90 ± 0.11	2.52 ± 0.18	0.58 ± 0.55	3.33 ± 0.07
		Two Way ANOVA: $F(3,108) = 1729$, $p < 0.001$, partial $\eta^2 = 0.980$		
P1/2	2.96 ± 0.10	2.62 ± 0.10	0.50 ± 0.07	1.71 ± 0.06
		Two Way ANOVA: $F(3,108) = 1440$, $p < 0.001$, partial $\eta^2 = 0.976$		
P3	1.69 ± 0.05	1.91 ± 0.09	0.57 ± 0.06	0.86 ± 0.06
		Two Way ANOVA: $F(3,108) = 495$, $p < 0.001$, partial $\eta^2 = 0.932$		
	$F(2,108) = 605.6$ $p < 0.001$ partial $\eta^2 = 0.918$	$F(2,108) = 177.6$ $p < 0.001$ partial $\eta^2 = 0.767$	$F(2,108) = 2.249$ $p = 0.110$ partial $\eta^2 = 0.040$	$F(2,108) = 1831$ $p < 0.001$ partial $\eta^2 = 0.971$
		Proportions		
	Bat FL	**Bat HL**	**Mouse FL**	**Mouse HL**
M	38.22± 0.83	35.33 ± 0.87	35.66 ± 1.00	56.30 ± 1.06
		One way ANOVA: $F(3,33) = 1087.78$, $p < 0.001$		
P1/2	33.33	24.90	11.85	8.17
		Kruskal-Wallis Test: *Statistic* = 30.8, d.f. = 3, $p < 0.001$		
P3	15.50	25.00	34.50	5.50
		Kruskal-Wallis Test: *Statistic* = 35.9, d.f. = 3, $p < 0.001$		

These differences also extended to the element proportions of DI (Figure 4.6B). The most dramatic differences were seen in the comparisons between the mouse DI, with the mouse HL having both the largest and proportionately largest metatarsal elements (Table 4.4). The proportions of P1/2 were not significantly different between bat limbs or between the mouse limbs, but there were significant differences between each intraspecies comparison ($p < 0.05$). Significant differences were found amongst the proportions of P3, with that of the mouse FL being longer than the mouse HL ($p < 0.001$). These data show that while the elements of DI have different overall lengths, those of the bat are the most similar in size and skeletal element proportion, with equivalently sized proximal elements and slightly shortened distal elements.

Overall these data indicate that, not only are the bat FL elements significantly longer than those of the HL and mouse limbs, but that they are not proportional, with distal elements appearing to be more highly elongated than the proximal ones. In addition, digit rays that are elongated in the bat FL autopod (digits II-V) correspond to those that express *Hoxd10*, *Hoxd11* and *Hoxd12*, during autopod formation.

4.3. Strong overexpression of the 5'HoxD genes is found in the bat forelimb as compared to the hindlimb

The co-regulation of the 5'HoxD genes is a central component of their complementary and integrated functionality (Montavon *et al.* 2008, 2011; Reno *et al.* 2008). In the limb and the autopod region the absolute dosage of *Hoxd* gene expression in a specific tissue region is an attribute of their functionality (Davis and Capecchi 1996; Goff and Tabin 1997; Zákány *et al.* 1997; Deschamps 2008; Montavon *et al.* 2008; Delpretti *et al.* 2012). The overexpression of *Hoxd11* in the bat forelimb autopods (FL) as compared to the hindlimb autopods (HL) suggests that neighbouring HoxD genes are similarly differentially expressed.

To validate the microarray results (Mason 2009) and explore the expressions of the 5'HoxD genes, I directly compared expression levels of *Hoxd10*, *Hoxd11*, *Hoxd12* and *Hoxd13* in the bat CS17 FL autopods to those of equivalently staged E13.5 mouse FL autopods. I included an associated 5' neighbouring gene, *Lunapark* (*Lnp*), situated 5' of the HoxD cluster (Figure 4.1) (Spitz *et al.* 2003), in this analysis to determine whether its expression was also differentially regulated in bat forelimbs and hindlimbs in character with its co-regulation and association with this 5'HoxD regulatory complex. Furthermore, to characterise the expression of these genes in *M. natalensis* I asked the question whether the 5'HoxD genes were differentially expressed in bat autopods across four bat developmental stages (CS15, CS16, CS17, CS18). In addition I quantified the absolute level of abundance for these transcripts in developing bat autopods to understand their contribution to HOX activity in this region.

4.3.1. Hoxd10 and Hoxd11 and Lnp have higher transcript abundance in the bat FL as compared to the mouse FL and are differentially expressed in bat limbs

In agreement with the microarray data, the relative expression levels of *Hoxd11* were higher in the CS17 bat FL as compared to the mouse E13.5 FL (Figure 4.7C & G). Significant upregulation was also found for *Lnp* (Figure 4.7F). While microarray data indicated significant upregulation of all 5'HoxD in the bat CS17 FL, this was not confirmed by the qPCR data (Figure 4.7). Strong fold differences were found for *Hoxd10* (2.4 fold higher in the bat FL), while *Hoxd11* (6.5) and *Lnp* (6.6) had the greatest fold differences between bat FLs and mouse FLs, (Figure 4.7G). Small fold differences were found for the more 5' genes (*Hoxd12*: 1.1, *Hoxd13*: 1.5). *Hoxd10* and *Hoxd11* were also over expressed in the CS16 and CS17 bat FL in comparison to their hindlimbs. While significant differences between bat limbs were found for *Hoxd12* (CS16) and *Hoxd13* (CS17), these were modest.

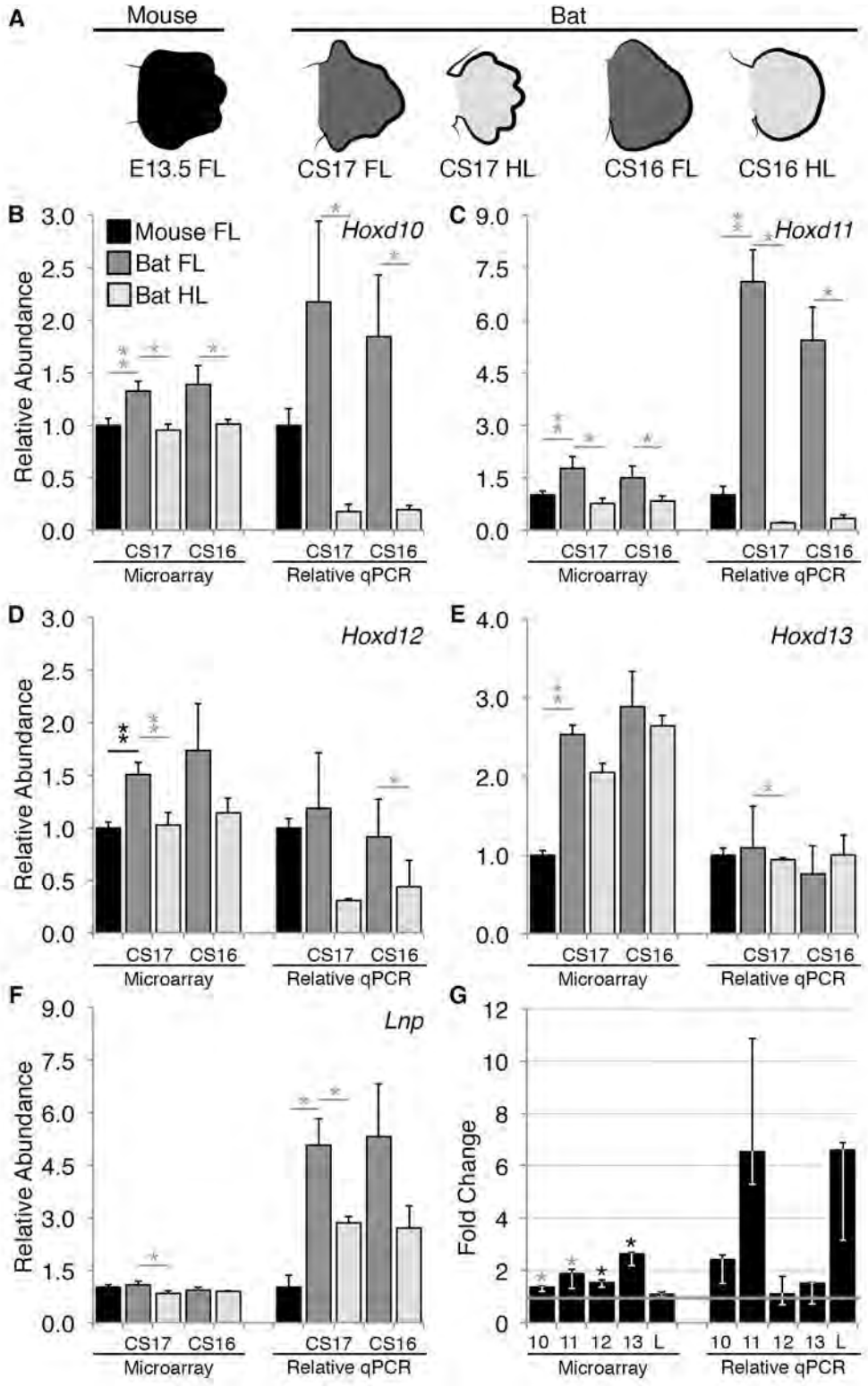

Figure 4.7: Comparisons between the relative abundance of 5'HoxD and *Lnp* transcripts in the microarray analysis as compared to the qPCR experiments. Mouse E13.5 forelimbs (FL) were compared to CS17 bat FL and hindlimbs (HL) with an additional stage of bat development (CS16) included. Microarray (N = 4) and qPCR (N = 3) data are presented as averages with positive error bars representing the standard errors. Fold changes are given as medians; Positive and negative error bars representing the maximum and minimum fold change respectively. Asterisks indicate significance (* $p < 0.05$, ** $p < 0.005$, Appendix C.2-C.3) with those in grey not passing correction for multiple comparisons.

4.3.2. *Hoxd10 and Hoxd11 are up-regulated in the bat FL and Hoxd10, Hoxd11 and Hoxd12 are down-regulated in the bat HL during stages of digit formation*

The transcript abundance of these genes was examined over four sequential stages of bat limb development (Figure 4.8A), finding that from CS15, *Hoxd10*, *Hoxd12* and *Hoxd13* transcripts progressively increased in the FL, with the highest transcript abundance at CS17, dropping at CS18 (Figure 4.8B, D-E). *Hoxd11* had the highest transcript abundance at CS15; this peaked slightly at CS17 (Figure 4.8C). In the HL transcripts decreased from CS15 onwards for *Hoxd10* and *Hoxd11*, while for *Hoxd12* and *Hoxd13* these rose at CS16, and decreased over later stages of development (Figure 4.8B-E). These data corresponded to high fold differences for *Hoxd10* and *Hoxd11* at all stages examined (Figure 4.8G). These differences in the limb type and stage wise expression patterns were only significant for *Hoxd10* (Two-way ANOVA: $F(3,16) = 4.66$, $p = 0.016$, partial $\eta^2 = 0.467$), where the FL samples had significantly different expressions, with significant differences being found between the FL and HL at each stage tested ($p < 0.05$) (Figure 4.8B).

For all 5'HoxD genes, fold differences were greatest at CS17 (Figure 4.8G). *Hoxd10* was over 6 fold higher in the CS16FL and over 11 fold higher in the CS17 FL, while *Hoxd11* was over 12 fold higher in the CS16 FL and over 28 fold higher in the CS17 FL (Figure 4.8G). Though *Hoxd12* transcripts were also more abundant in the FL autopods, these fold differences were relatively moderate, with transcripts over 2 fold higher in the FL (Figure 4.8G). *Hoxd13* did not show strong differences in transcript abundance between the FL and HL autopods, with the median fold difference ranging from 1 (CS18) to 1.6 (CS15 and CS16) (Figure 4.8G) (Appendix C.4).

The profile of *Lnp* transcript abundance appeared unique, with upregulation in both the FL and HL samples from CS15 to CS16, similar transcript abundance from CS16 to CS17, and then a drop at CS18. These differences were not significant, although *Lnp* transcripts were more abundant in the FL as compared to the HL at all stages (Figure 4.8F). Fold differences were greatest at CS15 with these differences decreasing as development progressed (Figure 4.8G).

Overall, the FL autopods had significantly higher transcript abundance than the corresponding HL autopods for all genes examined. This difference was highly significant for *Hoxd10*, *11*, *12* and *Lnp* (Related Samples Sign test: -3.18, N = 12, $p < 0.001$) and weakly significant for *Hoxd13* (Related Samples Sign test: -2.02, N = 12, $p = 0.039$).

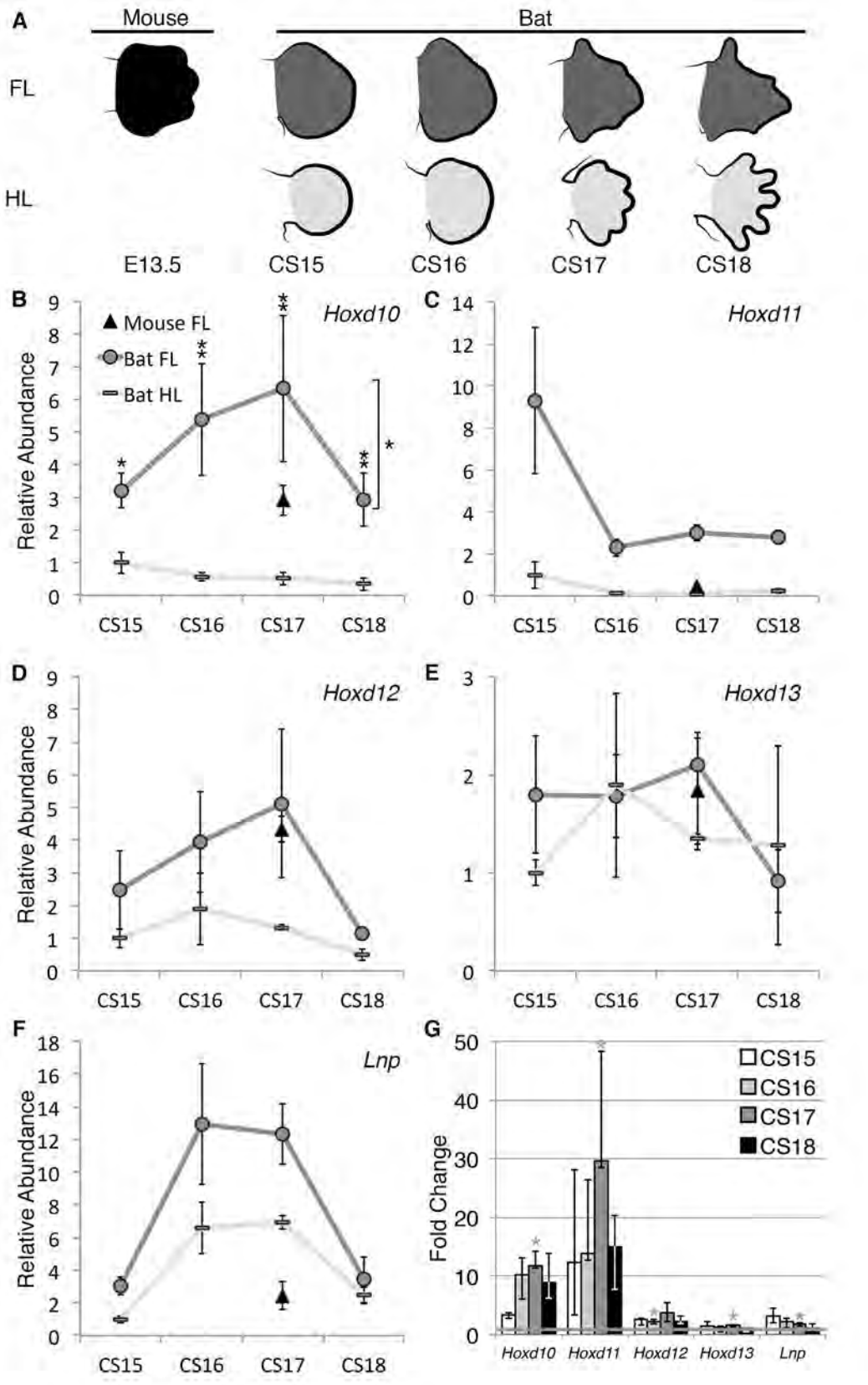

Figure 4.8: Relative expression levels of 5'HoxD and *Lnp* transcripts in bat forelimbs (FL) and hindlimbs (HL) over developmental series (CS15 - CS18). Data are the average of 3 biological repeats with the standard errors given. Fold changes are median values with error bars representing the maximum and minimum fold change. Asterisks denote significance (* $p < 0.05$, ** $p < 0.001$; Appendix C.3), with those in grey not passing correction for multiple comparisons.

4.3.3. A break in quantitative collinearity is found for Hoxd10 in both the bat forelimb and the hindlimb

The finding that *Hoxd10* and *Hoxd11* were overexpressed in the CS17 bat forelimb as compared to the E13.5 mouse, while the expression of *Hoxd12* and *Hoxd13* expressions were equivalent has interesting implications for the regulatory strategy of this cluster in the bat. In the mouse these genes are tightly co-regulated. In E13.5 distal digit tissues, their expressions have a specific and robust relationship, with highest expression of *Hoxd13*, intermediate expression of *Hoxd12* and *Hoxd11* (~35% of *Hoxd13* expression), and low expression of *Hoxd10* (~10%) (Montavon *et al.* 2008).

To determine the relationship among the 5'HoxD genes in bat autopods at each stage of development, their absolute transcript abundances were measured using a calibrated standard curve. Data confirmed those presented previously, with the exception that *Hoxd13* was not significantly differentially expressed between the FL and the HL in these analyses (data not shown). Absolute quantification determined that *Hoxd10* was the most abundant 5'HoxD gene at all stages of development. *Hoxd10* expression was significantly higher than that of *Hoxd11* at all developmental stages and significantly higher than *Hoxd12* at CS15, CS16 and CS18 ($p < 0.05$) (Figure 4.9A-B; Appendix C.5-C.6).

The relationship among the expressions of these genes was similar in all limb samples, with lowest expression of *Hoxd11*, higher expression of *Hoxd12* then *Hoxd13* and highest expression of *Hoxd10* (Figure 4.9A-B). These relationships were examined by looking at the fold change between each gene's transcript abundance and that of *Hoxd13* for both the FL and HL samples (Figure 4.9C, Appendix C.7). This illustrated the loss of quantitative collinearity of *Hoxd10*, which had a transcript abundance that was ~10 fold higher than that of *Hoxd13* in the bat FL at CS15, CS16 and CS17 and over 17 fold higher at CS18. Fold differences were smaller in the HL where *Hoxd10* was only 4 fold higher at CS15, 2 fold higher at CS18 under 2 fold higher at CS16 and CS17 (Figure 4.9C, Appendix C.7).

In contrast, *Hoxd11* and *Hoxd12* did appear to follow the established quantitative collinear relationship with *Hoxd13*. *Hoxd12* had moderately lower transcript levels (~3 fold lower in the FL and between 3.3 to 9.0 fold lower in the HL), while those of *Hoxd11* were dramatically lower. *Hoxd11* transcript levels in the FL were ~15 fold lower than that of *Hoxd13* at CS15 and CS18 while at CS16 and CS17 it was over 25 fold lower (Figure 4.9C). These fold differences were larger in the HL with the smallest median fold change found in CS15 (-64.2) and the largest found at CS17 (-449.5) with these value varying widely among biological replicates (Figure 4.9C, Appendix C.7).

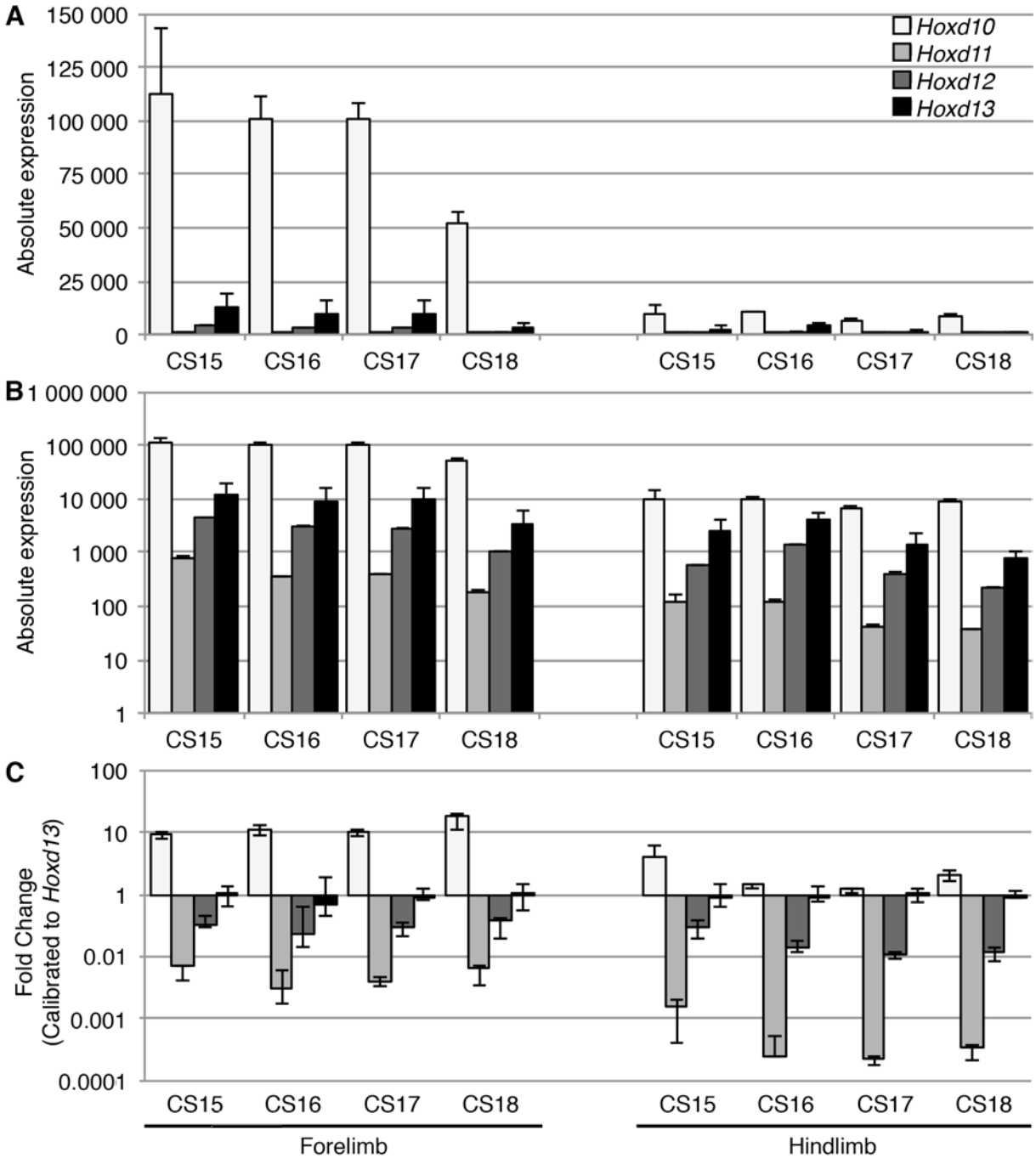

Figure 4.9: Absolute expression (copies/reaction) of the 5'HoxD genes. These show the high abundance of *Hoxd10* (**A**) and, when shown on a logarithmic scale, the quantitative collinear expression of *Hoxd13*, *Hoxd12* and *Hoxd11* (**B**). This relationship is highlighted when the absolute expressions are shown relative to that of *Hoxd13*.

4.3.4. *Verification of Hoxd10 expression*

The massive overexpression of *Hoxd10*, relative to the other 5'HoxD genes was unexpected, as these data do not align with the model of quantitative collinearity, as described in the mouse (Montavon *et al.* 2008). Additionally, recently published data that examined gene expression in developing *M. schreibersii* autopods found relatively low normalised read counts for *Hoxd10* in comparison to the other 5'HoxD genes (Wang *et al.* 2014). The *M. schreibersii* dataset was re-examined to confirm and compare expressions of these genes, including that of *Hoxd9*. Normalised read counts do not take into account contig size differences, potentially introducing read coverage biases amongst genes. This was taken into account by normalising the read counts to contig size to allow for a comparison among these genes. While this calibration to contig size did result in a reduction of the differences in the normalised read counts between *Hoxd10* (which had the smallest contig size) and the other 5'HoxD genes (which had larger contig sizes), this gene still had very low values relative to that of *Hoxd13* (Figure 4.10).

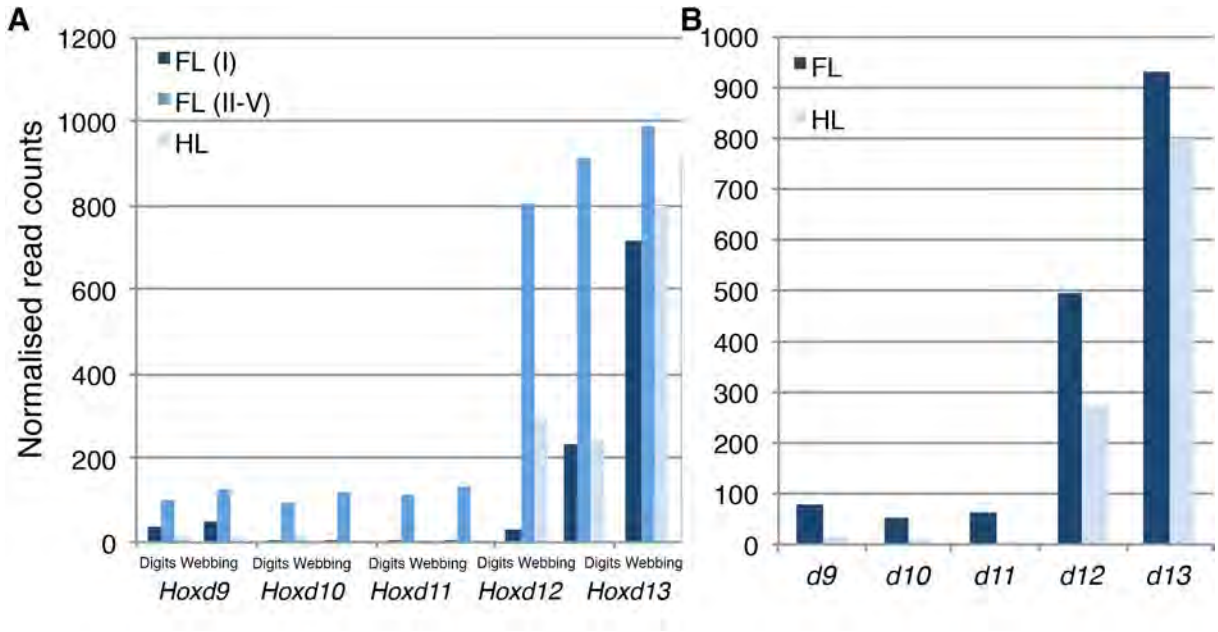

Figure 4.10: RNA-seq normalised read counts for the bat, *M. schreibersii* for genes in the 5'HoxD cluster. Normalised read counts were obtained for digit and webbing tissue, for the FL (dark blue indicates digit I or webbing associated with digit I, blue indicates digits II-V and the webbing associated with digits II-V) and the HL (light blue). These data show that *Hoxd9-11* were expressed at very low levels as compared to *Hoxd12* and *Hoxd13*. Normalised read counts have been normalised to their respective contig size. Data extracted from the GEO dataset (GSE50699) of Wang et al. (2014).

It must be noted that these two datasets are not equivalent. The qPCR data originated from whole autopod tissues, measured at distinct developmental stages (CS15, CS16, CS17 and CS18) while the RNA-seq normalised read counts originated from distinct tissues (digital and interdigital) within pooled autopods (pooled FL: 2x CS15, 1x CS16L and 5x CS17; pooled HL: 1x CS16L and 5x CS17). As

such, these data are not expected to replicate one another, but were expected to correspond to some degree.

The dramatic inconsistency between the qPCR and RNA-seq data for *Hoxd10* transcript abundance was not due to incorporation of technical errors, either in qPCR wet-work (sample, preparation, amplification, calibration standards preparation) or in computation (calibration and data analysis). Sample contamination (either by DNA or by amplicons) would be expected to result in either a uniform background of contamination across samples, or increases in some samples. Instead, biological repeats had values that were fairly similar, while samples varied among stages with the greatest differences being found between the FL and the HL for these data. Checks of post-run reports (QIAgility Pipetting Robot) indicated that the qPCR sample preparations were consistent between runs (data not shown). The quantified standard curves of *Hoxd10* did show high variations for the lowest dilution (1×10^2), and had slightly higher Cq values than those of the other genes. However, these samples did not deviate from expected values and had a comparable performance to that of the other *Hox* genes examined (Appendix C.8). The raw Cq values of the *Hoxd10* samples corresponded (inversely) to those of the calibrated data, with the much lower Cq values indicative of the relatively higher target abundance in this sample (Appendix C.8). It should also be noted that this relationship was also found for independently performed relative qPCR experiments. This indicates that sample calibration and data analysis steps did not incorporate errors into the dataset that would account for the large differences found in the *Hoxd10* dataset.

SYBR green qPCR technology is prone to mis-amplification of products and careful primer design is required to avoid this issue (Bustin *et al.* 2009). When designed and tested, *Hoxd10* primers were found to meet all criteria for target specificity. A 146 bp amplicon, corresponding to the *Hoxd10* locus, was the only hit found for *in silico* PCR in *M. lucifugus* (Broad Institute Myoluc2.0/myoLuc2, GL429772: 7095400-7095545), *P. vampyrus* (Broad/pteVam1, scaffold: 488:119073+119218) (UCSC Genome Browser), *M. musculus* (GRCm38/mm10, chr2: 74694210+74694355) and *H. sapiens* (GRCh37/hg19, chr2: 176983801+176983946) (UCSC Genome Browser). Sequences annotated as *Hoxd10* were the only targets identified through primer-BLAST (Appendix C.9; NCBI, Ye et al. 2012).

In all experimental runs the *Hoxd10* qPCR product had melt curves that produced a single sharp peak (86.4 °C, min = 86.0 °C, max = 86.6 °C), matching those of the standards (confirmed homogenous *Hoxd10* amplicon) (Table 2.3 and Table 2.4). This product was visualised as a single band of the expected size (146 bp) on a 2% agarose gel, and when sequenced it was confirmed to be that of *Hoxd10*, indicating that *Hoxd10* transcript targets were amplified by qPCR.

Hox gene paralogs are highly similar and, due to the lack of available bat sequence at the time of design, the *Hoxd10* qPCR primers amplify a conserved region that encompasses the homeobox, with the result that the mis-amplification of a *Hox10* paralog would produce a highly similar amplicon that may not be discriminated in gel or melt curve checks. To explore this possibility, *Hox10* paralog sequences (*M. schreibersii,* Wang *et al.* 2014) were aligned to that of the *Hoxd10* amplicon (Table 4.5, Appendix C.10). While *Hoxa10* and *Hoxc10 in silico* amplicons had the same size and a fairly high sequence similarity to that of *Hoxd10*, they had a large number of total mismatches over the primer binding regions (Table 4.5). The predicted melt peak of *Hoxc10* was much lower than that of *Hoxd10* excluding this product as a potential amplicon, however that of *Hoxa10* was fairly similar (Table 4.5). *Hoxa10* was excluded as a potential mistarget based on RNA-seq normalised read counts (*M. schreibersii,* Wang *et al.* 2014), which were low and not differentially expressed (Figure 3.15).

Table 4.5: Summary of aligned *Hox10* sequences from *M. schreibersii*. The predicted amplicon size, amplicon sequence similarity and number (#) of nucleotide differences for regions of interest are given. Predicted melting temperatures were given for each sequence. These were generated using uMELT v2.0.2 (Unified SantaLucia; $Mono^{+}$ = 10; free Mg^{++} = 1, DMSO = 0%) (Dwight *et al.* 2011).

Gene	Sequence name	Size (bp)	Similarity (%)	No. of Differences			Melt (°C)
				Amplicon (/146)	Fwd (/20)	Revs (/19)	
Hoxa10	comp913_c0_seq5/7	146	80.8	28	3	4	86.5
Hoxc10	comp13621_c0_seq1	146	80.8	28	5	6	83.0
Hoxd10	comp294_c0_seq2	146	99.3	1	0	0	87.0

The *M. schreibersii* RNA-seq sequence database (Wang *et al.* 2014) was examined to determine if an alternative bat transcript existed with the potential to be amplified using the *Hoxd10* primer set. The top BLAST (blastn, Max EVal = 10) hit for both primers corresponded to regions within a 7 977 bp 'unmatched sequence', comp294_c0_seq2 (Fwd interval: 7 834 – 7 816; Rvs interval: 7 689 – 7 708; Eval < 1e-02; Pairwise identity = 100%; Grade = 75%, Query coverage = 100%). This sequence was also the top hit found when the canonical mouse *Hoxd10* sequence and the *Hoxd10* qPCR amplicon were used as the BLAST query sequence (Eval = 3e-07; Pairwise identity = 99.3%; Grade = 99.7%, Query coverage = 100%). A BLAST analysis (blastn) of the full sequences of comp294_c0_seq2 against the Chiroptera (taxid:9397) nucleotide collection (nr) database revealed that the majority (1484-6525; 63% query cover) of this sequence matched to *splicing factor proline/glutamine-rich* (*Sfpq*), predicted mRNA for *M. davidii* (1257-6278; XM_006777411.1; 92% identity). The top five hits matched this gene (data not shown), while the sixth hit matched to a short region (400bp; 7557-7957; 5% query cover), that when extracted could be annotated as *Hoxd10*, predicted mRNA for *Eptesicus fuscus* (952-1352; XM_008138530.1; 97% identity), and subsequent hits for this specific region annotated as

Hoxd10 in several bat species. These findings indicate that some read counts for the transcript sequence of *Hoxd10* in the *M. schreibersii* dataset have been misincorporated into alternative contigs. This may be due to the *de novo* assembly of this RNA-seq dataset, and this may result in an underestimation of the transcript abundance for this dataset. *De novo* sequence assembly may present a specific problem for *Hox* paralogs, as these have high sequence similarities, particularly for the region encompassing their homeobox.

In summary, the incongruences between the qPCR data for *M. natalensis* and the RNA-seq data for *M. schreibersii* were not due to experimental errors in the qPCR measurements. Underestimation of the transcript abundance for this gene may have occurred in the RNA-seq dataset through the mis-incorporation of reads into alternative transcripts. In addition, it must be noted that differences in sampling strategy, may also underlie these differences.

4.4. The 5'HoxD genes have unique expressions in the bat forelimb and hindlimb

In the previous section I examined the relative and absolute expressions of the 5'HoxD genes in the autopod of bat forelimbs and hindlimbs. I have shown that there was strong overexpression of *Hoxd10*, *Hoxd11* and *Hoxd12* in the bat forelimb (FL) as compared to its hindlimb (HL). In addition, comparisons with an equivalently staged mouse forelimb revealed that *Hoxd10* and *Hoxd11* were over expressed in the CS17 bat forelimb. Absolute quantification of these four genes revealed that there is a massive overrepresentation of *Hoxd10* transcripts as compared to the neighbouring 5'HoxD genes. In this section I complement the previous analysis by examining 5'HoxD gene expression patterns in developing bat autopods to understand their spatio-temporal dynamics. What follows is a description of the expression pattern of these genes in the different limb types, similarities between the patterns of expression are highlighted and differences noted.

4.4.1. Expression of 5'HoxD genes during early limb bud outgrowth and autopod formation is similar between the FL and the HL of the bat

I examined the expression pattern of the 5'HoxD genes in early stages of bat limb bud outgrowth and early autopod formation (CS14E-CS15) to determine whether these patterns and progression of expression in the bat differed from that described for the mouse and to understand how the differences in the levels of transcript abundance, seen at CS15, are established. Over these stages of limb bud outgrowth and autopod formation, the HL lags behind the FL in terms of its development (Hockman *et al.* 2008). As such, expression patterns should not be directly compared between the FL and the HL between these early stages.

Prior to autopod formation in the bat (CS14E), the FL showed strong expression of *Hoxd10* in the distal limb bud that was restricted distally in the anterior half, extending proximally to the trunk of the embryo in the posterior half (Appendix C.11). The expression pattern of *Hoxd11* was similar, it was concentrated in the posterior-distal portion of the FL bud with the proximal boundary expression nested within that of *Hoxd10* (Appendix C.15). *Hoxd12* expression differed from that of these more 3' genes. It was posteriorly restricted, extending from the distal limb to the embryonic trunk. Expression was strongest in the distal tip, becoming weaker in the proximal portion (Appendix C.13). *Hoxd13* expression was limited to a focused region of the posterior-distal CS14E FL bud (Appendix C.14), and appeared to be nested within that of the more posterior HoxD genes. For all genes, expression was strongest in the posterior-distal portion of the limb bud, diminishing proximally.

At a slightly later stage (CS14) the FL extends outwards with the distal region forming a very slight bulge along it's A-P axis (Figure 4.11A A). Expressions of *Hoxd10* and *11* remained indistinguishable (Figure 4.11A A-B). Two distinct domains of expression became evident, a proximal domain that corresponded to the 'early-phase' of HoxD expression and a distal domain that corresponds to the 'late-phase' of 5'HoxD expression. The proximal expression domain arcs from the anterior half (beginning mid-way between the proximal and distal ends) to the posterior half of the limb (ending at the juncture between the limb bud and trunk) with diffuse expression seen in the centre of the limb bud. Distal expression was focused in the posterior-distal portion of the limb as a strongly expressed, semi-circle of expression. This appeared larger on the ventral surface of the bud but appeared to be more restricted than found in the comparative mouse limb (Figure 4.11B A-B). A clear stripe of signal-free tissue separates these two domains as in the mouse. *Hoxd11* had strong signal for both proximal and distal domains at this stage, while the signal for *Hoxd10* was more intense in the distal domain (Figure 4.11A A-B). Unlike *Hoxd10* and *Hoxd11*, *Hoxd12* had only a single domain of strong expression at CS14 (Figure 4.11A C). This was localised to the posterior half of the proximal bud, swept anteriorly, covering the majority of the distal bud, and was excluded from the most anterior portion. Though this sample may be slightly earlier than that of the mouse in terms of its development, these two regions were not clearly separable slightly later in development (CS14L).

At this later stage, expression remained excluded from the anterior edge of the bud, becoming focused in the distal-posterior portion with more proximal expression becoming lost. *Hoxd13* expression was not examined at CS14 (as the distal portion of the FL was damaged during processing), expression was still found in the posterior portion of the proximal limb bud but was weak and did not extend proximally as did *Hoxd12* (Appendix C.13**).** By CS14L, strong distal expression was evident across the autopod regions, this domain of expression had a posterior bias and was strongest in the posterior-distal portion of the limb bud, with a proximal boundary that appears nested within that of *Hoxd12* (Appendix C.13**)**. There was a slight extension of weak anterior-distal *Hoxd13* expression as compared to the more 3' genes, but *Hoxd13* also appeared to be restricted from, or very weakly expressed in, this portion of the limb at this stage. In a slightly older embryo of this stage, the proximal boundary of distal *Hoxd13* expression was lost over the region where digit IV forms. This loss in expression was evident from both a dorsal and a ventral perspective (Appendix C.13**)**. A distinct region of expression was also found on the posterior edge of the limb bud, adjacent to the most proximal-posterior boundary of the distal expression domain.

At early CS15 the A-P axis of the distal FL bud expands, but the bud remains fairly symmetrical. The posterior expression domains of *Hoxd10* and *Hoxd11* extended from the anterior to the posterior portion in a curve (arrow-shape) that was more extensive than found in the mouse (Figure 4.11A E-F, Figure 4.11B E-F Appendix C.11-C.12). Expression was strongest in the distal domain, and was concentrated in the distal edge of the autopod and extended proximally into the posterior portion. This expression domain appeared larger on the ventral surface, and expression became lost over the region where digit IV forms. At this stage, diffuse proximal *Hoxd12* expression was evident, with distal expression appearing strongest in the regions where the presumptive digits form (Appendix C.13). Strong expression of *Hoxd13* was found in the region of digit IV and its expression appeared to extend anteriorly (Figure 4.11A E-F, Appendix C.11-C.12)**.**

By CS15 the posterior half of the distal bud is broader than that of the anterior half. Proximal expressions of *Hoxd10* and *Hoxd11* occurred in the zeugopod as a large anterior domain that did not extend to the edge of the limb, and a smaller posterior domain, that did. (Figure 4.11A E-F). Distal expression was triangular; its base extended along the distal edge of the autopod and narrowed proximally. This domain extended along the posterior edge of the autopod and became weaker proximally. As the FL becomes progressively more asymmetrical, this triangular domain became more distinct, with strong signal along the distal edge (Appendix C.11-C.12). Slight differences, particularly along the posterior edge of the distal limb, were found among biological repeats (and between *Hoxd10* and *Hoxd11* expressions) at this stage, possibly attributable to technical variations. Based on these results, *Hoxd10* and *Hoxd11* are likely to be weakly expressed this region. Proximal and distal domains of *Hoxd12* became distinct in the CS15 FL autopod (Figure 4.11A F). Proximal domain expression was weak, found on the proximal-posterior margin, which joined a diagonal 'stripe' of expression that extended anteriorly and then distally to meet the distal domain of expression. Distal domain expression extended from the posterior margin of the proximal autopod, across the autopod, appearing to be excluded from (or much weaker in) the anterior portion where the presumptive digit I forms. Expression was strongest in the interdigital tissue between presumptive digits III and IV, and the no distinct 'triangular' domain was found. At this stage, *Hoxd13* expression extended from the anterior edge of the autopod to the posterior edge (presumptive digit I to V). Though strongly expressed across the entire autopod, an intense domain of expression was visible in interdigital tissue between digits III and V, strongest in the distal portion of the autopod (Figure 4.11A H**)**. In equivalently staged mice, digits II-IV were visible as regions of reduced 5'HoxD gene expression, and expression was localised to the more proximal regions of the interdigits. Though *Hoxd11* and *Hoxd12* expressions did appear more restricted (over digits II-IV), the strong triangular domain of distal expression was not evident.

Expressions of the 5'HoxD genes appeared altered at several stages of early HL development. At CS14E, *Hoxd10* and *Hoxd11* expression occurred in a small, domain, restricted to the posterior-distal portion of the limb bud, and did not extend to the trunk of the embryo (Appendix C.11-C.12). *Hoxd11* was more distally restricted. Expression of *Hoxd12* could not be described (due to sample loss) and *Hoxd13* expression was not evident (Appendix C.14). At CS14, *Hoxd10* and *Hoxd11* expression domains expand, appearing strongest on the ventral surface, with a clear domain of more proximal and posterior expression (Figure 4.11A A'-B', Appendix C.11-C.12). This single domain of expression appeared to separate with the appearance of a region of low to no *Hoxd10* expression that extended from the centre of the posterior edge of the distal limb to a midpoint in the distal limb bud (Appendix C.11). *Hoxd12* expression was found in the posterior-distal domain, weakly extending to the trunk (Figure 4.11A C'). By CS14L this proximal domain of expression was indistinct, however the posterior-distal domain of expression remained strong, and was clearly excluded from the most anterior portion of the distal limb bud (Appendix C.13). At CS14, *Hoxd13* expression was seen in the posterior-distal tip of the limb bud (Figure 4.11A D'). This domain expanded posteriorly (CS14L), maintaining a slight posterior bias (Appendix C.14). At CS15E, the limb bud has grown outwards. *Hoxd10* and *Hoxd11* expression domains separate along the posterior half of the limb bud, but appeared to merge along the anterior edge (Appendix C.11-C.12). The domain of distal *Hoxd12* expression become larger, and remained excluded from the anterior region (Appendix C.13). Signal for *Hoxd13* extended in a crescent from the anterior to a broad posterior domain in the distal limb bud (Appendix C.14).

At CS15E, *Hoxd10* and *Hoxd11* had strong proximal expression (Figure 4.11A E'-F') that curved downwards from the anterior to the posterior edge, meeting a small posterior region of strong expression. Uniform distal expression extended across the anterior to the posterior region. At later stages (CS15) expression remained uniform across the distal limb bud and was not excluded from the anterior portion (where presumptive digit I will develop). On formation of the HL autopod, the proximal and distal expression domains were completely separated. At later stages, the distal expression domain appeared symmetrical, with slightly weaker signal in the posterior region (Figure 4.11A E'-F'). It is interesting to note that in a slightly advanced embryo of this stage, expression in the HL appeared faint (Appendix C.11-C.12). *Hoxd12* maintained a diffuse stripe of very weak proximal expression. The distal expression domain was still strong, had a posterior bias and appeared weaker in the anterior margin where presumptive digit I forms (Figure 4.11A G'). *Hoxd13* had a strong and uniform signal across the distal domain, with broader and more proximally extended posterior expression. Expression becomes lost in the proximal boundary, where digit IV forms, with diffuse expression seen at this interface (Figure 4.11A H').

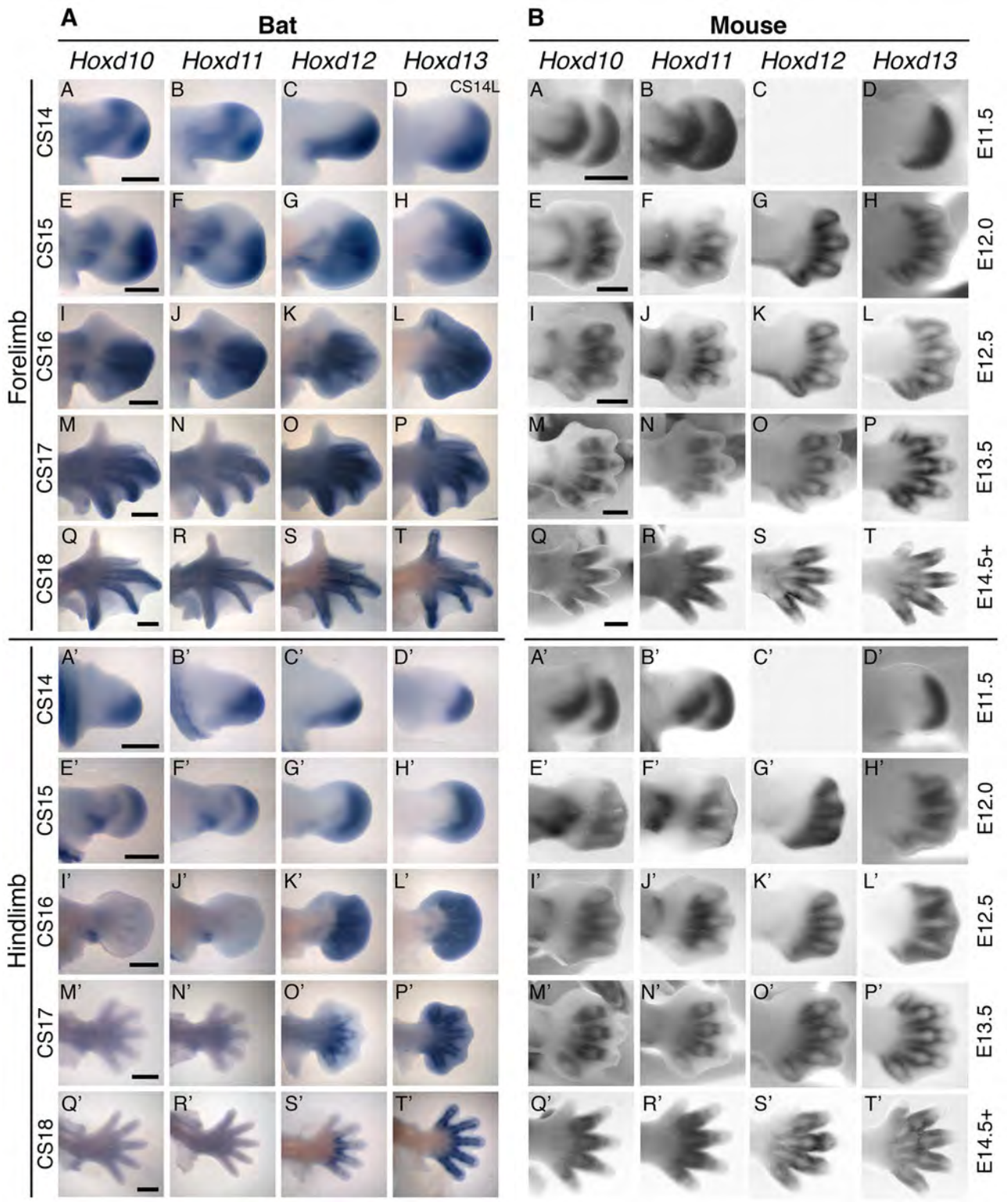

Figure 4.11: Expression pattern of the 5'HoxD genes. Bat forelimb (FL) and hindlimb (HL) autopods in a developmental series (CS14-CS18) (**A**). Expression of these genes is well defined in the FL with the distal domain of 5'HoxD gene expressions clearly defined during early autopod formation (CS14-CS15). Expression becomes focused over the region of digit III (CS16), and then restricted to the region surrounding the elongating digits at later stages (CS17-CS18). In the HL, genes show clear expression in the distal domain during early autopod formation (CS14-CS15). From CS16 onwards, expression of *Hoxd10* and *Hoxd11* is lost in the HL and at CS17 and CS18 *Hoxd12* expression is reduced. Comparative expressions corresponding to published data, are given in grey scale for the mouse in an equivalent developmental series (E11.5-E14.5+) (**B**) Dorsal view, scale bar represents 500 μm.

4.4.2. Expression of 5'HoxD genes during autopod formation and growth shows strong expression in the bat FL while exhibiting reduction of Hoxd10-12 expression in the HL

I examined the expression pattern of the 5'HoxD genes at later stages of bat limb autopod development (CS16-CS18). At CS16, the autopod has expanded, becoming highly asymmetrical and the anterior interdigital tissue develops a slightly scalloped edge (Hockman *et al.* 2009). In forelimbs, expressions of *Hoxd10* and *11* were maintained in proximal domains, specifically the anterior and posterior regions of the zeugopod, where they were excluded from the forming elements (Figure 4.11A I-J). *Hoxd12* signal was seen in the proximal, posterior region (Figure 4.11A K). All genes were strongly expressed in the distal autopod (Figure 4.11A I-L)**.** *Hoxd10* and *11* expressions were indistinguishable, and extended from the posterior side of digit II to the anterior side of digit V. Expressions were strongest over the area extending from DIII to DV, focused over the digit rays, and were excluded from DI and its associated webbing. *Hoxd12* expression expanded between DIII-IV, and was strongest in the proximal autopod (Figure 4.11A K). Interestingly, there did appear to be evidence of very weak expression of *Hoxd12* in the tissue surrounding digit I (but not in the digit ray itself) (Appendix C.17). *Hoxd13* expression extended across the entire autopod, was slightly weaker in the most anterior and posterior region, and strongest in the interdigital tissue between digits III-IV (Figure 4.11A L). For all genes, signal was concentrated in the regions surrounding the presumptive digits (Figure 4.11A K).

By CS17, the forelimb digit rays are clearly visible, and the edge of the interdigital tissue becomes scalloped. *Hoxd10* and *11* expressions were found proximally, in the region surrounding the distal radius and ulnar. Distal autopod expression of *Hoxd10, 11* and *12* was focused over the digit rays, particularly in the tissue surrounding DII-V. *Hoxd10* and *Hoxd11* expressions were not seen in DI, were weakest in DII, with strong expression found in the regions alongside the forming phalanges of DIII-V and surrounding the digit tips (Figure 4.11A M-N). *Hoxd12* expression appeared concentrated alongside the metacarpals and P1s of DIII-V (Figure 4.11A O). Interdigital expression was reduced for all genes (Figure 4.11A M-P). At a slightly later stage (CS17 L) embryo, a faint domain of *Hoxd12* expression was found in P1/2 of DI, as a weak band across the midline of this digit ray (Appendix C.17). *Hoxd13* expression occurred in the tissues surrounding all digit rays, focused in the distal ends of the metacarpals and proximal end of P1 and in P2 of DIII-V (Figure 4.11A O). Weak interdigital expression was evident for all of the genes, and was posteriorly restricted for *Hoxd12* and *13* (Figure 4.11A O-P). At a later stage of development (CS18) expression patterns appeared unchanged, with intense expression found in digit tips and lowered expression in the distal interdigital tissues (Figure 4.11A Q-T).

In the CS16 bat hindlimb, the autopod flattens and expands, and digit rays are clearly apparent (Hockman *et al.* 2009). In one of these samples, both *Hoxd10* and *11* had clear, strong signal from the posterior edge of the distal zeugopod, adjacent to the autopod in the region where the calcar develops (Figure 4.11A I'-J'), and, from the ventral surface, expression surrounded the distal edge of the zeugopod elements (Appendix C.15-C.16). *Hoxd12* had weak posterior proximal expression in the zeugopod (Figure 4.11A K'), and *Hoxd13* expression was also diffuse in this region (Figure 4.11A L', Appendix C.18). Remarkably, at this stage, *Hoxd10* and *11* expression was lost or very reduced in the distal autopod, with only weak, speckled signal in the regions surrounding the forming digit rays found in one sample (Figure 4.11A I'-J'). In contrast *Hoxd12* had clear autopod expression in the tissue surrounding digits II-V, this was concentrated alongside and over the distal tip of these digit rays (Figure 4.11A K'). Weak signal was also found in the region surrounding DI, this was not focused around the digit ray (Figure 4.11A K'). *Hoxd13* was strongly expressed across the entire autopod, there was only a slight weakening of expression in the most anterior portion of the autopod (adjacent to DI). Again, strong expression outlined the digit rays, which themselves had a reduced expression (Figure 4.11A L').

In subsequent stages (CS17), the digit rays are clearly visible and the interdigital tissue becomes scalloped. *Hoxd10* and *11* expressions were not found in the autopod, but did occur proximally in the zeugopod region (Figure 4.11A M'). In one sample (CS17L), faint signal for both *Hoxd10* and *Hoxd11* was found in the proximal interdigital tissue, at the base of DII-V (Appendix C.15-C.16). Expression for *Hoxd12* became lost from the distal interdigital tissue (evident at a slightly earlier stage). Expression was strongest alongside the developing metatarsals and outlined the digit tips at CS17E, with weak expression found in the distal cartilage elements at later stages (Figure 4.11A O'). Signal for *Hoxd13* was strong alongside all digit rays but was not found in the proximal end of the digit ray elements, and only weak expression found in the digit tips. Expression was evident throughout the interdigital tissue at this stage but became weaker at later stages (Figure 4.11A P').

No signal was seen for *Hoxd10* and *11* at later stages (CS18) of development (Figure 4.11A Q'-R'). Expression of *Hoxd12* and *Hoxd13* was still evident, with *Hoxd12* signal focused in the regions surrounding the distal metatarsals (DII-V), with weak bands of expression seen in the digits on either side of the putative joint regions. It was not seen in the joint regions or the digit tips (Figure 4.11A S'). *Hoxd13* expression was found in all digits, remained focused in the distal metacarpals and in the proximal and intermediate phalanges, but was weaker or excluded from the digit tips (Figure 4.11A T').

4.4.3. Expression of Hoxd10 and Hoxd11 is found in novel limb domains of the developing bat limb

In addition to the conventional domains of limb expression described previously, novel expression domains were found. At CS15, expressions of both *Hoxd10* and *Hoxd11* were found in the plagiopatagium, the tissue that develops from the flank region posterior to the outgrowing forelimb bud (Figure 4.11A A-B, E-F). Though expression of *Hoxd12* did appear to extend posteriorly into this region at CS14, expression was not clearly evident at later stages (Figure 4.11A C & G) and there was no evidence of *Hoxd13* expression in this developing tissue (Figure 4.11A D & H). At later stages of development (CS16–CS17), low expression of *Hoxd10* and *Hoxd11* were found in the most distal, growing tip of this tissue in some samples (Figure 4.11A I, J, M-N). This staining became indistinct and was not reproducible at later stages (Appendix C.15-C.16).

In contrast the uropatagium, which can be seen to form at later stages of development (CS15-CS16), did not appear to have a clear domain of expression that corresponded to the outgrowth of this tissue. However, a strong domain of *Hoxd10* and *Hoxd11* expression was seen (in the CS15 and one CS16 embryo) adjacent to the uropatagium and the autopod. (Figure 4.11A E'-F', I'-J'). This region may correspond to the developing calcar of the bat. Expression in this region was not reproducible at later stages of development with only diffuse expression found in one CS17 sample (Appendix C.15-C.16).

4.5. Analysis of protein coding and regulatory regions of the 5'HoxD cluster in bat species

I have shown that gene expression profiles of the 5'HoxD genes differ between the bat forelimbs and hindlimbs during their second phase of expression in the autopod. In the mouse limb, long-range enhancers regulate this phase of expression. A highly conserved Prox enhancer is found in a region 5' of the HoxD cluster (Figure 4.1), with interactions among this region, the GCR and the regulatory archipelago, shown to drive 5'HoxD gene expression in the developing autopod (Spitz *et al.* 2003; Montavon *et al.* 2011; Noordermeer and Duboule 2013). Conserved regions within the Prox enhancer, the CsC, drives digit specific LacZ expression in transgenic mice (Gonzalez *et al.* 2007). Changes in this sequence may modify conserved transcription factor (TF) binding motifs, affecting their protein binding and so altering the enhancer activity. In this section, I examine the CsC region, to determine whether this sequence has been altered in bat species as compared to other vertebrates. In addition to alterations in enhancer sequences, changes in the sequence of protein coding regions of genes have the potential to alter their protein activities. In transcription factors, such as the 5'HoxD genes, this has the potential to affect protein-protein and protein-DNA binding sites (Carroll 2008; Di-Poï *et al.* 2010). In this section, I examine the protein coding sequences of the 5'HoxD genes to determine whether they have undergone positive selection, and check for amino acid changes with the potential to alter their functioning in bat species.

4.5.1. 5'HoxD genes have a highly conserved nucleotide sequence similarity over their CDS with few conserved changes found in bat species

The 5'HoxD genes of *M. natalensis* were sequenced to analyse and compare their coding sequences (CDS) with those of other bat species and vertebrates. Full-length sequences were obtained for *Hoxd10* and *Hoxd12* and partial sequences were generated for *Hoxd11* and *Hoxd13* (Table 4.6, Appendix C.19-C22). The *Hoxd11* 3' RACE reactions amplified non-specific products, likely due to mis-priming, and this consensus sequence lacked the last 92 nt of the CDS and the 3' UTR. The consensus sequence of *Hoxd13* lacked the 5' UTR and the first 216 nt of the CDS. Reactions failed to amplify past a region with a high GC content (51 nt of 88% GC in human) that corresponded to an important conserved poly amino acid tract (15 Alanine residues). Advances in technologies now allow the direct sequencing of genomes and transcripts to produce high quality protein coding sequences, making additional cloning and sequencing work defunct. Subsequent alignments were performed using these partial sequences in addition to whole genome shotgun (WGS) sequences from additional bat species.

The CDS of all 5'HoxD genes for *M. natalensis* had very high sequence similarities to those of *M. schreibersii*, and with sequences of other bats and mammals, though conservation did drop in comparisons that included non-mammalian species (Table 4.6, Appendix C.19-C22). Average pairwise identities were also high when comparing all sequences in the alignment, indicating high conservation of these genes and their protein products.

Table 4.6: The average pairwise sequence similarity of 5'HoxD genes CDS generated for *M. natalensis*. The average pairwise identity (PWI) was used to compare *M. natalensis* with *M. schreibersii* (*M. sch*), and Miniopteridae to bats (B) mammals (M) and non-mammalian vertebrates (NM). *Hoxd10* and *Hoxd11* had high average PWIs. *Hoxd12* nucleotide and residue sequences had lower PWI values in both bats and mammals. *Hoxd13* nucleotide sequences had lower PWIs but the residue sequence similarity of bats and other mammals was comparable to that of *Hoxd10*.

Gene	Sequence	Length	Miniopterus Average PWI (%)				All Average PWI (%)		
			M sch.	**B**	**M**	**NM**	**B**	**M**	**NM**
Hoxd10	Full CDS	1026 bp	99.8	96.6	96.7	84.6	98.2	97.1	85.5
	Full Protein	340 aa	99.7	96.1	97.2	87.7	98.8	98.3	88.0
Hoxd11	Partial CDS	799 bp	97.8	97.1	95.4	80.3	96.8	96.5	80.6
	Partial protein	264 aa	95.9	98.8	98.9	87.0	99.2	99.6	90.7
Hoxd12	Full CDS	819 bp	99.8	91.8	88.6	69.6	91.4	88.0	70.0
	Full Protein	272 aa	100	92.8	90.6	71.8	91.6	89.2	71.0
Hoxd13	Partial CDS	810 bp	100	94.0	91.2	74.2	93.7	91.0	73.4
	Partial Protein	269 aa	100	97.7	96.1	82.0	97.0	97.3	79.6

For the *Hoxd11* translated CDS alignment, the protein sequence of *M. lucifugus* differed from residue 2, resulting in a stop codon at residue 5, and there were insertions of three cytosines. This resulted in a loss of protein sequence similarity with other bats, giving a pairwise identity of only 14.3% for the translated sequence. This may be due to incorrect sequencing or sequence assembly and this sequence was subsequently disregarded, resulting in the average pairwise identity of the translated CDS of bats (99.2%) being similar to that of mammals (99.3%).

Tests for non-neutral evolution (likelihood ratio test, LRT) were not supported for any of the 5'HoxD CDS alignments (*Hoxd10* Null model: Log(L) = -2046.35, Alt. model: Log(L) = -2046.35, LRT = 3.8531e-05, p = 0.99998; *Hoxd11* Null model: Log(L) = -3411.35, Alt. model: Log(L) = -3411.37, LRT = -0.222805, p = 1; *Hoxd12* Null model: Log(L) = -3419.73, Alt. model: Log(L) = -3417.56, LRT = 4.34087, p = 0.114128; *Hoxd13*: Null model: Log(L) = -2702.76, Alt. model: Log(L) = -2702.76, LRT = = 6.8951e-06, p = 0.99999). These results show that there was no evidence of positive selection in the alignments given (Appendix C.19-C22).

An integrated selection analysis found weak evidence of positive selection for the CDS of *Hoxd10* at consensus site 208 (a conserved Gly was altered to Ile in the Pteropodidae due to a change in two

nucleotides, GGC->ATC); *Hoxd11* at consensus site 220 (a conserved Glycine was altered to Alanine in Miniopteridae, Val in *Eptesicus fuscus* and Alanine in *Bos taurus*), however sequence coverage over this region was poor) and *Hoxd12* at consensus site 92 (conserved Alanine was altered in several species: Threonine in Armadillo, Serine in Dog, Threonine in *R. leschenaultii* and *C. perspicillata*, and Glycine in Miniopteridae). Amino acid properties did not show a selection change. All genes were strongly conserved, with robust evidence of negative (purifying) selection evident in *Hoxd10* (6 sites, 2% of CDS) and prevalent in *Hoxd11* (16 sites, 13%), *Hoxd12* (59 sites, 22%) and *Hoxd13* (50 sites, 20%). (Appendix C.23-C26). Overall, these alignments do not show evidence of positive selection, with only weak support given for amino acid alterations that were not conserved within the bat species tested.

Four polyamino stretches (tracts of an amino acids, > 75% composition in the human, longer than 4 residues) were found in HOXD11 and HOXD13. These were highly similar or invariant with the bat equivalents (Table 4.7). In HOXD11, the first polyglycine stretch was not highly conserved among vertebrates (76%) as compared to that of the other stretches (> 90%), which showed no conserved differences in bats. In HOXD13, polyamino tracts were highly conserved, with the second polyalanine tract (15 residues that are expanded in the *spdh* mouse mutant) fully conserved in all species. The second polyserine tract had an alteration of one residue into Alanine, while the third polyalanine tract had a loss of one residue into Glycine. All alterations found were not specific to bats as they were all also found in the cow.

Table 4.7: Summary of poly amino tracts in the translated CDS of the 5'HoxD genes. Their start position (relative to the human protein sequence), predominant amino acid (Gly, Glycine; Ala, Alanine; Pro, Proline; Ser, Serine) length and % composition of the predominant amino acid. The pairwise identity (PWI) between the human tract and that of a representative bat species is given, along with the bat species used in each comparison.

Name	Start posit. (UniProt)	Amino acid	Length (aa)	% Comp.	PWI (%)	Bat species
HOXD11	77 (90-102)	Gly	27	76.9	73.1	*M.nat, P.vam*
	108 (108-120)	Ala	13	100	100	*P.vam*
	193	Pro	12	75	100	*M.nat, M.sch, E.Fuc*
	218	Gly	5	100	100	*M.nat, M.sch P.vam E.Fuc*
HOXD13	25 (25-30)	Ser	6	100	100	*C.per, H.arm T.mel, R.les*
	32 (32-36)	Ala	5	100	100	*T.mel*
	57 (57-71)	Ala	15	100	100	*C.per, H.arm, T.mel, R.les, M.lyr, P.ale*
	85 (85-92)	Ser	8	100	87.5	*C.per, H.arm, T.mel, R.les, M.nat, M.sch, M.lyr, P.ale*
	113 (113-118)	Ala	6	100	83.3	*C.per, H.arm, T.mel, R.les, M.nat, M.sch, M.lyr, P.ale*

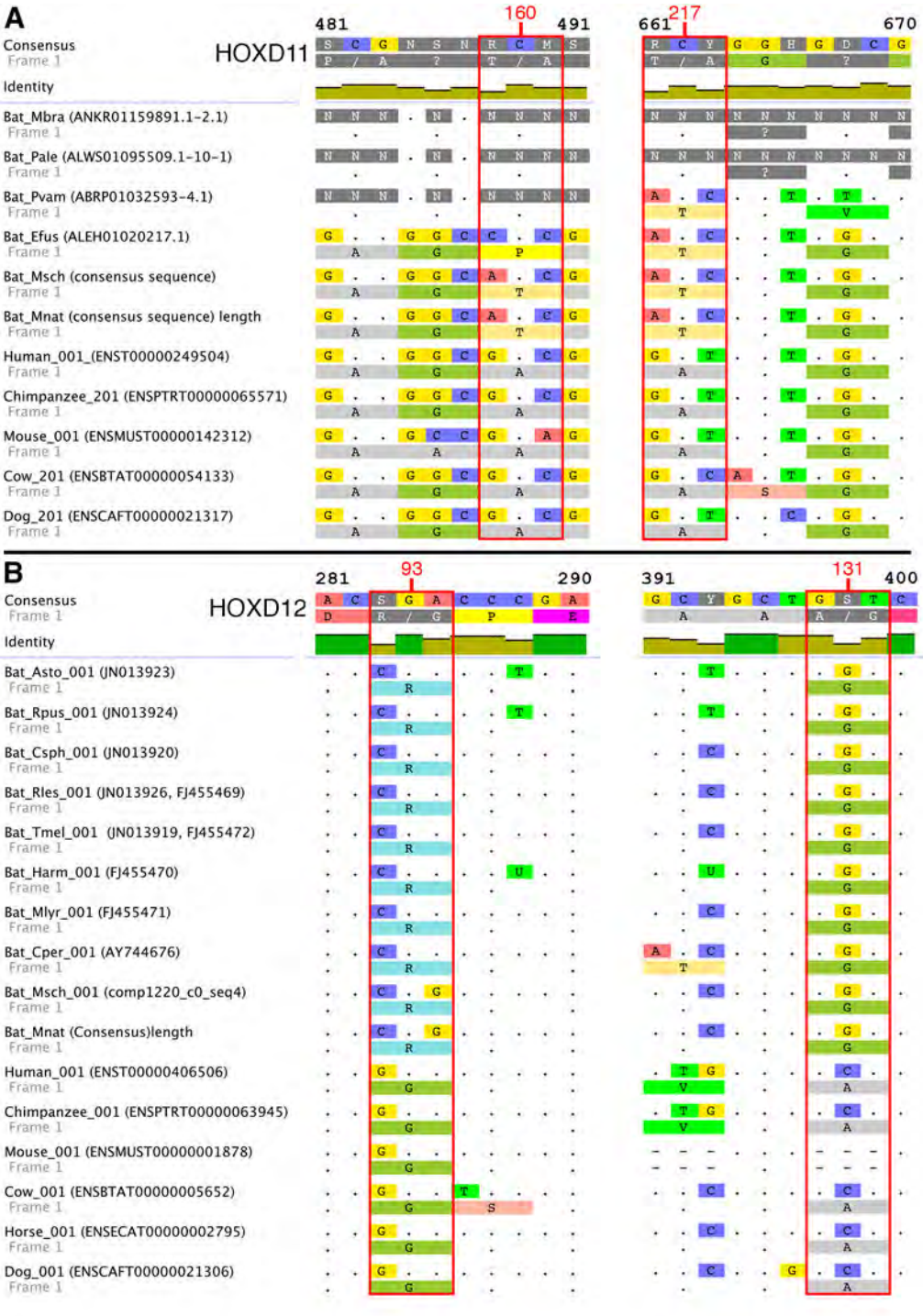

Figure 4.12: Alignments of protein coding sequence for *Hoxd11* and *Hoxd12*. HOXD10 (**A**) and HOXD12 (**B**), each show two nucleotide changes each that result in an altered amino acid as compared to other vertebrate species examined.

When examining the highly conserved DNA binding domain (Homeodomain), no amino acid alterations, common to all bats, were found. The homeodomain of HOXD10 (amino acids 266-325 in the human) was fully conserved. That of HOXD11 (266-325) had isolated residue changes in *M. natalensis* (Asparagine to Aspartic Acid, AAC->GAC) and *P. vampyrus* (Arginine to Asparagine; CGC->AAC). HOXD12 (202-261) had an alteration in the mouse, human and chimp (Leucine to Valine; CTC->GTC) and another altered residue in the mouse alone (Leucine to Glutamine; CTG->CAG). HOXD13 (276-335) was highly conserved, with one altered residue in the cow (Isoleucine to Valine, ATT->GTT).

A closer examination of the aligned translated CDS for each gene revealed two bat specific changes in the protein coding sequence of both HOXD11 and HOXD12 (Figure 4.12; Appendix C.20-C21). In HOXD11 at residue 160 (of the human sequence), Alanine was replaced by Threonine in *M. natalensis* and *M. schreibersii* and Proline in *E. fucus*. However, this did not appear to result in conserved changes to side-chain properties. At residue 217, Alanine was replaced with Threonine in all aligned bat species (4) resulting in a change from a non-polar to a polar, less hydrophobic side-chain with the charge remaining neutral (Figure 4.12A). In HOXD12 at residue 93 Glycine was substituted for Arginine in all bat species aligned (10). This changed the non-polar, neutral and slightly hydrophobic side chain into a polar, basic, positively charged and highly hydrophobic one. Residue 131, was changed from an Alanine to Glycine in bats (10), and did not appear to alter the properties of the side chain (Figure 4.12A). A previously found alteration of HOXD13 amino acid 159 (Alanine to Serine) found in two bat species (*M. lucifugus*, *C. perspicillata*) (Ray and Capecchi 2008), was not altered in representative species of Pteropodinae, Hipposiderinae and Megaderatidae. The above alterations did not correspond to natural variants or mutations annotated in human sequences (UniProt).

4.5.2. Alterations in the highly conserved CsC region of PROX are specific to bats

To determine whether bat species had acquired specific mutations in the CsC region, and to understand whether these may correspond to alterations in their regulatory strategy, I aligned and compared a portion of CsC, that encompassed two highly conserved regions, CsC1 and CsC2 (Homo_sapiens_(CsC); Figure 4.13; Gonzalez *et al.* 2007) from several bat and vertebrate species (Appendix C.27). This alignment had high sequence similarity across all species (83.4%), with tracts of strong conservation apparent. These were termed highly conserved regions (HCR) and noted for their high pairwise identities. This was most apparent in the two longest tracts, HCR_1_259 (95.9%), which was found within the CsC1 region and HCR_1_789 (94.4) and which was found within the CsC2 region (Figure 4.13; Appendix C.28).

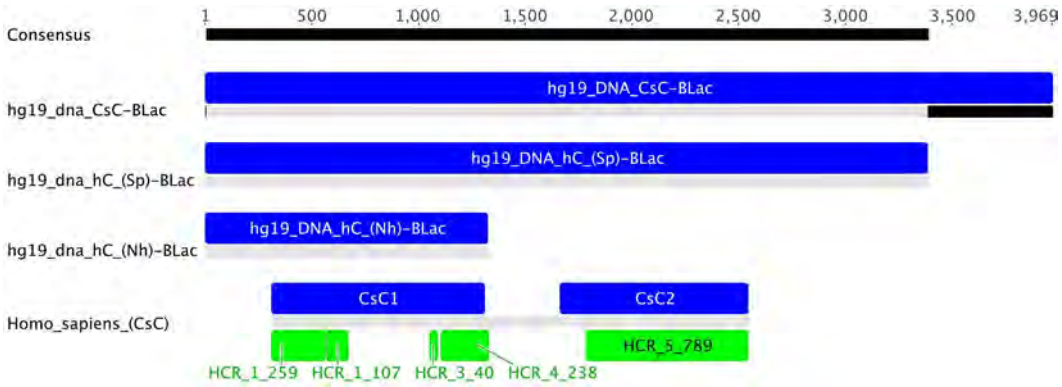

Figure 4.13: Alignment of the human CsC regions used in transgenic assays as compared to cloned sequence region encompassing CsC1 and CsC2. CsC enhancer regions used in transgenic assays are given (blue) (Gonzalez *et al.* 2007). The region cloned and sequenced in this study, Homo_sapiens_(CsC), is shown for comparison with highly conserved regions (HCR) identified and in annotated (green).

Eight regions contained nucleotide changes specific to bat species, five of these were associated with changes in predicted transcription factor (TF) binding motifs (Table 4.8). ConsCsC_0643 appeared within a conserved region of CsC1, resulting in a loss of the 'footprint II site' bound by the factor F2F. Two bat specific nucleotide changes were found in a relatively conserved region between CsC1 and CsC2. The first, consCsC_0960, resulted in the loss of the POU domain, class 1, transcription factor 1a (POU1F1a) core binding motif, in bats. The second, consCsC_1297, created a core binding motif of the Nuclear factor I (NF-I) family of TFs. In the CsC2 region, consCsC_2152 had the potential to result in a gain of a binding motif for c-Ets-2, and the gain of a TATA Binding Protein (TBP) site. These last two motifs were not conserved in the Pteropodidae (Table 4.8).

These annotations were based on the publically available data of TransFac database 7.0 (2005) and are not exhaustive. To complement these, TF binding sites from other databases were explored. Three previously identified TF binding regions identified through ChIP-seq experiments (UCSC Genome Browser, Encode Transcription Factor ChIP-seq) were examined (Table 4.9). These included the TF binding sites for STAT1, POLR2A and FOXP2. Four nucleotide changes, conserved in bats, were associated with these regions. Predicted transcription factors, common to the human, mouse and rat (UCSC Genome Browser, HMR, Conserved Transcription Factor Binding Sites; hg19/GRCh37), were annotated on the alignment (Appendix C.29). For the most part these were highly conserved in vertebrates, finding only two with nucleotide changes that were not specific to the bat lineage (Table 4.9).

Table 4.8: Nucleotide changes CsC region alignments that are conserved within bat species. The pairwise identity (PWI%) of a 50 nt window surrounding the altered nucleotide is given. The bat consensus and human sequence of 9-11 nt surrounding the nucleotide change (in bold) is given and the regional annotation shown. Transcription factor (TF) binding motif alterations are described, Transfac accession number and binding motif indicated.

Nucleotide	PWI%	Bat Cons (9-11 nt) (Human cons)	Alignment Annotations	Tf motif	Transfac accession
485	62.4	TCAT**G**CAGA (TCAC**A**CTCA)	CsC1; H19_dna_hC_(Nh)-Blac; H19_dna_hC_(Sp)-Blac	None	_
643	74.8	TAAA**G**TTAA (CAAA**A**TTAA)		Loss of F2F	T01506 TAAAA**T**
882-3	68.0	TTTAAG**CA**CAGGTA (TTTAAG**AG**CAGAGA)		None	_
960	76.9	TAAA**C**TGAG (TAAA**T**AAAG)	H19_dna_hC_(Sp)-Blac	Loss of Pou1f1a	T00691 TAAA**T**
1297	75.4	TTTT**G**CCAG (TTTG**A**CTAA)		Gain of NF-I	T00537 **G**CCA
1693	69.5	TTGG**A**GGTG (TTCA**T**GGTG)	CsC2; H19_dna_hC_(Sp)-Blac	Loss of non conserved TF	_
2152	86.6	CTAT**T**CCTT (CTAC**A**CCTT)	CsC2; HCR_5_789; H19_dna_hC_(Sp)-Blac	Gain of c-Ets-2	T00113 **TT**CCTT
				Possible gain of TBP	T00798 **TT**CC
2369	96.4	GGTT**T**AAGG (GGTT**C**AAGG)		None	_

Additional analyses were performed to look for factors that are differentially expressed in the forelimb and hindlimb. *Tbx5* and *Tbx4* are specifically expressed in the developing forelimb and hindlimb respectively. The binding motif of TBX5, (A/G)GGTGT(C/ T/G)(A/G) (Ghosh *et al.* 2001), also allow interactions with TBX4, who's unique binding sites are currently unknown (Glaser *et al.* 2014). Two regions were found with similarities to the core of this motif (A/G)GGTGT. The first (2009-2014) was highly conserved in all species. The second (2150-2155) was found over the regions of nucleotide change consCsC_2152, resulting in a loss of this motif in bats. However this binding motif was also not conserved in other vertebrates. These proteins are also known to interact with the binding site of Brachyury, T(G/C)ACACCT/AGGTGTGAAATT, another T-box transcription factor, however this motif was not present in this alignment. *Pitx1* is uniquely expressed in the hindlimb. Four putative PITX1 binding sites, (G/A)GATTA (JASPER Database Ver. 5.0_ALPHA, (Quirk *et al.* 2001), were found in the CsC alignment (151-156; 585-591; 743-751, 1040-1045 in the nucleotide alignment), the first was fully conserved in all species examined, while the others showed some alterations in several species. No sites had alterations that were specific to bat species alone.

Table 4.9: Annotated and conserved Transcription Factor (TF) binding sites in the CsC region of Prox identified using the UCSC Genome Browser Reference genomes, NCBI36/ hg18 and GRCh37/ hg19 were used. Location and size of the motif is given along with its position on the CsC multispecies alignment. Nucleotide changes within these regions are noted.

Genome reference	TF	Location	Region Size (bp)	CsC alignment	Nucleotide alteration
NCBI36/ hg18	STAT1	chr2:176598204-176598476	273	2292-2569 (CsC2)	consCsC_2369
GRCh37/ hg19	POLR2A	chr2:176888024-176888359	336	18-378 (CsC1)	None
		chr2:176888845-176889180	336	1017-1400	consCsC_1297
		chr2:176889538-176889873	336	1848-2200 (CsC2)	consCsC_2152
GRCh37/ hg19	FOXP2	chr2:176888859-176889154	296	1031-1371	consCsC_1297

Conserved TF	Item (Transfac matrix)	Location	Size (bp)	CsC alignment	Sequence
CsC1_HMR1	CDPCR3 (M00105)	chr2:176888078-176888092	15	72-86 (CsC1)	Deletion in Pteropodidae
CsC1_HMR2	GATA1_05 (M00346)	chr2:176888277-176888286	10	296-305 (CsC1)	Conserved
CsC2_HMR1	NKX61 (M00424)	chr2:176889530-176889542	13	1840-1852 (CsC2)	Lost in Laurasiatheria, Guinea pig and Squirrel.
CsC2_HMR2	OCT1/ POU2F1a (M00135)	chr2:176889580-176889598	19	1891-1910 (CsC2)	Conserved
CsC2_HMR3	NKX2-5 (M00241)	chr2:176889651-176889658	8	1963-1970 (CsC2)	Conserved
CsC2_HMR4	NKX6-1 (M00424)	chr2:176889689-176889701	13	2001-2024 (CsC2)	Conserved
	FOXJ2 (M00422)	chr2:176889695-176889712	18		
	HFH3 (M00289) FOXI1	chr2:176889697-176889709	13		
CsC2_HMR5	FOXJ2 (M00422)	chr2:176889974-176889991	18	2308-2325 (CsC2)	Conserved
	HNF-3beta (M00131)	chr2:176889977-176889991	15		
	FOXD3 (M00130)	chr2:176889978-176889989	12		
CsC2_HMR6	CHX10 (M00437)	chr2:176890118-176890131	14	2456-2469 (CsC2)	Conserved
CsC2_HMR7	S8 (M00099)	chr2:176890158-176890173	16	2496-2511 (CsC2)	Conserved
CsC2_HMR8	HOXA3 (M00395)	chr2:176890190-176890198	9	2528-2536 (CsC2)	Conserved
CsC2_HMR9	HNF-3beta (M00131)	chr2:176890224-176890238	15	2563-2578 (CsC2)	Conserved
	HOXA3 (M00395)	chr2:176890236-176890244	9		

4.6. Discussion

Hox genes are key regulators of developmental processes, with expressions of the 5'HoxD genes being necessary for events involved in limb bud patterning, digit formation and growth (Reno *et al.* 2006; Deschamps 2008; Montavon *et al.* 2008; Woltering and Duboule 2010). While similarly expressed in mouse forelimbs and hindlimbs (Dollé and Duboule 1989; Dollé *et al.* 1989; Dollé, Izpisúa-Belmonte, Boncinelli, *et al.* 1991), these genes have different patterns of expression in the divergent limbs (wing and leg) of the chick, and are thought to contribute to the formation of these distinct skeletal morphologies (Mackem and Mahon 1991; Mackem *et al.* 1993; Nelson *et al.* 1996; Wellik and Capecchi 2003; Kamiyama *et al.* 2012). This is supported by transgenic work in the mouse, with alterations in the level or pattern expressions of the 5'HoxD genes resulting in phenotypic changes in digit skeletal elements, with a loss in expression typically resulting reductions in lengths (Davis and Capecchi 1996; Zákány *et al.* 1997; Montavon *et al.* 2008; Delpretti *et al.* 2012). The 5'HoxD genes have been implicated in bat wing development, with early candidate gene studies finding few differences in *Hoxd13* gene expression patterns, in the forelimb and hindlimb of the bat, while high-throughput transcriptome analyses indicate that the 5'HoxD genes are upregulated in the developing bat forelimb (Chen *et al.* 2005; Ray and Capecchi 2008; Wang *et al.* 2010, 2014; Mason *et al.* 2015). In this chapter I examined the relative skeletal element lengths of adult bat and mouse autopods, corresponding these with 5'HoxD gene expressions measured over several stages of bat limb development, and verifying differential expression. I compared the bat 5'HoxD gene coding sequences with those of other mammals to confirm that protein activities were unchanged in the bat, and CsC enhancer sequences to identify potential functional alterations in regulatory sequences. These results are discussed in the context of digit development and skeletal element elongation.

4.6.1. Early limb bud expression of 5'HoxD genes may be integrated with the enhanced SHH-FGF feedback loop in the bat forelimb

The broad domains of early proximal 5'HoxD gene expressions in the outgrowing limb buds in the bat (CS14) were fairly similar to those of the mouse, however close examination revealed subtle expansion of expression in the forelimbs as compared to the hindlimb of a slightly later stage (to compensate for developmental lag evident at this stage). This included a more proximal extension of the expression boundary for *Hoxd10*, *Hoxd11* and *Hoxd12* and an anterio-posteriorly expanded domain of distal expression of *Hoxd10* and *Hoxd11* in the in the bat forelimb. Though not quantifiable, WISH staining

in the forelimb appeared more intense. RNA-seq supports the upregulation of *Hoxd10-13* in the forelimb in pooled CS14 samples in *M. schreibersii* (Wang *et al.* 2014).

5'HoxD gene products triggers *Shh* expression in the early limb bud (Zákány *et al.* 2004; Kmita *et al.* 2005) with HOXD10-13 shown to have the ability to bind directly to and activate expression from the *Shh* limb enhancer, the ZPA regulatory sequence (ZRS) (Capellini *et al.* 2006; Tarchini *et al.* 2006). The strong expression of the 5'HoxD genes in the bat forelimb bud may result in the expansion of *Shh* and *Fgf8* expression, reported in the CS14 forelimb, resulting in the enhancement of the early SHH-FGF feedback loop and a greater enlargement of this limb (Cretekos *et al.* 2008; Hockman *et al.* 2008). However, this feedback loop has a complex interaction with the HoxA/HoxD genes in the early limb bud, as it promotes Hox gene expression subsequent to its own initiation (Litingtung *et al.* 2002; Te Welscher *et al.* 2002; Sheth *et al.* 2013). More detailed analyses, that include earlier stages of development, is required to determine whether the upregulation of the 5'HoxD genes expression is a cause or an effect of the enhanced SHH-FGF signalling in the limb bud. This work would be critical in determining whether these genes contribute towards specifying the earliest developmental events that underlie forelimb and hindlimb specific morphologies in the bat limb.

4.6.2. 5'HoxD overexpression in the early autopod prefigures the reactivation of the SHH-FGF feedback loop in bat limbs

This enhancement of these early signalling events is suggested to promote proliferation and posterior expansion of the outgrowing limb bud and subsequent autopod (Hockman *et al.* 2008). However, the enlargement of the bat autopod, seen at CS15, must be integrated with digit ray patterning events to form a pentadactyl rather than a polydactyl autopod. The 5'HoxD genes have been shown to regulate the size of digit-interdigit patterning through altering the wavelength of a Turing patterning mechanism in this region (Sheth *et al.* 2012; Raspopovic *et al.* 2014; Zúñiga and Zeller 2014; Cooper 2015). The higher expressions of *Hoxd10, 11* and *Hoxd12* in the bat forelimb are positioned to mediate a scaling response, maintaining the pentadactyl digit pattern in the expanded bat autopod.

During early autopod formation, *Hoxd10* and *Hoxd11* are expressed in a uniquely patterned triangular distal domain, that prefigures the reactivation of *Shh* at CS16VE (Hockman *et al.* 2008). *Shh* has a transient burst of expression that expands throughout the forelimb autopod mesenchyme, becoming restricted to the interdigits between digit III and IV before it is lost (Hockman *et al.* 2008). This region of *Shh* expression lies within the distal domain of all 5'HoxD genes but unlike these genes, which have most intense expressions in the region encompassing digit III, *Shh* expression is graded with strong

posterior expression and weaker anterior expression. Based on their interactions in the early limb bud, these overlapping expressions may indicate that the 5'HoxD genes play a role in the reactivation of *Shh* expression in the bat autopod. While these two domains overlap, they do not resemble one another, this may be due to the fact that *Shh* activation is dependant on cooperative binding by HAND2 (encoded by *dHand*) in the mouse limb bud (Galli *et al.* 2010), and may require this or other cofactors in the bat autopod, which play a part in determining the pattern and intensity of *Shh* expression. As mentioned previously, 5'HoxD genes are able to activate *Grem1* expression in the limb bud, which is required for FGF activation (Sheth *et al.* 2013). Both *Grem1* and *Fgf8* are expressed throughout the bat (*C. perspicillata*) forelimb and hindlimb autopods at CS16, with their expressions becoming lost from the interdigital mesenchyme of the bat hindlimb at CS17 (Weatherbee *et al.* 2006). The continued expressions of these three genes in the bat forelimb autopod mesenchyme is suggested to increase cell-survival and proliferation signals, contributing to digit elongation and interdigital tissue retention (Weatherbee *et al.* 2006; Hockman *et al.* 2008). These findings support the reactivation of the SHH-FGF feedback loop in the bat autopods, and suggest that the 5'HoxD genes are positioned to orchestrate this event through multiple inputs. The continued strong expression of these genes in the forelimb and loss of *Hoxd10* and *Hoxd11* and reduction of *Hoxd12* in the hindlimb (at CS16), may alter the strength and duration of this signalling loop in the different limb types.

4.6.3. Quantitative differences in temporal expression of the 5'HoxD genes in bat forelimbs and hindlimbs

At CS17 significant upregulation of expression in the bat forelimb as compared to the equivalently staged mouse forelimb was only found for *Hoxd10*, *Hoxd11* and *Lnp*. While not involved in limb development, *Lnp* expression is activated by the centromeric HoxD enhancers (Spitz *et al.* 2003), with its upregulation supporting an enhanced activation of all the 5'HoxD genes in bat forelimbs as compared to the mouse . This was not the case, with strong differential expressions between the bat and the mouse forelimb only found for *Hoxd10*, *11* and to a lesser degree *Hoxd12*. While it is possible that this is a function of their reverse collinear expression (finding smaller fold changes in highly expressed genes and larger fold changes in lowly expressed genes), this does not fit in with the finding that *Hoxd10*, was one of the most highly expressed 5'HoxD genes in the bat.

While upregulation of *Hoxd10* and *11* was only measured at a late stage of autopod development (CS17), earlier expression patterns of these genes (CS15 and CS16) corresponded to the initial expression of *Shh* in the bat (CS16 E). *Hoxd10* and *11* may therefore play a primary part in activating

Shh expression. This is supported by experiments in transgenic mice, which show that the loss of *Hoxd9/10/11* paralogs (*aaDD, aaDd, aadd*) reduces *Shh* expression in a dose-dependent manner, implicating these paralogs as the primary mediators of *Shh* activation in the limb bud, and indicating that their loss limits *Shh* activation (Raines *et al.* 2015). If the activation and duration of *Shh* expression in the bat autopod is dependent on *Hoxd10* and *11* expressions, their loss in the CS16 hindlimb may underlie the lowered expression of *Shh* in this tissue.

All 5'HoxD genes had significantly higher expression in the bat forelimb than the hindlimb. This was not a strong effect for *Hoxd12* and *Hoxd13*, nor was this differential expression maintained for *Hoxd13* when analysing additional absolute expression data. Elevated levels of expression in the forelimb were found at all stages of development for *Hoxd10-12*, and at CS15 and CS17 for *Hoxd13*. Data for *Hoxd10* and *Hoxd11* corresponded well with, and confirmed previous microarray analyses, while that of *Hoxd12*, *Hoxd13* and *Lnp* were not consistent, possibly due to subtler differential expressions found for these latter genes. These results confirm and complement a transcriptome study that found significant upregulation of all 5'HoxD genes, including *Hoxd9*, in *M. schreibersii* autopods (Wang *et al.* 2014). In this study, transcript abundance of digit and interdigital regions were measured by RNA-seq, allowing high-resolution comparisons to be made among divergent tissues. However, pooling of a large, biased range of developmental stages precluded gene expression dynamics from being resolved in a stage-wise manner. WISH analysis did reveal that *Hoxd10* and *Hoxd11* expressions were not evident in the CS15 hindlimb autopod of *M. schreibersii*, while clear expression of all 5'HoxD genes, were found in *M. natalensis* at this stage. These findings indicate that the second phase of 5'HoxD expressions is initiated in the *M. natalensis* hindlimb. This was confirmed by qPCR, which showed that expression decreased in the hindlimbs between the CS15 and CS16, supporting a loss in expression. Reduction and subsequent loss of *Hoxd12* expression in *M. schreibersii* hindlimbs was reported from CS17 onwards, this is consistent with what was found in *M. natalensis*, though expression still surrounded the metatarsal elements at CS18, and transcripts were still detectable by qPCR.

In addition to the dramatic reduction of *Hoxd10-12* expressions in the hindlimbs, *Hoxd10* and *11* expressions appeared to increase in the forelimbs as development continued. When excluding the CS15 autopod (which may include a more proximal expression domain for *Hoxd10* and *Hoxd11*), the highest transcript abundance of these genes was found at CS17, a stage where the digits have become dramatically elongated and expression is found in the digit rays and partially maintained in the interdigital tissue. The subsequent drop in expression at CS18 may reflect the loss of this interdigital expression, as strong expression remains in the elongating digit rays. While these differences are

reported as 'overexpression' of the 5'HoxD gene in the bat limb, comparisons with the mouse support the idea that these genes are both upregulated in the bat FL, with the strongest effect seen for *Hoxd10* and *Hoxd11* and down regulated in the bat HL, with the strongest effect seen for *Hoxd10* and *11* and then *Hoxd12* (as compared to the mouse). In *M. schreibersii* there was evidence of significant differential expression of *Hoxd13* in digit rays II-V as compared to the hindlimb digit rays at CS18. When examining independent stages in *M. natalensis*, strong differential expression was not supported, with clear expression of *Hoxd13* in the bat hindlimb still evident at CS18. The strong expression, and subsequently high variance of *Hoxd13* make resolving potential differential expression difficult. This study does not exclude the possibility that there is biologically relevant, lowered expression of the highly abundant *Hoxd13* transcripts in bat hindlimbs.

Differences in the quantitative data between *M. schreibersii* and *M. natalensis* may be attributed to the differing sampling strategies (digits and interdigital webbing) and effects of pooling samples of multiple stages (pooled FL: 2x CS15, 1x CS16L and 5x CS17; pooled HL: 1x CS16L and 5x CS17), with the lack of biological variance in these samples reducing the stringency of significance testing. The differences in expression patterns, may be species specific, however these two species are closely related, and differences are more likely attributable to experimental differences in the WISH protocol itself, specifically at later stages where probe penetration becomes affected.

The strong differential expression found between bat forelimbs and hindlimbs is not evident in mouse WISH experiments. However, *Hoxd11* expression has been reported to be significantly higher in the E12.5 mouse forelimb autopod with *Hoxd10* and *Hoxd13* also showing slightly elevated expressions (Shou *et al.* 2005). A more detailed examination of the quantitative differences in the expression levels of these genes over stages of mouse autopod development is lacking. The progression of expression in bat digits did not appear to differ dramatically from that of the mouse, though novel domains of expression were noted in the patagia, and calcar region, two bat specific features.

It is important to note that differential expressions of the 5'HoxD genes are maintained in bat digit ray elements at later fetal stages (Wang *et al.* 2010, 2014), implicating these genes in the continued elongation of forelimb growth plates both during fetal development and postnatally, when the majority of skeletal element elongation occurs (Sears *et al.* 2006; Cretekos *et al.* 2008; Farnum *et al.* 2008b; Farnum *et al.* 2008a). This corresponds with reports of 5'HoxD expression being maintained in digit rays at late stages in the mouse (up to E17.5; Reno *et al.* 2008). Interestingly, the continued growth of bat forelimb skeletal elements corresponds to an enhancement of all chondrocytic performance parameters (number of cells, cellular height and volume, axial ratio in metacarpal and P1 of DIII) that

lead to postnatal bone elongation as compared to the mouse. In addition, hypertrophy appeared to occur rapidly, with these cells reaching their final, much larger, size early on in this process as compared to mouse forelimb elements (Farnum *et al.* 2008a). Based on these differential expression analyses, a role for the 5'HoxD genes in mediating these processes, in the growth plate at later stages of development, should be examined.

4.6.4. Role of 5'HoxD genes in mediating skeletal element elongation in the bat

Hox genes regulate a large variety of gene networks in the developing autopod and zeugopod (Cobb and Duboule 2005; Raines *et al.* 2015). In addition to their role in early patterning, these genes have been shown to mediate later growth events (Goff and Tabin 1997). In *aadd* compound mutants (lacking *Hox9/10/11* paralog expression), resting chondrocytes of the zeugopod are arrested and show downregulation of several genes involved in chondrogenic progression (*Runx3*, *Shox2*, *Bmp7*, *Lef1* and *Gli1*) and upregulation of genes involved in the delay of chondrogenesis and endochondral ossification (*Pknox*, *Zfp467*, *Hand2*, *Osr1*) in addition to the downregulation of other processes (BMP signalling, growth arrest, apoptosis and reduced proliferation) (Raines *et al.* 2015).

Interestingly 5'HoxD loss of function mutants show a reduction in the expression of *Runt-related transcription factor* paralogs (*Runx2/3*), and *Short-stature homeobox gene 2* (*Shox2*) (Cobb *et al.* 2006; Villavicencio-Lorini *et al.* 2010; Gross *et al.* 2012; Raines *et al.* 2015). *Runx2* is directly activated by several HOX proteins, at varying efficacies and both *Runx2* and *Runx3* are required for chondrocyte maturation, mediated through their activation of *Indian hedgehog* (*Ihh*) expression (Yoshida *et al.* 2004). *Ihh* is a key regulator of endochondral ossification and is expressed in prehypertrophic cells, playing a vital role in regulating the rate of hypertrophic transition (Vortkamp *et al.* 1996; St-Jacques *et al.* 1999; Kronenberg and Kronenberg 2003). In CS17 bat forelimbs, strong expression of *Patched1* (*Ptc1*), a downstream target of hedgehog signalling, is found alongside the metacarpal anlages, reflecting a potentially broadened domain of *Ihh* signalling in comparison to the mouse forelimb (Kronenberg and Kronenberg 2003; Hockman *et al.* 2008). Overexpression of *Ihh* in cultured chick limbs results in a delay in the onset of hypertrophic differentiation, and the upregulation of bone morphogenic protein (BMP) signalling in the perichondrium and the proliferating chondrocytes (Pathi *et al.* 1999; Minina *et al.* 2001). BMPs play multiple roles during chondrogenesis and are also involved in osteogenesis, *Bmp2/4/5/7* are expressed in the perichondrium, *Bmp7* is also expressed in proliferating chondrocytes and *Bmp6* is expressed in prehypertrophic and hypertrophic chondrocytes (Pathi *et al.* 1999; Minina *et al.* 2001; Yoon and Lyons 2004; Yoon *et al.* 2006; Chen *et al.* 2012). In the bat (*C. perspicillata*), an

increase in the expression of *Bmp2*, and BMP activity (indicated by the phosphorylation of SMAD proteins) was shown to occur the CS20 bat metacarpal (digit ray V) perichondrium (Sears *et al.* 2006). This was shown to stimulate cell proliferation events in the growth plates. In addition, it promoted hypertrophic differentiation, while inhibiting terminal hypertrophic differentiation, resulting in an increase in the proportion of the metacarpal hypertrophic cell zone (as compared to the mouse forelimb). This increase, was suggested to result in the exponential growth of bat forelimb bones during fetal development (Sears *et al.* 2006). In addition to the fast transition into hypertrophy, and short lifespan of terminal hypertrophic cells reported, the hypertrophic cells of the bat forelimb are uniquely large, a feature that contributes to the majority of skeletal element elongation (Farnum and Wilsman 2001; Farnum *et al.* 2008a). While this feature has not been examined earlier in development, it is likely that similar mechanisms are at play during late chondrogenesis and early endochondral ossification in bat digits. The strong expression of the 5'HoxD genes in the bat forelimb, particular the notable overexpression of *Hoxd10* and *Hoxd11* (CS17), as compared to the mouse forelimb, found in this study, position these genes to mediate a regulatory cascade upstream of the reported increase in *Bmp2* expression in the perichondrium of CS20 bat metacarpals (Sears *et al.* 2006). In addition, the 5'HoxD genes continue to be differentially expressed between bat forelimbs and hindlimbs during later fetal growth (Wang *et al.* 2010, 2014), in this context 5'HoxD genes may play a role in mediating the rapid transition to hypertrophy reported for postnatal bat skeletal elements (Farnum *et al.* 2008a).

Recent work has shown 5'HoxD gene expression in the autopod plays a direct role in specifying cell polarity in the developing metacarpal, a key feature in the organisation of cells during chondrogenesis (Romereim and Dudley 2011; Kuss *et al.* 2014). *Hoxd13* and *Wnt5a* are co-expressed in the region surrounding the metacarpal condensations, and HOXD13 is able to drive both *Wnt5a* and *Wnt5b* expression in DF1 cell lines (Kuss *et al.* 2014). The reduction of HOXD activity in the *Spdh* mouse mutant caused a similar loss of cell orientation in both growth plates and perichondrial cells as found in *Wnt5a* mutant mice (Kuss *et al.* 2014). It is interesting to note that when *Hox9/10/11* paralog gene expressions are lost (*aaDd* and *Aadd* mouse mutants) in developing zeugopod elements, this results in the misorientation of dividing prehypertrophic chondrocytes with *aadd* mutants showing a reduction of *Lef1* (a transcription factor effector of Wnt signalling) in these elements (Raines *et al.* 2015), indicating that 5'HoxD genes may also play a role in mediating interaction with *Wnt* genes. The specification of cell polarity plays a key role in chondrogenesis, positioning perichondrial cells to form a constraining sheath, organising chondrocytes into clonal columns prior to hypertrophic differentiation, and orientating cell growth events (Romereim and Dudley 2011). Events that are key in driving bone elongation. The upregulation of 5'HoxD genes in the bat forelimb and loss of expression in the bat

hindlimb, may, at later stages of chondrogenesis, drive elongation events through regulating Wnt signalling in the digit element condensations.

4.6.5. Upregulation of Hoxd10 and Hoxd11 expression in the bat forelimb is positioned to selectively elongate the digits II-V

The high transcript abundance of *Hoxd10* and *Hoxd11* in the CS17 bat forelimb as compared to the mouse is intriguing, as these genes are specifically involved in digit skeletal element growth of the posterior digits (II-V) in the mouse, (Montavon *et al.* 2008; Delpretti *et al.* 2012). These are the digits that undergo elongation in the bat forelimb. At these stages *Hoxd10* and *11* expression patterns are indistinguishable from one another, and are found surrounding the cartilage templates of DII-V in bat and mouse forelimb autopods. They are not expressed in the perichondrium, as originally reported (Dollé and Duboule 1989; Yokouchi *et al.* 1991; Davis and Capecchi 1994), but rather in the mesenchymal cell layer adjacent to this tissue and in forming joint regions (Suzuki and Kuroiwa 2002).

In zeugopod elements, *Hoxd10* and *Hoxd11* play predominant roles and loss of function mutants have been well characterised. *Hox11* mutants (*Hoxd11*$^{-/-}$;*Hoxa11*$^{-/-}$ and *Ulnaless*) had smaller condensation sizes, proliferating chondrocytes lost their ability to differentiate into round and columnar chondrocytes, and, at later stages in the ulnar, hypertrophic cells were misorientated (Boulet and Capecchi 2004; Gross *et al.* 2012; Raines *et al.* 2015). In more severe compound (6 *Hox* genes) deletion/frame-shift mutants (*Hoxa9/10/11*$^{-/-}$*; Hoxd9/10/11*$^{-/-}$ or *aadd*), the highly reduced zeugopod elements were composed of resting chondrocytes (E14.5) that were not competent to undergo hypertrophy (Raines *et al.* 2015). This indicates that during chondrogenesis *Hoxd10* and *11* mediate both the initial growth of condensations (resting cells) and play a role in their differentiation to round and columnar chondrocytes and subsequent hypertrophy, a process that plays a vital role in skeletal element elongation during endochondral ossification (Farnum and Wilsman 2001).

Similar phenotypes are found in the autopod when there was a loss of 5'HoxD gene expression, either through the triple deletion of *Hoxd11-13*, *Hoxd*$^{Del11-13}$, or in the mouse *Spdh* mutant that encodes an aberrant, dominant negative HOXD13 protein (Kuss *et al.* 2014). These mutants did not form a competent perichondrium, and exhibited a delay of chondrocyte differentiation in the metacarpals, with cells maintained as reserve chondrocytes that did not undergo differentiation into columnar chondrocytes or mature into hypertrophic cells (González-Martín *et al.* 2014; Kuss *et al.* 2014). An organised growth plate was not apparent, with cells in the cartilage templates being randomly orientated and undergoing isotropic growth (Villavicencio-Lorini *et al.* 2010; González-Martín *et al.* 2014). These

elements failed to form cortical bone; instead undergoing chondrocyte maturation postnatally with ossification resembling that found in carpals/tarsals (Villavicencio-Lorini *et al.* 2010). The activity of the 5'HoxD genes in mediating long bone growth is suggested to be quantitative, with the different paralogs and flanking genes contributing to an overall phenotype (González-Martín *et al.* 2014). Based on these studies, the high levels of expression of *Hoxd10* and *Hoxd11* in the bat forelimb digits II-V may up-regulate genetic networks that favour cartilage condensation and elongation. This is supported for *Hoxd11* where ectopic expression of this gene in presumptive digit I (using retroviral constructs in the chick) resulted in increased condensation size, elongation of these elements and the formation of an additional joint region (Goff and Tabin 1997). In the mouse, duplication of *Hoxd11*, leading to a two-fold overexpression of this gene in its endogenous expression domains, resulted in the significant elongation of several autopod elements (metacarpals of DII, DIII, DIV and DII P1 and P2) (Boulet and Capecchi 2002). Interestingly, further gain of function mutants have not been reported. Further characterisation of 5'HoxD gene expressions in bat limbs, by quantifying specific digit ray expression, and corresponding these with element lengths, should provide a better insight into the role that they play.

4.6.6. Symmetrical bat hindlimb digits have a loss 5'HoxD expression during their formation

In addition to a gain in expression of these genes, WISH and qPCR analyses support the loss of *Hoxd10*, *11* and reduction in *Hoxd12* expressions in the developing hindlimb from CS16 onwards. This represents a modulated activity of these genes targeted to digits II-V, which appear shortened in the bat hindlimb, relative to the mouse hindlimb. No differences in expression pattern could be found for *Hoxd13*, as reported previously (Chen *et al.* 2005; Ray and Capecchi 2008). Several loss of function experiments support a dose-dependant effect of 5'HoxD gene expression on digit length, with digits becoming progressively shortened with the loss of additional 5'HoxD genes (Davis and Capecchi 1996; Zákány *et al.* 1997; Montavon *et al.* 2008; Delpretti *et al.* 2012). 5'HoxD gene expression has been shown to be involved in both the initial growth of condensations and in growth plate formation (Villavicencio-Lorini *et al.* 2010; Gross *et al.* 2012; Raines *et al.* 2015), and have been suggested to alter the growth rates of proliferating cells in the cartilage template (Goff and Tabin 1997). Low levels of 5'HoxD gene expression in the bat hindlimb can be corresponded to the symmetrical reductions in these digit ray elements, indicating that these may have low, uniform growth rates, as found in the growth plates of all hindlimb elements in the postnatal bat (*Eptesicus fuscus*) (Farnum *et al.* 2008b). However, this does not fit well with the finding that the mouse forelimb, which maintains clear 5'HoxD expression until late stages of development, has the shortest autopod skeletal elements of all

limb types compared. Nor is it supported by the mouse *del9-11* mutant that, like the bat hindlimb, exhibits reduced *Hoxd12,* and loss of *Hoxd9*, *10* and *11,* expression in the autopod. This mutant has shortened, asymmetrical digit rays, with DI and DV being noticeably shorter than those of DII-IV (Delpretti *et al.* 2012). This indicates that factors, in addition to the decrease in *Hoxd10-12* expression, may be at play in forming the shortened, symmetrical bat digits.

The generation of bat hindlimb digit symmetry involves two processes, the expansion of the footplate at early stages of autopod development to promote the initiation of uniform digit rays (Hockman *et al.* 2008, 2009), and the maintenance of equivalent growth rates or compensatory elongation of specific elements to generate uniformity (Farnum *et al.* 2008b). Prior to the loss of expression of *Hoxd10*, *11* and *12*, the 5'Hoxd genes are expressed uniformly across the bat CS15 distal hindlimb autopod, in a similar domain as *Shh* expression seen at CS16, potentially playing a role in its reactivation (Hockman *et al.* 2009). This late phase of uniform distal *Shh* expression in the CS16E bat hindlimb is suggested to promote mesenchymal expansion of the autopod over the anterior-posterior axis, and allow for uniform condensations to be generated and underlying early patterning symmetry in the hindlimb autopod (Hockman *et al.* 2008). The loss of modular domains of 5'HoxD activities (i.e. regions of differing levels of expressions of *Hoxd10*, *11* and *12*) may have an effect on subsequent cartilage template growth, to create more uniform, reduced chondrogenic parameters, maintaining the initial hindlimb symmetry. It is interesting to note that low levels of expression of *Hoxd12* were found in digit I, of both the bat forelimb and hindlimb. This may correspond to their relative elongation as compared to the mouse.

4.6.7. Quantitative reverse collinear expression of the 5'HoxD genes is not maintained in bat limbs

The 5'HoxD genes have an integrated regulatory strategy and are expressed in a reverse collinear manner in the autopod. In mouse digits, expressions of these genes are driven by long-range interactions among centromeric enhancer regions and conserved non-coding elements (Spitz *et al.* 2003; Montavon *et al.* 2008, 2011). Proximity to this 5' enhancer region alters gene expression levels, with deletions of the more 5' *Hoxd* genes causing a successive upregulation in the expressions of their 3' neighbours. This gene ranking system appears to play the primary role in determining the relative level of 5'HoxD gene expression, but is not the only mechanism at play (Montavon *et al.* 2008). In the mouse autopod, these enhancer regions (bound proteins along the GCR and Prox regions and possibly the regulatory archipelago) first interact with the intergenic region between *Hoxd13* and *Evx2* (a gene

adjacent to the 5' region of *Hoxd13*), binding to promoter sequences in this region. This enhancer then undergoes a 'microscanning' process, in which it has short-range interactions with promoters in nearby regions (in an affinity dependent manner) driving the expressions of associated genes at different levels (Montavon *et al.* 2008).

Based on this regulatory strategy, *Hoxd13* has the highest levels of expression, *Hoxd12* and *Hoxd11* intermediate levels and *Hoxd10* very low levels of expression in mouse distal digits (Montavon *et al.* 2008). In the mouse model of quantitative collinearity, *Hoxd12* and *11* appear to have similar promoter 'affinities' as they have similar wildtype expression levels, and similar gains in expressions in mutants (increasing in a similar manner in either deletions of the more 5' genes or when duplicated) (Montavon *et al.* 2008). However, in the bat (*M. natalensis*) autopods, significant differences were found between *Hoxd12* and *11* expression levels, with lower expression of *Hoxd11* that was more dramatic within the hindlimb. *Hoxd11-13* did appear to follow the trend of reverse quantitative collinearity whereby the more 3' genes were expressed at lower levels than their 5' neighbours.

The finding that *Hoxd10* expression was over 10 fold higher in the FL as compared to *Hoxd13* does not agree with the mouse model of quantitative collinearity in the HoxD locus. This is difficult to resolve with current knowledge supporting a high conservation of this cluster in bats as compared to other vertebrates (Cretekos *et al.* 2005; Ray and Capecchi 2008), and RNA-seq data indicating low expression of this gene in the digit regions of the bat, *M. schreibersii* (Wang *et al.* 2014). These anomalous results are attributed to incorporation of more proximal tissue (distal zeugopod and basipod), which does have high expression of the more 3' 5'HoxD genes (Andrey 2013). This is supported by the finding of strong array signal for *Hoxd10* in the E12.5 mouse autopods that were dissected off at a similar region (Shou *et al.* 2005).

4.6.8. Loss of Hoxa13 expression in the bat forelimb autopod may underlie the upregulation of Hoxd10 and Hoxd11

The 5'Hox paralogs have the capacity to regulate their own activities. When Hox genes are co-expressed, the more 5' genes are functionally dominant (a feature known as posterior prevalence), with the activities of *Hoxa13* and *Hoxd13* in the autopod region playing a primary role in growth, patterning and skeletal elongation (Duboule and Morata 1994). *Hoxa13* plays a dominant role, with its expression in the autopod separating early proximal Hox expression in the zeugopod from the later expression in the autopod (Sheth *et al.* 2014). The loss of *Hox13* paralog expressions ($Hoxa13^{-/-}$;$Hoxd11\text{-}13^{-/+}$) or activities (through the disruption of the HOXA13 homeodomain) results in the ectopic expression of

Hoxd10 and *Hoxd11* (in conjunction with the loss of *Hoxd13* expression) in the most anterior portion of the autopod (digit I) in the E12.5 mouse (Sheth *et al.* 2014). The loss of *Hoxa13* expression alone appears to increase the expression domain and levels of *Hoxd10* throughout the entire autopod region (in conjunction with an expansion of *Hoxa11*). Loss of expression of these genes (*Hoxa13*$^{-/-}$;*Hoxd13*$^{-/-}$) allows the expansion of the expression of more anterior Hox genes across the entire autopod (Sheth *et al.* 2014). This is suggested to be due to the gain of the early phase of enhancer activity (ELCR) in the autopod and/or extension of the late phase enhancer activities more 3' *Hox* genes (Sheth *et al.* 2014). *Hoxa13* expression defines the boundary of the transition between these two regulatory strategies, and is suggested to be a central component in regulating their balance, however the mechanism by with this occurs is currently unknown.

In the bat, the loss of *Hoxa13* in the posterior distal domain of the forelimb autopod (over digit III) corresponds to the domain of intense expression of *Hoxd10* and *Hoxd11*. In the mouse, the complete absence of *Hoxa13* expression results in the distal expansion of the earlier proximal expression domain into the autopod region (Sheth *et al.* 2014). It is possible that the loss of *Hoxa13* expression within a domain of the autopod could result in the upregulation of more anterior 5'HoxD genes in this region through a similar mechanism. Either through the loss of Histone/chromatin modifications of the early first phase (telomeric) enhancer region, or through the local disruption of chromatin conformation within the HoxD cluster. This may result in the generation of elongated digit ray condensation in this region, in a similar manner to what is found when *Hoxd11* is ectopically activated in digit I of the chick (Goff and Tabin 1997).

4.6.9. 5'HoxD gene protein coding regions are highly conserved in bats and other vertebrates

In support of previous studies, the 5'HoxD genes and their encoded proteins show strong conservation in vertebrates and in the bat species examined (Chen *et al.* 2005; Ray and Capecchi 2008; Wang *et al.* 2014). No robust evidence of positive selection events was found, while these genes showed signals of strong purifying selection. HOX proteins have several well-characterised poly (amino acid) motifs that, when altered, affect protein availability, function, and have associated phenotypic effects during development (Tut *et al.* 1997; Anan *et al.* 2007). The expansion of a poly-alanine motif in HOXD13, also identified in HOXA13, RUNX2 and SOX9, results in misfolding, cytoplasmic localization, aggregation and degradation of these transcription factors (Albrecht *et al.* 2002). The expansion of this motif in HOXD13, results in the mouse mutant, synpolydactyly homolog (*spdh*), that exhibits limb patterning and cartilage growth defects by acting as a dominant negative inhibitor of HOXD11-13

protein function (Johnson *et al.* 1998; Bruneau *et al.* 2001; Kuss *et al.* 2009). Polymotifs were present in HOXD11 and HOXD13 but were unaltered in bats as compared to the vertebrates examined. HOXD11 and HOXD12 each had two amino acid changes in bat lineages, with one of these appearing to alter side chain properties. However these regions are not currently associated with functional differences in protein activities. Previously identified alteration of an amino acid in the CDS of HOXD13 (Ray and Capecchi 2008) was not supported in this analysis. Overall the protein sequences of these genes are highly conserved in bats and likely have similar activities during development.

4.6.10. Alterations in digit enhancer may result in differential expression of the 5'HoxD genes

The tight regulation of the HoxD cluster is dependant on its genomic organisation; with epigenetic mechanisms co-ordinating each gene's sequential and restricted expression in specific tissue regions at specified times (reviewed by Srivastava *et al.* 2015). Chromatin conformation and locus availability allows interactions between long-range enhancers and local locus control elements, through binding transcription factor complexes to drive or repress transcription (Kmita and Duboule 2003; Montavon and Duboule 2013). The long range enhancer regions controlling digit specific 5'HoxD gene expression have been well characterised, and are thought to be a recent evolutionary development (Kmita, Fraudeau, *et al.* 2002; Kmita, Tarchini, *et al.* 2002; Spitz *et al.* 2003; Montavon *et al.* 2011; Tschopp *et al.* 2011; Andrey 2013; Andrey *et al.* 2013; Montavon and Duboule 2013), while local regulatory elements within the clusters are thought to have much deeper evolutionary origins (Spitz *et al.* 2001; Srivastava *et al.* 2015). The interactions between multiple conserved enhancer and gene loci within this complex have the potential to allow for modulated expressions of this metagene, conferring an evolutionary plasticity to the autopod digit regions that may lead to the generation of morphological diversity seen both within and amongst organisms (Montavon *et al.* 2011).

Alterations in cis-regulatory regions potentially mediate gene expression differences both temporally and spatially, through the modification of transcription factor binding sites (Wittkopp and Kalay 2011). In the forelimb and hindlimb this can be through the loss of an enhancer region that drives expression in a limb specific manner, or through the loss of a binding site that is responsive to a limb specific binding factor. In a simplistic model, the gain of a transcription factor binding site that is responsive to a forelimb specific factor may result in increased expression in this limb type while the loss of a transcription factor in this enhancer region that requires a hindlimb specific transcription factor may result in the loss of expression in the bat hindlimb. A small number of transcription factors are known for their limb type specific expression, key amongst these are *Tbx5* (expressed in the forelimb only),

Tbx4 and *Pitx1* (expressed in the hindlimb only) (Gibson-Brown *et al.* 1996; Logan and Tabin 1999; Glaser *et al.* 2014).

In mouse digits expression is driven, in a reverse-collinear fashion, by centromeric enhancer regions that include the GCR, Prox and a series of conserved noncoding elements found within 800 kb of the cluster (Montavon *et al.* 2011; Tschopp and Duboule 2011; Tschopp *et al.* 2011). Transgenic mouse assays have shown that both the GCR and Prox sequences are required to recapitulate endogenous distal *Hoxd13* expression (Gonzalez *et al.* 2007). The GCR contains two conserved sequences, CsA and CsB, and drives both neural expression and limb specific expression (Spitz *et al.* 2003; Gonzalez *et al.* 2007), this region was highly conserved in vertebrates, but did show several changes that were specific to bats (*R. ferrumequinum* and *M. lucifugus*), including seven nucleotide changes in ultra conserved regions. The bat (*R. ferrumequinum*) GCR was able to drive expression in novel domains in transgenic mice, this included activity in the stylopod, and zeugopod, from E11.5 to E16.5 (Ray and Capecchi 2008).

The conserved enhancer region, Prox, can drive expression in the distal region from E11.5 to E15.5 in both the forelimb and the hindlimb, early expression is predominantly interdigital with later expression localising around the condensing digits (Gonzalez *et al.* 2007). Prox contains the evolutionarily conserved element CsC, that itself has two highly conserved regions, CsC1 and CsC2, with transgenic assays indicating that CsC2 is required for the digit enhancer function of this region (Gonzalez *et al.* 2007). Several nucleotide alterations in transcription factor binding sites specific to bats were noted in these regions, however, based on a limited motif analysis, they did not represent convincing candidates for mediating bat specific alterations in 5'HoxD gene expressions. Examinations of sequence regions bound by factors that are expressed in either the forelimb (*Tbx5*) or the hindlimb (*Tbx4*, *Pitx1*) also indicated strong conservation of these binding motifs.

Further work is needed to characterise the non-coding regions surrounding the HoxD cluster to determine what alterations in regulatory regions underlie the novel expression of this cluster in bats. It would be of particular interest to focus on motifs bound by either forelimb or hindlimb factors. It is expected that the loss the binding site of a limb specific transcription factor would underlie the divergence of these two limb types, possibly through driving altered downstream gene expressions such as that of the 5'HoxD genes.

5. Conclusions and future work

5.1. Conclusions

This study has examined the expression of genes in the developing bat limbs in the context of interdigital webbing retention and skeletal elongation. Several novel findings have resulted from this work, which complements recent work performed in other bat species. The characterisation of *Meis2* and the 5'HoxD gene expression in *M. natalensis* confirms the two most dramatic changes found in bat development to date (Dai *et al.* 2014; Wang *et al.* 2014), providing a clear resolution of their expressions at several developmental stages in the bat autopod.

This is the first quantitative analysis of *Meis2* expression in bat limbs over a full series of autopod development (CS15-CS18). Expressions of this gene were examined in the mouse and the bat giving a full comparative description and finding unique expression domains. Results suggest that upregulation of *Meis2* transcripts in the interdigital webbing of the developing bat forelimb is a feature of tissue retention, and possibly stimulates the expansion of the chiropatagium and supports the outgrowth of digits II-V in the bat. The lower expression of *Meis2* in developing mouse forelimb and hindlimb autopods may play a similar, albeit reduced part in sculpturing the tetrapod hand and foot, by maintaining a pool of proliferating interdigital cells that stimulates digit outgrowth, and marks marginal interdigital tissue. Importantly, expression of *Meis2* in the autopod was activated independently of RA, with interdigital *Meis2* expression present in a mouse mutant that lacks RA signalling and maintains interdigital tissue (*Rdh10*^{wrex}), and absent in the bat hindlimb that maintains RA signalling while undergoing interdigital regression. *Meis2* expression domains did not correlate with RA availability, however genes involved in RA synthesis (*Aldh1a2*) and degradation (*Cyp26b1*) had a modulated pattern of expression in the bat forelimb. Lowered RA availability corresponded to shorter anterior digits and higher availability corresponded to elongated posterior digits during later stages of digit development (CS17). This differing availability is positioned to modulate digit specific formation and growth, through altering differentiation events. Unlike in early limb bud development, *Meis2* was expressed in the presence of *Hoxa13* in the mouse interdigits. While *Hoxa13* expression did become lowered in the bat forelimb as compared to the hindlimb, the expression patterns of *Meis2* did not correspond with this loss. Instead this reduction in *Hoxa13* expression may allow the increased local activation of 5'HoxD gene expression during early bat forelimb autopod development, integrating events involved in interdigital webbing expansion, with those that underlie digit formation and growth.

The examination of adult limb skeletal element lengths in this species, commonly used in limb developmental studies (Hockman *et al.* 2008, 2009; Mason *et al.* 2015), represents the first characterisation of the adult limb phenotype of *M. natalensis*, and corresponds with the elongation of their posterior digits with the early autopod expressions of *Hoxd10-12*. This work provides novel contributions regarding the relationships among these 5'HoxD gene expressions in the bat forelimb and hindlimb, and is the first direct comparison of relative gene expressions in bat and mouse forelimbs. Strongly elevated expressions of *Hoxd10* and *11* were found in the bat forelimb, these two genes were the also highly differentially expressed between the bat forelimb and hindlimb. *Hoxd10* and *11* are positioned to underlie the reactivation of the SHH-FGF feedback loop in bat autopods and likely contribute to the divergent skeletal element lengths of the forelimb and hindlimb. This represents the first analysis of absolute levels of transcript abundance in bat limbs, finding that *Hoxd10* transcripts were overrepresented in the bat autopod. This may be attributed to an alteration in the conventionally reverse-collinear gene activation mechanism, however sampling strategy artefacts cannot be discounted. This study provides the first analysis of the a highly conserved regions (CsC) within the digit specific enhancer Prox, in multiple bat species, examining these regions in an alternative species to that of the mouse, and finding several sites that show a unique conservation in bats as compared to other vertebrate species.

5.2. Limitations of this study

The focus on characterising the expressions of eleven genes of interest in this study was necessarily limited, with examination of expressions restricted to the window of autopod development. Sample numbers were constrained, with stage-wise biological repeats not performed for some WISH experiments (*Hoxa11* and *Hoxa13*), in these cases presence or loss of signal was confirmed by examining transcript abundance. Wild-caught bat embryos were used, and these did not typically allow for direct stage wise comparisons, therefore emphasis was put on performing *in situ* analyses of each gene as a developmental series to elucidate the expression dynamics.

The incorporation of more proximal tissue into the autopod sample analysed during early limb development (CS15), necessitates a careful interpretation of the data. In this study the entire autopod was selected, this was done to ensure that the point of dissection had clear markers and resulted in an unbiased, biologically repeatable sampling of the forelimb and the hindlimb tissues at several stages of development (Hockman *et al.* 2009). While this is a successful strategy for high throughput comparisons (Mason *et al.* 2015) and did not appear to be an issue with the other genes examined

(*Meis2*, *Hoxa13*, RA genes), this approach suffers when attempting to resolve the digit specific expressions of the 5'HoxD cluster. This is due to the proximity of their proximal and distal expressions of *Hoxd10* and *11*. Based on analyses of *Hoxa11*, this does not bias differential expression analyses comparing forelimb and hindlimb expressions, but must be taken into account when comparing developmental stages. In future, the late, distal expressions of the 5'HoxD genes should be examined in tissues that only include the distal digit regions. This will facilitate comparisons of digit specific expression with that of the literature, (Montavon *et al.* 2008; Wang *et al.* 2014), and ensure the accurate interpretation of data. This was not possible in this study due to the original sampling strategy and subsequent limited sample availability, however future work on these genes in the bat must take this into consideration.

The developing autopod is a complex system, composed of several different tissues. Autopods have a modular development and can be separated into regions, tissues and cell types that have distinct identities and gene expressions (Reno *et al.* 2008; Wang *et al.* 2014). The qPCR experiments were designed to examine the change in gene expression over progressive stages of development, and autopods were not subdivided to resolve expression in the different autopod regions. However, WISH shows that *Hoxd10* expression in the distal zeugopod, posterior interdigital tissue and in the FL digit rays (II-V). To understand whether the high levels of expression of *Hoxd10* originate from the distal zeugopod, additional samples need to be obtained, and this tissue should be dissected out (in both the forelimb and the hindlimb), and quantified in separately, as performed for the mouse (Andrey 2013). Expressions of specific digit and interdigit regions could be also examined independently, as performed in the chick (Wang, Young, *et al.* 2011) to quantify expression in the specific digit rays and interdigital tissue. This extends to the examination of the 5'HoxD expression in the digit rays and/or growth plates, where a greater understanding of their relationship would be obtained from examining their expressions in isolated tissues and/or cells.

While offering a first, broad view of gene expressions, the whole-mount approach used in this thesis suffers from low resolution and potential for artefacts. Section *in situ* work on these tissue regions would offer cell-level resolution, while florescent *in situ* hybridisation (FISH) has the potential to probe for multiple transcripts and examine deep tissue expression when paired with confocal microscopy. FISH could be combined with immunofluorescence signals to visualise overlap with protein products in 3 dimensions (Neufeld *et al.* 2013). Specifically, it would be informative to examine the overlap of transcripts and the cellular localisation (cytoplasmic or nuclear) of MEIS2 in the interdigital tissues,

along with that of potential, or identified, co factors and characterise the expressions of the 5'HoxD genes in at higher resolution in the autopod and growth plates.

On a final note, it would be beneficial to explore the role of genes that have been implicated in processes unique to bat limb development. It would be particularly informative to functionally characterise *Meis2*, as the role of this gene has not been examined during autopod development. The 5'HoxD genes have been functionally characterised in several systems with a plethora of literature exploring the role that they play in limb patterning and skeletal element growth (Morgan *et al.* 1992; Goff and Tabin 1997; Delpretti *et al.* 2012; González-Martín *et al.* 2014). While loss of function mutations clearly show that a threshold of HOX activity is required for the formation and growth of long bones (González-Martín *et al.* 2014), the effect of increased expression in specific regions of the autopod is not clear and could be informed by a more detailed examination in both the bat and mouse development.

Overall, this work offers several new insights into interdigital webbing retention, and skeletal elongation, two integrated processes that are involved in forming the highly modified limbs of bats and contributes novel findings to the growing body of knowledge that examines the genes and genetic networks involved in specifying the unique morphologies of bat forelimbs and hindlimbs.

5.3. Future work

This work provides a foundation for additional research questions to be asked and tested.

5.3.1. How are the morphologies and early patterning events altered in bat limbs?

Much of the work on *Meis2* in the developing limb has focused on characterising its expression in the context of limb patterning and outgrowth. The early, seemingly upregulated expression of *Meis2* in the bat hindlimb (Dai *et al.* 2014) was not explored. This thesis focused specifically on the development of the bat autopod, with sample limitations precluding the study of these earlier patterning events. To gain a further understanding of this observation, proximodistal patterning events should be characterised during early limb bud formation and outgrowth in bat limbs. The expression domains of this gene along with those of zeugopod and autopod markers (*Hoxa11* and *Hoxa13*) should be corresponded to alterations in the morphologies in the early limb bud before further conclusions can be made. Examination of these expression domains could be complemented by characterising the formations of the cartilage templates (through *Sox9* expression) to create a model of outgrowth for the bat autopod.

Examination of these processes over early stages of limb bud formation and outgrowth would provide novel insight into its early patterning and inform on how a pentadactyl autopod structure is maintained in a handplate that experiences asymmetric mesenchymal expansion (Cooper *et al.* 2014; Raspopovic *et al.* 2014).

5.3.2. Does overexpression of Meis2 in the interdigital mesenchyme result in the maintenance or expansion of this tissue?

This work clearly illustrates the expression of *Meis2* in the distal limb, specifically in the interdigital tissues of bat and mouse autopod. It does not address the functional role of this gene in this context, with this line of work being a necessary component to understanding the mechanism of interdigital webbing retention in bats. The overexpression and ectopic expression of *Meis2* in the developing chick and mouse limb bud leads to shortening and truncations of distal limb elements, in addition to the retention of interdigital webbing (Mercader *et al.* 1999, 2009; Capdevila and Izpisúa Belmonte 2001). These studies explore the function of *Meis1/2* in early patterning events, using viral integration and vector injections of chick limb buds and transgenic activation of this gene in the full mouse limb from limb bud formation onwards, to distalise early proximal expression. Resulting phenotypes are likely due to massive permutations of the early patterning events that occur during limb bud outgrowth. Endogenous interdigital expression of this gene in the mouse is very low, indicating that if this gene has a function in this region, it is likely to be localised, therefore a targeted approach is required to characterise the function of *Meis2* expression in this region, with overexpression in the interdigital tissues (ectoderm and mesoderm) from E13.0 onwards. This could be performed using a recently developed conditionally targeted transgenic mouse (Bmp2CreER) that uses *Bmp2* regulatory elements to drive expression in the distal interdigital mesenchyme. This mouse has tamoxifen-inducible Cre-LoxP and shows appreciable activity in the E13.5 interdigital tissues 24 hrs after treatment (Huang and Mackem 2015). Other transgenic mouse lines that could be considered are Hoxb6CreER^{T} (Nguyen *et al.* 2009), and Osr1Cre (Grieshammer *et al.* 2008), however these have less localised interdigital transgene activities. These transgenic mice provide systems in which the effects of *Meis2* overexpression (in addition to other genes identified in the bat) can be examined in the interdigital tissue of the mouse. In addition to describing the resulting phenotype through cartilage staining and taking measurements of interdigital tissue areas, assays for cell death and proliferation should be performed to quantify the differences in these parameters between transgenic and wild type mice (Hernández-Martínez *et al.* 2009). Similar experiments can be performed in the chick using stable gene transfer though electroporation (Tol2 Tet-on system) (Wang, Song, *et al.* 2011; Nakamura and Funahashi 2013).

5.3.3. What are the targets of MEIS2 in the developing limbs?

Though well described in other systems, the targets of *Meis2* in the developing limb are currently unknown. The role of *Meis2* in promoting cell cycle events in neuroblastoma cell lines is mediated through the transcriptional activation of *Forkhead box protein M1* (*Foxm1*), through the binding of MEIS2 with its promoter (Zha *et al.* 2014). FOXM1 forms part of a larger complex (MuvB-BMYB-FOXM1) that functions as a regulator of late cell-cycle gene expression (Sadasivam *et al.* 2012). *Foxm1* is expressed in both the forelimb and hindlimb bud of the mouse, strongest in the distal regions during early stages of limb bud outgrowth (E10.5, EMAGE:1313; Gray *et al.* 2004). It has weak interdigital expression (E12.0, EMAGE:28289) and can be seen in digit tips of later stages (E14.5, Genepaint:MH632), with overexpression of this gene being found in mouse strains that are able to rapidly regenerate their digit tips (Chadwick *et al.* 2007). While this gene is expressed in the autopods of *M. schreibersii* (pooled CS15, CS16, and CS17) it does not appear to be differentially expressed in response to the high levels of *Meis2* found in the forelimb webbing (Wang *et al.* 2014). Another candidate is *SRY (sex determining region Y)-Box 3* (*Sox-3*), an early marker of neuronal fate, which has been shown to be activated by MEIS1/PBX1 binding in NT2/D1 cell lines after exposure to RA (Mojsin and Stevanovic 2010). *Sox3* transcripts can be detected in the E11.5 mouse limb (Collignon *et al.* 1996). Bat patagia are composed of a complex network of nerves and muscles (Tokita *et al.* 2012) and a role for *Meis2* in organising the migration and development of these cells should be considered. The only known target gene of MEIS2 in limb tissues is *Prod1*, a gene expressed in the regenerating limbs blastema of urodele amphibians (salamanders) (Da Silva *et al.* 2002; Mercader *et al.* 2005; Shaikh *et al.* 2011). *Prod1* encodes a cell-surface protein belonging to the three finger-protein superfamily, and encodes proximodistal identity of the regeneration blastula through regulation cell adhesion, migration and division (Da Silva *et al.* 2002; Echeverri and Tanaka 2005; Kumar *et al.* 2007). Interestingly *Prod1* is an 'orphan' gene, with no recognised ortholog in vertebrates, its evolution in salamanders, and role in conferring positional identity in the adult limb, has been linked to the unique capability of extensive appendage regeneration in this group (Garza-Garcia *et al.* 2009, 2010; Geng *et al.* 2015).

More work is needed to determine the downstream targets of *Meis2* overexpression during limb and autopod development. In the bat recently published RNA-seq data sets can be used to identify genes and pathways that show an upregulation in response to *Meis2* forelimb interdigital expression (Wang *et al.* 2014). Potential gene targets can be characterised, examining surrounding conserved non-coding elements or promoter sequences, in a range of bat species, to select those are enriched for conserved MEIS2 binding sites (Merabet and Hudry 2013; Amin *et al.* 2015; Grice *et al.* 2015; Merabet and

Lohmann 2015). Chromatin immunoprecipitation (ChIP) assays can also be used to identify target sequences that are bound to MEIS2 (Huang *et al.* 2005). Due to the limited availability of bat embryonic tissues, these experiments are best performed in the mouse, and should identify a set of genes with a high probability of interacting with MEIS2. The expressions of these target genes should be examined in this tissue through qPCR and their relationships can be explored in cell lines that overexpressed *Meis2* in response to RA signalling (Freemantle *et al.* 2002).

5.3.4. What cofactors does MEIS2 interact with in the bat limb?

Both HOXA13 and HOXD13 have been shown to have the potential to directly interact with MEIS proteins (specifically MEIS1 isoforms) through multiple interaction domains (Williams *et al.* 2005). Three *Meis2* transcript variants are expressed in bat limbs, RNA-seq analysis of *M. schreibersii* revealed *Meis2a* and *Meis2b,* while cDNA RACE found *Meis2a* and *Meis2d.* These share strong sequence similarity to vertebrate homologs, do not appear to be under positive selection in the bat and are expected to function in a similar manner as those in the mouse (Curry 2014; Dai *et al.* 2014). *Meis2e*, a transcript that encodes a homeodomain-less protein that acts as a dominant negative regulator of *Meis2d* transcription (Bürglin 1997; Yang *et al.* 2000), was not found and can be excluded. *Meis2a* includes all exons from the *Meis2* locus, while *Meis2b* has a truncated exon 11 (originally identified as exon 3A), these isoforms terminate at an early stop codon (within exon 12a, originally identified as exon 4), with the protein encoded by *Meis2a* containing an additional stretch of 7 amino acids after the homeodomain. *Meis2d* also has a truncated exon 11 and has lost exon 12a; this isoform terminates at a later stop codon (within exon 12b) (Yang *et al.* 2000; Irimia *et al.* 2011). These transcripts correspond to MEIS2A.1, Meis2A.2 and MEIS2B.2 respectively.

These isoforms have all been shown to have the ability to bind to DNA with differing activities. The more predominant A isoform has a reduced protein activity both in terms of its ability to induce transcription and its responsiveness to cell signalling (Maeda *et al.* 2001; Huang *et al.* 2005; Shim *et al.* 2007; Irimia *et al.* 2011; Sánchez-Guardado, Irimia, *et al.* 2011). Co-immunoassays using these specific isoforms may be able to identify stable interactions with protein binding partners, possibly HOX or PBX proteins (Williams *et al.* 2005).

5.3.5. Validation of the break in quantitative collinear expression bat limbs

While this study points only towards the upregulation of *Hoxd10* and *Hoxd11* in the bat as compared to the mouse, this does not easily align with the tight co-regulation of this cluster in the distal autopod.

Though the downregulation of *Hoxa13* does imply that alternative (telomeric) enhancer regions may mediate this interaction in the bat limb (Sheth *et al.* 2014), this must be confirmed. Care must be taken to account for the effect of absolute transcript abundance on these fold change analyses, which bias analyses towards finding strong fold changes in genes that are expressed at low levels. In addition, strong variation exists amongst the biological samples of these highly expressed genes, contributing towards a loss of resolution of any potential differential expression. While a clear upregulation of both *Hoxd10* (which is in fact expressed at high levels) and *Hoxd11* is shown in this work, it may be likely that this extends to the more 5'HoxD genes (as found in the microarray data) as indicated by Wang *et al.* (2014). This qPCR data may be reconfirmed prior to publication through alternative methods of quantification such as sigmoidal curve fitting (e.g. Linear regression of efficiencies, LRE, which do not require the generation of multiple standard calibration curves) (Liu and Saint 2002; Rutledge 2004; Rutledge and Stewart 2010) of the use of hydrolysis probes (e.g. TaqMan®) or dual hybridisation probes (e.g. FRET probes). These methods link the specific hybridisation of a labelled probe to the target of interest with the generation of fluorescence in the sample (VanGuilder *et al.* 2008). Additional analysis, potentially through RNA-seq analysis of mouse and bat autopods would also clarify this issue.

5.3.6. What pathways and processes are affected by the expression of Hoxa13 and the 5'HoxD genes in bat autopods?

While loss of function mutations clearly show that a threshold of HOX activity is required for the formation and growth of long bones (González-Martín *et al.* 2014), the effect of increased expression in this region is not clear. Overexpression studies of these key developmental genes in the chick limb, involving the ectopic activation (at the stage of limb bud outgrowth, stage 22) of either *Hoxd11* and *Hoxd13* using retroviral constructs, only resulted in elongation events of digit I where *Hoxd11* was ectopically expressed, with ectopic expression of *Hoxd13* causing reductions of stylopod and zeugopod element lengths (Goff and Tabin 1997). *Hoxd11* overexpression at early stages (stage 10) of limb development resulted in shortening of both the zeugopod and autopod elements, affecting the growth of these elements at later stages of development (Morgan *et al.* 1992). These experiments were resolved with a model of Hox activity whereby all HOXD proteins could positively regulate growth, albeit to differing degrees. *Hoxd13* is suggested to have a weak effect on growth with *Hoxd11* having a stronger effect on growth. This corresponds to the tight control and low expression of *Hoxd11* in the distal autopod, which have relatively short elements, and the predominant expressions of *Hoxd10* and *Hoxd11* in the stylopod and zeugopod, which have larger and longer elements (Goff and Tabin 1997). In this context HOX activities may be modulated by their differing protein or DNA binding potential

or mediated through the presence of specific cofactors (Moens and Selleri 2006; Mann *et al.* 2009; Ladam and Sagerström 2014).

Only a few experiments have illustrated a gain in skeletal element length from the ectopic or enhanced expression of these genes (Boulet and Capecchi 2002). An understanding of their role may therefore be inhibited by intrinsic mechanisms in model systems that inhibit their activities. Further examination of the expressions and interactions of *Hoxd10* and *Hoxd11,* within the context of bat limb development (where their overexpression appears to correspond to an asymmetrically elongated skeletal elements while their loss of expression corresponds to symmetrical short elements) has the potential to give a fascinating insight into these genes. Possibly informing the role that they play in the process of chondrogenesis and endochondral ossification and complementing studies performed in the chick and the mouse.

5.3.7. What chromatin interactions are occurring during 5'HoxD expression in bat limbs?

The complex regulation of the HoxD locus has been well characterised in the mouse limb (Andrey 2013; Noordermeer *et al.* 2014; Woltering *et al.* 2014). Activation of late autopod expression of the 5'HoxD genes requires interactions between multiple enhancer regions (and possibly involves many protein complexes) to alter the genomic landscape to favour their transcription (Montavon *et al.* 2011; Lonfat and Duboule 2015). In addition to the GCR and Prox (Spitz *et al.* 2003; Gonzalez *et al.* 2007), there are several sequence elements, termed 'islands' in the telomeric genomic region. These are highly conserved across vertebrates and have been shown to drive digit specific activity (Montavon *et al.* 2011). In addition there are several highly conserved sequences both 5' of and within the HoxD locus that serve as enhancers or insulators which, when removed, modulate 5'HoxD expression in the autopod (i.e. RX, RXI, RXII; Beckers and Duboule 1998; Hérault *et al.* 1998; Kmita, Fraudeau, *et al.* 2002; Tarchini and Duboule 2006; Montavon *et al.* 2008).

This single *in silico* analysis of Prox has not revealed strong transcription factor candidates for mediating differential expression in the bat limb due to the complex nature of the regulation of the 5'HoxD genes. A more focused approach would be to first characterise the dynamic chromatin architecture of this region in bat autopod development to identify the particular interactions that occur within this context. In the mouse limb this has been done using both Chromosome Conformation Capture (3C), and 4C-sequencing in conjunction with ChIP-seq experiments that indicate loci that are bound by histones with marks of activity (H3K4me3) or repression (H3K27me3) (Montavon *et al.* 2011; Noordermeer *et al.* 2014). These signatures are difficult to resolve in complex (heterogeneous) tissues and would require

careful sampling of tissues to obtain the signal of interest. In this study a particular region of interest found was the triangular domain of strong *Hoxd10* and *Hoxd11* expression in the forelimb autopod at CS15, and the CS16 hindlimb autopod (where there was a distal loss of *Hoxd10* and *Hoxd11* expressions). Examination of the active or repressive marks in these tissues, in combination analyses of regions of sequence interactions will clarify the mechanisms underlying the differential expression of these genes.

5.4. Final words

Overall this study elucidated the expression patterns of previously uncharacterised limb development genes in the bat autopod, in addition to corroborating recently published RNA-seq and WISH experiments that examine *Meis2* and 5'HoxD expressions in a closely related bat species (Dai *et al.* 2014; Wang *et al.* 2014). This work also contributed towards the analysis of the protein coding regions of the 5'HoxD genes (Liang *et al.* 2013), and expanded on limb specific enhancer analyses of the HoxD locus (Chen *et al.* 2005; Ray and Capecchi 2008). These findings make several novel contributions towards the study of bat limb development, and limb development in general, particularly in the context of autopod patterning, digit formation and interdigital regression in vertebrates.

6. References

Abu-Shaar, M., Ryoo, H.D., Mann, R.S. (1999) 'Control of the nuclear localization of extradenticle by competing nuclear import and export signals', *Genes & Development*, 13(8), 935–945.

Ackert-Bicknell, C., Beamer, W.G., Rosen, C.J., Sundberg, J.P. (2011) Aging Study: Bone Mineral Density and Body Composition of 32 Inbred Strains of Mice. MPD:25001 [online], *Mouse Phenome Database web site*, available: http://phenome.jax.org/ [accessed 3 Sep 2015].

Adams, R.A. (1992) 'Stages of development and sequence of bone formation in the little brown bat, *Myotis lucifugus*', *Journal of Mammalogy*, 73(1), 160–167.

Adams, R.A., Pedersen, S.C. (2000) *Ontogeny, Functional Ecology, and Evolution of Bats*, Cambridge University Press: Cambridge, UK.

Adams, R.A., Shaw, J.B. (2013) *Bat Evolution, Ecology, and Conservation*, Springer New York: New York, NY.

Afonja, O., Smith, J.E., Cheng, D.M., Goldenberg, a S., Amorosi, E., Shimamoto, T., Nakamura, S., Ohyashiki, K., Ohyashiki, J., Toyama, K., Takeshita, K. (2000) 'MEIS1 and HOXA7 genes in human acute myeloid leukemia.', *Leukemia Research*, 24(10), 849–855.

Agnarsson, I., Zambrana-Torrelio, C.M., Flores-Saldana, N.P., May-Collado, L.J. (2011) 'A time-calibrated species-level phylogeny of bats (Chiroptera, Mammalia)', *PLoS Currents*, 3, RRN1212.

Agoston, Z., Heine, P., Brill, M.S., Grebbin, B.M., Hau, A.-C., Kallenborn-Gerhardt, W., Schramm, J., Götz, M., Schulte, D. (2014) 'Meis2 is a Pax6 co-factor in neurogenesis and dopaminergic periglomerular fate specification in the adult olfactory bulb.', *Development*, 141(1), 28–38.

Agoston, Z., Li, N., Haslinger, A., Wizenmann, A., Schulte, D. (2012) 'Genetic and physical interaction of Meis2, Pax3 and Pax7 during dorsal midbrain development', *BMC Developmental Biology*, 12(1), 10.

Agoston, Z., Schulte, D. (2009) 'Meis2 competes with the Groucho co-repressor Tle4 for binding to Otx2 and specifies tectal fate without induction of a secondary midbrain-hindbrain boundary organizer.', *Development*, 136(19), 3311–3322.

Akiyama, H., Chaboissier, M.C., Martin, J.F., Schedl, A., De Crombrugghe, B. (2002) 'The transcription factor *Sox9* has essential roles in successive steps of the chondrocyte differentiation pathway and is required for expression of *Sox5* and *Sox6*', *Genes & Development*, 16, 2813–2828.

Akiyama, H., Kim, J.-E., Nakashima, K., Balmes, G., Iwai, N., Deng, J.M., Zhang, Z., Martin, J.F., Behringer, R.R., Nakamura, T., de Crombrugghe, B. (2005) 'Osteo-chondroprogenitor cells are derived from *Sox9* expressing precursors', *Proceedings of the National Academy of Sciences*, 102(41), 14665–14670.

Albrecht, A.N., Schwabe, G.C., Stricker, S., Böddrich, A., Wanker, E.E., Mundlos, S. (2002) 'The synpolydactyly homolog (spdh) mutation in the mouse – a defect in patterning and growth of limb cartilage elements', *Mechanisms of Development*, 112, 53–67.

Altschul, S.F., Gish, W., Miller, W., Myers, E.W., Lipman, D.J. (1990) 'Basic local alignment search tool', *Journal of Molecular Biology*, 215(3), 403–410.

Amali, A.A., Sie, L., Winkler, C., Featherstone, M.S. (2013) 'Zebrafish *Hoxd4a* acts upstream of *Meis1.1* to direct vasculogenesis, angiogenesis and hematopoiesis.', *PLoS ONE*, 8(3), e58857.

Amin, S., Donaldson, I.J., Zannino, D.A., Hensman, J., Rattray, M., Losa, M., Spitz, F., Ladam, F., Sagerström, C.G., Bobola, N. (2015) '*Hoxa2* selectively enhances *Meis* binding to change a branchial arch ground state', *Developmental Cell*, 32(3), 265–277.

Anan, K., Yoshida, N., Kataoka, Y., Sato, M., Ichise, H., Nasu, M., Ueda, S. (2007) 'Morphological change caused by loss of the taxon-specific polyalanine tract in *Hoxd-13*', *Molecular Biology and Evolution*, 24(1), 281–287.

Andrey, G. (2013) *Regulatory Switches Underlie Hoxd Gene Activation in Tetrapod Limbs*, PhD Thesis.

Andrey, G., Montavon, T., Mascrez, B., Gonzalez, F., Noordermeer, D., Leleu, M., Trono, D., Spitz, F., Duboule, D. (2013) 'A switch between topological domains underlies HoxD genes collinearity in mouse limbs', *Science*, 340(6137), 1234167.

Audesirk, T., Audesirk, G. (1999) *Biology: Life on Earth*, 5th ed, Pearson College Division: Upper Saddle River, N.J.

Azcoitia, V., Aracil, M., Martínez-A, C., Torres, M. (2005) 'The homeodomain protein *Meis1* is essential for definitive hematopoiesis and vascular patterning in the mouse embryo.', *Developmental Biology*, 280(2), 307–320.

Bandyopadhyay, A., Kubilus, J.K., Crochiere, M.L., Linsenmayer, T.F., Tabin, C.J. (2008) 'Identification of unique molecular subdomains in the perichondrium and periosteum and their role in regulating gene expression in the underlying chondrocytes', *Developmental Biology*, 321(1), 162–174.

Bar-Or, C., Czosnek, H., Koltai, H. (2007) 'Cross-species microarray hybridizations: A developing tool for studying species diversity.', *Trends in Genetics*, 23(4), 200–207.

Barna, M., Niswander, L.A. (2007) 'Visualization of cartilage formation: insight into cellular properties of skeletal progenitors and chondrodysplasia syndromes', *Developmental Cell*, 12(6), 931–941.

Barrett, T., Wilhite, S.E., Ledoux, P., Evangelista, C., Kim, I.F., Tomashevsky, M., Marshall, K.A., Phillippy, K.H., Sherman, P.M., Holko, M., Yefanov, A., Lee, H., Zhang, N., Robertson, C.L., Serova, N., Davis, S., Soboleva, A. (2013) 'NCBI GEO: archive for functional genomics data sets--update.', *Nucleic acids research*, 41(Database issue), D991–5.

Beckers, J., Duboule, D. (1998) 'Genetic analysis of a conserved sequence in the HoxD complex: regulatory redundancy or limitations of the transgenic approach?', *Developmental Dynamics*, 213(1), 1–11.

Bénazet, J.-D., Bischofberger, M., Tiecke, E., Gonçalves, A., Martin, J.F., Zúñiga, A., Naef, F., Zeller, R. (2009) 'A self-regulatory system of interlinked signaling feedback loops controls mouse limb patterning', *Science*, 323(5917), 1050–1053.

Bénazet, J.-D., Zeller, R. (2009) 'Vertebrate limb development: moving from classical morphogen gradients to an integrated 4-dimensional patterning system.', *Cold Spring Harbor Perspectives in Biology*, 1(4), a001339.

Bennett, S.C. (2000) 'Pterosaur flight: The role of actinofibrils in wing function', *Historical Biology*, 14(4), 255–284.

Ten Berge, D., Brugmann, S.A., Helms, J.A., Nusse, R. (2008) 'Wnt and FGF signals interact to coordinate growth with cell fate specification during limb development', *Development*, 135(19), 3247–3257.

Berthelsen, J., Kilstrup-Nielsen, C., Blasi, F., Mavilio, F., Zappavigna, V. (1999) 'The subcellular localization of PBX1 and EXD proteins depends on nuclear import and export signals and is modulated by association with PREP1 and HTH.', *Genes & Development*, 13(8), 946–953.

Berthelsen, J., Zappavigna, V., Mavilio, F., Blasi, F. (1998) 'Prep1, a novel functional partner of Pbx proteins.', *The EMBO Journal*, 17(5), 1423–1433.

Bessa, J., Gebelein, B., Pichaud, F., Casares, F., Mann, R.S. (2002) 'Combinatorial control of Drosophila eye development by eyeless, homothorax, and teashirt.', *Genes & Development*, 16(18), 2415–27.

Bi, W., Deng, J.M., Zhang, Z., Behringer, R.R., De Crombrugghe, B. (1999) '*Sox9* is required for cartilage formation.', *Nature Genetics*, 22(1), 85–89.

Bickley, S.R.B., Logan, M.P.O. (2014) 'Regulatory modulation of the T-box gene Tbx5 links development, evolution, and adaptation of the sternum.', *Proceedings of the National Academy of Sciences*, 111(50), 17917–17922.

Biemar, F., Devos, N., Martial, J.A., Driever, W., Peers, B. (2001) 'Cloning and expression of the TALE superclass homeobox *Meis2* gene during zebrafish embryonic development.', *Mechanisms of Development*, 109(2), 427–431.

Biesecker, L.G. (2011) 'Polydactyly: How many disorders and how many genes? 2010 update', *Developmental Dynamics*, 240(5), 931–942.

Bininda-Emonds, O.R.P., Jeffery, J.E., Sanchez-Villagra, M.R., Hanken, J., Colbert, M.W., Pieau, C., Selwood, L., ten Cate, C.J., Raynaud, A., Osabutey, C.K., Richardson, M.K. (2007) 'Forelimb-hindlimb developmental timing differences across tetrapod phylogeny', *BMC Evolutionary Biology*, 7(1), 182.

Bishop, K.L. (2008) 'The evolution of flight in bats: narrowing the field of plausible hypotheses.', *The Quarterly review of biology*, 83(2), 153–69.

Bouillet, P., Oulad-Abdelghani, M., Vicaire, S., Garnier, J.-M., Schuhbaur, B., Dollé, P., Chambon, P. (1995) 'Efficient cloning of cDNAs of retinoic acid-responsive genes in P19 embryonal carcinoma cells and characterization of a novel mouse gene, *Stra1* (mouse LERK-2/Eplg2).', *Developmental Biology*, 170(2), 420–433.

Boulet, A.M., Capecchi, M.R. (2002) 'Duplication of the Hoxd11 gene causes alterations in the axial and appendicular skeleton of the mouse.', *Developmental Biology*, 249(1), 96–107.

Boulet, A.M., Capecchi, M.R. (2004) 'Multiple roles of *Hoxa11* and *Hoxd11* in the formation of the mammalian forelimb zeugopod.', *Development*, 131(2), 299–309.

Bruneau, S., Johnson, K.R., Yamamoto, M., Kuroiwa, A., Duboule, D. (2001) 'The mouse *Hoxd13(spdh)* mutation, a polyalanine expansion similar to human type II synpolydactyly (SPD), disrupts the function but not the expression of other *Hoxd* genes.', *Developmental Biology*, 237(2), 345–353.

Bürglin, T.R. (1997) 'Analysis of TALE superclass homeobox genes (MEIS, PBC, KNOX, Iroquois, TGIF) reveals a novel domain conserved between plants and animals.', *Nucleic Acids Research*, 25(21), 4173–4180.

Bustin, S.A., Benes, V., Garson, J.A., Hellemans, J., Huggett, J., Kubista, M., Mueller, R., Nolan, T., Pfaffl, M.W., Shipley, G.L., Vandesompele, J., Wittwer, C.T. (2009) 'The MIQE guidelines: minimum information for publication of quantitative real-time PCR experiments.', *Clinical Chemistry*, 55(4), 611–622.

Capdevila, J., Izpisúa Belmonte, J.C. (2001) 'Patterning mechanisms controlling vertebrate limb development', *Annual Review of Cell and Developmental Biology*, 17(17), 87–132.

Capdevila, J., Tsukui, T., Rodríquez Esteban, C., Zappavigna, V., Izpisúa Belmonte, J.C. (1999) 'Control of vertebrate limb outgrowth by the proximal factor *Meis2* and distal antagonism of BMPs by Gremlin.', *Molecular Cell*, 4(5), 839–849.

Capellini, T.D., Di Giacomo, G., Salsi, V., Brendolan, A., Ferretti, E., Srivastava, D., Zappavigna, V., Selleri, L. (2006) '*Pbx1/Pbx2* requirement for distal limb patterning is mediated by the hierarchical control of *Hox* gene spatial distribution and *Shh* expression.', *Development*, 133(11), 2263–2273.

Carroll, S.B. (2008) 'Evo-devo and an expanding evolutionary synthesis: A genetic theory of morphological evolution', *Cell*, 134(1), 25–36.

Casanova, J.C., Badia-Careaga, C., Uribe, V., Sanz-Ezquerro, J.J. (2012) '*Bambi* and *Sp8* expression mark digit tips and their absence shows that chick wing digits 2 and 3 are truncated.', *PLoS ONE*, 7(12), e52781.

Casanova, J.C., Sanz-Ezquerro, J.J. (2007) 'Digit morphogenesis: Is the tip different?', *Development Growth and Differentiation*, 49(6), 479–491.

Castelli-Gair Hombría, J., Lovegrove, B. (2003) 'Beyond homeosis - HOX function in morphogenesis and organogenesis', *Differentiation*, 71(8), 461–476.

Cecconi, F., Proetzel, G., Alvarez-Bolado, G., Jay, D., Gruss, P. (1997) 'Expression of *Meis2*, a *Knotted*-related murine homeobox gene, indicates a role in the differentiation of the forebrain and the somitic mesoderm', *Developmental Dynamics*, 210(2), 184–190.

Chadwick, R.B., Bu, L., Yu, H., Hu, Y., Wergedal, J.E., Mohan, S., Baylink, D.J. (2007) 'Digit tip regrowth and differential gene expression in MRL/Mpj, DBA/2, and C57BL/6 mice', *Wound Repair and Regeneration*, 15(2), 275–284.

Chang, C.P., Jacobs, Y., Nakamura, T., Jenkins, N.A., Copeland, N.G., Cleary, M.L. (1997) 'Meis proteins are major in vivo DNA binding partners for wild-type but not chimeric Pbx proteins.', *Molecular and Cellular Biology*, 17(10), 5679–5687.

Chang, C.P., Shen, W.F., Rozenfeld, S., Lawrence, H.J., Largman, C., Cleary, M.L. (1995) 'Pbx proteins display hexapeptide-dependent cooperative DNA binding with a subset of Hox proteins.', *Genes & Development*, 9(6), 663–674.

Chen, C.-H., Cretekos, C.J., Rasweiler, J.J., Behringer, R.R. (2005) '*Hoxd13* expression in the developing limbs of the short-tailed fruit bat, *Carollia perspicillata*', *Evolution & Development*, 7(2), 130–141.

Chen, G., Deng, C., Li, Y.-P. (2012) 'TGF-β and BMP signaling in osteoblast differentiation and bone formation.', *International Journal of Biological Sciences*, 8(2), 272–288.

Cheney, J.A., Konow, N., Middleton, K.M., Breuer, K.S., Roberts, T.J., Giblin, E.L., Swartz, S.M. (2014) 'Membrane muscle function in the compliant wings of bats', *Bioinspiration & Biomimetics*, 9(2), 025007.

Chew, K.Y., Yu, H., Pask, A.J., Shaw, G., Renfree, M.B. (2012) 'HOXA13 and HOXD13 expression during development of the syndactylous digits in the marsupial Macropus eugenii.', *BMC Developmental Biology*, 12(2).

Chiang, C., Litingtung, Y., Harris, M.P., Simandl, B.K., Li, Y., Beachy, P.A., Fallon, J.F. (2001) 'Manifestation of the limb prepattern: limb development in the absence of sonic hedgehog function', *Developmental Biology*, 236(2), 421–435.

Chimal-Monroy, J., Abarca-Buis, R.F., Cuervo, R., Díaz-Hernández, M., Bustamante, M., Rios-Flores, J.A., Romero-Suárez, S., Farrera-Hernández, A. (2011) 'Molecular control of cell differentiation and programmed cell death during digit development.', *IUBMB life*, 63(10), 922–929.

Choe, S.-K., Vlachakis, N., Sagerström, C.G. (2002) 'Meis family proteins are required for hindbrain development in the zebrafish.', *Development*, 129(3), 585–595.

Coates, M.I. (1996) 'The Devonian tetrapod *Acanthostega gunnari Jarvik*: postcranial anatomy, basal tetrapod interrelationships and patterns of skeletal evolution', *Transactions of the Royal Society of Edinburgh: Earth Sciences*, 87(3), 363–421.

Coates, M.I., Cohn, M.J. (1998) 'Fins, limbs, and tails: Outgrowths and axial patterning in vertebrate evolution', *BioEssays*, 20(5), 371–381.

Cobb, J., Dierich, A., Huss-Garcia, Y., Duboule, D. (2006) 'A mouse model for human short-stature syndromes identifies Shox2 as an upstream regulator of Runx2 during long-bone development.', *Proceedings of the National Academy of Sciences*, 103(12), 4511–4515.

Cobb, J., Duboule, D. (2005) 'Comparative analysis of genes downstream of the *Hoxd* cluster in developing digits and external genitalia', *Development*, 132(13), 3055–3067.

Cohn, M.J., Bright, P.E. (1999) 'Molecular control of vertebrate limb development, evolution and congenital malformations', *Cell & Tissue Research*, 296(1), 3–17.

Collignon, J., Sockanathan, S., Hacker, A., Cohen-Tannoudji, M., Norris, D., Rastan, S., Stevanovic, M., Goodfellow, P.N., Lovell-Badge, R. (1996) 'A comparison of the properties of Sox-3 with Sry and two related genes, Sox-1 and Sox-2', *Development*, 122(2), 509–520.

Conte, I., Carrella, S., Avellino, R., Karali, M., Marco-Ferreres, R., Bovolenta, P., Banfi, S. (2010) 'miR-204 is required for lens and retinal development via Meis2 targeting.', *Proceedings of the National Academy of Sciences*, 107(35), 15491–15496.

Cooper, K.L. (2015) 'Self-organization in the limb: a Turing mechanism for digit development', *Current Opinion in Genetics & Development*, 32, 92–97.

Cooper, K.L., Hu, J.K.-H., ten Berge, D., Fernández-Terán, M.A., Ros, M.Á., Tabin, C.J. (2011) 'Initiation of proximal-distal patterning in the vertebrate limb by signals and growth.', *Science*, 332(6033), 1083–1086.

Cooper, K.L., Sears, K.E., Uygur, A., Maier, J., Baczkowski, K.-S., Brosnahan, M., Antczak, D., Skidmore, J.A., Tabin, C.J. (2014) 'Patterning and post-patterning modes of evolutionary digit loss in mammals.', *Nature*, 511(7507), 41–45.

Cooper, L.N., Cretekos, C.J., Sears, K.E. (2012) 'The evolution and development of mammalian flight', *WIREs Developmental Biology*, 1, 773–779.

Cooper, L.N., Sears, K.E. (2013) 'How to grow a bat wing', in Adams, R.A. and Pedersen, S.C., eds., *Bat Evolution, Ecology, and Conservation*, Springer New York: New York, NY, 3–20.

Corsetti, E., Azpiazu, N. (2013) 'Functional dissection of the splice variants of the Drosophila gene homothorax (hth).', *Developmental Biology*, 384(1), 72–82.
Covarrubias, L., Hernández-García, D., Schnabel, D., Salas-Vidal, E., Castro-Obregón, S. (2008) 'Function of reactive oxygen species during animal development: Passive or active?', *Developmental Biology*, 320, 1–11.
Coy, S.E., Borycki, A.-G. (2010) 'Expression analysis of TALE family transcription factors during avian development.', *Developmental Dynamics*, 239(4), 1234–1245.
Cretekos, C.J., Deng, J.-M., Green, E.D., Rasweiler, J.J., Behringer, R.R. (2007) 'Isolation, genomic structure and developmental expression of *Fgf8* in the short-tailed fruit bat, *Carollia perspicillata*.', *The International Journal of Developmental Biology*, 51(4), 333–338.
Cretekos, C.J., Rasweiler, J.J., Behringer, R.R. (2001) 'Comparative studies on limb morphogenesis in mice and bats: a functional genetic approach towards a molecular understanding of diversity in organ formation.', *Reproduction, Fertility and Development*, 13, 691–695.
Cretekos, C.J., Wang, Y., Green, E.D., Martin, J.F., Rasweiler, J.J., Behringer, R.R. (2008) 'Regulatory divergence modifies limb length between mammals.', *Genes & Development*, 22(2), 141–151.
Cretekos, C.J., Weatherbee, S.D., Chen, C., Badwaik, N.K., Niswander, L.A., Behringer, R.R., Rasweiler, J.J. (2005) 'Embryonic staging system for the short-tailed fruit bat, *Carollia perspicillata*, a model organism for the mammalian order Chiroptera, based upon timed pregnancies in captive-bred animals.', *Developmental Dynamics*, 233(3), 721–738.
Crowley, M.A., Conlin, L.K., Zackai, E.H., Deardorff, M.A., Thiel, B.D., Spinner, N.B. (2010) 'Further evidence for the possible role of MEIS2 in the development of cleft palate and cardiac septum', *American Journal of Medical Genetics, Part A*, 152(5), 1326–1327.
Cunningham, T.J., Chatzi, C., Sandell, L.L., Trainor, P.A., Duester, G. (2011) '*Rdh10* mutants deficient in limb field retinoic acid signaling exhibit normal limb patterning but display interdigital webbing.', *Developmental Dynamics*, 240(5), 1142–1150.
Cunningham, T.J., Duester, G. (2015) 'Mechanisms of retinoic acid signalling and its roles in organ and limb development', *Nature Reviews Molecular Cell Biology*, 16(2), 110–123.
Cunningham, T.J., Zhao, X., Sandell, L.L., Evans, S.M., Trainor, P.A., Duester, G. (2013) 'Antagonism between retinoic acid and fibroblast growth factor signaling during limb development', *Cell Reports*, 3(5), 1503–1511.
Curry, L. (2014) *Characterization of Transcripts Expressed from the Meis2 Locus in the Natal Long-Fingered Bat (Miniopterus Natalensis)*, MSc. Thesis.
Dahn, R.D., Fallon, J.F. (2000) 'Interdigital regulation of digit identity and homeotic transformation by modulated BMP signaling.', *Science*, 289, 438–441.
Dai, M., Wang, Y., Fang, L., Irwin, D.M., Zhu, T., Zhang, J., Zhang, S., Wang, Z. (2014) 'Differential expression of *Meis2, Mab21l2* and *Tbx3* during limb development associated with diversification of limb morphology in mammals', *PLoS ONE*, 9(8), e106100.
Darwin, C.R. (1859) *On the Origin of Species by Means of Natural Selection, or the Preservation of Favoured Races in the Struggle for Life*, 1st Ed. ed, John Murry: London.
Davis, A.P., Capecchi, M.R. (1994) 'Axial homeosis and appendicular skeleton defects in mice with a targeted disruption of *hoxd-11*.', *Development*, 120(8), 2187–2198.
Davis, A.P., Witte, D.P., Hsieh-Li, H.M., Potter, S.S., Capecchi, M.R. (1995) 'Absence of radius and ulna in mice lacking *hoxa-11* and *hoxd-11*.', *Nature*, 375(6534), 791–795.
Davis, M.C. (2013) 'The deep homology of the autopod: Insights from *Hox* gene regulation', *Integrative and Comparative Biology*, 53(2), 224–232.
Davis, M.C., Dahn, R.D., Shubin, N.H. (2007) 'An autopodial-like pattern of *Hox* expression in the fins of a basal actinopterygian fish.', *Nature*, 447(7143), 473–476.
Davis, P., Capecchi, M.R. (1996) 'A mutational analysis of the 5' *HoxD* genes: dissection of genetic interactions during limb development in the mouse.', *Development*, 122(4), 1175–1185.
Decker, R.S., Koyama, E., Pacifici, M. (2014) 'Genesis and morphogenesis of limb synovial joints and articular cartilage', *Matrix Biology*, 39, 5–10.
Delport, W., Poon, A.F.Y., Frost, S.D.W., Kosakovsky Pond, S.L. (2010) 'Datamonkey 2010: A suite of phylogenetic analysis tools for evolutionary biology', *Bioinformatics*, 26(19), 2455–2457.
Delpretti, S., Zákány, J., Duboule, D. (2012) 'A function for all posterior *Hoxd* genes during digit development?', *Developmental Dynamics*, 241(4), 792–802.
Derveaux, S., Vandesompele, J., Hellemans, J. (2010) 'How to do successful gene expression analysis using real-time PCR', *Methods*, 50(4), 227–230.
Deschamps, J. (2008) 'Tailored *Hox* gene transcription and the making of the thumb', *Genes & Development*, 22, 293–296.
Deschamps, J., van den Akker, E., Forlani, S., De Graaff, W., Oosterveen, T., Roelen, B., Roelfsema, J. (1999) 'Initiation, establishment and maintenance of *Hox* gene expression patterns in the mouse.', *The International Journal of Developmental Biology*, 43(7), 635–650.
Di-Poï, N., Montoya-Burgos, J.I., Miller, H., Pourquié, O., Milinkovitch, M.C., Duboule, D. (2010) 'Changes in Hox genes' structure and function during the evolution of the squamate body plan.', *Nature*, 464(7285), 99–103.

Díaz-Hernández, M., Rios-Flores, A., Abarca-Buis, R.F., Bustamante, M., Chimal-Monroy, J. (2014) 'Molecular control of interdigital cell death and cell differentiation by retinoic acid during digit development', *Journal of Developmental Biology*, 2(2), 138–157.

DiIorio, P., Alexa, K., Choe, S.-K., Etheridge, L., Sagerström, C.G. (2007) 'TALE-Family homeodomain proteins regulate endodermal sonic hedgehog expression and pattern the anterior endoderm', *Developmental Biology*, 304(1), 221–231.

Dixey, F.A. (1880) 'On the ossification of the terminal phalanges of the digits', *Proceedings of the Royal Society of London*, 31(206-211), 63–71.

Dollé, P., Dierich, A., LeMeur, M., Schimmang, T., Schuhbaur, B., Chambon, P., Duboule, D. (1993) 'Disruption of the *Hoxd-13* gene induces localized heterochrony leading to mice with neotenic limbs', *Cell*, 75, 431–441.

Dollé, P., Duboule, D. (1989) 'Two gene members of the murine HOX-5 complex show regional and cell-type specific expression in developing limbs and gonads.', *The EMBO Journal*, 8(5), 1507–1515.

Dollé, P., Izpisúa-Belmonte, Falkenstein, H., Renucci, A., Duboule, D. (1989) 'Coordinate expression of the murine *Hox-5* complex homoeobox-containing genes during limb pattern formation.', *Nature*, 342(6251), 767–772.

Dollé, P., Izpisúa-Belmonte, J.C., Boncinelli, E., Duboule, D. (1991) 'The *Hox-4.8* gene is localized at the 5' extremity of the *Hox-4* complex and is expressed in the most posterior parts of the body during development.', *Mechanisms of Development*, 36(1-2), 3–13.

Dollé, P., Izpisúa-Belmonte, J.C., Brown, J.M., Tickle, C., Duboule, D. (1991) 'Hox-4 genes and the morphogenesis of mammalian genitalia', *Genes and Development*, 5(10), 1767–1776.

Dollé, P., Ruberte, E., Leroy, P., Morriss-kay, G., Chambon, P. (1990) 'Retinoic acid receptors and cellular retinoid binding proteins. I. A systematic study of their differential pattern of transcription during mouse organogenesis.', *Development*, 110(4), 1133–1151.

Domínguez, M., Casares, F. (2005) 'Organ specification-growth control connection: New in-sights from the Drosophila eye-antennal disc', *Developmental Dynamics*, 232(3), 673–684.

Dranse, H.J., Sampaio, A. V., Petkovich, M., Underhill, T.M. (2011) 'Genetic deletion of Cyp26b1 negatively impacts limb skeletogenesis by inhibiting chondrogenesis.', *Journal of Cell Science*, 124, 2723–2734.

Duboc, V., Logan, M.P.O. (2009) 'Building limb morphology through integration of signalling modules.', *Current Opinion in Genetics & Development*, 19(5), 497–503.

Duboule, D. (1995) 'Vertebrate *Hox* genes and proliferation: an alternative pathway to homeosis?', *Current Opinion in Genetics & Development*, 5, 525–528.

Duboule, D. (2007) 'The rise and fall of *Hox* gene clusters.', *Development*, 134(14), 2549–2560.

Duboule, D., Morata, G. (1994) 'Colinearity and functional hierarchy among genes of the homeotic complexes.', *Trends in genetics*, 10(10), 358–64.

Dudley, R., Byrnes, G., Yanoviak, S.P., Borrell, B., Brown, R.M., McGuire, J.A. (2007) 'Gliding and the Functional Origins of Flight: Biomechanical Novelty or Necessity?', *Annual Review of Ecology, Evolution, and Systematics*, 38(1), 179–201.

Dupé, V., Ghyselinck, N.B., Thomazy, V., Nagy, L., Davies, P.J., Chambon, P., Mark, M. (1999) 'Essential roles of retinoic acid signaling in interdigital apoptosis and control of BMP-7 expression in mouse autopods.', *Developmental Biology*, 208(1), 30–43.

Durston, A.J. (2012) 'Hox Genes : Master Regulators of the Animal Bodyplan', in Sato, K.-I., ed., *Embryogenesis*, InTech, 652.

Dwight, Z., Palais, R., Wittwer, C.T. (2011) 'uMELT: Prediction of high-resolution melting curves and dynamic melting profiles of PCR products in a rich web application', *Bioinformatics*, 27(7), 1019–1020.

Echeverri, K., Tanaka, E.M. (2005) 'Proximodistal patterning during limb regeneration', *Developmental Biology*, 279(2), 391–401.

Egawa, S., Miura, S., Yokoyama, H., Endo, T., Tamura, K. (2014) 'Growth and differentiation of a long bone in limb development, repair and regeneration.', *Development Growth and Differentiation*, 56(5), 410–424.

Eiting, T.P., Gunnell, G.F. (2009) 'Global Completeness of the Bat Fossil Record', *Journal of Mammalian Evolution*, 16(3), 151–173.

Erdogan, F., Ullmann, R., Chen, W., Schubert, M., Adolph, S., Hultschig, C., Kalscheuer, V., Ropers, H.-H., Spaich, C., Tzschach, A. (2007) 'Characterization of a 5.3 Mb deletion in 15q14 by comparative genomic hybridization using a whole genome "tiling path" BAC array in a girl with heart defect, cleft palate, and developmental delay', *American Journal of Medical Genetics, Part A*, 143A(2), 172–178.

Eshkar-Oren, I., Krief, S., Ferrara, N., Elliott, A.M., Zelzer, E. (2015) 'Vascular patterning regulates interdigital cell death by a ROS-mediated mechanism.', *Development*, 142(4), 672–680.

Farnum, C.E. (2007) 'Postnatal growth of fins and limbs through endochondral ossification', in Hall, B.K., ed., *Fins into Limbs: Evolution, Development and Transformation*, University of Chicago Press: Chicago, 118–151.

Farnum, C.E., Tinsley, M., Hermanson, J.W. (2008a) 'Postnatal bone elongation of the manus versus pes: analysis of the chondrocytic differentiation cascade in Mus musculus and Eptesicus fuscus.', *Cells Tissues Organs*, 187(1), 48–58.

Farnum, C.E., Tinsley, M., Hermanson, J.W. (2008b) 'Forelimb versus hindlimb skeletal development in the big brown bat, Eptesicus fuscus: functional divergence is reflected in chondrocytic performance in Autopodial growth plates.', *Cells Tissues Organs*, 187(1), 35–47.

Farnum, C.E., Wilsman, N.J. (2001) 'Converting a differentiation cascade into longitudinal growth: stereology and analysis of transgenic animals as tools for understanding growth plate function', *Current Opinion in Orthopaedics*, 12(5), 428–433.

Fedak, T.J., Hall, B.K. (2004) 'Perspectives on hyperphalangy: Patterns and processes', *Journal of Anatomy*, 204(3), 151–163.

Ferran, J.L., Sánchez-Arrones, L., Sandoval, J.E., Puelles, L. (2007) 'A model of early molecular regionalization in the chicken embryonic pretectum.', *The Journal of Comparative Neurology*, 505(4), 379–403.

Fisher, M.C., Meyer, C., Garber, G., Dealy, C.N. (2005) 'Role of IGFBP2, IGF-I and IGF-II in regulating long bone growth', *Bone*, 37(6), 741–750.

Flicek, P., Amode, M.R., Barrell, D., Beal, K., Billis, K., Brent, S., Carvalho-Silva, D., Clapham, P., Coates, G., Fitzgerald, S., Gil, L., Girón, C.G., Gordon, L., Hourlier, T., Hunt, S., Johnson, N., Juettemann, T., Kähäri, A.K., Keenan, S., Kulesha, E., Martin, F.J., Maurel, T., McLaren, W.M., Murphy, D.N., Nag, R., Overduin, B., Pignatelli, M., Pritchard, B., Pritchard, E., Riat, H.S., Ruffier, M., Sheppard, D., Taylor, K., Thormann, A., Trevanion, S.J., Vullo, A., Wilder, S.P., Wilson, M., Zadissa, A., Aken, B.L., Birney, E., Cunningham, F., Harrow, J., Herrero, J., Hubbard, T.J.P., Kinsella, R., Muffato, M., Parker, A., Spudich, G., Yates, A., Zerbino, D.R., Searle, S.M.J. (2014) 'Ensembl 2014.', *Nucleic Acids Research*, 42(Database issue), D749–755.

Freemantle, S.J., Kerley, J.S., Olsen, S.L., Gross, R.H., Spinella, M.J. (2002) 'Developmentally-related candidate retinoic acid target genes regulated early during neuronal differentiation of human embryonal carcinoma', *Oncogene*, 21, 2880–2889.

Friedman, M., Coates, M.I., Anderson, P. (2007) 'First discovery of a primitive coelacanth fin fills a major gap in the evolution of lobed fins and limbs', *Evolution & Development*, 9(4), 329–337.

Fromental-Ramain, C., Warot, X., Messadecq, N., LeMeur, M., Dollé, P., Chambon, P. (1996) '*Hoxa-13* and *Hoxd-13* play a crucial role in the patterning of the limb autopod.', *Development*, 122(10), 2997–3011.

Galis, F., van Alphen, J.J.M., Metz, J.A.J. (2001) 'Why five fingers? Evolutionary constraints on digit numbers', *Trends in Ecology & Evolution*, 16(11), 637–646.

Galli, A., Robay, D., Osterwalder, M., Bao, X., Bénazet, J.-D., Tariq, M., Paro, R., Mackem, S., Zeller, R. (2010) 'Distinct roles of *Hand2* in initiating polarity and posterior *Shh* expression during the onset of mouse limb bud development', *PLoS Genetics*, 6(4), e1000901.

Gañan, Y., Macias, D., Basco, R.D., Merino, R., Hurle, J.M. (1998) 'Morphological diversity of the avian foot is related with the pattern of msx gene expression in the developing autopod.', *Developmental Biology*, 196(1), 33–41.

Garcia-Fernández, J. (2005) 'The genesis and evolution of homeobox gene clusters', *Nature Reviews. Genetics*, 6(12), 881–892.

Garza-Garcia, A.A., Driscoll, P.C., Brockes, J.P. (2010) 'Evidence for the local evolution of mechanisms underlying limb regeneration in salamanders', *Integrative and Comparative Biology*, 50(4), 528–535.

Garza-Garcia, A.A., Harris, R., Esposito, D., Gates, P.B., Driscoll, P.C. (2009) 'Solution structure and phylogenetics of *Prod1*, a member of the three-finger protein superfamily implicated in salamander limb regeneration', *PLoS ONE*, 4(9), e7123.

Gehring, W.J., Kloter, U., Suga, H. (2009) 'Evolution of the Hox gene complex from an evolutionary ground state', in *Current Topics in Developmental Biology*, Elsevier Inc., 35–61.

Gehrke, A.R., Schneider, I., de la Calle-Mustienes, E., Tena, J.J., Gomez-Marin, C., Chandran, M., Nakamura, T., Braasch, I., Postlethwait, J.H., Gómez-Skarmeta, J.L., Shubin, N.H. (2015) 'Deep conservation of wrist and digit enhancers in fish', *Proceedings of the National Academy of Sciences*, 112(3), 803–808.

Geng, J., Gates, P.B., Kumar, A., Guenther, S., Garza-Garcia, A.A., Kuenne, C., Zhang, P., Looso, M., Brockes, J.P. (2015) 'Identification of the orphan gene Prod 1 in basal and other salamander families', *EvoDevo*, 6(1), 4–7.

Ghosh, T.K., Packham, E. a, Bonser, a J., Robinson, T.E., Cross, S.J., Brook, J.D. (2001) 'Characterization of the TBX5 binding site and analysis of mutations that cause Holt-Oram syndrome.', *Human Molecular Genetics*, 10(18), 1983–1994.

Ghyselinck, N.B., Dupé, V., Dierich, A., Messadecq, N., Garnier, J.-M., Rochette-Egly, C., Chambon, P., Mark, M. (1997) 'Role of the retinoic acid receptor beta (RARbeta) during mouse development.', *The International Journal of Developmental Biology*, 41(3), 425–447.

Giannini, N., Goswami, A., Sánchez-Villagra, M.R. (2006) 'Development of integumentary structures in *Rousettus amplexicaudatus* (Mammalia: Chiroptera: Pteropodidae) during late-embryonic development and fetal stages', *Journal of Mammalogy*, 87(5), 993–1001.

Giannini, N.P. (2012) 'Toward an integrative theory on the origin of bat flight', in Gunnell, G.F. and Simmons, N.B., eds., *Evolutionary History of Bats*, Cambridge University Press: Cambridge, 353–384.

Gibson-Brown, J.J., Agulnik, S.I., Chapman, D.L., Alexiou, M., Garvey, N., Silver, L.M., Papaioannou, V.E. (1996) 'Evidence of a role for T-box genes in the evolution of limb morphogenesis and the specification of forelimb/hindlimb identity.', *Mechanisms of Development*, 56(1-2), 93–101.

Giguère, V., Lyn, S., Yip, P., Siu, C.H., Amin, S. (1990) 'Molecular cloning of cDNA encoding a second cellular retinoic acid-binding protein.', *Proceedings of the National Academy of Sciences*, 87(16), 6233–6237.

Glaser, A., Arora, R., Hoffmann, S., Li, L., Gretz, N., Papaioannou, V.E., Rappold, G. a. (2014) 'Tbx4 interacts with the short stature homeobox gene Shox2 in limb development', *Developmental Dynamics*, 243(5), 629–639.

Goff, D.J., Tabin, C.J. (1997) 'Analysis of *Hoxd-13* and *Hoxd-11* misexpression in chick limb buds reveals that Hox genes affect both bone condensation and growth.', *Development*, 124(3), 627–636.

Goldring, M.B., Tsuchimochi, K., Ijiri, K. (2006) 'The control of chondrogenesis', *Journal of Cellular Biochemistry*, 97, 33–44.

Gonzalez, F., Duboule, D., Spitz, F. (2007) 'Transgenic analysis of *Hoxd* gene regulation during digit development', *Developmental Biology*, 306(2), 847–859.

González-Martín, M.C., Mallo, M., Ros, M.Á. (2014) 'Long bone development requires a threshold of *Hox* function.', *Developmental Biology*, 392(2), 454–465.

Gray, P.A., Fu, H., Luo, P., Zhao, Q., Yu, J., Ferrari, A., Tenzen, T., Yuk, D.-I., Tsung, E.F., Cai, Z., Alberta, J.A., Cheng, L.-P., Liu, Y., Stenman, J.M., Valerius, M.T., Billings, N., Kim, H.A., Greenberg, M.E., McMahon, A.P., Rowitch, D.H., Stiles, C.D., Ma, Q. (2004) 'Mouse brain organization revealed through direct genome-scale TF expression analysis.', *Science*, 306(5705), 2255–2257.

Grice, J., Noyvert, B., Doglio, L., Elgar, G. (2015) 'A simple predictive enhancer syntax for hindbrain patterning is conserved in vertebrate genomes', *PLoS ONE*, 10(7), e0130413.

Grieshammer, U., Agarwal, P., Martin, G.R. (2008) 'A cre transgene active in developing endodermal organs, heart, limb, and extra-ocular muscle', *Genesis*, 46(2), 69–73.

Gross, S., Krause, Y., Wuelling, M., Vortkamp, A. (2012) '*Hoxa11* and *Hoxd11* regulate chondrocyte differentiation upstream of *Runx2* and *Shox2* in mice.', *PLoS ONE*, 7(8), e43553.

Grüneberg, H., Lee, A.J. (1973) 'The anatomy and development of brachypodism in the mouse.', *Journal of Embryology and Experimental Morphology*, 30(1), 119–141.

Gyurján, I., Sonderegger, B., Naef, F., Duboule, D. (2011) 'Analysis of the dynamics of limb transcriptomes during mouse development.', *BMC Developmental Biology*, 11(47).

Haack, H., Gruss, P. (1993) 'The establishment of murine *Hox-1* expression domains during patterning of the limb.', *Developmental Biology*, 157, 410–422.

Hall, B.K. (2003) 'Descent with modification: The unity underlying homology and homoplasy as seen through an analysis of development and evolution.', *Biological reviews of the Cambridge Philosophical Society*, 78(3), 409–433.

Hall, B.K. (2007) *Fins into Limbs*, The University of Chicago Press: Chicago and London.

Hall, B.K., Miyake, T. (1992) 'The membranous skeleton: The role of cell condensations in vertebrate skeletogenesis', *Anatomy and Embryology*, 186, 107–124.

Hall, B.K., Miyake, T. (1995) 'Divide, accumulate, differentiate: Cell condensation in skeletal development revisited', *International Journal of Developmental Biology*, 39, 881–893.

Hall, B.K., Miyake, T. (2000) 'All for one and one for all: condensations and the initiation of skeletal development', *BioEssays*, 22(2), 138–147.

Hamrick, M.W. (2001) 'Development and evolution of the mammalian limb: Adaptive diversification of nails, hooves, and claws', *Evolution & Development*, 3(5), 355–363.

Hamrick, M.W. (2003) 'Evolution and development of mammalian limb integumentary structures', *Journal of Experimental Zoology*, 298B(1), 152–163.

Han, M., Yang, X., Lee, J., Allan, C.H., Muneoka, K. (2008) 'Development and regeneration of the neonatal digit tip in mice', *Developmental Biology*, 315(1), 125–135.

Hanken, J., Wasersug, R. (1981) 'The Visible Skeleton', *Functional Photography*, 16(4), 23–27.

Harfe, B.D., Scherz, P.J., Nissim, S., Tian, H., McMahon, A.P., Tabin, C.J. (2004) 'Evidence for an expansion-based temporal *Shh* gradient in specifying vertebrate digit identities', *Cell*, 118(4), 517–528.

Heine, P., Dohle, E., Bumsted-O'Brien, K., Engelkamp, D., Schulte, D. (2008) 'Evidence for an evolutionary conserved role of *homothorax/Meis1/2* during vertebrate retina development.', *Development*, 135(5), 805–811.

Hérault, Y., Beckers, J., Kondo, T., Fraudeau, N., Duboule, D. (1998) 'Genetic analysis of a Hoxd-12 regulatory element reveals global versus local modes of controls in the HoxD complex.', *Development*, 125(9), 1669–1677.

Hermanson, J.W., Wilkins, K.T. (2008) 'Growth and Development of Two Species of Bats in a Shared Maternity Roost', *Cells Tissues Organs*, 187(1), 24–34.

Hernández-Martínez, R., Castro-Obregón, S., Covarrubias, L. (2009) 'Progressive interdigital cell death: regulation by the antagonistic interaction between fibroblast growth factor 8 and retinoic acid.', *Development*, 136(21), 3669–3678.

Hernández-Martínez, R., Covarrubias, L. (2011) 'Interdigital cell death function and regulation: New insights on an old programmed cell death model', *Development Growth and Differentiation*, 53(2), 245–258.

Hinoi, E., Bialek, P., Chen, Y.T., Rached, M.T., Groner, Y., Behringer, R.R., Ornitz, D.M., Karsenty, G. (2006) 'Runx2 inhibits chondrocyte proliferation and hypertrophy through its expression in the perichondrium', *Genes & Development*, 20(21), 2937–2942.

Hisa, T., Spence, S.E., Rachel, R.A., Fujita, M., Nakamura, T., Ward, J.M., Devor-Henneman, D.E., Saiki, Y., Kutsuna, H., Tessarollo, L., Jenkins, N.A., Copeland, N.G. (2004) 'Hematopoietic, angiogenic and eye defects in *Meis1* mutant animals.', *The EMBO Journal*, 23(2), 450–459.

Hockman, D., Cretekos, C.J., Mason, M.K., Behringer, R.R., Jacobs, D.S., Illing, N. (2008) 'A second wave of Sonic hedgehog expression during the development of the bat limb.', *Proceedings of the National Academy of Sciences*, 105(44), 16982–16987.

Hockman, D., Mason, M.K., Jacobs, D.S., Illing, N. (2009) 'The role of early development in mammalian limb diversification: a descriptive comparison of early limb development between the Natal long-fingered bat (*Miniopterus natalensis*) and the mouse (*Mus musculus*).', *Developmental Dynamics*, 238(4), 965–979.

Holland, P.W.H. (2013) 'Evolution of homeobox genes', *WIREs Developmental Biology*, 2(1), 31–45.

Howell, D.J., Pylka, J. (1977) 'Why bats hang upside down: A biomechanical hypothesis', *Journal of Theoretical Biology*, 69(4), 625–631.

Huang, B.-L., Mackem, S. (2015) 'Tamoxifen-dependent, inducible Bmp2CreER drives selective recombinase activity in early interdigital mesenchyme and digit collateral ligaments', *PLoS ONE*, 10(4), e0123325.

Huang, H., Rastegar, M., Bodner, C., Goh, S.-L., Rambaldi, I., Featherstone, M.S. (2005) 'MEIS C termini harbor transcriptional activation domains that respond to cell signaling.', *The Journal of Biological Chemistry*, 280(11), 10119–10127.

Hueber, S.D., Weiller, G.F., Djordjevic, M.A., Frickey, T. (2010) 'Improving *Hox* protein classification across the major model organisms.', *PLoS ONE*, 5(5), e10820.

Hyman-Walsh, C., Bjerke, G.A., Wotton, D. (2010) 'An autoinhibitory effect of the homothorax domain of Meis2', *FEBS Journal*, 277(12), 2584–2597.

Irimia, M., Maeso, I., Burguera, D., Hidalgo-Sánchez, M., Puelles, L., Roy, S.W., Garcia-Fernández, J., Ferran, J.L. (2011) 'Contrasting 5' and 3' evolutionary histories and frequent evolutionary convergence in *Meis/hth* gene structures.', *Genome Biology and Evolution*, 3, 551–564.

Jacobs, Y., Schnabel, C.A., Cleary, M.L. (1999) 'Trimeric association of *Hox* and TALE homeodomain proteins mediates *Hoxb2* hindbrain enhancer activity.', *Molecular and Cellular Biology*, 19(7), 5134–5142.

Jiang, H., Soprano, D.R., Li, S.W., Soprano, K.J., Penner, J.D., Gyda, M., Kochhar, D.M. (1995) 'Modulation of limb bud chondrogenesis by retinoic acid and retinoic acid receptors', *International Journal of Developmental Biology*, 39(4), 617–627.

Johanson, Z., Joss, J., Boisvert, C.A., Ericsson, R., Sutija, M., Ahlberg, P.E. (2007) 'Fish fingers: Digit homologues in sarcopterygian fish fins', *Journal of Experimental Zoology Part B: Molecular and Developmental Evolution*, 308B(6), 757–768.

Johansson, S., Berland, S., Gradek, G.A., Bongers, E., de Leeuw, N., Pfundt, R., Fannemel, M., Rødningen, O., Brendehaug, A., Haukanes, B.I., Hovland, R., Helland, G., Houge, G. (2014) 'Haploinsufficiency of MEIS2 is associated with orofacial clefting and learning disability', *American Journal of Medical Genetics, Part A*, 164(7), 1622–1626.

Johnson, K.R., Sweet, H.O., Donahue, L.R., Ward-Bailey, P., Bronson, R.T., Davisson, M.T. (1998) 'A new spontaneous mouse mutation of Hoxd13 with a polyalanine expansion and phenotype similar to human synpolydactyly', *Human Molecular Genetics*, 7(6), 1033–1038.

Jung, J.C., Tsonis, P. a. (1998) 'Role of 5' HoxD genes in chondrogenesis in vitro', *International Journal of Developmental Biology*, 42(4), 609–615.

Kamiyama, N., Seki, R., Yokoyama, H., Tamura, K. (2012) 'Heterochronically early decline of Hox expression prior to cartilage formation in the avian hindlimb zeugopod', *Development Growth and Differentiation*, 54(6), 619–632.

Kashimada, K., Svingen, T., Feng, C.-W., Pelosi, E., Bagheri-Fam, S., Harley, V.R., Schlessinger, D., Bowles, J., Koopman, P. (2011) 'Antagonistic regulation of Cyp26b1 by transcription factors SOX9/SF1 and FOXL2 during gonadal development in mice', *The FASEB Journal*, 25(10), 3561–3569.

Kawakami, Y. (2013) 'Redefining the role of retinoic acid in limb development', *Cell Reports*, 3(5), 1337–1338.

Kent, W.J. (2002) 'BLAT: The BLAST-Like Alignment Tool', *Genome Research*, 12(4), 656–664.

Kent, W.J., Sugnet, C.W., Furey, T.S., Roskin, K.M., Pringle, T.H., Zahler, A.M., Haussler, A.D. (2002) 'The Human Genome Browser at UCSC', *Genome Research*, 12(6), 996–1006.

Kim, E.J., Cho, S.W., Shin, J.O., Lee, M.J., Kim, K.S., Jung, H.S. (2013) '*Ihh* and *Runx2/Runx3* signaling interact to coordinate early chondrogenesis: A mouse model', *PLoS ONE*, 8(2), e55296.

Kmita, M., Duboule, D. (2003) 'Organizing axes in time and space; 25 years of colinear tinkering.', *Science*, 301(5631), 331–333.

Kmita, M., Fraudeau, N., Hérault, Y., Duboule, D. (2002) 'Serial deletions and duplications suggest a mechanism for the collinearity of Hoxd genes in limbs.', *Nature*, 420(6912), 145–150.

Kmita, M., Tarchini, B., Duboule, D., Hérault, Y. (2002) 'Evolutionary conserved sequences are required for the insulation of the vertebrate Hoxd complex in neural cells.', *Development*, 129(23), 5521–5528.

Kmita, M., Tarchini, B., Zákány, J., Logan, M., Tabin, C.J., Duboule, D. (2005) 'Early developmental arrest of mammalian limbs lacking *HoxA/HoxD* gene function.', *Nature*, 435(7045), 1113–1116.

Knoepfler, P.S., Calvo, K.R., Chen, H., Antonarakis, S.E., Kamps, M.P. (1997) 'Meis1 and pKnox1 bind DNA cooperatively with Pbx1 utilizing an interaction surface disrupted in oncoprotein E2a-Pbx1.', *Proceedings of the National Academy of Sciences*, 94(26), 14553–14558.

Knosp, W.M., Saneyoshi, C., Shou, S., Bächinger, H.P., Stadler, H.S. (2007) 'Elucidation, quantitative refinement, and in vivo utilization of the HOXA13 DNA binding site', *Journal of Biological Chemistry*, 282(9), 6843–6853.

Knosp, W.M., Scott, V., Bächinger, H.P., Stadler, H.S. (2004) 'HOXA13 regulates the expression of bone morphogenetic proteins 2 and 7 to control distal limb morphogenesis.', *Development*, 131(18), 4581–4592.

Komori, T. (2011) 'Signaling networks in RUNX2-dependent bone development', *Journal of Cellular Biochemistry*, 112(3), 750–755.

Komori, T. (2015) 'The functions of Runx family transcription factors and Cbfb in skeletal development', *Oral Science International*, 12(1), 1–4.

Kosher, R.A., Kulyk, W.M., Gay, S.W. (1986) 'Collagen gene expression during limb cartilage differentiation', *Journal of Cell Biology*, 102, 1151–1156.

Kozhemyakina, E., Lassar, A.B., Zelzer, E. (2015) 'A pathway to bone: signaling molecules and transcription factors involved in chondrocyte development and maturation', *Development*, 142(5), 817–831.

Kronenberg, H.M. (2007) 'The role of the perichondrium in fetal bone development', *Annals of the New York Academy of Sciences*, 1116, 59–64.

Kronenberg, H.M., Kronenberg, H.M. (2003) 'Developmental regulation of the growth plate.', *Nature*, 423(6937), 332–6.

Kulyk, W.M., Coelho, C.N.D., Kosher, R.A. (1991) 'Type IX collagen gene expression during limb cartilage differentiation', *Matrix*, 11(4), 282–288.

Kumar, A., Gates, P.B., Brockes, J.P. (2007) 'Positional identity of adult stem cells in salamander limb regeneration', *Comptes Rendus - Biologies*, 330, 485–490.

Kuss, P., Kraft, K., Stumm, J., Ibrahim, D., Vallecillo-Garcia, P., Mundlos, S., Stricker, S. (2014) 'Regulation of cell polarity in the cartilage growth plate and perichondrium of metacarpal elements by HOXD13 and WNT5A.', *Developmental Biology*, 385(1), 83–93.

Kuss, P., Villavicencio-Lorini, P., Witte, F., Klose, J., Albrecht, A.N., Seemann, P., Hecht, J., Mundlos, S. (2009) 'Mutant *Hoxd13* induces extra digits in a mouse model of synpolydactyly directly and by decreasing retinoic acid synthesis.', *The Journal of Clinical Investigation*, 119(1), 146–156.

Ladam, F., Sagerström, C.G. (2014) 'Hox regulation of transcription: more complex(es).', *Developmental Dynamics*, 243(1), 4–15.

Lalevée, S., Anno, Y.N., Chatagnon, A., Samarut, E., Poch, O., Laudet, V., Benoit, G., Lecompte, O., Rochette-Egly, C. (2011) 'Genome-wide in Silico identification of new conserved and functional retinoic acid receptor response elements (direct repeats separated by 5 bp)', *Journal of Biological Chemistry*, 286(38), 33322–33334.

Lande, R. (1978) 'Evolutionary mechanisms of limb loss in tetrapods', *Evolution*, 32(1), 73–92.

Lefebvre, V., Bhattaram, P. (2010) 'Vertebrate skeletogenesis.', *Current topics in developmental biology*, 90, 291–317.

Lefevre, C., Imagawa, M., Dana, S., Grindlay, J., Bodner, M., Karin, M. (1987) 'Tissue-specific expression of the human growth hormone gene is conferred in part by the binding of a specific trans-acting factor.', *The EMBO journal*, 6(4), 971–981.

Lewis, E.B. (1978) 'A gene complex controlling segmentation in Drosophila', *Nature*, 276, 565–570.

Li, D., Sakuma, R., Vakili, N.A., Mo, R., Puviindran, V., Deimling, S., Zhang, X., Hopyan, S., Hui, C.C. (2014) 'Formation of proximal and anterior limb skeleton requires early function of Irx3 and Irx5 and is negatively regulated by shh signaling', *Developmental Cell*, 29(2), 233–240.

Liang, L., Shen, Y., Pan, X., Zhou, T., Yang, C., Irwin, D.M., Zhang, Y.-P. (2013) 'Adaptive evolution of the *Hox* gene family for development in bats and dolphins.', *PLoS ONE*, 8(6), e65944.

Litingtung, Y., Dahn, R.D., Li, Y., Fallon, J.F., Chiang, C. (2002) 'Shh and Gli3 are dispensable for limb skeleton formation but regulate digit number and identity.', *Nature*, 418(6901), 979–983.

Liu, W., Saint, D.A. (2002) 'Validation of a quantitative method for real time PCR kinetics', *Biochemical and Biophysical Research Communications*, 294(2), 347–353.

Logan, M., Tabin, C.J. (1999) 'Role of Pitx1 Upstream of Tbx4 in Specification of Hindlimb Identity', *Science*, 283(5408), 1736–1739.

Lonfat, N., Duboule, D. (2015) 'Structure, function and evolution of topologically associating domains (TADs) at HOX loci', *FEBS Letters*, 589, 2869–2876.

Long, F., Ornitz, D.M. (2013) 'Development of the endochondral skeleton', *Cold Spring Harbor Perspectives in Biology*, 5, a008334.

Longobardi, E., Blasi, F. (2003) 'Overexpression of PREP-1 in F9 teratocarcinoma cells leads to a functionally relevant increase of PBX-2 by preventing its degradation.', *The Journal of Biological Chemistry*, 278(40), 39235–39241.

Longobardi, E., Penkov, D., Mateos, D., De Florian, G., Torres, M., Blasi, F. (2014) 'Biochemistry of the tale transcription factors PREP, MEIS, and PBX in vertebrates', *Developmental Dynamics*, 243(1), 59–75.

Louw, J.J., Corveleyn, A., Jia, Y., Hens, G., Gewillig, M., Devriendt, K. (2015) 'MEIS2 involvement in cardiac development, cleft palate, and intellectual disability', *American Journal of Medical Genetics, Part A*, 167(5), 1142–1146.

Mackem, S., Mahon, K.A. (1991) 'Ghox 4.7: a chick homeobox gene expressed primarily in limb buds with limb-type differences in expression.', *Development*, 112(3), 791–806.

Mackem, S., Ranson, M., Mahon, K. (1993) 'Limb-type differences in expression domains of certain chick Hox-4 genes and relationship to pattern modification for flight.', *Progress in clinical and biological research*, 383A, 21–30.

MacLean, G.A., Abu-Abed, S., Dollé, P., Tahayato, A., Chambon, P., Petkovich, M. (2001) 'Cloning of a novel retinoic-acid metabolizing cytochrome P450, Cyp26B1, and comparative expression analysis with Cyp26A1 during early murine development.', *Mechanisms of Development*, 107(1-2), 195–201.

Maeda, R., Mood, K., Jones, T.L., Aruga, J., Buchberg, A.M., Daar, I.O. (2001) '*Xmeis1*, a protooncogene involved in specifying neural crest cell fate in *Xenopus* embryos.', *Oncogene*, 20(11), 1329–1342.

Mann, R.S., Lelli, K.M., Joshi, R. (2009) 'Hox specificity unique roles for cofactors and collaborators.', *Current Topics in Developmental Biology*, 88, 63–101.

Margulies, E.H., Kardia, S.L., Innis, J.W. (2001) 'A comparative molecular analysis of developing mouse forelimbs and hindlimbs using serial analysis of gene expression (SAGE)', *Genome Research*, 11(10), 1686–1698.

Mariani, F. V., Ahn, C.P., Martin, G.R. (2008) 'Genetic evidence that FGFs have an instructive role in limb proximal-distal patterning', *Nature*, 453(7193), 401–405.

Martin, P. (1990) 'Tissue patterning in the developing mouse limb', *International Journal of Developmental Biology*, 34, 323–336.

Mason, M.K. (2009) *Cross-Species Microarray Analysis of Limb Development in the Bat, Miniopterus Natalensis*, MSc. Thesis.

Mason, M.K., Hockman, D., Curry, L., Cunningham, T.J., Duester, G., Logan, M., Jacobs, D.S., Illing, N. (2015) 'Retinoic acid-independent expression of Meis2 during autopod patterning in the developing bat and mouse limb', *EvoDevo*, 6(1), 6.

Matys, V., Fricke, E., Geffers, R., Gössling, E., Haubrock, M., Hehl, R., Hornischer, K., Karas, D., Kel, A.E., Kel-Margoulis, O. V, Kloos, D.-U., Land, S., Lewicki-Potapov, B., Michael, H., Münch, R., Reuter, I., Rotert, S., Saxel, H., Scheer, M., Thiele, S., Wingender, E. (2003) 'TRANSFAC: transcriptional regulation, from patterns to profiles.', *Nucleic Acids Research*, 31(1), 374–8.

Mendelsohn, C., Ruberte, E., LeMeur, M., Morriss-kay, G., Chambon, P. (1991) 'Developmental analysis of the retinoic acid-inducible RAR-beta 2 promoter in transgenic animals.', *Development*, 113(3), 723–734.

Merabet, S., Hudry, B. (2013) 'Hox transcriptional specificity despite a single class of cofactors: are flexible interaction modes the key? Plasticity in Hox/PBC interaction modes as a common molecular strategy for shaping Hox transcriptional activities.', *BioEssays*, 35(2), 88–92.

Merabet, S., Lohmann, I. (2015) 'Toward a new Twist in Hox and TALE DNA-binding specificity', *Developmental Cell*, 32(3), 259–261.

Mercader, N., Leonardo, E., Azpiazu, N., Serrano, A., Morata, G., Martínez-A, C., Torres, M. (1999) 'Conserved regulation of proximodistal limb axis development by *Meis1/Hth*', *Nature*, 402(6760), 425–429.

Mercader, N., Leonardo, E., Piedra, M.E., Martínez-A, C., Ros, M.Á., Torres, M. (2000) 'Opposing RA and FGF signals control proximodistal vertebrate limb development through regulation of Meis genes.', *Development*, 127(18), 3961–3970.

Mercader, N., Selleri, L., Criado, L.M., Pallares, P., Parras, C., Cleary, M.L., Torres, M. (2009) 'Ectopic *Meis1* expression in the mouse limb bud alters P-D patterning in a *Pbx1*-independent manner.', *The International Journal of Developmental Biology*, 53(8-10), 1483–94.

Mercader, N., Tanaka, E.M., Torres, M. (2005) 'Proximodistal identity during vertebrate limb regeneration is regulated by *Meis* homeodomain proteins.', *Development*, 132(18), 4131–4142.

Merino, R., Gañan, Y., Macias, D., Economides, A.N., Sampath, K.T., Hurle, J.M. (1998) 'Morphogenesis of digits in the avian limb is controlled by FGFs, TGFbetas, and noggin through BMP signaling.', *Developmental Biology*, 200(1), 35–45.

Mic, F.A., Haselbeck, R.J., Cuenca, A.E., Duester, G. (2002) 'Novel retinoic acid generating activities in the neural tube and heart identified by conditional rescue of Raldh2 null mutant mice.', *Development*, 129(9), 2271–82.

Miller-Butterworth, C.M., Eick, G., Jacobs, D.S., Schoeman, M.C., Harley, E.H. (2005) 'Genetic and Phenotypic Differences Between South African Long-Fingered Bats, With a Global Miniopterine Phylogeny', *Journal of Mammalogy*, 86(6), 1121–1135.

Minina, E., Wenzel, H.M., Kreschel, C., Karp, S., Gaffield, W., McMahon, a P., Vortkamp, A. (2001) 'BMP and Ihh/PTHrP signaling interact to coordinate chondrocyte proliferation and differentiation.', *Development*, 128(22), 4523–4534.

Moens, C.B., Selleri, L. (2006) '*Hox* cofactors in vertebrate development.', *Developmental Biology*, 291(2), 193–206.

Mojsin, M., Stevanovic, M. (2010) 'PBX1 and MEIS1 up-regulate SOX3 gene expression by direct interaction with a consensus binding site within the basal promoter region', *Biochemical Journal*, 425(1), 107–116.
Montavon, T., Duboule, D. (2013) 'Chromatin organization and global regulation of *Hox* gene clusters', *Philosophical Transactions of the Royal Society B: Biological Sciences*, 368(1620), 20120367–20120367.
Montavon, T., Le Garrec, J.-F., Kerszberg, M., Duboule, D. (2008) 'Modeling *Hox* gene regulation in digits: Reverse collinearity and the molecular origin of thumbness.', *Genes & Development*, 22(3), 346–359.
Montavon, T., Soshnikova, N., Mascrez, B., Joye, E., Thevenet, L., Splinter, E., de Laat, W., Spitz, F., Duboule, D. (2011) 'A regulatory archipelago controls *Hox* genes transcription in digits.', *Cell*, 147(5), 1132–1145.
Morgan, B.A., Izpisúa-Belmonte, J.C., Duboule, D., Tabin, C.J. (1992) 'Targeted misexpression of *Hox-4.6* in the avian limb bud causes apparent homeotic transformations.', *Nature*, 358(6383), 236–239.
Morgan, B.A., Tabin, C.J. (1994) '*Hox* genes and growth: early and late roles in limb bud morphogenesis.', *Development*, 186, 181–186.
Moskow, J.J., Bullrich, F., Huebner, K., Daar, I.O., Buchberg, A.M. (1995) 'Meis1, a PBX1-related homeobox gene involved in myeloid leukemia in BXH-2 mice', *Molecular and Cellular Biology*, 210(2), 184–190.
Murrell, B., Wertheim, J.O., Moola, S., Weighill, T., Scheffler, K., Kosakovsky Pond, S.L. (2012) 'Detecting individual sites subject to episodic diversifying selection', *PLoS Genetics*, 8(7).
Nagai, H., Mak, S.-S., Weng, W., Nakaya, Y., Ladher, R., Sheng, G. (2011) 'Embryonic development of the emu, *Dromaius novaehollandiae*.', *Developmental Dynamics*, 240(1), 162–175.
Nakamura, H., Funahashi, J. (2013) 'Electroporation: Past, present and future', *Development, Growth & Differentiation*, 55(1), 15–19.
Nakamura, T., Jenkins, N.A., Copeland, N.G. (1996) 'Identification of a new family of *Pbx*-related homeobox genes', *Oncogene*, 13(10), 2235–2242.
Nelson, C.E., Morgan, B.A., Burke, A.C., Laufer, E., DiMambro, E., Murtaugh, L.C., Gonzales, E., Tessarollo, L., Parada, L.F., Tabin, C.J. (1996) 'Analysis of *Hox* gene expression in the chick limb bud', *Development*, 122, 1449–1466.
Neufeld, S.J., Zhou, X., Vize, P.D., Cobb, J. (2013) 'mRNA fluorescence in situ hybridization to determine overlapping gene expression in whole-mount mouse embryos', *Developmental Dynamics*, 242(9), 1094–1100.
Neuweiler, G. (2000) *The Biology of Bats*, Oxford University Press, USA.
Newman, S.A., Frisch, H.L. (1979) 'Dynamics of skeletal pattern formation in developing chick limb.', *Science*, 205(4407), 662–668.
Nguyen, M.T., Zhu, J., Nakamura, E., Bao, X., Mackem, S. (2009) 'Tamoxifen-dependent, inducible Hoxb6CreERT recombinase function in lateral plate and limb mesoderm, CNS isthmic organizer, posterior trunk neural crest, hindgut, and tailbud', *Developmental Dynamics*, 238(2), 467–474.
Niederreither, K., Dollé, P. (2008) 'Retinoic acid in development: towards an integrated view', *Nature Reviews Genetics*, 9(7), 541–553.
Di Nino, D.L., Long, F., Linsenmayer, T.F. (2001) 'Regulation of endochondral cartilage growth in the developing avian limb: cooperative involvement of perichondrium and periosteum.', *Developmental Biology*, 240(2), 433–442.
Niswander, L.A., Jeffrey, S., Martin, G.R., Tickle, C. (1994) 'A positive feedback loop coordinates growth and patterning in the vertebrate limb', *Nature*, 371(6498), 609–612.
Nolte, M.J., Hockman, D., Cretekos, C.J., Behringer, R.R., Rasweiler, J.J. (2009) 'Embryonic staging system for the Black Mastiff Bat, *Molossus rufus* (Molossidae), correlated with structure-function relationships in the adult.', *The Anatomical Record*, 292(2), 155–168.
Noordermeer, D., Duboule, D. (2013) *Chromatin Architectures and Hox Gene Collinearity*, 1st ed, Current Topics in Developmental Biology, Elsevier Inc.
Noordermeer, D., Leleu, M., Schorderet, P., Joye, E., Chabaud, F., Duboule, D. (2014) 'Temporal dynamics and developmental memory of 3D chromatin architecture at Hox gene loci', *eLife*, 2014(3), 1–21.
Norberg, U.M. (1969) 'An arrangement giving a stiff leading edge to the hand wing in bats', *Journal of Mammalogy*, 50(4), 766–770.
Norberg, U.M. (1981) 'Allometry of bat wings and legs and comparison with bird wings', *Philosophical Transactions of the Royal Society B: Biological Sciences*, 292(1061), 359–398.
Norberg, U.M. (1990) *Vertebrate Flight*, Zoophysiology, Springer Berlin Heidelberg: Berlin, Heidelberg.
Norberg, U.M., Rayner, J.M. (1987) 'Ecological morphology and flight in bats (mammalia; Chiroptera): Wing adaptations, flight performance, foraging strategy and ecolocation', *Philosophical Transactions of the Royal Society B: Biological Sciences*, 316(1179), 335–427.
Ohuchi, H., Nakagawa, T., Yamamoto, A., Araga, A., Ohata, T., Ishimaru, Y., Yoshioka, H., Kuwana, T., Nohno, T., Yamasaki, M., Itoh, N., Noji, S. (1997) 'The mesenchymal factor, FGF10, initiates and maintains the outgrowth of the chick limb bud through interaction with FGF8, an apical ectodermal factor.', *Development*, 124(11), 2235–2244.
Oulad-Abdelghani, M., Chazaud, C., Bouillet, P., Sapin, V., Chambon, P., Dollé, P. (1997) '*Meis2*, a novel mouse Pbx-related homeobox gene induced by retinoic acid during differentiation of P19 embryonal carcinoma cells', *Developmental Dynamics*, 210(2), 173–183.

Paige, S.L., Thomas, S., Stoick-Cooper, C.L., Wang, H., Maves, L., Sandstrom, R., Pabon, L., Reinecke, H., Pratt, G., Keller, G., Moon, R.T., Stamatoyannopoulos, J., Murry, C.E. (2012) 'A temporal chromatin signature in human embryonic stem cells identifies regulators of cardiac development', *Cell*, 151(1), 221–232.

Pajni-Underwood, S., Wilson, C.P., Elder, C., Mishina, Y., Lewandoski, M. (2007) 'BMP signals control limb bud interdigital programmed cell death by regulating FGF signaling.', *Development*, 134, 2359–2368.

Panyutina, A.A., Korzun, L.P., Kuznetsov, A.N. (2015) *Flight of Mammals: From Terrestrial Limbs to Wings*, Igarss 2014, Springer International Publishing.

Pathi, S., Rutenberg, J.B., Johnson, R.L., Vortkamp, A. (1999) 'Interaction of Ihh and BMP/Noggin signaling during cartilage differentiation.', *Developmental Biology*, 209(2), 239–253.

Penkov, D., San Martín, D.M., Fernandez-Díaz, L.C., Rosselló, C.A., Torroja, C., Sánchez-Cabo, F., Warnatz, H.J., Sultan, M., Yaspo, M.L., Gabrieli, A., Tkachuk, V., Brendolan, A., Blasi, F., Torres, M. (2013) 'Analysis of the DNA-binding profile and function of TALE homeoproteins reveals their specialization and specific interactions with hox genes/proteins.', *Cell Reports*, 3(4), 1321–1333.

Perez, W.D., Weller, C.R., Shou, S., Stadler, H.S. (2010) 'Survival of *Hoxa13* homozygous mutants reveals a novel role in digit patterning and appendicular skeletal development.', *Developmental Dynamics*, 239(2), 446–457.

Pfaffl, M.W. (2004) 'Quantification strategies in real-time PCR', in Bustin, S.A., ed., *A-Z of Quantitative PCR*, International University Line: La Jolla, 87–112.

Pillay, L.M., Forrester, A.M., Erickson, T., Berman, J.N., Waskiewicz, A.J. (2010) 'The Hox cofactors Meis1 and Pbx act upstream of *gata1* to regulate primitive hematopoiesis.', *Developmental Biology*, 340(2), 306–317.

Pitsillides, A.A., Ashhurst, D.E. (2008) 'A critical evaluation of specific aspects of joint development', *Developmental Dynamics*, 237, 2284–2294.

Pond, S.L.K., Frost, S.D.W. (2005) 'Datamonkey: Rapid detection of selective pressure on individual sites of codon alignments', *Bioinformatics*, 21(10), 2531–2533.

Probst, S., Kraemer, C., Demougin, P., Sheth, R., Martin, G.R., Shiratori, H., Hamada, H., Iber, D., Zeller, R., Zúñiga, A. (2011) 'SHH propagates distal limb bud development by enhancing CYP26B1-mediated retinoic acid clearance via AER-FGF signalling.', *Development*, 138(10), 1913–1923.

Qin, P., Cimildoro, R., Kochhar, D.M., Soprano, K.J., Soprano, D.R. (2002) 'PBX, MEIS, and IGF-I are potential mediators of retinoic acid-induced proximodistal limb reduction defects.', *Teratology*, 66(5), 224–234.

Quinn, T.H., Baumel, J.J. (1993) 'Chiropteran tendon locking mechanism', *Journal of Morphology*, 216(2), 197–208.

Quirk, C.C., Lozada, K.L., Keri, R.A., Nilson, J.H. (2001) 'A single Pitx1 binding site is essential for activity of the LHbeta promoter in transgenic mice.', *Molecular Endocrinology*, 15(5), 734–746.

Raines, A.M., Magella, B., Adam, M., Potter, S.S. (2015) 'Key pathways regulated by HoxA9,10,11/HoxD9,10,11 during limb development', *BMC Developmental Biology*, 15(1), 28.

Raspopovic, J., Marcon, L., Russo, L., Sharpe, J. (2014) 'Modeling digits. Digit patterning is controlled by a Bmp-Sox9-Wnt Turing network modulated by morphogen gradients.', *Science*, 345(6196), 566–570.

Rasweiler, J.J., Cretekos, C.J., Behringer, R.R. (2009) 'Whole-mount in situ hybridization of short-tailed fruit bat (*Carollia perspicillata*) embryos with RNA probes.', *Cold Spring Harbor Protocols*, 2009(3), pdb.prot5164.

Ray, R., Capecchi, M.R. (2008) 'An examination of the Chiropteran *HoxD* locus from an evolutionary perspective.', *Evolution & Development*, 10(6), 657–670.

Reno, P.L., Horton, W.E., Lovejoy, C.O. (2013) 'Metapodial or phalanx? An evolutionary and developmental perspective on the homology of the first ray's proximal segment.', *Journal of Experimental Zoology Part B: Molecular and Developmental Evolution*, 320(5), 276–285.

Reno, P.L., McBurney, D.L., Lovejoy, C.O., Horton, W.E. (2006) 'Ossification of the mouse metatarsal: Differentiation and proliferation in the presence/absence of a defined growth plate', *The Anatomical Record - Part A*, 288(1), 104–118.

Reno, P.L., McCollum, M.A., Cohn, M.J., Meindl, R.S., Hamrick, M.W., Lovejoy, C.O. (2008) 'Patterns of correlation and covariation of anthropoid distal forelimb segments correspond to Hoxd expression territories.', *Journal of Experimental Zoology Part B: Molecular and Developmental Evolution*, 310(3), 240–258.

Rhinn, M., Dollé, P. (2012) 'Retinoic acid signalling during development', *Development*, 139(5), 843–858.

Rice, P., Longden, I., Bleasby, A. (2000) 'EMBOSS: the European Molecular Biology Open Software Suite.', *Trends in genetics*, 16(6), 276–7.

Richardson, L., Venkataraman, S., Stevenson, P., Yang, Y., Moss, J., Graham, L., Burton, N., Hill, B., Rao, J., Baldock, R. a., Armit, C. (2014) 'EMAGE mouse embryo spatial gene expression database: 2014 update', *Nucleic Acids Research*, 42(D1), 1–10.

Richardson, M.K., Gobes, S.M.H., van Leeuwen, A.C., Polman, J.A.E., Pieau, C., Sánchez-Villagra, M.R. (2009) 'Heterochrony in limb evolution: developmental mechanisms and natural selection.', *Journal of Experimental Zoology Part B: Molecular and Developmental Evolution*, 312(6), 639–664.

Riddle, R.D., Johnson, R.L., Laufer, E., Tabin, C.J. (1993) 'Sonic hedgehog mediates the polarizing activity of the ZPA.', *Cell*, 75(7), 1401–1416.

Riskin, D.K., Bertram, J.E.A., Hermanson, J.W. (2005) 'Testing the hindlimb-strength hypothesis: non-aerial locomotion by Chiroptera is not constrained by the dimensions of the femur or tibia.', *The Journal of Experimental Biology*, 208(Pt 7), 1309–1319.

Riskin, D.K., Fenton, M.B. (2001) 'Sticking ability in Spix's disk-winged bat, Thyroptera tricolor (Microchiroptera: Thyropteridae)', *Canadian Journal of Zoology*, 79(12), 2261–2267.

Riskin, D.K., Racey, P.A. (2010) 'How do sucker-footed bats hold on, and why do they roost head-up?', *Biological Journal of the Linnean Society*, 99(2), 233–240.

Rodriguez-Leon, J., Merino, R., Macias, D., Gañan, Y., Santesteban, E., Hurle, J.M. (1999) 'Retinoic acid regulates programmed cell death through BMP signalling.', *Nature Cell Biology*, 1(2), 125–6.

Romereim, S.M., Dudley, A.T. (2011) 'Cell polarity: The missing link in skeletal morphogenesis?', *Organogenesis*, 7(3), 217–228.

Rooney, P., Archer, C.W. (1992) 'The development of the perichondrium in the avian ulna.', *Journal of Anatomy*, 181(3), 393–401.

Roselló-Díez, A., Arques, C.G., Delgado, I., Giovinazzo, G., Torres, M. (2014) 'Diffusible signals and epigenetic timing cooperate in late proximo-distal limb patterning', *Development*, 141(7), 1534–1543.

Roselló-Díez, A., Ros, M.Á., Torres, M. (2011) 'Diffusible signals, not autonomous mechanisms, determine the main proximodistal limb subdivision', *Science*, 332(6033), 1086–1088.

Rutledge, R.G. (2004) 'Sigmoidal curve-fitting redefines quantitative real-time PCR with the prospective of developing automated high-throughput applications.', *Nucleic Acids Research*, 32(22), e178.

Rutledge, R.G., Stewart, D. (2010) 'Assessing the performance capabilities of LRE-based assays for absolute quantitative real-time PCR', *PLoS ONE*, 5(3), e9731.

Ryoo, H.D., Marty, T., Casares, F., Affolter, M., Mann, R.S. (1999) 'Regulation of Hox target genes by a DNA bound Homothorax/Hox/Extradenticle complex.', *Development*, 126(22), 5137–5148.

Sadasivam, S., Duan, S., DeCaprio, J.A. (2012) 'The MuvB complex sequentially recruits B-Myb and FoxM1 to promote mitotic gene expression', *Genes & Development*, 26(5), 474–489.

Sagerström, C.G., Kao, B. a., Lane, M.E., Sive, H. (2001) 'Isolation and characterization of posteriorly restricted genes in the zebrafish gastrula', *Developmental Dynamics*, 220(4), 402–408.

Salas-Vidal, E., Valencia, C., Covarrubias, L. (2001) 'Differential tissue growth and patterns of cell death in mouse limb autopod morphogenesis.', *Developmental Dynamics*, 220(4), 295–306.

Salsi, V., Vigano, M.A., Cocchiarella, F., Mantovani, R., Zappavigna, V. (2008) 'Hoxd13 binds in vivo and regulates the expression of genes acting in key pathways for early limb and skeletal patterning.', *Developmental Biology*, 317(2), 497–507.

Salsi, V., Zappavigna, V. (2006) '*Hoxd13* and *Hoxa13* directly control the expression of the *EphA7* ephrin tyrosine kinase receptor in developing limbs', *Journal of Biological Chemistry*, 281(4), 1992–1999.

Salzberg, A., Elias, S., Nachaliel, N., Bonstein, L., Henig, C., Frank, D. (1999) 'A Meis family protein caudalizes neural cell fates in Xenopus', *Mechanisms of Development*, 80(1), 3–13.

Sánchez-Guardado, L.Ó., Ferran, J.L., Rodríguez-Gallardo, L., Puelles, L., Hidalgo-Sánchez, M. (2011) '*Meis* gene expression patterns in the developing chicken inner ear.', *The Journal of Comparative Neurology*, 519(1), 125–147.

Sánchez-Guardado, L.Ó., Irimia, M., Sánchez-Arrones, L., Burguera, D., Rodríguez-Gallardo, L., Garcia-Fernández, J., Puelles, L., Ferran, J.L., Hidalgo-Sánchez, M. (2011) 'Distinct and redundant expression and transcriptional diversity of MEIS gene paralogs during chicken development.', *Developmental Dynamics*, 240(6), 1475–1492.

Sandell, L.L., Sanderson, B.W., Moiseyev, G., Johnson, T., Mushegian, A., Young, K., Rey, J.-P., Ma, J., Staehling-Hampton, K., Trainor, P.A. (2007) 'RDH10 is essential for synthesis of embryonic retinoic acid and is required for limb, craniofacial, and organ development.', *Genes & Development*, 21(9), 1113–1124.

Sanz-Ezquerro, J.J., Tickle, C. (2003) 'Digital development and morphogenesis', *Journal of Anatomy*, 202, 51–58.

Saunders, J.W. (1948) 'The proximo-distal sequence of origin of the parts of the chick wing and the role of the ectoderm', *Journal of Experimental Zoology*, 108(3), 363–403.

Savory, J.G. a., Edey, C., Hess, B., Mears, A.J., Lohnes, D. (2014) 'Identification of novel retinoic acid target genes', *Developmental Biology*, 395(2), 199–208.

Scheffler, K., Martin, D.P., Seoighe, C. (2006) 'Robust inference of positive selection from recombining coding sequences', *Bioinformatics*, 22(20), 2493–2499.

Schneider, I., Shubin, N.H. (2013) 'The origin of the tetrapod limb: From expeditions to enhancers', *Trends in Genetics*, 29(7), 419–426.

Schutt Jr., W.A., Simmons, N.B. (2006) 'Quadrapedal bats: Form, function, and evolution', in Akbar, Z., McCracken, G.F. and Kunz, T., eds., *Functional and Evolutionary Ecology of Bats*, Oxford University Press, USA, 145–159.

Scott, M.P. (1993) 'A rational nomenclature for vertebrate homeobox (HOX) genes', *Nucleic Acids Research*, 21(8), 1687–1688.

Scotti, M., Kmita, M. (2012) 'Recruitment of 5' Hoxa genes in the allantois is essential for proper extra-embryonic function in placental mammals', *Development*, 139(4), 731–739.

Sears, K.E. (2008) 'Molecular determinants of bat wing development.', *Cells Tissues Organs*, 187(1), 6–12.

Sears, K.E. (2009) 'Differences in the timing of prechondrogenic limb development in mammals: the marsupial-placental dichotomy resolved.', *Evolution*, 63(8), 2193–2200.
Sears, K.E. (2011) 'Novel insights into the regulation of limb development from "natural" mammalian mutants', *BioEssays*, 33(5), 327–331.
Sears, K.E., Behringer, R.R., Rasweiler, J.J., Niswander, L.A. (2006) 'Development of bat flight: Morphologic and molecular evolution of bat wing digits.', *Proceedings of the National Academy of Sciences*, 103(17), 6581–6586.
Shaikh, N., Gates, P.B., Brockes, J.P. (2011) 'The Meis homeoprotein regulates the axolotl Prod 1 promoter during limb regeneration', *Gene*, 484(1-2), 69–74.
Shanmugam, K., Green, N.C., Rambaldi, I., Saragovi, H.U., Featherstone, M.S. (1999) 'PBX and MEIS as non-DNA-binding partners in trimeric complexes with HOX proteins.', *Molecular and Cellular Biology*, 19(11), 7577–7588.
Shapiro, M.D., Hanken, J., Rosenthal, N. (2003) 'Developmental basis of evolutionary digit loss in the Australian lizard Hemiergis', *Journal of Experimental Zoology*, 297B(1), 48–56.
Shen, W.F., Montgomery, J.C., Rozenfeld, S., Moskow, J.J., Lawrence, H.J., Buchberg, A.M., Largman, C. (1997) 'AbdB-like Hox proteins stabilize DNA binding by the *Meis1* homeodomain proteins.', *Molecular and Cellular Biology*, 17(11), 6448–6458.
Sheth, R., Bastida, M.F., Kmita, M., Ros, M.Á. (2014) '"Self-regulation," a new facet of *Hox* genes' function', *Developmental Dynamics*, 243(1), 182–191.
Sheth, R., Grégoire, D., Dumouchel, A., Scotti, M., Pham, J.M.T., Nemec, S., Bastida, M.F., Ros, M.Á., Kmita, M. (2013) 'Decoupling the function of *Hox* and *Shh* in developing limb reveals multiple inputs of *Hox* genes on limb growth.', *Development*, 140(10), 2130–2138.
Sheth, R., Marcon, L., Bastida, M.F., Junco, M., Quintana, L., Dahn, R.D., Kmita, M., Sharpe, J., Ros, M.Á. (2012) 'Hox genes regulate digit patterning by controlling the wavelength of a Turing-type mechanism.', *Science*, 338, 1476–1480.
Shim, S., Kim, Y., Shin, J., Kim, J., Park, S. (2007) 'Regulation of *EphA8* gene expression by TALE homeobox transcription factors during development of the mesencephalon.', *Molecular and Cellular Biology*, 27(5), 1614–1630.
Shou, S., Carlson, H.L., Perez, W.D., Stadler, H.S. (2013) 'HOXA13 regulates *Aldh1a2* expression in the autopod to facilitate interdigital programmed cell death.', *Developmental Dynamics*, 242(6), 687–698.
Shou, S., Scott, V., Reed, C., Hitzemann, R., Stadler, H.S. (2005) 'Transcriptome analysis of the murine forelimb and hindlimb autopod.', *Developmental Dynamics*, 234(1), 74–89.
Shubin, N.H. (2002) 'Origin of evolutionary novelty: Examples from limbs', *Journal of Morphology*, 252(1), 15–28.
Shubin, N.H., Alberch, P. (1986) 'A morphogenetic approach to the origin and basic organization of the tetrapod limb', *Evolutionary Biology*, 20, 319–387.
Shubin, N.H., Daeschler, E.B., Jenkins, F.A. (2006) 'The pectoral fin of *Tiktaalik roseae* and the origin of the tetrapod limb', *Nature*, 440(7085), 764–771.
Shubin, N.H., Tabin, C.J., Carroll, S.B. (1997) 'Fossils, genes and the evolution of animal limbs', *Nature*, 388(6643), 639–648.
Shubin, N.H., Tabin, C.J., Carroll, S.B. (2009) 'Deep homology and the origins of evolutionary novelty', *Nature*, 457(7231), 818–823.
Da Silva, S.M., Gates, P.B., Brockes, J.P. (2002) 'The newt ortholog of CD59 is implicated in proximodistal identity during amphibian limb regeneration', *Developmental Cell*, 3(4), 547–555.
Simmons, N.B., Seymour, K.L., Habersetzer, J., Gunnell, G.F. (2008) 'Primitive Early Eocene bat from Wyoming and the evolution of flight and echolocation.', *Nature*, 451, 818–821.
Smits, P., Li, P., Mandel, J., Zhang, Z., Deng, J.M., Behringer, R.R., De Crombrugghe, B., Lefebvre, V. (2001) 'The Transcription Factors L-Sox5 and Sox6 Are Essential for Cartilage Formation', *Developmental Cell*, 1(2), 277–290.
Soshnikova, N., Dewaele, R., Janvier, P., Krumlauf, R., Duboule, D. (2013) 'Duplications of *hox* gene clusters and the emergence of vertebrates', *Developmental Biology*, 378(2), 194–199.
Spitz, F., Gonzalez, F., Duboule, D. (2003) 'A global control region defines a chromosomal regulatory landscape containing the *HoxD* cluster', *Cell*, 113(3), 405–417.
Spitz, F., Gonzalez, F., Peichel, C., Vogt, T.F., Duboule, D., Zákány, J. (2001) 'Large scale transgenic and cluster deletion analysis of the *HoxD* complex separate an ancestral regulatory module from evolutionary innovations', *Genes & Development*, 15, 2209–2214.
Srivastava, S., Dhawan, J., Mishra, R.K. (2015) 'Epigenetic mechanisms and boundaries in the regulation of mammalian Hox clusters', *Mechanisms of Development*, 138, 160–169.
St-Jacques, B., Hammerschmidt, M., McMahon, A.P. (1999) 'Indian hedgehog signaling regulates proliferation and differentiation of chondrocytes and is essential for bone formation.', *Genes & Development*, 13(16), 2072–2086.
Stadler, H.S., Higgins, K.M., Capecchi, M.R. (2001) 'Loss of *Eph-receptor* expression correlates with loss of cell adhesion and chondrogenic capacity in *Hoxa13* mutant limbs.', *Development*, 128(21), 4177–4188.
Sterbing-D'Angelo, S., Chadha, M., Chiu, C., Falk, B., Xian, W., Barcelo, J., Zook, J.M., Moss, C.F. (2011) 'Bat wing sensors support flight control', *Proceedings of the National Academy of Sciences*, 108(27), 11291–11296.
Summerbell, D. (1974) 'A quantitative analysis of the effect of excision of the AER from the chick limb-bud', *Journal of Embryology and Experimental Morphology*, 32(3), 651–660.

Sun, X., Mariani, F. V, Martin, G.R. (2002) 'Functions of FGF signalling from the apical ectodermal ridge in limb development.', *Nature*, 418(6897), 501–508.
Suzuki, M., Kuroiwa, A. (2002) 'Transition of *Hox* expression during limb cartilage development', *Mechanisms of Development*, 118(1-2), 241–245.
Suzuki, T. (2013) 'How is digit identity determined during limb development?', *Development Growth and Differentiation*, 55, 130–138.
Suzuki, T., Hasso, S.M., Fallon, J.F. (2008) 'Unique SMAD1/5/8 activity at the phalanx-forming region determines digit identity.', *Proceedings of the National Academy of Sciences*, 105(11), 4185–4190.
Swartz, S.M. (1997) 'Allometric patterning in the limb skeleton of bats: Implications for the mechanics and energetics of powered flight', *Journal of Morphology*, 234(3), 277–294.
Swartz, S.M., Iriarte-Diaz, J., Riskin, D.K., Tian, X., Song, A., Breuer, K.S. (2007) 'Wing structure and the aerodynamic basis of flight in bats', in *45th AIAA Aerospace Sciences Meeting and Exhibit*, American Institute of Aeronautics and Astronautics: Reston, Virigina, 1–10.
Swartz, S.M., Middleton, K.M. (2008) 'Biomechanics of the bat limb skeleton: Scaling, material properties and mechanics.', *Cells Tissues Organs*, 187(1), 59–84.
Szeto, D.P., Ryant, A.K., O'Connellt, S.M., Rosenfeldt, M.G. (1996) 'P-OTX: A PIT-1-interacting homeodomain factor expressed during anterior pituitary gland development', *Proceedings of the National Academy of Sciences*, 93, 7706–7710.
Tabin, C.J., Wolpert, L. (2007) 'Rethinking the proximodistal axis of the vertebrate limb in the molecular era.', *Genes & Development*, 21(12), 1433–1442.
Tamura, K., Yonei-Tamura, S., Yano, T., Yokoyama, H., Ide, H. (2008) 'The autopod: its formation during limb development.', *Development, Growth & Differentiation*, 50, S177–S187.
Tanaka, M. (2013) 'Molecular and evolutionary basis of limb field specification and limb initiation.', *Development Growth and Differentiation*, 55(1), 149–163.
Tarchini, B., Duboule, D. (2006) 'Control of Hoxd genes' collinearity during early limb development', *Developmental Cell*, 10(1), 93–103.
Tarchini, B., Duboule, D., Kmita, M. (2006) 'Regulatory constraints in the evolution of the tetrapod limb anterior-posterior polarity.', *Nature*, 443(7114), 985–988.
Teeling, E.C., Springer, M.S., Madsen, O., Bates, P., O'brien, S.J., Murphy, W.J. (2005) 'A molecular phylogeny for bats illuminates biogeography and the fossil record.', *Science*, 307(5709), 580–584.
Tokita, M. (2006) 'Normal embryonic development of the Japanese pipistrelle, *Pipistrellus abramus*.', *Zoology*, 109(2), 137–147.
Tokita, M. (2015) 'How the pterosaur got its wings', *Biological Reviews*, 90(4), 1163–1178.
Tokita, M., Abe, T., Suzuki, K. (2012) 'The developmental basis of bat wing muscle.', *Nature Communications*, 3(1302), 1–9.
Toresson, H., Parmar, M., Campbell, K. (2000) 'Expression of *Meis* and *Pbx* genes and their protein products in the developing telencephalon: implications for regional differentiation.', *Mechanisms of Development*, 94(1-2), 183–187.
Tschopp, P., Duboule, D. (2011) 'A genetic approach to the transcriptional regulation of *Hox* gene clusters.', *Annual Review of Genetics*, 45, 145–166.
Tschopp, P., Fraudeau, N., Béna, F., Duboule, D. (2011) 'Reshuffling genomic landscapes to study the regulatory evolution of Hox gene clusters.', *Proceedings of the National Academy of Sciences*, 108, 10632–10637.
Tucker, E.S., Lehtinen, M.K., Maynard, T., Zirlinger, M., Dulac, C., Rawson, N., Pevny, L., Lamantia, A.-S. (2010) 'Proliferative and transcriptional identity of distinct classes of neural precursors in the mammalian olfactory epithelium.', *Development*, 137(15), 2471–2481.
Turing, A.M. (1952) 'The chemical basis of morphogenesis', *Philosophical Transactions of the Royal Society of London B: Biological Sciences*, 237(641), 37–72.
Tut, T.G., Ghadessy, F.J., Trifiro, M. a, Pinsky, L., Yong, E.L. (1997) 'Long polyglutamine tracts in the androgen receptor are associated with reduced trans-activation, impaired sperm production, and male infertility.', *The Journal of Clinical Endocrinology and Metabolism*, 82(11), 3777–82.
Untergasser, A., Cutcutache, I., Koressaar, T., Ye, J., Faircloth, B.C., Remm, M., Rozen, S.G. (2012) 'Primer3-new capabilities and interfaces', *Nucleic Acids Research*, 40(15), 1–12.
Uzkudun, M., Marcon, L., Sharpe, J. (2015) 'Data-driven modelling of a gene regulatory network for cell fate decisions in the growing limb bud', *Molecular Systems Biology*, 8(815), 1–15.
VanGuilder, H.D., Vrana, K.E., Freeman, W.M. (2008) 'Twenty-five years of quantitative PCR for gene expression analysis', *BioTechniques*, 44(5), 619–626.
Vaughan, T.A. (1970) 'Flight patterns and aerodynamics', in Wimsatt, W., ed., *Biology of Bats, Volume 1*, Elsevier, 195–216.
Vaughan, T.A., Ryan, J.M., Czaplewski, N.J. (2011) *Mammalogy*, 5th ed, Jones & Bartlett Publishers.

Villavicencio-Lorini, P., Kuss, P., Friedrich, J., Haupt, J., Farooq, M., Türkmen, S., Duboule, D., Hecht, J., Mundlos, S. (2010) 'Homeobox genes d11-d13 and a13 control mouse autopod cortical bone and joint formation.', *The Journal of Clinical Investigation*, 120(6), 1994–2004.

Vlachakis, N., Choe, S.-K., Sagerström, C.G. (2001) '*Meis3* synergizes with *Pbx4* and *Hoxb1b* in promoting hindbrain fates in the zebrafish.', *Development*, 128(8), 1299–1312.

Vlachakis, N., Ellstrom, D.R., Sagerström, C.G. (2000) 'A novel Pbx family member expressed during early zebrafish embryogenesis forms trimeric complexes with *Meis3* and *Hoxb1b*', *Developmental Dynamics*, 217(1), 109–119.

Vortkamp, A., Lee, K., Lanske, B., Segre, G. V., Kronenberg, H.M., Tabin, C.J. (1996) 'Regulation of rate of cartilage differentiation by Indian hedgehog and PTH-related protein.', *Science*, 273(5275), 613–622.

Wagner, G.P., Lynch, V.J. (2010) 'Evolutionary novelties', *Current Biology*, 20(2), R48–R52.

Wanek, N., Muneoka, K., Holler-Dinsmore, G., Burton, R., Bryant, S.V. (1989) 'A staging system for mouse limb development', *The Journal of Experimental Zoology*, 249(1), 41–49.

Wang, X., Song, X., Glass, C.K., Rosenfeld, M.G. (2011) 'The long arm of long noncoding RNAs: roles as sensors regulating gene transcriptional programs.', *Cold Spring Harbor Perspectives in Biology*, 3(1), a003756.

Wang, Z., Dai, M., Wang, Y., Cooper, K.L., Zhu, T., Dong, D., Zhang, J., Zhang, S. (2014) 'Unique expression patterns of multiple key genes associated with the evolution of mammalian flight.', *Proceedings of the Royal Society B*, 281(1783), 20133133.

Wang, Z., Dong, D., Ru, B., Young, R.L., Han, N., Guo, T., Zhang, S. (2010) 'Digital gene expression tag profiling of bat digits provides robust candidates contributing to wing formation.', *BMC Genomics*, 11(619).

Wang, Z., Young, R.L., Xue, H., Wagner, G.P. (2011) 'Transcriptomic analysis of avian digits reveals conserved and derived digit identities in birds', *Nature*, 477(7366), 583–586.

Warot, X., Fromental-Ramain, C., Fraulob, V., Chambon, P., Dollé, P. (1997) 'Gene dosage-dependent effects of the Hoxa-13 and Hoxd-13 mutations on morphogenesis of the terminal parts of the digestive and urogenital tracts.', *Development*, 124(23), 4781–4791.

Waskiewicz, A.J., Rikhof, H.A., Hernandez, R.E., Moens, C.B. (2001) 'Zebrafish Meis functions to stabilize Pbx proteins and regulate hindbrain patterning.', *Development*, 128(21), 4139–4151.

Weatherbee, S.D., Behringer, R.R., Rasweiler, J.J., Niswander, L.A. (2006) 'Interdigital webbing retention in bat wings illustrates genetic changes underlying amniote limb diversification.', *Proceedings of the National Academy of Sciences*, 103(41), 15103–15107.

Wellik, D.M., Capecchi, M.R. (2003) '*Hox10* and *Hox11* genes are required to globally pattern the mammalian skeleton.', *Science*, 301(5631), 363–367.

Te Welscher, P., Fernández-Terán, M.A., Ros, M.Á., Zeller, R. (2002) 'Mutual genetic antagonism involving GLI3 and dHAND prepatterns the vertebrate limb bud mesenchyme prior to SHH signaling', *Genes & Development*, 16(4), 421–426.

Williams, T.M., Williams, M.E., Innis, J.W. (2005) 'Range of HOX/TALE superclass associations and protein domain requirements for HOXA13:MEIS interaction.', *Developmental Biology*, 277(2), 457–471.

Wilsman, N.J., Farnum, C.E., Leiferman, E.M., Fry, M., Barreto, C. (1996) 'Differential growth by growth plates as a function of multiple parameters of chondrocytic kinetics.', *Journal of Orthopaedic Research*, 14(6), 927–936.

Witte, F., Chan, D., Economides, A.N., Mundlos, S., Stricker, S. (2010) 'Receptor tyrosine kinase-like orphan receptor 2 (ROR2) and Indian hedgehog regulate digit outgrowth mediated by the phalanx-forming region.', *Proceedings of the National Academy of Sciences*, 107(32), 14211–14216.

Wittkopp, P.J., Kalay, G. (2011) 'Cis-regulatory elements: molecular mechanisms and evolutionary processes underlying divergence', *Nature Reviews Genetics*, 13(1), 59–69.

Woltering, J.M., Duboule, D. (2010) 'The origin of digits: Expression patterns versus regulatory mechanisms.', *Developmental Cell*, 18(4), 526–532.

Woltering, J.M., Noordermeer, D., Leleu, M., Duboule, D. (2014) 'Conservation and divergence of regulatory strategies at *Hox* loci and the origin of tetrapod digits', *PLoS Biology*, 12(1), e1001773.

Yang, Y., Hwang, C.K., D'Souza, U.M., Lee, S.H., Junn, E., Mouradian, M.M. (2000) 'Three-amino acid extension loop homeodomain proteins *Meis2* and TGIF differentially regulate transcription.', *The Journal of Biological Chemistry*, 275(27), 20734–20741.

Yashiro, K., Zhao, X., Uehara, M., Yamashita, K., Nishijima, M., Nishino, J., Saijoh, Y., Sakai, Y., Hamada, H. (2004) 'Regulation of retinoic acid distribution is required for proximodistal patterning and outgrowth of the developing mouse limb.', *Developmental Cell*, 6(3), 411–422.

Ye, J., Coulouris, G., Zaretskaya, I., Cutcutache, I., Rozen, S., Madden, T.L. (2012) 'Primer-BLAST: a tool to design target-specific primers for polymerase chain reaction.', *BMC Bioinformatics*, 13(134).

Yokouchi, Y., Sasaki, H., Kuroiwa, A. (1991) 'Homeobox gene expression correlated with the bifurcation process of limb cartilage development.', *Nature*, 353(6343), 443–445.

Yoon, B.S., Lyons, K.M. (2004) 'Multiple functions of BMPs in chondrogenesis.', *Journal of Cellular Biochemistry*, 93(1), 93–103.

Yoon, B.S., Pogue, R., Ovchinnikov, D.A., Yoshii, I., Mishina, Y., Behringer, R.R., Lyons, K.M. (2006) 'BMPs regulate multiple aspects of growth-plate chondrogenesis through opposing actions on FGF pathways.', *Development*, 133(23), 4667–78.

Yoshida, C.A., Yamamoto, H., Fujita, T., Furuichi, T., Ito, K., Inoue, K.I., Yamana, K., Zanma, A., Takada, K., Ito, Y., Komori, T. (2004) 'Runx2 and Runx3 are essential for chondrocyte maturation, and Runx2 regulates limb growth through induction of Indian hedgehog', *Genes and Development*, 18(8), 952–963.

Zákány, J., Duboule, D. (1996) 'Synpolydactyly in mice with a targeted deficiency in the HoxD complex.', *Nature*, 384(6604), 69–71.

Zákány, J., Duboule, D. (2007) 'The role of Hox genes during vertebrate limb development', *Current Opinion in Genetics & Development*, 17(4), 359–366.

Zákány, J., Fromental-Ramain, C., Warot, X., Duboule, D. (1997) 'Regulation of number and size of digits by posterior Hox genes: A dose-dependent mechanism with potential evolutionary implications.', *Proceedings of the National Academy of Sciences*, 94(December), 13695–13700.

Zákány, J., Kmita, M., Duboule, D. (2004) 'A dual role for Hox genes in limb anterior-posterior asymmetry', *Science*, 304(5677), 1669–1672.

Zeller, R. (2010) 'The temporal dynamics of vertebrate limb development, teratogenesis and evolution.', *Current Opinion in Genetics & Development*, 20(4), 384–390.

Zeller, R., López-Ríos, J., Zuniga, A. (2009) 'Vertebrate limb bud development: moving towards integrative analysis of organogenesis', *Nature Reviews Genetics*, 10(12), 845–858.

Zerucha, T., Prince, V.E. (2001) 'Cloning and developmental expression of a zebrafish *meis2* homeobox gene.', *Mechanisms of Development*, 102(1-2), 247–250.

Zha, Y., Xia, Y., Ding, J., Choi, J.-H., Yang, L., Dong, Z., Yan, C., Huang, S., Ding, H.-F. (2014) 'MEIS2 is essential for neuroblastoma cell survival and proliferation by transcriptional control of M-phase progression', *Cell Death and Disease*, 5(9), e1417.

Zhao, X., Brade, T., Cunningham, T.J., Duester, G. (2010) 'Retinoic acid controls expression of tissue remodeling genes Hmgn1 and Fgf18 at the digit-interdigit junction.', *Developmental Dynamics*, 239(2), 665–671.

Zhao, X., Sirbu, I.O., Mic, F.A., Molotkova, N., Molotkov, A., Kumar, S., Duester, G. (2009) 'Retinoic acid promotes limb induction through effects on body axis extension but is unnecessary for limb patterning', *Current Biology*, 19(12), 1050–1057.

Zhu, J., Nakamura, E., Nguyen, M.T., Bao, X., Akiyama, H., Mackem, S. (2008) 'Uncoupling sonic hedgehog control of pattern and expansion of the developing limb bud', *Developmental Cell*, 14(4), 624–632.

Zhu, J., Zhang, Y.T., Alber, M.S., Newman, S.A. (2010) 'Bare bones pattern formation: A core regulatory network in varying geometries reproduces major features of vertebrate limb development and evolution', *PLoS ONE*, 5(5), e10892.

Zhulyn, O., Li, D., Deimling, S., Vakili, N.A., Mo, R., Puviindran, V., Chen, M.H., Chuang, P.T., Hopyan, S., Hui, C.C. (2014) 'A switch from low to high shh activity regulates establishment of limb progenitors and signaling centers', *Developmental Cell*, 29(2), 241–249.

Zúñiga, A., Zeller, R. (2014) 'In Turing's hands--the making of digits', *Science*, 345, 516–517.

Appendices

Appendix A

A.1: *Table of BLAST results for absolute qPCR amplicons*

Table A.1: NCBI BLAST (megablast or *blastn) results for qPCR amplicons against the nucleotide collection (nr/nt) for the mouse (*Mus musculus*, taxid:10090) and the bat (Chiroptera, taxid:9397) giving the description and accession number of the top hit for each search.

Amplicon	Description	Accession	Query Cover (%)	E value	Identity (%)
b5'Meis2	*Mus musculus* 10 days neonate cortex cDNA, RIKEN full-length enriched library, clone:A830011L22	AK043601.1	100	3.00 E-48	97
	PREDICTED: *Pteropus vampyrus Meis homeobox 2* (*Meis2*), transcript variant X8, mRNA	XM_011354887.1	100	3.00 E-54	99
b3'Meis2	PREDICTED: *Mus musculus Meis homeobox 2* (*Meis2*), transcript variant X13, mRNA	XM_006498871.2	100	4.00 E-73	95
	Miniopterus fuliginosus Meis homeobox 2 (*Meis2*) mRNA, complete cds	KJ670370.1	100	2.00 E-87	100
bHoxd10	*Mus musculus homeobox D10* (*Hoxd10*), mRNA	NM_013554.5	100	2.00 E-65	98
	PREDICTED: *Eptesicus fuscus homeobox D10* (HOXD10), mRNA	XM_008138530.1	100	7.00 E-70	99
bHoxd11	**Mus musculus homeobox D11* (*Hoxd11*), transcript variant 1, mRNA	NM_008273.2	98	2.00 E-31	93
	PREDICTED: *Myotis brandtii homeobox D11* (HOXD11), mRNA	XM_005857731.1	98	8.00 E-42	100
bHoxd12	*Mus musculus homeobox D12* (*Hoxd12*), mRNA	NM_008274.3	99	5.00 E-50	100
	Taphozous melanopogon homeobox D12, mRNA, partial cds	FJ455472.1	97	4.00 E-40	94
bHoxd13	*Mus musculus homeobox D13* (*Hoxd13*), mRNA	NM_008275.3	99	1.00 E-42	91
	PREDICTED: *Eptesicus fuscus homeobox D13* (HOXD13), partial mRNA	XM_008138753.1	99	2.00 E-55	97
bHoxa11	**Mus musculus homeobox A11* (*Hoxa11*), mRNA	NM_010450.3	78	7.00 E-21	84
	PREDICTED: *Myotis davidii homeobox A11* (HOXA11), mRNA	XM_006779084.1	99	4.00 E-31	87
bHoxa13	**Mus musculus* chromosome 6, clone RP24-103E20, complete sequence	AC113985.11	89	4.00 E-18	78
	PREDICTED: *Myotis lucifugus homeobox A13* (HOXA13), mRNA	XM_006088760.1|	100	2.00 E-56	96
bTbpl1	*Mus musculus TATA box binding protein-like 1* (*Tbpl1*), mRNA	NM_011603.5	98	6.00 E-55	98
	PREDICTED: *Myotis davidii TBP-like 1* (TBPL1), mRNA	XM_006776214.1	98	2.00 E-59	99

A.2: *Analysis of the suitability of the reference gene, Tbpl1, for use in normalisation*

To confirm that the expression of *Tbpl1* did not differ among the groups tested, the Ct values (not corrected for efficiency) of this gene were examined (Figure A.1). Nine experiments were performed on this reference gene (three biological samples with three cDNA synthesis repeats) and the Ct values compared both among the dilutions, which were expected to differ (Figure A.1A & B) and among the limb samples, which were expected to be similar (Figure A.1C & D). This was done both without averaging the data from the cDNA synthesis technical repeats (Figure A.1A & C) and when the three repeats were averaged (Figure A.1B & D). There were no outliers (data points that were more or less than 1.5 times the interquartile range of that group) in either dataset, the data within all groups were normally distributed, and the variances were not significantly different among the limb samples (Levene's Test of Homogeneity of Variance: *Statistic* = 0.241, d.f.(1,2) = 8, 72, p = 0.982) and nor among the dilution samples (Levene's Test of Homogeneity of Variance: *Statistic* = 0.246, d.f.(1,2) = 4, 40, p = 0.999).

An examination of the distribution of the Ct values of the limb samples show that they are slightly lower in the E13.5 FL and the CS15 FL and HL (Figure A.1C & D). There also appeared to be an incremental increase in the Ct values as the developmental stage increased (Figure A.1D). However, a one-way Analysis of Variance (ANOVA) found no statistically significant differences among the Ct values of the limb samples both when the technical repeats were included ($F_{(8,72)}$ = 0.492, p = 0.858) (Figure A.1C) and when they were averaged (One-Way ANOVA: $F_{(8,18)}$ = 0.300, p = 0.957) (Figure A.1D). This test also did not reveal significant differences among the averaged mouse E13.5 FL and the bat CS17 FL and HL (One-Way ANOVA: $F_{(2,6)}$ = 0.423, p = 0.673) (Figure A.1D). No significant differences were seen between the medians of the bat FL and HL groups (Related-Samples Wilcoxon Signed Rank Test: z = 0, N = 12, p = 1.0), nor among the means of the four developmental stages (One-Way ANOVA: $F_{(3,20)}$ = 0.596, p = 0.625). These data indicate that there are no significant differences in the expression of *Tbpl1* among the tissue samples tested. The Ct values of this gene were therefore considered to be suitable normalisation factors for these experiments, slight variations in this gene's expression within these tissues were assumed to reflect technical differences among the samples.

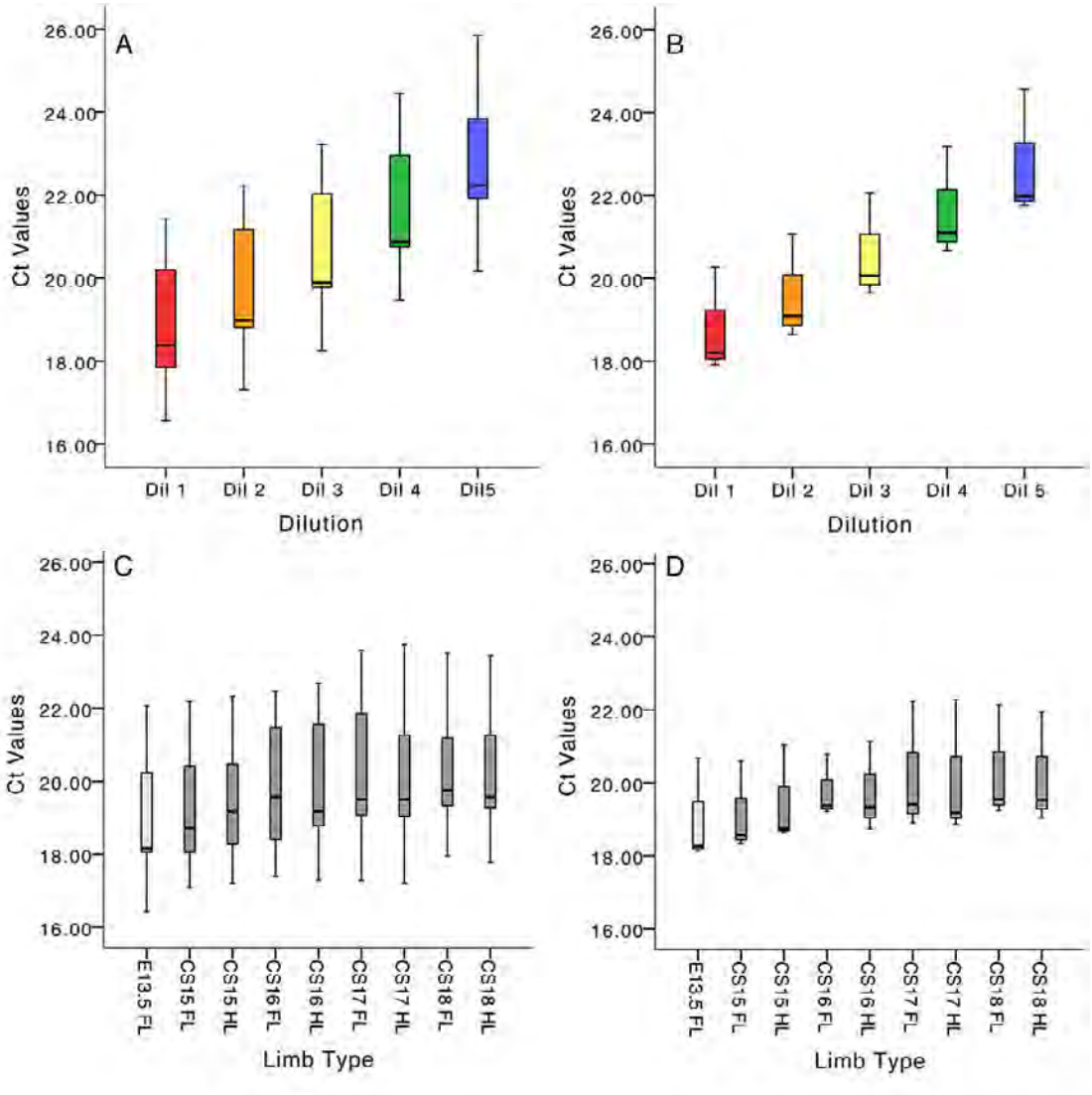

Figure A.1: Box plots of the Ct values for the normalisation gene, *Tbpl1*. These are shown for the serial dilution samples (**A**, **B**) and the limb samples (**C**, **D**). Data that included all biological and technical repeats (**A**, **C**; N = 9) had large ranges within groups. The shape of the distribution was similar among the serial dilution samples and this appears slightly altered among the limb type samples, with the mouse E13.5 FL having the lowest average Ct value and the CS15 FL and CS15 HL also tending to have lower Ct values. This difference is most apparent when the technical repeats are averaged (N = 3), with the average Ct value appearing to increase slightly with stage in the limb samples (**D**) while being unaffected in the serial dilutions (**B**). However these differences were not significant.

A.3: *Table of BLAST results for WISH probe amplicons*

Table A.2: NCBI BLAST (megablast) results for the WISH probe amplicons against the nucleotide collection (nr/nt) for bat (Chiroptera, taxid:9397) giving the description and accession numbers for all hits of the species with the of the top hit.

Amplicon	Description	Variant	Accession	Query Cover (%)	E value	Identity (%)
b5'-Meis2	PREDICTED: *Myotis davidii Meis homeobox 2* (MEIS2), transcript variant X5, mRNA	X5	XM_006778105.1	100	2.00 E-174	89
b3'-Meis2	PREDICTED: *Myotis lucifugus Meis homeobox 2* (MEIS2), transcript variant X4, mRNA	X4	XM_006087500.1	100	0.0	98
		X7	XM_006087503.1	98	0.0	98
		X3	XM_006087499.1	100	0.0	96
		X5	XM_006087501.1	84	0.0	98
		X2	XM_006087498.1	92	0.0	98
		X1	XM_006087497.1	92	0.0	95
		X6	XM_006087502.1	90	0.0	95
	PREDICTED: *Myotis lucifugus Meis homeobox 1* (MEIS1), transcript variant mRNA	X3	XM_006092997.1	99	0.0	79
bHoxa11	PREDICTED: *Myotis lucifugus homeobox A11* (HOXA11), mRNA		XM_006088761.1	100	0.0	86
bHoxa13	PREDICTED: *Myotis lucifugus homeobox A13* (HOXA13), mRNA		XM_006088760.1	98	0.0	93
bRdh10	PREDICTED: *Myotis lucifugus retinol dehydrogenase 10* (all-trans) (RDH10), mRNA		XM_006086358.1	100	0.0	94
bRaldh2	PREDICTED: *Myotis lucifugus aldehyde dehydrogenase 1 family, member A2* (ALDH1A2), transcript variants mRNA	X1	XM_006085903.1	99	0.0	95
		X2	XM_006085904.1	84	4.00 E-163	95
bCyp26b1	PREDICTED: *Eptesicus fuscus cytochrome P450 26B1* (LOC103291433), transcript variants mRNA	X1	XM_008147459.1	99	0.0	95
		X2	XM_008147460.1			
bRar*β*	PREDICTED: *Myotis brandtii retinoic acid receptor*, beta (RARB), transcript variants mRNA	X1	XM_005856593.1	100	0.0	98
		X2	XM_005856594.1			
		X3	XM_005856595.1			
		X4	XM_005856596.1			
		X5	XM_005856597.1			
bHoxd10	PREDICTED: *Myotis davidii homeobox D10* (HOXD10), mRNA		XM_006760592.1	100	0.0	98
bHoxd11	PREDICTED: *Eptesicus fuscus homeobox D11* (HOXD11), mRNA		XM_008138752.1	77	0.0	95
bHoxd12	*Taphozous melanopogon homeobox D12,* mRNA, partial cds		FJ455472.1	100	0.0	95

A.4: *Whole mount in situ hybridisation (WISH) protocol*

Background:

Originating from D. Wilkinson, as modified and taught to A.C. Burke by M. Hollyday in the McMahon lab at Roche, March, 1993, and further modified in the Tabin lab with additional modifications by the Logan Lab (National Institute for Medical Resesarch, 2011).

Sample preparation:

Dissect embryos into PBS, remove membranes and dissect as necessary. Using forceps or a needle, make a hole in the roof of the hindbrain, and/or open the forebrain.

Fix in 15 to 30 ml 4% paraformaldehyde (PFA) in 50 ml falcon tubes, 4 °C, overnight with gentle rocking.

Note: PFA should be made fresh.

All wash steps are performed in volumes of 5-10 ml (minimum of 10x tissue volume), in scintillation vials, rocking at room temperature (RT) for a minimum of 5 min unless otherwise specified.

Wash in PBT, 2X for 5 min at 4 °C, gentle rocking, in volume of 5-10 ml (10x volume).

Wash; 25%, 50%, 75%, PBT: MeOH, 5 min at RT.

Wash 2X in 100% MeOH, 5 min at RT, rocking.

Store in 100% methanol (MeOH) at -20 °C (good for several months).

DAY 1, Pre-treatment and hybridization:

1. Transfer embryos to clean scintillation vials (optional, may be taken to Prehyb. in 50 ml tubes).
2. Rehydrate samples in 75%, 50%, 25% PBT:MeOH.
   Wash 2X in PBT for 5 min at RT.
   Note: for large embryos increase the wash times (up to 20 min).
3. Bisect the embryos (if you are conserving samples) along their longitudinal axis. Put embryos in a sterile petridish covered by ice-cold PBT. Use microdissection scissors or sharp
   forceps to cut embryo along its neural tube and half from back to front, be careful not to damage the limbs.
4. Bleach with 6% Hydrogen Peroxide in PBT for 1 hr. at RT, rocking.
   Wash 3X with PBT for 5-20 min at RT.
5. Treat with 10 µg/ml Proteinase K in PBT for the recommended time at RT, rocking.
   Note: See table for a guideline of digestion times
   Wash with 2mg/ml glycine in PBT- 10' at RT, make fresh and filter.
   Wash 2X in PBT for 5 min at RT.
6. Postfix with 4% paraformaldehyde and 0.2% gluteraldehyde in PBT for 20 min at RT
   Wash 2X in PBT 5 min at RT
   Note: You can transfer embryos to 1.5 ml o-ring screw-topped eppendorf tubes or further steps may be continued in Scintillation vials, adjust volumes accordingly.
7. Add **Prehybridisation Solution** to vials (10x volume), mix gently by inversion
   Remove solution and repeat step.
   Prehybridize at 70 °C for 1 hr.
   Note: Can store in prehyb. solution at -20 °C, before or after heating
8. Make up and/or pre-warm the **Hybridisation solution**
   Note: this is prehybridisation solution with approximately 1 µg/ml digoxygenin probe, keep it liquid at 37 °C.
   You can recover and reuse this hybridization solution (with probe) from previous experiments, this can be stored at -20 °C, thawed before use (these cannot be reused indefinitely)
9. Remove the prehybridisation solution and add hybridisation solution. Mix gently by inversion.
   Hybridize overnight at 70 °C with gentle rocking.

DAY 2, Post-hybridization washes and Antibody hybridization:

Note: This protocol omits RNase treatment.

1. Recover Hybridisation solution into original 10 ml vials, let it sit at RT until cool and then put at -20 °C for reuse.
2. If using eppendorfs then rinse original scintillation vials with a couple of ml of Solution 1 and transfer embryos from 1.5 ml vials into pre-warmed Solution 1 in scintillation vials. If using original scintillation vials, then perform a rinse (gently inverting the scintillation vial) with pre-warmed Solution 1.
3. Wash with Solution 1
   Wash 3X in Solution 1 for 30 min at 70 °C, rocking.
4. Wash with Solution 3
   Wash 3X in Solution 3 for 30 min at 65 °C, rocking
5. Wash with fresh and filtered TBST (1% Tween-20 and 2 mM Levimasole)
   Wash 3X for 10 min at RT, rocking.
6. Preblock embryos with 10% Heat Inactivated (HI) sheep serum in TBST
   Wash for a min. of 2.5 hrs at RT, rocking.
7. Remove blocking serum from embryos and add Ab mix which consists of 1% HI sheep serum with anti-Dig AP (1:50 000) in a minimum of 10x volume of embryos.
   Wash overnight at 4 °C, gently rocking.

DAY 3, Post-Ab hybridization washes:

1. Remove Ab mix and rinse vials with TBST (1% Tween-20 and 2 mM Levimasole) in scintillation vials.
   Wash 3X for 10 min in TBST at RT, rocking.
2. Wash 5X for 1 to 1.5 hrs. in TBST at RT, rocking.
3. Wash over night in TBST, rocking at 4 °C.
   Note: This time can be increased (overnight to 2 days if required)

DAY 4, Detection:

1. Wash in NTMT (1% Tween-20 and 2 mM Levimasole),
   Wash 3X in NTMT for 10 min at RT, rocking.
2. Incubate with freshly made reaction mix of NBT and BCIP
   NBT (0.075 g/1 ml 70% dimethyl formamide)
   BCIP (0.050 g/1 ml H_2O)
   Reaction Mix:
   6.75 µl NBT/DMF
   5.25 µl BCIP/DMF
   2 ml NTMT
   Remove NTMT.
   Add 1 ml Reaction Mix to embryos and mix gently.
3. Cover tubes with foil (protect from light), place on rocker for 20 min at RT
   Monitor about once every 30 min to check on reaction progress.
   When judged complete proceed to step 4.
4. Wash in NTMT in the dark (colour reaction will still be progressing)
   Wash 2X in NTMT for 10 min at RT, rocking.
5. Stop reaction by washing in PBT (pH 5.5)
   Wash 2x in PBT (pH 5.5) for 10 min at RT, rocking.
6. Postfix with 4% PFA, 0.1% Glut. in PBS for 1 hr at RT
7. Wash 2X in PBT.
8. Store at 4 °C overnight.

To Clear:

Put embryos through a MeOH dehydration series (25%, 50%, 75%, 100%, 100% -20 min each step)

Embryos can then be stored at -20 °C

OR

Wash in increasing concentrations of glycerol (30%, 50%, 70%, 80% for 15'- 1hr. each depending on embryo size)

Add azide 0.05% for long-term storage at 4 °C

WISH Solutions

Note: Filtration should be done in Nalgene-type tissue culture filter units, 0.45 - 0.2 µm pore size.
PFA and formamide are hazardous chemicals. Follow health and safty guidelines

Phosphate Buffered Saline (PBS) 10X stock (1 L):

Dissolve:

80 g NaCl
2 g KCl
14.4 g Na_2HPO_4
2.4 g KH_2PO_4
in 800 ml H_2O

Adjust the pH to 7.4 (or 7.2 if needed) with HCl
Add H_2O to 1 L
Dispense the solution into aliquots
Sterilize by autoclaving for 20 min at 1.05 kg/cm^2 on liquid cycle or by filter sterilization.
Store PBS at room temperature.

DEPC H_2O:

0.1% DEPC in H_2O shake, leave rocking overnight and autoclave.

PBT:

Make with DEPC H_2O. Filter before use.
PBS / 0.1% Tween-20

Paraformaldehyde (PFA) 20% :

Dissolve:

250 g PFA powder
in 1 L DEPC H_2O
Add:
4 ml NaOH (10 N)

Heat at 60 °C (do not go over this temperature) until fully dissolved (6-8 hrs).
Add more NaOH in 0.5 ml increments if PFA does not fully dissolve.
When dissolved and cool adjust the pH to 7.4.
Adjust volume to 1.25 L with DEPC H_2O.
Filter the solution into aliquots and store in 50 ml falcon tubes at -20 °C.
Before use thaw gently at RT and dilute to 4% with PBS.

Prehybridisation Solution:

50% Formamide
5x SSC (pH 4.5 - use citric acid to pH)
50 µg/ml yeast RNA

All components should be made up with DEPC H_2O. Filter before use

1% SDS
50 µg/ml Heparin

Aliquot and store in 50 ml falcon tubes at -20 °C

Hybridisation Solution:

Add approx. 1 µg probe/ml, to premade prehybridisation solution (~10 µl/ml)
Store in 10 ml tubes at -20 °C

Solution 1:

Make up fresh and filter, approx. 25 ml/tube

50% formamide
5X SSC (pH 4.5)
1% SDS

Solution 3:

Make up fresh and filter, approx. 25 ml/tube

50% formamide
2X SSC (pH 4.5)

HI Sheep Serum:

Inactivate by heating to 55 °C for 60'. Can then be stored in aliquots at -20 °C.

TBST:

Make from stock of 10X TBS, dilute to 1X and add Tween-20 and Levimasole (inhibits Alk. Phos. activity), then filter. Does not require DEPC water.

10X TBS (100 ml):

8 g NaCl
0.2 g KCl
25 ml of 1 M TrisHCl (pH 7.5)
75 ml H_2O

1X TBST (100 ml): Dilute 10X TBS to 1X
add 2 mM Levimasole (0.048 g/100ml)
add 1% Tween-20

NTMT:

Make up fresh and filter

1X NTMT (100 ml);

2 ml of 5 M NaCl (100 Mm NaCl)
5 ml of 2 M TrisHCl, pH 9.5 (100 mM TrisHCl, pH 9.5)
5 ml of 1 M $MgCl_2$ (50 mM $MgCl_2$)
0.1 ml Tween-20 (0.1% Tween-20)
0.048 g Levimasole (2 mM Levimasole)
88 ml H_2O

NBT :

Make from powder and store at -20 °C

0.075 g NBT
1 ml 70% dimethyl formamide.

BCIP:

Make from powder and store at -20 °C

0.050 g BCIP
1 ml H_2O for sodium salt or 0.050 g/ml DMF for toluidine salt

Reaction Mix:

Make prior to adding to embryos

6.75 µl NBT/DMF
5.25 µl BCIP/H_2O
2 ml NTMT

A.5: *WISH antisense and sense probe signal in mouse*

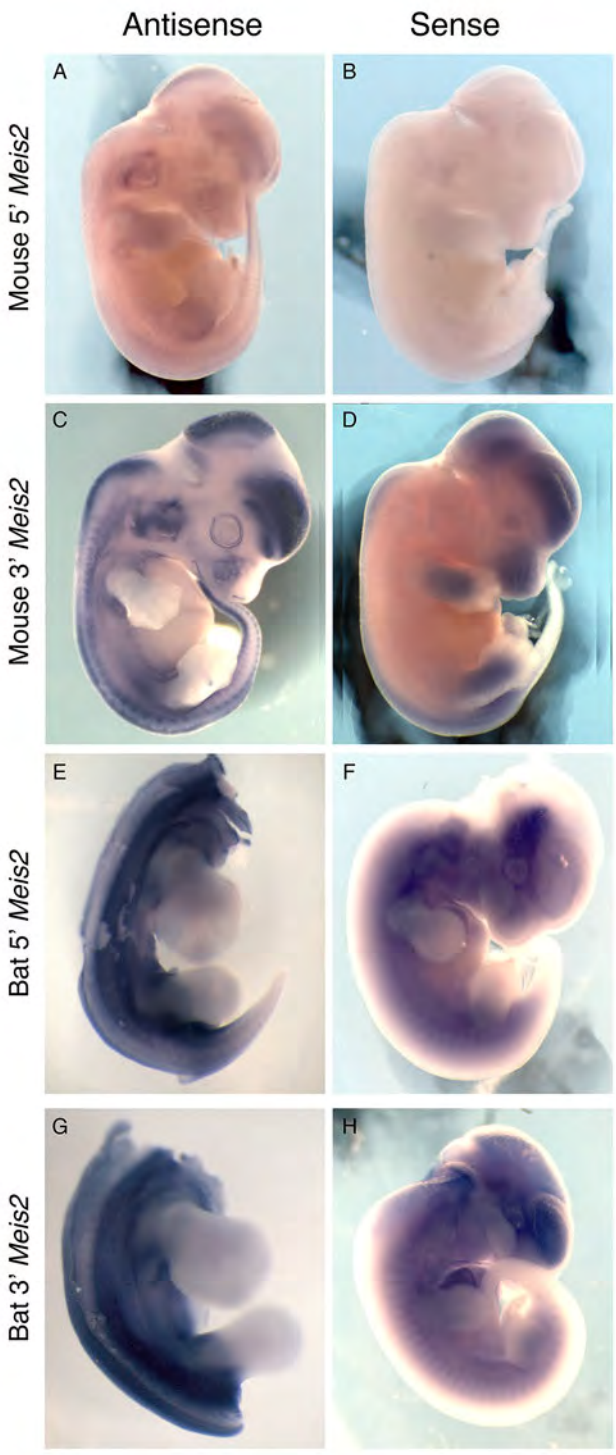

Figure A.2: Lateral views of mouse (E13.5) and bat (CS15) embryos showing the signal from Antisense (AS) and sense (S) probes. Neural tube and limbs did tend to colour non-specifically if the colour detection step was prolonged, but this background staining was very distinct from the probe signal.

A.6: *Table of BLAST results for Hoxd10 RACE amplicons*

Table A.3: NCBI BLAST (megablast) results for the *Hoxd10* RACE amplicons against the nucleotide collection (nr/nt) for bat (Chiroptera, taxid:9397) giving the description and accession numbers for the top hit. Values in red were not found and grey values had no significant similarity.

Sequence ID	Primer	Length	Description	Sequence ID	Query cover	E Value	Identity
Hoxd10	**5' Race**						
NA	NA	NA	NA	NA	NA		NA
Hoxd10	**3' Race**						
3RR_H10_A4_raw	SMARTer II NUP	Full	No significant similarity found				
3RR_H10_A5_raw	SMARTer II NUP	Full	No significant similarity found				
3RR_H10_A6_raw	SMARTer II NUP	Full	No significant similarity found				
3RR_H10_A7_raw	SMARTer II NUP	Full	PREDICTED: *Myotis lucifugus LUC7-like (S. cerevisiae)* (LUC7L), transcript variant X2, mRNA	XM_006103684.1	40	**0.0**	**89**
3RR_H10_A8_raw	SMARTer II NUP	Full	No significant similarity found				
3RR_H10_B0_con	RACE_Hoxd10_GSP2	828	PREDICTED: *Myotis lucifugus homeobox D10* (HOXD10), mRNA	XM_006083088.1	89	**0.0**	**91**
3RR_H10_B1_con	RACE_Hoxd10_GSP2	1068	PREDICTED: *Eptesicus fuscus homeobox D10* (HOXD10), mRNA	XM_008138530.1	94	**0.0**	**94**
3RR_H10_B2_con	SMARTer II UPM	Full	No significant similarity found				
3RR_H10_B4_con	RACE_Hoxd10_GSP2	1053	PREDICTED: *Eptesicus fuscus homeobox D10* (HOXD10), mRNA	XM_008138530.1	95	**0.0**	**94**
3RR_H10_B5_con	RACE_Hoxd10_GSP2	1067	PREDICTED: *Eptesicus fuscus homeobox D10* (HOXD10), mRNA	XM_008138530.1	94	**0.0**	**95**

A.7: *Table of BLAST results for Hoxd11 RACE amplicons*

Table A.4: NCBI BLAST (megablast) results for the *Hoxd11* RACE amplicons against the nucleotide collection (nr/nt) for bat (Chiroptera, taxid:9397) giving the description and accession numbers for the top hit.

Sequence ID	Primer	Length	Description	Sequence ID	Query cover	E Value	Identity
5' RACE							
5NR_H11_A0_con	RACE_Hoxd11_NGSP1	261	PREDICTED: *Myotis brandtii homeobox D11* (HOXD11), mRNA	XM_005857731.1	88	3.00E-111	98
5NR_H11_A1_con	RACE_Hoxd11_NGSP1	261	PREDICTED: *Myotis brandtii homeobox D11* (HOXD11), mRNA	XM_005857731.1	88	2.00E-111	98
5NR_H11_A2_con	RACE_Hoxd11_NGSP1	261	PREDICTED: *Myotis brandtii homeobox D11* (HOXD11), mRNA	XM_005857731.1	88	2.00E-111	98
5NR_H11_A3_con	RACE_Hoxd11_NGSP1	261	PREDICTED: *Myotis brandtii homeobox D11* (HOXD11), mRNA	XM_005857731.1	88	3.00E-111	98
5NR_H11_A4_con	RACE_Hoxd11_NGSP1	261	PREDICTED: *Myotis brandtii homeobox D11* (HOXD11), mRNA	XM_005857731.1	88	2.00E-111	98
5NR_H11_A5_con	SMARTer II A	Full	No significant similarity found				
5NR_H11_A6_con	RACE_Hoxd11_NGSP1	261	PREDICTED: *Myotis brandtii homeobox D11* (HOXD11), mRNA	XM_005857731.1	88	3.00E-111	98
5NR_H11_A7_con	RACE_Hoxd11_NGSP1	242	PREDICTED: *Myotis brandtii homeobox D11* (HOXD11), mRNA	XM_005857731.1	87	3.00E-101	98
3' RACE							
3RR_H11_A0_con	RACE_Hoxd11_NGSP1 (reversed)	809	PREDICTED: *Eptesicus fuscus tumor protein, translationally-controlled 1* (TPT1), transcript variant X1, mRNA	XM_008145559.1	91	0.0	96
3RR_H11_A1_con	RACE_Hoxd11_NGSP1 (reversed)	811	PREDICTED: *Eptesicus fuscus tumor protein, translationally-controlled 1* (TPT1), transcript variant X1, mRNA	XM_008145559.1	91	0.0	96
3RR_H11_A2_con	RACE_Hoxd11_NGSP1 (reversed)	810	PREDICTED: *Eptesicus fuscus tumor protein, translationally-controlled 1* (TPT1), transcript variant X1, mRNA	XM_008145559.1	91	0.0	96
3RR_H11_A4_con	RACE_Hoxd11_NGSP1 (reversed)	813	PREDICTED: *Eptesicus fuscus tumor protein, translationally-controlled 1* (TPT1), transcript variant X1, mRNA	XM_008145559.1	91	0.0	96
3RR_H11_A5_con	RACE_Hoxd11_NGSP1 (reversed)	821	PREDICTED: *Eptesicus fuscus tumor protein, translationally-controlled 1* (TPT1), transcript variant X1, mRNA	XM_008145559.1	91	0.0	96
3RR_H11_B0_raw	SMARTer II NUP	Full	PREDICTED: *Myotis lucifugus CDC-like kinase 1* (CLK1), mRNA	XM_006082389.1	38	0.0	85
3RR_H11_B1_raw	SMARTer II UPM	Full	No significant similarity found				
3RR_H11_B2_raw	SMARTer II NUP	Full	*Artibeus jamaicensis clone 1A13*, complete sequence	AC144636.4	23	9.00E-69	78
3RR_H11_B3_raw	SMARTer II UPM	Full	No significant similarity found				
3RR_H11_B4_raw	SMARTer II NUP	Full	No significant similarity found				
3RR_H11(H10)_C0_con	RACE_Hoxd11_NGSP1 (reversed)	Full	No significant similarity found				
3RR_H11(H10)_C1_con	RACE_Hoxd11_NGSP1 (reversed)	Full	No significant similarity found				
3RR_H11(H10)_C2_con	RACE_Hoxd11_NGSP1 (reversed)	1087	PREDICTED: *Myotis lucifugus uncharacterized* LOC102441917 (LOC102441917), ncRNA	XR_330857.1	74	0.0	93
3RR_H11(H10)_C4_con	RACE_Hoxd11_NGSP1 (reversed)	1134	PREDICTED: *Myotis davidii tumor protein, translationally-controlled 1* (TPT1), mRNA	XM_006757177.1	88	0.0	92

A.8: *Table of BLAST results for Hoxd12 RACE amplicons*

Table A.5: NCBI BLAST (megablast) results for the *Hoxd12* RACE amplicons against the nucleotide collection (nr/nt) for bat (Chiroptera, taxid:9397) giving the description and accession numbers for the top hit.

Sequence ID	Primer	Length	Description	Sequence ID	Query cover	E Value	Identity
5' RACE							
5NR_H12_A0_con	RACE_Hoxd12_NGSP1	184	PREDICTED: *Myotis brandtii homeobox D12* (HOXD12), mRNA	XM_006760699.1	83	1.00E-68	97
5NR_H12_A1_con	RACE_Hoxd12_NGSP1	181	PREDICTED: *Myotis davidii homeobox D12* (HOXD12), mRNA	XM_006760699.1	82	1.00E-68	98
5NR_H12_A2_fwd	RACE_Hoxd12_NGSP1	181	PREDICTED: *Myotis davidii homeobox D12* (HOXD12), mRNA	XM_006760699.1	82	1.00E-68	98
5NR_H12_A3_con	RACE_Hoxd12_NGSP1	180	PREDICTED: *Myotis davidii homeobox D12* (HOXD12), mRNA	XM_006760699.1	83	1.00E-68	98
5NR_H12_A4_con	RACE_Hoxd12_NGSP1	164	PREDICTED: *Myotis davidii homeobox D12* (HOXD12), mRNA	XM_006760699.1	81	3.00E-59	98
5NR_H12_A5_con	RACE_Hoxd12_NGSP1	191	PREDICTED: *Myotis davidii homeobox D12* (HOXD12), mRNA	XM_006760699.1	83	4.00E-74	98
5NR_H12_A6_rvs	RACE_Hoxd12_NGSP1	181	PREDICTED: *Myotis davidii homeobox D12* (HOXD12), mRNA	XM_006760699.1	79	1.00E-64	98
5NR_H12_A7_con	RACE_Hoxd12_NGSP1	164	PREDICTED: *Myotis davidii homeobox D12* (HOXD12), mRNA	XM_006760699.1	81	3.00E-59	98
5NR_H12_B0_con	RACE_Hoxd12_NGSP1	250	PREDICTED: *Myotis davidii homeobox D12* (HOXD12), mRNA	XM_006760699.1	87	1.00E-103	98
5NR_H12_B1_con	RACE_Hoxd12_NGSP1	184	PREDICTED: *Myotis davidii homeobox D12* (HOXD12), mRNA	XM_006760699.1	77	9.00E-65	98
5NR_H12_B2_con	RACE_Hoxd12_NGSP1	188	PREDICTED: *Myotis davidii homeobox D12* (HOXD12), mRNA	XM_006760699.1	76	9.00E-65	98
5NR_H12_B3_con	RACE_Hoxd12_NGSP1	188	PREDICTED: *Myotis davidii homeobox D12* (HOXD12), mRNA	XM_006760699.1	76	9.00E-65	98
5NR_H12_B4_con	RACE_Hoxd12_NGSP1	180	PREDICTED: *Myotis davidii homeobox D12* (HOXD12), mRNA	XM_006760699.1	79	8.00E-65	98
5NR_H12_B5_con	RACE_Hoxd12_NGSP1	162	PREDICTED: *Myotis davidii homeobox D12* (HOXD12), mRNA	XM_006760699.1	80	4.00E-58	98
5NR_H12_B6_con	RACE_Hoxd12_NGSP1	251	PREDICTED: *Myotis davidii homeobox D12* (HOXD12), mRNA	XM_006760699.1	56	1.00E-64	98
5NR_H12_B7_ con	RACE_Hoxd12_NGSP1	180	PREDICTED: *Pteropus alecto homeobox D12* (HOXD12), mRNA	XM_006921226.1	79	4.00E-63	97
3' RACE							
3NR_H12(H13)_A0_join	RACE_Hoxd12_NGSP2	1500	PREDICTED: *Eptesicus fuscus homeobox D12* (HOXD12), mRNA	XM_008138531.1	20	3.00E-137	96
3NR_H12(H13)_A1_join	RACE_Hoxd12_NGSP2	1499	PREDICTED: *Eptesicus fuscus homeobox D12* (HOXD12), mRNA	XM_008138531.1	20	3.00E-137	96
3NR_H12(H13)_A4_join	RACE_Hoxd12_NGSP2	1504	PREDICTED: *Eptesicus fuscus homeobox D12* (HOXD12), mRNA	XM_008138531.1	20	3.00E-137	96
3NR_H12(H13)_A5_join	RACE_Hoxd12_NGSP2	1502	PREDICTED: *Eptesicus fuscus homeobox D12* (HOXD12), mRNA	XM_008138531.1	20	3.00E-137	96
3NR_H12(H13)_A6_join	RACE_Hoxd12_NGSP2	1492	PREDICTED: *Eptesicus fuscus homeobox D12* (HOXD12), mRNA	XM_008138531.1	20	4.00E-137	96
3NR_H12(H13)_D0_con	RACE_Hoxd12_NGSP2	933	PREDICTED: *Eptesicus fuscus homeobox D12* (HOXD12), mRNA	XM_008138531.1	32	2.00E-137	96
3NR_H12(H13)_D1_rvs	RACE_Hoxd12_NGSP2	721	*Carollia perspicillata* HOXD13 (Hoxd13) and HOXD12 (Hoxd12) genes, complete cds	AY744676.1	91	1.00E-143	87
3NR_H12(H13)_D2_con	RACE_Hoxd12_NGSP2	699	PREDICTED: *Eptesicus fuscus homeobox D12* (HOXD12), mRNA	XM_008138531.1	29	1.00E-93	97
3NR_H12(H13)_D3_con	RACE_Hoxd12_NGSP2	948	PREDICTED: *Eptesicus fuscus homeobox D12* (HOXD12), mRNA	XM_008138531.1	30	2.00E-131	96
3NR_H12(H13)_D4_con	RACE_Hoxd12_NGSP2	988	PREDICTED: *Eptesicus fuscus homeobox D12* (HOXD12), mRNA	XM_008138531.1	22	1.00E-104	97
3NR_H12(H13)_D5_fwd	RACE_Hoxd12_NGSP2	730	PREDICTED: *Eptesicus fuscus homeobox D12* (HOXD12), mRNA	XM_008138531.1	41	2.00E-137	96

A.9: *Table of BLAST results for Hoxd13 RACE amplicons*

Table A.6: NCBI BLAST (megablast) results for the *Hoxd13* RACE amplicons against the nucleotide collection (nr/nt) for bat (Chiroptera, taxid:9397) giving the description and accession numbers for the top hit.

Sequence ID	Primer	Length	Description	Sequence ID	Query cover	E Value	Identity
5' RACE							
5NR_H13_A0_con	RACE_Hoxd13_NGSP1	224	PREDICTED: *Myotis lucifugus homeobox D13* (HOXD13), mRNA	XM_006083259.1	75	6.00E-78	98
5NR_H13_A1_con	RACE_Hoxd13_NGSP1	Full	No significant similarity found				
5NR_H13_A2_con	RACE_Hoxd13_NGSP1	154	PREDICTED: *Myotis lucifugus homeobox D13* (HOXD13), mRNA	XM_006083259.1	68	3.00E-44	97
5NR_H13_A3_con	RACE_Hoxd13_NGSP1	246	PREDICTED: *Eptesicus fuscus homeobox D13* (HOXD13), partial mRNA	XM_008138753.1	88	2.00E-92	95
5NR_H13_A4_con	RACE_Hoxd13_NGSP1	254	PREDICTED: *Eptesicus fuscus homeobox D13* (HOXD13), partial mRNA	XM_008138753.1	86	4.00E-99	96
5NR_H13_A5_con	RACE_Hoxd13_NGSP1	227	PREDICTED: *Myotis lucifugus homeobox D13* (HOXD13), mRNA	XM_006083259.1	70	6.00E-73	98
5NR_H13_A6_rvs	RACE_Hoxd13_NGSP1	280	PREDICTED: *Eptesicus fuscus homeobox D13* (HOXD13), partial mRNA	XM_008138753.1	88	2.00E-107	95
5NR_H13_A7_con	RACE_Hoxd13_NGSP1	146	PREDICTED: *Eptesicus fuscus homeobox D13* (HOXD13), partial mRNA	XM_008138753.1	67	2.00E-36	95
3' RACE							
3NR_H13(H12)_A0_con	RACE_Hoxd13_NGSP2	1222	PREDICTED: *Pteropus alecto homeobox D13* (HOXD13), mRNA	XM_006921451.1	75	6.00E-179	87
3NR_H13(H12)_A1_con	RACE_Hoxd13_NGSP2	1085	PREDICTED: *Pteropus alecto homeobox D13* (HOXD13), mRNA	XM_006921451.1	95	0.0	90
3NR_H13(H12)_A2_join	RACE_Hoxd13_NGSP2	1496	PREDICTED: *Pteropus alecto homeobox D13* (HOXD13), mRNA	XM_006921451.1	75	0.0	93
3NR_H13(H12)_A3_join	RACE_Hoxd13_NGSP2	1491	PREDICTED: *Pteropus alecto homeobox D13* (HOXD13), mRNA	XM_006921451.1	73	0.0	93
3NR_H13(H12)_A5_con	RACE_Hoxd13_NGSP2	535	PREDICTED: *Pteropus alecto homeobox D13* (HOXD13), mRNA	XM_006921451.1	90	0.0	93
3NR_H13(H12)_B0_cons	RACE_Hoxd13_NGSP2	1388	PREDICTED: *Pteropus alecto homeobox D13* (HOXD13), mRNA	XM_006921451.1	97	0.0	89
3NR_H13(H12)_B2_fwd	RACE_Hoxd13_NGSP2	729	PREDICTED: *Pteropus alecto homeobox D13* (HOXD13), mRNA	XM_006921451.1	100	0.0	92
3NR_H13(H12)_B4_cons	RACE_Hoxd13_NGSP2	1401	PREDICTED: *Pteropus alecto homeobox D13* (HOXD13), mRNA	XM_006921451.1	96	0.0	89
3NR_H13(H12)_B5_ join	RACE_Hoxd13_NGSP2	1489	PREDICTED: *Pteropus alecto homeobox D13* (HOXD13), mRNA	XM_006921451.1	49	0.0	93
3NR_H13(H12)_B6_ join	RACE_Hoxd13_NGSP2	1503	PREDICTED: *Pteropus alecto homeobox D13* (HOXD13), mRNA	XM_006921451.1	95	0.0	92
3NR_H13_B0_con	RACE_Hoxd13_NGSP2	535	PREDICTED: *Pteropus alecto homeobox D13* (HOXD13), mRNA	XM_006921451.1	89	0.0	94
3NR_H13_B1_con	RACE_Hoxd13_NGSP2	539	PREDICTED: *Pteropus alecto homeobox D13* (HOXD13), mRNA	XM_006921451.1	90	0.0	93
3NR_H13_B2_con	RACE_Hoxd13_NGSP2	539	PREDICTED: *Pteropus alecto homeobox D13* (HOXD13), mRNA	XM_006921451.1	90	0.0	93
3NR_H13_B3_con	RACE_Hoxd13_NGSP2	540	PREDICTED: *Pteropus alecto homeobox D13* (HOXD13), mRNA	XM_006921451.1	89	0.0	94
3NR_H13_B4_con	RACE_Hoxd13_NGSP2	501	PREDICTED: *Pteropus alecto homeobox D13* (HOXD13), mRNA	XM_006921451.1	88	0.0	94
3NR_H13_C0_ con	RACE_Hoxd13_NGSP2	704	PREDICTED: *Pteropus alecto homeobox D13* (HOXD13), mRNA	XM_006921451.1	91	0.0	93
3NR_H13_C1_ con	RACE_Hoxd13_NGSP2	1329	PREDICTED: *Pteropus alecto homeobox D13* (HOXD13), mRNA	XM_006921451.1	86	0.0	87
3NR_H13_C2_ con	RACE_Hoxd13_NGSP2	538	PREDICTED: *Pteropus alecto homeobox D13* (HOXD13), mRNA	XM_006921451.1	89	0.0	93
3NR_H13_C3_ con	RACE_Hoxd13_NGSP2	786	PREDICTED: *Pteropus alecto homeobox D13* (HOXD13), mRNA	XM_006921451.1	93	0.0	92

A.10: *Vertebrates used in multiple species alignments (Hoxd10)*

Table A.7: Names and accession numbers of *Hoxd10* protein coding sequences used in multi-species alignment.

Group	Common name	Scientific name	Sequence ID	CDS Length (bp)	Sequence origin	Type
Bat	Big brown bat	*Eptesicus fuscus (Efus)*	XM_008138530	1023	DNA	PREDICTED
	Straw-coloured fruit bat	*Eidolon helvum (Ehel)*	AWHC01171157.1*	1023	DNA	WGS
	Brandt's bat	*Myotis brandtii (Mbra)*	XM_005857609	1023	DNA	PREDICTED
	Mouse-eared bat	*Myotis davidii (Mdav)*	XM_006760592	1023	DNA	PREDICTED
	Little brown bat	*Myotis lucifugus (Mluc)*	XM_006083088	1023	DNA	PREDICTED
	Black flying fox	*Pteropus alecto (Pale)*	XM_006921227	1023	DNA	PREDICTED
	Large flying fox	*Pteropus vampyrus (Pvam)*	ABRP01032596.1*	1023	DNA	WGS
	Natal long fingered bat	*Miniopterus natalensis (Mnat)*	Consensus	1023	RNA	RACE, PCR
	Common bent-wing bat	*Miniopterus schreibersii (Msch)*	JN013877, comp11192_c0_seq1, comp294_c0_seq2(BLAST Hit), JN013855	1023	RNA	RNA-Seq, PCR
Mammal	Human	*Homo sapiens*	ENST00000249501	1023	RNA	KNOWN protein coding
	Chimpanzee	*Pan troglodytes*	ENSPTRT00000023468	1023	RNA	KNOWN protein coding
	Mouse	*Mus musculus*	ENSMUST00000061745	1023	RNA	KNOWN protein coding
	Dog	*Canis familiarus*	ENSCAFT00000021329	1023	DNA	PROJECTION_protein_coding
	Horse	*Equus caballus*	ENSECAT00000021893	1023	DNA	PROJECTION_protein_coding
	Cow	*Bos taurus*	ENSBTAT00000021334	1023	RNA	KNOWN protein coding
	Hyrax	*Procavia capensis*	(ENSPCAT00000015605	1023	DNA	PROJECTION_protein_coding
	Sloth	*Choloepus hoffmanni*	ENSCHOT00000011906	1020	DNA	PROJECTION_protein_coding
	Armadillo	*Dasypus novemcinctus*	ENSDNOT00000038323	1023	DNA	PROJECTION_protein_coding
Vertebrate	Opossum	*Monodelphis domestica*	ENSMODT00000012197	1020	DNA	PROJECTION_protein_coding
	Chicken	*Gallus gallus*	ENSGALT00000038688	1023	DNA	PROJECTION_protein_coding
	Frog	*Xenopus tropicalis*	ENSXETT00000016491	1017	RNA	KNOWN protein coding

A.11: *Vertebrates used in multiple species alignments (Hoxd11)*

Table A.8: Names and accession numbers of *Hoxd11* protein coding sequences used in multi-species alignment.

Group	Common name	Scientific name	Sequence ID	CDS Length (bp)	Sequence origin	Type
Bat	Big brown bat	*Eptesicus fuscus (Efus)*	ALEH01020217.1*	1017	DNA	WGS
	Brandt's bat	*Myotis brandtii (Mbra)*	ANKR01159891.1-2.1*	1014	DNA	WGS
	Little brown bat	*Myotis lucifugus (Mluc)*	AAPE02004650.1*	1015	DNA	WGS
	Black flying fox	*Pteropus alecto (Pale)*	ALWS01095509.1-10-1*	1017	DNA	WGS
	Large flying fox	*Pteropus vampyrus (Pvam)*	ABRP01032593-4.1*	1017	DNA	WGS
	Natal long fingered bat	*Miniopterus natalensis (Mnat)*	Consensus	799	RNA	RACE, PCR
	Common bent-wing bat	*Miniopterus schreibersii (Msch)*	comp7027_c0_seq1, JN013897.1, comp6458_c0_seq2, comp3957_c0_seq1	956	RNA	RNA-Seq, PCR
Mammal	Human	*Homo sapiens*	ENST00000249504	1017	RNA	KNOWN protein coding
	Chimpanzee	*Pan troglodytes*	ENSPTRT00000065571	1020	DNA	PROJECTION_protein_coding
	Mouse	*Mus musculus*	ENSMUST00000142312	1011	RNA	KNOWN protein coding
	Dog	*Canis familiarus*	ENSCAFT00000021317	1023	DNA	PROJECTION_protein_coding
	Cow	*Bos taurus*	ENSBTAT00000054133	1014	RNA	KNOWN protein coding
	Armadillo	*Dasypus novemcinctus*	ENSDNOT00000035668	1026	DNA	PROJECTION_protein_coding
Vertebrate	Opossum	*Monodelphis domestica*	ENSMODT00000012176	846	DNA	PROJECTION_protein_coding
	Chicken	*Gallus gallus*	ENSGALT00000015085	843	RNA	KNOWN protein coding
	Frog	*Xenopus tropicalis*	ENSXETT00000060673	828	DNA	PROJECTION_protein_coding

A.12: *Vertebrates used in multiple species alignments (Hoxd12)*

Table A.9: Names and accession numbers of *Hoxd12* protein coding sequences used in multi-species alignment.

Group	Common name	Scientific name	Sequence ID	CDS Length (bp)	Sequence origin	Type
Bat	Stoliczka's trident bat	*Aselliscus stoliczkanus (Asto)*	JN013923	461	RNA	PCR
	Seba's short-tailed bat	*Carollia perspicillata (Cper)*	AY744676*	813	DNA	CLONE
	Greater short-nosed fruit bat	*Cynopterus sphinx (Csph)*	JN013920	516	RNA	PCR
	Least horseshoe bat	*Rhinolophus pusillus (Rpus)*	JN013924	466	RNA	PCR
	Leschenault's Rousette	*Rousettus leschenaultii (Rles)*	JN013926, FJ455469	738	RNA	PCR
	Greater false vampire bat	*Megaderma lyra (Mlyr)*	FJ455471	720	RNA	PCR
	Great roundleaf bat	*Hipposideros armiger (Harm)*	FJ455470	720	RNA	PCR
	Black-bearded tomb bat	*Taphozous melanopogon (Tmel)*	JN013919, FJ455472	744	RNA	PCR
	Natal long fingered bat	*Miniopterus natalensis (Mnat)*	Consensus	819	RNA	RACE, PCR
	Common bent-wing bat	*Miniopterus schreibersii (Msch)*	comp1220_c0_seq4	819	RNA	RNA-Seq, PCR
Mammal	Human	*Homo sapiens*	ENST00000406506	813	RNA	KNOWN protein coding
	Chimpanzee	*Pan troglodytes*	ENSPTRT00000063945	813	DNA	PROJECTION_protein_coding
	Mouse	*Mus musculus*	ENSMUST00000001878	807	RNA	KNOWN protein coding
	Dog	*Canis familiarus*	ENSCAFT00000021306	813	DNA	PROJECTION_protein_coding
	Horse	*Equus caballus*	ENSECAT00000002795	813	DNA	PROJECTION_protein_coding
	Cow	*Bos taurus*	ENSBTAT00000005652)	816	RNA	KNOWN protein coding
	Hyrax	*Procavia capensis*	ENSPCAT00000015567	843	DNA	PROJECTION_protein_coding
	Armadillo	*Dasypus novemcinctus*	ENSDNOT00000049723	822	DNA	PROJECTION_protein_coding
Vertebrate	Opossum	*Monodelphis domestica*	ENSMODT00000012163	804	DNA	PROJECTION_protein_coding
	Chicken	*Gallus gallus*	ENSGALT00000015086	801	RNA	KNOWN protein coding

A.13: *Vertebrates used in multiple species alignments (Hoxd13)*

Table A.10: Names and accession numbers of *Hoxd13* protein coding sequences used in multi-species alignment.

Group	Common name	Scientific name	Sequence ID	CDS Length (bp)	Sequence origin	Type
Bat	Greater horseshoe bat	*Rhinolophus ferrumequinum (Rfer)*	AWHA01051979.1*	848	RNA	WGS
	Seba's short-tailed bat	*Carollia perspicillata (Cper)*	AY744676	1026	RNA	PCR
	Leschenault's Rousette	*Rousettus leschenaultii (Rles)*	FJ455490	969	RNA	PCR
	Greater false vampire bat	*Megaderma lyra (Mlyr)*	FJ455492	960	RNA	PCR
	Great roundleaf bat	*Hipposideros armiger (Harm)*	FJ455491	963	RNA	PCR
	Black-bearded tomb bat	*Taphozous melanopogon (Tmel)*	FJ455493	969	RNA	PCR
	Little brown bat	*Myotis lucifugus (Mluc)*	XM_006083259	840	RNA	PCR
	Black flying fox	*Pteropus alecto (Pale)*	ALWS01095508.1*	827	DNA	WGS
	Large flying fox	*Pteropus vampyrus (Pvam)*	ABRP01032590.1*	992	DNA	WGS
	Natal long fingered bat	*Miniopterus natalensis (Mnat)*	Consensus	810	RNA	RACE, PCR
	Common bent-wing bat	*Miniopterus schreibersii (Msch)*	comp611_c0_seq1	840	RNA	RNA-Seq, PCR
Mammal	Human	*Homo sapiens*	ENST00000392539	1032	RNA	PUTATIVE protein coding
	Chimpanzee	*Pan troglodytes*	ENSPTRT00000023465	1032	RNA	KNOWN protein coding
	Mouse	*Mus musculus*	ENSMUST00000001872	1020	RNA	KNOWN protein coding
	Rat	*Rattus norvegicus*	NM_001105886.1	1019	DNA	PROJECTION_protein_coding
	Cat	*Felis domesticus*	ENSFCAT00000031543	688	DNA	PROJECTION_protein_coding
	Cow	*Bos taurus*	UMD3.1:2:20853099:20857159:-1	1026	DNA	Genomic
	Armadillo	*Dasypus novemcinctus*	ENSDNOT00000019799	951	DNA	PROJECTION_protein_coding
Vertebrate	Opossum	*Monodelphis domestica*	ENSMODT00000012158	1023	DNA	PROJECTION_protein_coding
	Chicken	*Gallus gallus*	NM_205434	916	RNA	mRNA
	Frog	*Xenopus tropicalis*	NM_001090481	855	RNA	mRNA

A.14: *Vertebrates used in multiple species alignments (CsC1 and CsC2)*

Table A.11: Names and accession numbers of CsC1 and CsC2 sequences used in multi-species alignment.

Group	Common name	Scientific name	Source	Sequence ID	Length (bp)
Bat	Straw-coloured fruit bat	*Eidolon helvum (Ehel)*	NCBI (WGS)	EH_contig_107520,	2222
	Black flying fox	*Pteropus alecto (Pale)*	NCBI (WGS)	contig95505	2228
	Large flying fox	*Pteropus vampyrus (Pvam)*	NCBI (WGS)	cont1.32580	2228
	Greater false vampire bat	*Megaderma lyra (Mlyr)*	NCBI (WGS)	ML_contig_113704	2208
	Greater horseshoe bat	*Rhinolophus ferrumequinum (Rfer)*	NCBI (WGS)	RF_contig_7393	2205
	Seba's short-tailed bat	*Carollia perspicillata (Cper)*	NCBI (WDS)	clone 21O6	2229
	Big brown bat	*Eptesicus fuscus* (*Efus*)	NCBI (WGS)	contig020223	2236
	Little brown bat	*Myotis lucifugus (Mluc)*	NCBI (WGS)	cont2.4653	2241
	David's myotis	*Myotis davidii (Mdav)*	NCBI (WGS)	contig78380	2231
	Brandt's bat	*Myotis brandtii (Mbra)*	NCBI (WGS)	contig159881	2236
Mammal	Cat	*Felis catus*	UCSC (felCat5_dna)	chrC1:164214385-164216626 (+)	2242
	Dog	*Canis lupus familiaris*	UCSC (canFam3_dna)	chr36:19836985-19839212 (+)	2228
	Rat	*Rattus norvegicus*	UCSC (rn4_dna)	chr3:57226479-57228494 (+)	2016
	Mouse	*Mus musculus*	UCSC (mm10_dna)	chr2:74617827-74620034 (+)	2208
	Squirrel	*Ictidomys tridecemlineatus*	UCSC (speTri2_dna)	H393319:5516626-5518773 (+)	2148
	Guinea Pig	*Cavia porcellus*	UCSC (cavPor3_dna)	scaffold_3:14280050-14282236 (+)	2187
	Rabbit	*Oryctolagus cuniculus*	UCSC (oryCun2_dna)	chr7:115588707-115590862 (+)	2156
	Rhesus	*Macaca mulatta*	UCSC (rheMac3_dna)	chr12:39364034-39366260 (+)	2227
	Human	*Homo sapiens*	UCSC (hg19_dna)	chr2:176888007-176890239 (+)	2233
	Dassie	*Procavia capensis*	UCSC (proCap1_dna)	scaffold_7529:10904-13157 (+)	2254
	Hedgehog	*Erinaceus europaeus*	UCSC (eriEur1_dna)	scaffold_332162:7345-8392|81455:9-769 **(+)**	1859

Appendix B

B.1: *Meis2 is expressed in the interdigital tissue of E14.5 mouse embryos*

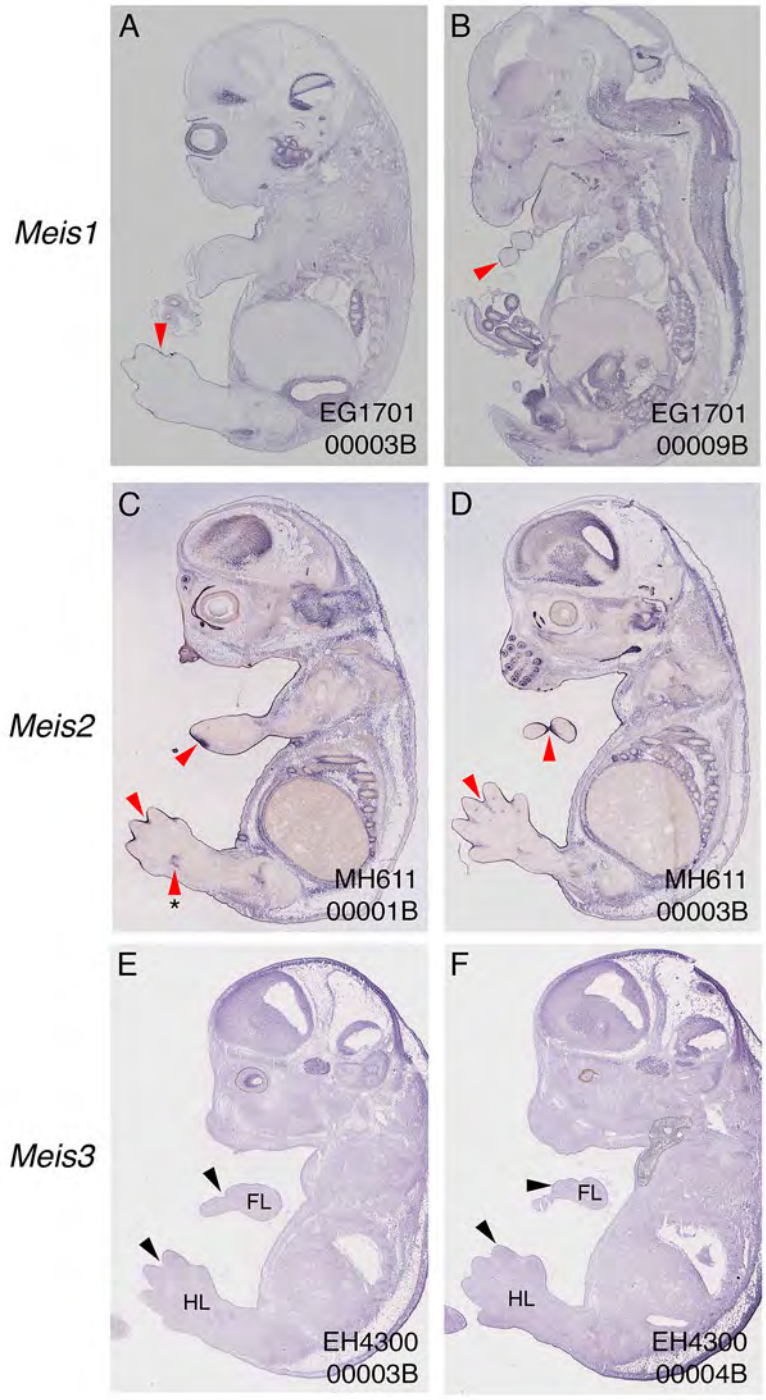

Figure B.1: Embryonic mouse (E14.5) sections show expression of *Meis1* (**A**, **B**); *Meis2* (**C**, **D**) and *Meis3* (**E**, **F**). Clear expression of *Meis2* is found in both the forelimb (FL) and the hindlimb (HL) interdigital tissue (red arrows **C**, **D**) and at the base of digit IV of the HL (red arrow with asterisk **C**). *Meis1* expression is restricted to the epidermal layer of the limb (red arrows **A**, **B**) while *Meis3* is absent from the limb tissues (black arrows **E**, **F**). The FL and HL regions are marked in E & F. Data adapted from the Genepaint digital atlas of gene expression, Set ID of each section given in the bottom right corner (Visel et al 2004).

B.2: *Graphs of relative qPCR comparisons among limb types (5'-Meis2 & 3'-Meis2)*

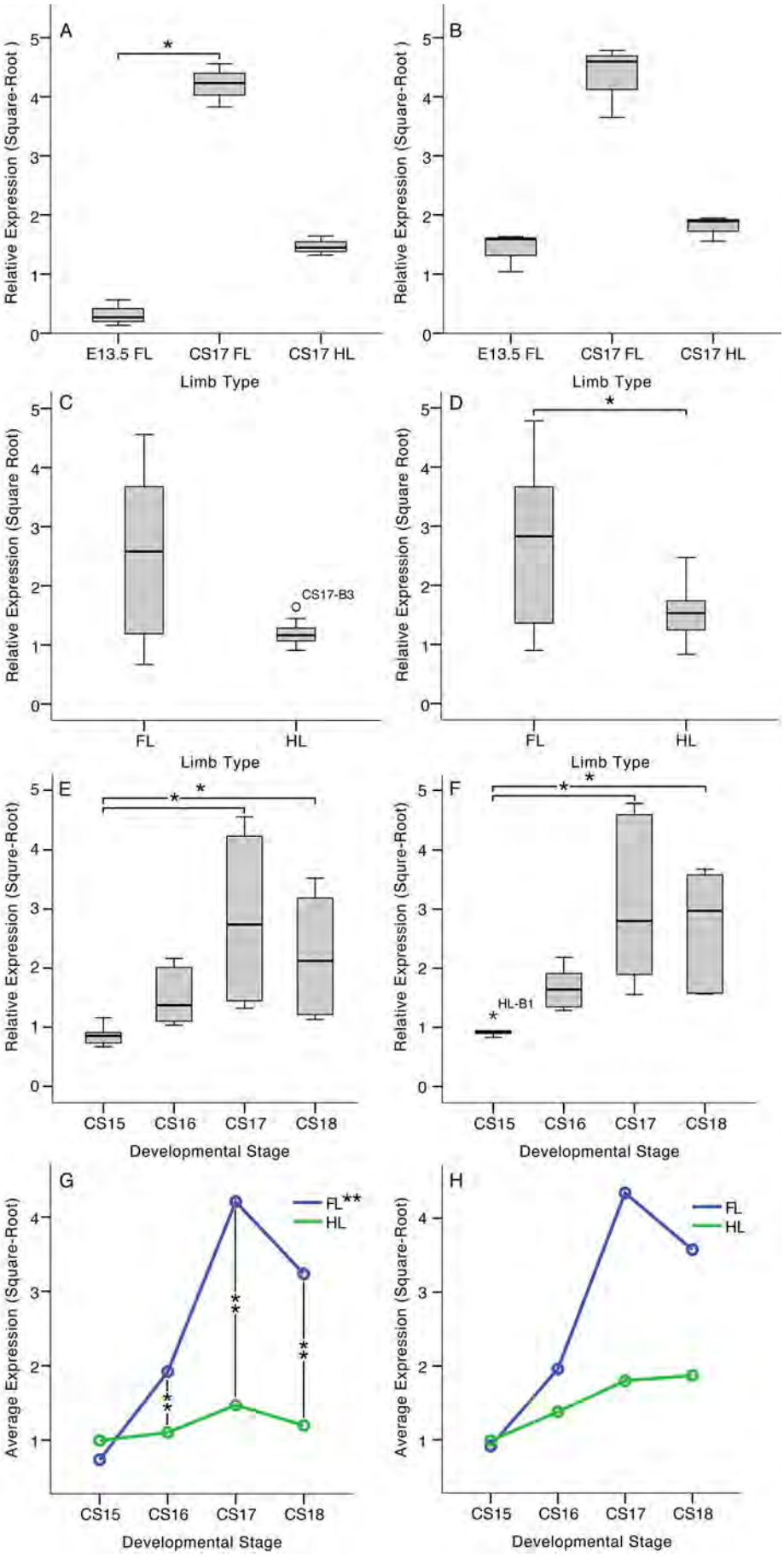

Figure B.2: An overview of the distributions for the relative expression (square root transformed) data for 5'-*Meis2* (**A**, **C**, **E**, **H**) and 3'-*Meis2* (**B**, **D**, **F**, **I**) qPCR experiments. The relative expression data among the mouse (E13.5) forelimb (FL) and bat (CS17 FL, CS17 HL) limbs samples (**A**, **B**) show that the bat CS17 FL had a much higher expression than the HL or the mouse E1.5 FL for both the 5'-*Meis2* and the 3'-*Meis2* experiments. This was significant for 5'-*Meis2* expression (Kruskal-Wallis H-test: H = 7.2, d.f. = 2, p = 0.027) with pairwise comparison revealing that the CS17 FL (mean rank = 8) was significantly higher than the E13.5 FL (mean rank = 2; p = 0.022), but that the differences between it and the CS17 HL (mean rank = 5) were not (p = 0.539). The differences seen among the mean ranks of these groups were not significant for 3'-*Meis2* (Kruskal-Wallis H-test: H = 5.9, d.f. = 2, p = 0.51). The distribution of the FL samples was much larger than that of the HL for both experiments (**C**, **D**), no significance could be attributed to the differences between the bat FL and HL samples for the 5'-*Meis2* (Related Samples Sign test: *Statistic* = -1.443, N = 12, p = 0.149), but this comparison was significantly different for the 3'-*Meis2* experiment (Related Samples Sign test: *Statistic* = -2.021, N = 12, p = 0.043). When the developmental stages were compared (**E**, **F**) these were found to be significantly different both for the 5'-*Meis2* experiment (One-way ANOVA: $F_{(3,20)}$ = 4.6, p = 0.014) and the 3'-*Meis2* experiment (Kruskal-Wallis H-test: H = 15.9, d.f. = 3, p = 0.01). For both experiments the differences among the developmental stages were attributable to the pairwise comparisons between the CS15 (mean rank 5'-*Meis2* = 4; mean rank 3'-*Meis2* = 3.5) with the CS17 (5'-*Meis2*: mean rank = 18.67, p = 0.002; 3'-*Meis2*: mean rank = 18, p = 0.002) and the CS18 groups (5'-*Meis2*: mean rank = 15.17, p = 0.037; 3'-*Meis2*: mean rank = 17, p = 0.006). When examining the FL and HL expression over the sequential stages of development (**G**, **H**), there were significant interactions between the limb type and developmental stage on the expression data for (**G**) 5'-*Meis2* (Two-way ANOVA: $F_{(3,16)}$ = 59.2, p < 0.001, partial η^2 = 0.92). The differences between the FL and HL were statistically significant for the older developmental stages: CS15 ($F_{(1,16)}$ = 2.24, p = 0.15, partial η^2 = 0.12); CS16 ($F_{(1,16)}$ = 22.5, p < 0.001, partial η^2 = 0.59), CS17 ($F_{(1,16)}$ = 252.7, p < 0.001, partial η^2 = 0.94), and CS18 ($F_{(1,16)}$ = 140.2, p < 0.001, partial η^2 = 0.90). There was also a statistically significant difference among developmental stages for the FL ($F_{(3,16)}$ = 155.3, p < 0.001, partial η^2 = 0.97), with a pairwise comparison finding significant differences among all stages (p < 0.001 for all comparisons). The HL samples were not significantly different ($F_{(3,16)}$ = 2.8, p = 0.072, partial η^2 = 0.35) samples. We could not determine the interaction effects of the 3'-*Meis2* experiment as the data contained an outlier (developmental stage CS15), and did not satisfy the assumption of homogeneity of variances. For the 3'-*Meis2* experiment the distributions of the developmental series were compared within each limb type and significant differences were found for both: FL (Kruskal-Wallis H-test: H = 9.97, d.f. = 3, p = 0.019); HL (Kruskal-Wallis H-test: H = 9.36, d.f. = 3, p = 0.025). With a significant pairwise difference found between the CS15 (mean rank = 2) and CS17 (mean rank = 10.67) stages in the FL comparison (p = 0.019) and no significant pairwise differences found in that of the HL. Outliers are given as empty circles in the boxplots. Asterisks denote a significantly different comparison with * signifying p < 0.05 and ** signifying p < 0.001.

B.3: *Statistical test of relative qPCR comparisons among limb types (5'-Meis2 & 3'-Meis2)*

Table B.1: Table summarising the comparisons made and tests used to determine the level of significance seen amongst the different samples. For each experiment the tests and their statistics are shown, with post hoc pairwise comparisons being performed.

Comparison	Region	Test				
		Kruskal-Wallis H Test			Pairwise comparison	
		H	d.f.	*p*	Samples	*p*
Interspecies (E13.5 FL, CS17 FL, CS17 HL)	5'-*Meis2*	7.2	2	0.027	E13.5 vs. CS17FL	0.022
					E13.5 vs. CS17HL	0.539
					CS17FL vs. CS17HL	0.539
	3'-*Meis2*	5.9	2	0.051		
		Related Samples Sign Test				
		Statistic	N	*p*		
Limb Type (FL, HL)	5'-*Meis2*	-1.44	12	0.149		
	3'-*Meis2*	-2.02	12	0.043		
		One-way Anova			Pairwise comparison	
		F	d.f.	*p*	Samples	*p*
Developmental Stage (CS15, CS16, CS17, CS18)	5'-*Meis2*	4.6	3, 20	0.014	CS15 vs. CS17	0.002
					CS15 vs. CS18	0.037
		Kruskal-Wallis H Test			Pairwise comparison	
		H	d.f.	*p*	Samples	*p*
	3'-*Meis2*	15.9	3	0.01	CS15 vs. CS17	0.02
					CS15 vs. CS18	0.006
		Univariate Anova				
		F	d.f.	*p*	partial η^2	
Limb Type and Developmental Stage	5'-*Meis2*	59.2	3, 16	< 0.001	0.92	
	FL	155.3	3,16	< 0.001	0.97	
	HL	2.8	3,16	0.072	0.35	
	CS15	2.24	1,16	0.15	0.12	
	CS16	22.5	1,16	< 0.001	0.59	
	CS17	252.7	1,16	< 0.001	0.94	
	CS18	140.2	1,16	< 0.001	0.9	

B.4: *Meis2 expression in the mouse footplate*

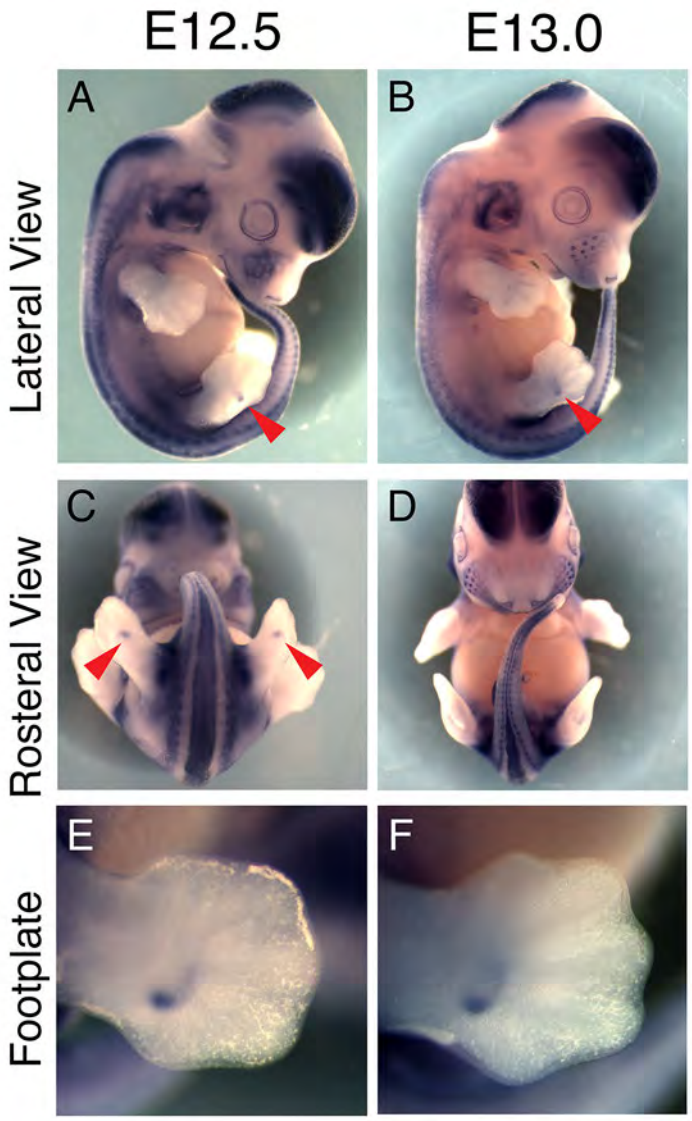

Figure B.3: A distinct 'comma-shaped' domain of expression is found in the mouse HL during early autopod formation. Lateral (**A** & **B**) and rostral (**C** & **D**) views of whole E12.5 and E13.0 embryos show the full extent of 5' *Meis2* probe signal with the distinct footplate signal occurring in both left and right limbs (white arrows **A**, **B** & **C**). A close up image of the footplate at E12.5 and E13.0 shows the full extent of this staining before it is lost at E13.5.

B.5: *Meis2 bat embryo biological replicates (Early autopod development)*

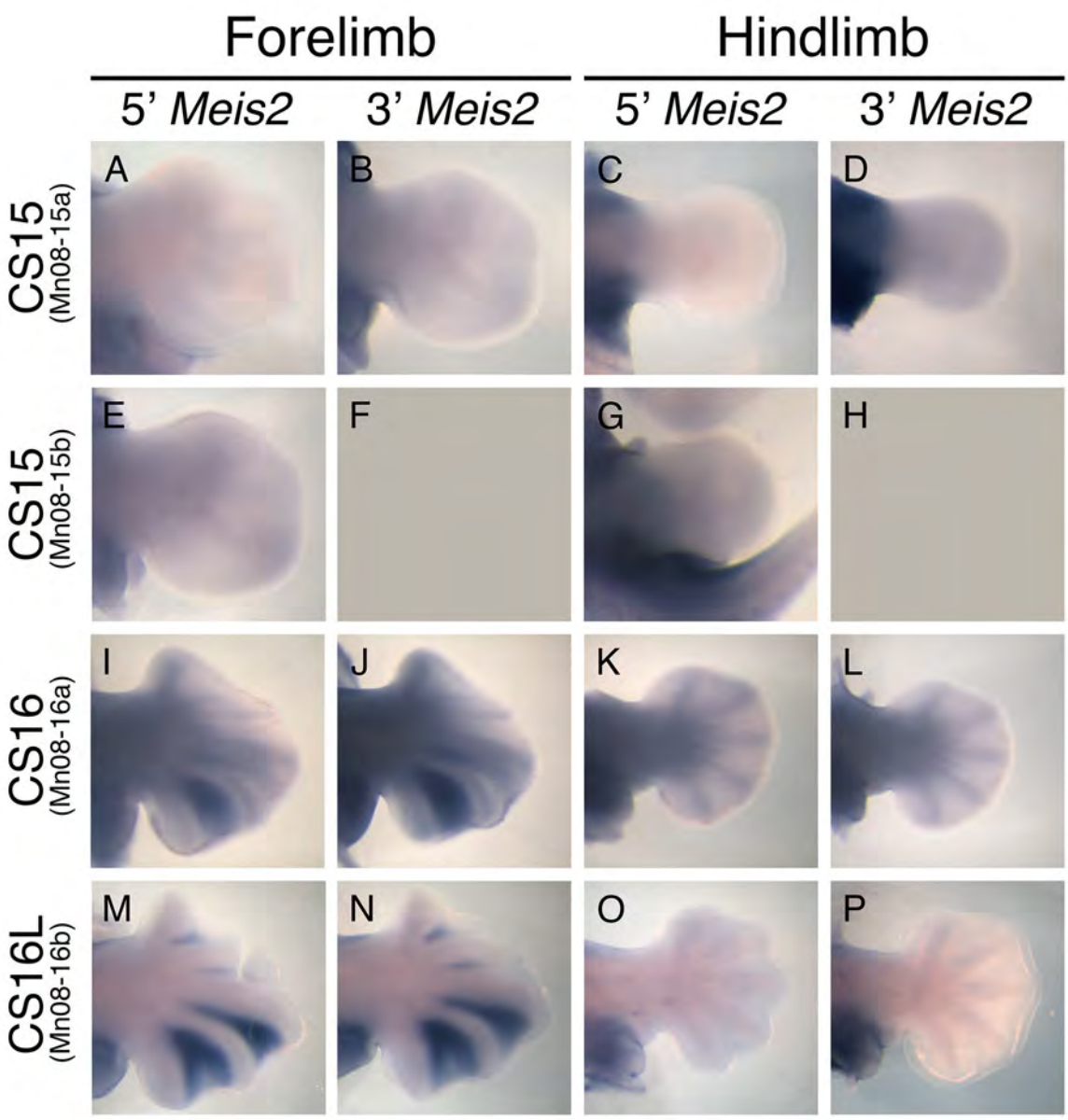

Figure B.4: *Meis2* expression in developing bat limbs showing the biological repeats that were performed with both the 5' *Meis2* probe and the 3' *Meis2* probe.

B.6: *Meis2 bat embryo biological replicates (Late autopod development)*

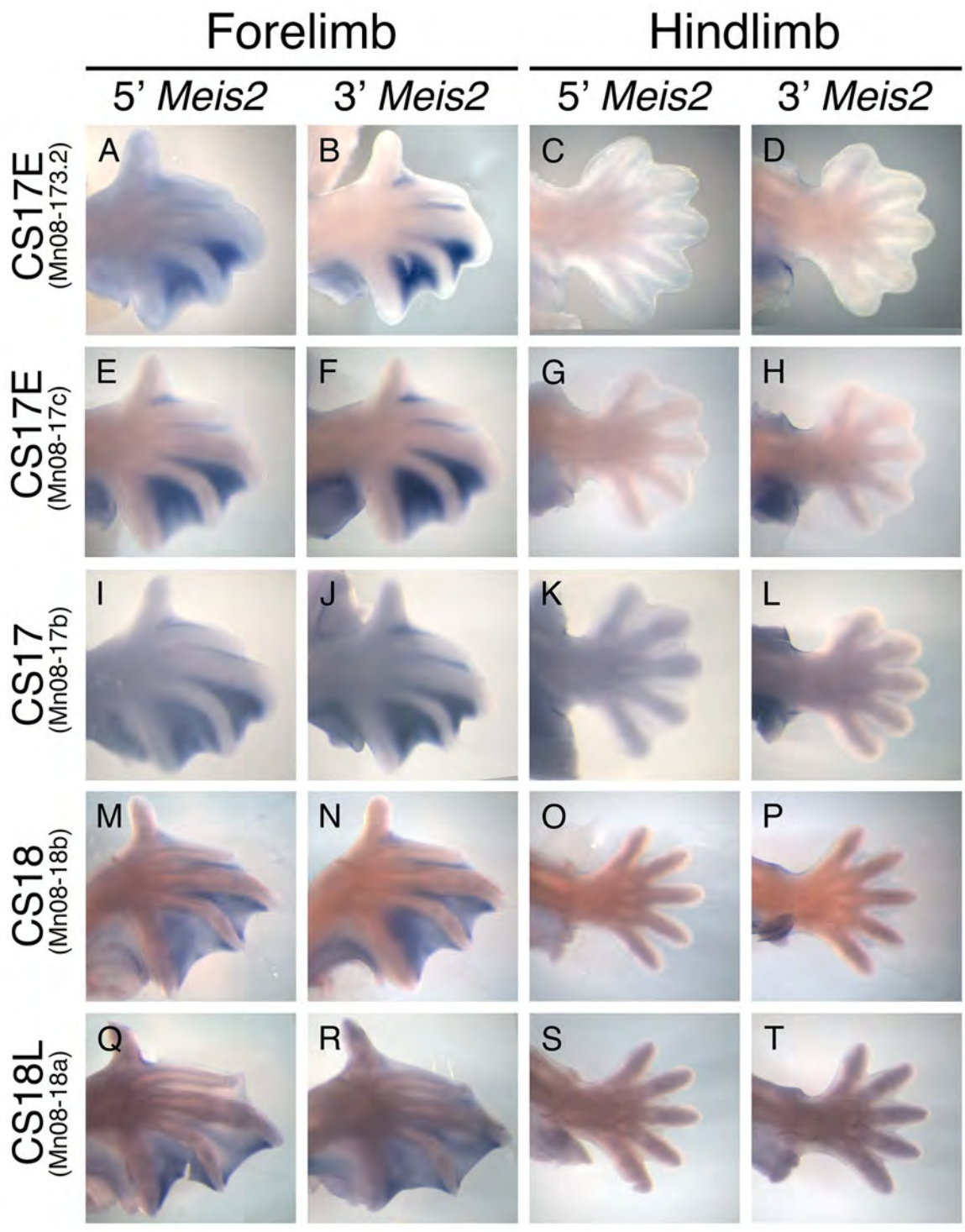

Figure B.5: *Meis2* expression in developing bat limbs showing the biological repeats that were performed with both the 5' *Meis2* probe and the 3' *Meis2* probe.

B.7: *Graphs of absolute qPCR comparisons among limb types (Hoxa13)*

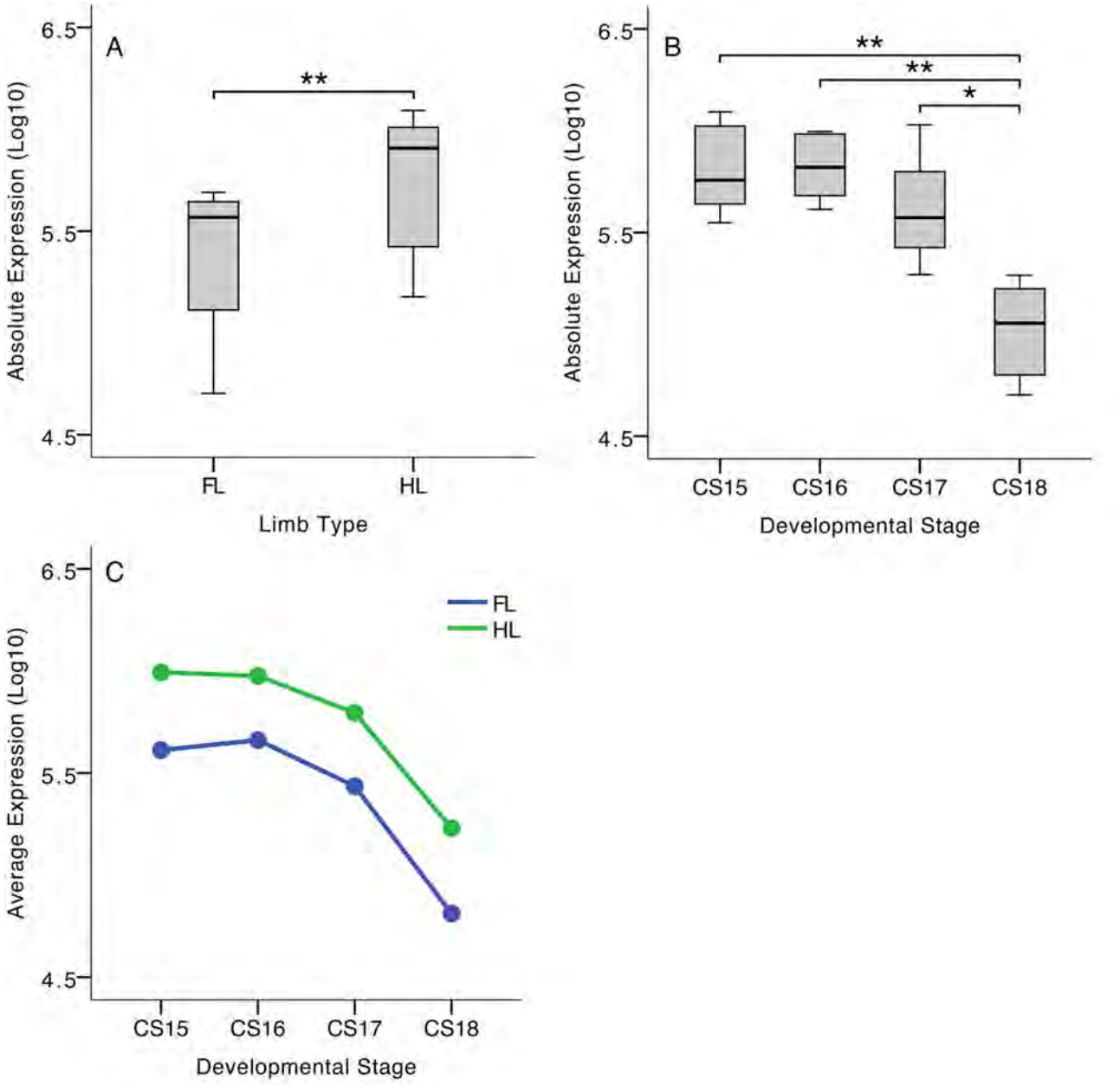

Figure B.6: The absolute expression values (Log_{10} transformed) for *Hoxa13* indicate that (**A**) the forelimb (FL) samples are significantly lower than the hindlimb (HL) samples (Related Samples Sign test: *Statistic* = 12.0 , N = 12, $p < 0.001$). (**B**) There were also significant differences among the developmental stages (One-Way ANOVA: $F_{(3,20)} = 16.02$, $p < 0.001$) with the oldest stage examined (CS18) being significantly different to all other stages examined: CS15 (Bonferroni: Mean Diff = 0.78, SE = 0.13, $p < 0.001$); CS16 (Bonferroni: Mean Diff = 0.93, SE = 0.13, p < 0.001); CS17 (Bonferroni: Mean Diff = 0.59, SE = 0.13, $p = 0.001$). (**C**) There were no significant interactions between the developmental stage and limb type expression (Two-way ANOVA: $F_{(3,16)} = 0.200$, $p = 0.895$, partial $\eta^2 = 0.036$). An examination of the main effects found significant differences between the expression of the limb types (Two-way ANOVA: $F_{(1,19)} = 66.16$, $p < 0.001$) and among the expressions of the developmental stages (Two-way ANOVA: $F_{(1,19)} = 68.2$, $p < 0.001$) with differences being attributable to pairwise comparisons between CS18 and that of all other developmental stages ($p < 0.001$ for all comparisons). Asterisks denote a significantly different comparison with * signifying $p < 0.05$ and ** signifying $p < 0.001$.

B.8: *Fold change data for Hoxa13 and Hoxa11 trancripts for the microarray and qPCR experiments.*

Table B.2: Fold change data for *Hoxa13* and *Hoxa11* trancripts for the microarray and qPCR experiments. Median fold changes of biological repeats are given with minimum and maximum fold changes bracketed. Four biological repeats were tested in the microarray experiments and three in the qPCR experiments.

Gene	Experiment	Mouse vs. Bat	Bat FL vs. HL			
		CS17 / E13.5	CS15	CS16	CS17	CS18
Hoxa13	Microarray	0.7 (0.6-0.8)	NA	1.1 (0.9-1.2)	1.0 (0.8-1.0)	NA
	qPCR	NA	-2.4 (-1.7- -3.5)	-2.0 (-1.9- -3.5)	-2.4 (-1.8- -2.8)	-2.4 (-2.3- -3.3)
Hoxa11	Microarray	3.8 (3.7-3.9)	NA	0.8 (0.7-1.0)	1.1 1.1-1.2)	NA
	qPCR	NA	-1.1 (-1.2-1.2)	-1.3 (-1.1- -1.4)	-1.1 (-1.4-1.1)	1.1 (-1.1-1.5)

B.9: *Graphs of absolute qPCR comparisons among limb types (Hoxa11)*

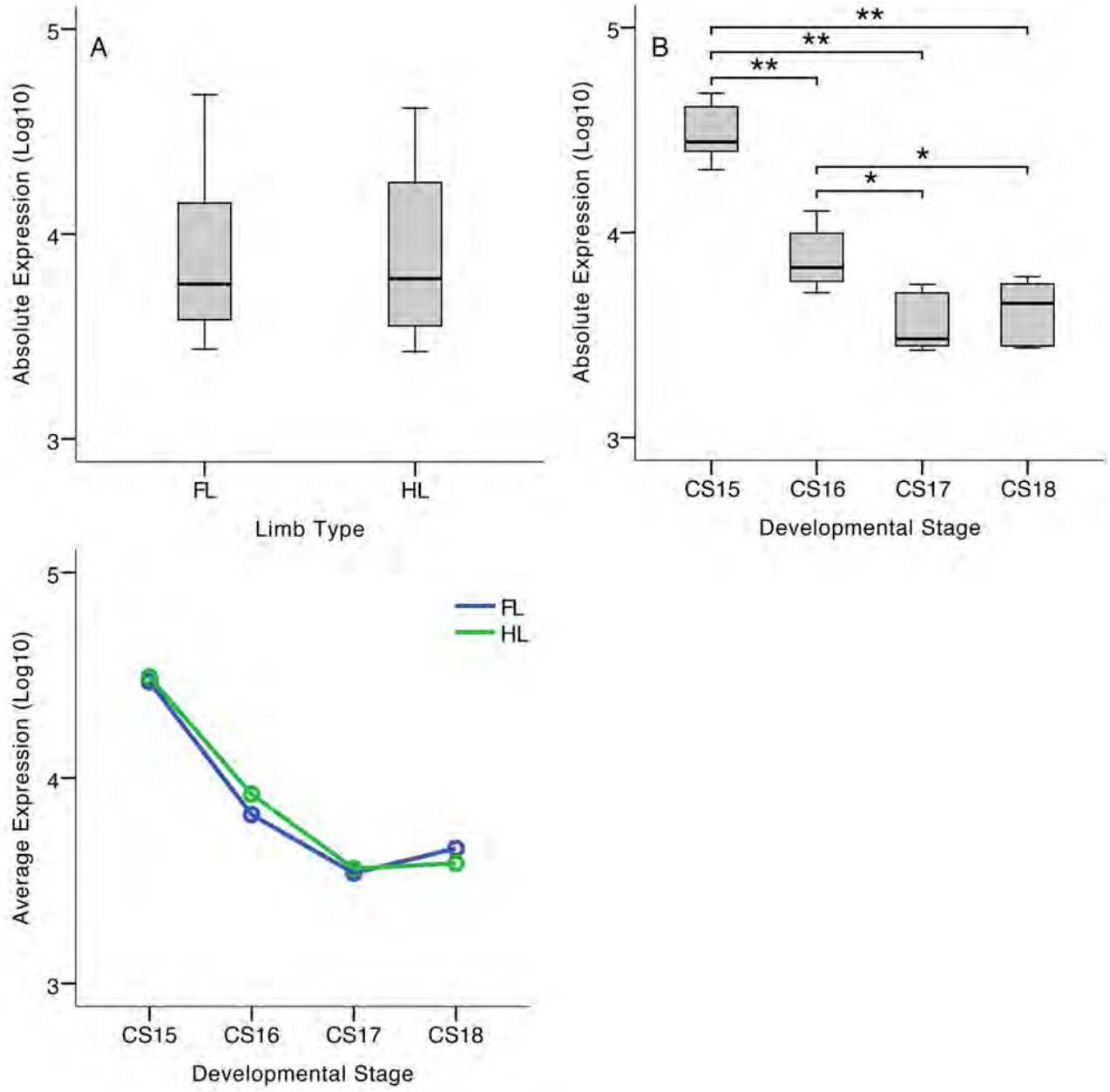

Figure B.7: The absolute expression values (Log_{10} transformed) for *Hoxa11* indicate that (**A**) the forelimb (FL) samples are not significantly different to their hindlimb (HL) counterparts ((Related Samples Wilcoxon Signed Rank test: *Statistic* = 53, N = 12, $p = 0.272$). (**B**) There were, however, significant differences among the developmental stages (One-Way ANOVA: $F_{(3,20)} = 50.39$, $p < 0.001$) with the CS15 being significantly different to all other stages examined: CS16 ($p < 0.001$); CS17 ($p < 0.001$); CS18 ($p < 0.001$) and the CS16 also being significantly different to all stages: CS17 ($p = 0.006$); CS18 ($p = 0.046$). (**C**) There were no significant interactions between the developmental stage and limb type expression (Two-way ANOVA: $F(3,16) = 0.293$, $p = 0.830$, partial $\eta^2 = 0.052$). Limb types were not significantly different (Two-way ANOVA: $F_{(1,19)} = 0.09$, $p = 0.768$), but differences among developmental stage were significant (Two-way ANOVA: $F_{(3,19)} = 48.10$, $p < 0.001$). Pairwise comparisons supported the previous findings that the CS15 was significantly higher than all other stages ($p < 0.001$ for all comparisons) and CS16 was also significantly higher than CS17 ($p = 0.08$). Asterisks denote a significantly different comparison with * signifying $p < 0.05$ and ** signifying $p < 0.001$.

Appendix C

C.1: *Statistical tests comparing the scaled metacarpal / metatarsal lengths*

Table C.1: Statistical analyses used to determine differences among the lengths of the scaled metacarpal/metatarsal both among and within the different limb types (ANCOVA). For all analyses N = 10.

Scaled metacarpal / metatarsal lengths				
	Bat FL	**Bat HL**	**Mouse FL**	**Mouse HL**
Digit III	3.643 ± 0.235	2.951 ± 0.094	3.025 ± 0.094	3.351 ± 0.047
	ANCOVA: $F_{(3, 35)} = 662.5$, $p < 0.001$, partial $\eta^2 = 0.983$			

Scaled metacarpal / metatarsal lengths				
	Digit II	**Digit III**	**Digit IV**	**Digit V**
Bat FL	NA	35.841± 0.851	43.496± 0.186	45.855± 0.792
	ANCOVA: $F_{(3, 35)} = 89.374$, $p < 0.001$, partial $\eta^2 = 0.882$			
Bat HL	NA	3.13 ± 0.021	3.108 ± 0.022	2.876 ± 0.021
	ANCOVA: $F_{(3, 35)} = 44.871$, $p < 0.001$, partial $\eta^2 = 0.782$			
Mouse FL	3.034± 0.035	3.192± 0.032	3.054± 0.020	NA
	ANCOVA: $F_{(3, 35)} = 8.540$, $p = 0.001$, partial $\eta^2 = 0.396$			
Mouse HL	NA	7.241± 0.054	7.386± 0.059	7.390± 0.097
	ANCOVA: $F_{(3, 35)} = 5.319$, $p = 0.012$, partial $\eta^2 = 0.290$			

C.2: *Statistical tests comparing 5'HoxD expression in microarray and qPCR experiments*

Table C.2: Statistical tests used to compare gene expressions in the microarray and qPCR experiments.

Experiment	Gene	Levene's Test for Equality of Variances		*t*-test for Equality of Means			
Independent Samples Tests: CS17 bat FL vs. E13.5 mouse							
		F	Sig.	*t*	d.f.	*p*-value	
						2-tailed	Bonreffoni
Microarray	*Hoxd10*	0.001	0.981	5.14	6	**0.002**	0.06
	Hoxd11	13.667	0.01	4.831	6	**0.003**	0.09
	Hoxd12	15.746	0.007	10.143	6	**0.000053**	**0.00159**
	Hoxd13	3.472	0.112	7.112	3.101	**0.005**	0.15
	Lnp	4.198	0.086	2.384	3.728	0.08	1
qPCR	*Hoxd10*	4.773	0.094	2.588	2.17	0.113	1
	Hoxd11	7.652	0.051	11.235	2.295	**0.005**	0.15
	Hoxd12	2.955	0.161	0.602	2.12	0.606	1
	Hoxd13	4.184	0.11	0.717	2.745	0.53	1
	Lnp	1.626	0.271	8.375	2.792	**0.005**	0.15
Paired Samples Test: Bat FL vs. Bat HL							
				t	d.f.	*p*-value	
						2-tailed	Bonreffoni
Microarray	*Hoxd10*	CS17		7.165	3	**0.006**	0.18
		CS16		4.135	3	**0.026**	0.78
	Hoxd11	CS17		5.772	3	**0.01**	0.3
		CS16		4.383	3	**0.022**	0.66
	Hoxd12	CS17		10.754	3	**0.002**	0.06
		CS16		2.348	3	0.1	1
	Hoxd13	CS17		2.084	3	0.128	1
		CS16		0.721	3	0.523	1
	Lnp	CS17		5.083	3	**0.015**	0.45
		CS16		0.965	3	0.406	1
qPCR	*Hoxd10*	CS17		4.922	2	**0.039**	1
		CS16		4.961	2	**0.038**	1
	Hoxd11	CS17		12.697	2	**0.006**	0.18
		CS16		8.863	2	**0.012**	0.36
	Hoxd12	CS17		2.956	2	0.098	1
		CS16		6.988	2	**0.02**	0.6
	Hoxd13	CS17		5.054	2	**0.037**	1
		CS16		-0.176	2	0.877	1
	Lnp	CS17		5.215	2	**0.035**	1
		CS16		2.292	2	0.149	1

C.3: *Statistical tests comparing 5'HoxD fold changes in microarray and qPCR experiments*

Table C.3: Statistical tests used to test fold changes in the microarray and qPCR experiments (Test Value = 1).

One-Sample Test: Fold Change (CS17 bat FL / E13.5 mouse FL)

Experiment	Gene	*t*	d.f.	*p*-value	
				2-tailed	Bonferroni
Microarray	*Hoxd10*	6.61	3	**0.007**	**0.07**
	Hoxd11	4.352	3	**0.022**	0.22
	Hoxd12	8.396	3	**0.004**	**0.04**
	Hoxd13	12.696	3	**0.001**	**0.01**
	Lnp	1.621	3	0.204	1
qPCR	*Hoxd10*	3.42	2	0.076	0.76
	Hoxd11	3.876	2	0.061	0.61
	Hoxd12	0.59	2	0.615	1
	Hoxd13	0.929	2	0.451	1
	Lnp	3.793	2	0.063	0.63

One-Sample Test: Fold Change (Bat FL / Bat HL)

Gene	Stage	*t*	d.f.	*p*-value	
				2-tailed	Bonferroni
Hoxd10	CS15	7.93	2	**0.016**	0.32
	CS16	4.321	2	0.05	1
	CS17	12.581	2	**0.006**	0.12
	CS18	3.851	2	0.061	1
Hoxd11	CS15	1.875	2	0.202	1
	CS16	3.794	2	0.063	1
	CS17	5.397	2	**0.033**	0.66
	CS18	3.646	2	0.068	1
Hoxd12	CS15	3.769	2	0.064	1
	CS16	5.007	2	**0.038**	0.76
	CS17	3.005	2	0.095	1
	CS18	3.796	2	0.063	1
Hoxd13	CS15	2.895	2	0.101	1
	CS16	0.364	2	0.751	1
	CS17	4.896	2	**0.039**	0.78
	CS18	-0.668	2	0.573	1
Lnp	CS15	3.165	2	0.087	1
	CS16	2.179	2	0.161	1
	CS17	5.331	2	**0.033**	0.66
	CS18	1.449	2	0.284	1

C.4: *Fold changes for microarray experiments as compared to all qPCR experiments*

Table C.4: Fold change data for 5' HoxD trancripts and *Lnp* for the microarray and relative and absolute qPCR experiments. Median fold changes of biological repeats are given with minimum and maximum fold changes bracketed. Four biological repeats were tested in the microarray experiments and three in the qPCR experiments. Values in bold highlight the largest median fold change (> 2) for each gene, and for the interspecies comparison.

Gene		Mouse vs. Bat	Bat FL vs. HL			
		CS17 FL	CS15	CS16	CS17	CS18
Hoxd10	Microarray	1.3 (1.2-1.4)	NA	1.4 (1.2-1.6)	1.2 (1.2-1.3)	NA
	Relative RT-qPCR	2.4 (1.5-2.6)	3.4 (2.8-3.8)	10.2 (6.1-13.1)	**11.8** (11.3-14.3)	8.9 (6.2-13.8)
	Absolute RT-qPCR		3.8 (3.3-4.2)	11.2 (7.6-11.3)	14.4 (11.2-16.8)	10.2 (6.1-13.3)
Hoxd11	Microarray	1.9 (1.3-2.1)	NA	2.1 (1.4-3.1)	2.4 (2.0-3.9)	NA
	Relative RT-qPCR	**6.5** (5.3-10.9)	12.2 (3.3-28.0)	13.9 (12.6-26.3)	**29.7** (28.5-48.2)	15.0 (7.7-20.4)
	Absolute RT-qPCR		6.6 (5.1-34.7)	16.2 (4.3-33.4)	28.7 (20.9-42.8)	22.7 (19.6-24.4)
Hoxd12	Microarray	1.5 (1.4-1.7)	NA	1.3 (1.1-2.0)	1.6 (1.4-1.7)	NA
	Relative RT-qPCR	1.1 (0.7-1.8)	2.7 (1.6-2.8)	2.2 (1.8-2.7)	**3.7** (2.2-5.5)	2.2 (1.9-3.2)
	Absolute RT-qPCR		2.3 (2.1-3.0)	2.2 (1.6-4.4)	3.9 (3.8-5.2)	4.4 (1.7-5.5)
Hoxd13	Microarray	2.6 (2.2-2.7)	NA	1.3 (0.7-1.4)	1.4 (1.0-2.2)	NA
	Relative RT-qPCR	1.5 (0.7-1.5)	1.6 (1.5-2.3)	1.3 (0.5-1.5)	1.6 (1.4-1.8)	1.0 (0.5-1.1)
	Absolute RT-qPCR		2.0 (1.8-2.1)	1.0 (0.7-1.8)	1.8 (1.2-2.0)	1.4 (0.6-1.8)
Lnp	Microarray	1.1 (1.0-1.1)	NA	1.1 (0.9-1.3)	1.3 (1.2-1.5)	NA
	Relative RT-qPCR	**6.6** (3.2-6.9)	**3.2** (2.0-4.5)	2.2 (1.2-2.9)	1.9 (1.5-2.0)	1.2 (1.1-1.9)

C.5: *Graphs of absolute qPCR comparisons among genes (5' HoxD genes)*

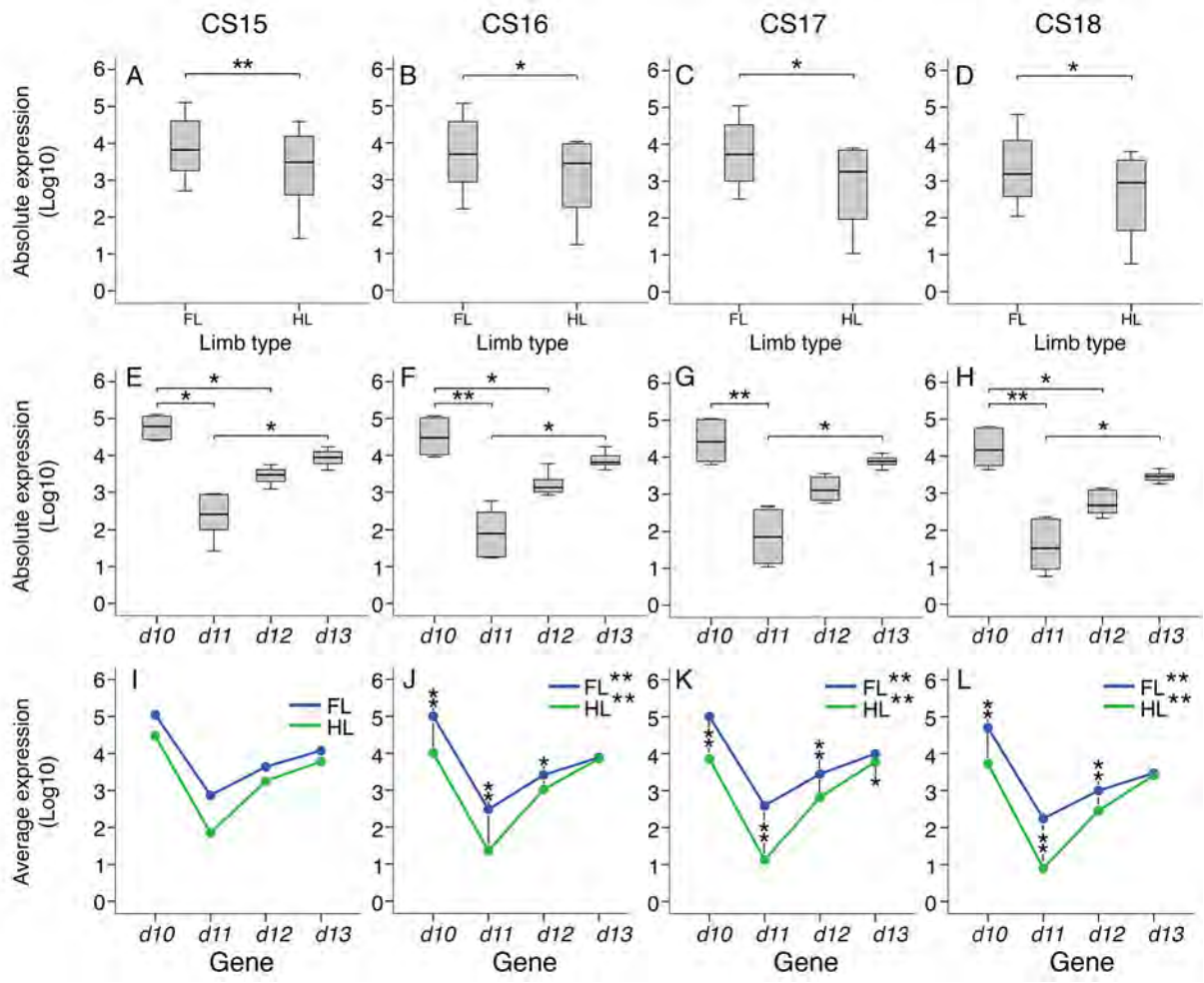

Figure C.1: Absolute qPCR data (Log_{10} transformed) for the 5' HoxD genes at successive stages of development: CS15 (**A**, **E**, **I**), CS16 (**B**, **F**, **J**), CS17 (**C**, **G**, **K**) and CS18 (**D**, **H**, **L**) revealed significant differences between the forelimb (FL) and the hindlimb (HL) at all stages (Related samples sign test, Table C.5). Expression levels of the different genes were significantly different at all stages (**E**-**H**). For CS15 (**E**), pairwise comparisons revealed significant differences between the median scores of *Hoxd10* (21.5) and *Hoxd11* (3.5) and *Hoxd12* (9.8) and between that of *Hoxd11* and *Hoxd13* (15.2) (p = 0.004 for these comparisons). Similar results were obtained for CS16 (**F**), the median score of *Hoxd10* (20.83) was significantly higher than both *Hoxd11* (3.5; $p < 0.001$) and *Hoxd12* (9.83; p = 0.042) while *Hoxd11* was significantly lower than *Hoxd13* (15.8; p = 0.015). For CS17 (**G**), pairwise comparisons revealed significant differences between the median score of *Hoxd11* (3.5) and that of *Hoxd10* (19.7; $p < 0.001$) and *Hoxd13* (17.3; p = 0.004), but no significant differences were found for comparisons with *Hoxd12* (9.5). CS18 (**H**) pairwise comparisons were similar to that found for CS15 and CS16 with *Hoxd10* (21.3) having significantly higher expression that *Hoxd11* (3.7; $p < 0.001$) and *Hoxd12* (9.4; p = 0.02), while *Hoxd11* had significantly lower expression than that of *Hoxd13* (15.7, p = 0.02). The interaction effects among the limb type and developmental stage could not be determined for CS15 (**I**), examination of the expression among genes within each limb type indicates that these were significantly different in both the FL and the HL (Kruskal-Wallis H test: H = 10.39, d.f. = 3, p = 0.016 for both) with pairwise comparisons indicating that there were significant differences between *Hoxd10* and *Hoxd11* (p = 0.022) for both tests. There were significant interaction effects among the limb type and developmental stage for CS16 (**J**), CS17 (**K**) and CS18 (**L**) (Two-way ANOVA, Table C.5). At all stages, significant differences were found among genes for both the FL and the HL samples (Two-way ANOVA, Table C.5). At CS16 (**J**) this could be attributed to significant differences between all pairwise comparisons excluding that of *Hoxd12* and *Hoxd13* in the FL (for all others: $p < 0.001$), and *Hoxd10* and *Hoxd11* in the HL (*Hoxd12* and *Hoxd13*: p = 0.01; for all others: $p < 0.001$). At CS17 (**K**) these were attributable to significant differences in all pairwise comparisons of the FL ($p < 0.001$) and most pairwise comparisons, with the exception of that between *Hoxd10* and *Hoxd13*, in the HL ($p < 0.001$). CS18 (**L**) showed the same relationship as CS17. For all stages significant differences were found between FL and HL were found for *Hoxd10*, *Hoxd11* and *Hoxd12. Hoxd13* was only significantly different between the FL and HL at CS17 (Two-way ANOVA, Table C.5). Outliers are given as empty circles in the boxplots. Asterisks denote a significantly different comparison with * signifying $p < 0.05$ and ** signifying $p < 0.001$.

C.6: *Statistical tests of absolute qPCR comparisons among genes*

Table C.5: Statistical tests used to compare gene expression amongst the 5' HoxD genes and limb types (FL & HL) examined for the transformed data (Log_{10}) of the absolute qPCR experiments. Tests in grey indicate non-significance ($p > 0.05$).

Comparison	Group	Test statistics
		Related samples (* Wilcoxon) sign test
FL vs. HL	CS15	*Statistic* = -3.18, N = 12, $p < 0.001$
	CS16	*Statistic* = -2.02, N = 12, $p = 0.039$
	CS17	*Statistic* * = -3.059, N = 12, $p = 0.002$
	CS18	*Statistic* * = -2.824, N = 12, $p = 0.005$
		Kruskal-Wallis *H* test
Genes	CS15	$H = 21.15$, d.f. = 3, $p < 0.001$
	CS16	$H = 20.24$, d.f. = 3, $p < 0.001$
	CS17	$H = 19.77$, d.f. = 3, $p < 0.001$
	CS18	$H = 21.13$, d.f. = 3, $p < 0.001$
		Two-way ANOVA
Interactions (CS16)	Genes & Limb type	$F_{(3,16)} = 8.766$, $p = 0.001$, partial $\eta^2 = 0.622$
	Hoxd10	$F_{(1,16)} = 33.09$, $p < 0.001$, partial $\eta^2 = 0.674$
	Hoxd11	$F_{(3,16)} = 42.0$, $p < 0.001$, partial $\eta^2 = 0.724$
	Hoxd12	$F_{(3,16)} = 5.113$, $p = 0.038$, partial $\eta^2 = 0.242$
	Hoxd13	$F_{(3,16)} = 0.038$, $p = 0.848$, partial $\eta^2 = 0.002$
	FL	$F_{(3,16)} = 73.31$, $p < 0.001$, partial $\eta^2 = 0.932$
	HL	$F_{(3,16)} = 98.17$, $p < 0.001$, partial $\eta^2 = 0.948$
Interactions (CS17)	Genes & Limb type	$F_{(3,16)} = 62.034$, $p < 0.001$, partial $\eta^2 = 0.921$
	Hoxd10	$F_{(1,16)} = 265.93$, $p < 0.001$, partial $\eta^2 = 0.943$
	Hoxd11	$F_{(3,16)} = 439.48$, $p < 0.001$, partial $\eta^2 = 0.965$
	Hoxd12	$F_{(3,16)} = 80.87$, $p < 0.001$, partial $\eta^2 = 0.835$
	Hoxd13	$F_{(3,16)} = 9.81$, $p = 0.006$, partial $\eta^2 = 0.380$
	FL	$F_{(3,16)} = 414.70$, $p < 0.001$, partial $\eta^2 = 0.987$
	HL	$F_{(3,16)} = 657.7$, $p < 0.001$, partial $\eta^2 = 0.992$
Interactions (CS18)	Genes & Limb type	$F_{(3,16)} = 21.928$, $p < 0.001$, partial $\eta^2 = 0.804$
	Hoxd10	$F_{(3,16)} = 67.37$, $p < 0.001$, partial $\eta^2 = 0.808$
	Hoxd11	$F_{(3,16)} = 129.12$, $p < 0.001$, partial $\eta^2 = 0.890$
	Hoxd12	$F_{(3,16)} = 21.05$, $p < 0.001$, partial $\eta^2 = 0.568$
	Hoxd13	$F_{(3,16)} = 0.249$, $p = 0.625$, partial $\eta^2 = 0.015$
	FL	$F_{(3,16)} = 151.37$, $p < 0.001$, partial $\eta^2 = 0.966$
	HL	$F_{(3,16)} = 230.76$, $p < 0.001$, partial $\eta^2 = 0.977$
		Pearson's (Spearman's) correlation
FL & HL	CS15	$r = 0.990$, N = 9, $p < 0.001$ ($r_s = 1.000$, N = 12, $p < 0.001$)
	CS16	$r = 0.951$, N = 9, $p < 0.001$ ($r_s = 0.951$, N = 12, $p < 0.001$)
	CS17	$r = 0.992$, N = 9, $p < 0.001$ ($r_s = 0.923$, N = 12, $p < 0.001$)
	CS18	$r = 0.940$, N = 9, $p < 0.001$ ($r_s = 0.930$, N = 12, $p < 0.001$)

C.7: *Fold changes of 5'HoxD genes relative to Hoxd13 in the FL and the HL*

Table C.6: Fold change data for 5' HoxD trancripts for the absolute qPCR experiments. Fold change is given relative to the average *Hoxd13* expression for that limb group and developmental stage. Median fold changes of biological repeats are given with minimum and maximum fold changes bracketed. Three biological repeats were tested in these experiments.

Gene	Limb Type	Bat FL vs. HL			
		CS15	CS16	CS17	CS18
Hoxd10	FL	9.2 (7.6, 10.2)	11.2 (8.9, 11.7)	10.4 (8.7, 11.0)	17.9 (10.6, 19.9)
	HL	4.2 (3.9, 6.0)	1.4 (1.3, 1.5)	1.3 (1.0, 1.3)	2.1 (1.6, 2.4)
Hoxd11	FL	-14.5 (-24.2, -13.7)	-31.1 (-56.9, -16.0)	-25.7 (-31.0, -21.4)	-15.7 (-28.9, -13.6)
	HL	-64.2 (-245.6, -49.1)	-397.0 (-419, -191.5)	-445.9 (-554.1, -393.2)	-292.0 (-463.5, -271.7)
Hoxd12	FL	-3.1 (-3.4, -2.3)	-4.2 (-7.0, -1.6)	-3.5 (-4.7, -2.8)	-2.7 (-5.2, -2.4)
	HL	-3.3 (-5.3, -2.7)	-7.2 (-8.6, -5.4)	-9.0 (-10.8, -8.2)	-8.7 (-12.1, -7.4)
Hoxd13	FL	1.0 (-1.6, 1.4)	-1.4 (-2.3, 1.9)	-1.1 (-1.3, 1.3)	1.0 (-1.8, -1.4)
	HL	-1.1 (-1.6, 1.5)	-1.1 (-1.3, 1.3)	1.0 (-1.4, 1.2)	1.0 (-1.8, 1.2)

C.8: *qPCR Cq values and calibrated values of quantified standard curves and samples*

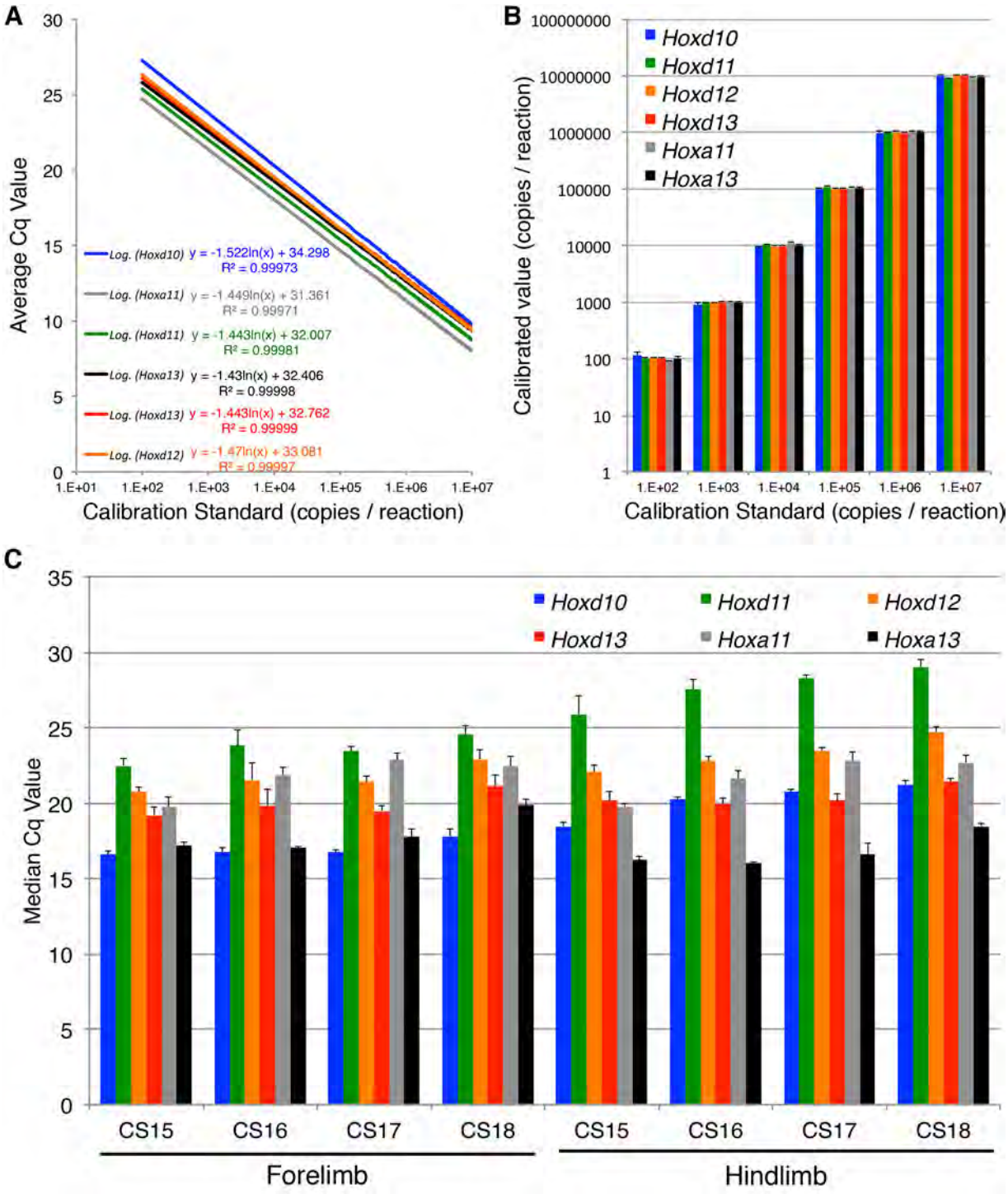

Figure C.2: The quantified standard curves of *Hoxd10* had slightly higher Cq values than those of the other genes (**A**). However, these samples did not deviate from expected values and had a comparable performance to that of the other *Hox* genes examined (**B**). The raw Cq values of the *Hoxd10* samples corresponded (inversely) to those of the calibrated data, with the much lower Cq values indicative of the relatively higher target abundance in this sample (**C**). Together these data show that the quantified standard curve was not miscalibrated and support a much higer abundance of the *Hoxd10* target in the limb samples.

C.9: *Table of primer-BLAST target hits for Hoxd10 qPCR primer set*

Table C.7: Primer-BLAST analyses were performed for the *Hoxd10* qPCR primer set against the Genome (chromosomes from all organisms) and RefSeq mRNA (refseq_rna) databases. Targets that had mismatches > 5 for either primer were ignored. These searches were limited to the organisms: *Homo sapiens*, Chiroptera (taxid:9397) and *Mus musculus* (10090). Description and accession number of the targets are given, with the amplicon length and primer coverage and percentage (%) identity to the target region given.

Description	Accession	Length	Query Cover (%)	Identity (%)
Genome (chromosomes from all organisms)				
Pteropus vampyrus isolate shadow unplaced genomic scaffold, Pvam_2.0 Scaffold2, whole genome shotgun sequence (Features associated with this product: *homeobox protein Hox-D10*)	NW_011888783.1	146	100	100
Myotis brandtii unplaced genomic scaffold, ASM41265v1 scaffold 112, whole genome shotgun sequence	NW_005353838.1	146	100	100
Myotis davidii unplaced genomic scaffold, ASM327334v1 scaffold370, whole genome shotgun sequence (Features associated with this product: *homeobox protein Hox-D10*)	NW_006288615.1	146	100	100
Pteropus alecto unplaced genomic scaffold, ASM32557v1 scaffold3, whole genome shotgun sequence (Features associated with this product: *homeobox protein Hox-D10*)	NW_006442484.1	146	100	100
Eptesicus fuscus isolate BU_THK_EF1 unplaced genomic scaffold, EptFus1.0 scaffold00008, whole genome shotgun sequence (Features associated with this product: *homeobox protein Hox-D10*)	NW_007370658.1	146	100	100
Homo sapiens chromosome 2, GRCh38.p2 primary assembly (Features associated with this product: *homeobox protein Hox-D10*)	NC_000002.12	146	100	100
Homo sapiens chromosome 2, alternate assembly CHM1_1.1, whole genome shotgun sequence (Features associated with this product: *homeobox protein Hox-D10*)	NC_018913.2	146	100	100
Myotis lucifugus unplaced genomic scaffold, Myoluc2.0 scafoold_5, whole genome shotgun sequence	NW_005871053.1	146	100	100
Mus musculus strain C57BL/6J chromosome 2, GRCm38.p3 C57BL/6J (Features associated with this product: *homeobox protein Hox-D10; homeobox protein Hox-D10 isoform X1*)	NC_000068.7	146	100	100
RefSeq mRNA (refseq-rna)				
PREDICTED: *Pteropus vampyrus homeobox D10* (HOXD10), mRNA	XM_011357150.1	146	100	100
PREDICTED: *Mus musculus homeobox D10* (HOXD10), transcript variant X1, mRNA	XM_006498789.2	146	100	100
PREDICTED: *Eptesicus fuscus homeobox D10* (HOXD10), mRNA	XM_008138530.1	146	100	100
PREDICTED: *Pteropus alecto homeobox D10* (HOXD10), mRNA	XM_006921227.1	146	100	100
PREDICTED: *Myotis davidii homeobox D10* (HOXD10), mRNA	XM_006760592.1	146	100	100
PREDICTED: *Myotis lucifugus homeobox D10* (HOXD10), mRNA	XM_006083088.1	146	100	100
PREDICTED: *Myotis brandtii homeobox D10* (HOXD10), mRNA	XM_005857609.1	146	100	100
PREDICTED: *Mus musculus homeobox D10* (HOXD10), mRNA	NM_013554.5	146	100	100
PREDICTED: *Homo sapiens homeobox D10* (HOXD10), mRNA	NM_002148.3	146	100	100

C.10: *Alignment of predicted amplicons for Hox10 paralogs*

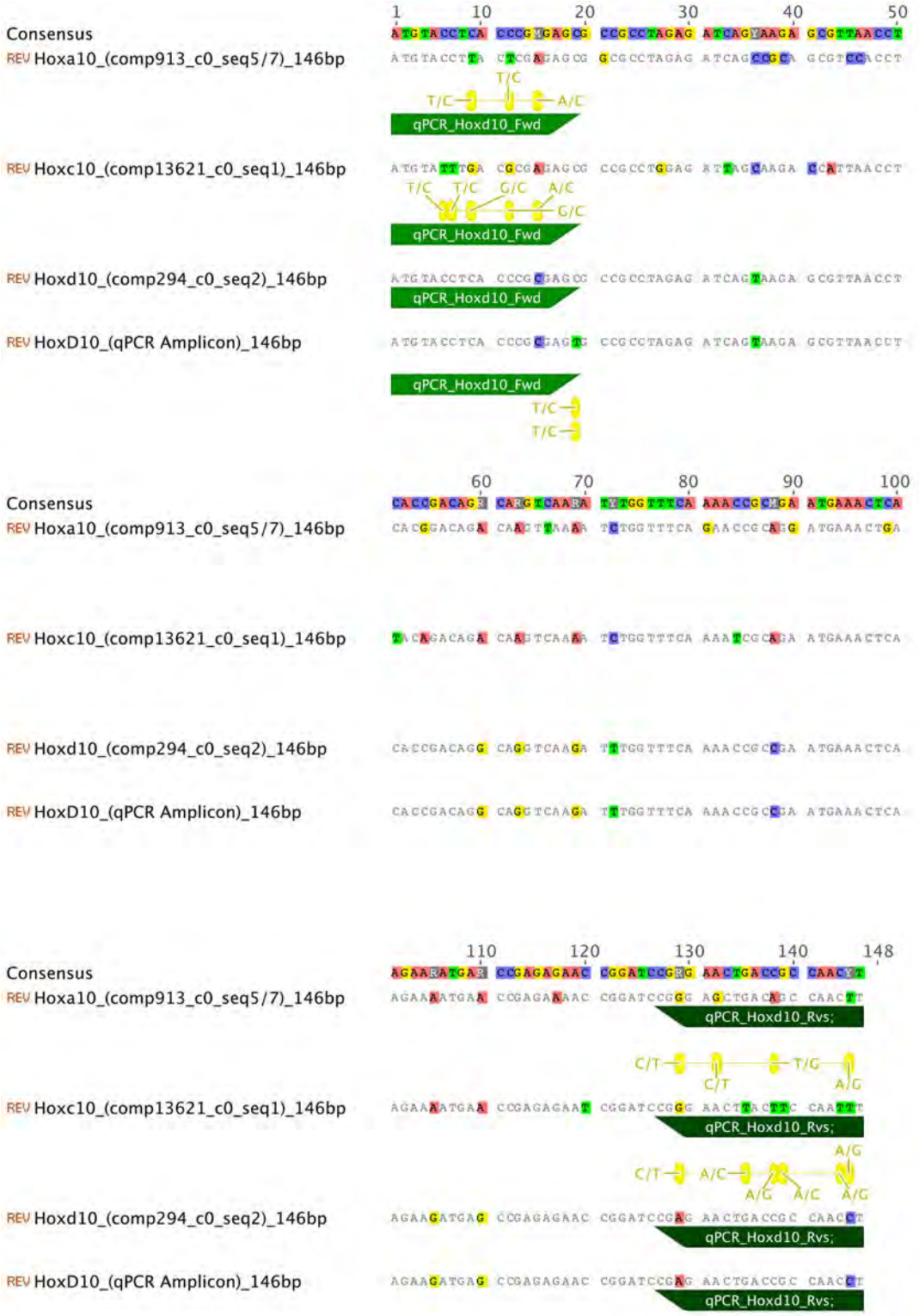

Figure C.3: Predicted qPCR amplicons for *Hox10* paralogs for *M. schreibersii* were generated by extracting sequences that had high sequence similarity to the amplicon of *Hoxd10* (*M. natalensis*). When aligned, these had high sequence similarity (mismatches highlighted), but showed several mismatches (annotated as yellow ellipses below sequence) in the predicted primer binding sites (annotated as green bars below sequence).

C.11: *Hoxd10 Expression (Early)*

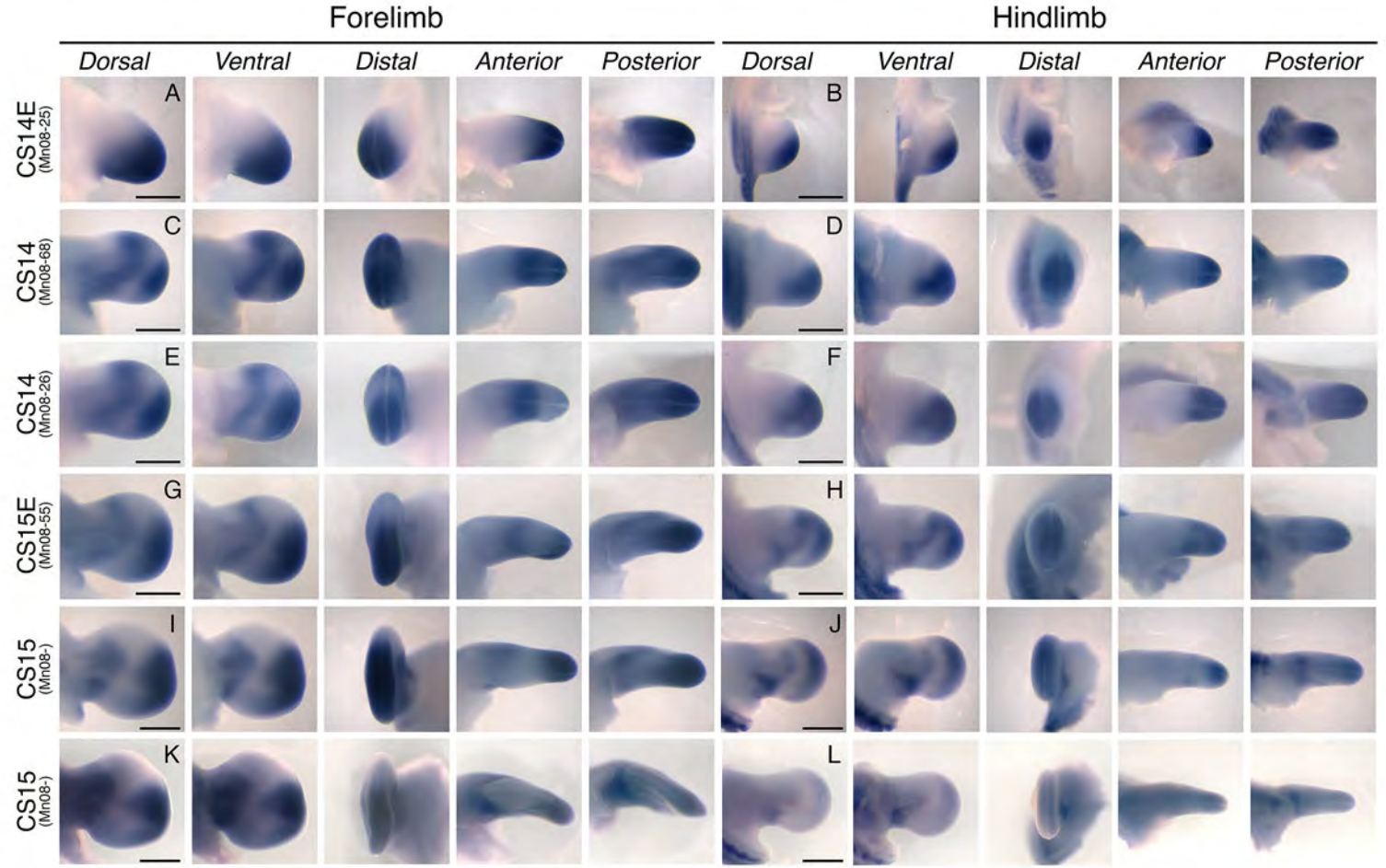

Figure C.4: Expression of *Hoxd10* in bat limbs during early autopod formation (CS14 – CS15).

C.12: *Hoxd11 Expression (Early)*

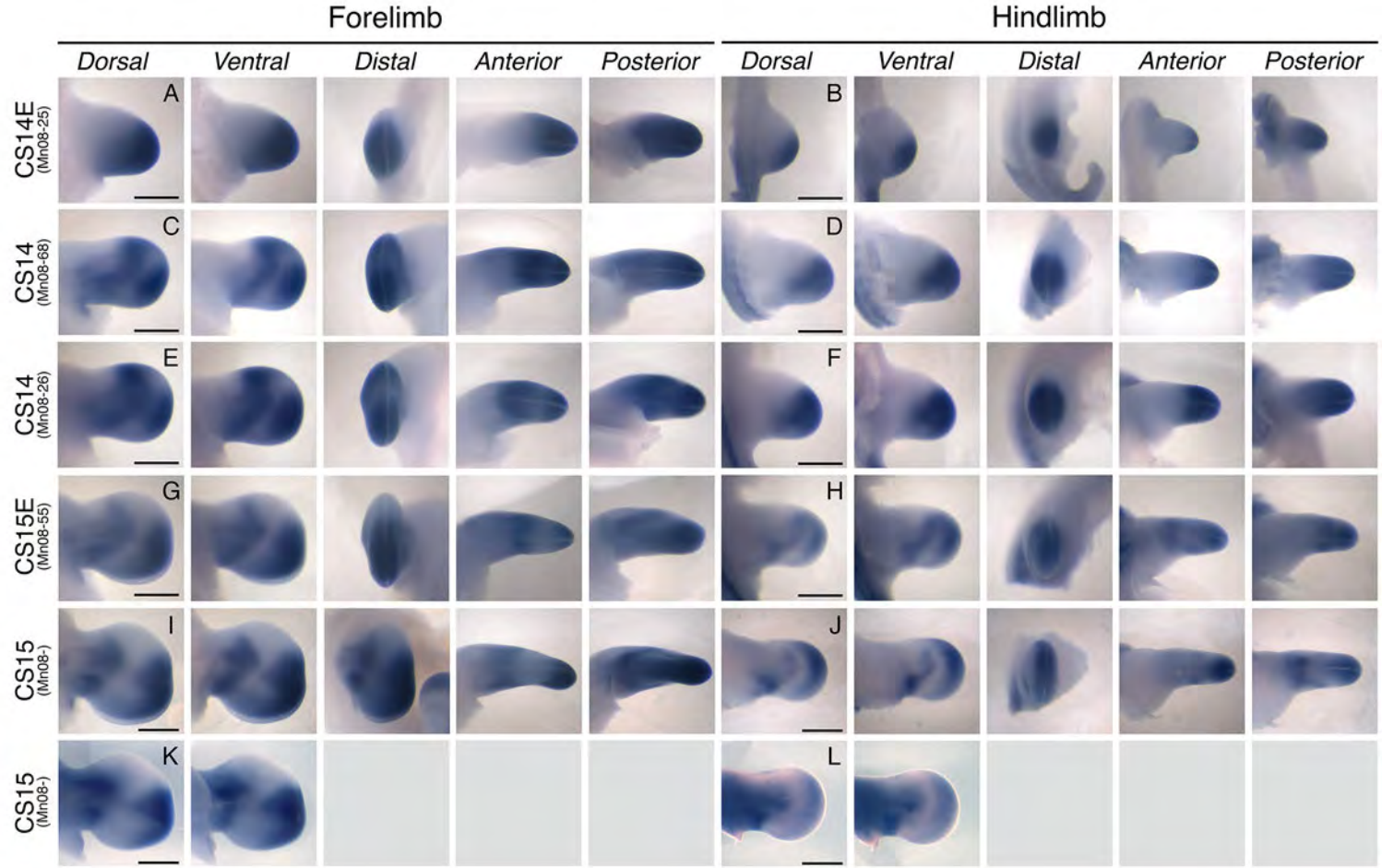

Figure C.5: Expression of *Hoxd11* in bat limbs during early autopod formation (CS14 – CS15).

C.13: *Hoxd12 Expression (Early)*

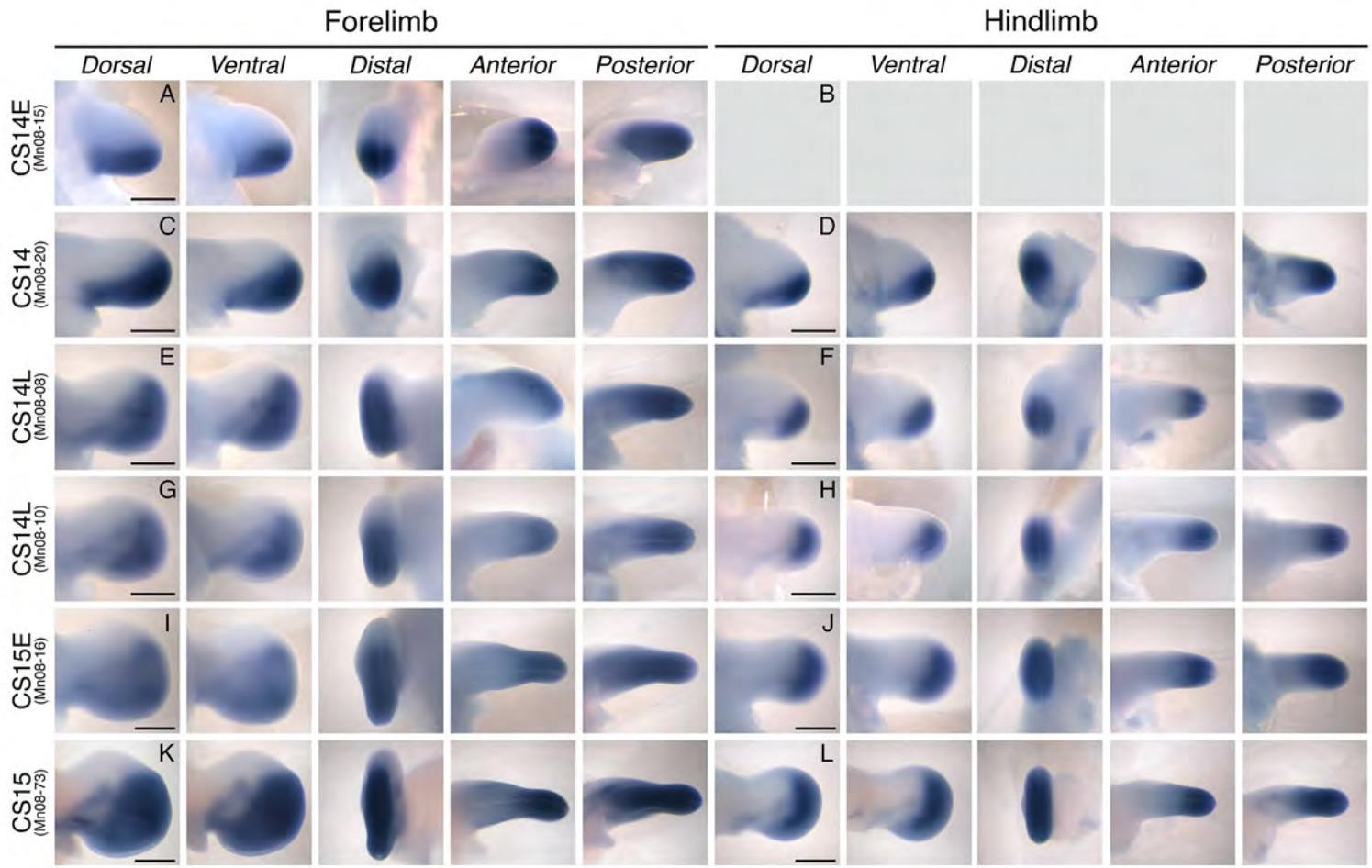

Figure C.6: Expression of *Hoxd12* in bat limbs during early autopod formation (CS14 – CS15).

C.14: *Hoxd13 Expression (Early)*

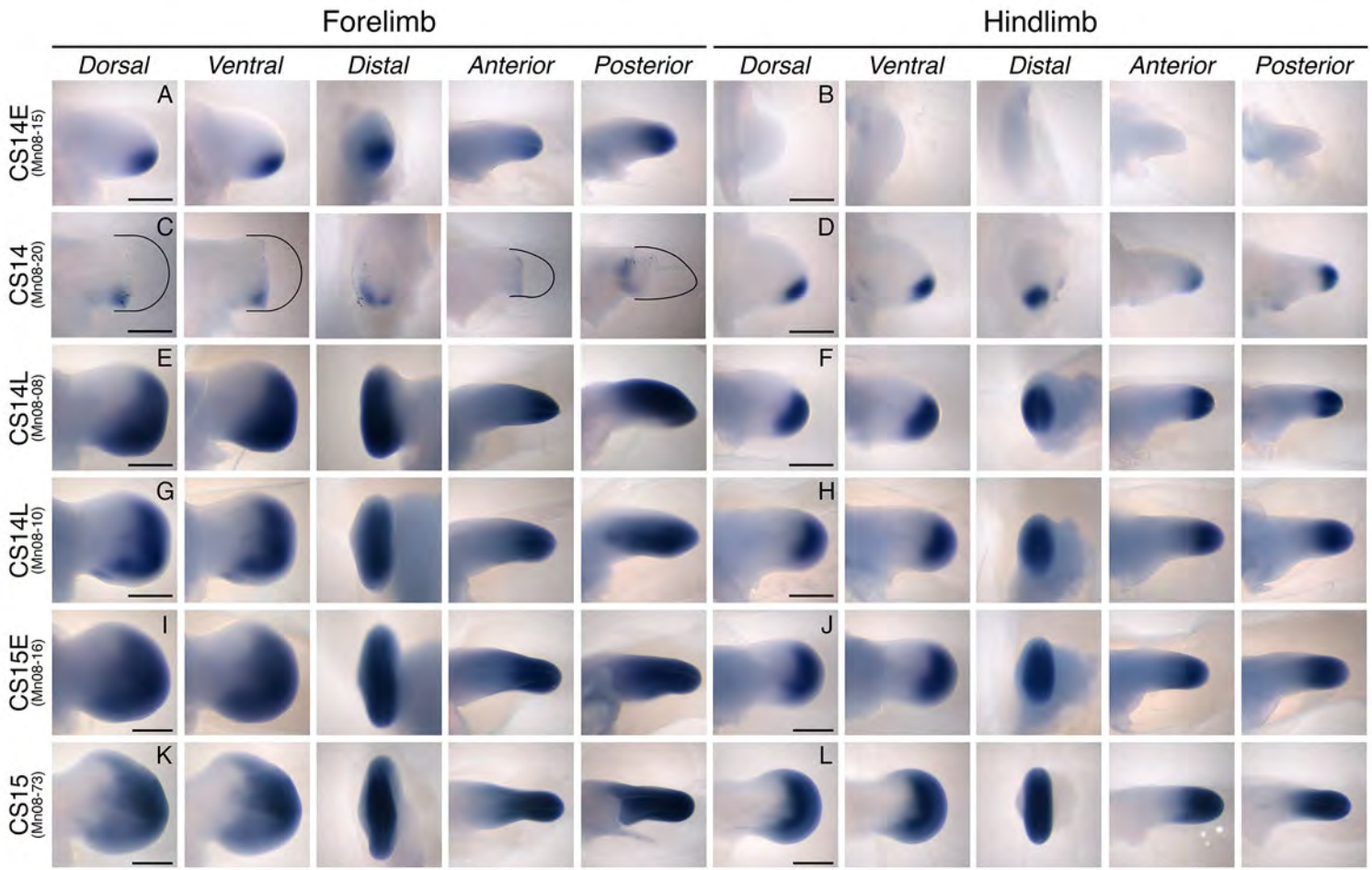

Figure C.7: Expression of *Hoxd13* in bat limbs during early autopod formation (CS14 – CS15).

C.15: *Hoxd10 Expression (Late)*

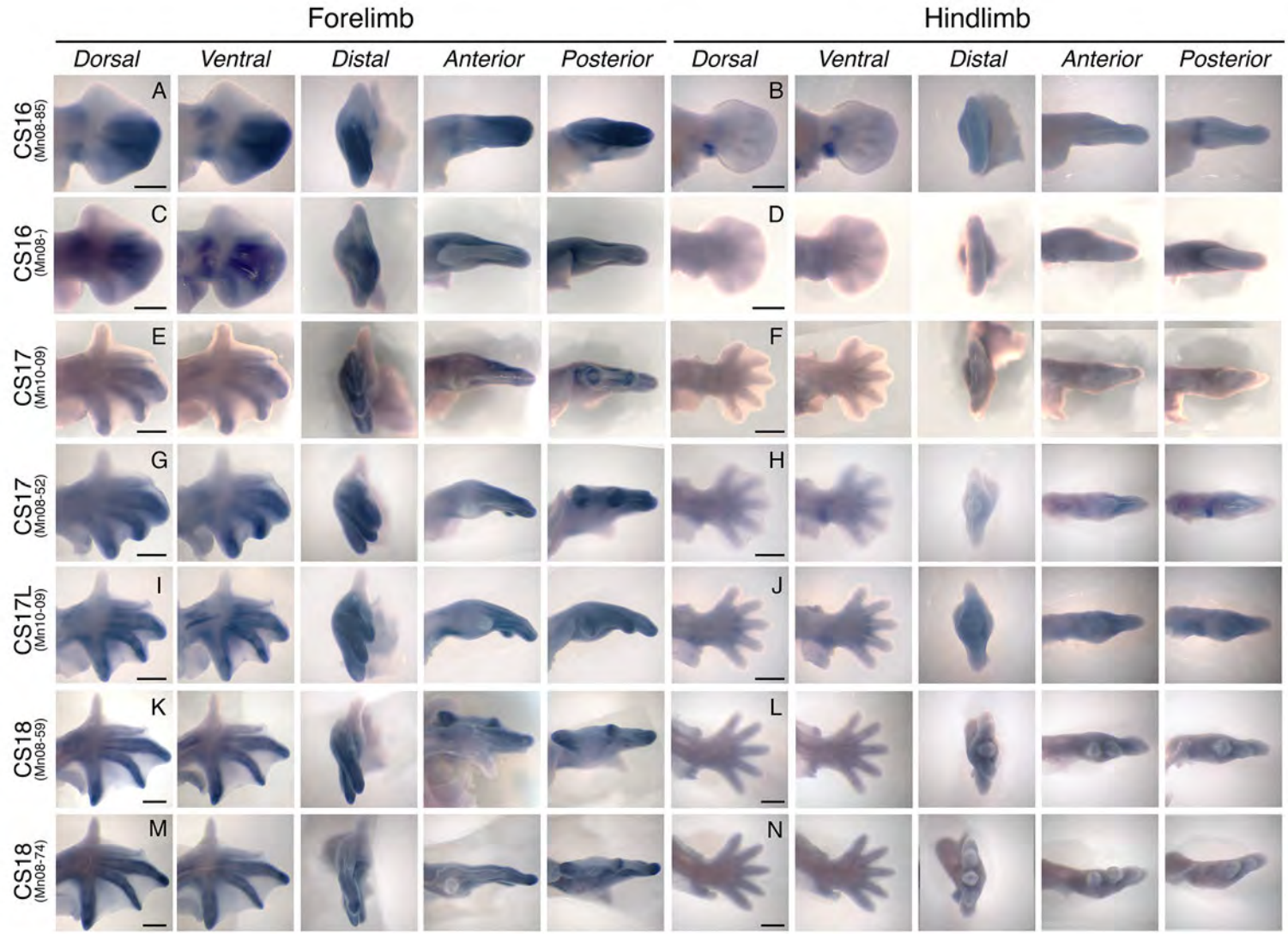

Figure C.8: Expression of *Hoxd10* in bat limbs during later autopod formation (CS16 and CS18).

C.16: *Hoxd11 Expression (Late)*

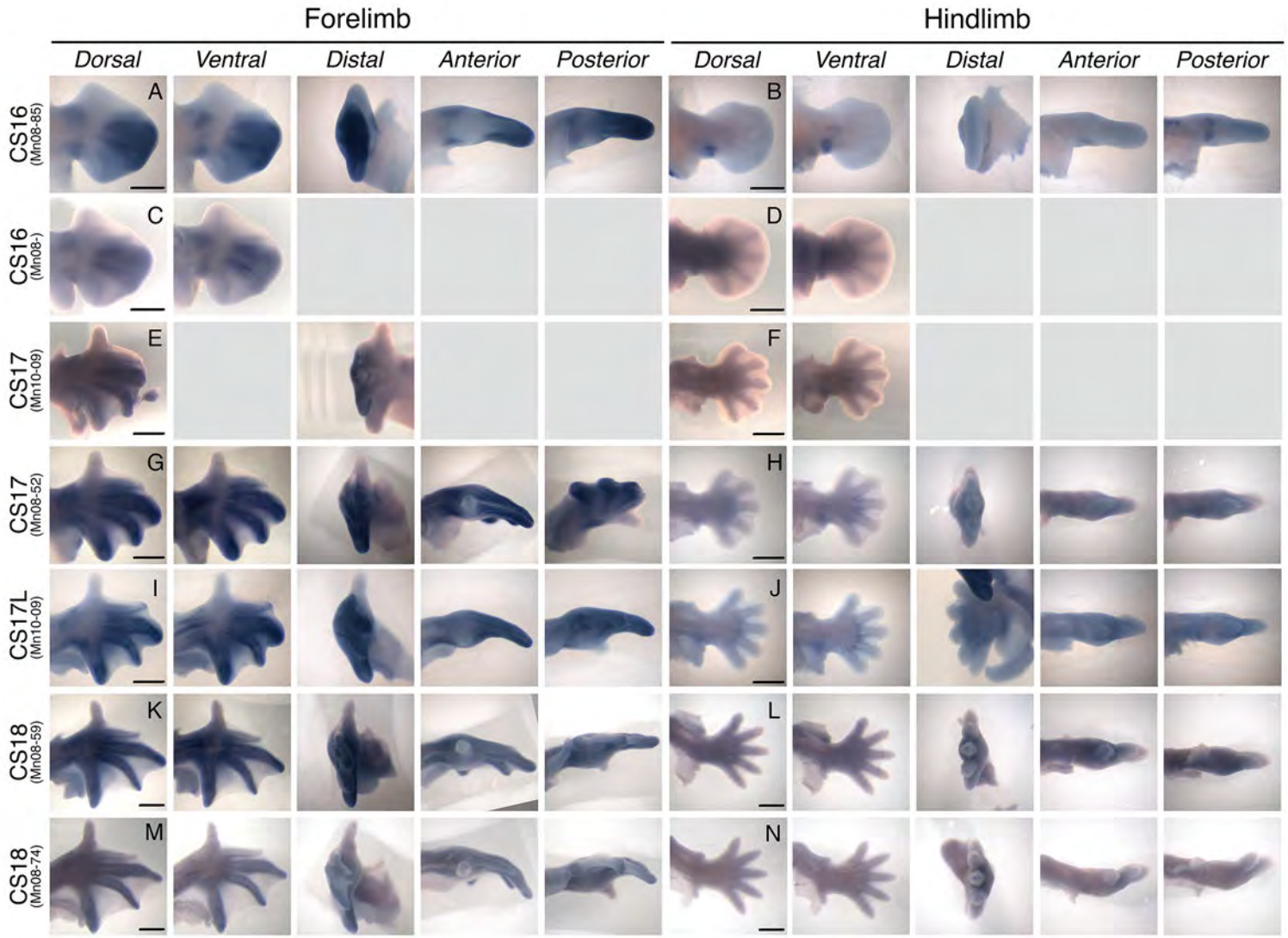

Figure C.9: Expression of *Hoxd11* in bat limbs during later autopod formation (CS16 and CS18).

C.17: *Hoxd12 Expression (Late)*

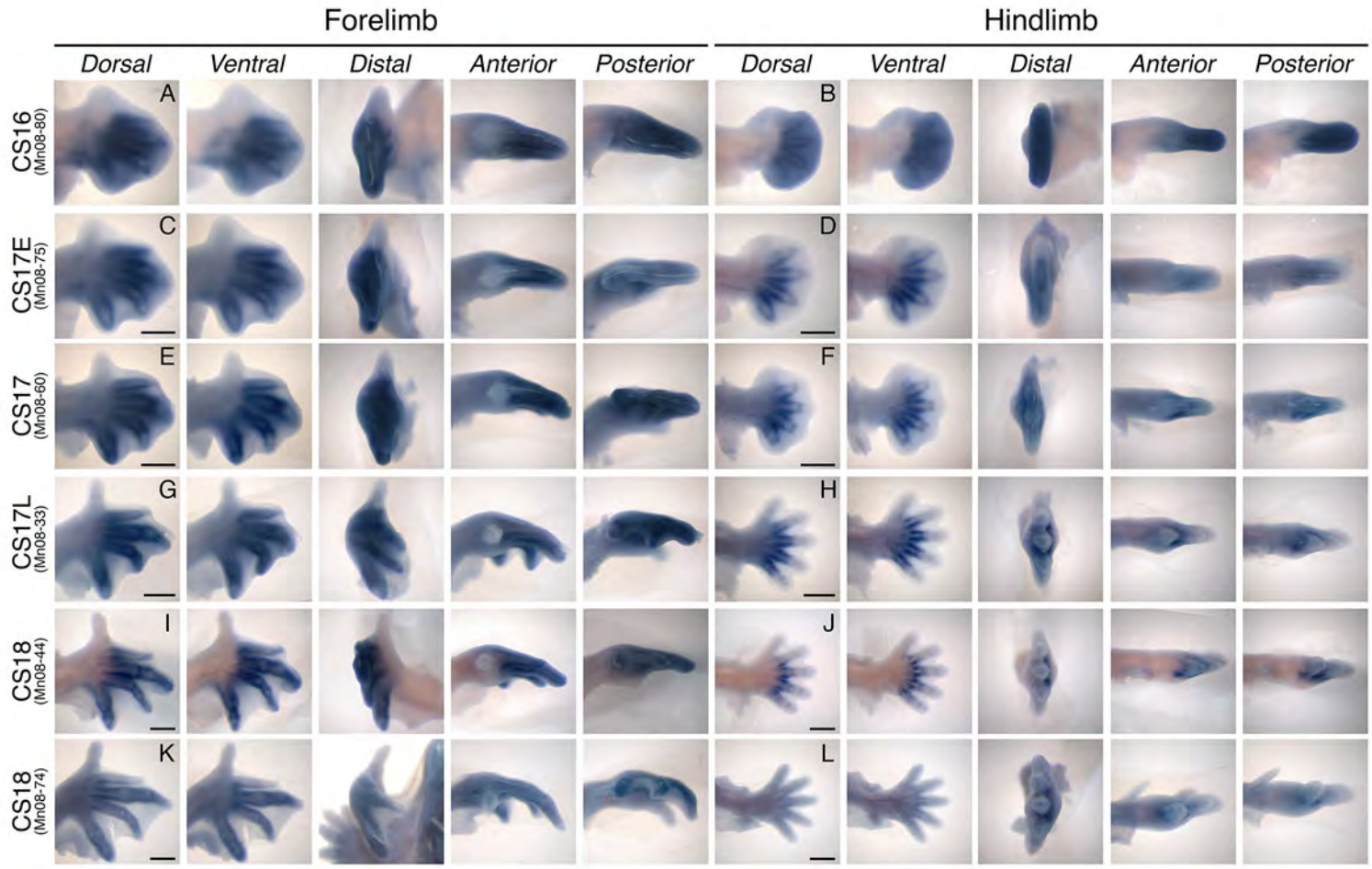

Figure C.10: Expression of *Hoxd12* in bat limbs during later autopod formation (CS16 and CS18).

C.18: *Hoxd13 Expression (Late)*

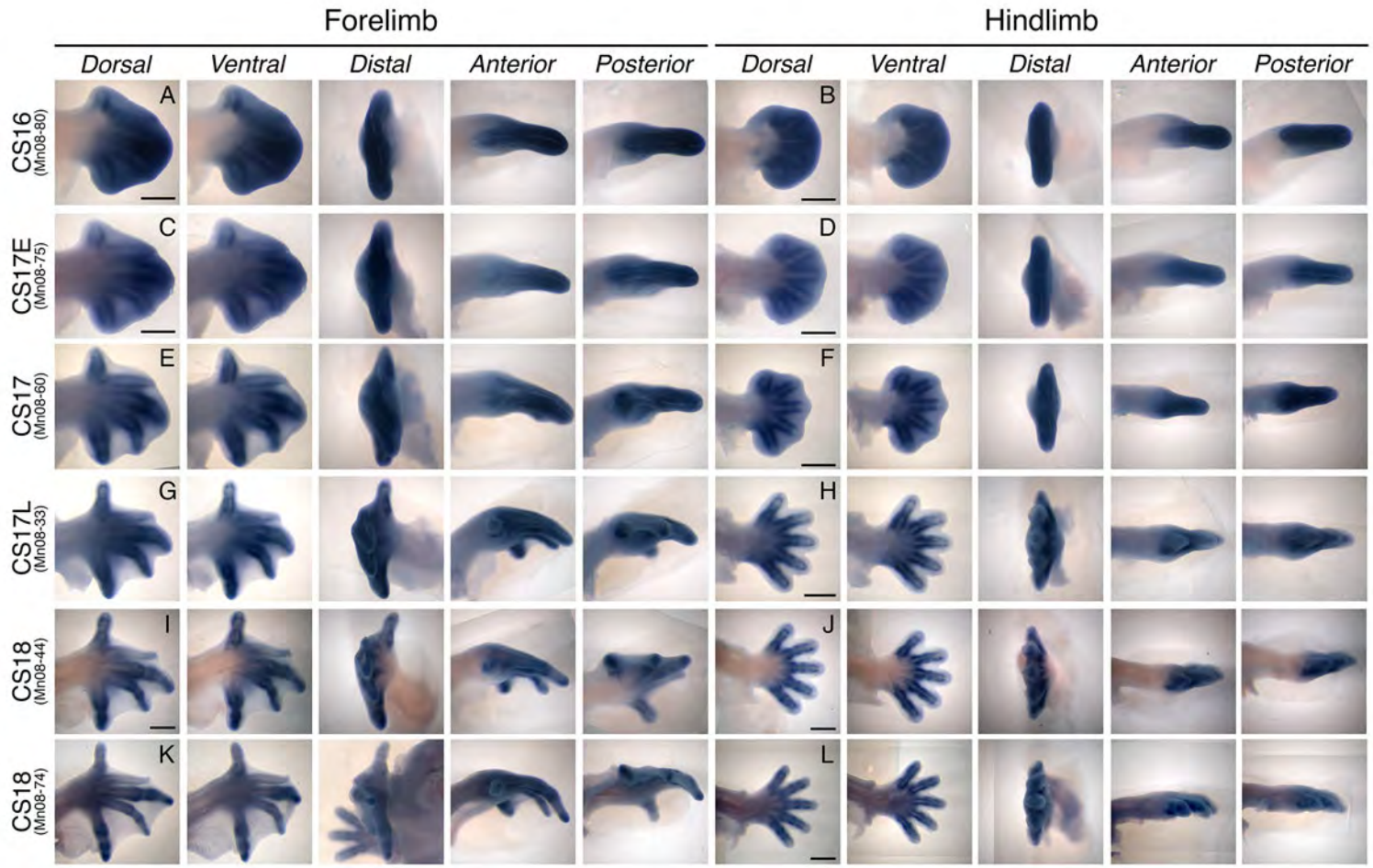

Figure C.11: Expression of *Hoxd13* in bat limbs during later autopod formation (CS16 and CS18).

C.19: *Protein alignments (Hoxd10)*

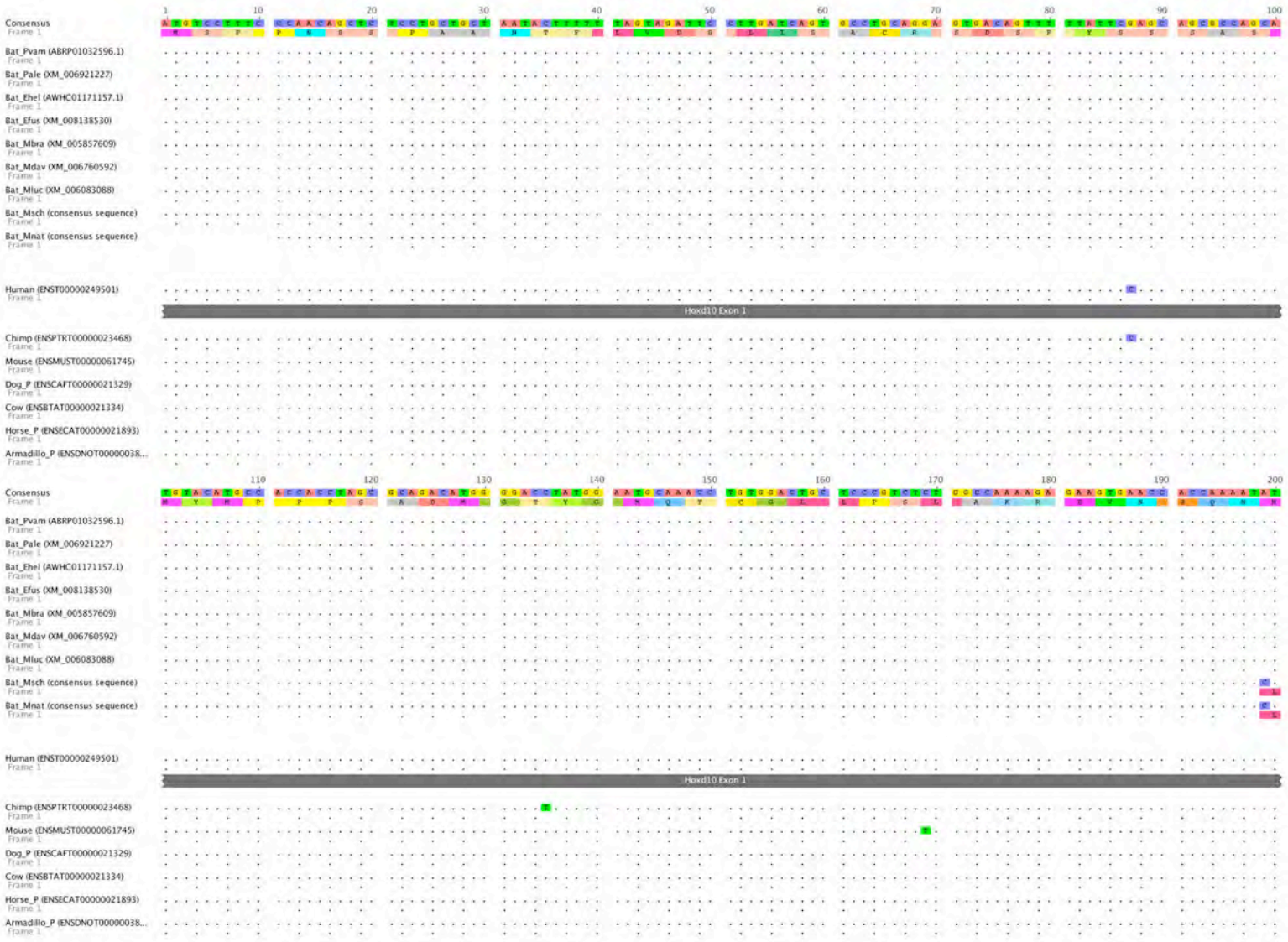

Figure C.12: Alignment of vertebrate protein coding sequences for HOXD10.

Figure C.12 cont.: Alignment of vertebrate protein coding sequences for HOXD10.

Figure C.12 cont.: Alignment of vertebrate protein coding sequences for HOXD10.

Figure C.12 cont.: Alignment of vertebrate protein coding sequences for HOXD10.

Figure C.12 cont.: Alignment of vertebrate protein coding sequences for HOXD10.

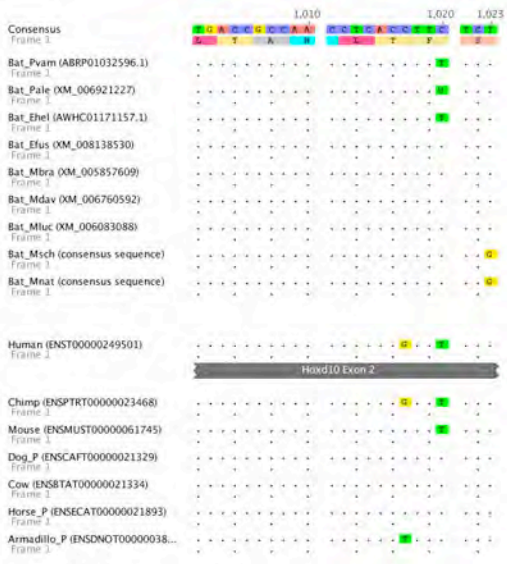

Figure C.12 cont.: Alignment of vertebrate protein coding sequences for HOXD10.

C.20: *Protein alignments (Hoxd11)*

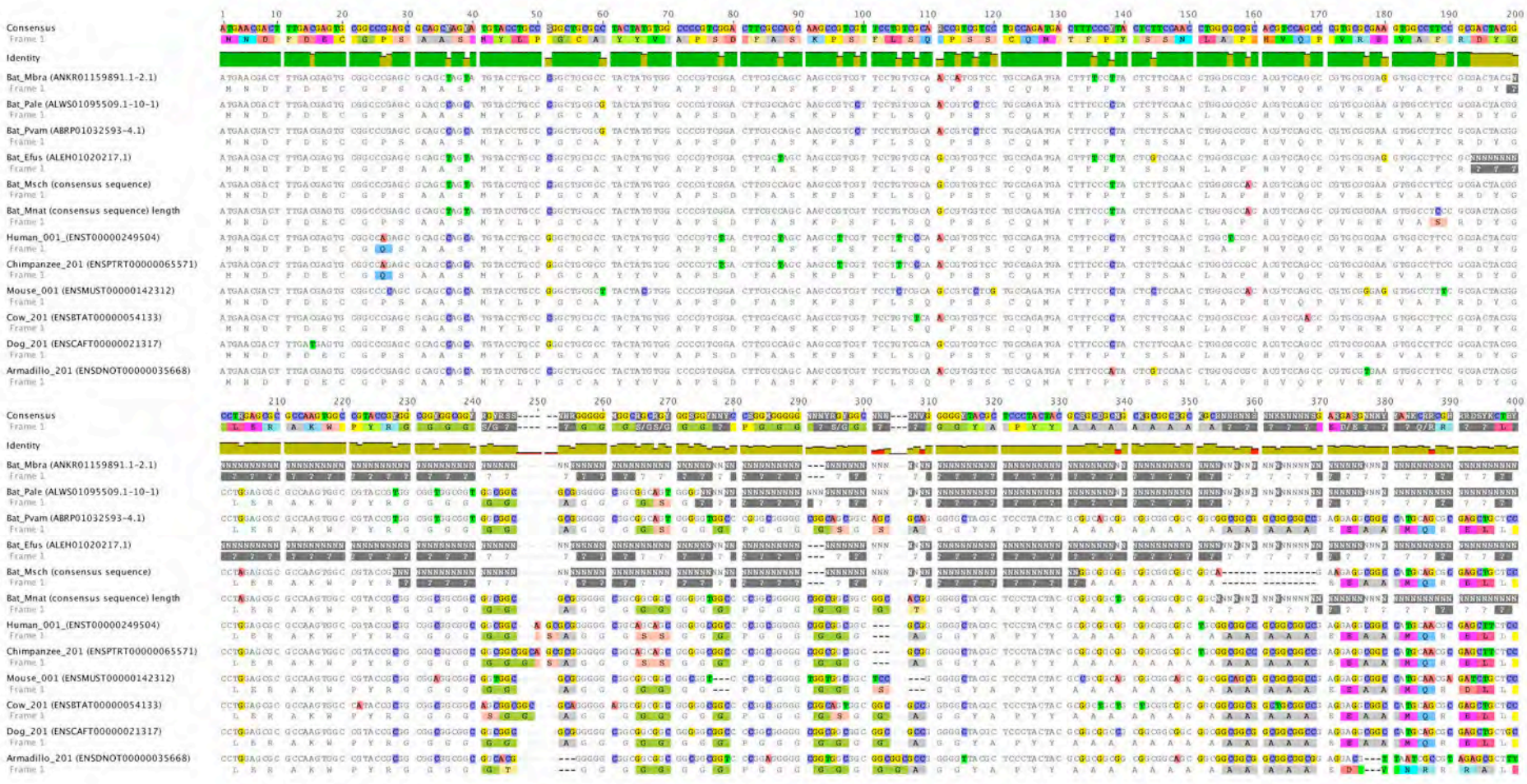

Figure C.13: Alignment of vertebrate protein coding sequences for HOXD11.

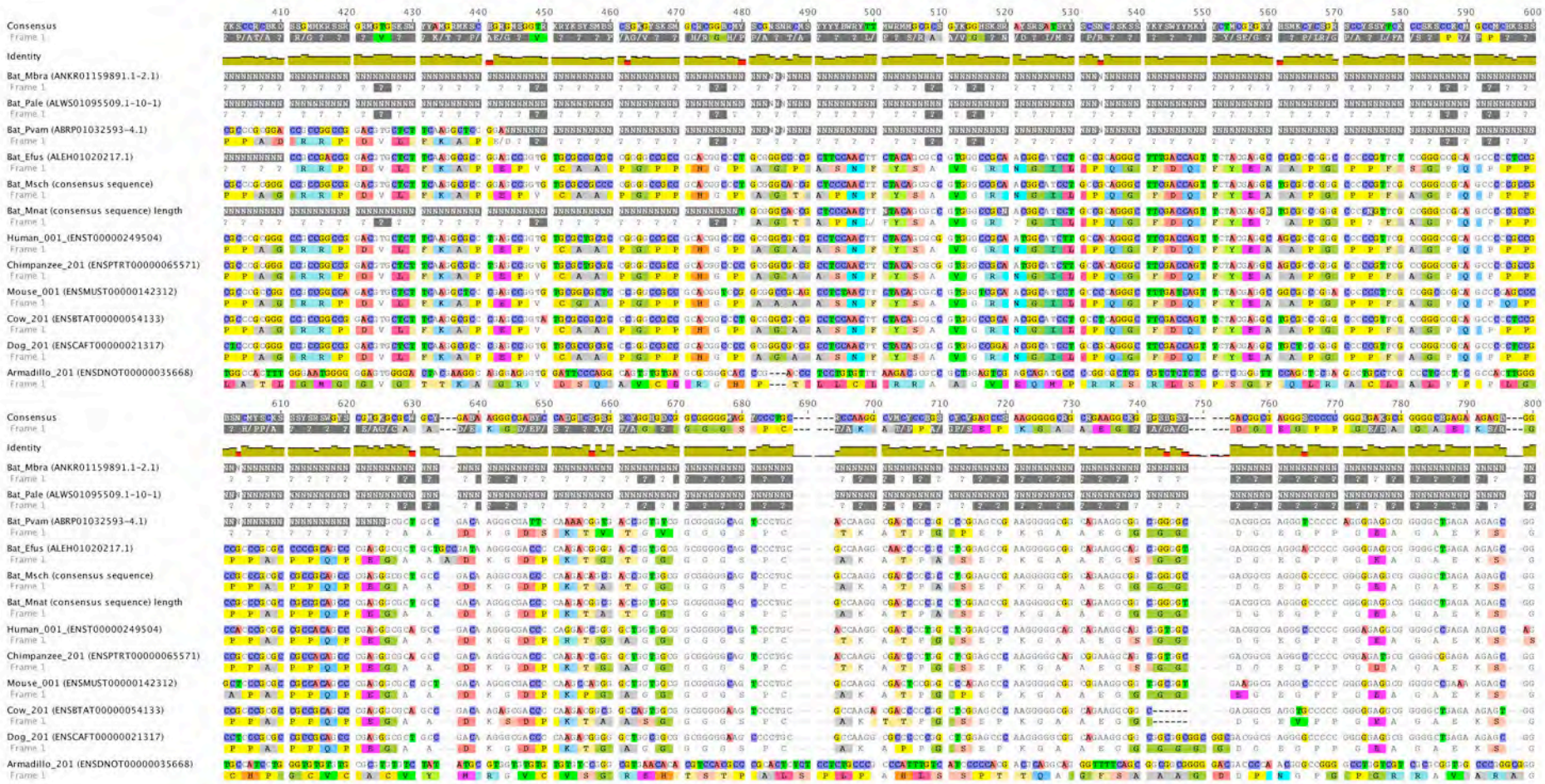

Figure C.13 cont.: Alignment of vertebrate protein coding sequences for HOXD11.

Figure C.13 cont.: Alignment of vertebrate protein coding sequences for HOXD11.

C.21: *Protein alignments (Hoxd12)*

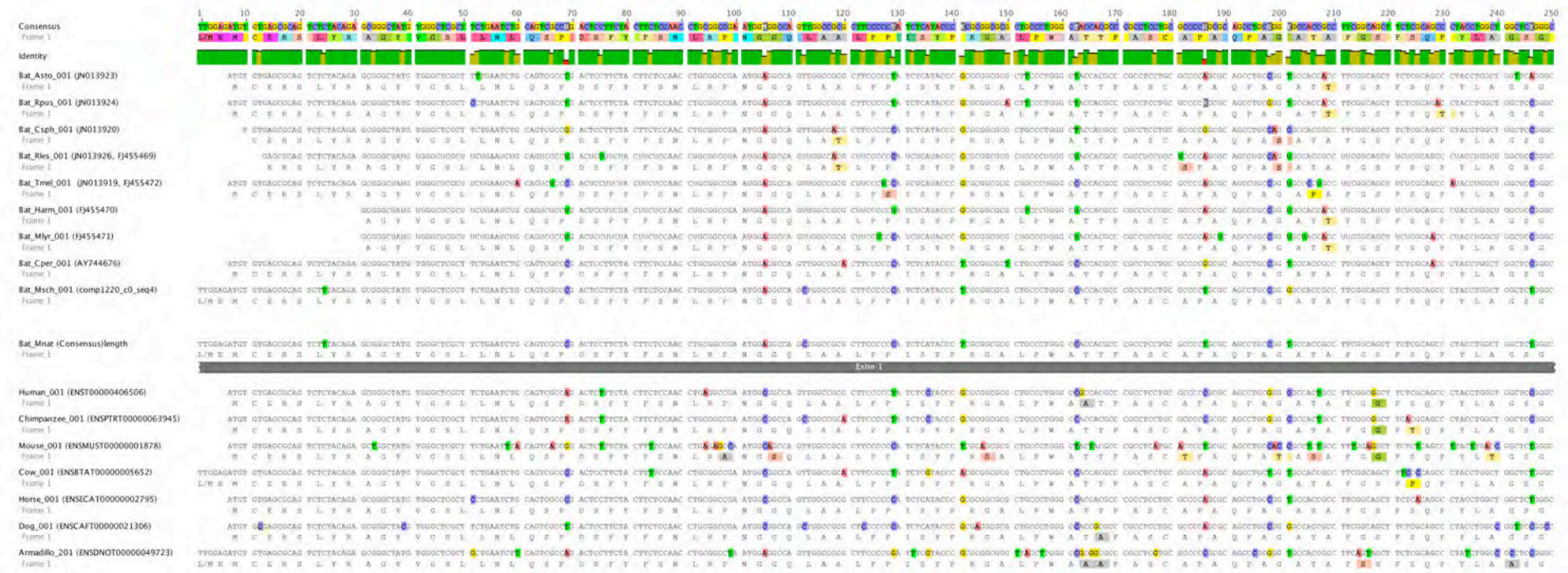

Figure C.14: Alignment of vertebrate protein coding sequences for HOXD12.

Figure C.14 cont.: Alignment of vertebrate protein coding sequences for HOXD12.

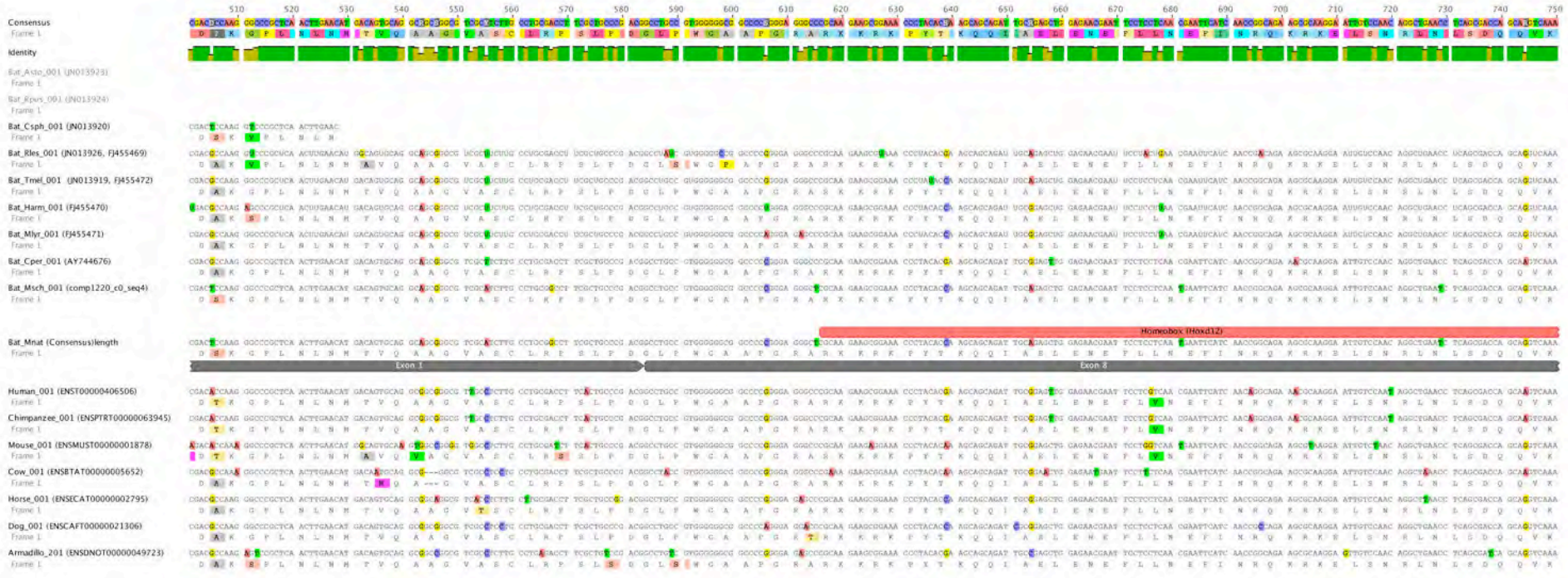

Figure C.14 cont.: Alignment of vertebrate protein coding sequences for HOXD12.

Figure C.14 cont.: Alignment of vertebrate protein coding sequences for HOXD12.

C.22: *Protein alignments (Hoxd13)*

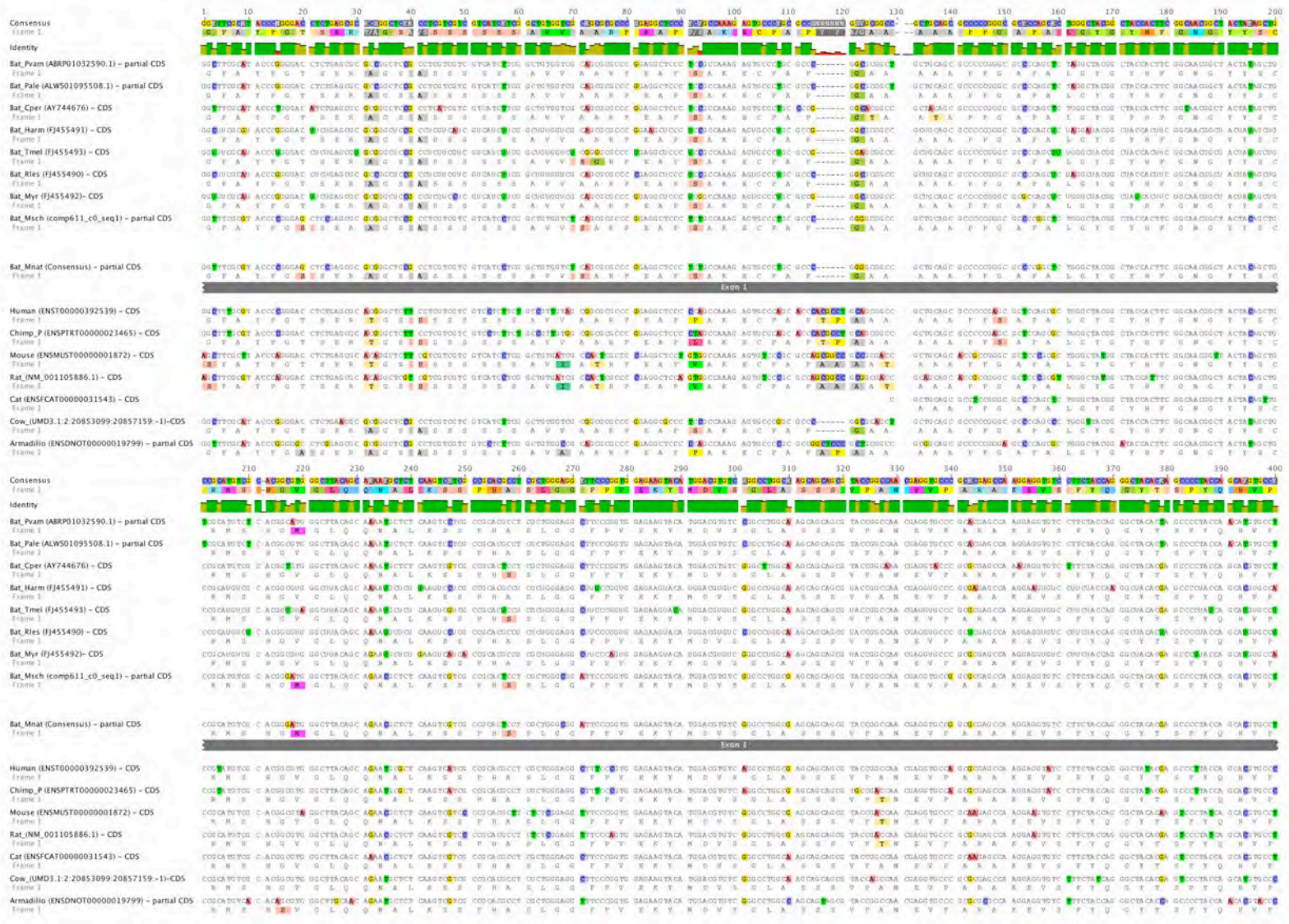

Figure C.15: Alignment of vertebrate protein coding sequences for HOXD13.

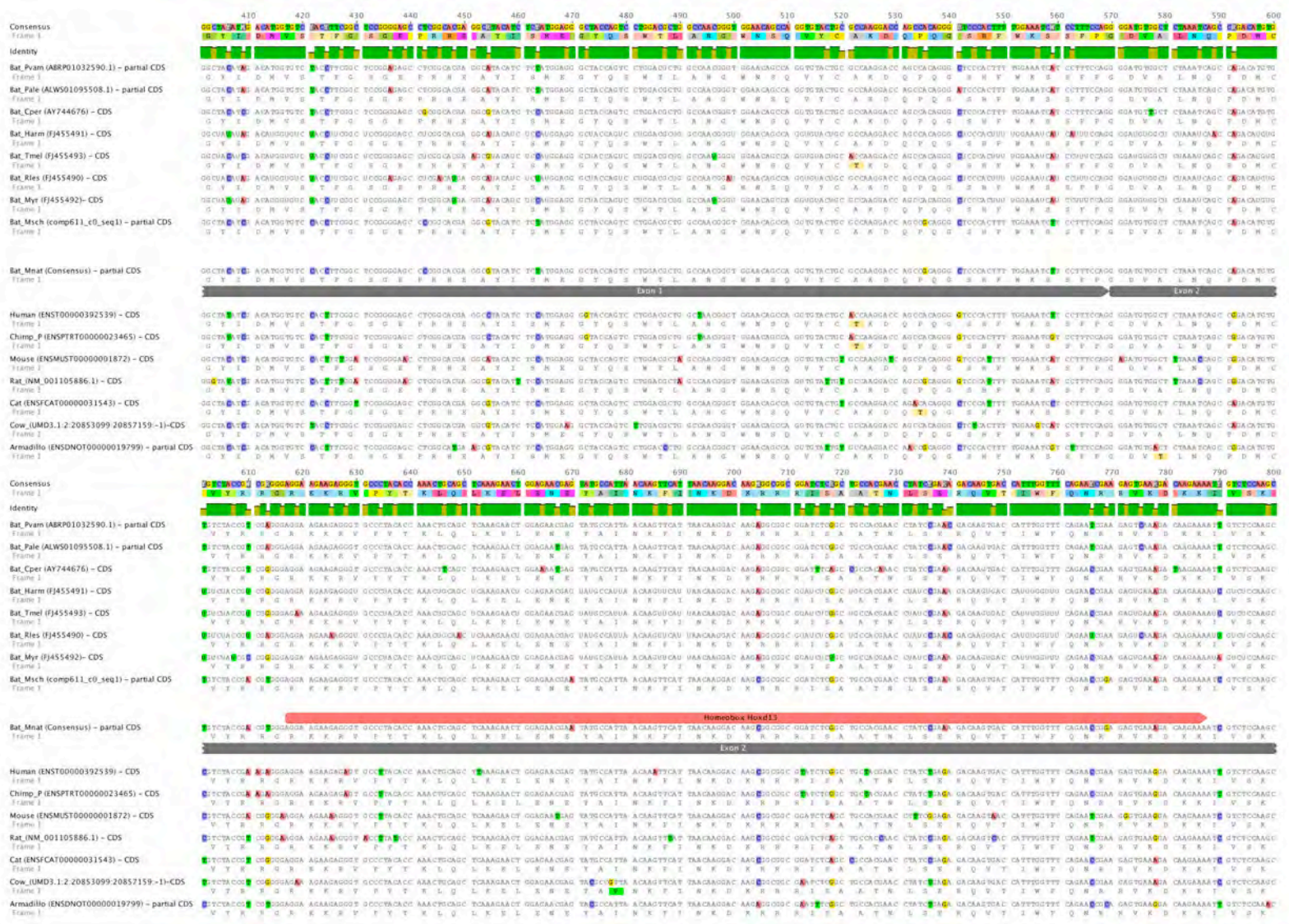

Figure C.15 cont.: Alignment of vertebrate protein coding sequences for HOXD13.

Figure C.15 cont.: Alignment of vertebrate protein coding sequences for HOXD13.

C.23: *Protein residue alterations (Hoxd10)*

Table C.8: Summary of protein residue changes found in the alignments of bat species coding sequence (CDS) for *Hoxd10*. The residue number of the translated sequence of the human is given alongside the average % pairwise identity of the translated alignment. The number of sequences containing the original residue is shown above the bat species that contains the changed residue. The abbreviated name of the substitution is shown alongside. The properties of each amino acid are given and the nucleotide change responsible for the substitution is also shown. No alterations are found in the highly conserved homeodomain (human residue 267 – 355).

Res. No.	ID (%)	Species	Substitution	P/ NP	Charge	HydropI ndex	Nt No.	Type	nt
67	83	7 bats, 12 other	Met	NP	Neut.	1.9	200	1st nt TV	A
		M. nat, M. sch	Leu	NP	Neut.	3.8			C
87	83	7 bats, 12 other	Ser	P	Neut.	-0.8	259	1st nt TS	T
		M. nat, M. sch	Pro	NP	Neut.	-1.6			C
90	83	7 bats, 12 other	Ile	NP	Neut.	4.5	268	1st nt TS	A
		M. nat, M. sch	Val	NP	Neut.	4.2			G
192	54	6 bats, 9 other	Ala (2 Ser, 1 Pro)	NP	Neut.	1.8	574	1st nt TS	G
		P. vam, P. ale, E. hel	Thr	P	Neut.	-0.7			A
205	32	7 bats, 4 other	Ala (3 Val, 2 Pro, 1 Ser, 1 Gly, 1 Asn)	NP	Neut.	1.8	617	2nd nt TV	C
		M. nat, M. sch	Gly	NP	Neut.	-0.4			G
207	53	6 bats, 9 other	Gly (1 Asn, 1 Ser, 1 Gln)	NP	Neut.	-0.4	622	1st nt TS	GG
		P. vam, P. ale, E. hel	Ile	NP	Neut.	4.5	& 623	2nd nt TV	AT
210	60	8 bats, 8 other	Pro (3 Ser, 1 Ala)	NP	Neut.	-1.6	632	2nd nt TS	C
		M. nat	Leu	NP	Neut.	3.8			T
211	50	7 bats, 6 other	Thr (5 Ala, 1 Gly)	P	Neut.	-0.7	635	2nd nt TV	C
		E. fus	Ser	P	Neut.	-0.8			G
232	91	8 bats, 12 other	Leu	NP	Neut.	3.8	698	1st nt TV	C/ T
		M. bra	Met	NP	Neut.	1.9			A

C.24: *Protein residue alterations (Hoxd11)*

Table C.9: Summary of protein residue changes found in the alignments of bat species coding sequence (CDS) for *Hoxd11*. The residue number of the translated sequence of the human is given alongside the average % pairwise identity of the translated alignment for that residue. The number of sequences containing the original residue is shown above the bat species that contains the changed residue, the abbreviated name of the substitution is shown alongside. The properties of each amino-acid are given and the nucleotide change responsible for the substitution is also shown. Alterations in the sequence that appear conserved in and unique to bats are highlighted in bold, those that appear within the highly conserved homeodomain region are highlighted in red.

Res. No.	ID (%)	Species	Substitution	P/ NP	Charge	HydropI ndex	Nt No.	Type	nt
63	76	5 bats, 9 other	Phe	NP	Neut.	2.8	189	2nd nt TS	T
		M. nat	Ser	P	Neut.	-0.8			C
100	15	1 bats, 5 other	Ala	NP	Neut.	1.8	308	1st nt TS	G
		M. nat	Thr	P	Neut.	-0.7			A
134	21	1 bats, 6 other	Gly (2 Asn, 1 Leu, 1 Ser)	NP	Neut.	-0.4	411	1st nt TS	G
		M. nat	Asp	Acidic P	Neg.	-3.5			A
160	**20**	**0 bats, 7 other**	**Ala**	**NP**	**Neut.**	**1.8**	**488**	**1st nt TS/TV**	**G**
		M. nat, M. sch (E. fus)	**Thr (1 Pro)**	**P**	**Neut.**	**-0.7**			**A/C**
162	33	1 bats, 8 other	Ser (1 Leu)	P	Neut.	-0.8	494	1st nt TS	T
		M. nat, M. sch	Pro	NP	Neut.	-1.6			C
191	20	2 bats, 6 other	Ala	NP	Neut.	1.8	581	1st nt TS	G
		E. fus	Ser	P	Neut.	-0.8			T
213	32	3 bats, 6 other	Pro	NP	Neut.	-1.6	651	1st nt TS	C
		P. vam	Ser	P	Neut.	-0.8			T
216	13	1 bat, 5 other	Gly (3 Ala, 1 Pro, 1 Gln)	NP	Neut.	-0.4	661	2nd nt TS	C
		P. vam	Val	NP	Neut.	4.2			T
217	**18**	**0 bats, 7 other**	**Ala (1 Arg, 1 His)**	**NP**	**Neut.**	**1.8**	**663 & 665**	**1st and 3rd nt TS**	**G T**
		P. vam, E. fus, M. nat, M. sch	**Thr**	**P**	**Neut.**	**-0.7**			**A C**
219	25	3 bat, 5 other	Gly (2 Ala, 1 His,1 Asn)	NP	Neut.	-0.4	670	2nd nt TS	G
		P. vam	Val	NP	Neut.	4.2			T
231	28	1 bat, 7 other	Gly (1 Ser,1 Thr)	NP	Neut.	-0.4	712	2nd nt TV	G
		E. fus, M. nat, M. sch	Ala	NP	Neut.	1.8			C
270	76	1 bat, 5 other	Arg	Basic P	Positive	-4.5	838 & 839	1st nt TV	CG
		P. vam	Asn	P	Neut.	-3.5		2nd nt TS	AA
286	76	1 bat, 5 other	Asn	P	Neut.	-3.5	904	1st nt TS	A
		M. nat	Asp	Acidic P	Neg.	-3.5			G

C.25: *Protein residue alterations (Hoxd12)*

Table C.10: Summary of protein residue changes found in the alignments of bat species coding sequence (CDS) for *Hoxd12*. The residue number of the translated sequence of the human is given alongside the average % pairwise identity of the translated alignment. The number of sequences containing the original residue is shown above the bat species that contain the changed residue, the abbreviated name of the substitution is shown alongside. The properties of each amino-acid are given and the nucleotide change responsible for the substitution is also shown. Alterations in the sequence that appear conserved in and unique to bats are highlighted in bold. No alterations are found in the highly conserved homeodomain (human residue 203 – 259).

Res. No.	ID (%)	Species	Substitution	P/NP	Charge	Hydrop. Index	Nt No.	Type	nt
38	84	8 bats, 11 other	Ala	NP	Neut.	1.8	118	1st nt TS	G
		C. sph, R. les	Thr	P	Neut.	-0.7			A
41	84	9 bats, 10 other	Pro (1 Thr)	NP	Neut.	-1.6	127	2nd nt TS	C
		T. mel	Ser	P	Neut.	-0.8			T
65	76	8 bats, 10 other	Gly (1 Thr)	NP	Neut.	-0.4	199	2nd nt TS	G
		C. sph, R. les	Ser	P	Neut.	-0.8			A
67	69	9 bats , 8 other	Thr	P	Neut.	-0.7	205 & 207	1st nt TS 3rd nt TS	AC
		T. mel	Pro	NP	Neut.	-1.6			CT
68	71	8 bats, 11 other	Ala	NP	Neut.	1.8	208	2nd nt TS	G
		A. sto, R.pus,H.arm, M.lyr	Thr	P	Neut.	-0.7			A
75	92	9 bats , 11 other	Thr	P	Neut.	-0.7	229	1st nt TS	C
		R. pus	Pro	NP	Neut.	-1.6			A
93	**45**	**0 bats, 10 other**	**Gly (1 Cys)**	**NP**	**Neut.**	**-0.4**	**283**	**1st nt TV**	**G**
		All	**Arg**	**Basic P**	**Positive**	**-4.5**			**C**
98	69	9 bats, 8 other	Ala (1 Ala, 1 Gly, 1 Ser)	NP	Neut.	1.8	298	1st nt TS	G
		C. sph	Thr	P	Neut.	-0.7			A
107	36	7 bats, 5 other	Ala (7 Ser, 2 Thr, 1 Pro)	NP	Neut.	1.8	326	2nd nt TS	C
		A. sto	Val	NP	Neut.	4.2			T
114	71	8 bats, 11 other	Arg	Basic P	Positive	-4.5	347	1st nt TS	G
		M. sch, M. nat	His	Basic P	Positive (10%) Neutral (90%)	-3.2			A
115	41	9 bats , 4 other	Ala (4 Thr, 1 Gly, 1 Pro, 1 Gln)	NP	Neut.	1.8	349	1st nt TS	G
		C. per	Ser	P	Neut.	-0.8			T
123	70	8 bats, 9 other	Ser (1 Ala)	P	Neut.	-0.8	373	1st nt TS	T
		R. les	Ala	NP	Neut.	1.8			G

Table C.10 cont.: Summary of protein residue changes found in the alignments of bat species coding sequence (CDS) for *Hoxd12*.

128	23	3 bats, 7 other	Ala (8 Gly, 2 Ser)	NP	Neut.	1.8	389	2nd nt TS	C
		M. nat, M. sch	Val	NP	Neut.	4.2			T
129	45	9 bats , 5 other	Ala (4 Val, 1 Gly)	NP	Neut.	1.8	391	1st nt TS	G
		C. per	Thr	P	Neut.	-0.7			A
131	**46**	**0 bats , 8 other**	**Ala**	**NP**	**Neut.**	**1.8**	**398**	**2nd nt TV**	**C**
		All	**Gly**	**NP**	**Neut.**	**-0.4**			**G**
134	36	5 bats, 8 other	Ala (2 Pro, 1 Gly, 1 Val)	NP	Neut.	1.8	406	2nd nt TS	G
		T. mel, C. per, M. sch, M. nat	Ser	P	Neut.	-0.8			T
142	69	9 bats, 8 other	Val (2 Met, 1 Leu)	NP	Neut.	4.2	431	2nd nt TS	T
		C. sph	Ala	NP	Neut.	1.8			C
147	56	8 bats, 7 others	Pro	NP	Neut.	-1.6	448	1st nt TS	C
		C. sph, R. les	Ser	P	Neut.	-0.8			T
166	36	5 bats, 6 other	Ala (4 Thr, 1 Ile)	NP	Neut.	1.8	508	1st nt TS	G
		C. sph, M. sch, M. nat	Ser	P	Neut.	-0.8			T
168	60	5 bats, 9 other	Gly (2 Ser, 1 Asn)	NP	Neut.	-0.4	515	2nd nt TS	G
		C. sph, R. les	Val	NP	Neut.	4.2			T

C.26: *Protein residue alterations (Hoxd13)*

Table C.11: Summary of protein residue changes found in the alignments of bat species coding sequence (CDS) for *Hoxd13*. The residue number of the translated sequence of the human is given alongside the average % pairwise identity of the translated alignment. The number of sequences containing the original residue is shown above the bat species that contain the changed residue, the abbreviated name of the substitution is shown alongside. The properties of each amino-acid are given and the nucleotide change responsible for the substitution is also shown. Alterations in the sequence that appear conserved in and unique to bats are highlighted in bold. No alterations are found in the highly conserved homeodomain (human residue 205 – 261).

Res. No.	ID (%)	Species	Substitution	P/NP	Charge	Hydrop. Index	Nt No.	Type	nt
24	40	5 bats, 4 other	Ala	NP	Neut.	1.8	70	1st nt TS	G
		H. arm	Thr	P	Neut.	-0.7			A
79	43	8 bats, 5 other	Thr (3 Ala, 1 Gly)	P	Neut.	-0.7	293	2nd nt TV	C
		M. nat, M. sch	Ser	P	Neut.	-0.8			G
96	81	6 bats, 8 other	Ala	NP	Neut.	1.8	353	1st nt TS	G
		T. mel, R. fer, M. luc, M. sch, M. nat	Ser	P	Neut.	-0.8			T
97	64	10 bats, 6 other	Ala	NP	Neut.	1.8	356	2nd nt TS	G
		T. mel	Gly	NP	Neut.	-0.4			A
114	72	10 bats, 6 other	Ala (1 Ser, 1 Pro)	NP	Neut.	1.8	406	1st nt TS	G
		C. per	Thr	P	Neut.	-0.7			A
117	73	10 bats, 8 other	Ala	NP	Neut.	1.8	418	1st nt TS	G
		C. per	Thr	P	Neut.	-0.7			A
135	91	10 bats, 10 other	Tyr	P	Neut.	-1.3	474	3rd nt TS	C
		R. fer	STOP	NA	NA	NA			A
144	60	6 bats, 10 other	Val	NP	Neut.	4.2	509	1st nt TS	G
		P. vam, M. luc, M. sch, M. nat	Met	NP	Neut.	1.9			A
157	62	5 bats, 10 other	Ala	NP	Neut.	1.8	548	1st nt TS	G
		C. per, T. mel, M. luc, M. sch, M. nat	Ser	P	Neut.	-0.8			T

C.27: *Sequence alignment (CsC region)*

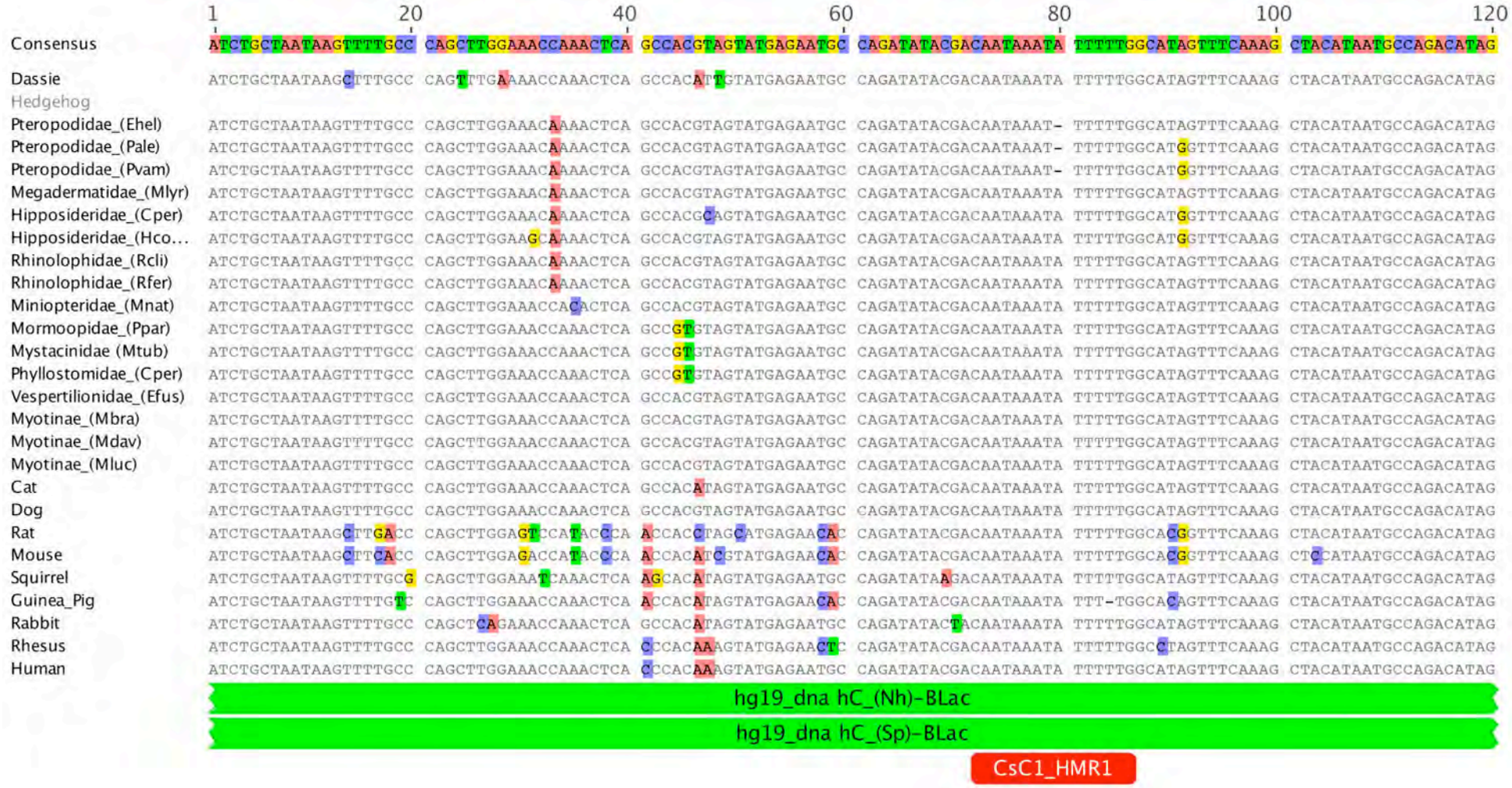

Figure C.16: Alignment of sequences for CsC region of the Prox enhancer for several vertebrate and 16 bat species.

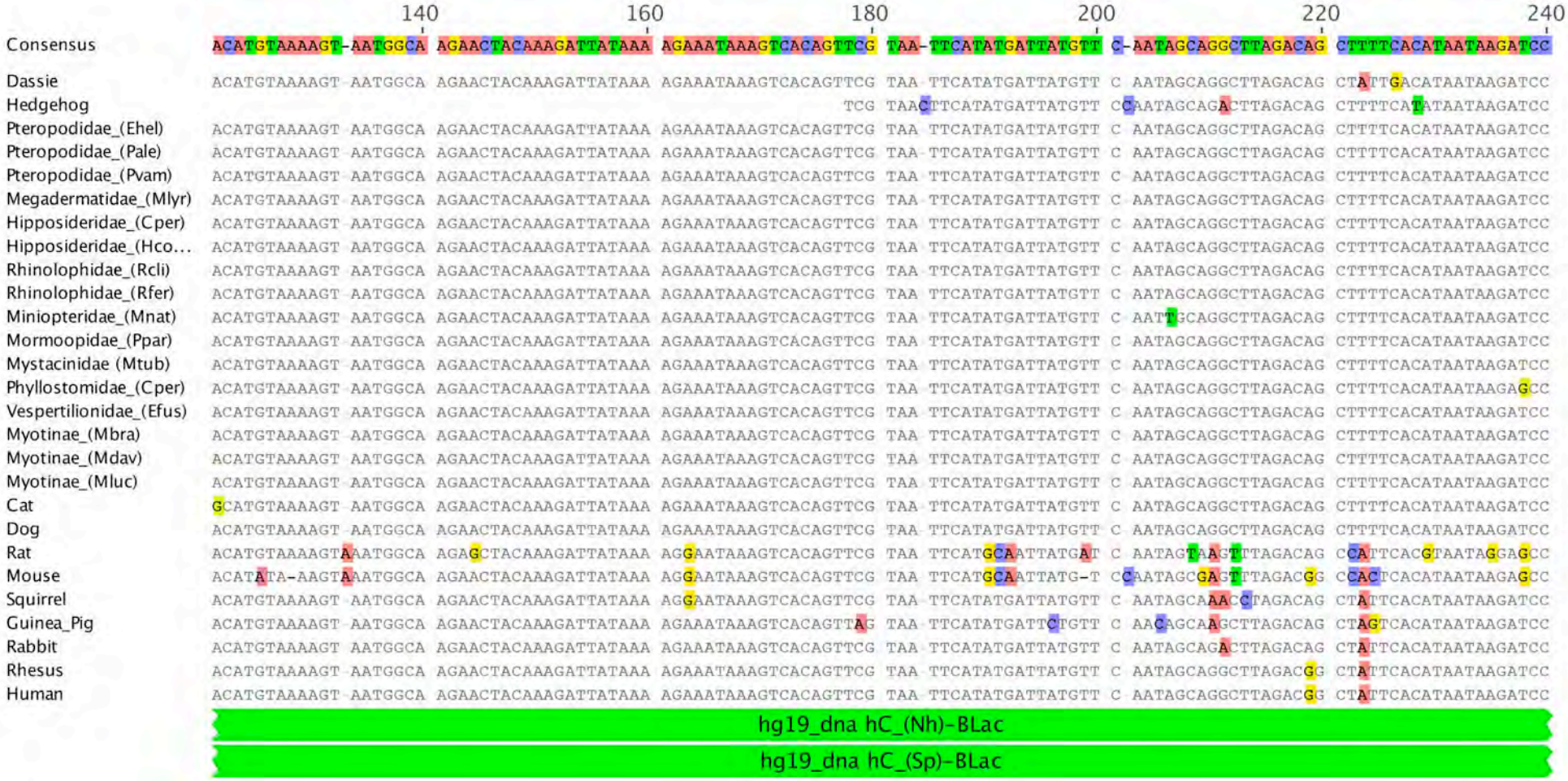

Figure C.16 cont.: Alignment of sequences for CsC region of the Prox enhancer for several vertebrate and 16 bat species.

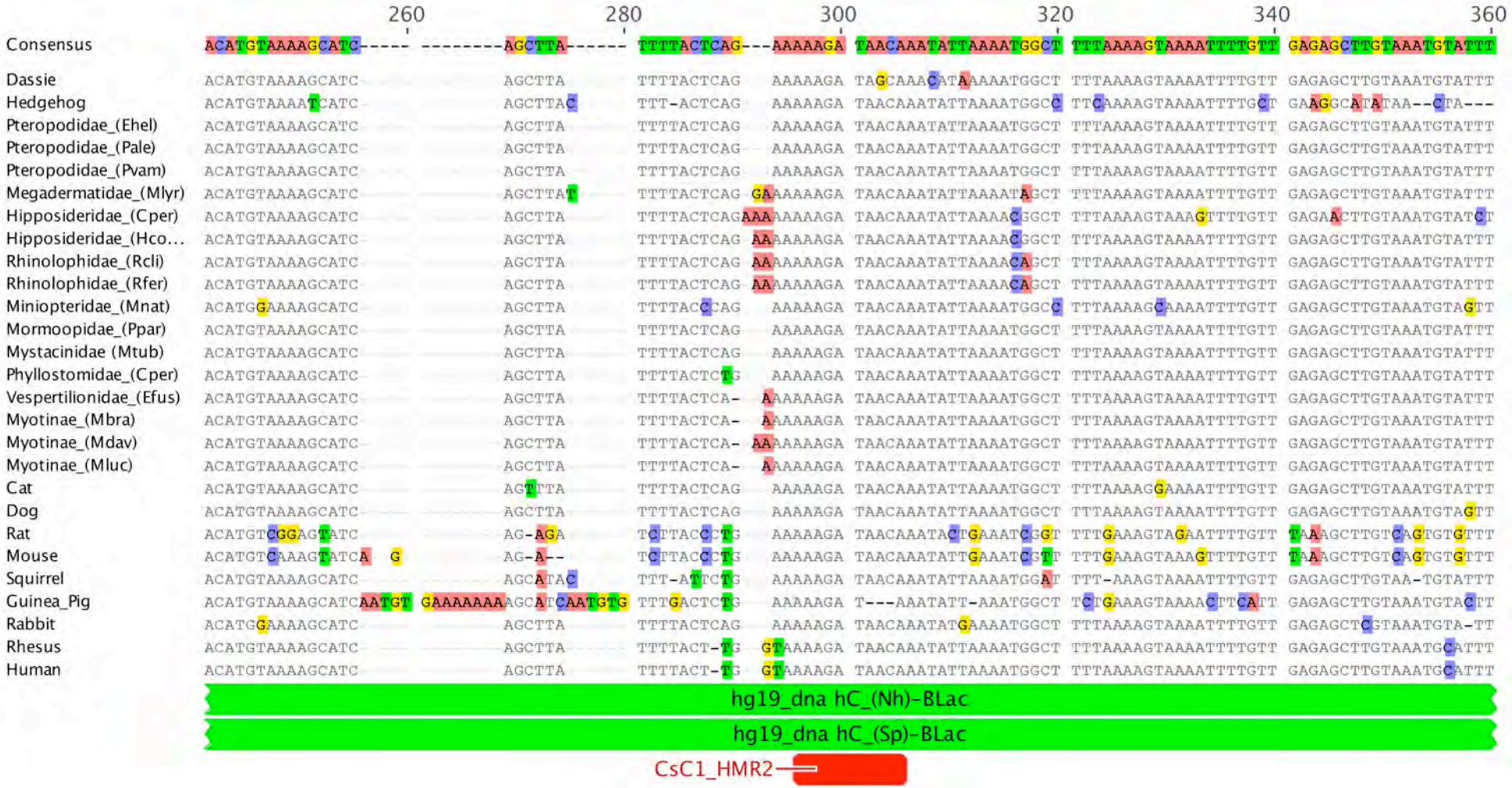

Figure C.16 cont.: Alignment of sequences for CsC region of the Prox enhancer for several vertebrate and 16 bat species.

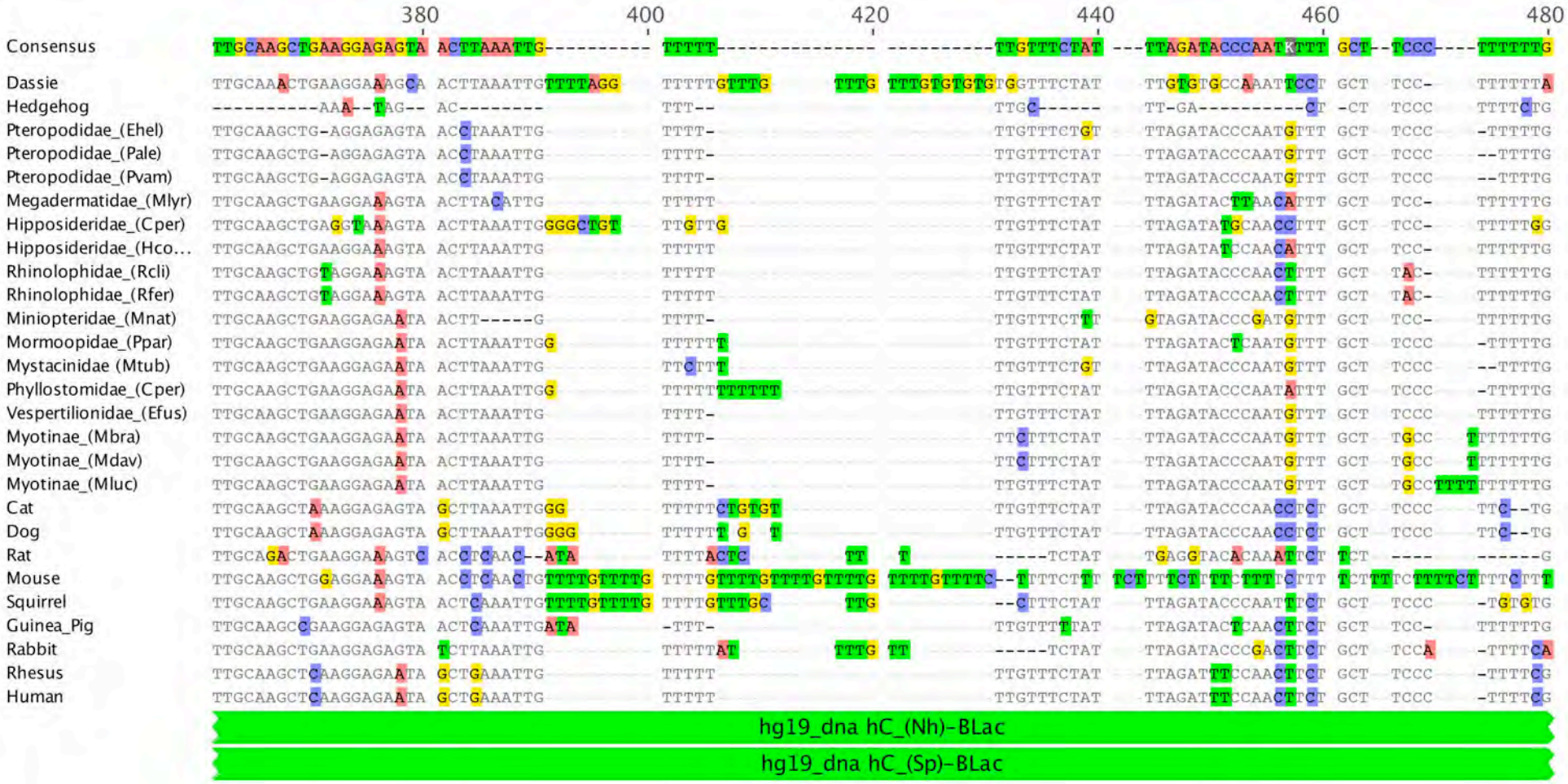

Figure C.16 cont.: Alignment of sequences for CsC region of the Prox enhancer for several vertebrate and 16 bat species.

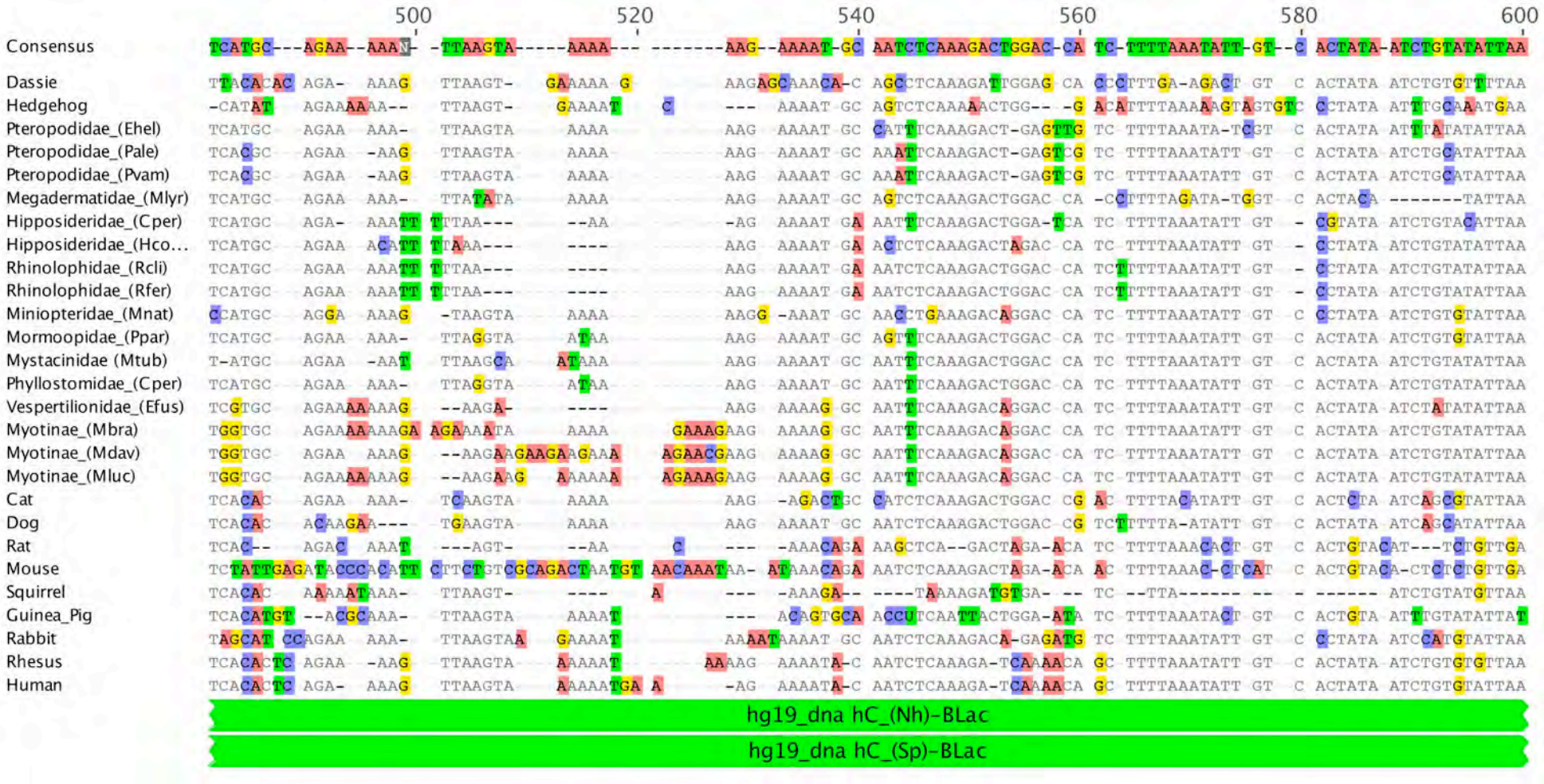

Figure C.16 cont.: Alignment of sequences for CsC region of the Prox enhancer for several vertebrate and 16 bat species.

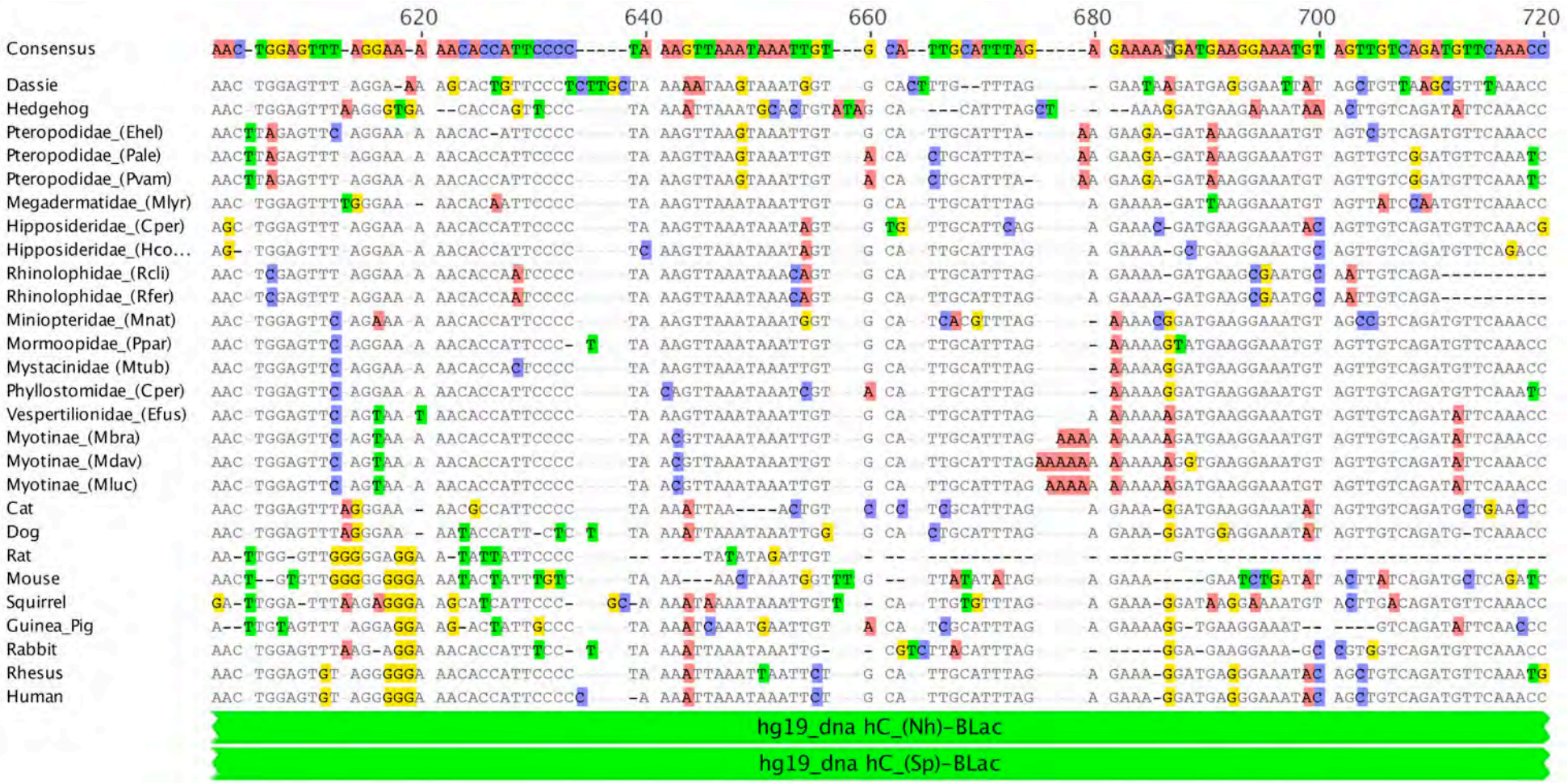

Figure C.16 cont.: Alignment of sequences for CsC region of the Prox enhancer for several vertebrate and 16 bat species.

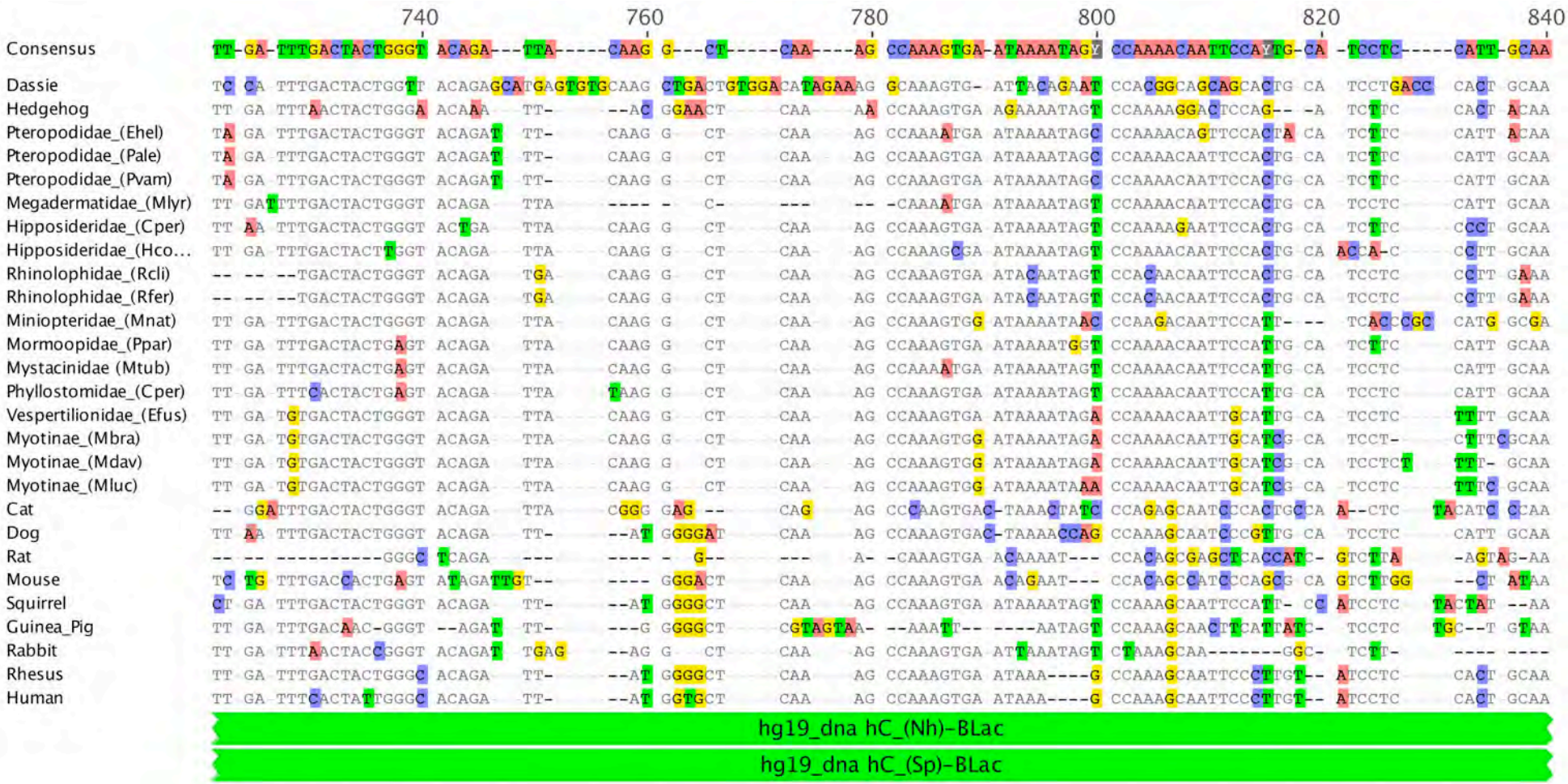

Figure C.16 cont.: Alignment of sequences for CsC region of the Prox enhancer for several vertebrate and 16 bat species.

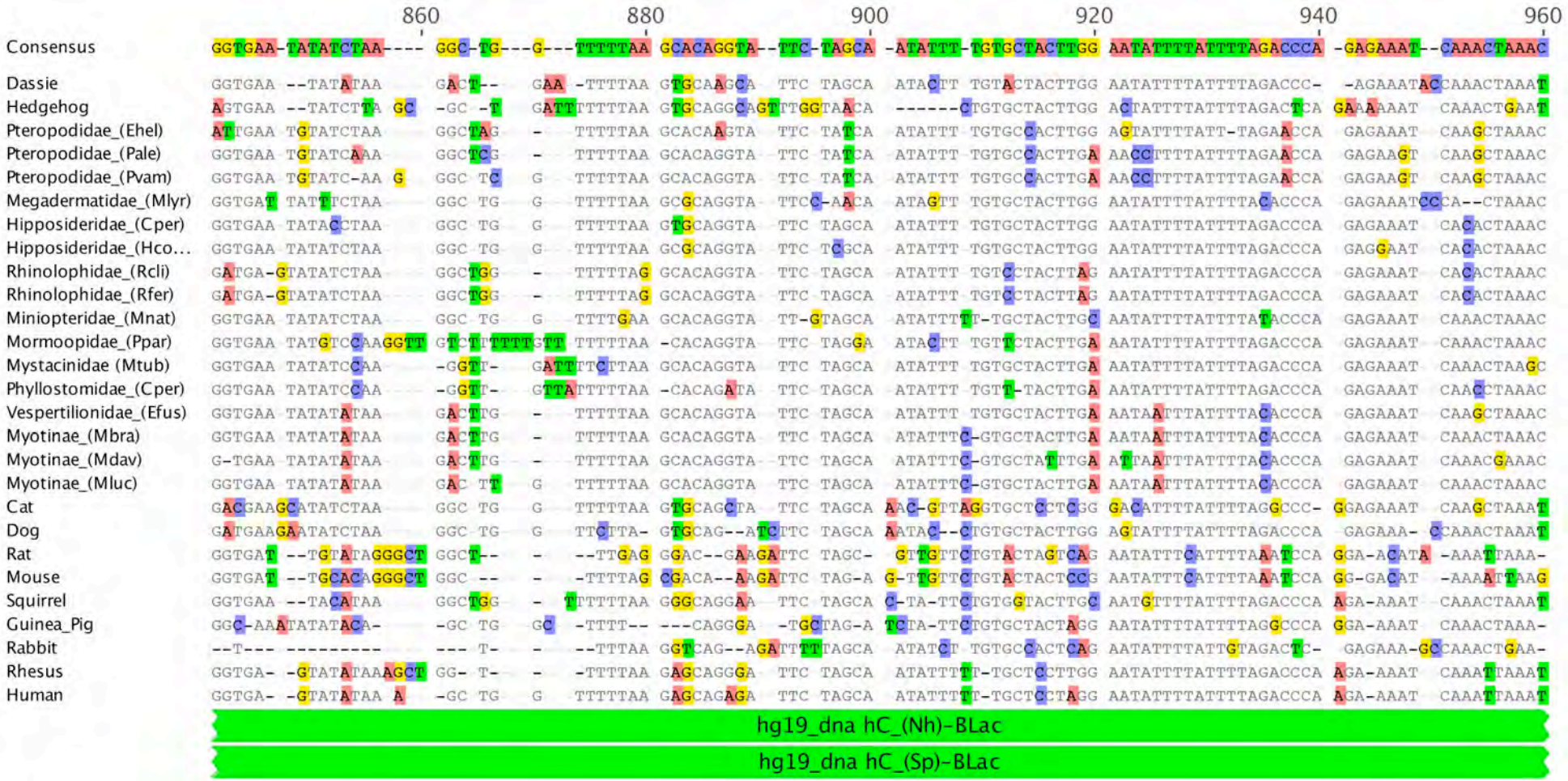

Figure C.16 cont.: Alignment of sequences for CsC region of the Prox enhancer for several vertebrate and 16 bat species.

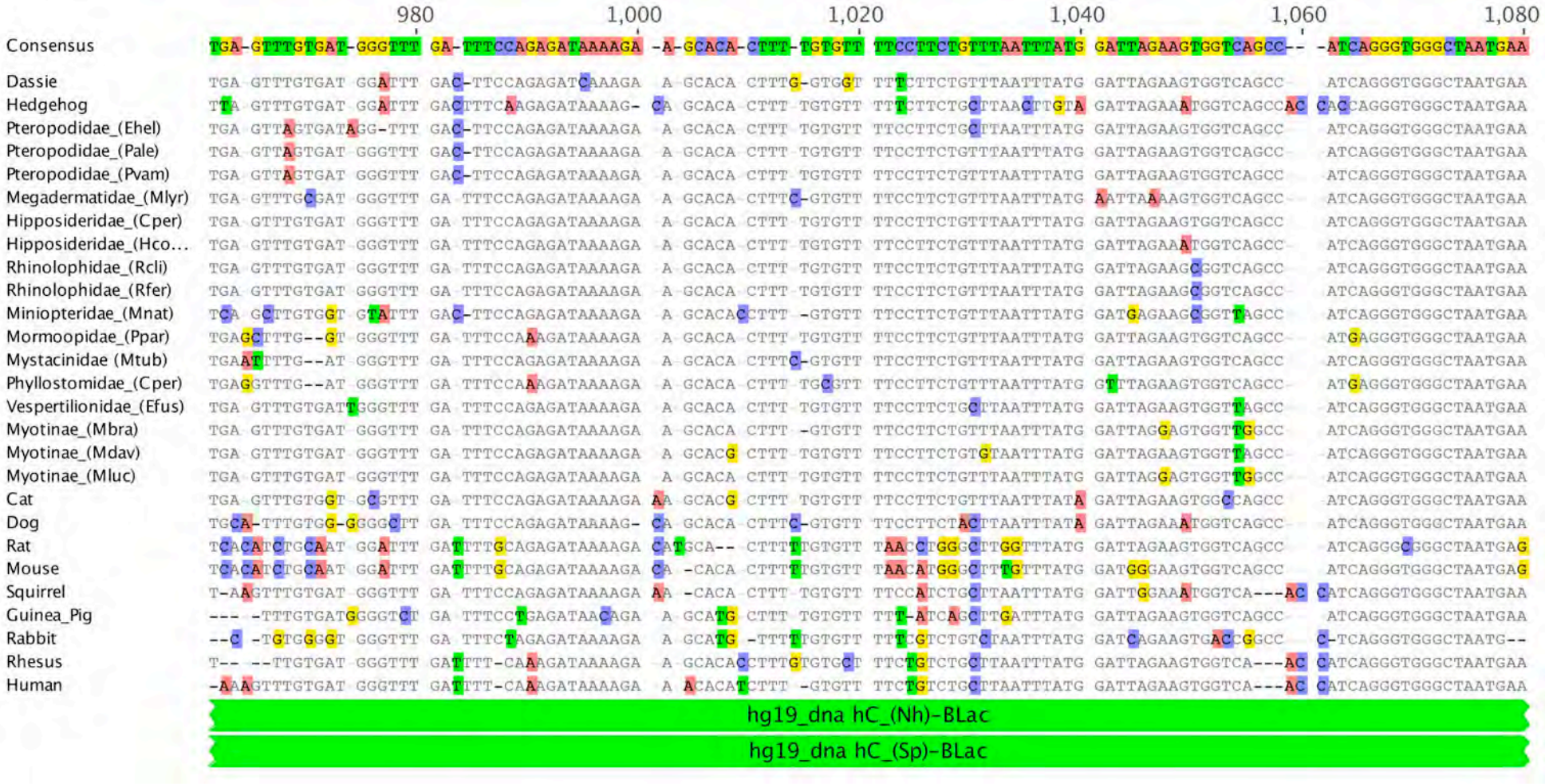

Figure C.16 cont.: Alignment of sequences for CsC region of the Prox enhancer for several vertebrate and 16 bat species.

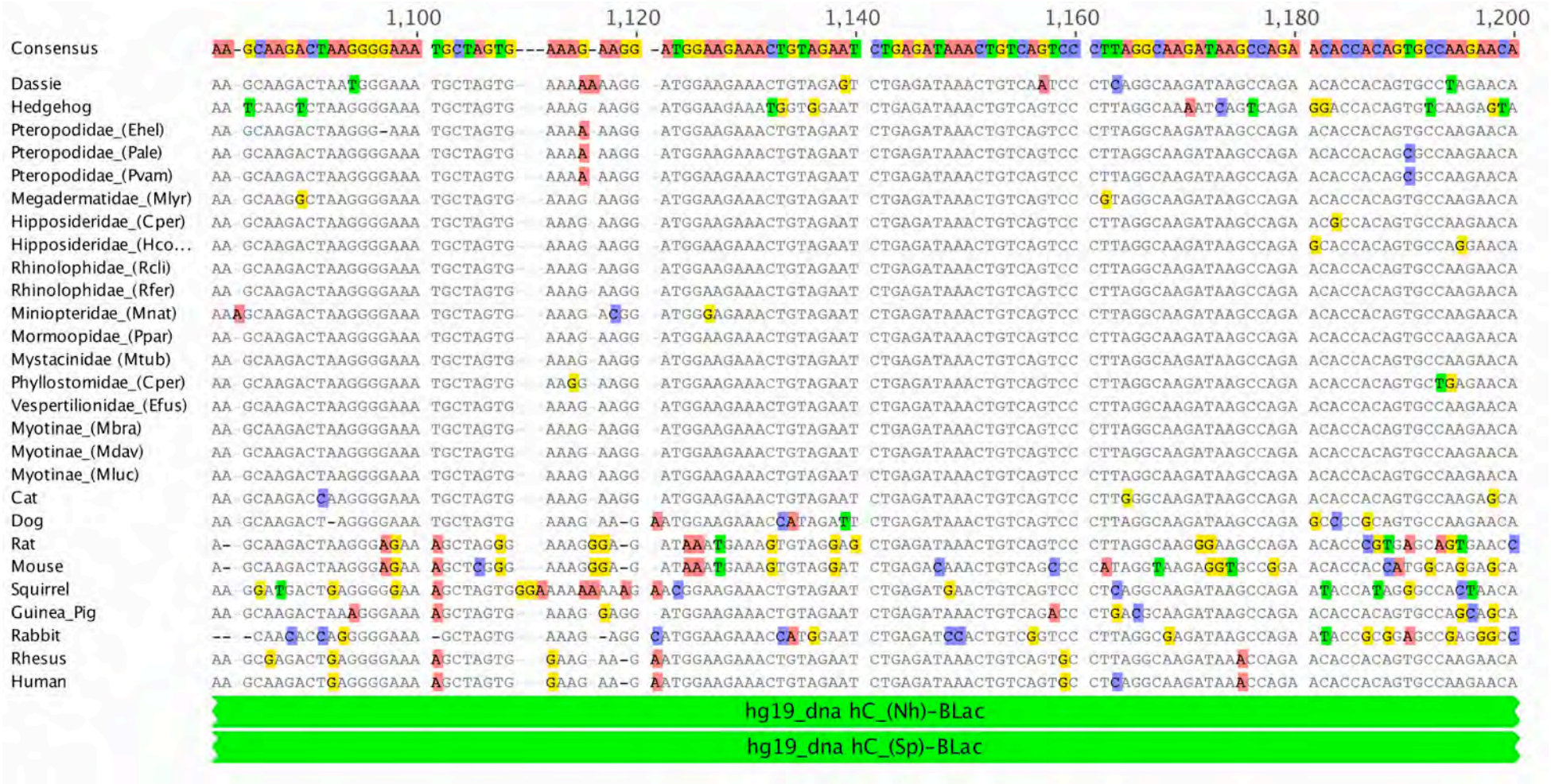

Figure C.16 cont.: Alignment of sequences for CsC region of the Prox enhancer for several vertebrate and 16 bat species.

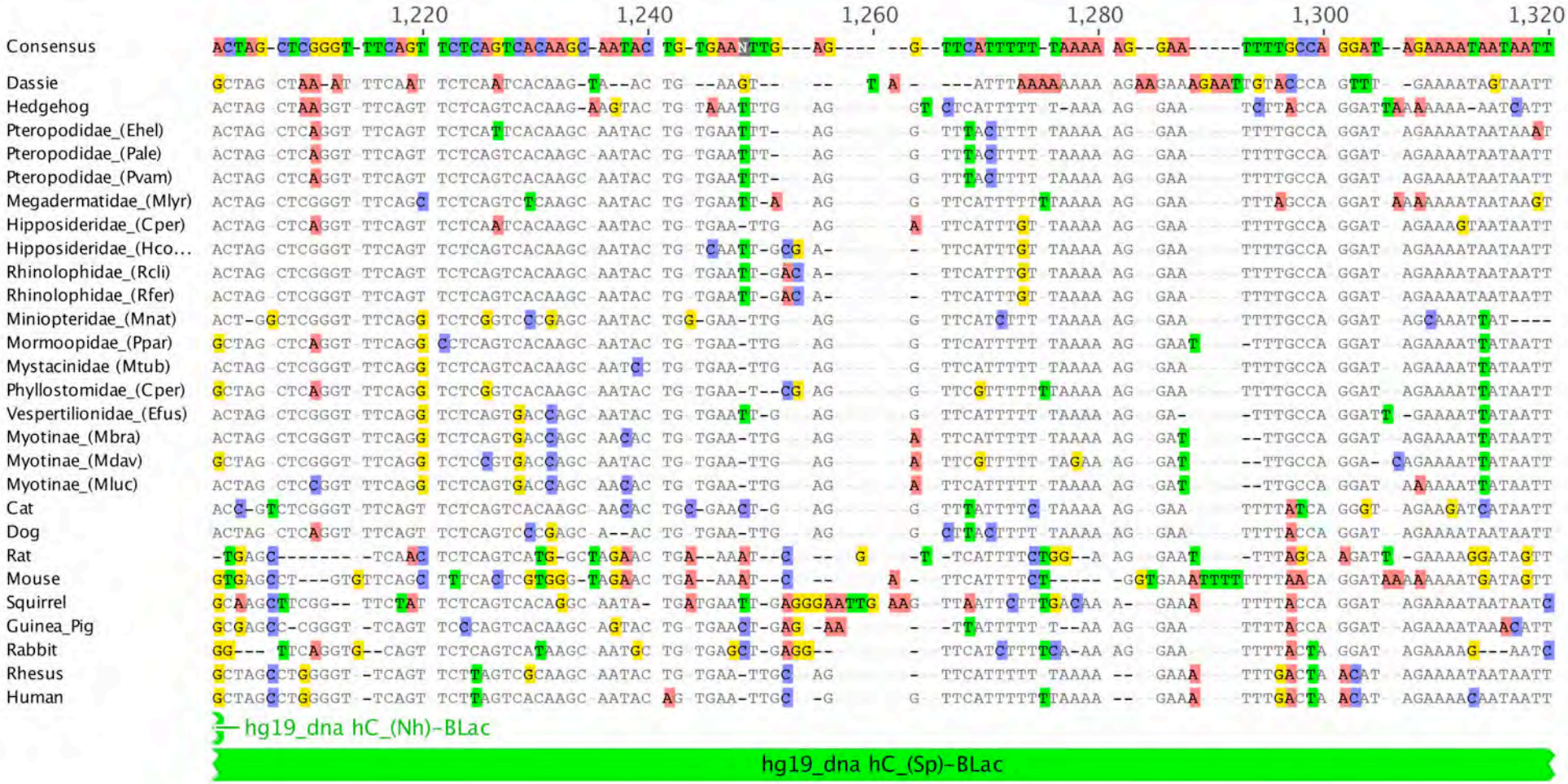

Figure C.16 cont.: Alignment of sequences for CsC region of the Prox enhancer for several vertebrate and 16 bat species.

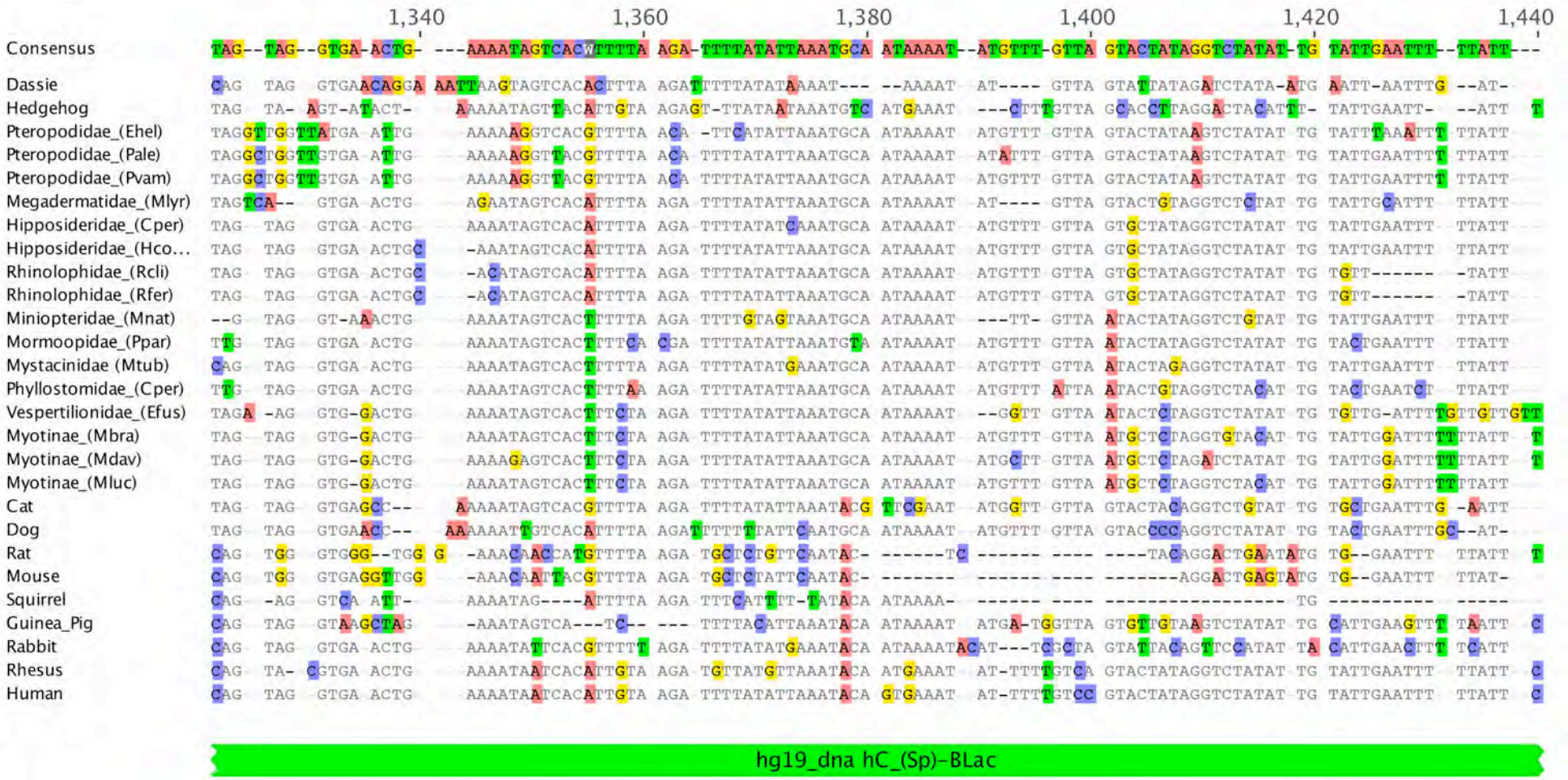

Figure C.16 cont.: Alignment of sequences for CsC region of the Prox enhancer for several vertebrate and 16 bat species.

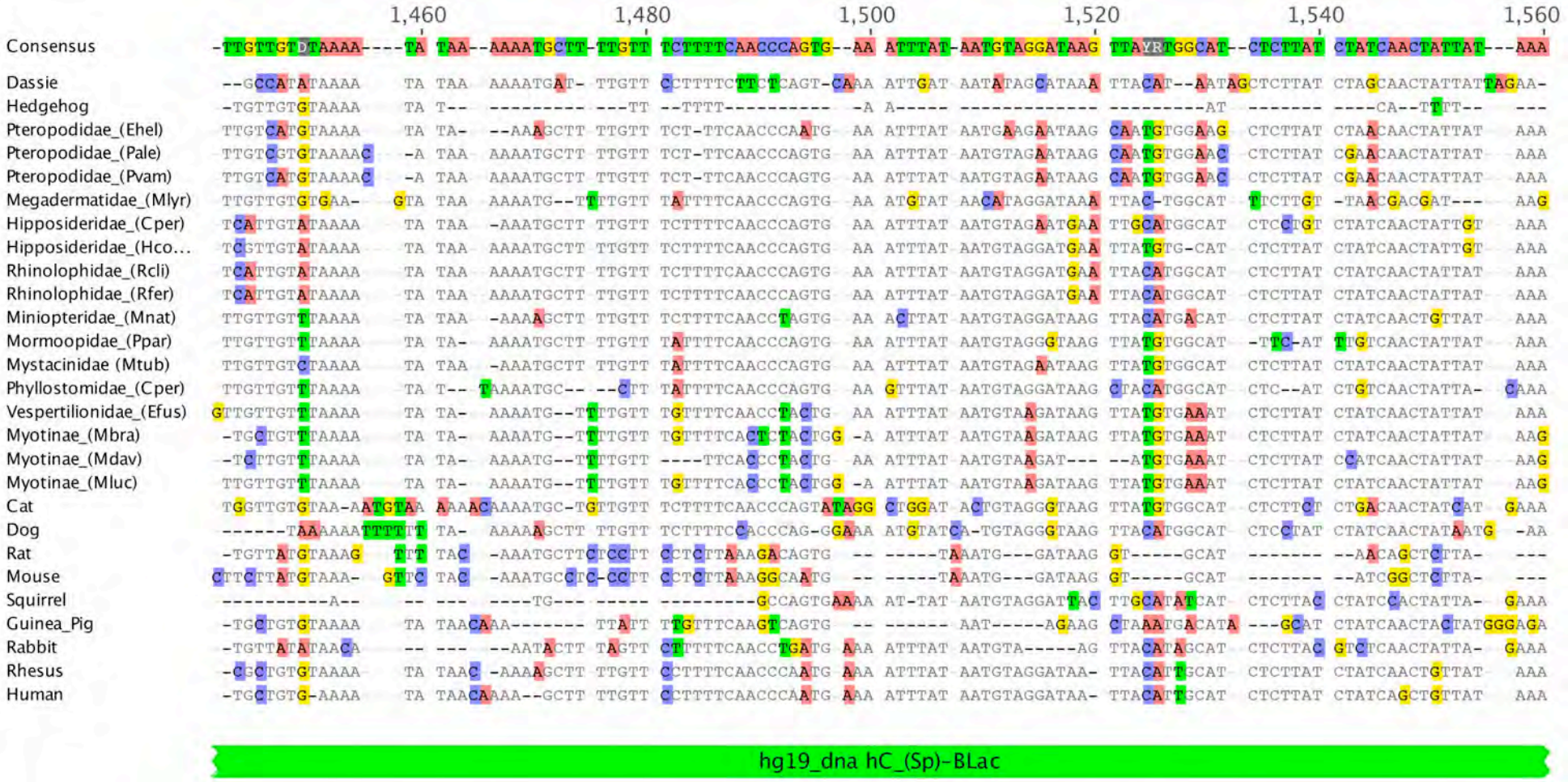

Figure C.16 cont.: Alignment of sequences for CsC region of the Prox enhancer for several vertebrate and 16 bat species.

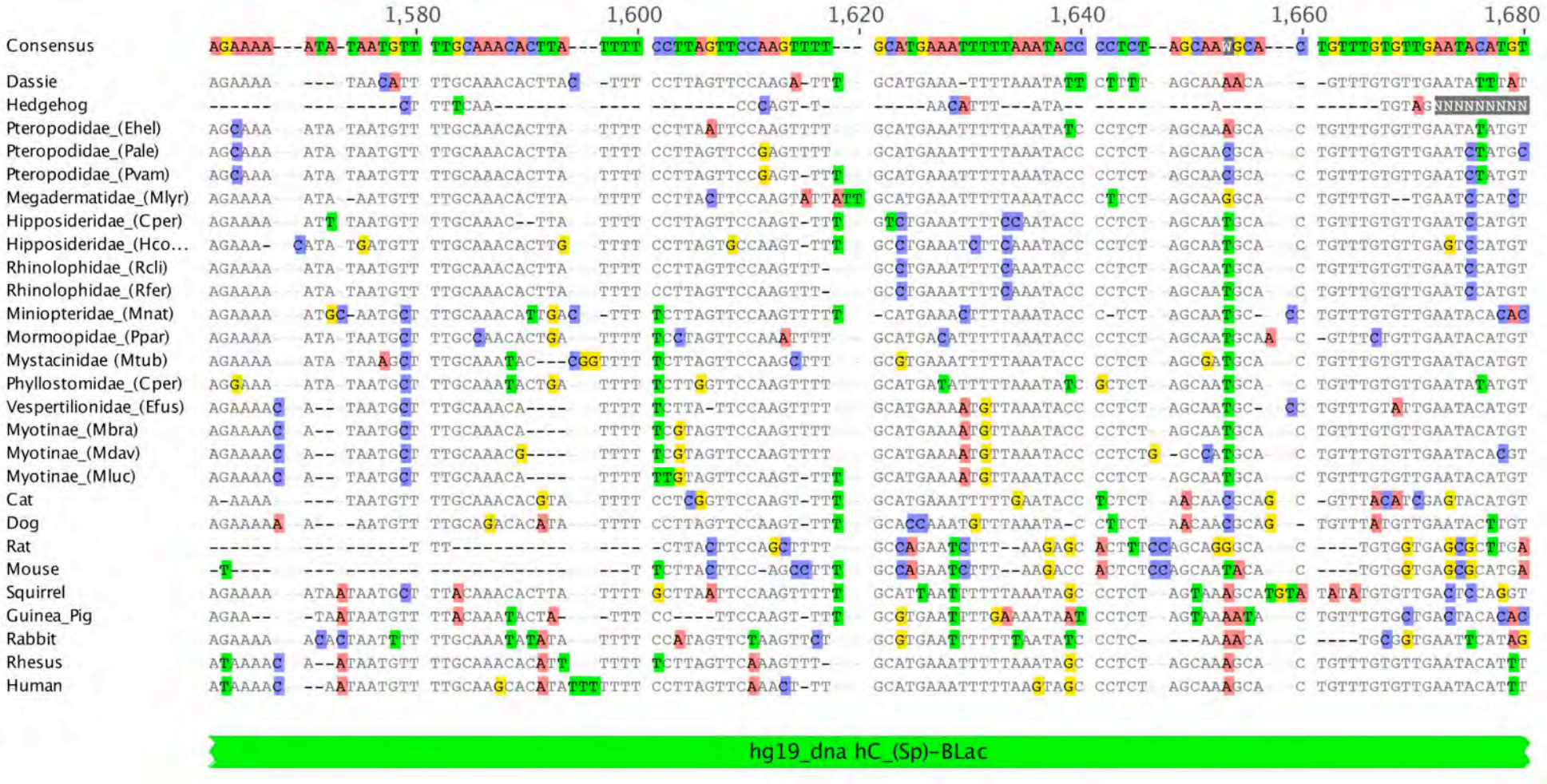

Figure C.16 cont.: Alignment of sequences for CsC region of the Prox enhancer for several vertebrate and 16 bat species.

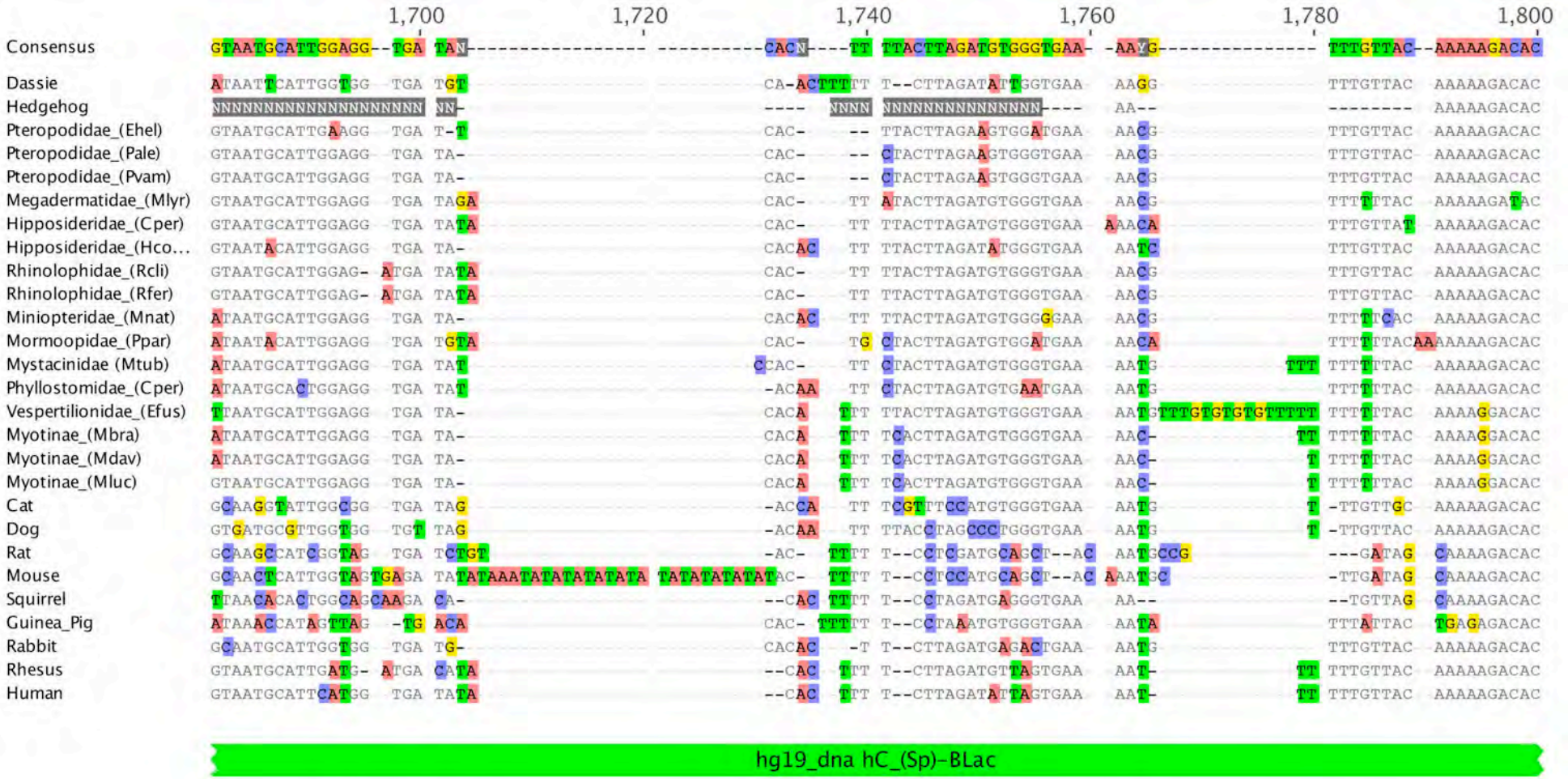

Figure C.16 cont.: Alignment of sequences for CsC region of the Prox enhancer for several vertebrate and 16 bat species.

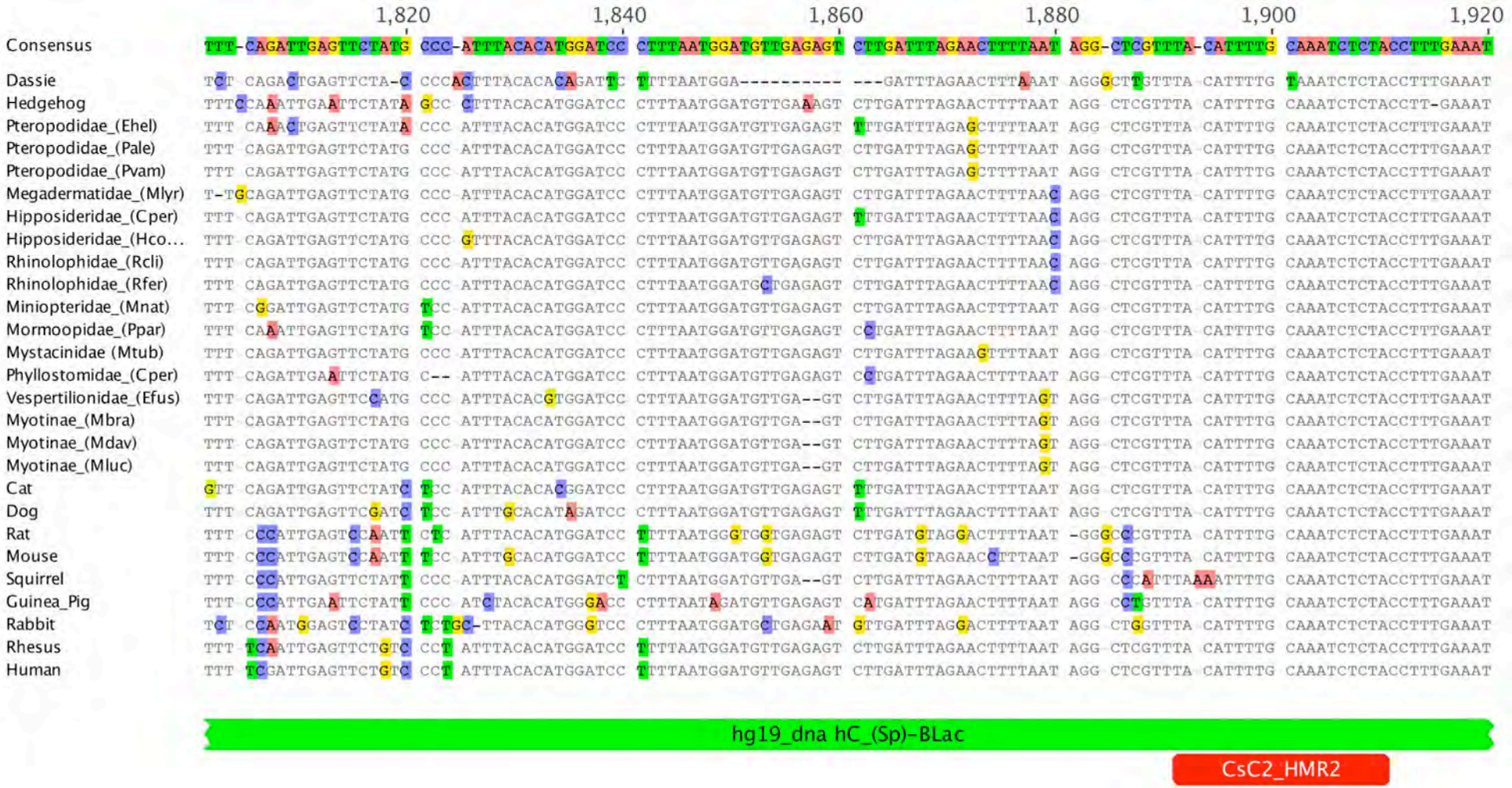

Figure C.16 cont.: Alignment of sequences for CsC region of the Prox enhancer for several vertebrate and 16 bat species.

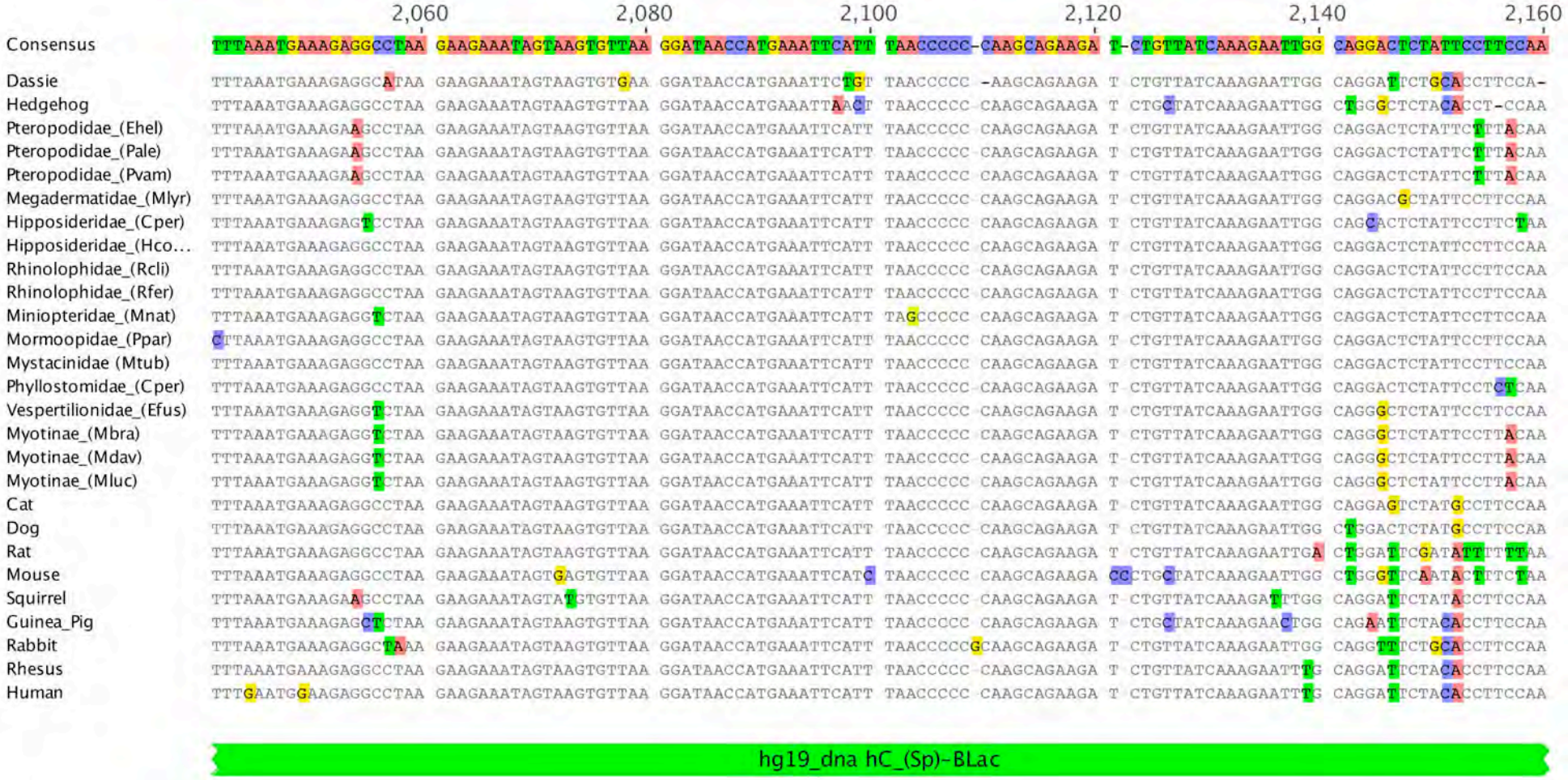

Figure C.16 cont.: Alignment of sequences for CsC region of the Prox enhancer for several vertebrate and 16 bat species.

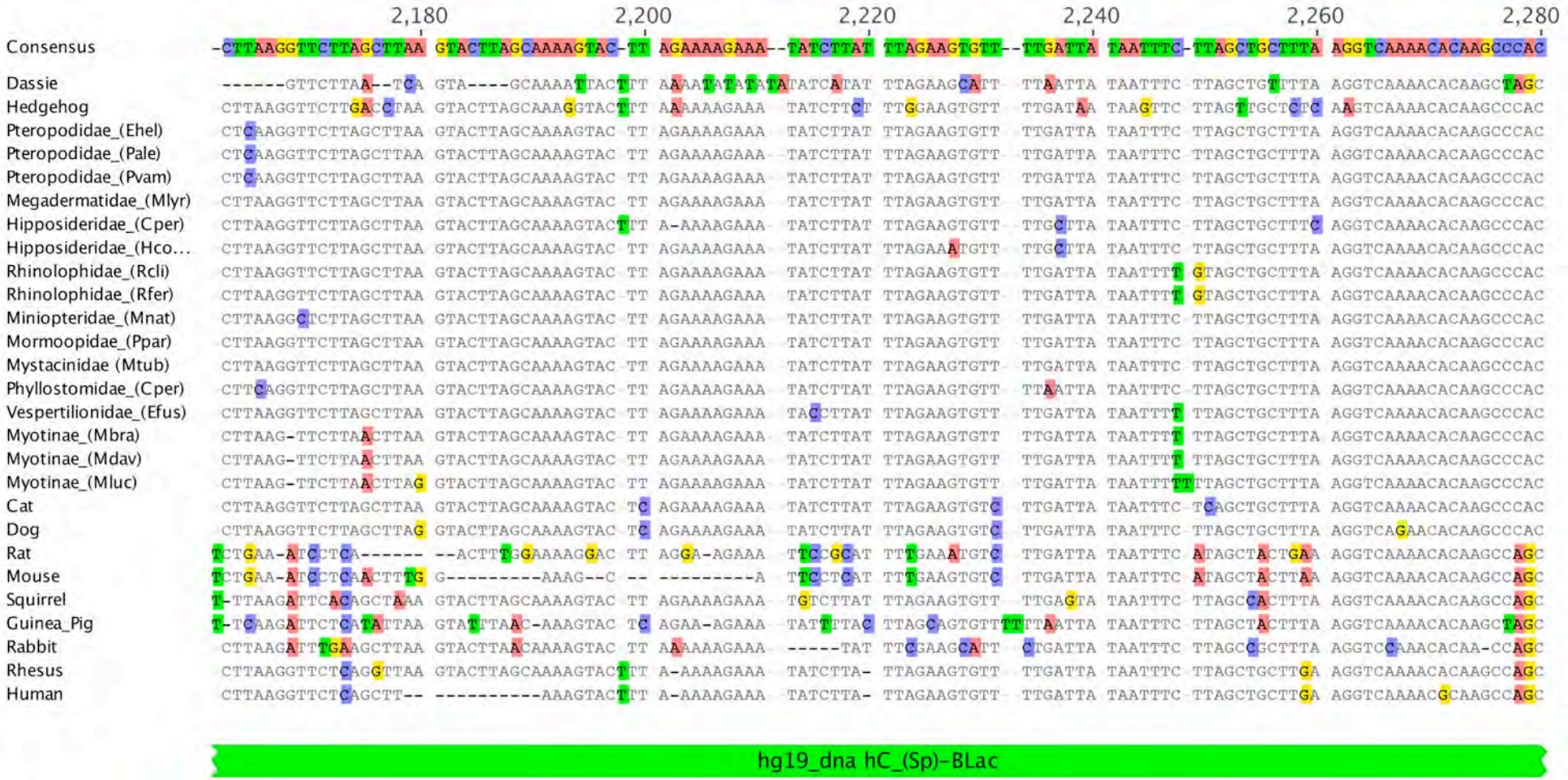

Figure C.16 cont.: Alignment of sequences for CsC region of the Prox enhancer for several vertebrate and 16 bat species.

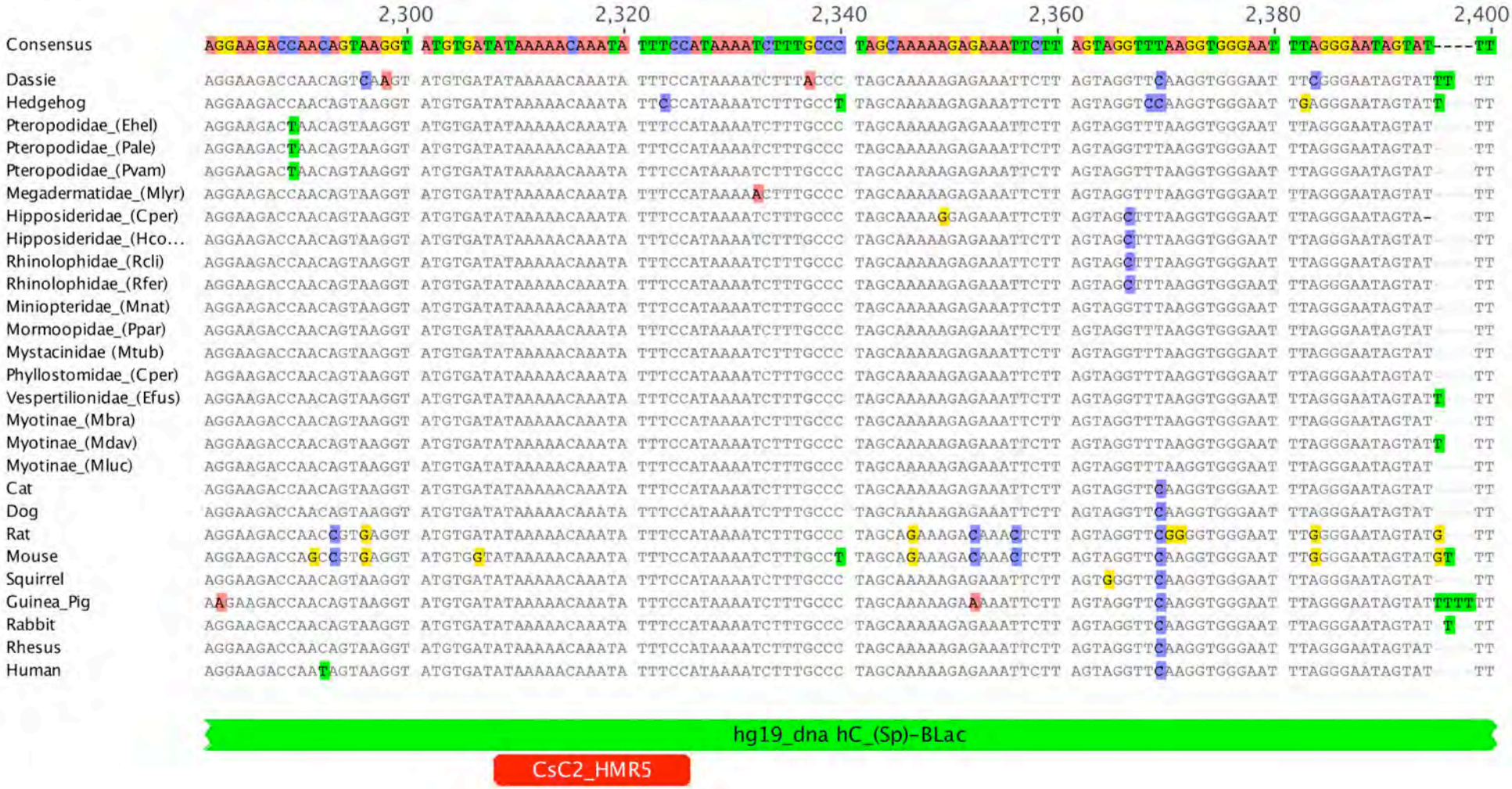

Figure C.16 cont.: Alignment of sequences for CsC region of the Prox enhancer for several vertebrate and 16 bat species.

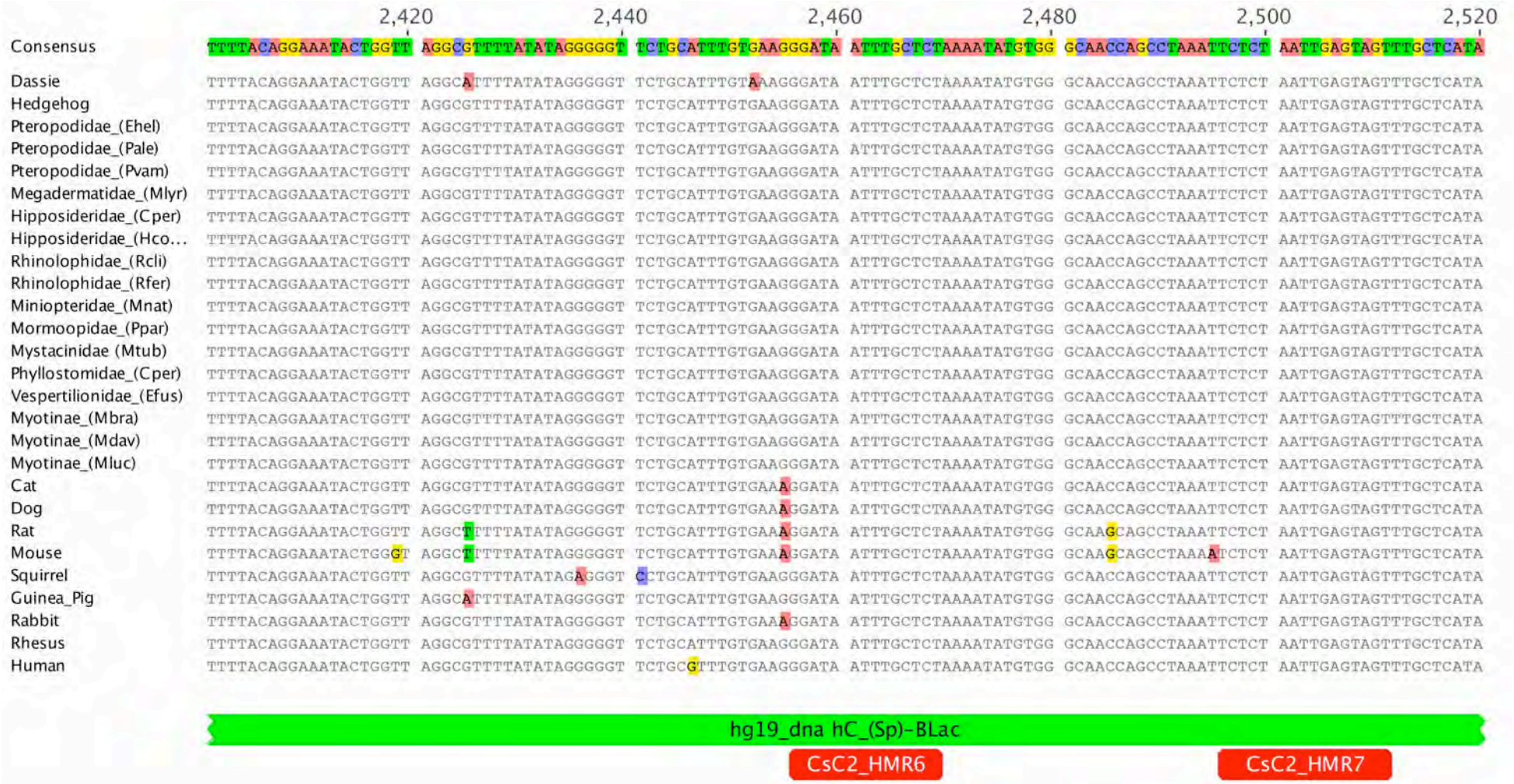

Figure C.16 cont.: Alignment of sequences for CsC region of the Prox enhancer for several vertebrate and 16 bat species.

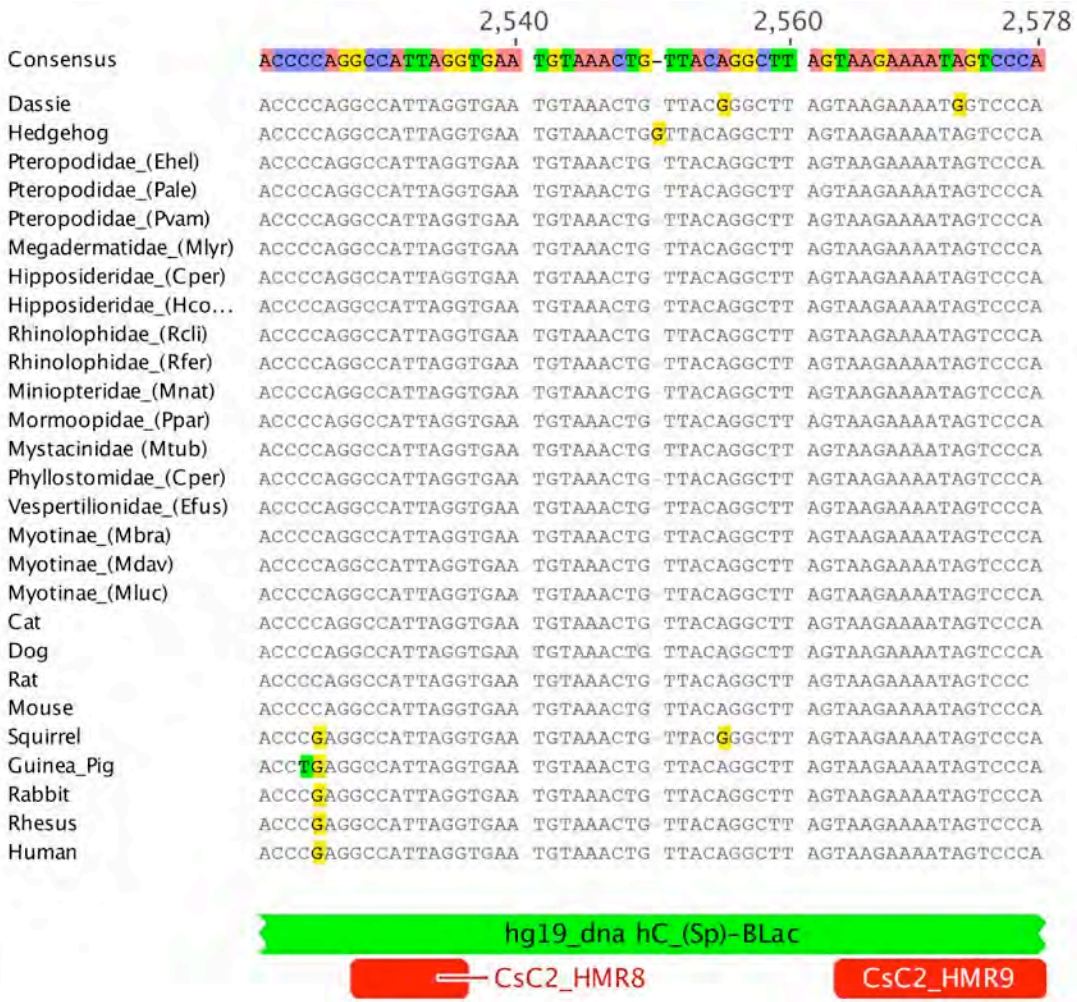

Figure C.16 cont.: Alignment of sequences for CsC region of the Prox enhancer for several vertebrate and 16 bat species.

C.28: *CsC sequence statistics*

Table C.12: Sequence statistics of partial Prox (CsC1 and CsC2) sequence alignment giving the number of identical sites, pairwise identities and GC content of the entire alignment, and regions identified as highly conserved sequences.

Alignment	Group	Identical sites	Pairwise % Identity	Ungapped lengths	GC %
Full Length (2578)	All (29)	886 (34.4%)	83.4	2 201.6±78.3 (1 859-2 254)	29.1
Full Length (2578)	Bats (18)	1653 (69.5%)	91.7	2 227.0±11.5 (2205-2241)	28.9
Full Length (2578)	Vertebrates (11)	964 (37.9%)	74	2 159.9±114.6 (1 859-2 254)	29.4
1-259 (259)	HCR_1_259	185 (71.4%)	95.9		33
281-388 (107)	HCR_2_107	33 (30.8%)	88.4		24.9
909-948 (40)	HCR_3_40	10 (25%)	81.9		29.7
968-1205 (238)	HCR_4_238	86 (36.1%)	88.7		39.5
1790-2578 (789)	HCR_5_789	516 (65.4)	94.4		34

C.29: *Conserved transcription factor binding sites in CsC region of Prox*

Table C.13: Annontated and conserved Transcription Factor (TF) binding sites in the CsC region of Prox identified using the UCSC Genome Browser (NCBI36/ hg18 and GRCh37/ hg19). Location and size of the motif is given along with its position on the CsC multispecies alignment. Nucleotide changes within these regions are noted.

Annotation	TF	Location	Size	CsC alignment	Nucleotide alteration
NCBI36/ hg18	STAT1	chr2:176598204-176598476	273	2292-2569 (CsC2)	consCsC_2369
GRCh37/ hg19	POLR2A	chr2:176888024-176888359	336	18-378 (CsC1)	None
		chr2:176888845-176889180	336	1017-1400	consCsC_1297
		chr2:176889538-176889873	336	1848-2200 (CsC2)	consCsC_2152
GRCh37/ hg19	FOXP2	chr2:176888859-176889154	296	1031-1371	consCsC_1297

Conserved TF	Item (Transfac matrix)	Location	Size	CsC alignment	Sequence
CsC1_HMR1	CDPCR3 (M00105)	chr2:176888078-176888092	15	72-86 (CsC1)	Deletion in Pteropodidae
CsC1_HMR2	GATA1_05 (M00346)	chr2:176888277-176888286	10	296-305 (CsC1)	Conserved
CsC2_HMR1	NKX61 (M00424)	chr2:176889530-176889542	13	1840-1852 (CsC2)	Lost in Laurasiatheria, Guinea pig and Squirrel.
CsC2_HMR2	OCT1/ POU2F1a (M00135)	chr2:176889580-176889598	19	1891-1910 (CsC2)	Conserved
CsC2_HMR3	NKX2-5 (M00241)	chr2:176889651-176889658	8	1963-1970 (CsC2)	Conserved
CsC2_HMR4	NKX6-1 (M00424)	chr2:176889689-176889701	13	2001-2024 (CsC2)	Conserved
	FOXJ2 (M00422)	chr2:176889695-176889712	18		
	HFH3 (M00289) FOXI1	chr2:176889697-176889709	13		
CsC2_HMR5	FOXJ2 (M00422)	chr2:176889974-176889991	18	2308-2325 (CsC2)	Conserved
	HNF-3beta (M00131)	chr2:176889977-176889991	15		
	FOXD3 (M00130)	chr2:176889978-176889989	12		
CsC2_HMR6	CHX10 (M00437)	chr2:176890118-176890131	14	2456-2469 (CsC2)	Conserved
CsC2_HMR7	S8 (M00099)	chr2:176890158-176890173	16	2496-2511 (CsC2)	Conserved
CsC2_HMR8	HOXA3 (M00395)	chr2:176890190-176890198	9	2528-2536 (CsC2)	Conserved
CsC2_HMR9	HNF-3beta (M00131)	chr2:176890224-176890238	15	2563-2578 (CsC2)	Conserved
	HOXA3 (M00395)	chr2:176890236-176890244	9		